Proceedings
Fifth International
Joint Military/Government-Industry
Symposium on
Structural Adhesive Bonding at

U.S. Army Armament Research
Development, and Engineering Center

Picatinny Arsenal
Dover, New Jersey
3-5 November 1987

DTIC DOES NOT HAVE THIS ITEM

-- 1 - AD NUMBER: D441283
-- 5 - CORPORATE AUTHOR: ARMY ARMAMENT RESEARCH DEVELOPMENT AND
--   ENGINEERING CENTER DOVER NJ ARMAMENT ENGINEERING DIRECTORATE
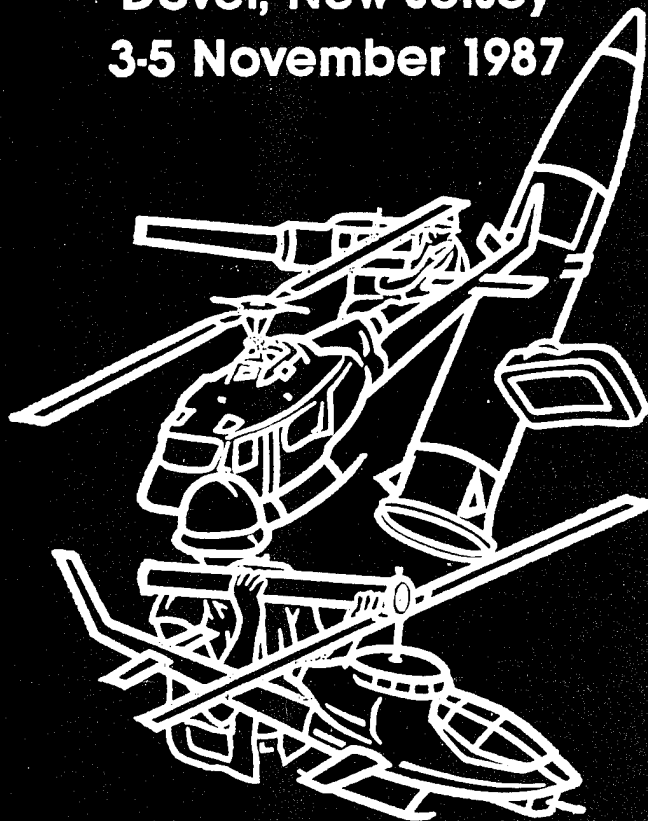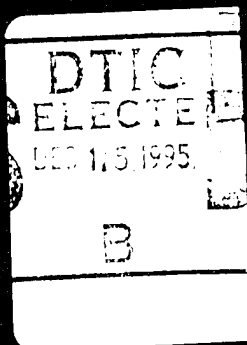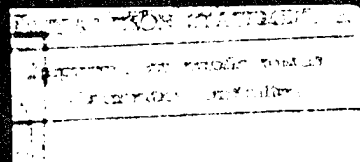-- 6 - UNCLASSIFIED TITLE: PROCEEDINGS FIFTH INTERNATIONAL JOINT
--   MILITARY/GOVERNMENT-INDUSTRY SYMPOSIUM ON STRUCTURAL ADHESIVE
--   BONDING.
--11 - REPORT DATE: NOV , 1987
--12 - PAGINATION: 508P
--20 - REPORT CLASSIFICATION: UNCLASSIFIED
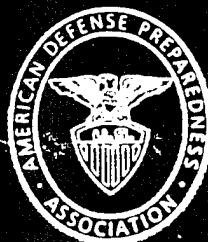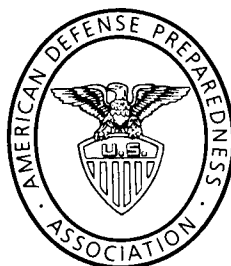--21 - SUPPLEMENTARY NOTE: IN PROCEEDINGS: THE FIFTH INTERNATIONAL
--   JOINT MILITARY/GOVERNMENT-INDUSTRY SYMPOSIUM ON STRUCTURAL ADHESIVE
--   BONDING, AT U.S. ARMY ARMAMENT RESEARCH DEVELOPMENT, AND
--   ENGINEERING CENTER, PICATINNY ARSENAL, DOVER, NJ, 3-5 NOV 1987,
--   (SEE PL-050930 - PL-050962).
--22 - LIMITATIONS (ALPHA):   APPROVED FOR PUBLIC RELEASE; DISTRIBUTION
--   UNLIMITED. AVAILABILITY: AMERICAN DEFENSE PREPAREDNESS ASSOCIATION
--   (ADPA), ROSSLYN CENTER, SUITE 900, 1700 NORTH MOORE ST, ARLINGTON,
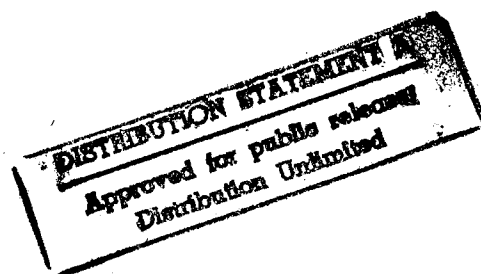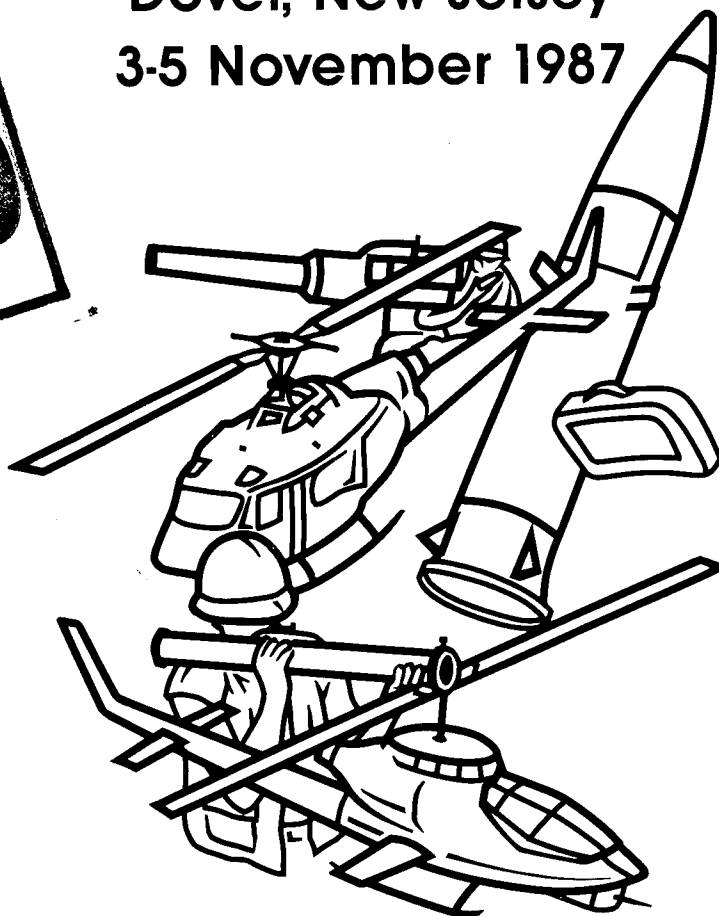--   VA 22209 ATTN: DAWN HIGGINS.
--33 - LIMITATION CODES: 1

Proceedings
Fifth International
Joint Military/Government-Industry
Symposium on
Structural Adhesive Bonding at

U.S. Army Armament Research Development, and Engineering Center

Picatinny Arsenal
Dover, New Jersey
3-5 November 1987

DTIC
S ELECTE D
DEC. 1.5.1995
B

AMERICAN DEFENSE PREPAREDNESS ASSOCIATION
U.S.

DTIC QUALITY INSPECTED 3

OBJECTIVE AND SCOPE

JOINT MILITARY/GOVERNMENT-INDUSTRY SYMPOSIUM ON

STRUCTURAL ADHESIVE BONDING

As a result of the US Army Materiel Command's "Adhesive Bonding Improvement Initiative," the US Army Armament Research, Development and Engineering Center (ARDEC) and the US Army Materiels Technology Laboratory (MTL) are conducting this international symposium with the theme "to improve the design, technology, production and testing of adhesive bonded joints for military and aerospace application."

The Army Materiel Command is placing increased emphasis on the proper application of adhesive bonding in structures and improved reliability and durability of adhesive bonded joints. Several failures of critical parts, primarily in aircraft, but also in other applications, have raised concerns that current technology may not have been properly used in design, manufacturing and quality controls, or that new technology may be needed in other instances. Areas of interest thus run the gamut from "high tech" surface analysis of failed parts to manufacturing methods and controls and testing. The whole picture must be considered to assure the fielding of reliable materiel which will meet military requirements.

In this Fifth International Symposium on Adhesive Bonding, we are honored by the many distinguished scientists and engineers from the United States and Allied and Friendly Nations who will make presentations concerning current and future technology on structural adhesive bonding. The topics covered in this symposium include:

* Army Materiel Command Perspectives
* Epoxy Systems
* New Polyimides
* Resins
* Fracture Mechanics
* Adhesion Phenomena
* Testing Techniques
* Adhesion Technology
* Air Force Bonding Applications & Operational Experience
* Epoxy Adhesives for Field Repair of Military Equipment

i

ORGANIZATIONAL COMMITTEES

GENERAL CHAIRMEN

Michael J. Bodnar
Chief, Adhesives Section
Organic Materials Branch, ATD, AED
US Army Armament Research, Development and
Engineering Center
Picatinny Arsenal, New Jersey 07806-5000

Stanley E. Wentworth
Research Chemist
US Army Materials Technology Laboratory
Watertown, Massachusetts 02172-0001

TECHNICAL PROGRAM COMMITTEE

Robert B. Bonk, Program Chairman, ARDEC

Robin L. De Caro, Editorial Assistant, ARDEC

Dean A. Martinelli, Arrangements, ARDEC

John E. Osterndorf, Planning, ARDEC

Michael J. Bodnar, ARDEC

Stanley Wentworth, MTL

Colonel Duquesne A. Wolf, US Army (Ret.), ADPA

Paula M. Beck, ADPA

PREFACE

As a result of the Army Materiel Command's (AMC) Adhesive Bonding Improvement Initiative, the American Defense Preparedness Association in cooperation with the U.S. Army Materials Technology Laboratory and the U.S. Army Armament Research, Development and Engineering Center is conducting a Joint Military/Government-Industry Symposium on Structural Adhesive Bonding. The symposium is scheduled for November 3-5, 1987 at the U.S. Army Armament, Research, Development and Engineering Center, Picatinny Arsenal, New Jersey.

The symposium theme is improved design, technology, production, and testing of adhesive bonded joints for military and aerospace applications. AMC is placing increased emphasis on the proper application of adhesive bonding in structures and improved reliability and durability of adhesive bonded joints.

This is the fifth national/international symposium on adhesives bonding that the Adhesives Section, Organic Materials Branch, Armaments Technology Division, Armament Engineering Directorate has organized and held since the early 1960's.

The symposium committee wishes to thank all of the authors and session chairmen for their participation in this symposium on Structural Adhesive Bonding. We would also like to thank ADPA for sponsoring this symposium and Colonel Duquesne Wolf for his assistance.

Michael J. Bodnar   Stanley E. Wentworth
General Co-Chairman   General Co-Chairman
ARDEC   MTL

Additional copies of this publication may be obtained
from the American Defense Preparedness Association:

ADPA
Rosslyn Center, Suite 900
1700 North Moore Street
Arlington, VA 22209
ATTN: Dawn Higgins
Telephone: (703) 522-1820

Disclaimer Clause

The findings, conclusions, or viewpoints expressed in this publication
and the presentations contained herein comprise the personal views of the
respective authors thereof and should not be construed as reflecting any
official position of the US Government, the US Army, or the American Defense
Preparedness Association. Also, no assurance can be implied that the
information contained herein is acceptable for use by others for any purpose,
and any liability respecting such use is specifically disclaimed. The use of
trade names or trade marks in this publication should not be construed as an
official endorsement of any product, nor an assurance of its suitability for
any purpose other than precisely in the context of the discussion wherein they
are mentioned. Responsibility for the content and security clearance of the
papers in this publication rests solely on the authors.

TABLE OF CONTENTS

November 3, 1987

Page

SESSION III

SESSION V

Fundamentals of Adhesion
The Science Beneath the Practice

K. W. Allen
Director of Adhesion Studies, Adhesion Science Group
The City University
London EC1V OHB, England

1. Introduction

Rather more than 60 years ago, the need for a proper understanding of the fundamental basis of adhesion was recognized by the Adhesions Research Committee of the Department of Scientific and Industrial Research of His Majesty's Government. In the First Report in 1922 it stated[1], "It is obviously necessary to investigate the nature of adhesion, be it physical or chemical. This problem, which has such an important bearing upon many branches of industry, is constantly before the Committee."

From that time until the present, various ideas and theories have been advanced to account for the observed phenomena. There has always been the hope, rarely fulfilled, that it would be possible to predict behaviour and to optimise conditions for practical application. The theories have been of differing depths of sophistication and development, but they have been slowly refined over the years. Frequently particular theories have suffered from the enthusiasm of their protagonists who have sometimes been inclined to promote their own view as a universal panacea--as improbable situation as the discovery of the alkahest! Although the fallacy of this misconception was recognised at quite an early date[2,3], it has only been accepted quite slowly. It is only comparatively recently that it has been possible to consider freely which mechanism is appropriate for any particular example of adhesion, and to attempt to resolve the way in which the contribution of different mechanisms might be combined to provide a fuller understanding of the observed phenomena.

Within this paper I shall give some account of the four principle mechanisms which have been advanced and which have gained reasonable credence. Then I shall consider the durability of adhesive joints quite broadly, and finally I shall try to draw those all together into a coherent whole.

Of these four principle mechanisms, two - diffusion processes and electrostatic interactions - are now clearly seen to be of significance in only a limited range of situations and I shall deal with those first. The other two - mechanical interlocking and adsorption interactions - are of much wider application and I shall consider them later. Since the endurance of adhesion joints is a vital factor in any real use, I

shall include a broad discussion of this before drawing some overall conclusions.

2. Diffusion Processess in Adhesion

The original work suggesting that diffusion plays an important role in at least some examples of adhesion is due to Voyutskii[4]. Fundamentally it depends upon the simple concept that if two polymer surfaces are in close contact, at a temperature above their glass transition temperature, then the long-chain molecules or at least segments of them will interdiffuse. This is undoubtedly true in the case of the adhesion of a polymer to itself (autohesion). Also when an adhesive is applied as a solution of a polymer in a volatile solvent to two surfaces, the solvent is allowed to evaporate and the two adhesive coated surfaces are brought together, it is a diffusion process which is responsible for the combination and eventual disappearance of the interface between the adhesive surfaces.

From this original idea, Vasenin[5] developed a more quantifiable theory. He started from the theories of mixing and interdiffusion of simple liquids and developed the necessary modifications to extend these to include polymers with only a small degree of liquid character. For the autohesion of a polymer to itself he deduced an expression for the force required for peeling separation in which this force was directly proportional to the rate of separation and to the fourth root of the time of contract as well as inversely proportional to the two-thirds root of the molecular weight. A number of series of experimental results by different investigators[6,7], are consistent with these relationships as is shown in Figure 1.

All this approach was criticised by Anand[8] who attributed the change with time to a slow increase in the effective area of intimate contact by rheological processes not involving diffusion. To this attack, Voyutskii[9] replied with qualitative evidence and additional interpretation and explanation.

Much of the evidence which was used in these considerations was indirect and only a proportion was direct and entirely convincing. However, now a number of workers have studied the structure of the interface by various methods including optical and electronic microscopy, radiothermoluminescence, UV luminescence, Fourier transform internal reflectance IR spectroscopy and paramagnetic probe[10]. In some instance the interface is clearly revealed as a band in which the density varies gradually from one phase to the other over a zone which ranges from 10Å to 1000Å thick--suggesting a region of interdiffusion of the two.

Vasenin's equation for the autohesion of a polymer to itself:

$$F = 11v \left\{ \left\{ \frac{d\,(2+p)}{M} \right\}^{2/3} K_D^{1/2} \right\} rt^{1/4}$$

where F - force to separate autohesion

v - vibration frequency of $-CH_2-$ group

d - density

p - number of chain branches in molecule

M - molecular weight

r - rate of separation

t - time of contact before test

K_D - constant characteristic of diffusing molecule
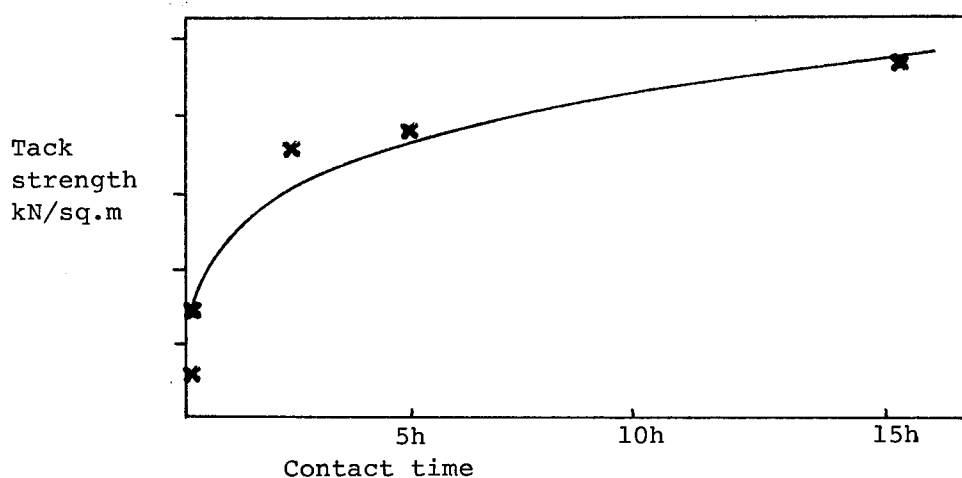
Data from Forbes & McLeod, line fitted to $t^{1/4}$
according to the equation.
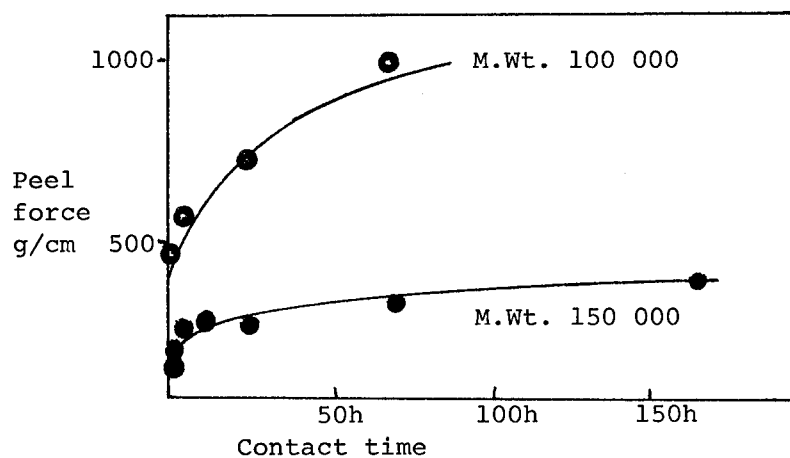
Data from Voyutskii & Shtarkh, one line fitted to $t^{1/4}$ and
other adjusted by molecular weight factor from the equation.

Figure 1.

In some examples the peeling strength of pairs of polymers varies with the temperature of bonding and shows sharp increases at temperatures which correspond with a change of the mode of failure from interfacial to cohesive. These changes can be attributed to the incidence of effective interdiffusion between the two adherents[11].

A fresh approach to this concept is by a consideration of the free volume within the polymer structure. Campion[12] developed this for a number of types of rubber and particularly considered the free space which inevitably occurs close to the chains because of their geometry. He was able to correlate the autoadhesive properties of the rubbers with the cross-sectional area of the holes associated with this configuration available for diffusion.

The usual technique for joining polycarbonates or polysulphones (sometimes also used for other polymers) is that known as "solvent welding"[13]. Either one or both surfaces are treated with an appropriate solvent and after a short time the two surfaces are brought together and pressure is applied. A good bond is produced in which the lines of the original interface cannot be discerned, although there is a zone where the polymer has evidently undergone some structural modification. It appears that the bond has been produced by interdiffusion within this zone but this is only possible when the solvent has loosened the molecular chains and allowed some mobility.

Thus overall it is apparent that for mutually compatible polymers of similar solubility parameters and at temperatures well above their glass transition temperatures then interdiffusion is a prime mechanism for adhesive bonding.

A similar mechanism to autohesion is involved when a coherent film is formed from a polymer latex. As the dispersing medium is lost by sorption or evaporation, there is a phase inversion and the polymer particles which were the disperse phase become the continuous phase. At the stage when this is occurring the long chain polymer molecules begin a process of interdiffusion which eventually eliminates the boundaries of the particles entirely.

It has been suggested that the mechanism whereby an adhesive penetrates the fine structure of a metal oxide is one of diffusion rather than simple flow. Certainly polymer does penetrate into pores and interstices which are of dimensions approaching the size of large molecules and diffusion must be a possible mechanism.

3. Electrostatic Interactions

About 30 years ago Derjaguin[14] and his co-workers developed an explanation for the properties of pressure sensitive tape based upon the development of an electrical double layer at the interface. The separation of the adherents by peeling, breaking the bond was accompanied by drawing apart of the two components of this double layer. They identified the Work of Adhesion with the electrical energy stored in the capacitor system. In qualitative terms they evinced the crackling noise and the light which are observed when a tape is peeled rapidly in dry conditions. They developed a quantitative theory and reported satisfactory agreement between theoretical and experimental results and account for the effect on peel strength of variation of the gas pressure of the situation. However, they do not appear ever to have taken account of the energy which is dissipated in the viscoelastic deformation of the adherents particularly in peeling tests.

The only attempt made in the West directly to explore this approach used direct tension tests instead of peeling tests. Great difficulty was reported in measuring the surface charge density and the bond strengths were considerably lower, even when due allowance was made for the different technique[15].

Adhesion of vacuum-deposited thin metal films on polymer substrates has been considered in terms of electrostatic interactions. Experiments showed that[16] the force needed to remove a thin metal film from a substrate by scratching with a stylus increased with the elapse of time. The suggestion that this might be due to slow oxidation processes leading to the development of chemical bonds between the metal and the insulator substrate were discounted because this effect occurred with gold as well as with base metals. Additionally if the metal was deposited and allowed to develop its full adhesive strength, and then the specimen was exposed to a corona discharge the bond strength dropped to zero. From this it was inferred, very reasonably, that there was an electrostatic origin to the adhesion.

The Russian workers argued that the origin of the electric double layer lay in electron transfer from the metal to the polymer to equalise their termi energy levels. Weaver[17] suggests that this is improbable since it would imply an excess energy of about 3eV to overcome the potential energy barrier at the interface. He suggested instead positive-hole injection with the electron moving from polymer to metal; although the nature of the charge-carrying bodies in the polymer is not clear. In any case the process would be expected to be slow both because of the relatively small number of conduction electrons in an insulator like the polymer and because they are likely to be in situations where their mobility is low. Thus the adhesion might be expected to develop quite slowly - exactly as is observed. Further, the final charge concentration might well depend upon the number of electrons available rather than upon their energy levels and no relationship would exist

between the work function of the metal and the adhesive forces developed.

If one turns from considering adhesion between plane surfaces to that of fine particles, then there is clear evidence that electrostatic forces are significant. This has been demonstrated particularly by experiments[18] with gold particles and it has been suggested as important in the retention of pollen on the stamen in flowers and in its removal by bees[19]. This is put to practical use in the installation of electrostatic precipitators to remove dust from flue gases.

Much more recently Derjaguin[20] has renewed discussion of the comparative importance of electrostatic forces as compared with the forces of molecular attraction. The particular point involved is that for a condensor, provided that the distance between the lates is small compared with the area, the mechanical force of attraction between them is independent of the distance apart. The forces of molecular attraction are inversely proportional to the cube of the distance apart. Thus at close distances the electrostatic forces may be small compared to those of molecular attraction but as the separation is increased the relative significance of these forces will change. When the process of breaking adhesive bonds is considered the electrostatic forces may contribute a not insignificant proportion to the total energy required for complete separation.

4. <u>Mechanical Interlocking</u>

The idea that attributes adhesion to the interlocking of the adhesive with irregularities and roughness of the adherent surface is both commonly advanced and surprisingly widely held. However, even a cursory review of the facts shows that it certainly cannot be of general application at least on a macro scale. Effective and strong adhesive bonds are easily made between optical glass flats which clearly demonstrates that rough surfaces are not essential.

The results for the bond strengths of maple wood samples of different roughness are clear evidence that this idea is fallacious, as is illustrated in Table 1[21].

Table 1.

Maple wood samples, bonded side grain, with U/F resin at 5 lbf in^{-2} pressure, tested in shear.

Surface	Roughness	Strength
Planed		3120 lbf.in^{-2}
Sanded		2360
Sawn		2690
Combed		2400

Nevertheless, there are some particular instances of adhesion where straightforward mechanical interlocking is important. The classical work of Wake and Boroff[22] on the adhesion of natural rubber to textile materials woven from spun staple of natural origin demonstrated that the bond strength depended upon the penetration of fibre ends from the spun yarn into the rubber. When the rubber and the textile are subjected to a stress which separates them, these fibre ends are broken. The strength of the bond depends upon the number of these fibre ends which were originally embedded.

The specific interaction between the rubber and the surface of the textile fibre is only of indirect significance in that it governs the length of fibre end which must be embedded before the interfacial shear strength exceeds the tensile strength of the fibre end. Penetration of the rubber between the yard into the weave of the fabric is of negligible importance. When the spun natural fibre was replaced by synthetic continuous monofilament the bond strength was very considerably reduced. Where, for other reasons, as in motor vehicle tyres, this replacement was desirable, then various special treatments for the textile has to be introduced to increase the specific adhesion between the rubber and the surface of the textile to achieve a satisfactory bond.

An instance which is broadly similar is that of adhesion to leather. Haines[23] showed that it was necessary to have a continuous film of adhesive between leather adherents into which the fibres of the corium must be imbedded. These fibres must be separated and raised by a roughening process which was not so vigorous that they were damaged and weakened.

Another example where it is well established that mechanical interpretation makes a significant contribution to the bond strength is in the plating of certain plastics by the electroless method. The base materials involved are either high impact polystyrene or ABS (acrylonitrile-butadiene-styrene copolymer) both of which consist of a continuous phase of a

glassy polymer with an elastomer dispersed in it. The process of plating involves an etching step which oxidises and removes the elastomer from the surface layer leaving a highly reticulate and porous structure. This is followed by a chemical reduction which deposits a first metal layer (usually copper) which is then built-up by conventional electroplating. Electron micrographs of sections show quite clearly the penetration and interlocking of the metal within the plastic to a depth of up to 10μm. A very similar process is used for plating polyalkenes, although these are homogeneous polymers. The acid etching attacks the crystal grain boundaries and various micro-inhomogeneities to produce a roughened surface. For these materials, a very thorough study by Perrers and Pettett[24] showed that there were two mechanisms involved, a specific interaction depending upon the exact chemical nature of the polymer surface and a mechanical interlocking. The final bond strength depended upon an interaction of these two components and could only be maximised if both mechanisms were operative.

These are all rather special cases and out of the main stream of adhesive technology for which it was at one time conventional to dismiss mechanical interlocking as irrelevant and unimportant. However, the view has begun to change and the beginning of the change can be traced to Packham's[25] work on the adhesion of molten polyethylene to aluminum. He studied the behaviour of polyethylene which had been sintered into the surface of aluminum which had been treated in various ways. It was already well known that anodising aluminum in an acidic electrolyte produced an oxide coating which comprised a compact and dense barrier layer immediately adjacent to the metal, surmounted by a layer of hexagonal cells each with a pore of circular cross-section at its centres. The size and number of these pores was controlled by the duration and electrical conditions of the anodising. Diameters ranged from 120 to 330Å. Experiment showed a direct correlation between the bond strength (measured by peeling) and the size and concentration of these pores in the oxide.

Electron micrographs of polymer surfaces which had been separated from the metal oxide revealed clusters of tufts. These clusters were about 1μm deep and 500 to 2000Å in diameter and correspond to groups of tufts or whiskers which had originally been inside the pores. Thus, there were very clear indications of an interlocking mechanism contributing significantly to the bond strength.

More recently, sophisticated surface analytical techniques have enabled Venables[26] and his colleagues to study the morphology of surfaces of aluminum and titanium which had been prepared for adhesive bonding by various established etching processes. These surfaces are covered with oxide whiskers and in some cases the oxide layer beneath these is porous, but all on a very small scale. The whiskers are 100 to 400Å long and

8

50 to 100Å diameter, depending upon the details of the treatment. Their evidence indicates that there is mechanical interlocking of the polymeric adhesive with the structure of this surface to give a bond which is much stronger than that achieved with a smooth surface. Indeed the bond only fails when the polymer itself yields by visco-elastic deformation. When the oxide lacks the roughness and porosity and the bond depends for its strength solely on physio-chemical forces across the interface, then separation occurs quite clearly at the boundary at much lower levels of stress which are unacceptable for structural purposes.

They have gone on to show that when these surfaces are exposed to a hostile environment, particularly high humidity, there are changes both in the chemistry and the morphology of the surface. The aluminum oxide is progressively hydrated and the characteristic whisker structure is lost, being replaced by a "cornflake" structure. The hydroxide is both itself mechanically weaker than the oxide and is much less strongly bound to the underlying metal surface. So the well known loss of strength of an adhesive bond is explained in these terms. Similar results have also been found for titanium, both by Venables[27] and indeed less precisely by Allen and Wake[28] rather earlier.

Thus, quite clear evidence has been provided and an explanation adduced for a significant mechanical component in the adhesion mechanism for structural adhesives as used in aerospace applications. But it is important to recognise that the whole scale of this mechanical interaction is very much smaller than that involved either in the other examples quoted or in the common view.

The fundamental explanation for this mechanical contribution to the total strength of an adhesive bond lies in the presence of a zone between the two materials - adhesive and adherent - where both are present. This zone results from the interpretation of the one material - the adhesive - into the roughness of the other - the adherent. The depth will depend upon the extent of this roughness and upon the degree to which the adhesive penetrates within it. In order to separate the two, energy will have to be used and work will have to be done in order to deform and draw the material of lower compliance and stiffness (the adhesive). This is always provided that the surface features of the roughness of the more rigid material (the adherent) are themselves strong enough and do not themselves fracture under the applied stress. It is this energy which is reflected in the bond strength attributable to this mechanism.

Before leaving the topic some explanation is needed of the practical experience that "roughening" a surface by mechanical abrasion does result in stronger bonds. It is important to realise that abrasion removes the outermost layers of the surface which is initially present. In doing this, a whole

variety of materials is removed; absorbed films of moisture and oil, intrinsically weak oxides and hydroxides, poorly adherent layers of oxide; all of which would have decreased the bond strength which might otherwise have been achieved. A fresh and comparatively clean surface is exposed without the weakness of the surface, rather than its roughness which enable better, stronger bonds to be achieved.

5. Adsorption Interactions

Any solid material has a mechanical strength which depends first upon the cohesion provided by the various forces of attraction between the ultimate fundamental particles of which it comprises. This strength in any real material will be reduced from the ideal value (except in very special circumstances) by various flaws, imperfections and ir-regularities in the structure. These defects are of particular effect when they occur in the surface as was demonstrated by Griffith[29] and by Irwin[30]. The forces of attraction are varied in their nature but include some ionic attractions, covalent bonds, hydrogen bonds, and van der Waals forces, differing both in their strength and in their range of effective action as is shown in Table 2.

Table 2.

Bond Type	Bond Energy (kj/mole)	Effective Range (nm)
Ionic	600 - 1200	0.2 - 0.4
Covalent	60 - 800	0.07 - 0.3
Metallic	100 - 350	0.2 - 0.6
Hydrogen	ca.50	0.3
van der Waals	ca.20	ca.1.0

Which of these forces are important in any particular material depends upon their chemistry but the van der Waals forces are universally present and effective whichever of the others are also involved. Moreover, as can be seen, they are effective over a significantly greater distance than either of the others and their rate of decrease with increase of distance is significantly less.

It has been recognised for a long time that all the forces which provide the cohesive strength of a homogenous solid are

also potentially available to provide adhesive strength across the interface between two materials in a joint[31]. The common feature of these forces as has already been indicated, is that all of them are effective over distances which are only comparatively short on an atomic scale. So if they are to be utilised across an interface between two materials it is a first and necessary requirement that they are in the closest and most intimate contact. It is from this requirement they have the necessity to apply any adhesive as a liquid springs and further leads to all our concern for the phenomena of wetting and spreading.

Perhaps it is worth indicating at this stage that it is this concept of the origin of the forces responsible for adhesion which links the whole of this part of the science of adhesion with the main stream of physical chemistry in several ways. First, there are all the classical studies of the adsorption of gases and to a lesser extent liquids, or solids. While the detailed mathematics and theories (associated with names like Longmuir and Brunauer) may have little immediate correlation with, for instance, the interaction of an epoxy adhesive system with a prepared aluminum surface, yet the fundamental ideas of interaction between two sets of different molecules are common to both. The considerations of physical and chemical adsorption have direct parallels in the exposition of the fundamentals of adhesion. Next, all that part of surface science which considers the energy relationships of interfaces and the origins of surface tension and energy is of direct and immediate relevance.

The magnitude of the theoretical attractions which can arise from these universal dispersion forces are, at first sight, surprisingly high. For two perfectly plane parallel plates when the centres of the molecules of the surface layers are separated by 1nm, the attractive force is $10^7 - 10^9$ Nm^{-2} (0.6 - 65 tons per square inch) and if the separation is increased to 10nm the force is reduced to $10^7 - 10^6$ Nm^{-2} (1 - 150 lbs per square inch)[32]. The magnitude of these forces depends, of course, upon the particular materials and is greatest between two metals and is about an order of magnitude less between two dielectrics. So clearly there is here a potential source of strength which is considerably greater than is normally achieved in real adhesive joints and this has been extensively considered.

Turning now to consider the thermodynamics involved in an adhesive joint, an outline is as follows.

The first relationship is due to Young[33] who considered the equilibrium of a drop of liquid on a solid surface and produced the well known equation:

$$\gamma_{SV} = \gamma_{SL} + \gamma_{LV}\cos\theta$$

This has been combined with Dupré's equation[34] for the reversible thermodynamic work of adhesion W_A to separate two phases, which were originally in intimate contact, to give clean surfaces which is:

$$W_A = \gamma_1 + \gamma_2 - \gamma_{12}$$

where γ_1, γ_2 are the surface free energies of the two phases and γ_{12} is the interfacial free energy between them.

Together they give:

$$W_A = \gamma_{LV}(1 + \cos) + \pi$$

where π is the spreading pressure, which allows for the effect of an adsorbed layer of vapour on the solid surface.

Good and Girifalco[35] estimated this interfacial free energy by considering the ratio of this free energy of adhesion to the geometric mean of the free energies of cohesion of the two pure phases:

$$\gamma_1 + \gamma_2 - \gamma_{12} \Big/ 2(\gamma_1 \gamma_2)^{\frac{1}{2}} = \Phi$$

where Φ is an interaction parameter which can be estimated from the properties of the two phases. They also showed that in the simplest cases Φ is approximately unity.

So $\gamma_{12} = \gamma_1 + \gamma_2 - 1 (\gamma_1 \gamma_2)^{\frac{1}{2}}$

and $W_A = 2(\gamma_1 \gamma_2)^{\frac{1}{2}}$

Fowkes[36] proposed that this work of adhesion was the result of contributions from a variety of interactions across the interface. These may include dispersion forces, hydrogen bonds, dipole/dipole and dipole/induced forces, acid/base interactions, and in addition, perhaps covalent bonds. Further, he suggested that these contributions might be combined by a simple addition, thus

$$W_A = W_A^d + W_A^h + W_A^x + W_A^i = W_A^{ab} + etc$$

and similarly the surface free energy (and the work of cohesion) could be expressed in terms of contributions from the various interactions.

$$\gamma = \gamma^d + \gamma^h + \gamma^x + \gamma^i + ab$$

where the superscripts represent d - dispersion forces, h - hydrogen bonding, x - dipole/dipole interactions, i - induced dipole/dipole interactions, ab - acid/base interactions.

These relationships were often contracted to

$$W_A{}^d = W_A{}^d + W_A{}^p$$

where the superscript p represented all the polar, non-dispersion forces involved.

Considerable success was achieved by correlations where only dispersion forces were relevant by using the Good and Girifalco relationship

$$W_A{}^d = 2 (\gamma_1{}^d \gamma_2{}^d)$$

However, this success led to the introduction of similar proposals to write

$$W_A{}^p - 2 (\gamma_1{}^p \gamma_2{}^p)$$

which are not justified in terms of the original derivation and in the terms of the approximation which put $\Phi = 1$; although they did lead to useful results in some cases.

More recently, as the fallacies of this type of extension have become recognised, considerable attention has been directed towards the nature and relative significant of the other, non-dispersion interactions.

The discussion of this was due to Bolger and Michaels[37] who, considering the case of (acidic) polar polymers and (basic) metallic oxides, suggested that the only forces other than dispersion forces which needed to be invoked were hydrogen bonds. These could best be treated using the Brönstead proton definition and theories of acid/base relationships, which gave satisfactory results for those particular examples of adhesion.

Then it was recognised[38] that this sort of treatment might be extended to a wider field by use of the Lewis acid/base definitions and theories, which consider electron donor/acceptor interactions, rather than the more limited Brönstead proton theories.

This most recent consideration[39] was based on the work of Drago[40] on the enthalpies (heats of reaction, ΔH), of acid/base pair reactions. For each conjugate pair he correlated experimental values with theoretical ones calculated on the basis of four constants, two for the acid (C_A; E_A) and two

for the base (C_B; E_B). The results demonstrated that the dipole interactions did not contribute measurably to the enthalpies of molecular interaction. This conclusion initially appeared to conflict with earlier work on intermolecular forces due to Keesom[41] and Debye[42] until the differences in the situations being considered were recognised. The latter considered gases where intermolecular distances are considerable and interactions principally involve only two molecules; whereas Drago was considering the situation in condensed phases where molecules are close and dipole interactions are minimised by multiple nearest-neighbours.

Thus the Work of Adhesion is now to be considered as effectively arising from two components, the dispersion forces and the polar forces concerned as acid/base interactions. Fowkes and his co-workers[43] have prepared a series of polymers of controlled acidity or basicity by copolymerisation of ethylene with either acrylic acid or vinyl acetate. For each of these solids they have estimated the acid-base contribution to the Work of Adhesion for a series of liquids of known basicity or acidity by measurement of contact angles. In each case a set of smooth curves was obtained relating the acid/base contribution to the Work of Adhesion with the degree of acidity or basicity. Additionally, for an acidic liquid there was nothing but dispersion forces interactions with the acidic polymers and similarly for a basic liquid with the basic polymers.

Adsorption studies of the interaction of polymers in solution in different solvents with inorganic solids confirmed this to be a three-way competition. It involved the dispersion force and acid/base interactions between polymer and solid, between polymer and solvent, and between solvent and solid. The differences in dispersion forces cancel out and it is the acid/base competition which controls the adsorption behaviour[44].

Direct effects upon adhesion can be illustrated by comparison of the adhesion of cast films of basic polymethyl methacrylate on an acidic glass (less than 0.1% alkali metal oxides) and on a basic glass (20% alkali metal oxide). It was difficult to remove the film from the acidic glass but it was quite easy to peel it away from the basic glass[45].

A survey of the practical use of adhesives indicates that acid/base (electron donor/acceptor) interactions have been utilised largely by empirical, trial and error methods and to explain rather than to predict. There is some hope that, for the future, results may be more directly achieved by considerations of the acid/base characteristics of the substrates and of the polymers used in the adhesives and selecting appropriate pairs.

14

So far this discussion has involved only the secondary interactions (van der Waals) forces in the form of dispersion forces, electron pair interactions, and dipole interactions (even if these last have been shown to be generally negligible). While, as was shown at the beginning, these secondary interactions are more than adequate to provide high bond strengths, yet there are instances where primary covalent bonding is believed to be involved. This is particularly the case where techniques have been developed to increase the durability of bonds and their resistance to deterioration in hostile environments.

Direct and positive evidence for this mechanism is somewhat sparse but there is considerable indirect evidence. The use of primers or coupling agents, particularly silane compounds, is now extensive especially for the manufacture of glass-fibre reinforced composites. The film of silane is itself polymerised and there is now clear evidence from Laser-Raman[47] that there are -X-O-Si- groups in the surface (where X represents the surface material) held by covalent bonds. It is believed that it is these covalent bonds which confer upon the interface the resistance to hydrolytic attack under wet conditions which is the particular object of the use of these primers. Indirect evidence also arises from studies where it has been shown by thermodynamic techniques that secondary interaction are insufficient to account for the observed properties of strength and durability[48].

Direct evidence also arises from introducing quite small amounts (0.001 - 0.1 mole fraction) of reactive functional groups into the adhesive which often greatly increases the adhesive bond strength[49]. For a number of cases a relationship of the form

$$\sigma_C = \sigma_O + kc^n$$

where σ_C is the adhesive strength when the concentration of functional group in the adhesive is C, and k and n are constants. Usually n is in the range of 0.6 - 1.0.

Moreover, as would be expected the effectiveness of functional groups in increasing adhesion shows considerable specificity with the adherent. Thus, particular functional groups may be selected for particular adherents where they may give rise to chemical bonding across the interface. For example, carboxyl groups (introduced by copolymerisation with acrylic, methacrylic, or maleic acid) will promote adhesion to metals.

6. Durability

If an adhesive joint is to be of practical utility then it must be able to carry a required load which may be constant or variable; for a sufficient period of time which may be as short as minutes for some military requirements or as long as decades or centuries for civil engineering structures; under particular service conditions which may be benign or harshly aggressive. While each of these factors can be examined independently, it is now common experience that they have mutual interactions.

For any structure, however constructed, there is a limit to the load which it can carry, which will normally be at a maximum for a stress steadily and smoothly applied. This is true for an adhesively bonded structure as much as for any other but generally it is probable that the adhesive bond will be the weakest part and hence the limiting factor. If the load is cyclic then, just as for metals, there is fatigue of an adhesive and failure will occur after a time at a load considerably less than test methods. There are indications[50] that this will occur at any cyclic load greater than a third of the ultimate tensile strength.

The effects of impact or shock loading have always been a severe problem for adhesives because whatever their strength they have been brittle. It is only in comparatively recent times that this has been overcome by the inclusion of an elastomeric component dispersed within the matrix of adhesive to give a toughened product. To achieve this dispersion satisfactorily with the elastomer dispersed in micron spheres which are graft copolymerised to the matrix is one of the triumphs of contemporary adhesive technology. The results and implications of this for the use of structural adhesive bonding are very considerable[51].

The service life of an adhesive is related to the maximum temperature to which it is exposed and it is in the military sphere that this has been most extensively studied. Missile structures must be able to withstand temperatures of more than 500°C but only for one minute. A supersonic transport aircraft on the other hand need only withstand half this temperature but has an expected service life of perhaps 100,000 hours[52]. To meet these varied requirements special polymers have been developed, the more extreme the demands the more exotic the polymer.

Generally, the most hostile environment which an adhesive joint encounters is moisture and this is considerably more aggressive when the joint is simultaneously under stress. The detail of this was demonstrated for a number of adhesives in a very extensive series of trials carried out by the Royal Aircraft Establishment, Farnborough. Over a period of four

years in a hot, wet climate the loss in strength varied from 5% to 25+% depending upon the simultaneous stress[53].

The mechanisms involved in this attack have been extensively explored and it now seems clear that water vapour primarily reaches the interface by diffusion through the body of the adhesive rather than via the interface itself. Once there, its effect depends upon the origin of the bonding. If this is mainly due to dispersion forces, then generally the water will displace the adhesive from the substrate. This is because, as can be demonstrated by study of the thermodynamics, this loads to a state of lower energy and is thus favourable. If in addition to dispersion forces the bond also involves primary chemical bonds between adhesive and substrate then the situation is rather different. These bonds are unlikely to be sensitive to hydrolysis and are not displaced so the bond remains intact. The corrosion which is often to be seen in metal joints which have failed due to moisture is now believed to occur subsequent to de-bonding and to be a result of rather than a cause of failure.

So it is important when a joint is to be exposed to moisture to take steps to increase the primary chemical bonding, commonly affected by the use of adhesion promoters or primers.

7. Conclusion

It should now be quite clear that none of the separate accounts of the mechanism of adhesion can reasonably claim to cover all situations. For any satisfactory account we have to look for a contribution from several to provide a combined explanation of the observed behaviour.

Undoubtedly in every case where two phases are brought together there will be dispersion forces acting between them tending to hold them together. How far these ubiquitous forces will be sufficient for practical bonding will depend upon the extent and intimacy of the contact, but they will inevitably contribute to the total interactions.

Supplementary to these there are the specific interactions which have been considered under the heading of adsorption. It now appears that the dipole interactions, which had been postulated, are insignificant compared with those arising from electron donor/acceptor interactions. These interactions are now considered in the Lewis view of acid/base behaviour and encompass hydrogen bonds. Clearly these are electrostatic forces and there must be a convergence of this approach with that of Derjaguir and his co-workers on the strictly electrostatic theory of adhesion. There appears to be a need for a fuller exploration of the relationship between these two methods of consideration.

If we turn to the mechanical component of adhesion it is evident that, other things being equal, a surface which is rough and porous on a sufficiently small scale will result in stronger bonds than one which is relatively smooth; always provided that the roughness is itself coherent and strong. There is even some indication that the precise morphology of the structure of the roughness has some effect upon the bonding behaviour. It is necessary that the surface, rough or smooth, is properly wetted by the adhesive, probably for two reasons. First of all, there must be proper intimate contact between the surfaces of the two phases so that the dispersion and electron interaction forces can be effective. Secondly, the interstices of the roughness must be penetrated so that advantage may be taken of the mechanical effect. As the extreme, the mechanism whereby this penetration is achieved, is one of diffusion so there is a relationship here with the fundamental concepts originated by Voyutskii even in circumstances remote from the areas which he was considering.

So we begin to see that an adhesive bond achieves its strength from the combination of a variety of sources; the adsorption interactions including dispersion forces, acid/base electron donor/acceptor forces, and chemical bonds, all of which may be described as electrostatic; mechanical inter-penetrations which depend both upon topography and flow and diffusion; and in the case of two polymers interdiffusion of polymer segments. For these various mechanisms, the relative importance and the proper way in which they should be combined will vary from one example to another, but none should be excluded without very careful consideration and exploration. The whole is, usually, greater than the sum of the parts.

REFERENCES

1. First Report of the Adhesives Research Committee HMSO, London 1922.

2. R. M. Vasenin, Adhesives Age, $\underline{8}$ (5), 21 and (6), 30 (1965).

3. K. W. Allen in Aspects of Adhesion 5, D. J. Alner Ed., (University of London Press Ltd, London 1969), Chap 1, p 23.

5. R. M. Vasenin (i) RAPRA Translations 1005, 1006, 1010, 1075 R. J. Mosely (1960-63) (ii) Adhesives Age $\underline{8}$, (5) 21 and (6) 30 (1965).

6. J. D. Skewis, Rubber Chem and Tech, $\underline{39}$, (2), 217 (1966).

7.   W. G. Forbes and L. A. McLeod, Trans Inst Rubber Ind, $\underline{34}$, 154 (1958).

8. J. N. Anand, J Adhesion, $\underline{1}$, 31 (1969); $\underline{2}$ 23 (1970), $\underline{5}$,

265 (1973).

9.   S. S. Voyutskii, J Adhesion 3, 69 (1971).

10. N. H. Sung, Polymer Eng Sci 19, 810 (1979).

11. S. S. Voyutskii Autohesion and Adhesion of High Polymers translated by S. Kaganoff and edited V. Vakula (Interscience, New York 1963).

12. R. P. Campion (i) J Adhesion, 7, 1 (1975), (ii) in Adhesion 1, K. W. Allen Ed (Applied Science Publishers London 1977), Chap 5.

13. W. V. Titow in Adhesion 2, K. W. Allen Ed (Applied Science Publishers London)   Chap 12.

14. (i) B. V. Derjaguin, N. A. Krotova, V. V. Karasev, Y. M. Krillova and I. N. Aleinokova, Proc 2nd Int Conf Surface Activity Div VI (c), DP 595 (1957). (ii) B. V. Derjaguin and V. P. Smilga in Adhesion Fundamentals and Practice (McLaren London 1969) p 152.   (iii) B. V. Derjaguin Research 8, 70 and 363 (1955).

15. S. M. Skinner, R. L. Savage and J. E. Rutzler, J App Phys 24, 438 (1953).

16. C. Weaver (i) in Adhesion: Fundamentals and Practice (McLaren London 1969) p 46.   (ii) in Aspects of Adhesion 5, D. J. Alner Ed. (Univ of London Press Ltd 1969) p 262.

17. As 16.

18. H. Krupp (i) J. Adhesion 4, 83 (1972) and 5, 269, (1973). (ii) in Aspects of Adhesion 8, K. W. Allen Ed. (Transcripta Books, London, 1975), p 187.

19. Sir James Beaumont, Private communication.

20. B. V. Derjaguin and Yu P. Toporov in Physiochemical Aspects of Polymer Surfaces K. L. Mittal Ed (Plenum New York and London 1983), p 605.

21. J. W. Maxwell, trans Am Soc Mech Engs, 67, 104 (1945).

22. E. M. Boroff and W. C. Wake, Trans Inst Rubber Industry, 25, 199 and 210 (1949).

23. B. M. Haines in Aspects of Adhesion 3, D. J. Alner Ed. (Univ of London Press 1967) Chap 3, p 40.

24. L. E. Perrins and K. Pettett, Plastics and Polymers, 30, 391 (1971).

25. D. E. Packham in Aspects of Adhesion 7, D. J. Alner and K. W. Allen Ed. (Transcripta Books, London 1973) p 51.

26. J. D. Venables (i) in Adhesion 7, K. W. Allen Ed. (Applied Science Publishers, London 1983) Chap 1 (ii) J Materials Sci 19, 2431 (1984).

27. J. D. Venables et al Proc 12th Nat SAMPE Tech Conf 1980 12 882.

28. K. W. Allen, N. S. Alsalem and W. C. Wake. J Adhesion 6, 153, 1974.

29. A. A. Griffith Phil Trans Royal Soc A221, 163, 1920.

30. G. R. Irwin in Treatise on Adhesion and Adhesives Vol 1, R. L. Patrick Ed (Edward Arnold Ltd, London 1966) Chap 7, P 233.

31. W. C. Wake, Adhesion and the Formulation of Adhesives 2nd Ed (Applied Science Publishers, London 1982) p 9.

32. J. R. Huntsberger in Treatise on Adhesion and Adhesives Vol 1, R. L. Patrick Ed. (Edward Arnold Ltd, London 1966), Chap 4, p 121.

33. T. Young, Phil Trans Royal Soc, 95, 64, 1805.

34. A. Dupré, Theorie Mechanique de la Chaleur (Paris 1869).

35. (i) L. A. Girifalco and R. J. Good, J Phys Chem 61, 904 (1957), (ii) R. J. Good in Aspects of Adhesion 7, D. J. Alner and K. W. Allen Ed. (Transcripta Books, London 1973), p 182.

36. F. M. Fowkes, (i) in Contact Angle, Wettability and Adhesion, Advances in Chemistry 43, (Am Chem Soc 1964), p 99 (ii) J. Adhesion 4, 155 (1972).

37. J. C. Bolger and A. S. Michaels in Interface Conversion for Polymer Coatings, P. Weiss and G. D. Cheevers Ed., (Elsevier, New York 1968), Chap 1.

38. K. L. Mittal, Pure and Applied Chem 52, 1295 (1980).

39. F. K. Fowkes, Physicochemical Aspects of Polymer Surfaces, K. L. Mittal Ed. (Planum New York and London 1985) Vol 2, p 583.

40. (i) R. S. Drago, G. C. Vogel and T. E. Needham, J Am Chem Soc 93, 6014 (1971), (ii) R. S. Drago, L. B. Parr and C. S. Chamberlain, J Am Chem Soc 99, 3203 (1977).

41. W. H. Keesom, Physik Zeit 22, 129 and 643 (1921).

42. P. Debye, Physik Zeit 21, 178 (1920), 22, 302 (1921).

43. F. M. Fowkes and S. Maruchi in Organic Coatings and Plastics Chemistry Preprints (Am Chem Soc 1977), 37, 605.

44. F. M. Fowkes and M. A. Mostafa Ind Eng Chem Prod Res & D, 17, 3 (1978).

45. F. M. Fowkes, Physicochemical Aspects of Polymer Surfaces, K. L. Mittal Ed (Planum New York and London 1985) Vol 2, p 583.

46. J. L. Koenig and P. T. K. Shih, J Colloid & Interface Sci 36, 247 (1971).

47. M. Gettings and A. J. Kinloch, (i) J Material Sci, 12, 2511 (1977), (ii) Surface Interf. Analysis 1, 189, (1980).

48. K. W. Allen, L. Greenwood and W. C. Wake, J Adhesion 16, 127, (1983).

49. S. Wu, Polymer Interface and Adhesion (Dekker, New York 1982), p 420.

50. K. W. Allen, S. M. Smith, S. C. Wake & A. L. van Raalte, Int J Adh and Adhesives 5, 23 1985.

51. W. A. Lees, J Adhesion, 12, 241, 1981.

52. A. K. St. Clair NASA Tech Memo 81884, 1980.

53. W. C. Wake in Adhesion and the Formulation of Adhesives (Applied Science Publishers London 1982) Chap 8.

BIOGRAPHY

Dr. Allen is the Director of Adhesion Studies at The City University, London, England. His work and published papers include preparation of surfaces for bonding titanium, stainless steel, and tantalum; properties of silane primer films; creep and effects of cyclic loading of joints; the concept of an endurance limit for bonds; encapsulation of electronic devices for implant with the human body, etc. Since its inception 25 years ago, he has organized the Annual Conference on Adhesion and Adhesives at City University--now recognized as one of the premier venues world-wide in this field. He has edited the proceedings since 1973. Dr. Allen has presented papers at many conferences, including ones in France, East Germany, Bulgaria,

Czechoslovakia, as well as in Britain and the United States. He was entirely responsible for the unique MSc course in Adhesion Science and Technology at City University until its unfortunate suspension. Dr. Allen was a founding member of the Adhesives Group of the Plastics and Rubber Institute and is at present Chairman of the Group.

ADHESIVE PROPERTIES OF A SEMI-CRYSTALLINE POLYIMIDE

P. M. Hergenrother
NASA Langley Research Center
Hampton, VA 23665-5225

and

S. J. Havens
PRC-Kentron, Inc.
Hampton, VA 23666

ABSTRACT

Adhesive and film properties of a new semi-crystalline polyimide, designated LARC-CPI, having a glass transition temperature of 222°C and a crystalline melt temperature of 350°C are presented. The films exhibited excellent resistance to solvents and strong base and 25 and 232°C tensile strengths, tensile moduli, and elongations of 23,000 and 8,400 psi, 630,000 and 340,700 psi and 8.3 and 9.6% respectively. Compact tension specimens from LARC-CPI moldings displayed a fracture energy (G_{Ic}) of 37.8 in lb/in^2. Titanium tensile shear specimens gave strengths of 6250 psi initially at 25°C, 7120 psi at 25°C after 1000 hours at 232°C, 2800 psi at 232°C after annealing for 5 hours at 300°C and 3670 psi at 232°C after 100 hours at 316°C in air.

INTRODUCTION

High temperature adhesives are needed to join ceramics, composites, metals and plastics to themselves and to each other and must often retain high strength under very severe environments. These adhesives are required for use in a variety of applications in the aerospace, electronic, energy, and household industry. A major part of our effort has focused on the development of high

temperature structural adhesives for the aerospace sector. For example, adhesives are required for hundreds to thousands of hours of performance around the engines on commercial airplanes where the temperature may be as high as ~370°C depending upon the application. High speed aircraft structures demand tens of thousands of hours at temperatures up to ~260°C. Space vehicles require performance for hundreds of hours at temperature to ~300°C. Missiles require mechanical integrity for less than a minute but temperatures can exceed 540°C. Adhesives for use in most of these applications require a unique combination of properties such as processability, environmental durability and high mechanical properties. Many experimental polymers have shown good adhesive properties for thousands of hours at 230°C and short term at temperatures as high as 540°C (1). However, only a few high temperature organic adhesives are commercially available* (2-4). Of these, LARC-TPI has displayed excellent retention of adhesive properties at 232°C after

32,000 hours at 232°C (5). In continuing work on high temperature structural resins for potential use on aerospace vehicles, a series of new polyimides, many semi-crystalline, were prepared (6). The chemistry, physical and mechanical properties of one of these new semi-crystalline polyimides, designated LARC-CPI, will be discussed herein with particular emphasis on the adhesive performance.

EXPERIMENTAL

Polymer Synthesis -
3,3',4,4'-Benzophenonetetra-carboxylic dianhydride (BTDA) was reacted with 1,3-bis(4-aminophenoxy-4'-benzoyl)benzene (1,3-BABB) in N,N-dimethylacetamide (DMAC) at 15% solids content to initially yield an extremely viscous solution of

*The use of trade names of manufacturers does not constitute an official endorsement of such products or manufacturers, ether expressed or implied, by NASA.

24

poly(amic acid) which dissipated after stirring overnight at ambient temperature to a less viscous amber solution. This solution was used to cast films, coat glass carrier to form adhesive tape or graphite fiber to form prepreg. Subsequent drying to 300°C converted the poly(amic acid) to the polyimide. More detailed discussion on the purification of BTDA and DMAC and the synthesis of 1,3-BABB, the poly(amic acid) and the corresponding polyimide has been described elsewhere (6).

In some cases, the stoichiometry of the polymerization of BTDA with 1,3-BABB was upset in favor of the BTDA in an attempt to obtain a lower molecular weight polymer with better processability. As an example, a poly(amic acid) with an inherent viscosity of 0.50 dL/g (measured as 0.5% concentration in DMAC at 25°C) was obtained when the stoichiometry was upset by at least 5 mole percent in favor of BTDA and the reaction was stirred at ambient temperature under nitrogen for 24 hours. This polymer was found to give improved processability without adversely affecting physical properties. The molecular weight of the poly(amic acid) as evidenced by inherent viscosity will change (decrease) upon longer exposure at ambient temperature. Cold storage of the poly(amic acid) solution will greatly lessen the change in molecular weight.

LARC-CPI powder (~170 microns in diameter) was obtained by heating a m-cresol solution of the monomers containing toluene (to azeotrope the water) to 180°C for 12 hours. A powder separated which was isolated by filtration, boiled in methanol and subsequently dried at 300°C for 1 hour.

Films - The poly(amic acid) solution (15% solids concentration) was centrifuged, the decantate cast onto plate glass using a 30 mil doctor blade, and dried to a tack-free form in a dust-free chamber. The films on glass were then thermally converted to the polyimide by heating in air at 100, 200, and 300°C for 1 hour at each temperature. In some cases, boiling in water was required to remove the polyimide films from the glass plates. Mechanical

properties of the 2.0 - 2.5 mil thick films were determined according to ASTM D882 using four to six specimens per test condition.

Moldings - In a 1.25 in.^{2} stainless steel mold, the LARC-CPI powder was compression molded at 400°C under 2000 psi. Miniature compact tension specimens (0.625 x 0.625 x 0.375 in. thick) were cut from the molding and subsequently tested to determine fracture toughness according to ASTM E399 using four specimens.

Adhesive Specimens - The as-made poly(amic acid) solution was used to brush coat 112 E-glass, with an A-1100 finish, secured on a frame. Each coat was dried in air for 1 hour each at 100, 200 and 300°C which converted the poly(amic acid) to polyimide. Generally, five coats were required to provide a 12 mil thick boardy tape which contained essentially no volatiles. Titanium (Ti, 6A1-4V) to Ti tensile shear specimens with a Pasa-Jell 107 surface were fabricated by increasing the temperature from 25 to 400°C under various pressures during ~1 hour and holding at 400°C under various pressures for 0.25 to 1.0 hour. Four specimens were tested for each condition according to ASTM D1002.

Characterization - Inherent viscosities were measured in 0.5% solution (w/v) in DMAC at 25°C. Differential scanning calorimetry (DSC) was performed at a heating rate of 20°C/min with the apparent glass transition temperature (Tg) taken at the inflection point of the ΔT vs. temperature curve. Thermogravimetric analysis (TGA) was conducted at a heating rate of 2.5°C/min in flowing air or nitrogen on powder samples. Wide angle x-ray scattering data (WAXS) was obtained on thin film specimens of the polyimide. With the x-ray diffractometer operated at 45 kV and 40 mA, using copper radiation with a flat sample holder and a graphite monochromator, the intensity of 1 s counts taken every 0.01° (2θ) was recorded on hard disk for the angular range: 10 - 40° (2θ). An external α-quartz standard was used in goniometer alignment. Polymer melt viscosity was measured using a Rheometrics System IV rheometer with a

parallel plate configuration with the top plate operating in an oscillating mode at different frequencies (0.1 to 100 radians/second) at a temperature of 375°C and 395°C.

RESULTS AND DISCUSSION

A new semi-crystalline polyimide, LARC-CPI, as depicted in Eq. 1 was prepared from the solution polymerization of BTDA and 1,3-BABB followed by thermal cyclodehydration of the precursor poly-(amic acid). LARC-CPI has good thermal stability as indicated by thermogravimetric analysis (Fig. 1) where the temperatures of 5% weight loss in air and in nitrogen were 488 and 525°C respectively. Films of LARC CPI can be easily formed by casting the precursor poly(amic acid) onto a suitable substrate and subsequently heating to remove the solvent and convert the precursor polymer to polyimide. The resulting transparent orange films exhibit excellent tensile properties, chemical and solvent resistance and thermal stability as evidenced in Table 1. In addition, films showed no change after soaking in methylene chloride. A poly(amic acid) (inherent viscosity = 1.26 dL/g) cast on plate glass and subsequently dried through 1 hour at 300°C provided tensile strength of 23,000 psi, tensile modulus of 630,000 psi and break elongation of 8.3% at 25°C. The film properties reported are without the benefit of optimization or drawing.

The properties of all the film specimens tested at 25°C after various exposures were within the variation in test values normally encountered in our laboratory. It is noteworthy that LARC-CPI films retained excellent properties after 100 hours in 30% aqueous sodium hydroxide. A commercial polyimide film, Kapton® (7), exhibited severe degradation in 30% aqueous sodium hydroxide after only a few hours. The crystalline regions in the LARC-CPI apparently protect the polymer from chemical and solvent attack. The effect of crystallinity is further evident in the higher strength and modulus of the films aged for 100 hours at 316°C and tested at 232°C versus those aged for 100 hours at 232°C

(1)
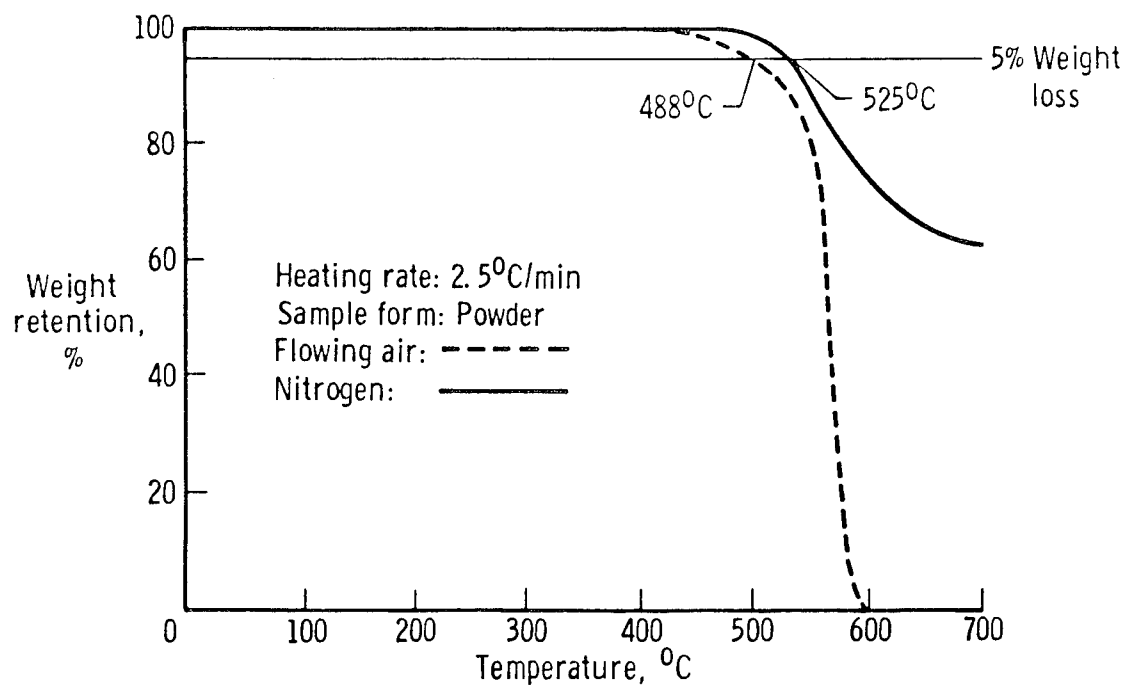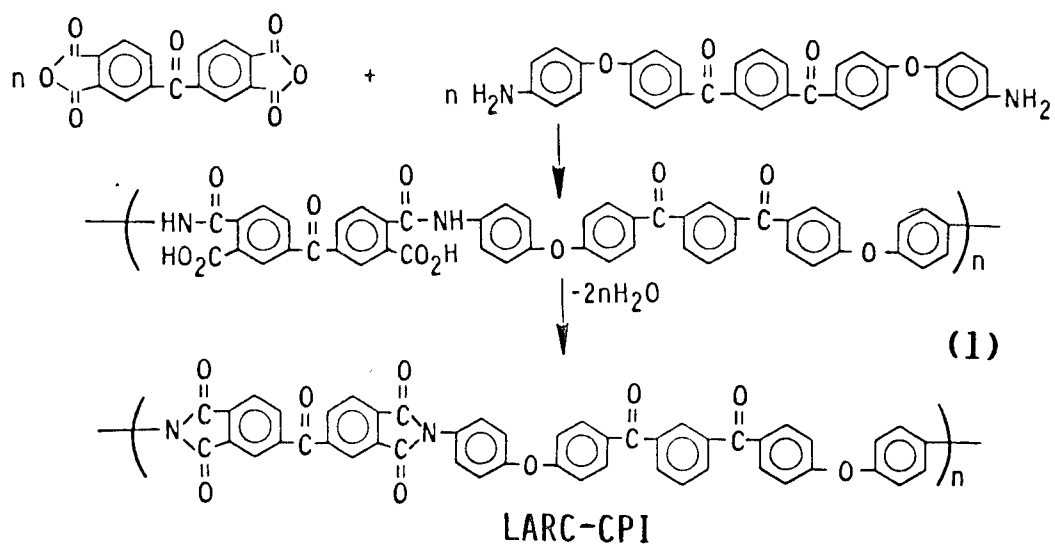
LARC-CPI

FIG. 1. THERMOGRAVIMETRIC ANALYSIS CURVES OF LARC-CPI

Table 1

LARC-CPI Thin Film Tensile Properties*

Test Condition	Tensile Strength, psi	Tensile Modulus, psi	Elongation, %
25°C	19,400	615,500	4.4
25°C after 3-day water boil	19,300	610,400	4.3
25°C after 100 hr soak in hydraulic fluid (SKydrol)	18,350	557,300	4.0
25°C after 100 hr soak in 30% aq. NaOH	20,300	589,500	5.0
25°C after 100 hr @ 232°C	20,000	555,500	5.1
25°C after 100 hr @ 316°C	17,480	616,400	4.1
232°C	4,600	239,400	39.2
232°C after 100 hr @ 232°C	4,800	256,000	61.2
232°C after 100 hr @ 316°C	8,400	340,700	9.6

*Inherent viscosity of poly(amic acid) = 0.82 dL/g, cast on stainless steel, dried 1 hr each @ 100, 200, and 300°C, cooldown rapid in the oven, average of four specimens
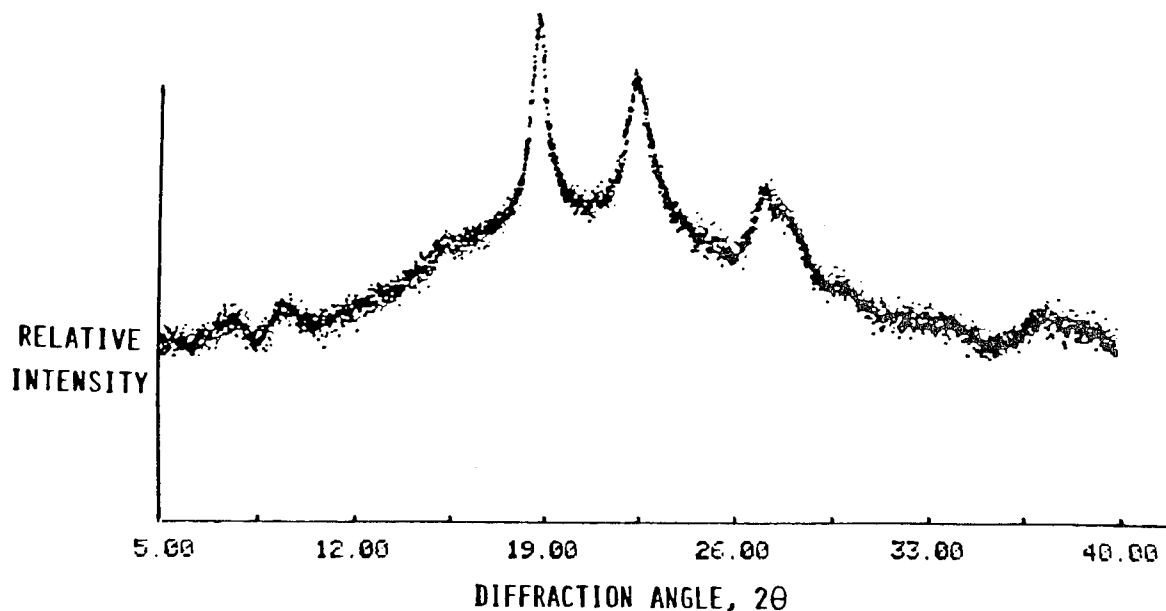
FIG. 2. X-RAY DIFFRACTOGRAM OF LARC-CPI FILM

and tested at 232°C. WAXS verified that the 316°C aged film was more crystalline than the 232°C aged film. A typical WAXS diffactogram of unoriented LARC-CPI film dried through 1 hour at 300°C in air on plate glass in Fig. 2 showed it to be semi-crystalline with three major reflections.

Further evidence for crystallinity in the LARC-CPI film was obtained from DSC measurements as shown in Fig. 3. Run 1 curve shows an intense endotherm peaking at 350°C due to melting of the crystalline regions. After quenching the sample from run 1 and reheating, a second order transition (Tg) is readily apparent at 222°C with a small melting endotherm present at 350 - 360°C. Run 3 is the sample from run 2 after cooling slowly and reheating. Again a well-defined Tg transition is apparent at 222°C with a slightly more intense melting endotherm in the 350 - 360°C range. Run 4 is the sample from run 3 which was held for 45 minutes at 300°C and slowly cooled. A Tg transition at 224°C and a more intense melting endotherm at 354°C are evident.

The melt viscosity of small molded discs of LARC-CPI powder were determined at 375 and 395°C over a frequency range of 10^{-1} to 10^{2} radians/second. As shown in Fig. 4, LARC-CPI undergoes shear thinning, evident from the decrease in melt viscosity of more than two decades as the frequency was increased from 10^{-1} to 10^{2} radians/second.

LARC-CPI powder was compression molded at 400°C under 2000 psi to yield moldings which were subsequently cut and machined into miniature compact tension specimens (8). DSC analysis of the molding was similar to that of the quenched film in run 2 of Fig. 4, indicating amorphism. Fracture energy (G_{Ic}, critical strain energy release rate) of 37.8 in lb/in^2 (6600 J/M^2) was obtained using the modulus (402,000 psi) of essentially amorphous LARC-CPI (6) in the calculations. The failed fracture surfaces of the specimens were very rough due to yielding and highly crazed, indicative of a fracture mechanism that absorbs energy
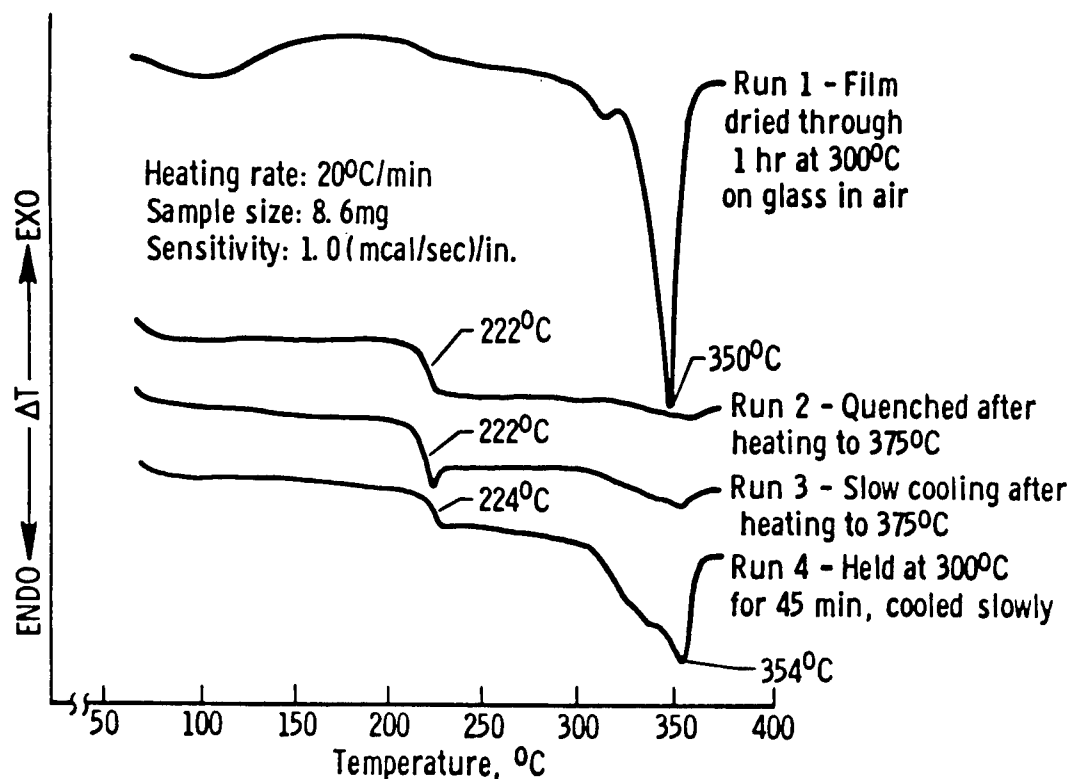
FIG. 3. DIFFERENTIAL SCANNING CALORIMETRIC CURVES OF LARC-CPI
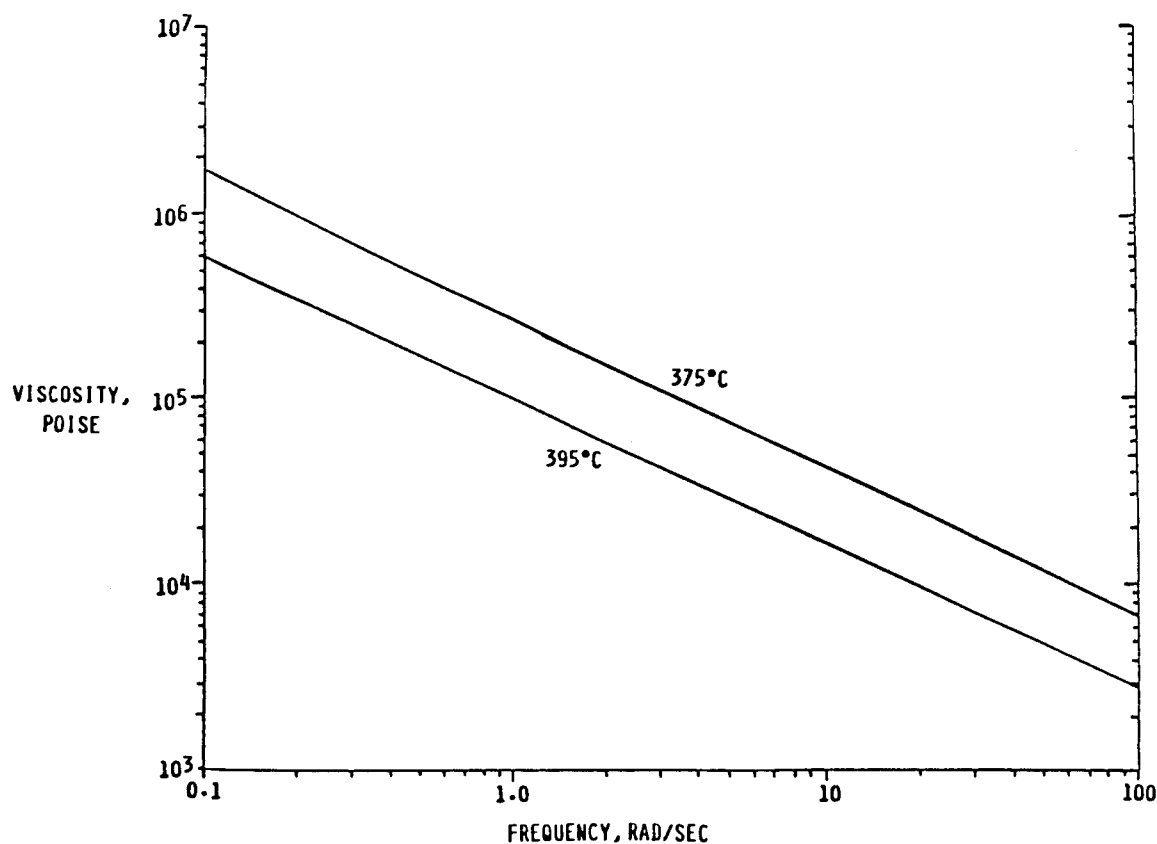
FIG. 4. MELT VISCOSITY CURVES OF LARC-CPI

by distributing it over a large surface area.

Since preliminary compression molding efforts indicated relatively high pressures were required to mold LARC-CPI at 400°C, a brief study was conducted to assess the effect of molecular weight on processability and adhesive properties. Three different molecular weight versions of LARC-CPI [based upon the inherent viscosities of the precursor poly(amide acid)] were prepared. As shown in Table 2, pressures from 200 to 2000 psi at 400°C were employed to fabricate tensile shear specimens. As the molecular weight of LARC-CPI increased, higher pressures were required to obtain good bonding and accordingly high strength. With the lowest molecular weight version of LARC-CPI, high bond strength was obtained at 500 psi. Work is currently underway to alter LARC-CPI to obtain good processability at lower pressure (e.g. 200 psi). Table 3 summarizes the tensile shear strengths of LARC-CPI under a variety of test conditions. Strength of 6250 psi was obtained at 25°C which decreased only to 5140 psi after a 3-day water boil. Pasa-Jell 107 surface treated Ti/Ti tensile shear specimens generally exhibit a drop in strength to the 2500 - 3000 psi level after a 3-day water boil. The change is due to water attacking the interface causing debonding. The 25°C strength surprisingly increased to 7120 psi after aging for 1000 hours at 232°C. Under these conditions, LARC-CPI becomes more crystalline which obviously is accompanied by some shrinkage. Perhaps this contraction enabled LARC-CPI to bond to the oxide layer more tenaciously. The initial strength at 232°C was 590 psi and the tested specimens exhibited ~95% adhesive type failure. After 5 hours at 300°C, the 232°C strength increased to 2800 psi and the failure mode changed to ~80% cohesive. This drastic change is attributed to increased crystallinity in LARC-CPI. The T_g is 222°C and excellent strength at 232°C is obtained because the crystalline regions carry the load. Further improvement in the 232°C strength to 3670 psi was observed for specimens aged for 100 hours at 316°C. This

Table 2

Effect of Bonding Pressure on LARC-CPI Adhesive Strength*

Inherent Viscosity of Poly(amic acid), dL/g	400°C Bonding Pressure, psi	25°C Ti/Ti Tensile Shear Data	
		Strength, psi	Failure
0.50	200 500 1000 2000	2250 5600 6250 5970	Incomplete bonding Cohesive ↓
0.70	500 1000 2000	5470 5730 6210	Cohesive ↓
1.10	200 500 1000 2000	3430 3770 4450 4870	Incomplete bonding ↓

*15 min

Table 3

LARC-CPI Ti/Ti Tensile Shear Data*

Test Condition	Strength, psi	Failure
25°C	6250	> 95% Cohesive
25°C after 3-day water boil	5140	~90% Cohesive
25°C after 72 hr hydraulic fluid soak	5590	~70% Cohesive
25°C after 1000 hr @ 232°C	7120	~100% Cohesive
25°C after 5 hr @ 300°C, 100 psi	6130	> 95% Cohesive
25°C after 100 hr @ 316°C	4590	~70% Cohesive
177°C	4510	> 95% Cohesive
177°C after 4 hr @ 300°C, 100 psi	4690	~100% Cohesive
232°C	590	~95% Adhesive
232°C after 100 hr @ 232°C	1840	~50% Cohesive
232°C after 1000 hr @ 232°C	2740	~50% Cohesive
232°C after 5 hr @ 300°C, 100 psi	2800	~80% Cohesive
232°C after 100 hr @ 316°C	3670	> 95% Cohesive

*Pasa-Jell 107 surface treatment, inherent viscosity of poly(amic acid) = 0.50 dL/g, bonding conditions, 400°C, 1000 psi, 15 min

excellent strength at 232°C after aging for 100 hours at 316°C in circulating air also reflects the good thermooxidative stability of LARC-CPI.

CONCLUSIONS

A new semi-crystalline polyimide with a Tg of 222°C and a T_m of 350°C exhibits the following attractive properties:

o Excellent thermal and thermooxidative stability
o High film mechanical properties
o Excellent resistance to solvents and strong bases
o High fracture energy
o High adhesive properties

REFERENCES

1. P. M. Hergenrother, Chemtech, August issue, 496 (1986); In Adhesive Chemistry (L. H. Lee, ed.), Plenum Publishing Co., New York, 1984, p. 447

2. Product Data Sheets on FM-34 and 36, American Cyanamid Company, Aerospace Products Department, Havre de Grace, Maryland 21078

3. Product Data Sheet on LARC-TPI Mitsui Toatsu Chemicals, Inc., Yokohama City, Japan

4. Product Data Sheet on Thermid, National Starch and Chemical Corporation, Bridgewater, NJ 08807

5. C. L. Hendricks and J. N. Hale in NASA Conference Publication 2387, p. 351 (1984)

6. P. M. Hergenrother, N. T. Wakelyn and S. J. Havens, J. Polym. Sci.: Pt. A.: Polym. Chem., 25, 1093 (1987)

7. E. I. DuPont De Nemours and Co., Industrial Film Division, Wilmington, DE 19898

8. J. A. Hinkley, J. Appld. Polym. Sci. 32, 5653 (1986)

Epoxy Systems with Increased Strength, Stiffness and Cure Rate

Andrew Garton[*] and Paul D. McLean[+]
Institute of Materials Science
University of Connecticut, Storrs, CT 06268
[*]author for correspondence
[+]National Aeronautical Establishment, Ottawa, K1A OR6, Canada

Unmodified epoxy adhesives are relatively brittle, which leads to low strength and poor impact properties in the presence of defects. Considerable effort has been expended to improve the fracture properties, and ease of curing (1,2). We describe here an alternative approach, which involves the addition of 5-15% of a low molecular weight material which can increase the tensile strength by 50%, the tensile modulus by 60%, yet not induce brittleness (tensile test specimens fail in a ductile fashion). Unlike the commonly-used rubber modified systems, these additives do not phase separate during the cure and function by modifying the free volume available for motion of the polymer chains (3-5). Versions of these additives are presently marketed by the licensee of this technology, Uniroyal Canada Ltd., under the trade name "Fortonox".

Two typical additive formulations are shown below. In general they consist of a stiff polar molecule (eg 4-hydroxyacetanilide) reacted with a mono- or non-symmetrical diepoxide to improve its solubility in the crosslinked epoxy matrix.
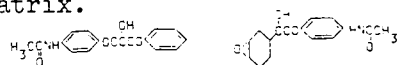
Structure I   Structure II

The additives are simply mixed with the resin and curing agent just before curing (some formulations may be pre-compounded with either the resin or curing agent before use).

Figures 1 to 4 show the benefits of addition of these materials (commonly known as "fortifiers"). Tensile stress-strain curves (Figure 1) show the increase in modulus and strength, and the occurrence of a ductile failure mode. Figure 2 shows the change in fracture toughness (an increase at low strain rates, no change at higher rates) that occurs for compact tension specimens. Figure 3 demonstrates that the improvement in mechanical properties is retained even after immersion in boiling water or aging at 75°C and 95% R.H. Subsequent redrying returns the tensile properties almost to their original values. Figure 4 illustrates that good mechanical properties can be obtained with a 60°C cure for a system which usually will not cure satisfactorily at <100°C. Lower temperature, cure systems show a similar increase in cure rate. Other important material properties are reported elsewhere (3-5), including a significant reduction in the coefficient of thermal expansion, which has obvious relevance to adhesives applications.

The effect of these additives on the modulus of the crosslinked epoxy have been explained in terms of the concept of "antiplasticization", i.e. a decrease in free volume produced by strong molecular interactions between the additive and the network. The decreased free volume reduces polymer segmental motion and so increases the modulus (3-5). The surprising occurrence of a ductile failure mode along with an increase in modulus is explained in terms of the low Poisson's ratio of these materials, i.e. their large increase in free volume with strain.

At strains of 4-5% the increase in free volume is sufficient to take the material through the glass to rubber transition, and so yielding occurs. This model can be placed on a quantitative basis by comparing thermal expansion data with strain-induced expansion data obtained with perpendicularly aligned strain gauges.

References

1. K. Dusek Ed., "Epoxy Resins and Composites" Adv. Polym. Sci., Series 72 (1985) and vol. 75 (1986).
2. C. K. Riew and J. K. Gillham Eds., "Rubber Modified Thermoset Resins" Adv. Chem. Series, 208 (1984).
3. J. Daly, A. Britten, A. Garton and P. D. McLean, J. Appl. Polym. Sci., 29, 1403 (1984).
4. P. D. McLean, A. Garton, W. T. K. Stevenson and K. E. MacPhee, Polymer Composites, 1, 330 (1980).
5. A. Garton, J. Clark, J. Daly, W. T. K. Stevenson and P. D. McLean, Polym. Eng. and Sci., in press.

Figure 2 Fracture toughness Epon 828-DDM Δ control o + 30 phr EPPHAA
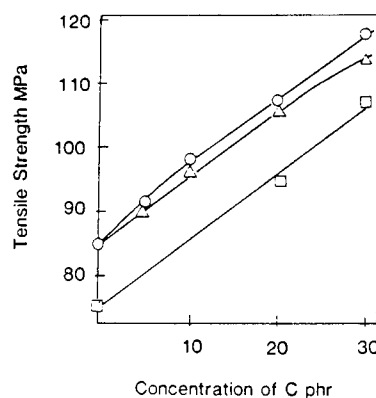
Figure 3 Retention of tensile properties o original plastic Δ boiled 15 min, ▣ 8 days 75°C, 95% R.H.

Figure 1 Tensile stress-strain. Epon 828-DDM (a) control (b) +15 phr EPPHAA (c) +30 phr EPPHAA
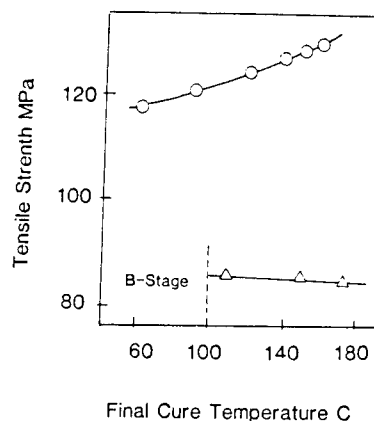
Figure 4 Tensile strength as a fuction of cure temperature. Δ control o + 30 phr EPPHAA

Adhesive Evaluation of New Polyimides

Terry L. St. Clair and Donald J. Progar
Polymeric Materials Branch
NASA Langley Research Center
Hampton, VA 23665-5225

ABSTRACT

During the past 10-15 years, the Materials Division at NASA Langley Research Center (LaRC) has developed several novel high temperature polyimide adhesives for anticipated needs of the aerospace industry. These developments have resulted from fundamental studies of structure-property relationships in polyimides. Recent research at LaRC has involved the synthesis and evaluation of copolyimides which incorporate both flexibilizing bridging groups and meta-linked benzene rings. The reason for this activity was to develop systems based on low cost, readily available monomers. Two of these copolyimides evaluated as adhesives for bonding titanium alloy, Ti-6A1-4V, are identified as LARC-STPI and STPI-LARC-2 and are compared with LARC-TPI. Lap shear strength (LSS) measurements were used to determine the strength and durability of the adhesive materials. LSS results are presented for LARC-TPI, STPI-LARC-2, and LARC-STPI lap shear specimens before and after thermal exposure in air for up to 5000 hrs and a 72-hour water-boil. LARC-TPI was shown to perform better than the copolymer LARC-STPI which exhibited poor thermooxidative performance possibly due to the amines used which would tend to oxidize easier than the benzophenone system in LARC-TPI. Lap shear strengths decreased after the water-boil test, however, useable strengths were retained at 204°C for LARC-STPI and STPI-LARC-2 and at 177°C for LARC-TPI.

INTRODUCTION

There are few materials available which can be used as aerospace adhesives at temperatures in excess of 200°C. During the past 10-15 years, the Materials Division at NASA Langley Research Center has developed several novel high temperature polyimide adhesives to fulfill the anticipated needs of the aerospace industry. These developments have resulted from fundamental studies of structure-property relationships in polyimides. Two materials that have exhibited exceptional adhesive properties are LARC-TPI[1-3] (Langley Research Center Thermoplastic Imide) and PISO2 (a thermoplastic polyimidesulfone).[4-6] The structures of these are illustrated.
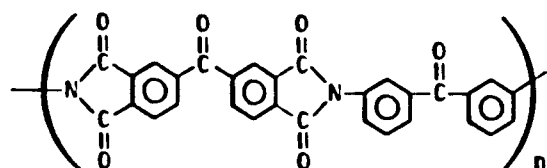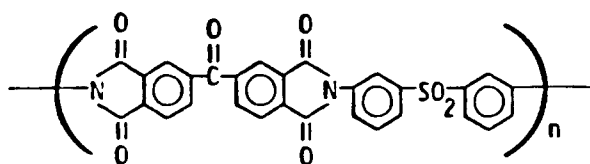
In examining these structures one should notice that the backbones are identical with one exception - a carbonyl group in LARC-TPI and a sulfone group in PISO2. The primary characteristic that imparts the thermoplastic nature, and hence good adhesive properties, to these systems is the degree of flexibility along the backbone. In this regard, the flexibility is introduced via the carbonyl bridging group in the anhydride-derived portion of the chain and from the sulfone and carbonyl groups in the diamine-derived portion of the chain.[7] In addition a key factor is the meta-oriented linkage to the benzene rings in the amine-derived segments. The corresponding systems with para-oriented linkages exhibit very little thermoplasticity. The structures are shown below for comparison.

LARC-TPI

PISO2
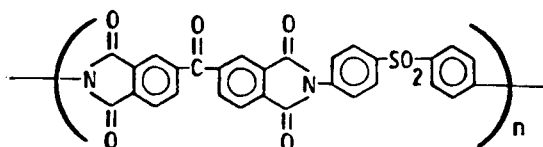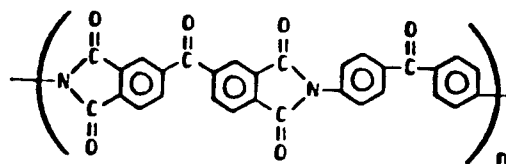
A recent research program at NASA Langley has involved the synthesis and evaluation of copolyimides which incorporate both flexibilizing bridging groups and meta-linked benzene rings. This activity was undertaken in order to develop systems based on low cost, readily available monomers. The approach involved the preparation of copolyimides of the following structure:
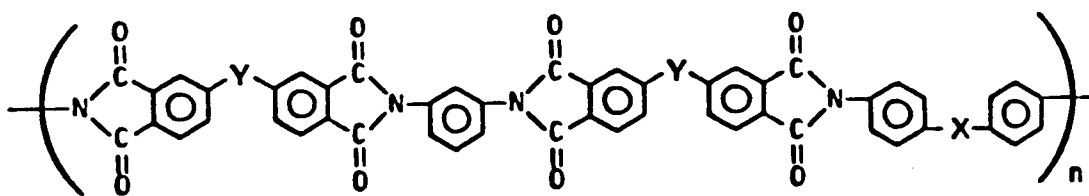
In the cases studied to date, x is an oxygen and y is either an oxygen or a carbonyl. Models of this system and of the LARC-TPI and PISO2 were prepared and compared. All systems exhibited similar long range flexibility with the LARC-TPI and PISO2 exhibiting more uniform short range flexibility.

The two copolyimides[8-9] that have been evaluated as adhesives for bonding a titanium alloy (Ti-6Al-4V) are on the following page.

MATERIALS

The chemicals were obtained from commercial sources. The list of chemicals, abbreviations and their sources follows: benzophenonetetracarboxylic acid dianhydride (BTDA), King Mar Laboratories; oxydiphthalic anhydride (ODPA), Ciba-Geigy (made on NASA contract); 4,4'-oxydianiline (ODA), Mallinckrodt, Inc.; meta-phenylenediamine (MPD), N,N-dimethylacetamide (DMAc), 2-methoxyethylether (diglyme), N-methylpyrrolidone (NMP), Fluka Chemical Co.; and phthalic anhydride (PA), Eastman Kodak Co.

SYNTHESIS

The preparation of the copolyimides were carried out at room temperature in a 1000 ml cylindrical reaction flask with a removable, four-necked
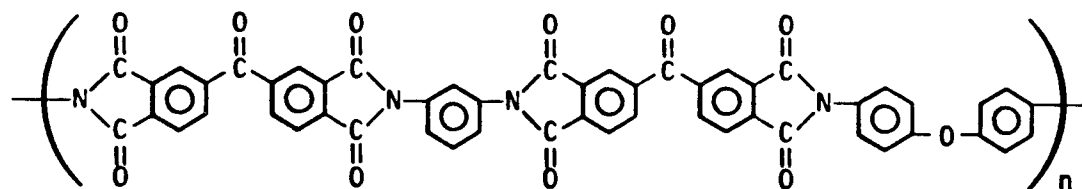
LARC-STPI
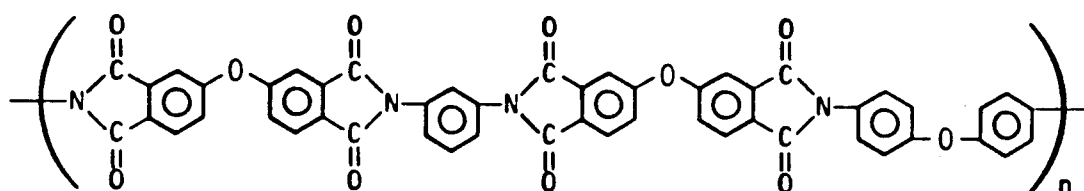
STPI-LARC-2

top. Stirring of the mixture was accomplished using an impeller blade driven by a constant-torque, overhead motor equipped with a variable speed control.

The BTDA or ODPA (0.050M) and PA (0.002M) were slurried in a mixed solvent system of diglyme with either NMP or DMAc. To this was added ODA (0.025M) and the mixture was allowed to stir for 15 min to form a solution. Next the MPD (0.025M) was added and the solution was stirred for an additional 35 min. The resin was decanted from the vessel. In this manner, a 15 wt % solids solution of LARC-STPI with a 3:1 ratio of amide/ether solvent was prepared. The STPI-LARC-2 was prepared as a 17.5 wt % solids solution with an approximate 1.6:1 ratio of amide/ether solvent. An inherent viscosity of 0.52 dl/g was obtained for the LARC-STPI resin and 0.65 for STPI-LARC-2.

CHARACTERIZATION

Lap shear strength was obtained according to ASTM D-1002 using a Model TT-C Instron Universal Testing Machine. The lap shear strengths reported represent an average of four lap shear

40

specimens per test condition. The range of the lap shear strengths is indicated by dashed lines in the bar graph figures. The average bondline thickness for LARC-STPI was 0.017 cm with a range of 0.014 cm to 0.020 cm. STPI-LARC-2 averaged 0.019 cm with a range of 0.015 cm to 0.021 cm. Due to the greater flow of the LARC-TPI adhesive, average bondline thickness for the LARC-TPI was 0.009 cm with a range of 0.007 cm to 0.011 cm. Specimens were heated in a clam-shell, quartz-lamp oven and were held at temperature for 10 minutes prior to testing except for the water-boil specimens which were tested as soon as the test temperature was reached. Temperatures were controlled to within ± 3°C for all tests. Glass transition temperatures (Tg) were determined by differential scanning calorimetry (DSC) for films of the polymers using a DuPont* Thermal Analysis System. DSC measurements were run in air at 50°C/min. The inherent viscosity reported is the average of three measurements on 0.5 wt % solids solutions in DMAc made at 35°C ± 0.01°C using a Cannon Ubbelohde viscometer.

ADHESIVE BONDING

Adhesive tapes for the LARC-STPI, STPI-LARC-2, and LARC-TPI prepared by brush coating a solution of the polyamic acid onto 112 E-glass cloth with A-1100 finish (γ-aminopropysilane). The glass cloth had been tightly mounted on a metal frame and dried in a forced-air oven for 30 min at 100°C prior to coating. The coated cloth was then air-dried for 1 hr and heated for 1 hr or more at each of three temperatures: 100°C, 150°C, and 175°C. Subsequent applications were treated in the same manner until a thickness of 0.020-0.025 cm was obtained.

The reaction scheme for LARC-TPI, developed at NASA Langley Research Center in the late 1970's from BTDA and 3,3'-diaminobenzophenone (3,3'-DABP) in diglyme solvent is shown in Figure 1.[1] LARC-TPI, Lot No. 26-001, was supplied by Mitsui Toatsu

---

*Use of trade names or company names does not constitute an official endorsement by NASA, either expressed or implied.

Chemicals, Incorporated, Tokyo, Japan, as a 29.1 wt % solids polyamic acid solution in diglyme with an inherent viscosity of 0.54 dl/g (35°C).
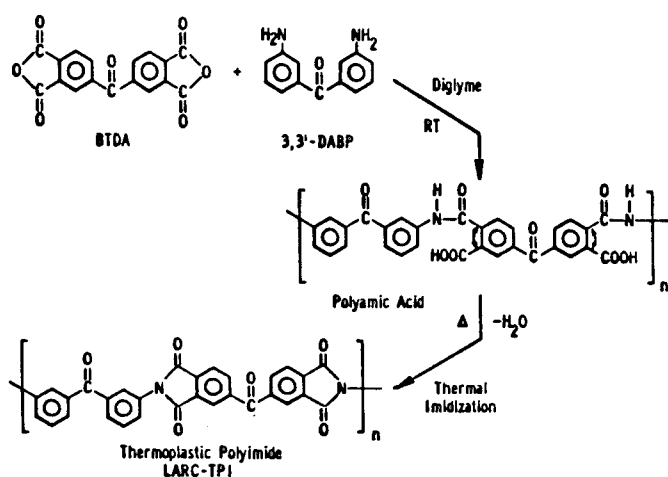
Figure 1. Reaction scheme for LARC-TPI.

The reaction schemes for LARC-STPI and STPI-LARC-2 are shown in Figure 2. The anhydride monomers had only partial solubility in the mixed solvent system of diglyme and DMAc (NMP). The difunctional anhydride allows for molecular weight buildup (chain growth); the PA was used as a method of controlling the molecular weight so that the level was high enough to yield tough, flexible polymers, but not so high as to inhibit the thermoplastic flow properties. The resulting polymer did

afford a flexible film when cast and cured to 300°C. There was adequate thermoplastic flow as evidenced by the softening that occurred during the adhesive bonding operation.

The prepared adhesive tapes were used to bond titanium adherends (Ti-6Al-4V, per Mil-T-9046E, Type III Ccmp. C) with a nominal thickness of 0.13 cm for the adherends. The Ti-6Al-4V panels were grit blasted with 120 grit aluminum oxide, washed with methanol, and treated with Pasa-Jell 107* to form a stable oxide on the surface. The adherends were washed with water and dried in a forced-air oven at 100°C for 5 min. The treated adherends were primed within two hrs of the surface treatment by applying a thin coat of the polyamic acid solution of the respective adhesives on the surfaces to be bonded. After air-drying in a forced-air oven for 30 min, they were heated for 15 min at 100°C and

_____

*Trade name for a titanium surface treatment available from Semco, Glendale, CA.

42

15 min at 150°C. Lap shear specimens were prepared by inserting the adhesive tape between the primed adherends using a 1.27 cm overlap (ASTM D-1002) and applying 2.1 MPa pressure in a hydraulic press during the heating schedule. Bonding temperature was monitored using a type K thermocouple spot-welded to the titanium adherend at the edge of the bondline. A bonding cycle was determined in a preliminary study (2.1 MPa, RT to 343°C, hold 1 hr) and used to prepare lap shear specimens for thermal exposure for up to 5000 hrs at 204°C and up to 5000 hrs at 232°C for LARC-TPI and LARC-STPI. Thermal exposure was performed in a forced-air oven controlled within ± 1% of the desired exposure temperature. Lap shear tests were conducted at room temperature, 177°C, 204°C and in some cases, 232°C before (controls) and after exposure.

A 72-hr water-boil test was conducted in laboratory glassware containing boiling distilled water. Lap shear specimens were immersed (above the bonded area) during the 72-hr period. Lap shear strengths were subsequently determined at room temperature, 177°C, and 204°C.

RESULTS AND DISCUSSION

An initial comparison of room temperature and 204°C lap shear strengths for the three primary adhesive systems of this study and PISO2 are shown in Table I.

All systems have excellent RT and 204°C lap shear strengths and relatively high Tgs (260°C to 283°C).

THERMAL EXPOSURE TESTS

The stability of the adhesives to long term thermal exposure was determined for the three adhesive systems by exposing lap shear specimens for up to 5000 hrs at 204°C in a forced-air oven. Lap shear strengths were determined at RT, 177°C, and 204°C before (controls) and after exposure.

Results for LARC-STPI are given in Figure 3. Little change in lap shear strength was observed due to the thermal exposure. The 500 and 1000 hr exposure strengths, approximately 23 MPa, are the same, but slightly lower than the controls strengths,
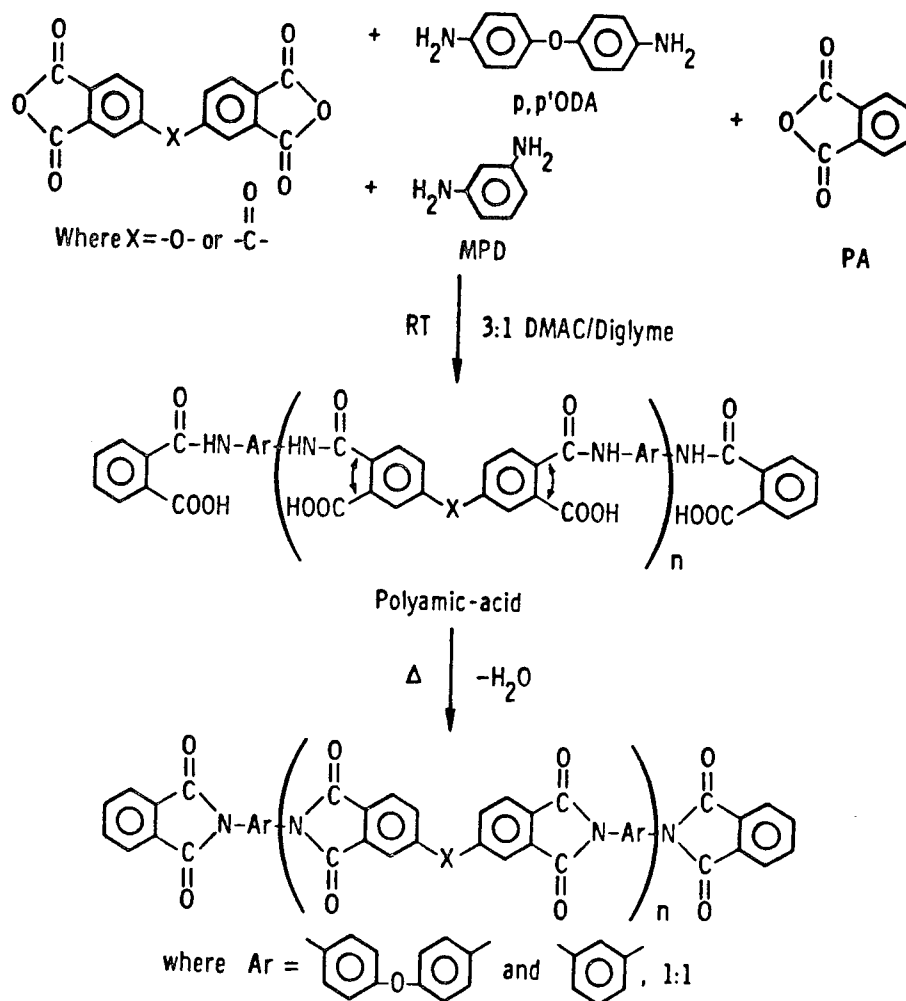
Figure 2. Reaction scheme for formation of LARC-STPI and STPI-LARC-2.

TABLE I

| Adhesive | Lap Shear Strength, MPa (psi) | | Tg, °C |
	RT	204°C	
LARC-TPI	33.0 (4791)	25.2 (3660)	260
PISO2	25.2 (3650)	20.1 (2920)	273
LARC-STPI	26.6 (3858)	25.0 (3626)	283
STPI-LARC-2	35.2 (5111)	26.8 (3890)	279

approximately 26 MPa. The primary failure mode of the fractured specimens was cohesive except for the 500 and 1000 hr exposure specimens tested at RT which were adhesive/cohesive and adhesive, respectively.

Results for STPI-LARC-2 adhesive are given in Figure 4. Little change in lap shear strength was noted due to thermal exposure at 204°C for up to 1000 hrs exposure. However, for the 5000 hr exposure, RT and the 204°C strengths decreased significantly but were still respectable (RT - 18 MPa, 204°C - 21 MPa). Strengths were retained for the 232°C test. A general decrease in RT lap shear strength was noted. A slight decrease in lap shear strength with test temperature was shown for the

control tests - RT, 35.1 MPa, 177°C, 32.7 MPa; and 204°C, 26.2 MPa. Failures were primarily cohesive except for the RT test for those given 1000 hr and 5000 hr thermal exposures which were primarily adhesive. Results in Figure 6 show a 55% strength retention at RT and 73% retention at 204°C for specimens aged 5000 hrs at 204°C.

Results are given in Figure 5 for the LARC-TPI adhesive. No significant difference was found in the lap shear strength with time of thermal exposure up to 1000 hrs for any one temperature (RT, 32.9 - 34.1 MPa; 177°C, 29.0 - 29.9 MPa; and 204°C, 25.2 - 27.8 MPa). There is a general trend of decreasing lap shear strength with increasing test temperature
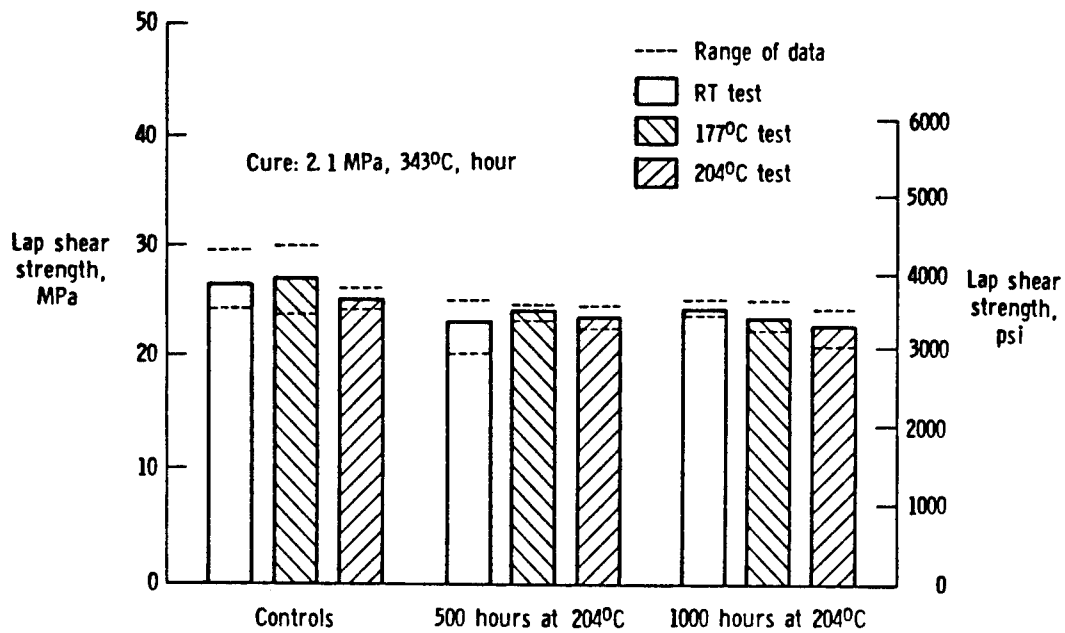
Figure 3. Effects of thermal exposure in air at 204°C on lap shear strength for titanium bonded with LARC-STPI adhesive.
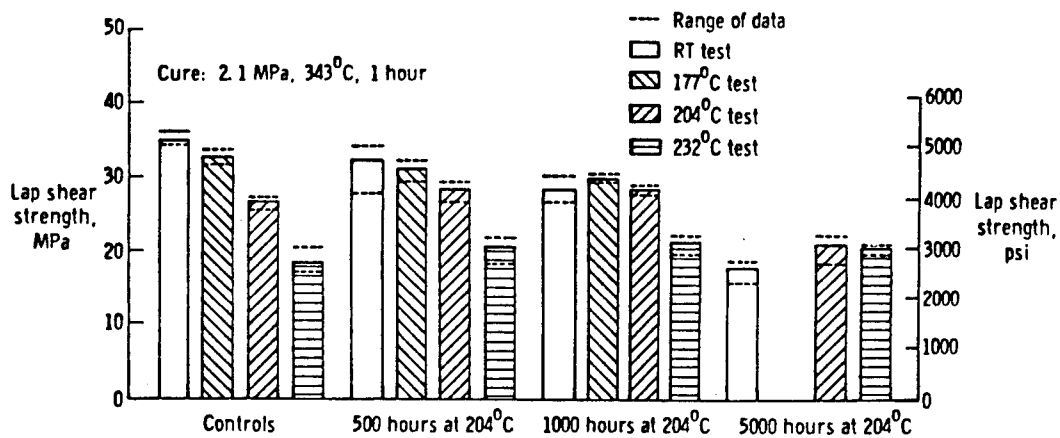
Figure 4. Effects of thermal exposure in air at 204°C on lap shear strength for titanium bonded with STPI-LARC-2 adhesive.
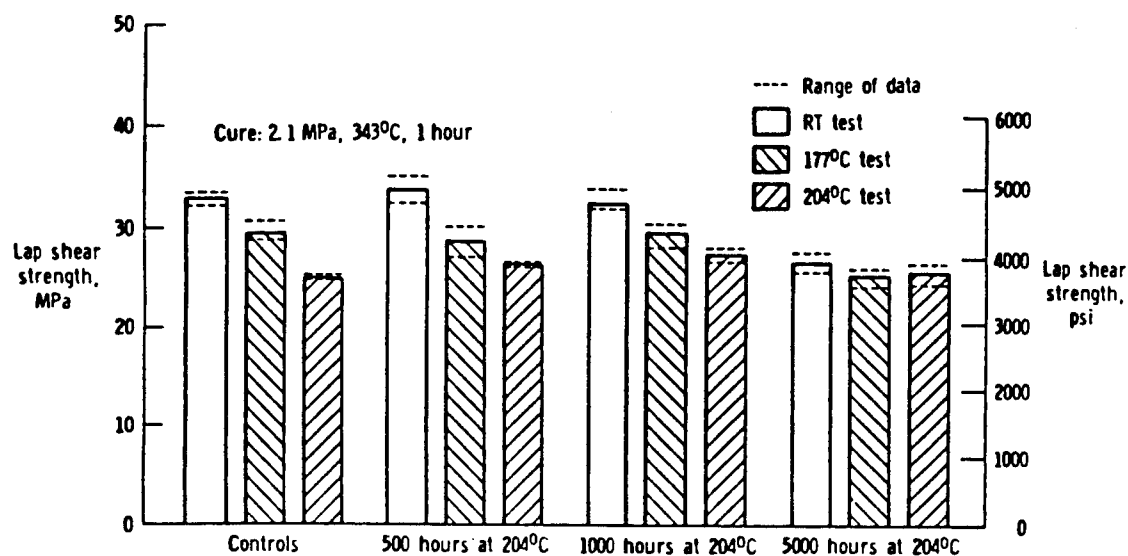
Figure 5. Effects of thermal exposure in air at 204°C on lap shear strength for titanium bonded with LARC-TPI adhesive.
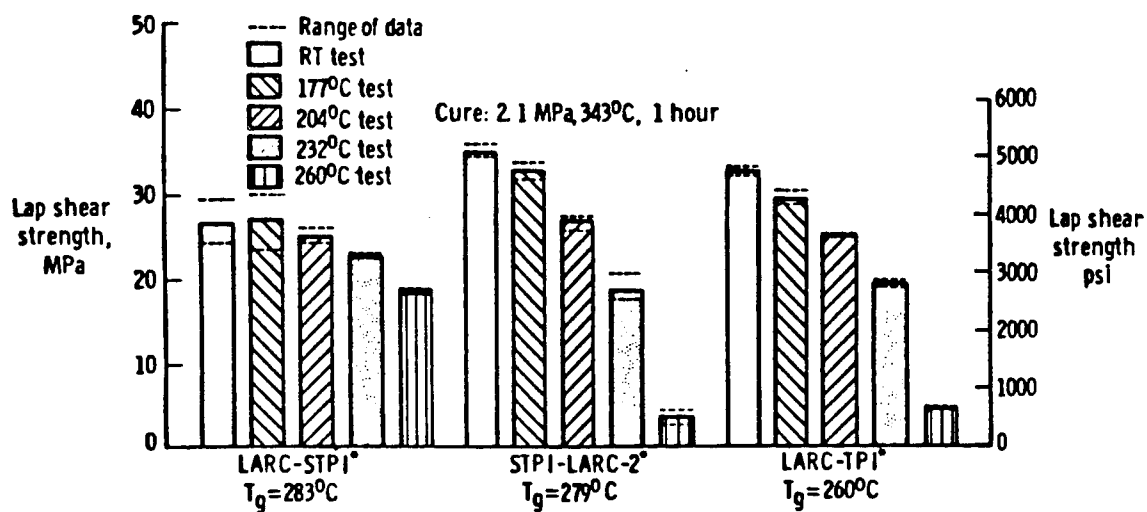
* Tg determined by DSC measurement made on films heated 1 hour at 100°C, 200°C, and 300°C for each adhesive film.

Figure 6. Lap shear strength results for tests up to 260°C of titanium bonded with LARC-STPI, STPI-LARC-2, and LARC-TPI adhesives.

47

except for the 5000 hr exposure results. All failures were 100% cohesive. Data obtained for 5000 hrs exposure show a small decrease for the RT and 177°C tests but no change for the 204°C test.

We chose to age the LARC-STPI system at 232°C for comparison with the data base of LARC-TPI. A comparison of the two systems is shown in Table II. As seen in the table, the copolymer does not perform as well as the LARC-TPI. After the postcure

possibly due to the amine portions of the LARC-STPI. The amines used in this polymer should have more tendency to oxidize than the benzophenone system used for LARC-TPI.

Lap shear strengths up to 260°C were obtained for the three adhesive systems to determine their possible use temperature capabilities (Figure 6). Quite obviously, STPI-LARC-2 and LARC-TPI decrease drastically at the 260°C test temperature because

TABLE II

Aging Time at 232°C, Hours	Lap Shear Strength,* MPa (psi)	
	LARC-TPI	LARC-STPI
0	13.6 (1970)	24.7 (3580)
168	19.6 (2840)	24.7 (3590)
2500	23.4 (3390)	17.7 (2570)
5000	23.7 (3440)	9.8 (1420)

*Tested at 232°C

effect, the LARC-TPI retained its strength whereas the LARC-STPI copolymer retained only 40 percent of its highest strength value. This poor thermooxidative performance is

the Tg of the adhesives were exceeded (all $\leq$ 246°C) (Tg determined by TMA of the adhesive on a fractured specimen). The Tgs given in Figure 6 were determined by DSC on films heated for one

hr each at 100°C, 200°C, and 300°C. Although the STPI-LARC-2 and LARC-TPI have high lap shear strengths at RT, 177°C, and 204°C, the LARC-STPI because of its high Tg has greater strength at 232°C and is the only one of the three with good strength at 260°C.

All three systems show promising results for the thermal exposure investigated. In general, LARC-TPI and STPI-LARC-2 had approximately the same range of lap shear strengths which were higher overall than the LARC-STPI system. However, the LARC-STPI system had a higher Tg than LARC-TPI and STPI-LARC-2 which generally indicates a higher potential use temperature. All failures for the LARC-TPI were 100% cohesive, whereas, the LARC-STPI and STPI-LARC-2 failed primarily cohesively with partial adhesive failures.

72-HOUR WATER-BOIL

The resistance of the three adhesives to water (humidity) was determined by immersing lap shear specimens in distilled boiling water for a 72-hour period and subsequently testing their lap

shear strengths at RT, 177°C, and 204°C. Results of those tests are given in Figure 7 for the LARC-STPI adhesive system, Figure 8 for STPI-LARC-2, and in Figure 9 for the LARC-TPI system.

The lap shear strengths of LARC-STPI specimens after water-boil were 88% of the control's RT strength, 62% of the control's 177°C strength, and 68% of the control's 204°C strength. The lap shear strengths for the STPI-LARC-2 were 52% of the control's RT strength and 50% of the control's 204°C strength. The lap shear strengths for the LARC-TPI were 84% of the control's RT strength, 67% of the control's 177°C strength, and 40% of the control's 204°C strength. From these results, it appears that the LARC-STPI and LARC-TPI adhesive systems retain a high percentage of the original RT strength. The LARC-STPI also retained the highest percentage, 68%, of the original strength for the 204°C test temperature. Failures were primarily cohesive for the LARC-STPI and LARC-TPI adhesive systems whereas they were cohesive/adhesive after water-boil for
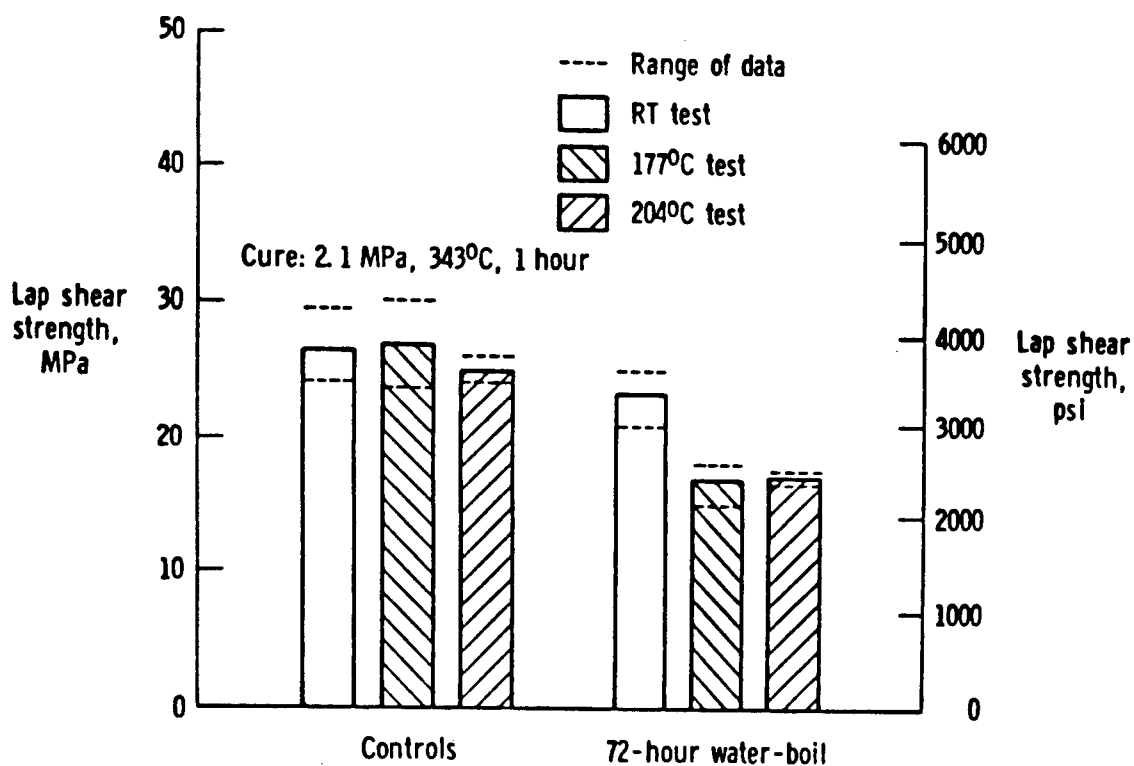
Figure 7. Effects of a 72-hour water-boil on lap shear strength
for titanium bonded with LARC-STPI adhesive.
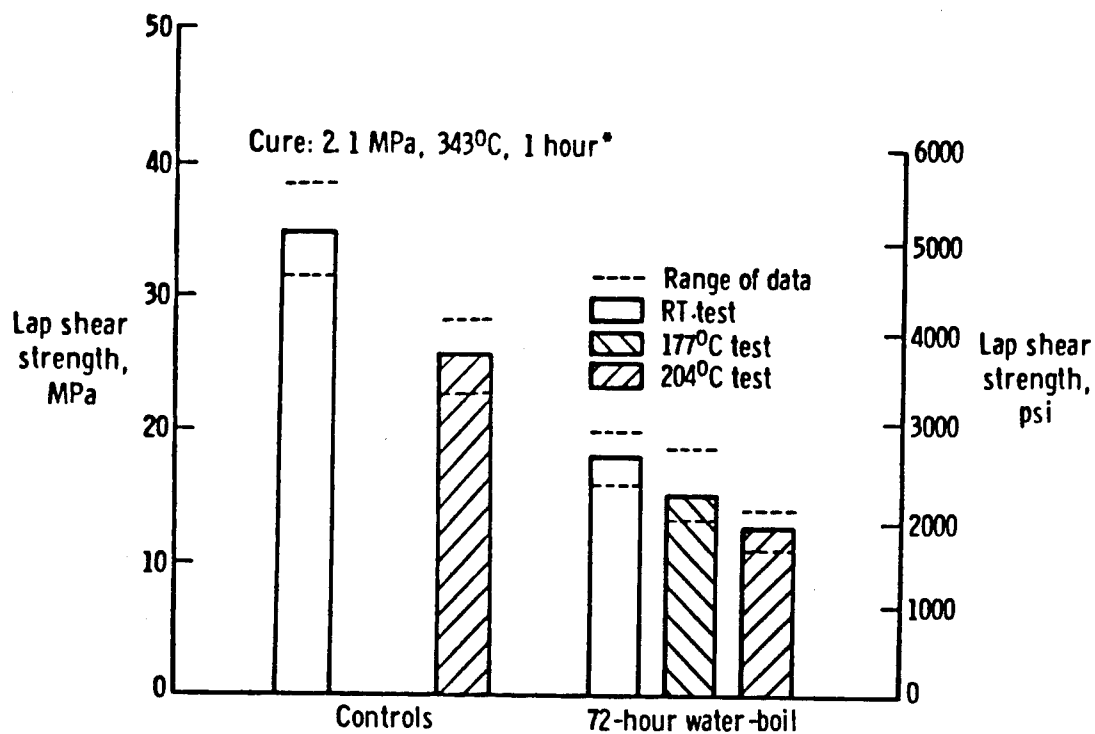
* Adhesive tape given an additional heat treatment of 0.5 hour at 343°C.

Figure 8. Effect of a 72-hour water-boil on the lap shear strength
for titanium bonded with STPI-LARC-2 adhesive.
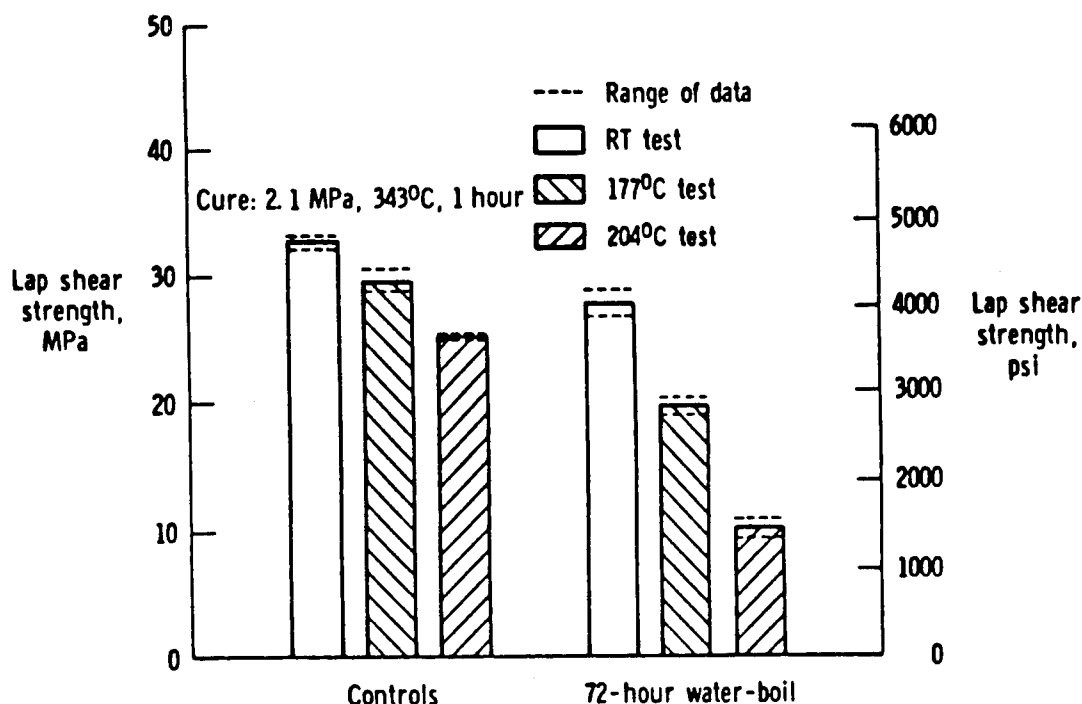
Figure 9. Effect of a 72-hour water-boil on the lap shear strength
for titanium bonded with LARC-TPI adhesive.

the STPI-LARC-2 adhesive system.

The LARC-TPI provided the highest lap shear strengths after water-boil for the RT and 177°C tests, whereas LARC-STPI retained the highest strength at 204°C after water-boil, 17.0 MPa compared to 10.1 MPa for LARC-TPI and 12.7 MPa for STPI-LARC-2.

CONCLUSIONS

A thermoplastic polyimide, LARC-TPI, has previously been shown to be an excellent adhesive for several applications. The reason for the thermoplastic nature of this polymer has been attributed to the flexibility of the backbone caused by the use of the meta-linked diamine-3,3'-diaminobenzophenone.

In this work the use of a combination of two flexibilizing diamines in the polymers, LARC-STPI and STPI-LARC-2, has resulted in copolyimides with adhesive performances that are very similar to LARC-TPI. The

experimental data on a commercially available LARC-TPI and on the experimental LARC-STPI and STPI-LARC-2 shows all three systems to possess exceptional lap shear strengths at room and elevated temperatures up to 204°C both before and after aging at 204°C. The copolymer, LARC-STPI, does not perform as well as the LARC-TPI for those exposed up to 5000 hrs at 232°C. The poor thermooxidative performance of the LARC-STPI is possibly due to the amine portions of the copolymer. The amines used in this portion should have more of a tendency to oxidize than the benzophenone system used for LARC-TPI. The LARC-STPI, because of its high Tg, provided high lap shear strengths up to 260°C. In general, the LARC-TPI and STPI-LARC-2 adhesive systems had approximately the same range of lap shear strengths, which were higher overall than the LARC-STPI system. The LARC-STPI system has a higher Tg than LARC-TPI and STPI-LARC-2 which generally indicates a higher potential use temperature. After a 72-hour water-boil exposure, LARC-TPI bonded specimens exhibited the highest lap shear strengths for room temperature and 177°C tests, whereas the LARC-STPI retained a higher percentage of its original strength when tested at 204°C after the water-boil exposure [68% versus 50% (STPI-LARC-2), 40% (LARC-TPI) retention].

An attractive feature of the LARC-STPI and STPI-LARC-2 is that they were prepared from relatively inexpensive, commercially available chemicals. Therefore, these flexible, thermoplastic copolyimides show considerable potential as adhesives based on this initial study.

REFERENCES

1. St. Clair, A. K.; and St. Clair, T. L.: A Multipurpose Thermoplastic Polyimide. SAMPE Quarterly, vol. 13, no. 1, 1981, pp. 20-25.
2. Hill, S. G.; Peters, P. D.; and Hendricks, C. L.: Evaluation of High Temperature Structural Adhesives for Extended Service. NASA CR-165944, July 1982.

3. Hendricks, C. L.; and Hale, J. N.: High Temperature Adhesive Development and Evaluation. NASA CP-2387, 1984.

4. St. Clair, T. L.; and Yamaki, D. A.: A Thermoplastic Polyimidesulphone. NASA TM-84574, 1984.

5. Progar, D. J.: Processing Study of a Polyimidesulfone Adhesive. NASA TM-85742, 1984.

6. Progar, D. J.: Processing Study of a High Temperature Adhesive. Int. J. of Adhesion and Adhesives, vol. 4, no. 2, 1984, pp. 79-86.

7. Bell, V. L.; Stump, B. L.; and Gager, H.: J. Polym. Chem. Ed. 14, 1976.

8. Progar, D. J.; and St. Clair, T. L.: STPI/LARC: A 200°C Polyimide Adhesive. NASA TM-86447, 1985.

9. Progar, D. J.; and St. Clair, T. L.: Flexibilized Copolyimide Adhesives. J. Adhesion, vol. 21, 1987, pp. 35-37.

NEW LOW TEMPERATURE CURING RESINS
AND ADHESIVES FOR COMPOSITE REPAIR

P. M. Puckett, W. D. White, and P. L. Wykowski
The Dow Chemical Company
Freeport, Texas
and
E. S. Caplan
Lockheed-Georgia Company
Marietta, Georgia

Abstract

New polymer systems were developed for the repair of composites in aircraft. Candidate systems were required to cure at or below 93°C (200°F) and provide service comparable to state-of-the-art epoxies cured at 177°C (350°F). Four chemical approaches were investigated: vinyl esters, styrene-terminated resins, cyanates, and epoxies. The initial test data indicated that several vinyl ester systems could perform as desired up to approximately 149°C (300°F) without serious degradation under wet conditions. The data on styrene-terminated resins revealed that additional process research beyond the scope of the program would be required in order to eliminate a chemical problem that inhibited the cure at low temperature. Cyanate systems were found to be in need of a few minor modifications directed at driving the last five to fifteen percent of the cure reaction to completion at low temperature. Finally, several of the new epoxy formulations investigated showed promise, but additional test data will be needed.

1. INTRODUCTION

Adhesives and laminating resins are used throughout today's aircraft in bonded assemblies, honeycomb sandwich structures, and components made of fiber-reinforced polymers. These structures pick up moisture from the environment during service, either by absorption into adhesive and matrix materials, or by accumulation through crevices into areas such as honeycomb cells. The acquisition of moisture can be accelerated by the presence of cracks, defects, or service-related damage.

The repair of such moisture-laden parts can be difficult.[1-4] The heat and pressure that are required to cure the repair materials also affect the moisture acquired during service. Water vapor is generated. If the partial pressure of the water vapor exceeds the applied pressure, then bubbles can nucleate in

54

uncured resins and adhesives, honeycomb core can blow apart, and composites can delaminate in the repair zone. Hence, in order to keep the induced vapor pressure low, repair materials are needed which can be cured at low temperatures.

The present study is part of an on-going Air Force effort to develop low temperature curing, high performance laminating resins and structural adhesives.[5] The long-term objective is to effect full-strength repairs to typical advanced composite aircraft structures without preliminary drying of the damaged components. The short-term objective, however, is simply to develop new polymeric repair materials which are capable of being cured at or below 93°C (200°F). The new materials must retain the elevated temperature performance of traditional repair materials cured at 177°C (350°F). The primary concern, therefore, is to ensure that the maximum use temperature of each candidate system is much higher than its cure temperature (T_{cure}).

In the next section of this paper, the scientific principles behind the selection of chemical approaches for this program will be discussed. Later, in Section 3, the development of specific candidate systems will be addressed. Finally, in Section 4, the initial test results obtained on these systems will be presented.

2. SELECTION OF APPROACHES

One material property that can be used to evaluate the service temperature of a polymer is its glass transition temperature (T_g). The relationship between T_g and T_{cure} for thermosetting polymers has been explored extensively by Gillham and co-workers.[6-9] They have proposed a time-temperature-transformation (TTT) state diagram to represent the isothermal cure of such materials. They have also confirmed that a thermosetting system attains its optimum mechanical properties and highest T_g when it is in a fully cured, highly crosslinked, glassy state. This condition, however, is difficult to achieve with a low temperature cure. Usually the system chemistry is such that the molecular excitation generated at low temperature is not enough to drive the cure reaction to the required state.

The easiest way, it would seem, to induce $T_g \gg T_{cure}$ in a system for which $T_{cure} < 93°C$ (200°F) is to design the polymer chemistry such that the likelihood of each reactive species to crosslink is unusually high. The surest technique, therefore, is to provide a large number of potential reaction sites by using materials with highly functional backbone structures. Another strategy is to use coreactant and catalyst molecules which are small so that they can undergo a great deal of molecular motion and can diffuse through a vitrified system.

Another option is the use of systems which contain a large amount of stored internal energy in their chemical bonds. Such systems react to generate heat faster than the heat can be dissipated. Hence, the externally applied temperature can be low, while the local cure temperature is elevated. A possible risk to this approach is that the moisture problems prevalent in high temperature repair may recur locally. Another disadvantage is that systems with a great deal of

energy stored in chemical bonds, such as peroxide-cured polymers, tend to be unstable in storage.

Finally, the effect of absorbed moisture on the T_g of a polymer must be considered. As illustrated in Figure 1, the hydrophobic backbone of the hydrocarbon epoxy novlac (HEN) reduces the amount of water absorbed by the polymer as compared to a conventional epoxy novolac system like D.E.N.^{R} 438*. Nevertheless, the absorbed moisture plasticizes the cured polymers and lowers its T_g. The primary goal of this program is to obtain $T_g \gg T_{cure}$, and it is important not to sacrifice this goal under wet conditions. A final chemistry principle for this program, therefore, is to seek materials with inherently low moisture uptake in both the cured and uncured states. Hydrophobic chemical groups such as hydrocarbons, aromatics, and halogens are beneficial to this cause. Hydrophilic chemical units, such as oxygen, sulfur, and nitrogen, need to be avoided or placed in molecules at locations where access is hindered by steric interference.

On the basis of the principles described in this section, four general chemical approaches were selected for development. They include vinyl ester resins, styrene-terminated resins, cyanates, and epoxies.

3. MATERIALS EVALUATED

Candidate systems within each chemical family were formulated, cured, and tested. The purpose of these tests was to identify promising candidates for further development and testing later in

*a Trademark of The Dow Chemical Co.

the program. These materials will be subjected to a more extensive test program that will include evaluation in bulk form, in graphite/resin composite patches, and in adhesive joints.

3.1 Vinyl Ester

The general structure of a vinyl ester is shown in Figure 2a. Vinyl ester resins are produced by the reaction of an epoxy resin with an acrylic or methacrylic acid. The methacrylate system is preferred for most applications because it is much more resistant to hydrolysis and environmental aging. Vinyl ester resins are generally copolymerized with an unsaturated molecule such as styrene, vinyltoluene, or divinylbenzene. The coreactant lowers the viscosity of the system and imparts processability. The cure mechanism is free radical polymerization, where free radicals are most often generated by the catalyzed decomposition of an organic peroxide with a metallic or amine promoter. The processing parameters may be altered by changing the nature of the base resin or the catalyst/initiator package.

Seventeen vinyl ester systems were formulated and tested. Base resins derived from epoxy novolacs were tried because it was believed their high functionality would promote crosslinking and thereby increase T_g. A novolac containing hydrocarbon in the backbone was introduced in an effort to reduce moisture uptake. Although systems based on bisphenol A epoxy resins were unlikely to offer the high T_g of the novolacs, they were also tried because they were likely to offer improved toughness. Other variations in the vinyl ester formulations included diluent

concentration and functionality (styrene and divinylbenzene were used to alter viscosity and crosslink density) and the incorporation of rubber into certain systems (vinyl- and carboxy-terminated butadiene acrylonitrile rubbers were used to improve toughness).

3.2 Styrene-Terminated Resins

The general structure of a styrene-terminated resin is shown in Figure 2b. These resins are produced by the reaction of a phenolic with a styrene-terminated alkylating agent in the presence of a base. They were patented by The Dow Chemical Company in 1978.[10] Their chemistry is similar to the vinyl esters in that polymerization proceeds through terminal vinyl unsaturation reacting via a free radical mechanism. Styrene-terminated resins, like vinyl esters, are highly viscous and must be copolymerized with unsaturated diluents for processability. There are, however, significant differences in behavior. The styrene-terminated resin molecules are less polar because of their lower oxygen content and therefore absorb less water. They also have a higher percentage of aromatic residue per reactive equivalent, so they are capable of producing higher T_g's. Because these systems are normally cured above 93°C (200°F), the main challenge for this program was to find a suitable catalyst or other means for driving the cure reaction to completion at temperatures below 93°C (200°F).

On the basis of the same rationale that was used to select the polymer backbones for vinyl ester systems, various base resins were selected for the production of a series of styrene-terminated resins. A phenol-formaldehyde novolac, a novolac containing a hydrocarbon segment, and a bisphenol A epoxy were used. These materials were diluted with styrene or methylmethacrylate. A total of four formulations were tested.

3.3 Cyanate

The general structure of a cyanate resin is shown in Figure 2c. Polycyanates were first synthesized in 1963 by Grigat and Putter.[11] The chemistry of the cyanate group is quite complex because of the wide variety of reactions that can occur with molecules containing a nucleophilic functional group. It is believed, however, that the polymerization of the cyanate, at least initially, is the result of a trimerization reaction which produces a triazine ring. The polymerization reaction is very exothermic and can release its energy very quickly when it is properly catalyzed. The temperatures produced can be high enough to cause decomposition in most polymers, but the polymers formed from cyanate resins have high intrinsic stability and do not normally decompose below 300°C (572°F).

Polycyanates have been of interest for years as potential systems for 177°C (350°F) service applications. Unfortunately, many of the early polycyanate resins were susceptible to long-term degradation by moisture. Recently, a unique system was developed which maintains excellent thermal and mechanical properties even after prolonged exposure to moisture.[12] This polycyanate is produced from a cycloaliphatic/aromatic hybrid backbone which is highly hydrophobic. The material is normally thinned with a reactive

diluent and processed with a transition metal catalyst at 177 to 240°C (350 to 464°F). The final properties, however, are so attractive that the material was selected for development in this program. The research effort focused on the identification of a catalyst system for low temperature cure. Two transition metal ion catalysts were evaluated: Fe(III) and Zn(II). In both cases, the resin was diluted with twenty percent vinyltoluene by weight.

3.4 Epoxy

The general structure of an epoxy resin is shown in Figure 2d. Epoxy systems represent one of the best known and most thoroughly studied families of thermosets. Most of the work to date on material development for composite repair has involved epoxies and epoxy prepregs.[13-15] No available system, however, was found which met all the requirements of this program, particularly the ability to provide $T_g \gg T_{cure}$.

Of the systems discussed in previous studies, the most promising were epoxy novolac formulations cured with either aliphatic or cycloaliphatic amines. The blends selected for this study were all mixtures of a bisphenol A-derived epoxy and novolac-derived epoxies of varying functionality, with low viscosity reactive amine hardeners.

4. TEST RESULTS AND DISCUSSION

A set of initial screening tests were performed on the candidate formulations in order to determine the most promising systems for further development and testing. Mechanical properties measured on cured samples of the candidate formulations included ultimate tensile strength, tensile modulus, and elongation at failure, as well as ultimate flexural strength and flexural modulus. Physical properties evaluated included the heat distortion temperature (HDT) and the weight percent water absorbed at weight gain equilibrium. Differential scanning calorimetry (DSC) was also used as a means to characterize the cure process thermally. From the DSC data, heat of reaction, degree of cure, and glass transition temperature were quantified when necessary. For the epoxy systems only, the full set of initial tests were not completed in time for inclusion in this paper, and only the DSC data were available for review.

4.1 Vinyl Ester

The seventeen vinyl ester systems formulated and their associated properties are shown in Table 1. System chemistries were identified by the components of the resin base and the diluents and additives used. The properties listed were measured on specimens that had been cured for two hours at 80°C (176°F). The mechanical properties were all measured at ambient conditions.

The mechanical property values were generally in the same range as comparable values for state-of-the-art epoxies cured at 177°C (350°F). HDT values suggested that satisfactory performance at 121 to 149°C (250 to 300°F) could be achieved by many of these systems, but that performance at 177°C (350°F) would be questionable. In addition, the low water absorption values relative to the five to six percent typical of baseline epoxies indicated that

performance should hold up well under wet conditions.

Several patterns were observed in the data. The presence of Tactix^R 742* or epoxy phenolic novolac in relation to other resin base components tended to increase the HDT; unfortunately, these materials also raised the water absorption level. Systems derived from epoxy phenolic novolac and hydrocarbon epoxy novolac were less sensitive to diluents than systems derived from bisphenol A epoxy and hydrocarbon epoxy novolac. The latter group, however, when diluted with styrene or styrene and divinylbenzene in a 9-to-1 ratio, provided the best mechanical properties of all the vinyl esters studied.

Patterns were also noted with regard to the diluents and additives. Divinylbenzene, in particular, showed strong, consistent effects. Its presence caused an increase in the HDT of systems but hurt their tensile properties, lowering both the ultimate strength and elongation at failure. These effects were moderated by rubber additives. In fact, for all systems investigated with rubber additives, a marked improvement in the elongation at failure was apparent. This improvement, however, came at the expense of a reduction in the HDT. Vinyl-terminated butadiene acrylonitrile (VTBN) rubbers, it should be noted, underwent phase separation from the vinyl esters, while carboxy-terminated butadiene acrylonitrile (CTBN) rubbers did not. Therefore, although the data at room temperature for VTBN-modified systems were acceptable, in order to ensure satisfactory performance at elevated temperatures, only CTBN rubbers should be considered as suitable toughening agents for vinyl esters.

4.2 Styrene-Terminated Resins

Although these materials were expected to process similarly to the vinyl esters because of their vinyl unsaturation, a problem was encountered in obtaining a complete cure below 93°C (200°F). The problem was a consequence of the starting materials and process chemistry. Styrene-terminated resins, as discussed earlier, are produced by capping phenolics. The failure to cap even 0.5 percent of a phenolic starting material leaves behind 5,000 ppm of a free radical phenolic inhibitor. This level of residual phenolic is higher than the level in many commercial inhibitor packages. In order to produce a material that is not self-quenching in free radical polymerization, it is critical to obtain nearly 100 percent conversion of the phenolic to a styrene-terminated resin. Future attempts to pursue this chemistry will necessarily involve process research to develop a more efficient conversion method for styrene-terminated resin production.

In order to prepare specimens sufficiently well-cured to evaluate properties, it was necessary to add a post-cure step above 93°C (200°F), a procedure contrary to the objectives of this program. All systems were cured overnight at room temperature, followed by two hours at 80°C (176°F) and a post-cure at 155°C (311°F) for two hours. The formulations and their properties are summarized in Table 2.

*a Trademark of The Dow Chemical Co.

59

The mechanical properties at ambient conditions were acceptable but not outstanding. HDT's were particularly disappointing considering the 155°C (311°F) post-cure. The only exceptional property was the extremely low water absorption of the novolac-based systems. This characteristic could be exploited in an application where low temperature cure is not essential. For the composite repair application, however, additional process research to develop a successful low temperature curing resin will be required.

4.3 Cyanate

Cyanate systems were cured with Fe(III) and Zn(II) catalysts at 80°C (176°F) for four hours. DSC analysis of the residual exotherm in these systems revealed conversion efficiencies of 85 to 95 percent. This degree of cure achieved at low temperature is noteworthy because the normal cure cycle for this cyanate resin is two hours at 177°C (350°F) followed by a post-cure for four hours at more than 200°C (392°F). The mechanical and physical properties measured for these systems are shown in Table 3. Also included are data for systems which had been post-cured for two hours at 177°C (350°F).

The test data confirmed that a partial cure had been achieved at 80°C (176°F). Of the two catalysts, Fe(III) provided better final properties. Additional work on this system indicated that the last 15% of cure is unlikely at temperatures below 93°C (200°F). Unfortunately, a substantial amount of a polymer's ultimate T_g is generated in the last 10-20% of cure. Therefore, the

use of cyanates in composite repair limited to low temperature cures seems improbable at this time.

4.4 Epoxy

Combinations of various epoxy resin blends and hardeners were cured at 80°C (176°F) for four hours. The resin blends were a bisphenol A-derived epoxy and four mixtures of a bisphenol A-derived epoxy and novolac-derived epoxies of varying functionality. The mixtures were labelled Blends 1 through 4. The hardening agents were three commercially available, low viscosity amines (Ancamine 1856*, Sylvamine 21**, and Amicure PACM-20***) and one proprietary aliphatic amine recently developed by The Dow Chemical Company and referred to as M1. The dry T_g of each system was measured by DSC. The data are presented in Table 4.

The T_g's of the systems hardened with Ancamine 1856 and Sylvamine 21 were not substantially different from T_{cure}. The results with Amicure PACM-20 hardener showed more promise. In particular, Blends 1 and 3 provided T_g's of 137°C (279°F) and 163°C (325°F), respectively. Finally, systems using the non-commercial hardener M1 gave the best results of all. Resin Blends 2, 3, and 4 had T_g's near 165°C (329°F).

These data were encouraging in that they demonstrated that T_g >> T_{cure} could be obtained with certain epoxy systems. They did not indicate what to expect from the systems in composite form or

*a product of Pacific Anchor
  Chem. Corp.
**a project of Sylvachem Corp.
***a product of Air Products

60

after water absorption. Nevertheless, appropriate modifications could make these materials useful for low temperature repair of composites.

5. CONCLUSIONS

New polymer systems are under development for the repair of composite structures in aicraft. Candidate systems are required to be cured at or below 93°C (200°F) but to provide service properties comparable with state-of-the-art epoxies cured at 177°C (350°F). Four chemical approaches were selected for investigation: vinyl esters, styrene-terminated resins, cyanates, and epoxies. Initial formulations for each approach have been prepared and tested.

In their current state of development, vinyl ester systems most closely fulfill the program objectives. The tensile and flexural properties measured at ambient conditions on specimens cured at 80°C (176°F) were in the same range as properties for state-of-the-art epoxies cured at 177°C (350°F). The heat distortion and water absorption characteristics of numerous formulations indicated that satisfactory performance will be obtained at 121 to 149°C (250 to 300°F) and will be maintained under wet conditions. The data also showed that CTBN rubber was a good toughening agent, despite a small sacrifice in elevated temperature performance capability.

Styrene-terminated resin systems in their current state of development are not good candidate materials. The cure at low temperature is inhibited by residual uncapped phenolic. Additional process research is needed to develop a more efficient conversion method for the production of styrene-terminated resins from phenolic starting materials. If this chemical problem can be solved, styrene-terminated resin systems should offer exceptional resistance to degradation by moisture.

Cyanate systems in their present form do not meet the requirements of this program for composite repair but do appear likely to succeed with further modifications to the catalyst and cure schedule. These systems have demonstrated an 85% cure at low temperatures, which is sufficient to produce green strength in the part. Additional curing of the part at temperatures of approximately 177°C (350°F) will be needed to obtain fully cured parts.

Finally, new epoxy systems may also offer potential. Several systems were formulated which produced T_g's approximately 80°C higher than T_{cure}. These formulations are currently being optimized. Mechanical properties and water absorption characteristics are being evaluated.

Ten candidate systems from the various chemical families will be selected for further development on the basis of the initial test data. These systems, in bulk form, in graphite/resin composite patches, and in adhesive joints, will be subjected to extensive physical and mechanical testing.

6. ACKNOWLEDGEMENTS

7. REFERENCES

1. T. M. Donnellan, J. G. Williams, and and R. E. Trabocco, "An Investigation of Void Formation in Adhesive Bonds Produced under Field Repair Conditions," NADC-84079-60, Feb. 1984.

2. J. M. Augl, "Moisture Transport in Composites During Repair Work," NSWC-TR-83-374, Sept. 1983.

3. R. S. Kiwek and L. J. Matienzo, "Moisture Problems in Repair," Proc. Tri-Service Composites Repair Technology Workshop, Dayton, V.2, Nov. 1984, p. 3.10-1.

4. R. C. Cochran, et al., "An Adhesive for Field Repair of Wet Composites," Proc. Second DoD/NASA Comp. Rep. Tech. Wkshp., San Diego, V. 2, Nov. 1986.

5. AF Contract No. F33615-85-C-5081, "Development of Low Temperature Curing Resins/Adhesives."

6. J. K. Gillham, "The Time-Temperature-Transformation (TTT) Cure Diagram of Thermosetting Polymeric Systems," Proc. ACS Div. Poly. Mat.: Sci. and Eng., V. 54, 1986, p. 8.

7. X. Peng and J. K. Gillham, "Time-Temperature-Transformation (TTT) Cure Diagrams: Relationship Between T_g and the Temperature and Time of Cure for Epoxy Systems," Proc. ACS Div. Poly. Mat.: Sci. and Eng., V. 54, 1986, p. 223.

8. J. K. Gillham, "The Time-Temperature-Transformation (TTT) State Diagram and Cure," The Role of the Polymeric Matrix in the Processing and Structural Properties of Composite Materials, J. C. Seferis and L. Nicolais, eds., New York: Plenum Press, 1983, p. 127.

9. H. N. Nae' and J. K.. Gillham, "Time-Temperature-Transformation (TTT) Cure Diagrams of High T_g Epoxy Resins: Competition Between cure and Degradation," ACS Div. Org. Plast. Chem. Preprints, V. 48, 1983, p. 566.

10. E. Steiner, U. S. Patent No. 4,116,936, "Polyvinylbenzyl Ethers of Polyphenols, Their Polymers, and Copolymers," Sept. 1978.

11. E. Grigat and R. Putter, German Patent Nos. 1,195,764 and 1,201,839, "Cyanic Acid Esters, Intermediates for Drugs," 1963.

12. E. Woo and D. V. Dellar, U.S. Patent No. 4,528,366, "Production of Polytriazines from Aromatic Polycyanates with Cobalt Salt of a Carboxylic Acid as Catalyst," July 1985.

13. L. J. Buckley and R. E. Trabocco, "Epoxy Resin Development for Composite Field Repair," NADC-80128-60, Oct. 1980.

14. D. J. Crabtree, "Adhesives for Field Repair of Graphite/Epoxy Composite Structures," NADC-79286-60, 1979.

15. D. J. Crabtree, "Room Temperature Curing Resin Systems for Graphite/Epoxy Composite Repair," NADC-78101-60, 1978.

8. BIOGRAPHIES

P. M. Puckett joined The Dow Chemical Company in 1984. His responsibilities at Dow include the design, synthesis, and characterization of thermoset resin systems. He is also involved in the formulation and evaluation of materials for resin transfer molding applications. He holds a B.S. degree in chemistry and mathematics from Harding University and a Ph.D. in organic synthetic chemistry from Texas A&M University.

W. D. White is a Research Associate with fifteen years' experience at The Dow Chemical Company in all phases of process and production research and development. He has worked on processes for urethanes, isocyanates, amines, styrene, ethyl benzenes, and epoxy resins. Dr. White has authored over thirty internal reports, ten scientific publications, and one U.S. patent. He earned his B.S. in chemical engineering and Ph.D. in chemistry at the University of Texas. He also conducted postdoctoral work in chemistry at the University of Illinois.

P. L. Wykowski has worked at The Dow Chemical Company since 1980. His experience encompasses plant process improvement, composite development for highway repair, flexibilized thermoset resin development, and maintenance coating development. He received a B.S. in chemistry from Loyola University in Chicago and an M.S. in analytical chemistry from the University of Kansas.

E. S. Caplan joined the Lockheed-Georgia Company in 1982. His work centers around the processing science of nonmetallic materials for aircraft, including rheology, modeling, and cure monitoring studies. He holds a B.S. from the Massachusetts Institute of Technology in materials science and engineering and an M.S. from Virginia Polytechnic Institute and State University in engineering mechanics.

TABLE 1. COMPARISON OF VINYL ESTER FORMULATIONS

RESIN BASE COMPONENTS	DILUENTS	RUBBER	TENSILE PROPERTIES STRENGTH MPa(KSI)	MODULUS GPa(KSI)	ELONG. %	FLEXURAL PROPERTIES STRENGTH MPa(KSI)	MODULUS GPa(KSI)	HDT °C(°F)	WATER ABSORPTION %
1. TACTIX^R 742	S	--	65.5(9.50)	3.45(500)	2.3	113(16.4)	3.72(540)	158(316)	1.80
2. DERAKANE^R 470 (3.6 functional)	S	--	77.2(11.2)	3.45(500)	2.8	143(20.7)	3.72(540)	160(320)	1.48
3. HEN, bis-A	S	--	77.9(11.3)	3.53(512)	2.9	121(17.6)	3.52(510)	139(283)	1.16
4. HEN, bis-A	S	CTBN	84.1(12.2)	3.05(442)	4.7	160(23.2)	3.51(509)	123(253)	1.16
5. HEN, bis-A	S/D (9:1)	--	62.3(9.03)	3.19(463)	2.3	139(20.1)	3.68(534)	146(295)	1.22
6. HEN, bis-A	S/D (9:1)	CTBN	77.9(11.3)	3.12(452)	4.1	130(18.8)	3.52(510)	116(241)	1.21
7. HEN, bis-A (variation)	S/D (9:1)	CTBN	85.5(12.4)	3.03(439)	4.5	146(21.2)	3.46(502)	129(264)	1.14
8. HEN, bis-A	S/D (9:1)	VTBN	69.6(10.1)	2.78(403)	4.7	127(18.4)	3.17(460)	139(282)	1.22
9. HEN, bis-A (variation)	S/D (9:1)	VTBN	59.3(8.60)	2.35(341)	5.2	101(14.6)	2.69(390)	136(277)	1.36
10. HEN, bis-A	S/D (4:1)	--	60.0(8.70)	3.28(475)	2.2	119(17.2)	3.79(550)	151(304)	1.23
11. HEN, bis-A	D	--	36.4(5.28)	3.59(520)	1.1	64.4(9.34)	3.72(540)	177(351)	1.32
12. HEN, EPN	S	--	68.4(9.92)	3.56(516)	2.4	123(17.8)	3.72(540)	153(307)	1.29
13. HEN, EPN	S/D (9:1)	--	69.6(10.1)	3.50(507)	2.5	139(20.1)	3.78(548)	158(316)	1.50
14. HEN, EPN	S/D (4:1)	--	62.4(9.05)	3.49(506)	2.1	129(18.7)	3.99(578)	161(322)	1.35
15. EPN, bis-A	S	CTBN	80.0(11.6)	3.09(448)	4.8	141(20.5)	3.47(504)	113(235)	1.47
16. HEN, EPN, bis-A	S/D (9:1)	CTBN	79.3(11.5)	3.01(437)	3.9	136(19.7)	3.44(499)	125(257)	1.30
17. EPN	S/D (4:1)	--	73.1(10.6)	3.43(497)	2.7	122(17.7)	3.86(560)	162(323)	1.74

KEY: R = trademark of the Dow Chemical Co.   HEN = hydrocarbon epoxy novolac   S = styrene
      HDT = heat distortion temperature   EPN = epoxy phenolic novolac   D = divinyl benzene
                                                bis-A = bisphenol-A epoxy

CTBN = carboxy-terminated butadiene acrylonitrile
VTBN = vinyl-terminated butadiene acrylonitrile
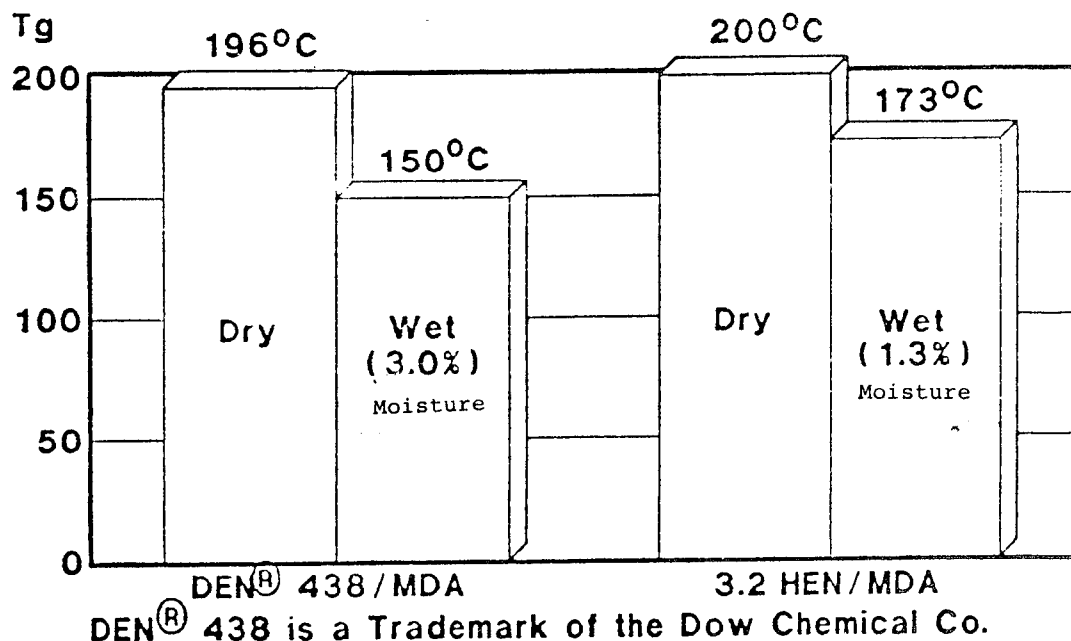
Figure 1.   Effects of Backbone Structure on Moisture Absorption
and Glass Transition Temperatures
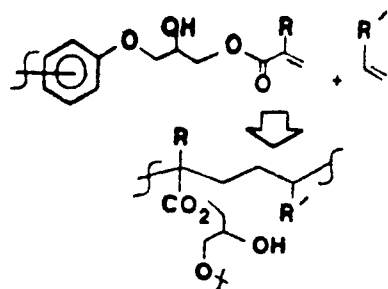
a. Vinyl Ester
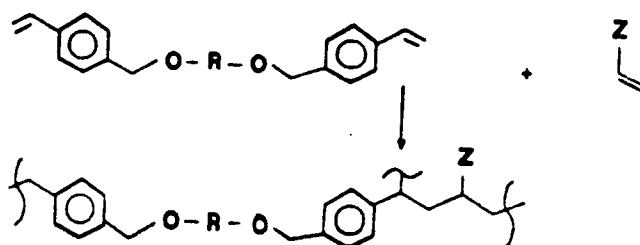
b. Styrene-Terminated Resin
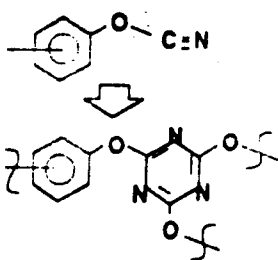
c. Cyanate
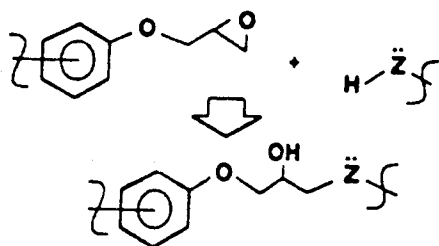
d. Epoxy

Figure 2. Chemical Approaches Selected

65

TABLE 2. PROPERTIES OF STYRENE-TERMINATED RESIN SYSTEMS

	3.6F Novolac 30% wt Styrene	3.6F Novolac 25% wt Parabisphenol A 25% wt Methylmethacrylate	Hydrocarbon Novolac 30% Wt Styrene	Trisphenol 30% wt Styrene
TENSILE				
Strength-MPa (ksi)	58.6 (8.5)	35.2 (5.1)	51.0 (7.4)	39.3 (5.7)
Modulus-GPa (ksi)	3.53 (512)	3.81 (552)	3.25 (471)	2.99 (434)
Elongation (%)	2.0	1.0	1.9	1.5
FLEXURAL				
Strength-MPa (ksi)	110.3 (16.0)	72.4 (10.5)	94.5 (13.7)	68.3 (9.9)
Modulus-GPa (ksi)	4.38 (635)	3.87 (561)	3.41 (495)	3.12 (452)
HDT - °C (°F)	140 (284)	133 (271)	131 (267)	130 (266)
H_2O ABSORPTION (%)	0.46	0.92	0.39	2.44

TABLE 3. PROPERTIES OF POLYCYANATE SYSTEMS

	Fe(III)	Fe(III)	Zn(II)	Zn(II)
Catalyst	2500 ppm	2500 ppm	2500 ppm	2500 ppm
Cure Cycle	4 hr/80°C	4 hr/80°C 2 hr/177°C	4 hr/80°C	4 hr/ 80°C 2 hr/177°C
TENSILE				
Strength-MPa (ksi)	37.9 (5.49)	48.6 (7.05)	42.3 (6.14)	61.6 (8.94)
Modulus-GPa (ksi)	1.99 (288)	3.28 (476)	1.95 (283)	3.56 (516)
Elongation (%)	1.5	0.8	1.87	1.03
FLEXURAL				
Strength-MPa (ksi)	64.9 (9.41)	99.3 (14.4)	65.2 (9.46)	144 (20.9)
Modulus-GPa (ksi)	1.83 (265)	3.18 (461)	1.91 (277)	3.19 (463)
HDT - °C (°F)	61.1 (142)	156 (313)	60.0 (140)	154 (309)
H_2O ABSORPTION (%)	3.18	1.76	>9*	2.12
Tg, dry - °C (°F)	85.7 (186)	211 (412)	82.1 (180)	217 (423)

*some decomposition of sample

TABLE 4. GLASS TRANSITION TEMPERATURES OF EPOXY SYSTEMS

RESIN

HARDENER	Bis A	Blend 1*	Blend 2*	Blend 3*	Blend 4*
M1**	117 (243)	113 (235)	164 (327)	168 (334)	163 (325)
PACM-20	108 (226)	137 (279)	125 (257)	163 (325)	141 (286)
Sylvamine 21	79 (174)	---	81 (178)	75 (167)	---
Ancamine 1856	76 (169)	---	89 (192)	100 (212)	---

NOTES: T_g reported in °C (°F) in parentheses
T_{cure} = 80°C (176°F) for all samples
*Blends 1 through 4 are all mixtures of bis A - derived epoxies
 and epoxy novolac resins of varying functionality
**M1 is an aliphatic amine

Dr. Anita E. Mizusawa
Hysol Aerospace & Industrial Products Div.
The Dexter Corporation
PO Box 312
Pittsburg, CA 94565-3299

Challenges of Adhesive
Formulation: Development
of a Room Temperature
Storage, Room Temperature
Curing Paste Adhesive

BACKGROUND

The first epoxy-based
adhesives were developed
in the 1940's. These
adhesives gained quick
acceptance during the
1950's for several
reasons: ease of
application, high
mechanical strength, the
ability to bond mismatched
parts and dissimilar
substrates. For
structural bonding
applications adhesives
have the ability to spread
the load over the entire
bond area as opposed to
mechanical fasteners which
concentrate the load at
the fasteners.

Adhesives are being widely
used in the aerospace
industry for bonding,
repair, potting, fairing
and liquid shim
applications. As the use
of adhesives increased,
the understanding of
adhesive requirements
became better understood.
Adhesives are developed to
accomodate the stresses
seen by the bonded part.
The four major types of
stresses include tensile,
shear, peel and cleavage.
Mechanical property tests
such as flatwise, lap
shear, T-peel, bell peel,
and wedge crack have been
developed to evaluate an
adhesive's performance
under those four types of

stress. Other factors
have become critical such
as environmental
conditioning and long term
exposures to stress or
heat.

With aerospace technology
advancing there exists a
need for higher
performance adhesives and
raw materials. Adhesive
formulation has become
better understood. It is
now possible to tailor
adhesives to the required
properties. By
understanding the function
of each adhesive
component, it becomes
possible to develop
adhesives for specific
applications.

One adhesive used
extensively in the
aerospace industry is
Hysol EA 934. This epoxy-
based adhesive has good
tensile lap shear
properties from -67^0F to
350^0F with a room
temperature cure.

The major disadvantage of
EA 934 is that it contains
asbestos. Due to the
increasing concerns about
asbestos, a development
program was initiated to
formulate a non-asbestos
adhesive with improved
properties over EA 934 (EA
934NA is available as a
non-asbestos replacement
with similar properties to
EA 934). EA 934 is
brittle and has a limited
shelf life at temperatures
above 40^0F.

The goals for the new
adhesive included
increased toughness over

67

EA 934 with improved
storage stability,
mechanical properties,
handling properties and
room temperature
curability.

ADHESIVE FORMULATING

The first step in the
formulation of a new
product is to define the
necessary adhesive
properties. These can
include processing
requirements, mechanical
properties, shelf
stability and toxicity.
This list can be divided
into two categories:
primary and secondary
goals. The primary goals
are properties that the
adhesive must have. These
are defined by the
customer's design
requirements. The
secondary goals are
desired features, such as
handling and processing
properties. These
properties are usually
defined by the customer, a
specification, or a
specific application area.
Secondary goals can be as
important to the customer
as primary goals, but if
the primary goals are not
met the adhesive will not
be used for that
application.
The next step is to
develop a formulation to
meet the required
properties. This can be
done either with new or
existing raw materials.
The basic components of a
paste adhesive formulation
are: resins, fillers,
additives, modifiers, and
curing agents. With the

goals in mind, these
components can be chosen
to give the optimum
properties.

A brief description of
each basic component is
given below. These topics
are covered in more detail
in Handbook of Epoxy
Resins by Lee and Neville.

RESINS

Resins are the foundation
of a formulation. The
final properties of the
product rely heavily on
the properties of the
resins selected. Shelf
stability is a good
example of this. It is
primarily determined by
the base resins. If the
base resins are not room
temperature stable, then
the formulated product is
likely to be as unstable
as its individual
components unless
chemically modified or
stabilized by an additive.

The resins used also have
a large effect on the
viscosity, reactivity,
cross-link density and
thermal stability
properties as well as
other bulk and adhesive
properties. The most
commonly used resins are
based on bisphenol A. New
resins in the marketplace
offer improved performance
over the bisphenol A type
resins. Improvements in
adhesive properties along
with thermal and
environmental stability
have been achieved using
new resins which have
become available.

FILLERS

There are many types of fillers. Aluminum, silica, talc, microballoons, and conductive fillers are a few of the available types. The filler selected can affect the potlife, peak exotherm temperature, shrinkage, density, electrical and mechanical properties of the adhesive. Large variations in compressive strength are possible based on the filler type. Fillers are also used to increase the thixotropy of a system for applications where sag resistance is needed.

ADDITIVES AND MODIFIERS

Additives and modifiers are used for a variety of reasons. Two such modifiers are colors and diluents. Colors are added to monitor the mixing of two components. Diluents are used to reduce viscosity. Other modifiers include wetting agents, toughners and stabilizers.

CURING AGENTS

The curing agent plays a major role in the cured adhesive properties. Curing agent selection is based on the desired potlife, cure temperature, and service temperature of the adhesive system. In formulations, the curing agent is as important to the final properties as the base resins.

EXPERIMENTAL DESIGN

When formulating, scaling up or manufacturing an adhesive system, there are several factors to be aware of. A major concern is the effects of lot-to-lot variations in the raw materials. This is overcome by obtaining several representative lots of raw materials and extensively evaluating the effect of their properties on the adhesive's properties. By narrowing down raw material specifications such as viscosity and epoxide equivalent weight, a more consistent product will be obtained. It is important to set the raw material specifications to get the desired result from the final product.

When screening adhesive properties, variations in testing technique, lay-up, metal etch and cure conditions can all affect the results. It is very important to include a control each time a new material is being evaluated.

Repetitive testing must be done to assure that the values obtained are consistent and not a "one time fluke". There are several things to consider when comparing two adhesives, A and B, whose performance follows a

bell-shaped distribution curve as shown below.

#1B #1A
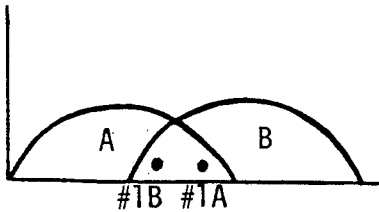
In the region where the two curves overlap there is possible misinterpretation of test results.
For test #1, A initially looks better than B. If enough tests are performed B should statistically outperform A. The more similar A and B are in performance, the greater their performance curves will overlap therefore the greater the possibility for misinterpretation of the test results.

When scaling up from the lab to production, processing parameters become a major consideration. Mass effects influence the heat-up rates, cool-down rates and total processing time. These changes must be monitored to determine their effect on the final adhesive properties.

By designing the experiments to accomodate the lot-to-lot variations, processing variations and statistical errors, the final product becomes more consistent.

A NEW PRODUCT, EA 9394

The preceding steps were taken when formulating Hysol's new adhesive EA 9394. The primary goals were to exceed the mechanical specifications required by MMMA-132 Rev A, to eliminate asbestos and increase room temperature shelf stability over EA 934.

The secondary goals were to have a thixotropic system for liquid shim applications, utilization of low toxicity materials, improved handling characteristics and good moisture resistance.

The following charts include data base information on EA 9394 and comparative information with EA 934 and EA 934NA. Bulk and adhesive properties are also given.

Primary Goals for Screening EA 9394

PROPERTY	TEST CONDITIONS	NO. OF SPEC.	MINIMUM REQUIREMENTS
TENSILE SHEAR	10 MIN. -67° $\pm$ 5° F	6	3000 psi
TENSILE SHEAR	75° $\pm$ 5° F	6	3000 psi
TENSILE SHEAR	10 MIN. 180° $\pm$ 5° F	6	2000 psi
TENSILE SHEAR	NORMAL TEMPERATURE 75° $\pm$ 5° F after 30 days at 120° $\pm$ 5° F 95-100% relative humidity	6	2750 psi
TENSILE SHEAR	75° $\pm$ 5° F. 7 days immersion in the respective fluid (4.5.5)	6	2750 psi

EA 9394

Secondary Goals Attained

EXCELLENT MECHANICAL PROPERTIES

TOUGHNESS

LONGER POTLIFE

ROOM TEMPERATURE STORAGE STABLE

THIXOTROPIC, NO SAG

HIGH TEMPERATURE COMPRESSIVE STRENGTH

GOOD HOT/WET COMPRESSIVE STRENGTH

ROOM TEMPERATURE CURE (3-5 days)

LOW EXOTHERM

SHORT CURE CYCLE AT ELEVATED TEMPERATURES

XEA 9394

PILOT PLANT AND PRODUCTION SCALE-UP

TENSILE LAP SHEAR VALUES (psi)

TEST TEMPERATURE	SPECIFICATION REQUIREMENT	PILOT PLANT LOT NUMBER			PRODUCTION LOT NUMBER
		6258	7047	7099	7160
$-67^{0}F$	3000	3300	3500	3500	3200
$77^{0}F$	3000	4100	3900	4200	4000
$180^{0}F$	2000	2900	3000	3100	3000
$300^{0}F$	1000	1900	1700	1700	1800

BULK PROPERTIES OF EA 9394

ADHESIVE	MIX RATIO	SHORE D HARDNESS
EA 9394	100:17	89

TENSILE STRENGTH (psi)	TENSILE MODULUS	% ELONGATION
6675	620,000	1.66

Tg (DMTA, DRY)	Tg (DMTA, WET;60 DAYS 100% RH)
$78^{0}C$	$68^{0}C$

SHEAR MODULUS (RDS)

$77^{0}F$	$180^{0}F$	$300^{0}F$	$500^{0}F$
212,040	118,130	74,470	7,985

COMPARISON OF EA 9394 VERSUS EA 934NA AND EA 934

	EA 9394	EA 934	EA 934NA
VISCOSITY (poises)			
PART A	5700-7500	7500	4000
PART B	42	30	30
DENSITY			
PART A	1.45	1.55	1.45
PART B	1.02	.98	.98
MIXED	1.33	1.35	1.30
SLUMP			
NICKEL	0	0	2"
3M JIG	0	>5"	>5"
POTLIFE (minutes)	100	40	40
MIX RATIO 100:	17	33	33
ROOM TEMPERATURE TENSILE LAP SHEAR VALUES AFTER EXPOSURE TO:			
JP4	4800	3100	3500
HYDRAULIC OILS	4400	3000	3500
IPA	4200	-	3500
WATER	4400	3600	3500
500 PSI TENSILE LAP SHEAR VALUES AT 77°F (HOURS)	7-8	6	6

73

EA9394 and EA934

Viscosity in Poise vs. Time

32 K
28 K
24 K
20 K
16 K
12 K
8 K
4 K
0

Initial   8 Weeks   10 Weeks   16 Weeks

9394 120F   9394 90F   9394 77F   9394 40F   934 90F   934 77F

934 40F
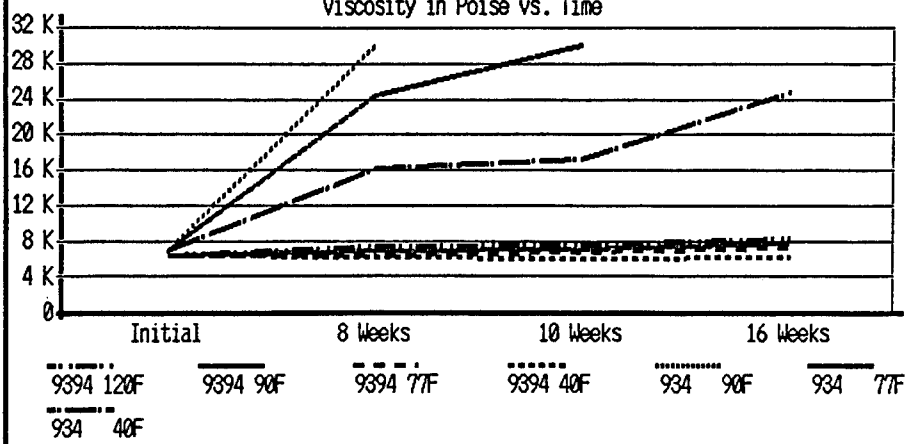
TENSILE STRENGTH VS CURE XEA 9394

4500
4000
3500
3000
2500
2000
1500
1000
500
0

15   30   45   60   90   120   150   180

TIME @ 125 F

Compressive Strength
77 F. Cure Temperature
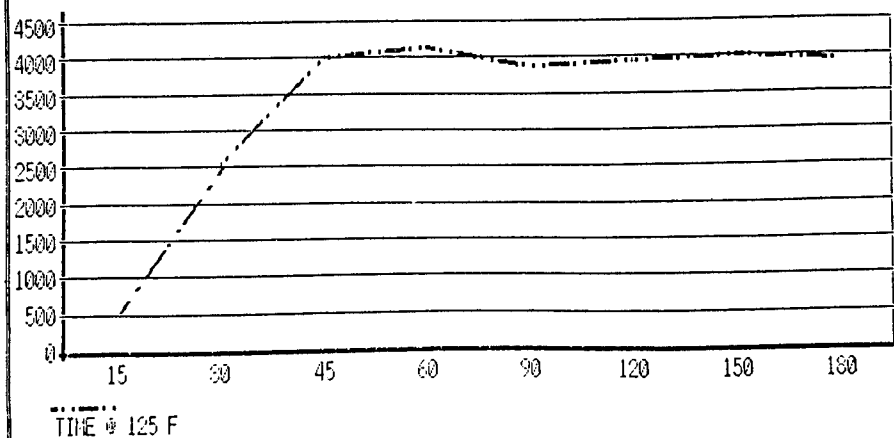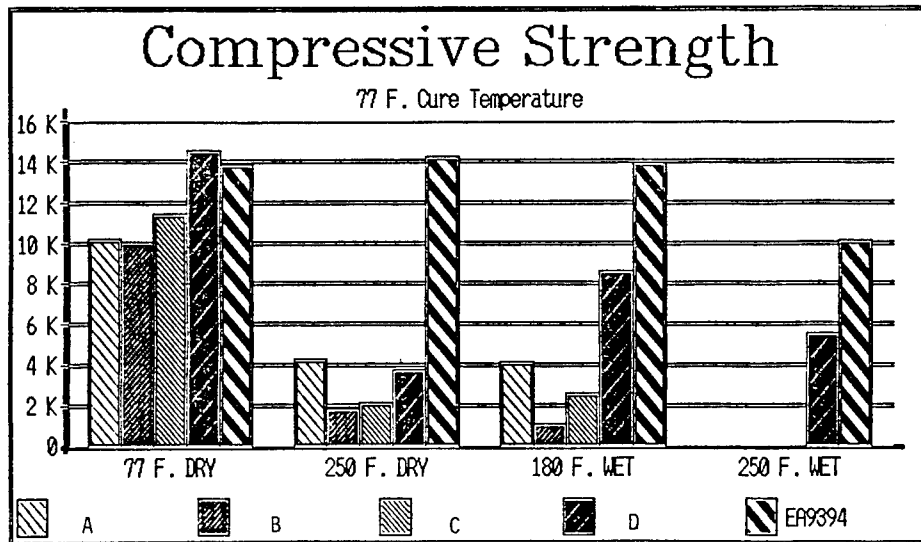
A, B, C AND D ARE MATERIALS TYPICALLY USED FOR LIQUID SHIM APPLICATIONS

Compressive Strength
Cure Temperature 190 F. Except "D" (260 F.)
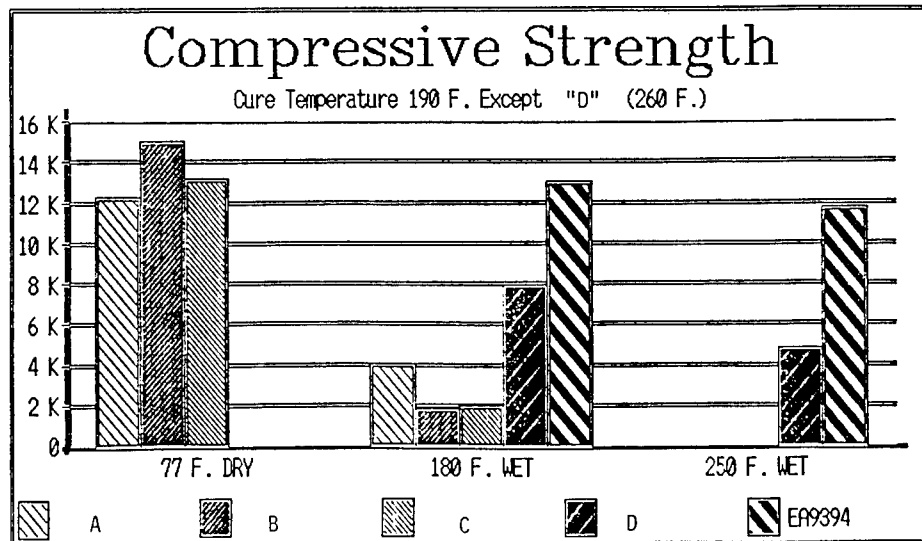
Synthesis and Adhesive Properties
of
Acetylene Terminated Resins

Dr. Yesh P. Sachdeva

Dr. C. Lynn Mahoney

Advanced Technology Group
Research and Development

Hysol Aerospace and Industrial Product Division
The Dexter Corporation
2850 Willow Pass Road
Pittsburg, CA 94565

Abstract

Acetylenic terminated resins are showing considerable promise as processable, moisture insensitive, thermally stable structural materials. While most of their past evaluation has been in composite systems, some have shown potential as adhesive candidates. Selected resins based on phenylene backbones have application and cure properties similar to familiar high-temperature epoxide adhesives. Their retention of strength and stabilities at elevated temperatures are considerably above such epoxide based systems, but they presently need improvements in toughness and adhesion properties. The solvent properties of the resins based on bisphenol A limit inclusion of modifying materials. Structural modifications and formulation work to gain such property improvement are part of this work. Through such toughness improvements, the mechanical strength properties of selected AT resins have been markedly increased over the ambient to over 500°F test temperature range.

1. INTRODUCTION

Over the past thirty years, a high level of synthesis effort has been expended in preparation and evaluation of potentially thermally and oxidatively stable fluids and polymers. Many of the

compositional factors leading to stability and required performance have been repeatedly examined and general ground rules have been well established. Not unexpectedly, conflicts exist between attainment of thermal and oxidative stability and the practical needs of ease of processing and fabrication, mechanical properties and cost, etc., and major compromises are generally needed.

A major limitation of many materials examined in the past for high temperature adhesive applications, including many of the materials carried to initial commercial stages, has been generation of volatile components during processing. Thus, successful formation of void-free bonds have been obtained only with very small overlap areas. Resins curing by addition mechanisms should not generate volatiles and adhesives based on maleimide, norbornene, and acetylenic end groups, etc., have received various levels of attention for use as elevated temperature adhesives. The norbornene, and maleimide systems have various

problems including some volatile generation, major application and cure challenges, and toughness deficiencies. The acetylenic terminated resins (Ref 1) based on various phenylene backbones do have application advantages similar to the much used epoxy resins, with low viscosities at reasonable temperatures and reasonable cure schedules. These resins cure by an addition mechanism (Figure 1)[2] forming a cross-linking conjugated polyene structure that has premium thermal and oxidation stability. They absorb only low levels of moisture so that mechanical properties are only moderately reduced in wet environments.

Since the most common acetylenic terminated resins, when cured, are brittle materials, improvements in toughness are needed to make them practical for adhesive applications. Examined approaches to such improvement include: 1. increase the cross-link distance through use of stable, more flexible backbone structures, and; 2. introduce more polar functionality into the

backbone structure so that the increased solvent power will allow inclusion of polymeric modifiers.

The work following is the result of a preliminary study to prepare and examine the properties of some new acetylenic terminated resins and access their potential for use as high temperature adhesives.

2. EXPERIMENTAL

2.1 Synthesis

Most of the new AT-Resins were synthesized in high yields (80+%) via a general three-step synthesis (Fig. 2).[1] The first step involves the condensation of an appropriate diphenol with excess dibromobenzene to yield (95+%) of the bromophenyl capped Ullmann ether. In the second step, the Ullmann product is reacted with 2-methyl-3-butyn-2-ol in the presence of a palladium catalyst to generate a blocked AT-Resin. The third step uses a base for deblocking to give the final resin (Figure 2).

Several products were also made using the reaction of dichloro-diphenyl sulfone with m- or p-bromophenol and/or a diphenol to produce a simple or oligomeric dibromo compound which was converted to an acetylenic resin by the above described route. The structures of the AT (acetylenic terminated) resins made for this study are shown in Figure 3.

2.2 Neat Resin Properties

The various acetylenic terminated resins synthesized for this study are listed in Table 1. Yields were generally high, their purity was also high (HPLC) and the residual metals (Cu, Pd from the catalysts used in their synthesis) were below 20 ppm. The oligomer content was dependent on the synthetic route and conditions used but was in the 15-20% range for the main resins studied. Their viscosities varied greatly, mainly dependent on the oligomer content. Viscosity temperature curves (Rheometric Viscoelastic Tester), shown in Figure 4, indicate that most of the resins, with 20% or less oligomer content, reached a 10 poise viscosity level by temperature of 65-87°C (Table 1). The p-ATS was a high melting point crystalline material, which

on melting, reached a low viscosity but at a temperature (160°C) which rapidly caused advancement towards cure.

The cure initiation temperatures [as indicated by DSC (Differential Scanning Calorimeter) scans at 10°C/min] were closely grouped in the 125-160°C range and the peak exotherm temperatures ranged from 205-245°C (Table 1).

The ATB (bisphenol A based) resins were poor solvents for many desired modifying polymers but were solvents for all the related acetylenic terminated resins studied in Table 1. The m-ATBF6 and m-ATDiB were poor solvents also. The m-ATS and m-ATBZ resins were much more polar and could dissolve up to 20-30% of modifying polymers. The m-ATBZ was selected for the formulation work of this study. The m-ATS resins have received much formulation attention for matrix resin applications in other studies.[3],[4].

2.3 Cured Resin Bulk Properties

The resin cure cycle developed by the Air Force Materials Laboratory for m-ATB and m-ATS resins[1] was modified for the following work. For cure of neat resin samples, as well as for lap shear specimen preparation, the general conditions used were: 2-5°C/min. heat up, hold at 121°C for 2 hrs., heat to 179°C and hold for 4-5 hours. Post cure at 290°C for 4 hours.

In the cured state, the series of neat resins listed in Table 2, showed the expected order of Tg's [as measured using DMTA equipment (Dynamic Mechanical Thermal Analysis)]. The highest Tg (TanΔ, 410°C) was as expected for the low oligomer content para substituted acetylenic terminated sulfone. The low oligomer content m-ATS's Tg was lower at 360°C. This was followed by m-ATBF6 at 325°C, the m-ATBZ at 290°C and the m-ATB at 275°C. The m-ATDiB was still lower at 260°C (Table 2).

The moisture absorption level of all these cured AT resins was relatively very low compared to more conventional adhesive and matrix resin systems. As shown in Figure 5,

79

during exposure at 160-200°F, 100% RH, over 6% water was absorbed by a BMI system and 5% by a typical high temperature epoxide system (tetraglycidyl methylene dianiline-diamina-diphenyl sulfone). In contrast, m-ATB and m-ATDiB absorbed only 0.5-0.6% water. The water absorption of the m-ATBZ was about 1.1% and the m-ATS about 2% under the same exposure. This increased water absorption of the m-ATS system reflects the tradeoff needed when polarity increases are made to improve solvency capabilities. This low absorption greatly reduces the influence of moisture on the mechanical properties of the AT resins. For example, in DMTA tests at rapid heat-up rates (20°C/min) to reduce water loss, the m-ATB resin showed a wet Tg loss of only 20°C (275°C dry-257°C wet) and the m-ATS only 40°C (360°C dry -320°C wet). This compares very favorably to the 120-140°C Tg loss of high temperature epoxides and bismaleimide systems when saturated with moisture.

When cured, all the above AT resins showed a high level of thermal and oxidation stability. In TGA (Thermogravimetric) test, using finely powdered samples to maximize the exposed surface area, the m-ATB resin showed a major increase in stability, both in the absence (N_2) and presence of oxygen (air) over current epoxide-based, high-temperature systems (Figure 6). A model BMI system showed similar thermal stability (N_2) but was significantly poorer in tests in air. In comparison to the m-ATB resin, both the m- and p-ATS resins were slightly more thermally and oxidatively stable (Table 2). The m-ATBF6 showed a similar high stability in these tests. The m-ATDiB showed an expected lower stability. All these results show a stability ordering expected from the known relative thermal and oxidative stability of the added central linking groups of the AT resins. This suggests that the cross-linking structure generated during cure of the acetylenic groups is not the weaker link in such materials. Theoretically, phenylene rings could form from the cross-linking

80

reaction of three acetylenic groups. However, studies by the Air Force Materials Laboratory have indicated that, at most, only a very minor amount of such reaction occurs. The main cross-linking reaction appears to involve formation of conjugated double bonds which, through their conjugation, develop a high level of oxidative and thermal stability[2].

2.4 Performance Properties

The tensile lap shear test specimen was deliberately chosen for this work because it greatly concentrates the stresses at the edges of the bond line. It thus serves as a rapid method of indicating not only the tensile strength of adhesive materials but shows also the order of the peel strength or toughness of the system.

In this initial screening work, the high temperature tempered 2024-T81 aluminum was used for ease of fabrication and test specimen preparation as well as for the peel stresses imposed. Phosphoric acid anodized surface preparation was used and the cure conditions were similar to those described in Section 2.3.

In initial screening work using m-ATB resins, tensile lap shear strengths were essentially linear (1600 psi) from ambient temperatures to 500°F and 600°F values were still 900 psi (Figure 7). Use of various support fabrics, fillers and primers has so far not increased the lower temperature strength properties. As shown by the failure pattern of the mx-ATB lap shear test specimen shown in the SEM photograph (Figure 8), the bond fails progressively in a highly brittle manner leaving almost a gridlike pattern of long rectangular bulk adhesive fragments. This brittle failure pattern is seen throughout the tested temperature range with the m-ATB resins and similar failure patterns were found with all the rigid unmodified AT resins (ATB, ATS, ATBZ, etc.).

Initial attempts to add high molecular weight polymers or addition curing coreactants or other potential tougheners were only marginally successful with

resins based on bisphenol A. Increased resin polarity to improve wetting and adhesion to specific substrates should be possible using stable polar linking groups for aromatic structures. Such changes should also increase the solvent power of such resins to allow formulating approaches involving addition of modifying polymer.

3. FORMULATION STUDIES

3.1 Reduction of Cross-Link Density

Several of the high oligomer content AT resins [p-AT(S-B) and p-AT(S-DiB)] showed quite high values in lap shear tests at relatively high temperatures (approx. 2.5K in the 300-500°F range) (Figure 7). However, their viscosities were much too high for practical application (Figure 4). As shown in Table 3, blends containing equal amounts (1/1) or excess (3/1) m-ATB reduced the viscosities to a more manageable level. With such blends, lap shear strength properties were reduced nearly to the level of the m-ATB (brittle failure modes) (Table 3). This

approach was set aside and formulation work with polymeric modifiers was emphasized.

3.2 Formulation with Polymeric Materials

Both the m-ATS and m-ATBZ are sufficiently polar to act as solvents for selected stable polymeric modifiers. The m-ATBZ resin was chosen for the following work. Screening studies with two polymer systems showed promise in generating toughness as measured with compact tension test specimens[4]. A major increase in G_{IC} was found with use of increasing concentrations of Modifier A (Table 4). Modifier B was less effective. Both polymeric modifiers made little change in the cure characteristics of their blends in m-ATBZ. The thermal and oxidation stability and moisture pick-up of Modifier A blends were very close to those of the neat m-ATBZ resin.

3.3 Strength Properties

In tensile lap shear tests, blends of Modifier B with m-ATBZ showed only modest improvement over results with the AT resin alone. With

Modifier A, however, and
reflecting the major increase
in G_{IC} values (Table 4)
obtained through its use, a
major increase in tensile lap
shear values was obtained over
a wide temperature range
(Figure 9). With bond line
control using either 0.5 mil
glass beads or a glass scrim
cloth, tensile shear values
were in the range of 2.0 KSI-
2.8 KSI over the ambient to
450°F test range. Comparable
tests with the neat m-ATBZ
resin gave values of 1.2-1.5
KSI. With the Modifier A-ATBZ
resin blends, strengths of over
1.2-KSI were retained to 550°F.
The failure mode was markedly
less brittle than with the neat
AT resin. Some bond failure at
or close to the metal surface
and from the glass scrim cloth
is partly responsible for the
observed data scatter and
offers directions for strength
improvement.

4. SUMMARY

Acetylenic terminated phenylene
resins show many properties
important for high temperature
adhesive application. They
absorb little water, have good
viscosity and cure properties,
and are thermally and oxida-
tively very stable. Their
strength properties have been
hindered by brittle failure
modes. Use of polymeric
modifiers has given major
improvement in toughness
properties and suggests future
attainment of useful adhesives
for the ambient to 550°F
temperature range.

5. REFERENCES

[1] B.A. Reinhardt, G.A.
    Loughran, F.E. Arnold and
    E.J. Soloski, "Synthesis
    and Properties of
    Acetylene Terminated Aryl-
    Aryl-Ether Oligomers"; New
    Monomers and Polymers, Eds
    B.M. Culbertson and C.U.
    Pittman, Jr. Plenum Press
    1984. Pages 29-40.

[2] J.M. Pickard, E.G. Jones
    and I.J. Goldfarb, "The
    Kinetics and Mechanism of
    the Bulk Thermal
    Polymerization of Bis-4-
    (3-ethynyl-phenoxy)
    phenylsulfone," Macromol.,
    12, 895 (1979).

[3] P.A. Steiner, J. Browne,
M.T. Blair and J.M.
McKillen, "Development of
Damage Tolerant Acetylene
Terminated Resin/Carbon
Fiber Composites,"
International SAMPE
Technical Conference, Vol.
18, 1986, pp 193-208.

[4] P.A. Steiner, J. Browne,
M.T. Blair and J.M.
McKillen, "Development of
Damage Tolerant Acetylene
Terminated Resin/Carbon
Fiber Composites: II,"
International SAMPE
Symposium, Vol. 32, 1987,
pp 807-821.

Table 1. Neat Resin Properties.

AT Resins[1]	Oligomer Content	Yield	Viscosity, Temp.°C for 10 poise	DSC Scan Exotherm, 0°C Init.	Peak	Solvency % Modifier
m-ATB	15	80	65	140	220	Low
mx[2]-ATB	24	80	65	(145)	(210)	Low
m-ATS	0	95	87	125	221	30
p-ATS	0	65	160 (100 poise)	165 (mpt.)	205	-
m-ATBZ	20	80	78	137	245	30
m-ATBF6	20	80	65	154	237	Low
m-ATDiB	20	80	87	160	235	Low
p-AT(S-B)	43	65	160 (200 poise)	135	220	-
p-AT(S-DiB)	32	80	168	130	220	-

[1] See Figure 3 for structures.
[2] mx - 85%m, 10%p, 5% 0 linkages.

Table 2. Summary of Cured Resin Bulk Properties.

	Tg °C	H$_2$O Abs. %	TGA Stab. Temp(°C), for 10% Wt. Loss N2	Air	G_{IC} in-lbs/in^2
m-ATB	275	0.6	-	-	~0.4
mx[a]-ATB	275	0.7	430	405	-
m-ATS	360	2.2 1.6	440	420	~0.1
p-ATS	410	3.0	455	425	~0.1
m-ATBZ	290	1.1	445	-	~0.1
m-ATBF6	325	1.7	435	-	-
m-ATDiB	260	0.5	360	-	0.45
p-AT(S-B)	285	1.5	430	410	-
p-AT(S-DiB)	245	1.1	430	395	-

[a] See Table 1.

85

Table 3. Performance Properties of mx-ATB Mixtures with
High Oligomer Content AT Resins.

Mixture	Viscosity, Temp., °C, for 10 poise	Tg °C	H_2O Abs. % w	Tensile Lap Shear, KSI, (°F)			
				RT	350	450	550
mx-ATB	65	276	0.8	1.5	1.6	1.5	1.0
p-AT(S-B)	160 (200 poise)	285	1.46	2.0	2.2	2.4	1.2
1/1[a)	110	280	1.04	1.6	1.6	1.90	0.8
3/1[b)	82	282	0.85	1.6	1.6	1.5	1.0
p-AT(S-DiB)	168	243	1.1	1.9	2.6	1.8	0.4
1/1[a)	124	264	0.90	1.7	1.8	1.7	0.6
3/1[b)	85	270	0.75	1.6	1.7	1.6	0.8

a) 1/1 mx-ATB/p-AT(S-B) (or p-AT(S-DiB) ratio.
b) 3/1 mx-ATB/p-AT(S-B) (or p-AT(S-DiB) ratio.

Table 4. Fracture Toughness of Formulated AT Resins
(Compact Tension Specimen).

Material	G_{IC}, in.lbs/in^2
m-ATBZ	0.01
+10% Modifier A	0.50
+20% Modifier A	0.80
+30% Modifier A	1.50
+10% Modifier B	0.26
+20% Modifier B	0.30
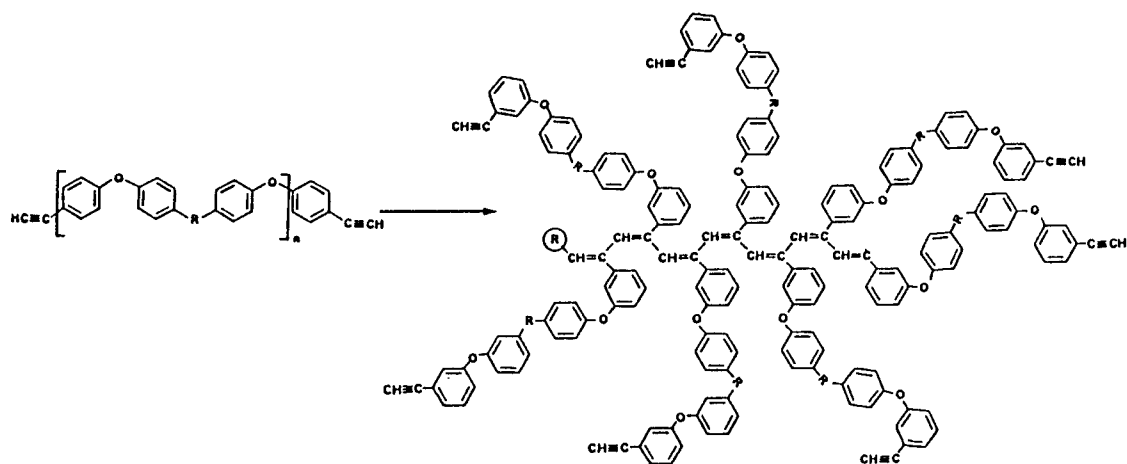
Conjugated Polyene

Figure 1. Mechanism of Polymerization of AT Resins

Synthesis of m-ATB
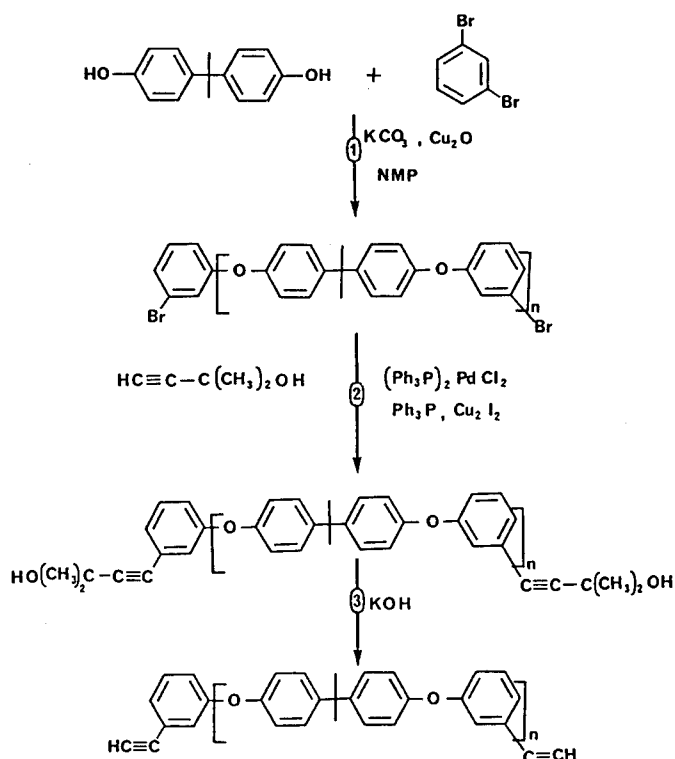
Figure 2. Synthesis Route to AT Resins

HC≡C-Ph-O-R-O-Ph-C≡CH

(Ph=Phenylene Group)

R	Abbreviation
-Ph-C(CH3)(CH3)-Ph-	ATB
-PH-S(O)(O)-Ph-	ATS
-Ph-C(O)-PH-	ATBZ
-Ph-C(CF3)(CF3)-Ph-	ATBF6
-Ph-C(CH3)(CH3)-Ph-C(CH3)(CH3)-Ph-	AT-DiB
-Ph-S(O)(O)-Ph-O-Ph-C(CH3)(CH3)-Ph-	AT(S-B)
-Ph-S(O)(O)-Ph-O-Ph-C(CH3)(CH3)-Ph-C(CH3)(CH3)-Ph-	AT(S-DiB)

Figure 3. Structures of Synthesized AT Resins
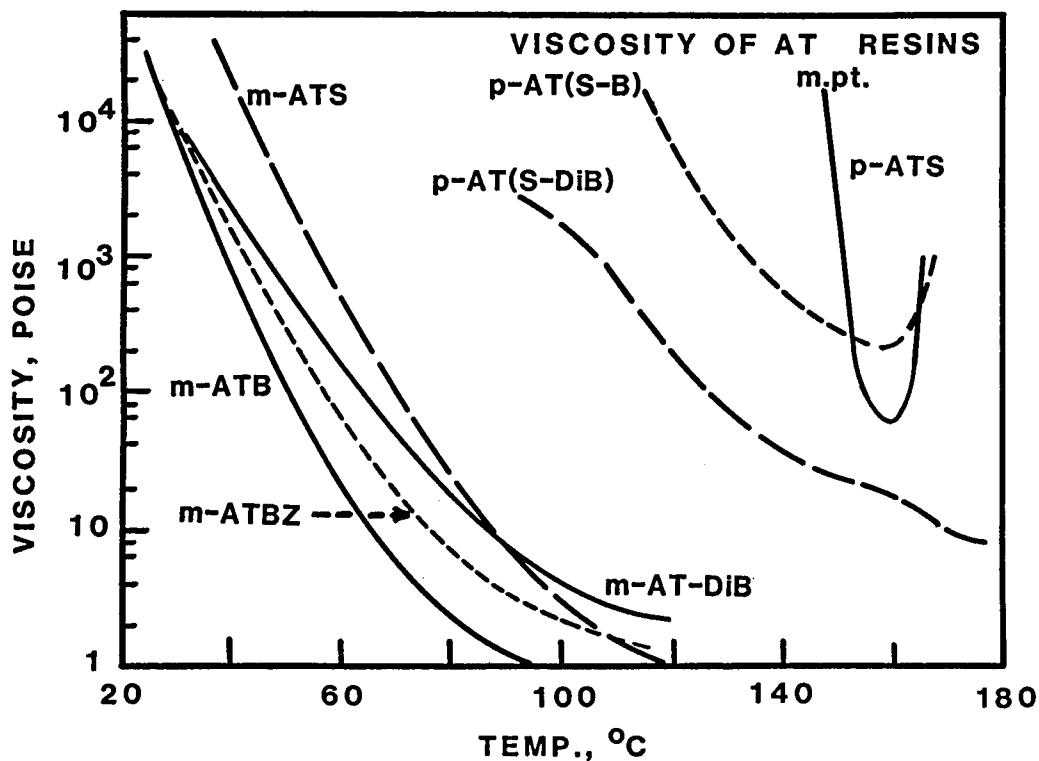
Figure 4. Viscosity-Temperature Properties

88
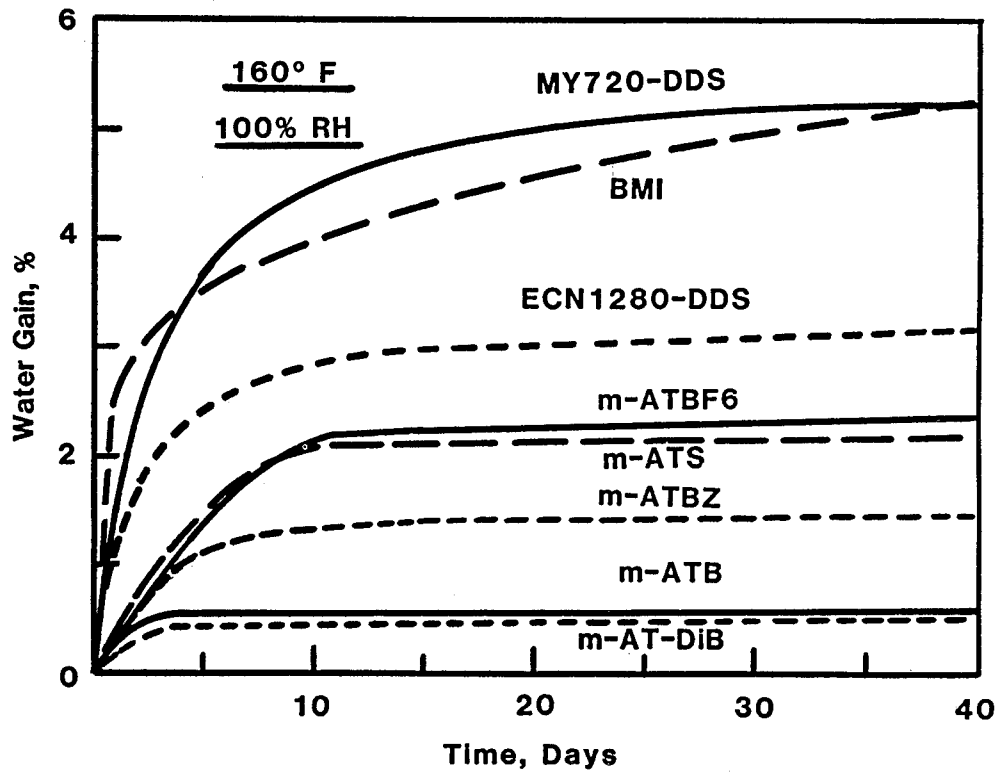
Figure 5. Water Absorption Levels of Cured AT Resins
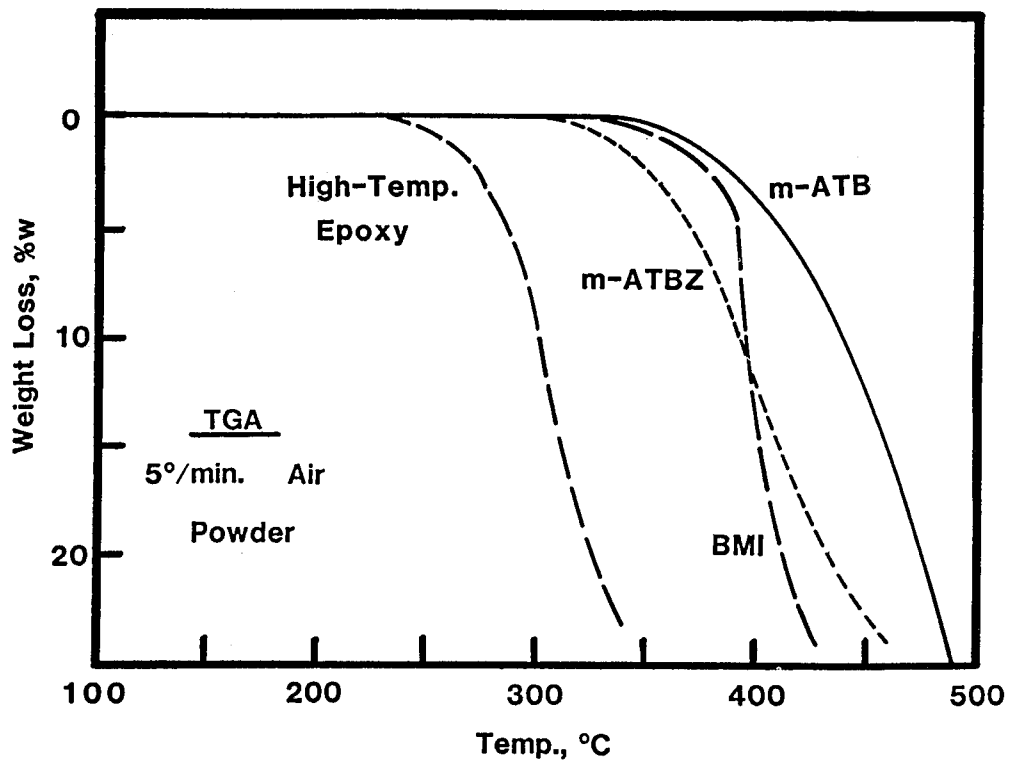
Figure 6. Thermal-Oxidation Resistance of AT Resins

89
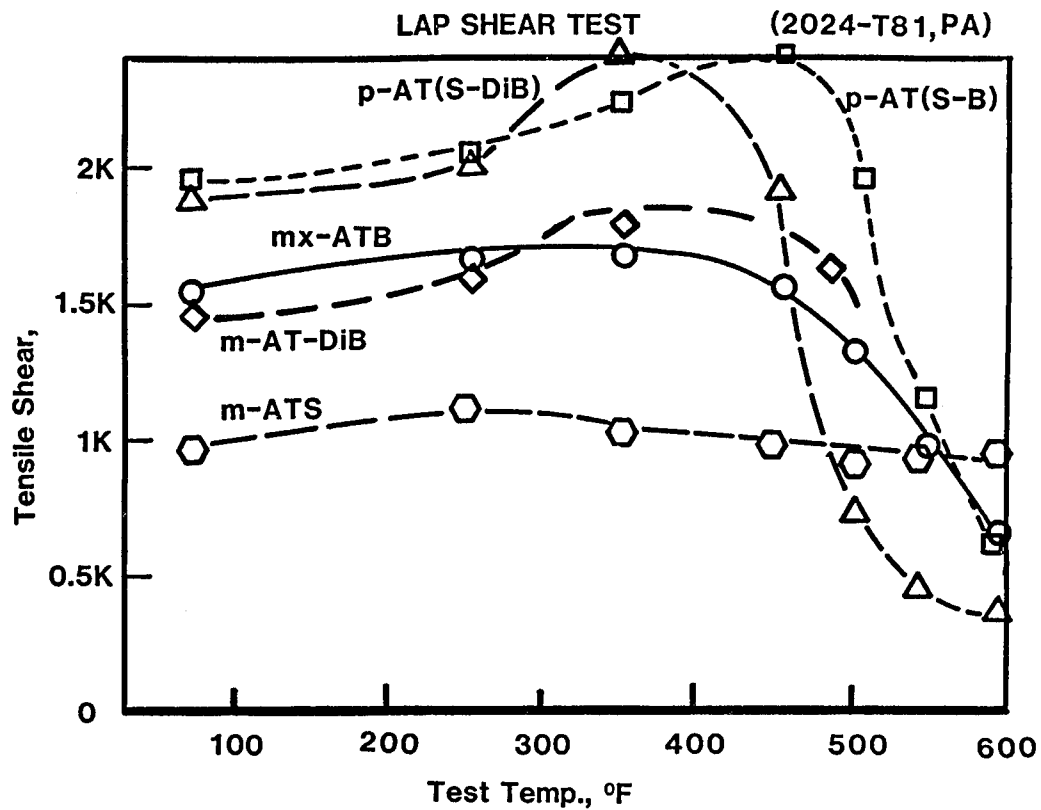
Figure 7. Tensile Lap Shear Test Performance of AT Resins
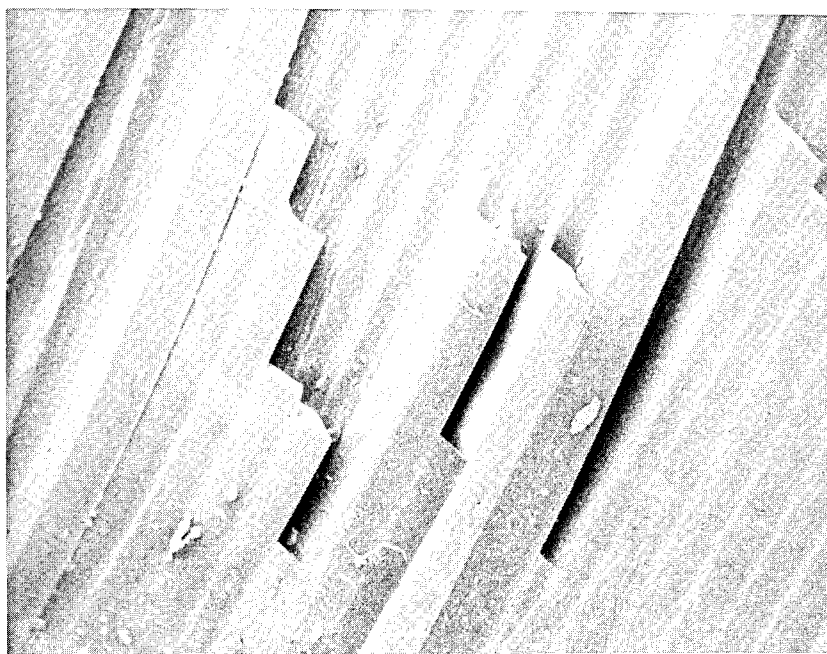
Figure 8. Brittle Fracture Pattern of Unmodified AT Resins
(Lap Shear Specimen, m-ATB, 30X)
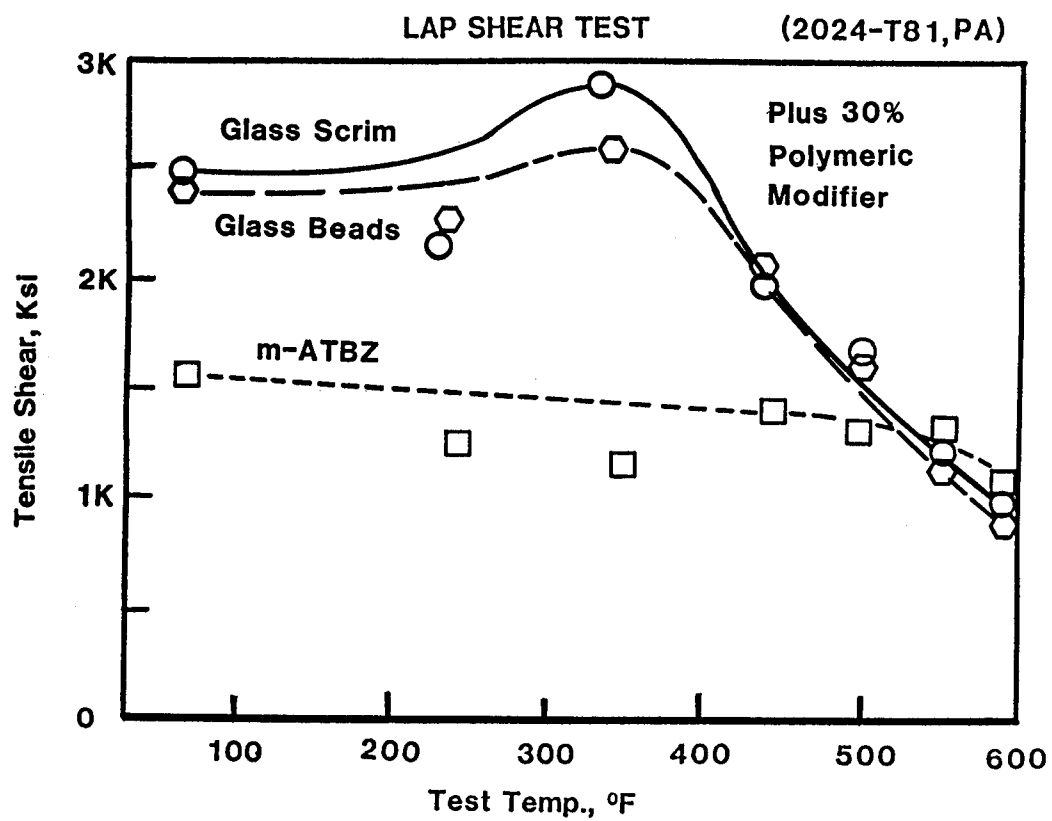
Figure 9. Tensile Lap Shear Test Performance of Toughened m-ATBZ.

PHYSICAL PROPERTIES AND DURABILITY OF
THIRD GENERATION TWO-PART EPOXY ADHESIVES

Alphonsus V. Pocius and Robert D. Waid
3M
Adhesives, Coatings and Sealers Division
St. Paul, MN 55144-1000

ABSTRACT

The evolution of physical properties and durability of two-part epoxy adhesives is discussed in terms of "generations" of products. Comparisons are made in regards to the general organic chemistry of these epoxy adhesives in relation to their performance. Of major importance is the comparison of second generation two-part epoxies and third generation two-part epoxies. Second generation epoxies rely upon the phase separation of a rubber (usually a functional butadiene-nitrile polymer) during cure to obtain their performance. Third generation epoxies improve upon this concept by providing a system where the rubber (an acrylic) is phase separated in the epoxy resin before cure. The lap shear and peel performance of adhesive bonds made with the four generations of adhesives are compared. The durability of adhesive bonds made with the four generations of adhesives are also compared on both steel and aluminum. The results indicate the superior performance of the third generation system. Dynamic mechanical analysis as well as electron microscopy are used to explain some of the results.

1. INTRODUCTION

The evolution of performance of two-part epoxy adhesives can be described in terms of "generations" of products in much the same way as this terminology has been applied to acrylics and to epoxy based film adhesives. The "zeroth" generation of two-part epoxy adhesives comprises those adhesives which consist of a single, unmodified epoxy resin and an unmodified curative, usually a polyamide. "Zeroth" generation two-part epoxy adhesives are characterized as being moderate to high shear strength adhesives but also as being very brittle materials. The first generation of two-part epoxy adhesives comprises those adhesives which consist of single or multiple epoxy resins as the base resin and a curative which imparts flexibility to the cured adhesive. First generation two-part epoxy adhesives are characterized as being moderate in shear strength but as having high elongation so that the adhesive is more elastomeric than brittle. The second generation of two-part epoxy adhesives comprises those adhesives whose base consists of epoxy resins modified by reactive liquid polymers and a curative selected such that

appropriate epoxy matrix properties would result. In this second generation of two-part epoxy adhesives, the reactive liquid rubber is initially soluble in the epoxy resin but the rubber phase separates from the epoxy phase as the adhesive cures. This results in a cured epoxy matrix having dispersed therein a discrete phase of rubbery particles. Second generation epoxy adhesives are character- ized as being "tough" or frac- ture resistant while maintaining the modulus of the unmodified epoxy. This fracture resistance is, for the most part, due to the presence of the two phase morphology.

Inherent to the second genera- tion technology is the depend- ence of the phase separation process upon the cure of the epoxy. Thus, factors such as the degree of mixing, the tem- perature of cure or maintenance of the proper stoichiometry of the base resin and the curative could affect the fracture resis- tance of the adhesive in that the phase separation could be affected. To address this con- cern, 3M has developed a new resin technology in which the proper phase separation of the rubber is complete in the **uncured** epoxy resin. Thus, the cure factors mentioned above will have no effect on the phase separation characteristics of the base resin. This new resin technology forms the basis of new third generation two-part epoxy adhesives.

2. EXPERIMENTAL

a. Adhesives

The "zeroth" and first genera- tion adhesives used in the work are 3M's EC-1838 B/A and EC-2216 B/A, respectively. Both adhesives have been successfully used for over 20 years in both aerospace and general industrial applications. The third generation adhesives used in this work are EC-3569 B/A and 1XA-3559 B/A. The base resin for the second generation adhesive used in this work was synthesized by the method of N.C. Paul, et. al.[1] The base resin generated had an epoxy equivalent weight of 242 as determined by the tetrabutyl- ammonium bromide/acetic acid/ perchloric acid titration method. This equivalent weight is identical to that of the resin in EC-3569-B. The second generation base resin was then further modified with the same fillers as used in EC-3569-B in such a way as to make this resin identical in every way to EC-3569-B except for the type of toughener. The curative used with the second generation base resin was EC-3569-A. We will designate the second generation adhesive as CTBN/3569-A. From this discussion it is seen that CTBN/3569-A is meant to be an exact 2nd generation analog to EC-3569 B/A; the only difference is the mode of toughening. Both parts of all of the adhesives were thoroughly deaerated in a vacuum oven at elevated temper- ature before weighing and mixing. They were also deaerat- ed as well as possible after mixing but before application.

b. Metals and Surface Preparation

Aluminum. The metals used as adherends in this study were 2024-T3 bare and clad aluminum alloy and 7075-T6 bare aluminum alloy. In one case, 5052H34 and 6061 aluminum alloy was used.

The surface preparation was the optimized FPL etch process. No priming of any sort was used in this work.

Steel. 1010 cold rolled steel was used. Coupons were degreased by wiping with methyl ethyl ketone (MEK) using a lint free cloth. Abraded samples were first MEK wiped then abraded with a Scotch-Brite® three dimensional abrasive pad and again MEK wiped. Grit blasted samples were first MEK wiped then grit blasted with 120 alumina grit at an air pressure of 0.55 MPa. Etched samples were MEK wiped then etched in a nitric/phosphoric acid solution at room temperature for 5 minutes, rinsed in tap water and allowed to air dry.[2]

c. Bonding Method

Aluminum. Lap shear specimens were generated using ASTM Method D1002 with the following exceptions. The metal had dimensions of 4" X 7" X 0.063". The adhesive was applied in a 1/2" wide stripe down the milled edge of the specimen. 4 mil thick shims were placed into the adhesive at three locations to maintain a constant bondline thickness for all of the adhesive bonds. The specimens were fixtured with pressure sensitive tape, placed between release liners, cardboard (for equalization of pressure) and then steel plates were placed on the assembly to apply a pressure of about 4 psi to the bonded areas. T-peel specimens were generated according to ASTM Method D1872 with the following exceptions. The metal had dimensions of 3" X 8" X 0.032". The adhesive was applied in a 2.5" wide, 25 mil thick stripe down the center of the metal panel (except in the case where EC-2216 B/A was used, where the applied thickness was 32 mils). Brass shims of 8 mil thickness were placed on both sides of the strip of adhesive (except in the case of EC-2216 B/A, where 25 mil thick shims were used) to control bondline thickness. The bond was fixtured with pressure sensitive adhesive tape, placed between release liners and cardboard and the assembly was placed under steel plates to apply a pressure of 0.4 psi to the bonded area. The adhesives were allowed to cure at ambient laboratory conditions under pressure for 24 hours, after which the bonds were placed in a constant temperature, constant humidity (CT) room (77°F/50% RH) for another 6 days. Several of the T-peel bonds were left in the CT-room for 40 and 90 days before testing.

Steel. Single coupon lap shear specimens were made with the surface prepared cold rolled steel. The adherend dimensions were 1" X 4" and the adherend thickness was 60 mils. The bonded area measured 1" X 0.5" and a uniform bondline thickness of 10 mils was maintained using steel spacer wires. The adhesive components were weighed, hand mixed and applied. Bonds were allowed to cure at room temperature for 7 days under a slight applied pressure.

d. Testing

Initial Physical Properties

Initial physical properties were determined on an MTS 880 Tensile Tester. The rate of crosshead displacement for lap shear specimens was 0.1"/min., while the rate of crosshead displacement for T-peel specimens was 20"/min.

94

At elevated and reduced temperatures, the lap shear strengths were determined in a Missimers environmental cabinet. The lap shear strength of a series of bonds was determined after 10, 11.5, 13.5, 15 and 16.5 minutes of exposure to the environment. This is important as it constitutes a post cure of the adhesive.

Durability Tests, Aluminum.
Durability of adhesive bonds made with the adhesives described in Section 2.a. (above) was evaluated by the 3M sustained load durability test as described by Pocius, et. al.[3] The samples used were "blister detection" specimens as described in Ref. 3. The bonds were placed into spring loaded fixtures with an applied stress of 25% or 10% of their ultimate strength when measured at 100°F (37.8°C). The fixtures are placed in a Blue M cabinet under conditions of 100°F and 95-100% RH. The fixtures were examined at least twice daily to determine the time to failure.

Durability Tests, Steel. The single lap shear specimens described in Section 2.c. were used and the method of test is described immediately above.

e. Dynamic Mechanical Analysis

Samples of mixed adhesive were placed between pieces of Teflon - FEP.® The samples were allowed to cure for seven days at ambient temperature. After 7 days, the sample was cut into three pieces. One of these pieces was postcured for one hour at 140°F (60°C) and the other for one hour at 180°F (82.2°C). The samples were then subjected to dynamic mechanical

analysis (DMA) using a DuPont 1090 Dynamic Mechanical Analyzer. The temperature scan rate was 5°C/min. Several samples of the room temperature cured adhesives were tested using various scan rates to be sure that the scan rate did not affect the results.

f. Electron Microscopy

Samples for electron microscopy were cut from T-peel specimens that were failed in order to determine peel performance (see Table 2). The samples were taken from T-peel specimens that were tested after 7 and 40 days ambient temperature cure. The sections of T-peel specimen were appropriately coated with conductive media and they were then analyzed using a JEOL Model 840 Scanning Electron Microscope used in the secondary electron emission mode. The JEOL Model 840 Microscope has a resolution of 100Å.

3. RESULTS

a. Lap Shear Performance

The lap shear performance of the various generations of adhesives is compared in Table 1. The most evident differentiation is the far superior performance in lap shear of the 2nd and 3rd generation two-part epoxies over that of the earlier generation systems. This superiority exists in the temperature range -67°F to 180°F. At 250°F, the 0th and 1st generation systems display better performance except in the case of 1XA-3559 B/A. 1XA-3559 B/A is a third generation adhesive formulated to give better high temperature lap shear strength. In comparing the 2nd and 3rd generation adhesives, the 2nd generation

adhesive displays a moderate superiority at room temperature and below. However, at elevated temperatures, the 3rd generation system displays a definite superiority. The differentiation is most marked with a comparison of EC-3569 B/A and CTBN/3569-A. Remembering that the amount of epoxy resin and the curative in these two adhesives is identical, this difference in performance at elevated temperature is surprising.

b. T-Peel Performance

The T-peel performance of the various generations of epoxy two-part adhesives is compared in Table 2. There is a substantial difference in performance between the 0th generation adhesive and the other adhesives. This is expected since the reason for the evolution of this type of product is the improvement of fracture resistance. The T-peel performance of the 2nd generation adhesive is surprisingly low (see discussion below). Very startling is the difference in performance as a function of bond aging at ambient conditions. It can be inferred from the literature that epoxies which cure at room temperature are incompletely cured after 7 days at room temperature.[4] There is also some suggestion that epoxies will "physically" age even when completely cured.[5] Usually more complete cure means a higher crosslink density in the epoxy matrix which usually means a more brittle material. "Physical" aging also usually leads to embrittlement of epoxies. The results in Table 2 clearly differentiate the generations of adhesive, in that the 0th and 1st generation seem

to become more brittle as they age while the 2nd and 3rd generation adhesives display constant or increasing peel performance. Particularly impressive is the doubling of peel performance of EC-3569 B/A and 1XA-3559 B/A and its comparison to the modest increase in peel strength for CTBN/3569-A in the same period of room temperature aging.

c. Durability Performance

Aluminum. The "control" strength, the ultimate shear at 100°F (37.8°C) of "blister detection" specimens made with the 4 generations of adhesives, is shown in Table 3. The shear strengths vary in much the same order as that seen in Table 1. The bonds were loaded at 25% and 10% of their "control" strength. The actual stress applied is also shown in Table 3. Also shown are the results of sustained load durability tests of adhesive bonds made with the 4 generations of adhesives. The 0th and 1st generation adhesives demonstrated bond failure at 25% of ultimate at very short times. Notwithstanding this result, these adhesives have been used successfully in the aerospace and other industries for over 20 years. The second generation adhesive displays improved performance in durability. This type of behavior has also been noted in the evolution of film adhesives and acrylic adhesives. Far greater improvement in durability performance in comparison to other 3 generations of adhesives is noted for the third generation adhesives. EC-3569 B/A displays 10 times better resistance to the aggressive environment than the 2nd generation adhesive. Once again, this is particularly surprising in light of the fact that

96

CTBN/3569-A and EC-3569 B/A differ only in the type of toughener and the toughener comprises only 15% of the final mixed adhesive for both systems. 1XA-3559 B/A gives extraordinary durability performance in that some specimens have been under load in high temperature, high humidity condition for over 3 years with no failures. This type of resistance to this aggressive environment was once thought only available from heat cured epoxy adhesives.

Steel. In the case of steel adherends, the durability data is presented in Table 4. Control strengths are shown in the last column of Table 4. The trends observed are similar to those discussed for aluminum and are also similar to those previously reported.[6] Thus, the third generation adhesive provides the best performance. Unfortunately, tests of this sort were not performed on the second generation adhesive. In terms of surface preparation, grit blasting provides the most durable joints followed by abrasion or a nitric/phosphoric acid etch. Solvent wiping generally leads to the poorest performance, although some results, particularly at the lower stress levels, appear to be as good as those obtained using abraded adherends.

d. Dynamic Mechanical Analysis

The result[5] of dynamic mechanical analysis of the cured monolithic adhesives as a function of cure are shown in Figures 1-5. The 0th generation adhesive shows two peaks in the loss spectrum, one at about -47°C and the other at about 48°C. The lower temperature peak is a β transition

which results from localized segmental motion in the polymer while the higher temperature peak is an α transition which results from major main chain motion in the polymer. The temperature of the α transition is also the glass transition temperature of the epoxy. All amine cured bisphenol-A based epoxy resins exhibit a β transition in the temperature range of -50°C. The α transition of EC-1838 B/A as a function of cure temperature varies in the expected manner as it increased slightly with more cure. EC-2216 B/A, Figure 2, shows a β transition at about the same temperature as the 0th generation adhesive. However, the α peak is at a much lower temperature, in fact below room temperature, attesting to the elastomeric character of this 1st generation adhesive. Surprisingly, there is very little effect of postcure.

The DMA results for the second generation adhesive are shown in Figure 3. The β transition has become very prominent for CTBN/3569 B/A in comparison to either the 0th or 1st generation adhesive. The increased loss is due to the fact that the adhesive has phase separated and the glass transition temperature of the rubber is at about -40°C. Thus the peak seen in this temperature range is a combination of the β transition of the epoxy and the α transition of the rubber. If the rubber was not phase separated, then the α temperatures of the epoxy would be lower than those seen for EC-1838 B/A and the β transition intensity would likely be the same as for the unmodified system. This is not seen, so the adhesive apparently displays a phase separated

character. The α transition peak as a function of postcure once again shows a modest increase in temperature, much as would be expected.

Figures 4 and 5 display the DMA results for the 3rd generation adhesives. Nominally, the look of the figures is much the same as that seen for the second generation adhesive shown in Figure 3. The height and position of the β peak at -40°C is similar to that seen for the 2nd generation adhesive indicating a phase separated system. The α transition peak as a function of postcure, displays a very curious effect in comparison to the other generations of adhesives. Where the other adhesives show modest increase in Tg as a function of postcure, the third generation adhesives give substantial, in excess of 20°C, increases in Tg with postcure at 180°F. Once again, these results are surprising in light of the chemical similarity between CTBN/3569-A and EC-3569 B/A. 1XA-3559 B/A, whose curative has been formulated for high temperature performance, gives a dramatic 34°C increase in Tg with a 180°F postcure.

e. Electron Microscopy

Electron micrographs of peel failure surfaces for the 4 generations of adhesives are shown in Figure 6. The electron micrographs clearly demonstrate the differences in the type and degree of deformation caused by propogation of a crack in the T-peel specimens. The micrograph for EC-1838 B/A shows a mostly brittle failure, the flat surfaces are believed to be the filler. The micrograph for EC-2216 B/A shows a somewhat greater degree of plastic deformation than EC-1838 B/A. The micrograph for the 2nd genera-

tion adhesive shows a massive amount of plastic deformation. The small bumps easily visible in the micrograph are likely the phase separated rubber particles. The micrographs for the third generation adhesives display massive amounts of plastic deformation and cavitation in the wake of the crack. The voids present in the failure surface are not due to entrapped air; all of the adhesives were completely deaerated in a vacuum oven before use. None of the other failure surfaces display the level of cavitation displayed by the third generation adhesives. This type of micrograph is very similar to the type observed for 2nd generation rubber toughened heat cured epoxy adhesives.[7]

4. DISCUSSION

The chemistry and physical properties of rubber modified structural adhesives have been reviewed by Pocius.[8] There are also many reviews of the chemistry which is utilized in second generation structural adhesives, i.e. the carboxy terminated butadiene-nitrile rubber[9] (Hycar CTBN-RLP® marketed by B. F. Goodrich). As discussed in the introduction, the mode of operation of the 2nd generation systems is the use of a rubber polymer which is prereacted with an epoxy, which is initially soluble in the epoxy resin but phase separates upon cure. Several authors have expressed concern about the effect of improper cure on the phase separation characteristics of 2nd generation systems.[10] To meet the concern, 3M has generated third generation adhesives in which the rubber is phase separated in the epoxy resin before cure.

The chemistry of third generation systems unites acrylic and epoxy technology. The key to the system is a unique amphiphilic molecule which has both acrylic and epoxy functionality. Acrylic monomers are chosen having appropriate solubility characteristics and elastomeric characteristics when they are polymerized by a method to which epoxy resins are not sensitive. Thus, the amphiphile is dissolved in an epoxy resin and then acrylic monomers and a free radical initiator are also dissolved into the epoxy resin. As the acrylic polymerization proceeds, the growing acrylic elastomer becomes insoluble in the epoxy resin. Normally, the acrylic polymer would catastrophically phase separate leading to a macroscopically phase separated system. However, the unique amphiphile used in the third generation adhesive base resin stabilizes the growing acrylic polymer as acrylic microdroplets suspended in the epoxy resin. The mechanism by which this occurs is known as "steric stabilization".[11]

The acrylic rubber, thus phase separated, is stable in suspension for periods in excess of five years. In addition, due to the bireactivity of the surfactant, the acrylic elastomer is chemically bound to the epoxy once the epoxy is cured. This chemical bond is known to be necessary to achieve toughness in a two phase rubber modified resin system.[12]

The performance advantages of the third generation system over the earlier generation systems are obvious in Tables 1 and 2. In addition to the excellent shear performance, the peel performance is exceptional for a system having high 180°F lap shear strength. Note, however, that all of the adhesives were exposed to the high temperature environment for periods of time in excess of 10 minutes. This does lead to some postcure of the adhesive, a fact seldom alluded to in data sheets on two-part adhesives.[13]

However, for the lap shear tests at elevated temperatures, the adhesive bonds were tested identically as discussed in Section 2.d., thus the comparisons are valid. The lap shear strengths at high temperatures should be correlated with the DMA results shown in Figures 1-5. The Tg of EC-1838 B/A is at about 50°C and its lap shear performance drops off after 60°C. The Tg of EC-2216 B/A is at about 21°C and its lap shear performance drops off after 35°C. The 2nd and 3rd generation systems, due to their curative system, offer higher Tg's and proportionally higher retention of shear strength at elevated temperature. The third generation adhesives, however, give substantially higher Tg's after postcure and this results in the much higher lap shear performance shown in Table 1. We believe that the effect is due to the much "cleaner" phase separation in the third generation system as exhibited in the micrographs in Figure 6. Less well phase separated particles, as are apparent in Figure 6c, leads to a lower Tg (due to retention of the CTBN-RLP® in solution) and hence lower high temperature lap shear performance.

The peel performance of the adhesive systems as displayed in Table 2, indicates the superiority of the 2nd and 3rd generation systems over earlier systems. In addition, even

though the peel strength of EC-3569 B/A and 1XA-3559 B/A is adequate for most aerospace applications after 7 days of room temperature cure, these adhesives display an increase in peel performance with time. Other data generated at 3M but not included here demonstrates that lap shear performance does not degrade as peel strength increases. The cause of the dramatic effect is not known, however, it could be due to more complete reaction of the amphiphile to the matrix as the resin continues to cure. The durability of adhesive bonds made with the newer 2nd and 3rd generation adhesives certainly exceeds that of the earlier systems. The third generation adhesives also show a marked improvement in bond durability over the second generation systems. Especially notable is the outstanding durability of bonds made with 1XA-3559 B/A. The reason for the exceptional durability of the 3rd generation adhesives is not known, but could be due to better wetting of the substrates by the adhesive since acrylic polymers are lower in surface energy than epoxies. It is possible that the combined system has a lower surface energy than the comparable second generation adhesive system. It is possible that the acrylic rubber sorbs less moisture than the nitrile rubber and this leads to a more durable bond. Moisture uptake experiments have not been performed to substantiate this proposition.

5. Summary

The geneology of 2 part epoxy adhesives was discussed and performance characteristics were compared. The results indicate that third generation two-part adhesives having a pre-phase separated acrylic elastomer provide improvements in performance, especially in durability, over previous generation adhesives.

7. References

1. N. C. Paul, D. H. Richards and D. Thompson., Polymer, 18, 945 (1977).

2. D. L. Trawinski, SAMPE Q, Oct. (1984), p. 1.

3. A. V. Pocius, D. A. Wangsness, C. J. Almer and A. G. McKown, in "Adhesive Chemistry - Developments and Trends", L-H. Lee, ed., Plenum Press, New York, 1984, pp. 617-642.

4. L. Shechter, J. Wynstra and R. P. Kurkjy, Ind. Eng. Chem., 48, 94 (1956).

5. E.S.W. Kong, G. L. Wilkes, J. E. McGrath, A. K. Banthia, Y. Mohajer, M. R. Taut, Polym. Eng., Sci., 21, 943 (1981).

6. W. Brockman, in "Durability of Structural Adhesive", A. J. Kinloch, ed., Applied Science Publishers, New York, 1983, pp. 281-316.

7. J. L. Bitner, J. L. Rushford, W. S. Rose, D. L. Hunston, C. K. Riew, J. Adhesion, 13, 3 (1981).

8. A. V. Pocius, Rubber Chem. Tech. 58, 622 (1985).

9. C. K. Riew, E. H. Rowe and A. R. Siebert, in "Advances in Chemistry Series", no. 154, R. D. Deanin and A. M. Crugnola, eds., American Chemical Society, Washington, D. C. (1976), pp. 326-343.

10. a. L. T. Manzione, J. K. Gillham, C. A. McPherson, Org. Coat. Plast. Chem., 41, 371 (1979).

    b. L. C. Chan, J. K. Gillham, A. J. Kinloch, S. J. Shaw, in "Advances in Chemistry Series", no. 208, C. K. Riew and J. K. Gillham, eds., American Chemical Society, Washington, D. C. 1984.

11. D. H. Napper, in "Colloidal Dispersons", J. W. Goodwin, ed., Special Publication of the Royal Society of Chemistry, Dorchester, Dorset, UK (1982), pp. 99-128.

12. F. J. McGarry and A. M. Willner, Am. Chem. Soc., Div. Org. Coat Plast. Chem. Pap., 28, 5112 (1968).

13. F. J. Keimel, Adhesives and Sealants Newsletter, August 13, 1984, p. 3.

TABLE 1

COMPARISON OF LAP SHEAR PERFORMANCE OF THE "GENERATIONS" OF ADHESIVES
(psi, values in parenthesis are in MPa)

Adhesive "Generation"	0th	1st	2nd	3rd	3rd
Adhesive Designation	EC-1838 B/A	EC-2216 B/A	CTBN/3569-A	EC-3569 B/A	1XA-3559 B/A
Temperature of Test					
-67°F	2254 + 135 (15.5 ± 0.9)	2442 + 136 (16.8 ± 0.9)	5530 + 723 (38.1 ± 5)	4598 + 796 31.7 ± 5.5	4603 + 736 (31.8 ± 5)
75°F	3085 + 169 (21.3 ± 1.2)	3304 + 199 (22.8 ± 1.4)	4915 + 276 (33.9 ± 1.9)	4597 + 155 (31.7 ± 1.1)	4809 + 144 (33.2 ± 1)
120°F	3562 + 96 (24.6 ± 0.7)	1645 + 159 (11.3 ± 1.1)	3365 + 223 (23.2 ± 1.5)	3591 + 197 (24.8 ± 1.4)	3285 + 187 (22.7 ± 1.3)
160°F	1781 + 51 (12.3 ± 0.4)	1084 + 88 (7.48 ± 0.6)	1886 + 215 (13 ± 1.5)	2632 + 376 (18.2 ± 2.6)	1817 + 366 (12.5 ± 2.5)
180°F	1353 + 74 (9.3 ± 0.5)	947 + 52 (6.53 ± 0.4)	1461 + 124 (10.1 ± 0.9)	2270 + 481 (15.7 ± 3.3)	1529 + 374 (10.5 ± 2.6)
250°F	738 + 62 (509 ± 0.43)	698 + 47 (4.81 ± 0.32)	358 + 89 (247 ± 0.61)	420 + 44 2.9 ± 0.3)	1113 + 86 (7.68 ± 0.59)

(Average of 5 specimens, 4 mil thick bondlines)

TABLE 2

COMPARISON OF ROOM TEMPERATURE T-PEEL PERFORMANCE OF
THE "GENERATIONS" OF ADHESIVES AS A FUNCTION OF
DAYS OF CURE

(pounds/inch width)

Adhesive "Generation"	0th	1st	2nd	3rd	3rd
Adhesive Designation	EC-1838B/A	EC-2216B/A	CTBN/ 3569-A	EC-3569B/A	1XA-3559B/A
Days of RT Cure					
7	3.5	20.5	14.2	24.7	21.8
40	3.6	11.8	13.7	31	27.3
90	3.0	10	17.7	45.8	36.7

(Average of 3 specimens)

(Bondlines were   8 mil thick except in the case of EC-2216 B/A
where the bondline was 20 mil thick)

TABLE 3

DURABILITY OF ADHESIVE BONDS MADE WITH THE FOUR
GENERATIONS OF ADHESIVES*. CONDITIONS ARE SUSTAINED LOAD AT 100°F/95-100% RH
(all metal is surface prepared by the optimized FPL etch method)

Adhesive	Metal	Control Strength (psi)**	Actual Applied Load (psi)	% of Ultimate Shear Strength	Results (Days to Failure)
EC-1838 B/A	2024-T3 Bare	2767 ± 44	852	25	0.007, 0.01, 0.014, 0.125 (Avg.=0.04)
EC-1838 B/A	2024-T3 Bare	2767 ± 44	276	10	55, 2 Not Failed at 66 Days
EC-2216 B/A	2024-T3 Bare	1975 ± 127	494	25	0.01, 0.007, 0.014, 0.017 (Avg.=0.012)
EC-2216 B/A	2024-T3 Bare	1975 ± 127	197	10	0.67, 1.71, 3.71 (Avg. = 2.03)
CTBN/3569-A	2024-T3 Bare	3766 ± 97	942	25	9, 1.9, 2.54, 0.92 (Avg. = 2.03)
CTBN/3569-A	2024-T3 Bare	3766 ± 97	377	10	69, 56, 39, (Avg. = 55)
EC-3569 B/A	2024-T3 Bare	3648 ± 68	912	25	24.5, 20.5, 27, 27.5 (Avg. = 24.9)
EC-3569 B/A	2024-T3 Bare	3648 ± 68	365	10	3 Not Failed at 66 Days
1XA-3559 B/A	2024-T3 Bare	3407 ± 234	852	25	4 Not Failed at 79 Days
1XA-3559 B/A	2024-T3 Bare	3407 ± 234	341	10	3 Not Failed at 66 Days
1XA-3559 B/A	5052/6061	3280 ± 98	800	24	4 Not Failed at 1160 Days
1XA-3559 B/A	2024-T3 Clad	3290 ± 68	800	24	4 Not Failed at 1160 Days
1XA-3559 B/A	2024-T3 Clad	3318	800	24	4 Not Failed at 984 Days

*As of 5/1/87
**Measured at 100°F without preapplication of humidity or stress

104

TABLE 4

SUSTAINED LOAD DURABILITY RESULTS FOR 1010 COLD-ROLLED STEEL LAP SHEAR SPECIMENS

Adhesive	Surface Prep.	Time to Failure (days)			Control Strength (psi)
		800 psi	400 psi	200 psi	
EC-2216 B/A	MEK wipe	1	1	1	486
	Abrade	1	1	1	581
	Prime	1	1	1	1671
	Grit blast	1	1	1	803
	Etch	1	1	1	793
EC-1838 B/A	MEK Wipe	1	1	60	2026
	Abrade	1	18	27	2833
	Prime	1	27	60+	3127
	Grit blast	1	20	60+	2567
	Etch	1	1	21	2540
1XA-3569 B/A	MEK wipe	1	49	56+	3073
	Abrade	21	40	42+	2867
	Prime	27	50	56+	2933
	Grit blast	32	57	56+	2940
	Etch	30	38	39+	2973

Exposure, 38°C/100% RH; control strength measured at 38°C; applied loads are shown at the tops of the Time to Failure columns.

D42:2

Dynamic Mechanical Analysis
as a Function of Cure
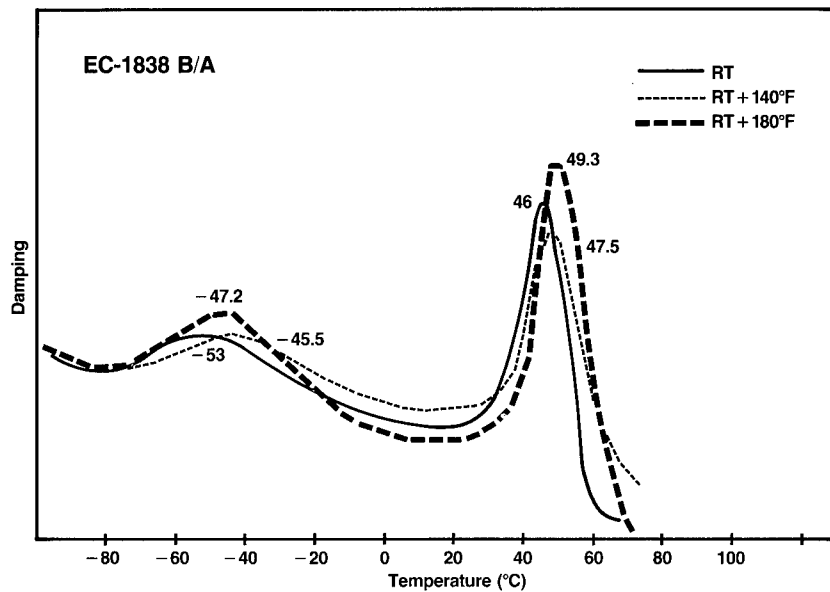
Figure 1

Dynamic Mechanical Analysis
as a Function of Cure

Figure 2

106

Dynamic Mechanical Analysis
as a Function of Cure

CTBN Epoxy/3569-A

RT
RT + 140°F
RT + 180°F

–44.5°C

–44.0°C
–44.5°C

56.0°C
63.5°C
64.0°C

Damping

Temperature (°C)
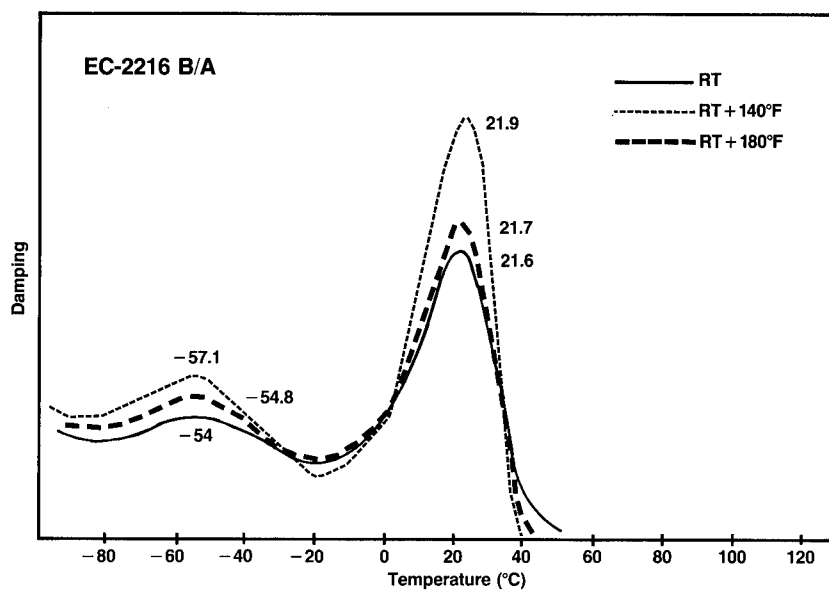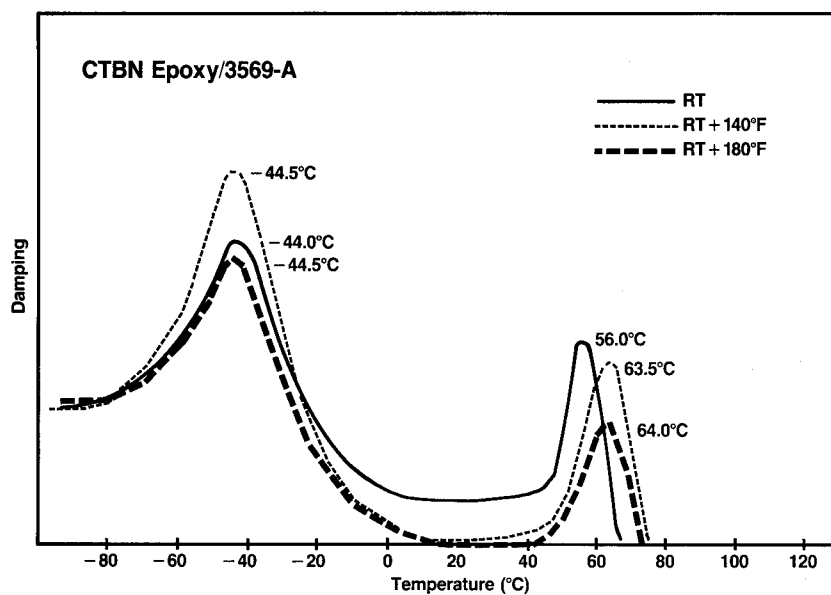
Figure 3

Dynamic Mechanical Analysis
as a Function of Cure

RT
RT + 140°F
RT + 180°F

EC-3569 B/A

–48.2
–48

–49.1

60
74.3
81.9

Damping

Temperature (°C)
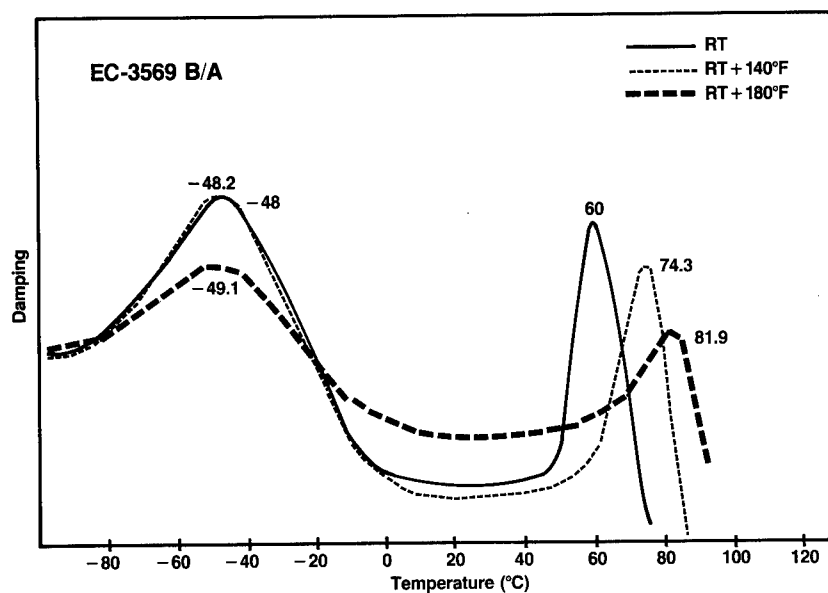
Figure 4

Dynamic Mechanical Analysis
as a Function of Cure
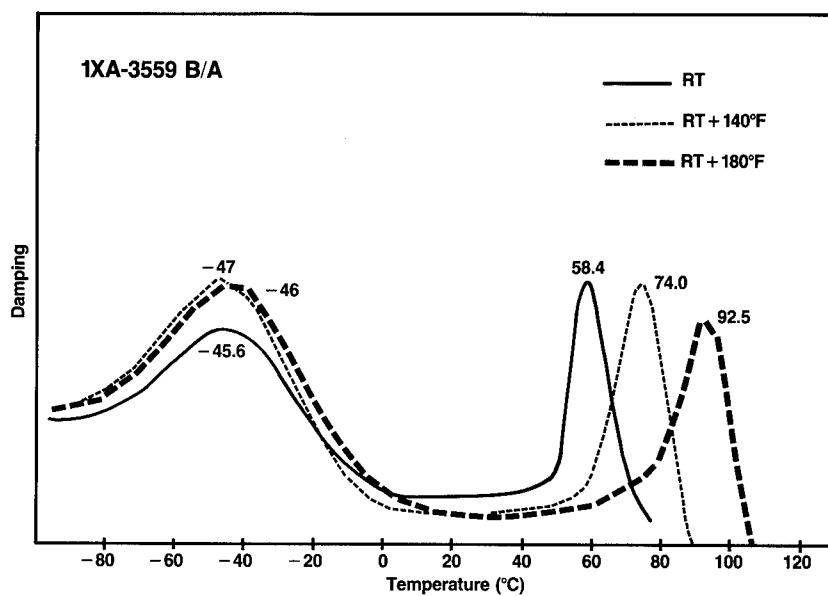
Figure 5

Figure 6

Electron Micrographs of T-Peel Failure
Surfaces
3000x Magnification
Bonds Pulled 40 Days After Bonding
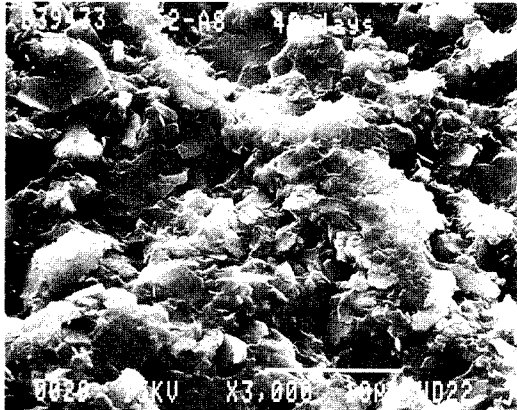
a. "0th" Generation
EC-1838 B/A
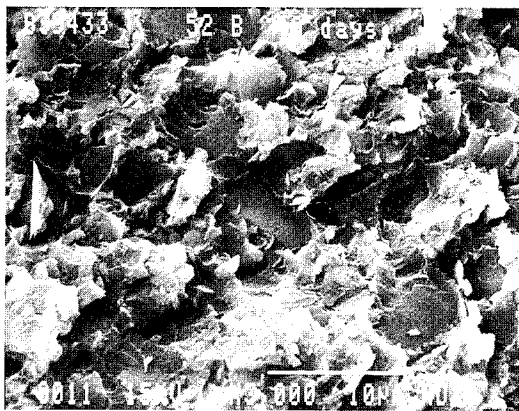
b. "1st" Generation
EC-2216 B/A
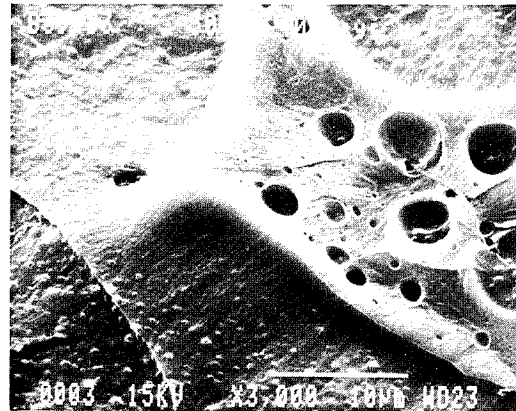
c. "2nd" Generation
CTBN/3569-A
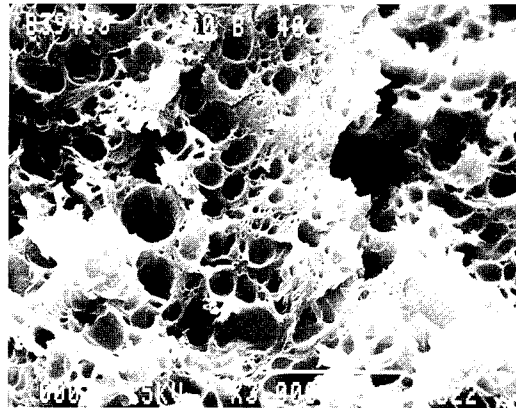
d. "3rd" Generation
EC-3569 B/A
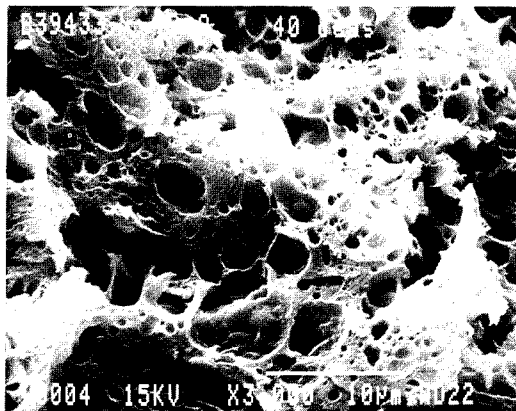
e. "3rd" Generation
1XA-3559 B/A

INHERENT WEAKNESSES OF STRUCTURAL ADHESIVES

By M.R. Piggott

Department of Chemical Engineering
and Applied Chemistry
University of Toronto, Toronto, Ontario, M5S 1A4
Canada

ABSTRACT

An examination of the basic processes leading to the failure of the bond between relatively high Young's modulus load bearing materials and the much lower elastic modulus materials used as matrices in fibre composites, e.g. tire cord in rubber, glass and carbon fibres an epoxy resins suggests that debonding is a brittle fracture process. Using an energy approach that successfully describes these debonding processes, two types of structural adhesive joint are examined. It is shown that for short bond lengths they can behave as if the adhesive has a yield stress, even though the process is a brittle fracture one. For longer bond lengths, failure is governed by (bond length)$^{1/2}$. The bond appears to behave in a way analogous to a Griffith crack. Thus, although it is important for the adhesive to be as tough as possible, further improvements in bond strength might be possible if the elastic modulus of the adhesive could be increased.

1. INTRODUCTION

Great advances have been made in developing structural adhesives which are useful for bonding metals and high performance composites. However, the factors important in developing a good bond are still imperfectly understood[1]. In the case of tire cord adhesion to rubber, it is thought that debonding can be considered to be a brittle fracture process. The debonding work, G_i, in this case is identified as the work of peeling the rubber from tire cord material: fibre pull out experiments and peeling experiments gave about the same values of G_i[2].

Work on fibres in plastics appear to be leading to a similar conclusion. Debonding processes are investigated by the same type of fibre pull out experiment as used for tire cord and rubber. Early work suggested that an approximately constant shear stress, τ_i, governed the debonding stage of pull out. Thus the debonding force, F_A, was thought to be at least roughly proportional to embedded length, L, i.e.

$$F_A = \pi dL\tau_i \qquad (1)$$

where d is the fibre diameter. This expression was found to fit very well results with fibres pulled out of metal matrices[3], and was used to explain the results from experiments with components of reinforced plastics by Favre and co-workers[4]. Chua and Piggott found that they needed to modify equation 1 by the addition of a constant term to the right hand side, for small values of L, and that for large values of L, F_A was independent of L[5]. However, this involved two distinct modes of failure and was unnecessarily complicated. Instead, a single curve

$$F_A = \pi d \sqrt{G_i n E_f L} \qquad (2)$$

was shown to fit the results somewhat better[6]. Fig. 1 compares these two interpretations, for the same set of results, i.e. glass fibres pulled out of cylindrical bars of polyester resin. It can be seen that the monotonically increasing curve (equation 2) is more in keeping with the trend in the results for L greater than about 1.2 mm. In addition, more recent results fit equation 2 much better than equation 1[7]. Results obtained with carbon fibres by Favre et al could also be fitted using equation 2, as also could results obtained with carbon fibres by Piggott et al [8]. In equation 2 E_f is the Young's modulus of the fibres, and n is a constant approximately equal to $0.327 \sqrt{E_m/E_f}$ for the dimensions of fibre and polymer cylinder used in the experiment (E_m is the Young's modulus of the polymer).
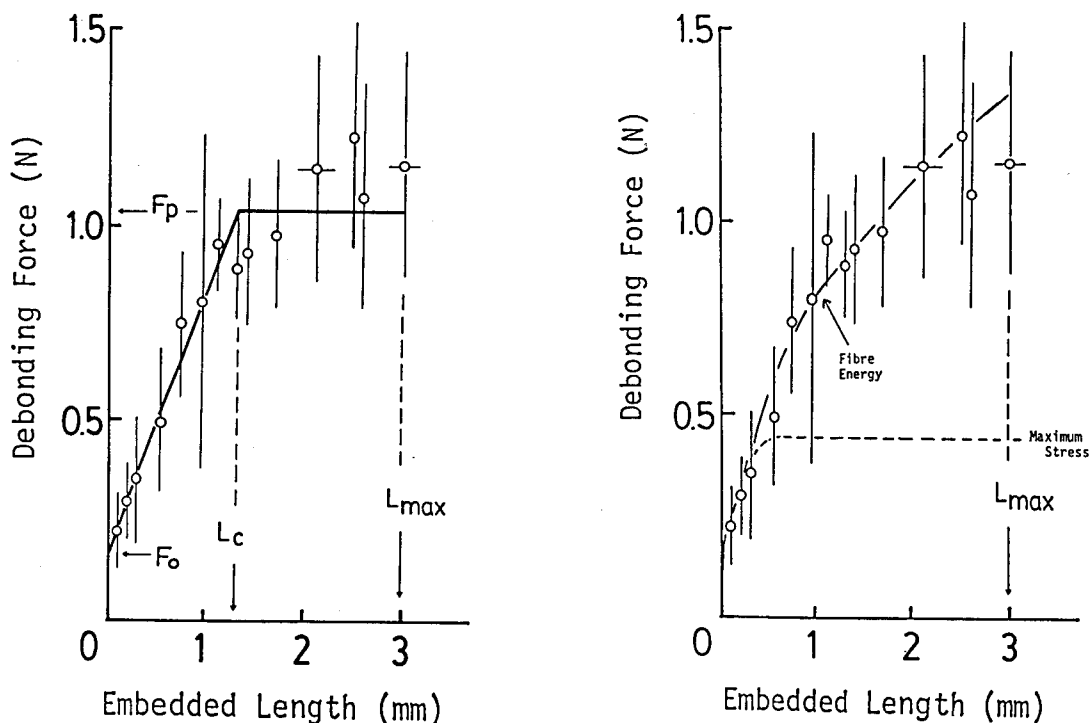
Fig. 1.   Two mode failure (left) compared with simple brittle failure in debonding of glass fibres from polyester resins[8]

111

Recently it was shown that for small values of nL/d, equation 2 should be written[9]

$$F_A = \pi d \sqrt{E_f G_i d/2} \sqrt{n s \tanh(n s)} \qquad (3)$$

where $s = 2L/d$. For $ns > 3$ equation 3 reduces to equation 2, but for $ns < 0.3$ equation 3 reduces to

$$F_A \cong \pi d L n \sqrt{2 E_f G_i/d} \qquad (4)$$

so that F_A is a linear function of L. Experiments in which steel rods were pulled out of epoxy resins gave results which agreed with equation 3, i.e. giving a linear region near the origin, and an $L^{1/2}$ variation for larger L[10].

The linear region near the origin can be misinterpreted. Comparing equation 4 with equation 1 we see that we now have a spurious shear stress, $\tau_i = \tau_s$, where

$$\tau_s \cong 0.327 \sqrt{2 E_m G_i/d} \qquad (5)$$

(n has been replaced by $0.327 \sqrt{E_m/E_f}$ in equation 5).

Thus, great care is needed in the interpretation of the results of pull out experiments. If short embedded lengths only are investigated, an erroneous interpretation of results is possible, i.e. that some sort of yielding is taking place, rather than fracture. For example, with the "microdebond" test[11] in which a small blob of resin is cured on a
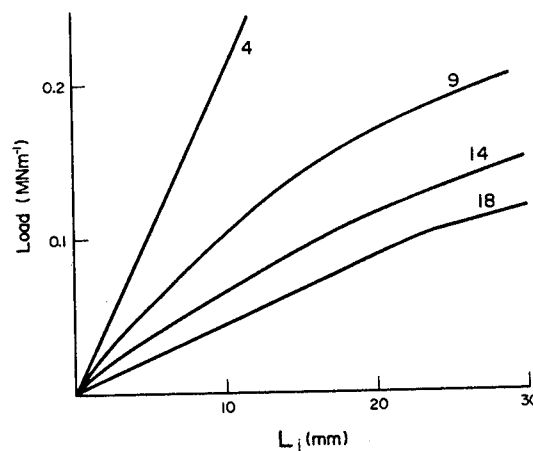
Fig. 2.   Failure load per ply unit width of joint as a function of lap length for glued double-lapped glass-polymer/aluminum joints. The figures on the curves indicate the number of layers in the laminates[11].

fibre, and then debonded by shear, the results appear to fit equation
1. However, with Kevlar, higher values of L could be used without the
fibre breaking, and a curved F_A vs L plot was obtained for the higher
L values. This could be fitted to equation 3 reasonably well, with
plausible values of the constants[9].

In this paper, the approximate energy analysis will be extended to the
case of flat adhesive joints. These joints can exhibit non-linear
behaviour. Figure 2[12] shows some results obtained with lap joints in
which the load bearing capacity is not always a linear function of
the joint length.

2. ENERGETICS OF FAILURE OF AN ADHESIVE JOINT

A joint made with a structural adhesive involves stress concentrations,
in just the same way as a single embedded fibre does. The stresses
involved have been well investigated, especially by finite element
methods, and some mitigation of the stress concentrating effect is
possible by rounding off the glue profiles at the ends of the joints[13].
The stress concentrating effect of the joint coupled with the sudden
changes of elastic modulus at the adherend-adhesive interface make
the joint analogous to a Griffith crack[14]. We will first consider what
is probably the simplest case, shown in fig. 3, where a sheet of material,
thickness d, and width b is glued to a solid block of material whose
elastic deformation may be neglected. The glue line has thickness t,
the bond length is L, and we consider the stresses and strains as a
function of distance x along the bond line.

If the stress in the sheet is σ_p, and the adhesive has a shear stress
τ_a, then for equilibrium between the force in the sheet and the surface
shear, we have

$$d\sigma_p/dx = \tau_a/d \qquad\qquad (6)$$
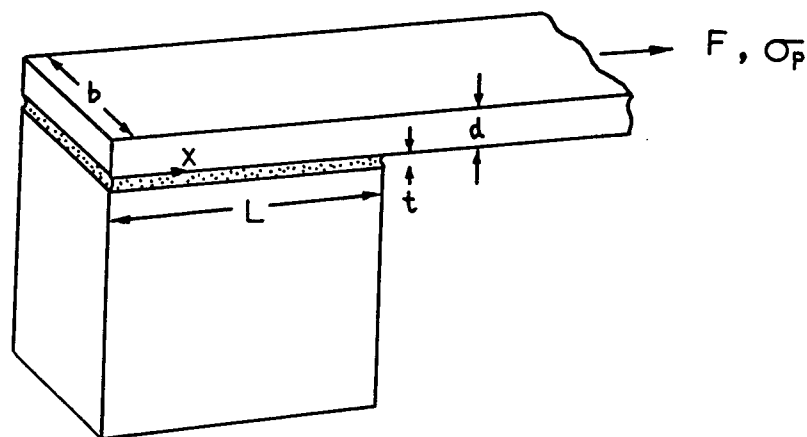
Fig. 3.   Joint between sheet and rigid block.

and τ_a can be determined from the displacement of the sheet, u, since the shear strain in the adhesive is u/t. Thus,

$$u/t = \tau_a/G_a \tag{7}$$

Similarly, the tensile strain in the sheet is $e_p = du/dx$. Thus

$$du/dx = \sigma_p/E_p \tag{8}$$

Differentiating equation 8 with respect to x, and using equations 6 and 7 gives

$$d^2\sigma_p/dx^2 = m^2\sigma_p \tag{9}$$

where

$$m = \sqrt{G_a/dtE_p} \tag{10}$$

The solution to equation 9, for $\sigma_p = 0$ at $x = 0$ and $\sigma_p = \sigma_{pe}$ at $x = L$ is

$$\sigma_p = \sigma_{pe} \sinh\{mx\}/\sinh\{mL\} \tag{11}$$

To estimate the energy in the system, first consider the energy U_p in the plate

$$U_p = (bd/2E_p) \int_0^L \sigma^2_p dx \tag{12}$$

which on substitution for σ_p from equation 11 gives, on integration

$$U_p = (bd\sigma_{pe}^2/4mE_p)(\coth\{mL\} - mL/\sinh^2\{mL\}) \tag{13}$$

In the adhesive, the energy U_a is

$$U_a = (bt/G_a) \int_0^L \tau^2_a dx \tag{14}$$

114

From equations 6 and the differential with respect to x of equation 11, we have

$$\tau_a = md\sigma_{pe}\cosh\{mx\}/\sinh\{mL\} \tag{15}$$

Substituting this into equation 14 and integrating gives

$$U_a = (bd\sigma_{pe}^2/4mE_p)(\coth\{mL\}+mL/\sinh^2\{mL\}) \tag{16}$$

so that the total energy, $U_T = U_p+U_a$ is

$$U_T = bd\sigma_{pe}^2\coth\{mL\}/2mE_p \tag{17}$$

For failure, with work of fracture G_i

$$U_T = bLG_i \tag{18}$$

and finally using equation 17 we have, for the force F_A for failure by brittle fracture

$$F_A = b\sqrt{2dE_pG_i}\ \sqrt{mL\tanh mL} \tag{19}$$

Equations 19 and 3 differ only by virtue of the different geometries.

The lap joint between two sheets with different Young's moduli E_{p1} and E_{p2}, and thickness d_1 and d_2 is equivalent to two joints of the type shown in figure 3. So, instead of equation 17, we have

$$U_T = b(d_1\sigma_{p1e}^2\coth\{m_1L\}/2m_1E_{p1}+d_2\sigma_{p2e}^2\coth\{m_2L\}/2m_2E_{p2}) \tag{20}$$

where

$$m_1 = \sqrt{2G_a/td_1E_{p1}} \tag{21}$$

$$m_2 = \sqrt{2G_a/td_2E_{p2}} \tag{22}$$

115

and the force F_A is given by the stresses σ_{p1e} and σ_{p2e} in the sheets

$$F_A = bd_1\sigma_{p1e} = bd_2\sigma_{p2e} \qquad (23)$$

In this case, failure occurs when $U_T = bLG_i$ as before, so that the failure force, F_A is given by

$$F_A = b\sqrt{2LG_i/(\coth\{m_1L\}/d_1m_1E_{p1}+\coth\{m_2L\}/d_2m_2E_{p2}} \qquad (24)$$

For sheets having the same thickness d and Young's modulus E_p this reduces to

$$F_A = b\sqrt{m_1E_pG_i}\sqrt{m_1L\tanh\{m_1L\}} \qquad (25)$$

with

$$m_1 = m\sqrt{2} \qquad (26)$$

3. DISCUSSION

This approximate treatment indicates that the failure of lap joints and other forms of adhesive joints may be governed by the same equations as debonding in fibre composites. In particular, for short bond lengths (small L, so that $mL < 0.3$) a pseudo shear strength τ_s may govern failure. This is because equation 19 reduces to

$$F_A \cong bmL\sqrt{2dE_pG_i} \qquad (27)$$

so that

$$\tau_s = \sqrt{2G_aG_i/t} \qquad (28)$$

For long bond lengths, $(mL > 3)$ by contrast

$$F_A = b(2G_iL)^{1/2}(dG_aE_p/t)^{1/4} \qquad (29)$$

Equation 28 can give quite high values for the pseudo shear stress. For example, for G_a = 1 GPA, typical of an epoxy, and for G_i = 200 Jm^{-2} (obtained in pull out experiments with steel[10] in epoxy) a glue line 0.1 mm thick gives τ_s = 63 MPa. Fig. 4 shows the theoretical F_A vs L plot for this system with E_p = 211 GPa (steel) and d = 1 mm. If the steel had a strength of 1 GPa, the steel strip would fail, rather than the bond, for L > 55 mm. The linear part of the curve ends at L = 2 to 3 mm.

Fig. 5 shows the predicted failure force for a steel-aluminum lap joint. Again, the glue line is 0.1 mm and the metal pieces are 1 mm thick and 10 mm wide. For an aluminum alloy having a strength of 500 MPa, failure would occur at about L = 52 mm. The curve, plotted using equations 20-22, has an almost identical shape to that shown in fig. 4, although the force transmitted for a given bond length is about one half that for the steel bonded to a rigid block. The inset has an expanded scale for L, and shows that the linear region extends to about 4 mm of joint. This linear part indicates a pseudo shear stress of about 41 MPa.
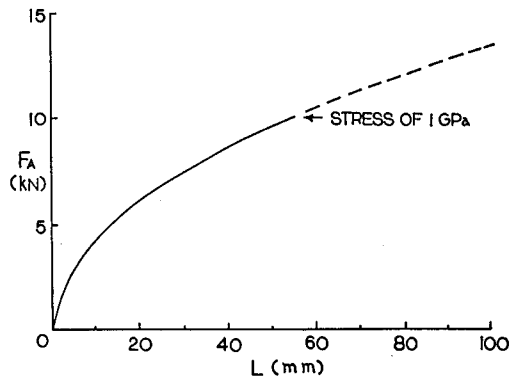
Fig. 4. Failure load vs joint length for steel sheet bonded to rigid block. Steel is 10 mm wide, 1 mm thick. Adhesive 0.1 mm thick.
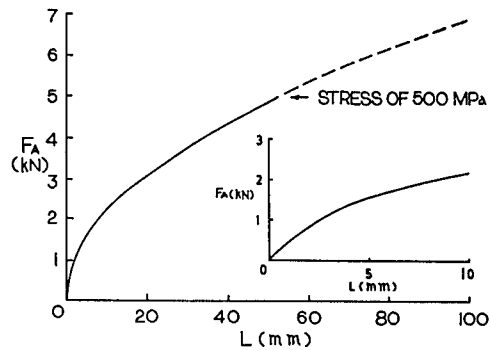
Fig. 5. Failure load vs joint length for a lap joint between steel and aluminum. Both strips 10 mm wide and 1 mm thick. Adhesive is 0.1 mm thick.

This type of joint failure corresponds well with the type of failure observed when relatively thick laminates are joined (see fig. 2) and agrees well with work on debonding of tire cord from rubber[2] (these workers observed non-linear F_A vs L plots) and work with glass and carbon debonded from polyester and epoxy[8]. Agreement is particularly good with steel rod debonded from epoxy[10]. The only difference between these cord, fibre, and rod studies, and a lap joint appears to be the different geometry. The governing equations are, apart from the geometrical factors, substantially the same.

The reason for this type of failure appears to be that, in joints using structural adhesives, there is a large difference in moduli between the materials being joined and the structural adhesive; typically 100 to 1 so that the discontinuity is akin to a Griffith crack. Thus an adhesive joint seems to be inherently weak.

Two approaches to the problem seem likely to be fruitful. The obvious one of making the adhesive tougher is being pursued with vigour. However, since the glue line is generally quite thin, the efficacy of this approach is limited[15]. The other, i.e. increasing the Young's modulus of the adhesive to close to that of the adherends, will not be easy with polymer adhesives and metal or composite adherends. However, it should be noted that joints between metals using solders and other metallic brazing materials can be extremely strong, and appear to fail by yielding rather than brittle fracture.

CONCLUSION

A joint made with a structural adhesive (i.e. a polymer) appears to be inherently weak because of the large difference in Young's modulus between the adhesive and adherend. The joint can thus behave in a way analogous to a Griffith crack, and the joint strength for moderately long and very long joints can be proportional to (joint length)$^{1/2}$ rather than directly proportional to joint length. Once the possibilities of tougher adhesives have been exhausted, it would be worth examining the effect on joint behaviour of increasing the elastic modulus of the adhesive.

ACKNOWLEDGEMENTS

REFERENCES

1. A.N. Gent, Plastics and Rubber International 6, (1981), 151.

2. A.N. Gent, G.S. Fielding-Russell, D. Livingston and D.W. Nicholson, J. Mater Sci., 16, (1981), 949.

3. A. Kelly, Strong Solids, (Clarendon, Press, Oxford, 1973), p. 203.

4. J.P. Favre and J. Perrin, J. Mater Sci., 7, (1972), 1113.

5. P.S. Chua and M.R. Piggott, Comp. Sci. Tech. 22, (1985), 107.

6. M.R. Piggott and P.S. Chua, Ind. Eng. Chem.-Product R/D, 26, (1986), 672.

7. P.S. Chua, Ph.D. thesis, University of Toronto, 1985.

8. M.R. Piggott, A. Sanadi, P.S. Chua and D. Andison, Proc. 1st Int. Conf. on the Comp. Interface (1986), 227.

9. M.R. Piggott, Accepted by Comp. Sci. & Tech. (August 1987), paper no. 1.

10. M.R. Piggott and S.R. Dai, Accepted by Comp. Sci. & Tech. (August 1987), paper no. 2.

11. B. Miller, P. Muri and L. Rebenfield, Comp. Sci. & Tech. $\underline{28}$, (1987), 17.

12. G.C. Grimes & L.F. Greimann, Composite Materials: $\underline{8}$, Structural Design and Analysis (Ed. Chamis C.C. Academic Press, 1974), p. 135.

13. P. Czarnocki and K. Piekarski, Int. J. Adh. & Adhvs, $\underline{6}$, (1986), 93.

14. A.A. Griffith, Phil. Trans. Roy Soc. $\underline{A221}$, (1970), 180.

15. M.R. Piggott, Submitted to J. Mater Sci., (1987).

ELASTOPLASTIC FRACTURE BEHAVIOR OF STRUCTURAL ADHESIVES UNDER MONOTONIC AND DYNAMIC LOADING

Erol Sancaktar
Associate Professor

Clarkson University
Mechanical and Industrial
Engineering Department
Potsdam, New York 13676 U.S.A

ABSTRACT

Elastoplastic fracture behavior of a rubber toughened solid film epoxy adhesive with and without carrier cloth (Metlbond 1113 and 1113-2) is studied using bulk and bonded specimens. The bulk specimens are tested under monotonic loading using single-edge-crack specimen geometry. The Independently Loaded Mixed Mode Specimen (ILMMS) geometry is used for mixed mode testing in the bonded form. The ILMMS geometry allows simultaneous but physically separate application of cleavage and shear loads.

The availability of K_{IC}, σ_y (yield stress), E and v (Poisson's ratio) values in the bulk mode makes the calculation of crack tip plastic zone radii (r_{yc}) and fracture energy (G_{IC}) values possible on the basis of Irwin's theory.

In the bonded form, the relationship between the bondline thickness and the crack tip plastic zone radius values calculated earlier is studied. Expressions developed on the basis of LEFM assumptions are utilized to calculate G_{IC} and G_{IIC} values in the bonded form. The G_{IC} values obtained in this manner are compared to the bulk G_{IC} values obtained earlier.

With the availability of P_I and P_{IC} (G_I and G_{IC}) values that result in failure in the bonded form, the fracture condition (i.e the fracture failure criterion) in mixed mode (modes I and II) loading is determined for adhesively bonded joints.

For cyclic loading, the first phase of the investigation involves determination of the threshold levels for crack propagation under cyclic mode I and static mode II loads. Experimental results reveal that the threshold cyclic load levels in mode I are reduced when the level of mode II static loads is increased.

Crack propagation rates (da/dN) are measured as a function of total strain energy release rate (G_{Tmax}) during the second phase. Functional relationship is established between (da/dN), (G_{Tmax}) and (ΔG).

Key Words: Elastoplastic Adhesive Fracture; Energy Balance Criterion; Principal Stress Criterion; Mixed Mode Adhesive Fracture; Plastic Deformation Zone, Cyclic Threshold Load, Crack Growth Law

A. ADHESIVE BEHAVIOR UNDER MONOTONIC LOADING

INTRODUCTION

Adhesively bonded joint failures are usually results of catastrophic crack propagations (brittle fracture) originating from inherent flaws (voids or trapped air bubbles) and impurities [1]. These flaws are mainly formed in the bulk of the adhesive material during the curing process if ideal bonding and surface preparation of adherends prevail. Hence, a complete characterization of adhesives requires investigation of flaw-related material properties as well as bulk tensile properties

as functions of cure and other service parameters. Since inherent flaws usually cause structural adhesives to fail in a brittle manner, the use of an LEFM (Linear Elastic Fracture Mechanics) method can be considered appropriate for characterizing their fracture behavior.

This paper presents data using model thermosetting adhesives Metlbond 1113 and 1113-2 which are commercially available from Narmco Materials, Inc. (Costa Mesa California) in 0.25 mm and 0.13 mm (respectively) thick solid film rolls. Metlbond 1113 is a 100% solids, modified nitrile epoxy film with a synthetic carrier cloth. Metlbond 1113-2 is the same adhesive without the carrier cloth.

Brinson et al. [2] determined that the mechanical behavior of bulk Metlbond 1113 and 1113-2 adhesives is affected by the rate of straining. They showed that the constant strain rate stress-strain behavior of the adhesives approaches a perfectly elastic-plastic behavior as the magnitude of strain rate is increased. This mechanical behavior was described with the use of modified Bingham visco-elastic-plastic model.

Since the stresses at a crack tip reach high values upon loading, yielding occurs in a zone called the "crack tip plastic zone." If this zone is small compared to crack length, it will not greatly disturb the elastic stress field around it. Consequently, the extent of the plastic zone can be defined by the elastic stresses. Apparently, the use of elastic-plastic material assumption in stress analysis problems greatly facilitates the solution.

The elastic-plastic material behavior assumption has been widely used for adhesive materials by a number of investigators such as Bascom [3] and Hart-Smith [4]. Bascom used a crack tip plane-strain assumption to relate the adhesive tensile yield stress, elastic mod-

ulus and the crack tip plastic zone radius to the fracture energy (G_{IC}). He calculated the plastic zone radius (r_{yc}) by using experimentally measured values of G_{IC}, σ_y and E [3].

In order to be able to interpret the bulk data to design bonded joints, however, on needs to understand the constraint mechanisms imposed on the adhesive material in the bonded form. Bascom [3] reports that the maximum fracture energy for an adhesive in the bonded form was obtained when the bond thickness was approximately equal to the plastic zone diameter $(2r_{yc})$. His investigations also revealed that this maximum G_{IC} value was equal to that obtained with the bulk form of the adhesive.

In adhesively bonded joints crack propagation is constrained within the adhesive layer regardless of the loading orientation. Because of this condition one needs to consider mixed mode fracture. The majority of practical adhesive applications involve only G_I and G_{II} due to the peel and in-plane-shear stresses that arise in the use of lap joint geometries. In such geometries, adhesive cracks are exposed to both tension and shear resulting in mixed mode cracking.

The Independently Loaded Mixed Mode Specimen (ILMMS) geometry is used during the current investigation for mixed mode testing of adhesives in the bonded form. This geometry was originally proposed by Ripling et al. [5]. It allows combined or independent application of cleavage and shear loads. Monotonic loading of the specimens with different P_I to P_{II} ratios enables us to determine the failure criterion for fracture of adhesively bonded specimens.

In order to determine the fracture toughness (K_{IC}) of bulk adhesives, the

single-edge-cracked specimen geometry shown in Figure 1 was chosen. The pertinent dimensions of plate specimens for K_{IC} testing are the crack length, thickness and the ligament (uncracked) length. According to ASTM standards [6] for a K_{IC} test to be valid, these dimensions should exceed a certain multiple of the quantity $(K_{IC}/\sigma_y)^2$. This quantity has been shown [6] to be directly proportional to the crack tip plastic zone radius. Based on the elastic-plastic material assumption, the LEFM solutions are valid beyond the plastically deformed zone around the crack tip, if the size of this zone is small.

ANALYTICAL CONSIDERATIONS

Irwin [7] showed that for an isotropic material in the bulk form and crack tip plane strain conditions the stress intensity factor can be expressed as

$$K_I = (G_I E / 1-v^2)^{1/2} \qquad (1)$$

where v is the Poisson's ratio.

For ductile materials the crack propagation process involves mainly plastic energy due to crack tip plastic deformation. Furthermore the mathematical formulation of the stress field based on perfectly elastic material behavior suffers from singularity at the crack tip. In order to resolve this problem, Irwin assumed elastic-plastic material behavior and stated that the failure stress at the crack tip is equal to the uniaxial yield stress acting over a region called the plastic zone. Beyond this zone the elastic stress distribution remains undisturbed. Irwin [7] calculated the size (diameter) of the plastic deformation zone by considering an infinite plate containing a single crack under the action of tensile in-plane loading perpendicular to the crack. The

diameter of the plastic (deformation) zone was thus shown to be

$$r_p = K^2_{IC}/\sigma_y^2 \pi \quad . \qquad (2)$$

Based on equations 2 and 1, the "corrected" critical strain energy release rate could then be written as

$$G_{IC} = \pi \sigma_y^2 r_p (1-v^2)/E . \qquad (3)$$

Irwin showed that the plane-strain elastic constraint will increase the tensile yield stress for plastic yielding and thus affect the size of the plastic zone. Such an increase in the yield strength was estimated to be by a factor of $\sim(3)^{1/2}$ [7]. The critical radius of crack tip deformation zone can, therefore, be written as

$$2r_{yc} = (1/\pi)(K_{IC}/\sqrt{3}\,\sigma_y)^2 \qquad (4)$$

for plane-strain conditions. Substitution into equation 1 results in

$$G_{IC} = 6\pi\sigma_y^2 r_{yc} (1-v^2)/E. \qquad (5)$$

For an elastic cracked structure subjected to some mode I load (P_I), the rate of strain energy release (G_I) has been related to the material and geometrical properties and applied load [8] with the equation

$$G_I = (P_I^2/2b)(\partial c/\partial a) \qquad (6)$$

where b = material thickness in the vicinity of crack; $\partial c/\partial a$ = change in compliance (c) with crack length (a).

The load level at which spontaneous crack growth occurs is called the critical

load (P_c) and the corresponding energy release rate is called the fracture energy (G_C). In order to utilize equation 6 one needs to determine the variation of compliance (ratio of displacement to the applied load) for different crack lengths of a given specimen geometry.

Determination of Fracture Energy in Bonded and Bulk Samples

A. Bonded Samples

There are three basic specimen geometries for mixed mode testing of adhesives in the bonded form. They are cracked lap-shear [9], scarf joint [10] and the Independently Loaded Mixed Mode Specimen (ILMMS) geometries. Among these, the only specimen geometry which allows independent measurement of P_I and P_{II} (and consequently G_I and G_{II}) is the ILMMS. The other two require finite element analysis to calculate G_I and G_{II} values from a load applied in only one direction. In order to avoid any inaccuracies which may be involved in the calculation of G_I and G_{II} values with the use of a finite element program and due to its practicality in load measurement, the ILMMS geometry is used during the current investigation. In order to test different P_I to P_{II} ratios, a hydraulic actuator force is applied statically in mode II and the specimen is loaded monotonically in mode I until failure. Subsequently, the static force is applied in mode I while the specimen is loaded monotonically in mode II until failure.

Examination of the literature and our experience show that the strain energy values are affected by the thickness of the adherend and the bondline. For this reason it is necessary first to determine ex-

perimentally, the adhesive and adherend thickness values that result in plane strain conditions. The following methods are used for this purpose:

As mentioned earlier, Bascom [3] reports that the maximum fracture energy for an adhesive in the bonded form is obtained when the bond thickness is approximately equal to the plastic zone diameter ($2r_{yc}$). His investigations also reveal that this maxium G_{IC} value is equal to that obtained with the bulk form of the adhesive.

Limited information is available in the literature regarding the effects of adherend thickness (b) (or crack front length) on G_{IC}. It is known that the stress condition at the crack tip of an adhesive bond varies from one of plane stress for short crack fronts (thin bonds) and at the edges of thicker bonds to one of plane strain near the center of thick bonds. We believe that the increased constraint present in plane strain conditions results in a smaller zone of plastic deformation. This indicates that as the adherend thickness increases, thereby increasing constraint on material deformation, then the fracture energy will decrease.

The advantage in using the ILMM specimens is the option of not having to calculate G_I or G_{II} values in order to determine the fracture criterion. The availability of separate P_I and P_{II} values is sufficient to obtain such criterion. However, calculation of G_I and G_{II} values is helpful in accounting for geometrical effects (when different geometries are used) and for comparison purposes.

Our experiments showed that P_{IIC} is a (linear) function of the bond length (L) and therefore necessary terms must be included in any G_{IIC} relation to render this material constant independent of

123

geometrical effects. For this purpose the following simplified approach is used: If we assume that the axial load varies linearly along the overlap direction [11] then the total elastic energy (W_T) stored in the adhesive and the adherends can be written as

$$W_T = \int_0^L \int_0^h \int_0^b (P_{II}^2/Eh^2b^2)(1-y/L)^2 \, dxdydz + nbL \, (\tau_{avg}^2/G_A) \qquad (7)$$

where G_A = elastic shear modulus for the adhesive, n = adhesive thickness, and τ_{avg} = P_{II}/Lb = average shear stress in the adhesive layer. Solution of equation 7 with the assumption

$$G_{II} = W_T/2Lb \qquad (8)$$

yields

$$G_{II} = (P_{II}^2/2b^2)(1/3hE + n/2L^2G_A) . \qquad (9)$$

Note that equation 9 accommodates the linear increase of P_{II} with L.

A widely accepted relation for G_1 in (bonded) double cantilever beam specimens is

$$G_{IC} = 4P_{IC}^2(3(a+a_0)^2 + h^2)/b^2h^3E . \qquad (10)$$

Experimentation shows that in addition to bending and shear deflections, there exists additional deflection due to rotation at the assumed "built in" end of the beam. It is assumed that this rotation can be treated as an increase in crack length and hence it is accounted for with the use of the empirical rotation factor a_0 in equation 10. The value of a_0, however, must be

determined experimentally when the geometrical parameters are varied. This is accomplished by means of experimental compliance calibration.

B. Bulk Samples

For the single-edge-crack geometry used for bulk samples Gross et al. [12] applied a boundary collocation procedure to the William's stress function to determine the elastic stress distribution at the tip of an edge crack in a finite-width specimen subjected to uniform tensile loading. The K-calibration for the single-edge-crack geometry is given by

$$K_{IC}bw/P_C a^{1/2} = 1.99 - 0.41(a/w) + 18.7(a/w)^2 - 38.48(a/w)^3 + 53.85(a/w)^4 \qquad (11)$$

where w is the specimen width. Examination of literature [6] reveals that in single-edge-crack samples plane strain condition is ensured when the minimum values for specimen thickness (b) and crack length (a) are given by:

$$a,b \geq 2.5(K_{IC}/\sigma_y)^2 . \qquad (12)$$

Determination of Failure Criterion

With the application of the famous energy balance criterion we get:

$$K_I^2 + K_{II}^2 = \text{constant} \qquad (13)$$

where the locus of failure is a quarter circle. However, previous experimentation by other researchers (primarily on metals) showed that an elliptical condition is more realistic i.e.

$$(P_I/P_{IC})^2 + (P_{II}/P_{IIC})^2 = 1 . \qquad (14)$$

124

A second criterion that must be considered involves the possibility of failure in mode I under the action of a principal stress even though a biaxial state of stress is applied globally. It should be noted that the mode I in such cases will be at an angle to the applied P_I load, with this angle being determined by the applied P_I to P_{II} ratio. Obviously such an inclined crack will have to connect with similar ones or simply continue propagating in the P_{II} direction (possibly close to or at the interface) to result in catastrophic failure. The likelihood of this type of failure is high especially for brittle adhesives.

We propose the following simplified approach to describe this type of failure: If one takes a biaxial stress element well ahead of the crack tip where the stresses are defined and uniform, then the elementary theory defines the principal stress as:

$$(\sigma/2) + [(\sigma^2/4)+\tau^2]^{1/2} = \text{constant} \qquad (15)$$

Assuming that loads and stresses are linearly related, substitution into equation 15 yields:

$$CAP_I + B^2 P_{II}^2 = C^2 . \qquad (16)$$

Note that equation 16 describes a parabolic failure condition while equation 14 described an elliptical one. Obviously equation 16 should contain at least an additional P_I^2 term resulting from the contribution of shear loading to the opening direction. However, this contribution is neglected, as it is assumed to be small.

It should also be noted that equation 16 can be rewritten in terms of the stress intensity factors as:

$$(K_I/K_{IC}) + (K_{II}/K_{IIC})^2 = 1 \qquad (17)$$

EXPERIMENTAL PROCEDURES

Details on sample preparation and testing of bulk specimens should be obtained from reference [13].

Bonded Samples

The original dimensions and geometry proposed by Ripling and Mostovoy were altered substantially on the basis of our experimental stress analysis through the use of reflection and transmission photoelasticity in order to minimize any interference between the two modes (i.e., cleavage loads resulting from shear loads, etc.) and to reduce the effects of stress discontinuities. This new geometry allows the use of a small hydraulic actuator inside the specimen. The geometries developed are shown in Figures 2 and 3. Since the width of the actuator used is larger than its height, it was necessary to develop two different specimen geometries with geometry A (Figure 2) being used for static loading in mode II and geometry B used for static loading in mode I. Examination of Figures 2 and 3 reveals the presence of frictional resistance affecting the loads applied orthogonal to the static loads. These frictional loads were measured experimentally and subtracted from the applied (monotonic) loads. Even though the frictional resistance existed only in the sliding mode during all our experiments, the validity of the subtraction procedure based on static equilibrium was checked with the use of rolling friction. For this purpose steel pins were placed in between the actuator face and the specimen. In both sliding and rolling friction cases the same G_I to G_{II} ratios were obtained.

Bonding of steel samples was done on the basis of the procedure supplied by the Narmco Corporation.

RESULTS AND DISCUSSIONS

A. Bulk Samples

As mentioned earlier, information on the size of the crack tip plastic zone radius makes it possible to relate the bulk properties to fracture properties in the form of fracture toughness and fracture energy. Such a relation is possible on the basis of "small scale" yielding assumption [10] and equations 5 and 1. Figures 4 and 5 show the effects of cure conditions on the plastic zone radius of Metlbond 1113 and 1113-2, respectively. Examination of these figures reveals that r_{yc} values corresponding to optimum K_{IC}'s for the fast or slow cool-down conditions are relatively constant. Therefore, it seems possible that one can use some average r_{yc} values (based on optimum K_{IC}'s) to represent the typical plastic zone radii sizes for either material subjected to the fast or slow cool-down conditions. Using this concept, it can be seen in Figure 5 that the average plastic zone radius for Metlbond 1113-2 with the slow cool-down condition is higher than that for the fast cool-down condition. As expected, this implies that the slow cool-down condition results in tougher adhesive matrix material as the availability of a larger plastic zone size at the crack tip enables relieving of higher stress levels at that location thus resulting in higher crack growth resistance. It is not possible to offer a similar argument for the adhesive with the carrier cloth as the values obtained with slow and fast cool-down conditions are about the same (Fig. 4). This result, however, is also expected since it is already known that the effect of cool-down conditions on Metlbond 1113 fracture toughness is minimal as attributed to the presence of the carrier cloth [13].

The availability of these r_{yc} values along with previously measured σ_y and E data made the calculations of G_{IC} values possible based on equation 5. These calculated values could also be compared with the G_{IC} values which were obtained on the basis of measured K_{IC} values and equation 1. In calculating fracture energies the value of Poisson's ratio (v) was assumed to be the constant value of 0.374 for both materials [2]. Figures 6 and 7 show the effects of cure conditions on the fracture energy of Metlbond 1113-2 and 1113, respectively. Comparison of Figures 6 and 7 confirms that: i) With the fast cool-down condition Metlbond 1113 yields higher G_{IC} values than Metlbond 1113-2; ii) With the slow cool-down condition the optimum G_{IC} values are significantly higher using Metlbond 1113-2 as compared with Metlbond 1113; iii) Cure temperature and time do not seem to have a significant effect on fracture energy for either material.

B. Bonded Samples

Experimental results indicate that for the adhesive without the carrier cloth the G_{IC} values are maximum when the adherend thickness (b) is equal to 6.35 mm. A plane strain condition is attained when b = 1.27 cm (Figure 8). For the adhesive with the carrier cloth (1113) the G_{IC} value is maximum when b = 3.18 mm and the plane strain condition is attained when b = 9.53 mm (Figure 9). For both adhesives b = 1.27 cm is used for plane strain condition. It should be noted that the maximum G_{IC} values obtained with 1113-2 and 1113 adhesives are close to the G_{IC} values previously measured by us [13] using bulk edge-cracked compact tension specimens and the values measured

by O'Conner [14] using bonded Tapered Double Cantilever Beam (TDCB) specimens.

As mentioned earlier, Bascom [3] reports that the G_{IC} values in the bonded form are maximum and equal to bulk G_{IC} values when the bond thicknesses (n) are equal to $2r_{yc}$. Our experimental results showed further confirmation of this assertion. For 1113-2 samples with b = 6.35 mm and b = 1.27 cm adherend thicknesses, G_{IC} is maximized and remains constant when the plane strain condition is attained slightly above n = 0.508 mm value (Figures 10,11). The adhesive thickness corresponding to the onset of plane strain condition is close to the $2r_{yc}$ value calculated by us based on our previous bulk fracture tests [13] (Figure 5). For the adhesive with the carrier cloth the plane strain condition is achieved slightly above n = 0.254 mm. This value is very close to our previously calculated $2r_{yc}$ value for the 1113 adhesive [13] (Figure 4). These results also reveal the stabilizing effect of the carrier cloth on G_{IC} values.

In order to be able to use equation 10 in determining G_{IC} values, it is necessary to evaluate first the rotation factor a_o experimentally. This is done by means of compliance calibration: The specimen compliance (c) is defined as

$$c = \partial/P \qquad (18)$$

where ∂ = crack opening displacement and P = applied opening load. Apparently, if δ vs. P values are determined for different crack lengths then the compliance equation

$$C = (2/3EI)[(a+a_O)^3 + h^2a] \qquad (19)$$

can be fitted to this data by using the appropriate a_o value. Figure 12 shows such

compliance calibration curves for different adherend thicknesses of specimen geometry A bonded with 0.635 mm thick Metlbond 1113-2 adhesive. Obviously, for geometry A with 6.35 mm <b ≤ 12.7 mm, the correction factor a_o is (0.7)h where h is the beam height. Other rotation factor (a_o) values were obtained by means of compliance calibration for different adherend thicknesses, adhesive thicknesses, specimen geometries (A or B) and adhesive types (with or without carrier cloth) as shown below:

1) For the adhesive without the carrier cloth (1113-2):

i) For geometry A with 6.35 mm ≤ b ≤ 12.7 mm (adherend thickness) and 0.178 mm ≤ n ≤ 0.635 mm (adhesive thickness): a_o = (0.7)h.

ii) Same as in 1-i except n = 1.27 mm: a_o = (0.85)h.

iii) For geometry B with 6.35 mm ≤ b ≤ 12.7 mm with n = 0.635 mm: a_o = (0.6)h.

2) For the adhesive with the carrier cloth (1113):

i) For geometry A with b = 6.35 mm and n = 0.63 mm: a_o (0.6)h.

ii) Same as in 2-i except b = 12.7 mm: a_o = (0.8)h.

iii) For geometry B with b = 12.7 mm and n = 0.635 mm: a_o = (0.8)h.

It should be noted that some of the a_o values reported above may be in error by as much as 25% due to experimental

difficulties and functional dependence of a_o on crack length.

Another geometrical consideration in fracture energy calculations involves the effect of bondline length on G_{II} values. Our experiments with double cantilever beams revealed that the mode II breaking force (P_{IIC}) increases with increasing bond length. This behavior was observed with two different beam thicknesses (b = 6.35 mm and 12.7 mm) and appeared to be a linear function between the P_{IIC} and the bond length (L) (Figure 13).

Failure criteria data and curves showing P_I vs P_{II} for 1113-2 and 1113 adhesives are depicted in Figures 14 thru 16. Results obtained using geometry A (monotonic in opening, static in shear) and B (monotonic in shear and static in opening) are combined in these figures. Since the two geometries have different crack lengths (5.08 cm for geometry A and 15.24 cm for geometry B), opening mode loads for geometry B were normalized with respect to those obtained with geometry A. This was done with the application of the G_I relation (equation 10). The data shown in Figures 14 and 15 were obtained with the adhesive without the carrier cloth using specimens with 6.35 mm and 12.7 mm thick adherends respectively. The data for the adhesive with the carrier cloth is shown in Figure 16 for the adherend thickness of 12.7 mm. Included in these figures are also correlation coefficients to indicate the goodness of fit for elliptical (equation 14) and parabolic (equation 16) functions based on energy balance and principal stress criteria respectively.

Examination of Figures 14 thru 16 reveal two important points common to all of them:

1) The presence of viscoelastic effects are observed in the application of the static load. In other words relaxation processes take place prior to failure. These effects are especially severe when the static load is applied in mode I. The presence of delayed failure in mode I at high loads is an indication of this behavior. It is therefore assumed that some relaxation takes place at the crack tip, rendering the actual static loads somewhat less than shown. This is why the data obtained using geometry B lays above those obtained using geometry A when the P_{II} values are the same in magnitude (note that their mode of application is different). The use of data from both geometries A and B in determining the failure criteria is thought to have some averaging effect on this behavior.

2) The parabolic (principal stress) criterion defined by equation 16 consistently provides better fit to the experimental data in comparison to the elliptical criterion given by equation 14.

The G_I vs. G_{II} behavior for the Metlbond 1113-2 adhesives is shown in Figure 17.

B. ADHESIVE BEHAVIOR UNDER CYCLIC LOADING

This phase of the investigation is concerned with the mixed mode fracture behavior of the same model adhesive under combined dynamic (cyclic) and static loads. The cyclic load fluctuates sinusoidally in time. The objectives of the study include obtaining the governing crack growth model for the Metlbond adhesive under cyclic opening and static shear loads using Independently Loaded Mixed Mode (ILMM) specimen geometry (Figure 2). The thresholds for stable and catastrophic crack propagations are determined and compared with the failure conditions of monotonically loaded fracture specimens.

ANALYTICAL CONSIDERATIONS

The general form of energy conservation principle can be expressed as

$$dF/da = d(U + W + D)/da \qquad (20)$$

where a is the crack length per unit crack width, F is the work done by external forces, U is the elastic strain energy, W is the energy needed to create the fracture surfaces, and D is the energy dissipated through heat generation, sound etc.

In a cyclic test, the inherent viscoelastic nature of the model adhesive becomes more effective on its fracture behavior due to the long duration of load application. During a lengthy cyclic test, heat dissipation due to the viscoelastic nature of the adhesive and creep deformation caused by the mean level of the sinusoidally fluctuating load become non-negligible factors. Consequently, the D term of equation 20 representing the irreversible work output is no longer negligible, unlike a fast fracture experiment performed under monotonic loading. Also, due to the viscoelastic effects cited, formation of micro cracks, voids (pores) and stretched fibrils is facilitated. Therefore, void coalescence and fibril rupture becomes more likely at lower loads in comparison to the fracture testing of the adhesive under fast monotonic loading.

In cyclic load dominated mixed mode fracture tests, K_I and K_{II} values increase as the crack propagates in a stable fashion. Consequently, the maximum principal stress failure theory (equation 17) is expected to be valid at the onset of catastrophic crack propagation when K_I and K_{II} approach K_{IC} and K_{IIC} values respectively. However, it should also be noted that the use of K_{II} and K_{IIC} values obtained from monotonic experiments in equation 17 is not expected to give accurate prediction of failure in a cyclic experiment. This is because both material properties and crack tip geometries may change due to the heat generation and plastic deformation processes described earlier. Furthermore, the crazing, microcracking and cavitation mechanisms which occur during plastic deformation of the material are thought to be more effective as the stress amplitude and its duration of application are increased. These mechanisms are believed to lower the fatigue resistance of the material. Therefore, catastrophic crack propagations proceeding from stable crack growth are expected to be much more random in comparison to the catastrophic crack propagations induced by monotonic loading of a starter crack.

The energy balance failure criterion is also not expected to be accurate in the form it was applied for the monotonic case due to the existence of the "D" term in equation 20.

Because of the reasons mentioned above, empirical formulas are usually adopted to fit the data obtained in cyclic dominant fracture tests and used as the governing model for crack propagation prediction.

In the cyclic load dominant fracture tests, although the loading level is relatively low compared to the loading level applied for catastrophic crack propagation in monotonic load dominant fracture, stresses around crack tip are still beyond the yield stress of adhesive in the whole cycle or in the part of cycle because of the singularity, so that crack propagation can still occur. Intuitively, it is easy to understand that the crack growth rate depends on P_{Imax} P_{Imin}, and P_{II} since it is induced by displacements (i.e. C.O.D). Therefore, in terms of elastic energies, the crack growth rate should depend on the

parameters such as: strain energy release rate range $\Delta G = G_{max} - G_{min}$, total strain energy release rate G_{Tmax}, crack length a, material properties, specimen geometry as well as environmental effects such as temperature T, etc..

Among these parameters, the strain energy release rate range ΔG due to the dynamic part of the loading plays the most important role in fatigue crack propagation, again, because it is proportional to the C.O.D.

Typically, for mode I loading, when we plot fatigue crack growth rate (da/dN) vs. strain energy release rate range ΔG on log-log paper, we obtain a multimodal curve with three different crack growth rate regions. The first region is identified by a threshold strain energy release rate range for non-propagation cracks. The second region is expected to be governed by a power law relationship between crack growth rate and strain energy release rate. The third region begins with the threshold for catastrophic crack propagation.

In this study, the threshold at which the crack starts growing is called the onset threshold. The threshold where the catastrophic failure occurs is called the catastrophic threshold.

For adhesively bonded joints, a widely used crack growth model for the second region described above is given by:

$$da/dN = c(\Delta G)^n. \qquad (21)$$

This relation, however, does not include any G_{II} term, and hence, is not expected to correlate mixed-mode crack propagation data efficiently even though the terms "c" and "n" can be expressed as functions of G_{II}.

A more efficient way to describe mixed-mode crack propagation data is to make (da/dN) an explicit function of G_{Tmax} and ΔG as given by [8]

$$da/dN = c\,G_{Tmax}^m(\Delta G)^n \qquad (22)$$

Note that the environmental effects are neglected in both equations 21 and 22.

As mentioned earlier, when a cracked component is loaded, a plastic deformation zone develops around the crack tip. When the crack is unloaded, the plastically deformed part keeps its size but the elastically deformed part tends to resume to its original size and position, so that a compressive stress is exerted on the plastic zone. From stretch to compression there must be a load level at which the stress on the plastic zone is zero. This load level is called the crack closure load (P_{cc}) level. In the load range of 0 to P_{cc}, no crack propagation is expected since the crack is kept closed.

Based on the mechanism of crack closure explained above, it follows that when the cyclic load is applied in the range of $0 - P_{cc}$, crack tip will not open and crack propagation will not occur. This verifies the existence of threshold in the first region theoretically. However, due to global geometrical effects threshold value in practice is usually higher than the one calculated according to the mechanism of crack closure.

EXPERIMENTAL CONSIDERATIONS

Fatigue Testing   All the cyclic load dominant mixed-mode fracture tests were performed on an Instron 1331 servo-hydraulic testing machine. The static shear load was applied in mode II direction through a piston, and the cyclic load was applied in mode I direction using sine wave load control with 10 Hz frequency and a load ratio with $R = (P_{max}/P_{min}) = 10$.

Each level of the static shear load was coupled by a number of cyclic opening loads in mode I direction. Five static load levels (0-17800 N) were applied in the

mode II direction. For each static load level, the onset threshold strain energy release rate range value G_{th} was determined first. In the present work, the G_{th} value was defined in such a way that the specimen should fail in one million cycles under the lowest P_{Imax} level. If the specimen did not fail in one million cycles, the P_{Imax} level was increased by 4450 N at a time until the onset threshold was reached. After the onset threshold was found, the P_{Imax} was increased by 4450 N at a time until the specimen failed in a very short time. This procedure was repeated for five different static load levels for both Metlbond 1113-2 and Metlbond 1113 adhesives.

The Dynamic Measurement of Rolling Friction Force

It was found that if a piston was directly inserted in the specimen to apply the static shear load as was in the case of montonic load dominant fracture, the fatigue life of the specimen did not correspond to the applied cyclic opening load even when the sliding friction force was deleted from the cyclic opening load. This is because the direct contact between the piston and the specimen surfaces increased the stiffness of the system considerably. To overcome this difficulty, a pin was placed to roll on two blades with lubricant Teflon to reduce the rolling friction force between the surfaces of the piston and the specimen.

The procedure for measuring the rolling friction force can be described as follows: (1) For no shear load, apply a certain level of cyclic load P_{Imax} and record the corresponding C.O.D amplitude. (2) After applying a certain level of static shear load P_{II}, the amplitude of C.O.D decreased due to the increase of rolling friction force. (3) Increase the cyclic

opening load to P'_{Imax} until the amplitude of C.O.D returns to its original level. (4) The rolling friction force P_f can now be calculated as $P_f = P'_{Imax} - P_{Imax}$.

The Measurement of Crack Closure Load By C.O.D. Method

In the present study, a simple C.O.D method based on the hysteresis curve of P_I vs. C.O.D was used to measure the crack closure load.

The measured results revealed that the crack closure load is relatively small compared to the P_I applied. This is attributed to the plane strain conditions of the specimen resulting in small plastic deformation zone and also to the absence of the necessary adhesive ductility to result in large closure loads.

RESULTS AND DISCUSSION

The Saw Teeth Phenomenon on the Fracture Surface

In the cyclic load dominant mixed mode fracture tests, the main crack in the adhesive bond was found to usually propagate near an adhesive/adherend interface. It was also found that many small cracks branched from the main crack and approached to the same interface with similar angles, resulting in the "saw teeth" appearance of the fracture surfaces. One hypothetical explanation of the saw tooth phenomenon is offered below:

An investigation by Wang (15) shows that the stress field very close to the crack tip in the Double Cantilever Beam (D.C.B) type adhesively bonded specimens is similar to that in monolithic specimens. So, with the understanding that the analysis is not very accurate due to the constraint imposed by the rigid adherends, the results obtained for monolithic specimens are introduced here. If a monolithic plate containing a central crack is loaded in combined mode I and mode

II, the relation between the angle θm corresponding to the maximum principal stress direction and the ratio of the stress intensity factors K_I and K_{II} in modes I and II can be plotted as shown in Figure 18a (8). It should be noted that the θm = -70.53° value calculated theoretically for the condition $K_I = 0$ varies by 26% from the

θm = -56° value determined experimentally using monolithic plates. Shown in Figure 18a are also our experimental data for mixed mode fracture (solid points 1 through 7) which reveal a variation from 0° to ~37° in the direction of crack propagation as the magnitude of P_{II} (K_{II}) is increased. Note that what is shown in Figure 18a is only theoretical prediction based on monolithic plate theory, but it has been confirmed qualitatively by visual observations on post fracture surfaces of bonded samples. As shown in Figure 18b, for bonded specimens under mixed mode loading, the crack should start propagating at an angle $θ_m'$ approximately equal to what is predicted in Figure 18a. The crack branch 1-2 shown is created in this fashion. But as soon as the crack gets to the inteface at point 2, it has to change the propagation direction due to the constraint of the adherend. Now, we assume that point 3 is weaker compared to point 2 due to stress concentration. Consequently, a new crack will initiate at point 3 and propagate towards point 4 in a direction $θ_m''$ close to $θ_m$ forming the saw tooth described by points 2-3-4. After the crack gets to point 4 on the interface, it might propagate along the interface for a while and then go back to the adhesive bond at point 5 due to defects such as flaws or voids inside the bond. The similar procedure will repeat at point 5 as occurred at point 1, so another saw tooth will be formed. Based

on the illustration in Figure 18b, we have main crack along route 1-3-4-5-7 and branched cracks 3-2 and 7-6. The branched cracks have angles close to the corresponding $θ_m$. Under different combinations of P_I and P_{II} or different ratios of K_I and K_{II}, the branch cracks will have different angles $θ_m$'s as shown in Figure 2a. The possibility of crack branching is cited here due to our consistent observations of crack tip crazing, cavitation, and microcracking mechanisms which occur in bulk samples. Furthermore, the presence of voids and flaws in adhesive bonds is a well documented phenomenon.

Fatigue Fracture Behavior   In order to determine the effect of static shear load on the cyclic dominant mixed-mode fracture, five different static shear load levels were applied to the ILMM specimens. Each level of static shear load was coupled with a number of cyclic opening load levels. A computer program subroutine "ZXSSQ" form the software package IMSL available in UNIX system at Clarkson University was used to determine the coefficients in equations 21 and 22 by fitting the experimental data. ZXSSQ is a finite difference, Levenberg-Marquardt routine for solving nonlinear least square problems.

Since the first model (equation 21) does not contain the strain energy release rate G_{II} due to the static shear load P_{II}, it should be fitted with the steady state (da/dN) vs. ΔG values corresponding to a variety of P_I's for each P_{II} level. Therefore, it governs crack growth rate (da/dN) vs.ΔG for one level of P_{II} coupled with different P_I levels. On the other hand, the second model (equation 22) contains one more parameter $G_{Tmax} = G_{Imax} + G_{II}$ which involves the strain energy re-

lease rates due to P_{Imax} and P_{II}. Hence, it can be fitted to all (da/dN) vs. G_{Tmax} and ΔG values corresponding to different P_I's for all five P_{II} levels. Consequently, it governs the crack growth rate under different P_{Imax} and P_{II} combinations.

Obviously, the first model requires five different values for the parameters c and n to describe the crack growth rates for five different P_{II} levels coupled with a variety of P_I's. The second model, however, requires only one set of the parameters c, m and n to describe all the data and therefore, may be considered more efficient for data fitting and representation purposes. Obviously, since the sums of square of errors for the two models are expected to be different, efficiency in data representation is not necessarily expected to provide accuracy also.

It was found that for most specimens steady state crack propagation prevailed under 7.52 cm crack length and catastrophic failures occurred when crack propagated to or beyond this length. So, 7.62 cm crack length was taken as threshold level for catastrophic crack propagation.

The material parameters "c" and "n" of equation 21 for the model adhesive with (Metlbond 1113) and without (Metlbond 1113-2) a carrier cloth are shown in Table 1. The parameters "c", "m" and "n" for the second model (i.e. equation 6) are 4.77 x 10^{-5}, 1.2533, and 3.6812 respectively for Metlbond 1113-2 and 3.65 x 10^{-5}, 0.77173, and 3.19886 for Metlbond 1113 if the G values are substitued in English units (i.e. in-lb/in^2). For 1113-2, the first model provides a better fit since the average error with the first model ($\sim$2.32 x 10^{-2}) is about half of that for the second model. For 1113, however, the average error is about the same for the first and

second models (2.48 x 10^{-2} and 2.68 x 10^{-2} respectively).

Threshold Levels   The onset threshold values for the 1113-2 and 1113 adhesives are shown in Tables 2 and 3 respectively. Examination of Tables 2 and 3 reveals that for both Metlbond 1113-2 and 1113 adhesive, the G_{Imax} values at onset threshold descrease with increasing satic shear load values in mode II. Tables 4 and 5 show the catastrophic threshold values for 1113-2 and 1113 adhesives respectively. Again, an increase in mode II loads result in a general decrease in ΔG and N_c (number of cycles at catastrophic crack propagation) values.

Comparison of P_I and P_{II} values corresponding to catastrophic crack progation under cyclic loading and the same values under monotonic loading reveal that catastrophic crack propagation occurs under lower P_I - P_{II} load combinations when the specimen is subjected to cyclic loading. In other words, P_{IC} and P_{IIC} values are reduced as a result of cyclic load application.

CONCLUSIONS

A) Mixed Mode Fracture Under Monotonic Loading

1) The application of the elastoplastic fracture behavior assumption proved adequate and useful for the model adhesive.

2) Excellent correlation was obtained between the measured bulk and bonded fracture properties.

3) The concept of plastic deformation zone is useful in determining optimum adhesive thickness in bonded mode.

4) When the energy balance criterion is used, the mixed I-II Mode fracture energy (total energy) values are lower than Mode I fracture energy values at failure.

5) The fracture data for the "brittle" model adhesive could be correlated better with the use of principal stress criterion in comparison to an energy criterion.

6) The fracture resistance of the model adhesive without the carrier cloth is higher than the fracture resistance of the same adhesive with the carrier cloth in both bonded (mixed mode) and bulk (cleavage only) modes.

7) The use of ILMMS geometry allows determination of a failure criterion on the basis of applied loads and hence makes it possible to compare the failure behavior of different adhesives under similar test conditions without calculating any G or K values.

B) Mixed Mode Fracture Under Cyclic loading

8) The strain energy release rate range ΔG due to the dynamic part of the sinusoidally flucturating load plays the most important role in cyclic load dominant mixed mode fracture

9) The G_{Imax} and ΔG values at onset and catastrophic threshold levels decrease with increasing static shear load values in Mode II.

10) The shear loads affect the crack propagation directions within the adhesive bonds.

11) An increase in the mean level of the sinusoidally fluctuating loads results in shorter fatigue life.

12) With cyclic loading, catastrophic crack propagation occurs under lower P_I and P_{II} load combinations in comparison to failure under fast monotonic loading.

13) The adhesive with the carrier cloth has slower crack propagation in comparison to the adhesive without the carrier cloth.

REFERENCES

1. Dwight, D.W., Sancaktar, E. and Brinson, H.F., 1980, Adhesion and Adsorption of Polymers, pp. 141-164, Plenum Press.

2. Brinson, H.F., Renieri, M.P. and Herakovich, C.T., 1975, ASTM STP 593, pp. 177-199.

3. Bascom, W.D., Cottington, R.L. and Timons, C.O., 1977, J. Applied Polymer Science: Applied Polymer Symposium 32, pp. 165-188.

4. Hart-Smith, B.J., 1972, Air force Conference on Fibrous Composites in Flight Vehicle Design, Dayton, Ohio.

5. Ripling, E.J., Mostovoy, S., and Patrick, R.L., 1963, ASTM STP No. 360.

6. ASTM E:399-81, Standard Test Method for Plane-Strain Fracture Toughness of Metallic Materials.

7. Irwin, G.R., 1960, Proc. 7th Sagamore Conf., pp. 4-63.

8. Broek, D., 1974, <u>Elementary Engineering Fracture Mechanics</u>, Noordhoff International Publishing, Leyden, Netherlands.

9. Mall, S., Johnson, W.S., and Everett, R.A., NASA Tech. Memo-84577, Nov. 1982.

10. Kinloch, A.J., 1981, "Developments in Adhesives-2"pp.83-124,AppliedScience Publishers.

11. Szepe, F., 1965, Proceedings of Second SESA International Congress on Experimental Mechanics.

12. Gross, B., Srawley, J.E., Brown, Jr., W.F.,1964,TechnicalNoteD-2395,NASA, August.

13. Jozavi, H., and Sancaktar, E., 1985, <u>J. Adhesion</u>, 18, 25.

14. O'Conner, D.G.,1979, <u>Factor Affecting the Fracture Energy for a Structural Adhesive</u>, M.S. Thesis, V.P.I and S.U. Blacksburg, VA.

15. Wang, S.S., Mandell, J.F., and McGarry, F.J., 1978, <u>Int. J. Fracture</u> 14, 39.

P_{II} (LB)	1113-2 ADHESIVE		1113 ADHESIVE	
	c	n	c	n
0	6.71×10^{-5}	4.2381	5.08×10^{-4}	2.36
1000	2.44×10^{-4}	3.507	6.15×10^{-7}	6.785
2000	3.49×10^{-4}	3.457	1.95×10^{-5}	4.357
3000	1.14×10^{-3}	2.612	2.41×10^{-5}	4.2689
4000	5.68×10^{-4}	3.3672	9.123×10^{-4}	2.365

Table 1. The Material Parameters for the Crack Growth Model $da/dN = c \, (\Delta G)^n$ where ΔG has the units (in-lb/in^2)

| P_{Imax}	P_{II}	G_{Tmax}	G_{Imax}	G_{II}	ΔG	N_C
LB (N)	LB (N)	$\frac{IN-LB}{IN^2}$ $(\frac{KJ}{M^2})$	$\frac{IN-LB}{IN^2}$ $(\frac{KJ}{M^2})$	$\frac{IN-LB}{IN^2}$ $(\frac{KJ}{M^2})$	$\frac{IN-LB}{IN^2}$ $(\frac{KJ}{M^2})$	Cycle
1400 (6230)	0 (0)	2.301 (402.94)	2.301 (402.94)	0 (0)	2.278 (398.92)	40142
1400 (6230)	1000 (4450)	2.317 (405.70)	2.301 (402.94)	0.016 (2.751)	2.278 (398.92)	181022
1300 (5785)	2000 (8900)	2.047 (385.5)	1.984 (374.44)	0.0632 (11.07)	1.9641 (343.95)	817273
1100 (4895)	3000 (13350)	1.563 (273.67)	1.420 (248.67)	0.143 (25.042)	1.41 (246.22)	84874
800 (3560)	4000 (17800)	1.004 (175.87)	0.751 (131.52)	0.253 (44.31)	0.7438 (130.25)	462256

Table 2. The Onset Threshold Values for 1113-2
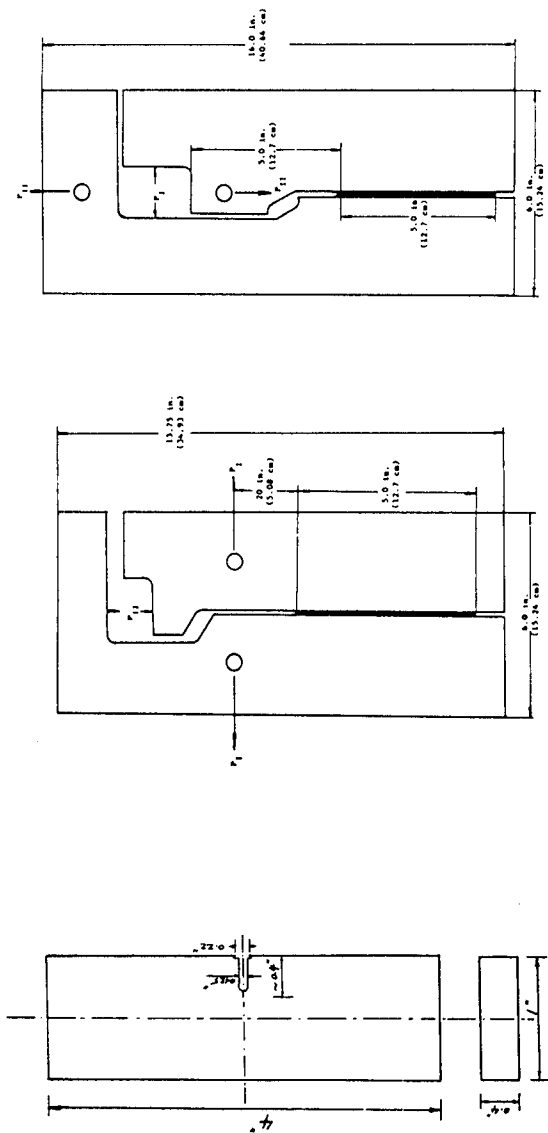
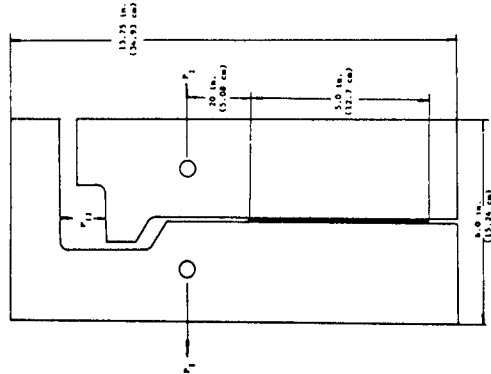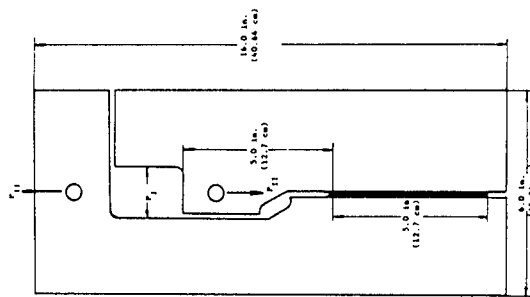Fig. 1 Single-Edge-Cracked Specimen Geometry

Fig. 2. ILMM Specimen Geometry A

Fig. 3 ILMM Specimen Geometry B
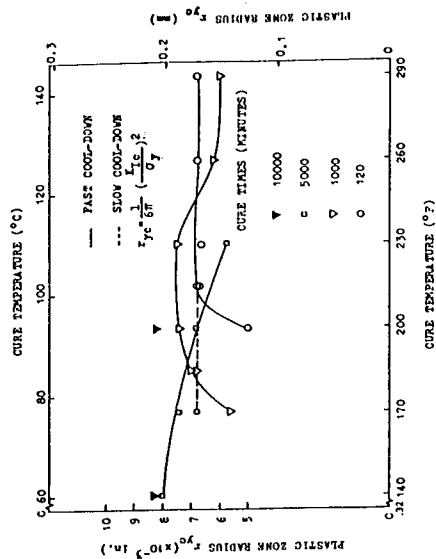
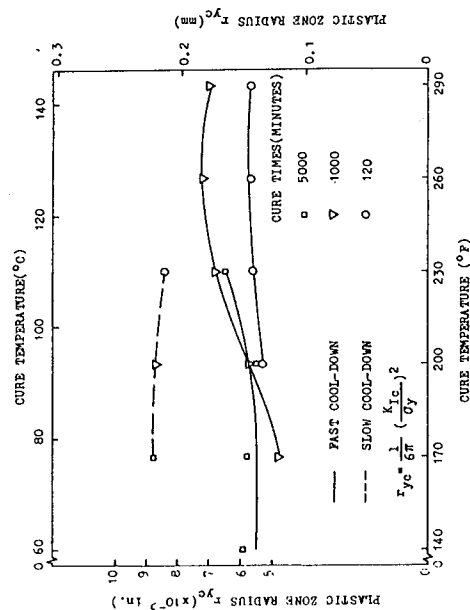Fig. 4 Effect of Cure on the ryc for Metlbond 1113 Based on Bulk Tensile and Fracture Data

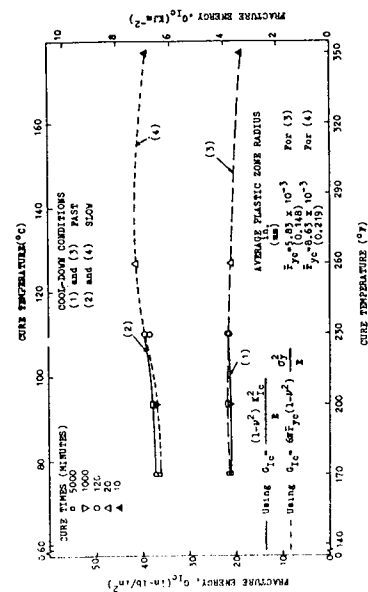Fig. 5 Effect of Cure on the ryc for Metlbond 1113-2 Based on Bulk Tensile and Fracture Data

Fig. 6 Fracture Energy-Cure Optimization Curves for Metlbond 1113-2 Based on Bulk Tensile and Fracture Data

Fig. 7 Fracture Energy-Cure Optimization Curves for Metlbond 1113 Based on Bulk Tensile and Fracture Data

136

Fig. 10 Variation of G_{IC} with Bond Thickness for 1113-2 Adhesive

Fig. 13 Variation of Mode II Breaking Force with Bond Length
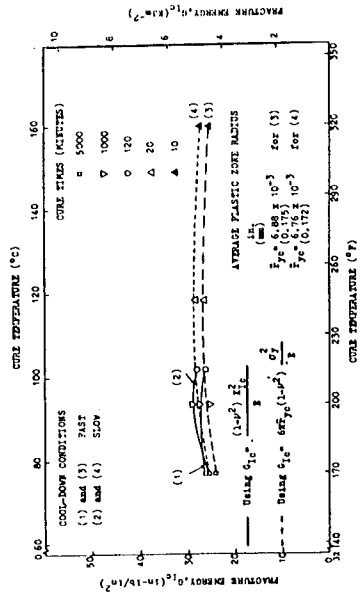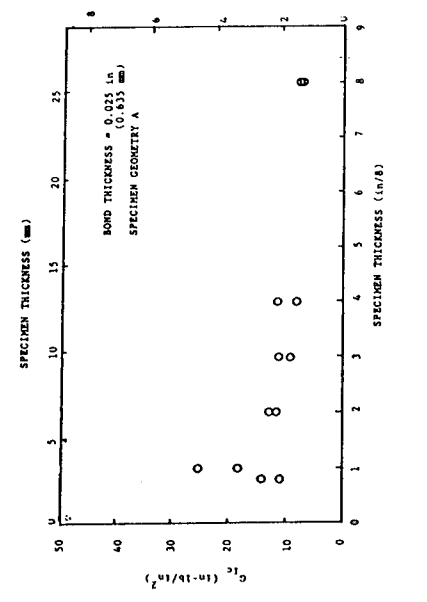
Fig. 9 Variation of G_{IC} with Specimen Thickness for 1113 Adhesive

Fig. 12 Compliance Calibration for Different Thicknesses of Geometry A Bonded with 0.635 mm Thick 1113-2 Adhesive
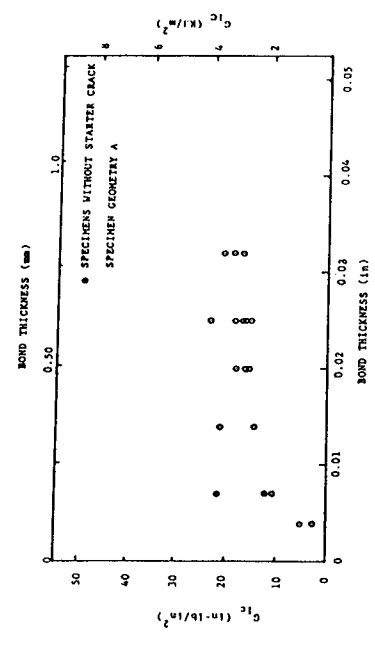
Fig. 8 Variation of G_{IC} with Specimen Thickness for 1113-2 Adhesive
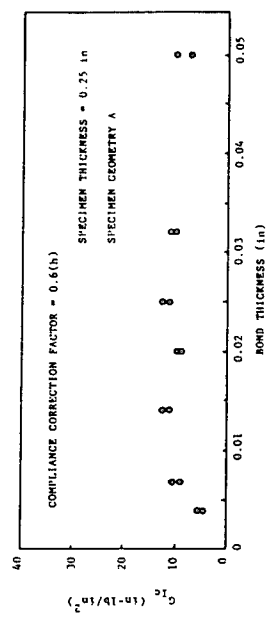
Fig. 11 Variation of G_{IC} with Bond Thickness for 1113 Adhesive

137

Fig. 15 Opening Load vs. In-Plane Shear Load for 12.7 mm Thick 1113-2 ILMM Specimens and Comparison with Theory

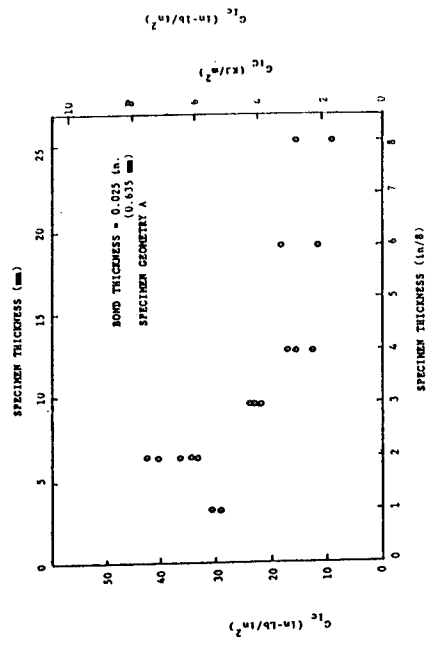**Fig. 17** G_I vs. G_{II} Behavior of 12.7 mm Thick Specimens Bonded with 1113-2 Adhesive

Fig. 14 Opening Load vs. In-Plane Shear Load for 6.35 mm Thick 1113-2 ILMM Specimens and Comparison with Theory

Fig. 16 Opening Load vs. In-Plane Shear Load for 12.7 mm Thick 1113 ILMM Specimens and Comparison with Theory. The Bond Thickness is 0.635 mm

Table 3. The Onset Threshold Values for 1113

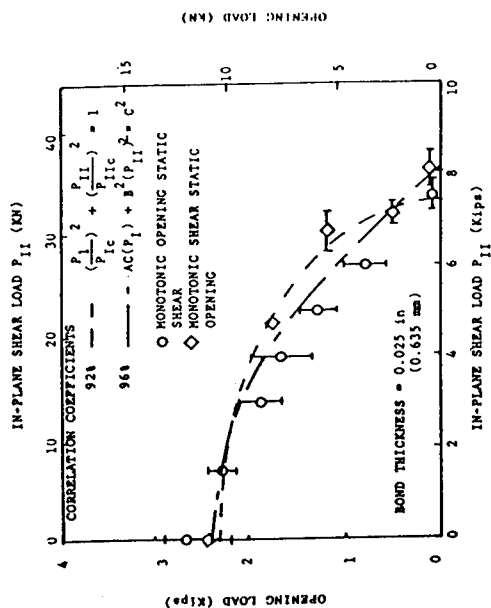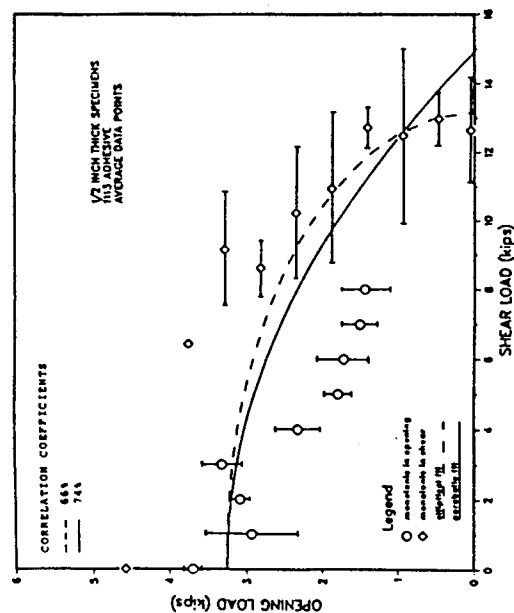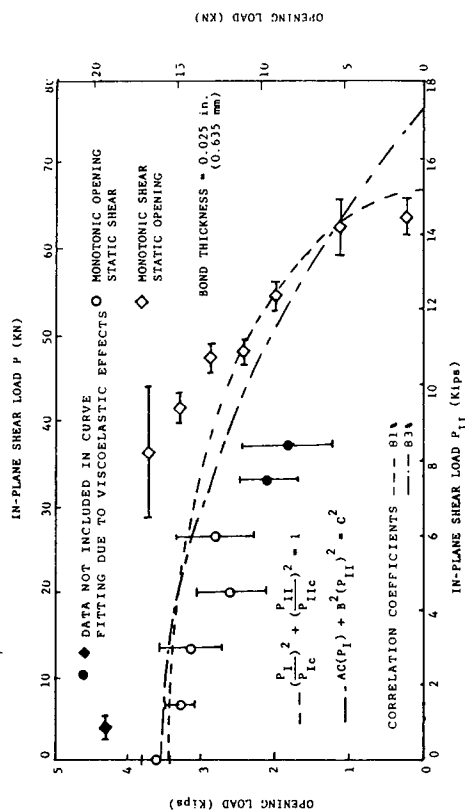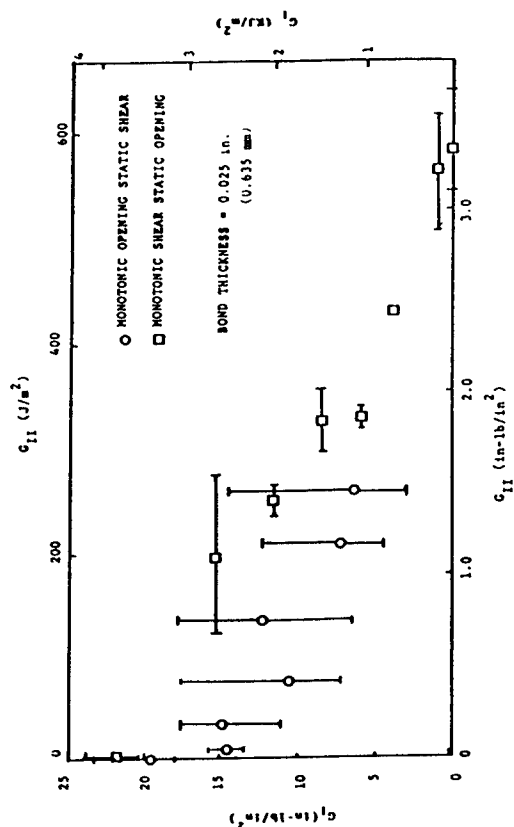| P_{Imax} LB (N)	P_{II} LB (N)	G_{Tmax} $\frac{IN-LB}{IN^2}$ $(\frac{KJ}{M^2})$	G_{Imax} $\frac{IN-LB}{IN^2}$ $(\frac{KJ}{M^2})$	G_{II} $\frac{IN-LB}{IN^2}$ $(\frac{KJ}{M^2})$	ΔG $\frac{IN-LB}{IN^2}$ $(\frac{KJ}{M^2})$	N_C Cycle
1400 (6230)	0 (0)	2.301 (402.95)	2.301 (402.95)	0 (0)	2.278 (398.92)	569002
1400 (6230)	1000 (4450)	2.317 (405.70)	2.301 (402.95)	0.016 (2.751)	2.278 (398.92)	511813
1400 (6230)	2000 (8900)	2.364 (414.00)	2.301 (402.95)	0.0632 (11.06)	2.278 (398.9)	426616
1300 (5785)	3000 (13350)	2.126 (372.3)	1.984 (347.44)	0.142 (24.87)	1.9641 (343.95)	897389
1300 (5785)	4000 (17800)	2.237 (391.73)	1.984 (347.44)	0.253 (44.31)	1.964 (343.95)	277469

Table 5. The Catastrophic Threshold Values for 1113

P_{Imax} LB (N)	P_{II} LB (N)	ΔG $\frac{IN-LB}{IN^2}$ $(\frac{KJ}{M^2})$	N_C Cycle
2400 (10680)	0 (0.0)	7.046 (1233.9)	9530
2300 (10235)	1000 (4450)	7.498 (1313.05)	3219
2300 (10235)	2000 (8900)	6.15 (1076.5)	1486
2200 (9790)	3000 (13350)	5.625 (985.4)	2741
2300 (10235)	4000 (17800)	6.15 (1076.6)	1271

Table 4. The Catastrophic Threshold Values for 1113-2

P_{Imax} LB (N)	P_{II} LB (N)	ΔG $\frac{IN-LB}{IN^2}$ $(\frac{KJ}{M^2})$	N_C Cycle
2300 (10235)	0 (0.0)	9.0032 (1576.6)	1618
2100 (9345)	1000 (4450)	5.3945 (944.7)	6388
2100 (9345)	2000 (8900)	5.3945 (944.7)	4536
2100 (9345)	3000 (13350)	5.3945 (944.7)	3692
2100 (9345)	4000 (17800)	5.3945 (944.7)	3623

1. $P_{II} = 0$
2. $P_{II} = 1000\ LB (4450\ N)$
3. $P_{II} = 1000\ LB (4450\ N)$
   $P_I = 2000\ LB (8900\ N)$
4. $P_I = 2000\ LB (8900\ N)$
5. $P_{II} = 3000\ LB (13350\ N)$
   $P_I = 1000\ LB (4450\ N)$
6. $P_{II} = 3000\ LB (13350\ N)$
   $P_I = 2000\ LB (8900\ N)$
7. $P_{II} = 4000\ LB (17800\ N)$
   $P_I = 1000\ LB (4450\ N)$

Fig. 18a Crack Extension Angle as Predicted by the Maximum Principal Stress Criterion

Fig. 18b The Saw Teeth Phenomenon

139

Predicting Bond Strength with a Fracture Mechanics Approach

D. H. Brinton and G. P. Anderson

Morton Thiokol Inc.
Box 524
Brigham City, Utah 84302

K. J. Ninow and K. L. DeVries

Dept of Mechanical and Industrial Engineering
University of Utah Salt Lake City, Utah 84112

Abstract

The most prevalent method in evaluating adhesive joint strength in the adhesive industry is the average stress criterion. It is shown that this method may be in error by an order of magnitude in many applications.

Fracture mechanics methods are presented that accurately predict failure of adhesive bonds. Failure in production adhesive joints may be reasonably predicted using fracture mechanics parameters obtained from simple test specimens.

A linear elastic fracture mechanics method is shown to give good results for predicting failure of a brittle high strength structural epoxy. This epoxy exhibits a nearly linear stress strain relationship. The method is applied to this epoxy for Mode I (tensile) loading. The results from one type of specimen are used to accurately predict failure in a radically different specimen which has the same loading mode. The effects of temperature and load rate on the method are quantified for this nearly linear elastic epoxy.

Nonlinear elastic fracture mechanics techniques are employed to predict failure in a nonlinear rubber modified epoxy in Mode I loading. Alternate failure criteria are also explored. Progress is given in extending the theory to Mode II (shear) loading. Several candidate specimens are identified.

Introduction

The most common method for assessing adhesive capability is the average stress criterion. This criterion is simply that an adhesive's load carrying capability is equal to the failure load divided by the bond area. This method may be in error by an order of magnitude in many applications. For example, the average stress failure criterion does not explain why specimens which differ only by bondline thickness exhibit failure loads which may differ by a factor of ten.[1]

Adhesive bonds are in a complex state of stress. A maximum stress criterion states that an adhesive bond will fail when any point in the bond exceeds a given stress. This localized failure stress is the maximum stress capability of the bond. This approach leads to problems too. If a linear elastic analysis is performed, points of singularity are encountered.[2] The stress is theoretically infinite at these points. Bond termination points are typically singular. On the other hand, if an elastic-perfectly plastic analysis is performed, the maximum stress is limited to the plastic stress or stress at which plastic flow

occurs. The bond does not fail at this stress until a critical value of strain is reached.(2) In this case it is ambiguous to use a stress failure criterion since the maximum stress does not occur at a discrete point.

An alternative to using a stress failure criterion is a fracture mechanics criterion. This approach is based on energy rather than stress required to break a bond. In this paper fracture mechanics techniques are given to predict failure in linear and nonlinear adhesives. Effects of load rate and temperature on fracture mechanics parameters are explored. A strain failure criterion is also explored for nonlinear adhesives. For the linear epoxy, progress is given on Mode II (shear) testing.

Linear Elastic Mode I Testing

A high strength structural epoxy, EA-934NA, a product of Dexter Hysol, Aerospace Division, was employed for the "linear elastic" testing. This brittle epoxy exhibits a nearly linear stress strain curve as shown in Figure 1. Linearity was assumed so linear elastic fracture mechanics (LEFM) could be used. LEFM states that when the energy release rate, G, the rate at which a specimen dissipates energy as a crack grows, goes above the critical energy release rate, Gc, energy will go into creating crack surfaces.

For this work it is assumed that microscopic inclusions, voids, or debonds exist in an adhesive bondline. Although these defects exist throughout a bondline, they are of most interest at the points of maximum stress or stress singularity. These defects are classified as inherent flaws, a_o. The size of these inherent flaws governs the amount of force required to achieve the critical energy release rate of the adhesive in a bond. The theory is that when the two parameters, G_c and a_o, are known, failure loads may be predicted in this linear adhesive.
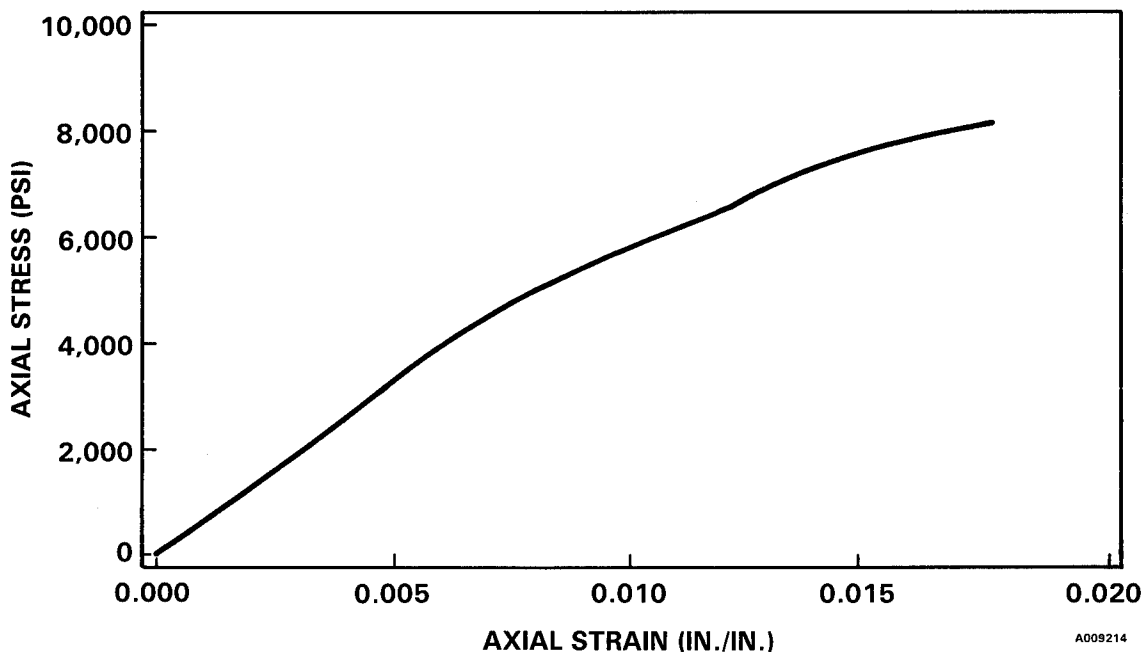

Figure 1. Stress Strain Curve for "Linear" Epoxy

The primary Mode I specimen used was the tensile adhesion button. A tensile button specimen consists of two short cylinders bonded together on the cylinder ends in a butt joint. Each cylinder has a groove machined into it so the specimen may be slid into a set of U-shaped grips which are mounted to a universal testing machine. A picture of this specimen and test grips is shown in Figure 2. This specimen was tested in several different configurations. The bondline geometry of the specimen was altered by using spacers to give different thicknesses and by creating intentional debonds by putting Teflon tape on the bonding surface of one button. This makes an initial flaw of known dimensions. This flaw is large enough that any effects of the inherent flaw are overridden. Since the flaw size is known in this case, a finite element technique (for example, the crack closure integral method) may be used to get the normalized energy release rate or square root of G per unit load. Using this parameter and

the failure load from lab testing, the critical energy release rate, G_c, may then be calculated. The G_c obtained for EA-934NA was 0.47 in-lb/in^2. The energy release rate is then calculated for a specimen with a constant bondline thickness over a range of small cracks. The failure load in tensile button specimens tested without an initial flaw (inherent flaw only) is used for these calculations. Thus the calculated energy release rates are critical energy release rates, G_c, for various inherent flaws. the flaw which produces a G_c, of 0.47 in-lb/in^2 is termed the inherent flaw size. The inherent flaw size obtained was 0.0016 inches.

As an independent verification of this test, a nontapered double cantilevered beam test was run according to ASTM D-3433. This test involves applying a tensile force normal to the bondline of two parallel plates. A crack is propagated incrementally by loading and unloading the specimen. From this testing a load versus displacement
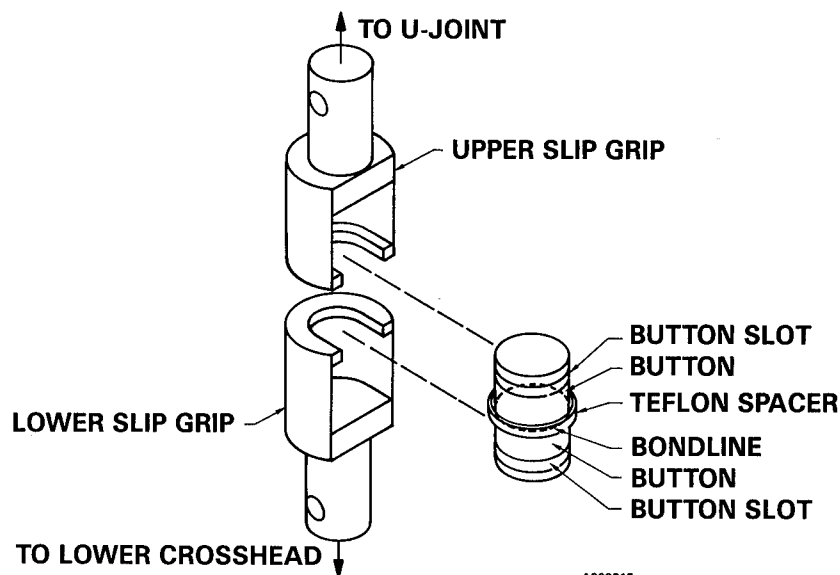
Figure 2. Tensile Adhesion Button Test Setup

142
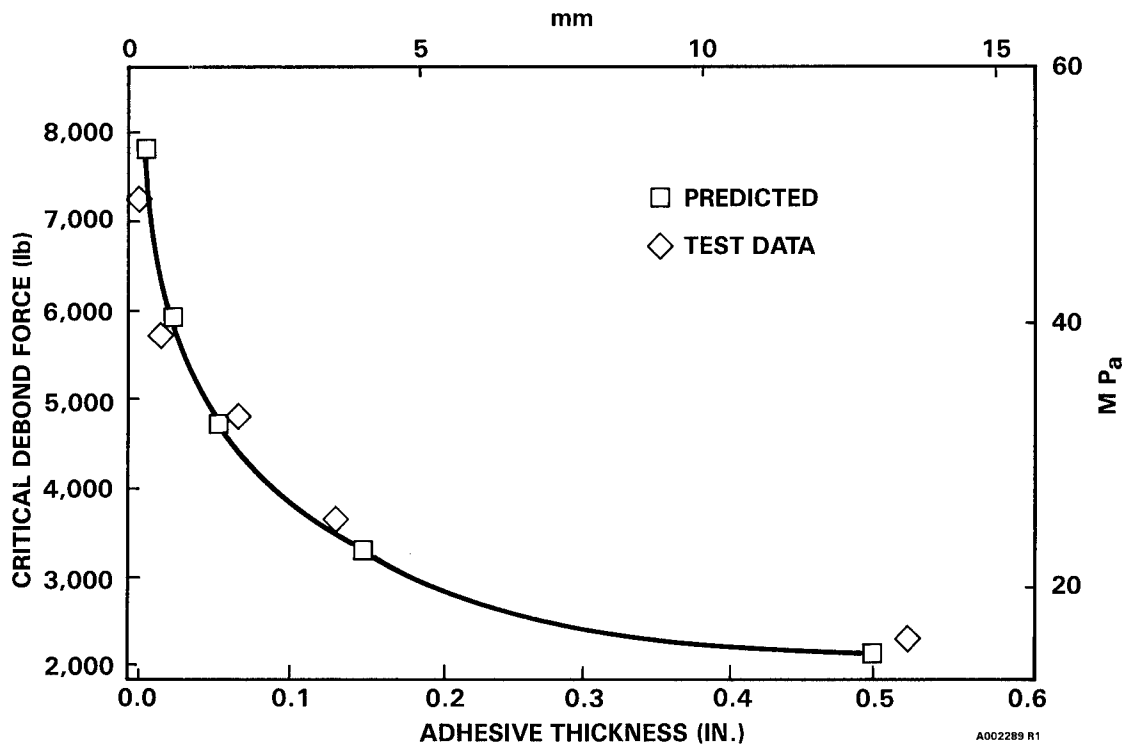
Figure 3. Effect of Thickness on Debond Load for "Linear" Epoxy

curve is obtained at different crack lengths. From these data the change in compliance of the specimen per change in crack length may be calculated. This allows calculation of G_c according to the following equation.

$$G_c = \frac{p^2}{2b} \frac{dc}{da}$$

Where p is the crack propagation load, b is the specimen width, and dc/da is the change in compliance with crack length. From this testing a G_c value of 0.52 in-lb/in^2 was obtained. This is in close agreement to 0.47 in-lb/in^2 which was obtained in the tensile adhesion tests.

Theoretically, G_c and a_o may now be used to predict failure in other Mode I specimens. In the first verification of the theory, failure was predicted in tensile buttons with the bondline thickness varying from 0.005 to 0.500 inches. A

comparison of measured and predicted data is shown in Figure 3. As may be seen, the theory correctly predicts the thickness effect. With this success a third Mode I specimen was used for further theory verification. This specimen was the modified blister test.

Blister Test Results

The blister test is shown in Figure 4. It was employed as an alternate Mode I (tensile) specimen to verify the Mode I failure theory developed with the buttons for the nearly linear elastic epoxy.

A blister specimen consists of a steel cylinder which has a cylindrical hole machined concentrically with the outer cylinder surface. A Teflon plug is inserted into this hole and a 0.125 inch layer of adhesive is cast on the cylinder end. The blister specimen was modified by adding a 0.625 inch thick steel plate on top of the uncured

143

ADHESIVE STEEL TOP PLATE

SHIM

TEFLON TAPE FOR STEEL
INITIAL DEBOND BUTTON

A000761 R1

Figure 4. Modified Blister Test
Specimen

adhesive to provide increased
stiffness and thus prevent
cohesive shear failure
initiation within the adhesive.
After the adhesive is cured the
Teflon plug is removed. The
blister is then tested by
pressurizing inside the hole
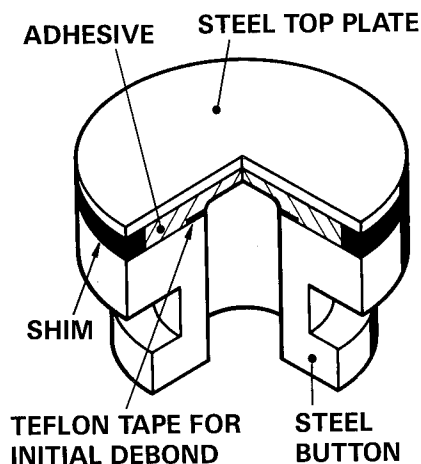until failure. Finite element
analysis showed that although
the tensile button and blister
specimens are radically
different in both specimen
geometry and loading method,
both specimens exhibit about 98
percent Mode I loading.

Using the G_c and a_o obtained
from the tensile buttons and
data from finite element runs on
the blister specimens, failure
pressure predictions were made
for blister specimens. These
predictions, along with the
actual test data, are shown in
Table 1.

As can be seen excellent
results are obtained when
predicting the blister specimen
failure pressure based on
fracture mechanics parameters
obtained from tensile button
tests. This verifies the
hypothesis that fracture
mechanics may be used to predict

Table 1. Blister Test Results

Debond Size (in.)	Failure Pressure (psi)		% Error
	Pred	Actual	
ao	3370	3320	2
0.2	860	910	6

failure in "linear elastic"
adhesives in Mode I loading.

Temperature and Load Rate
Effects

Using the button specimen shown
in Figure 2, testing was
completed to determine the
effects of varying temperature
and load rate on G_c and a_o. It
was assumed that a_o would not
change since it is a geometric
parameter. The critical energy
release rate, G_c, is an energy
derived parameter and would be
expected to change. Testing was
at 20°, 75°, and 150°F. The
three load rates were 0.005,
0.050, and 0.500 inches per
minute. The viscoelastic
properties of the
adhesive were taken into account
by using the effective modulus
obtained from relaxation modulus
testing. The effective modulus
is obtained by integrating a
relaxation modulus curve for a
constant strain rate loading.
The relaxation modulus curve is
obtained by rapidly loading a
specimen to a constant strain
and allowing the stress to relax
with time. The relaxation stress
is converted to relaxation
modulus using Hooke's Law. A
master curve of the effective
modulus for a constant strain
rate loading is shown in Figure
5.

144
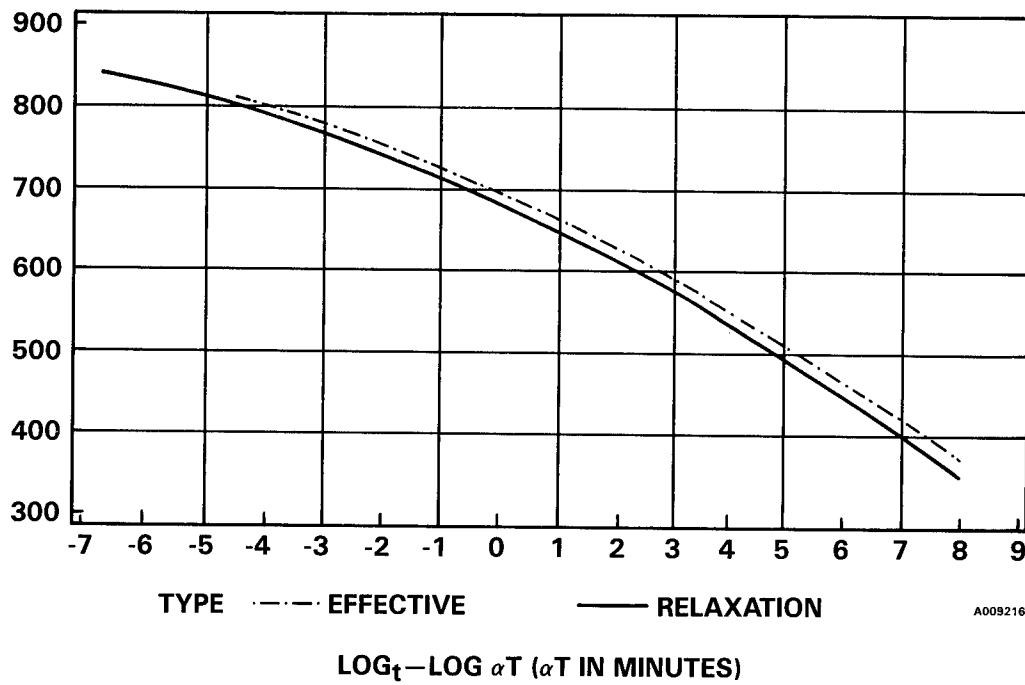
Figure 5. Effective Modulus for "Linear" Epoxy
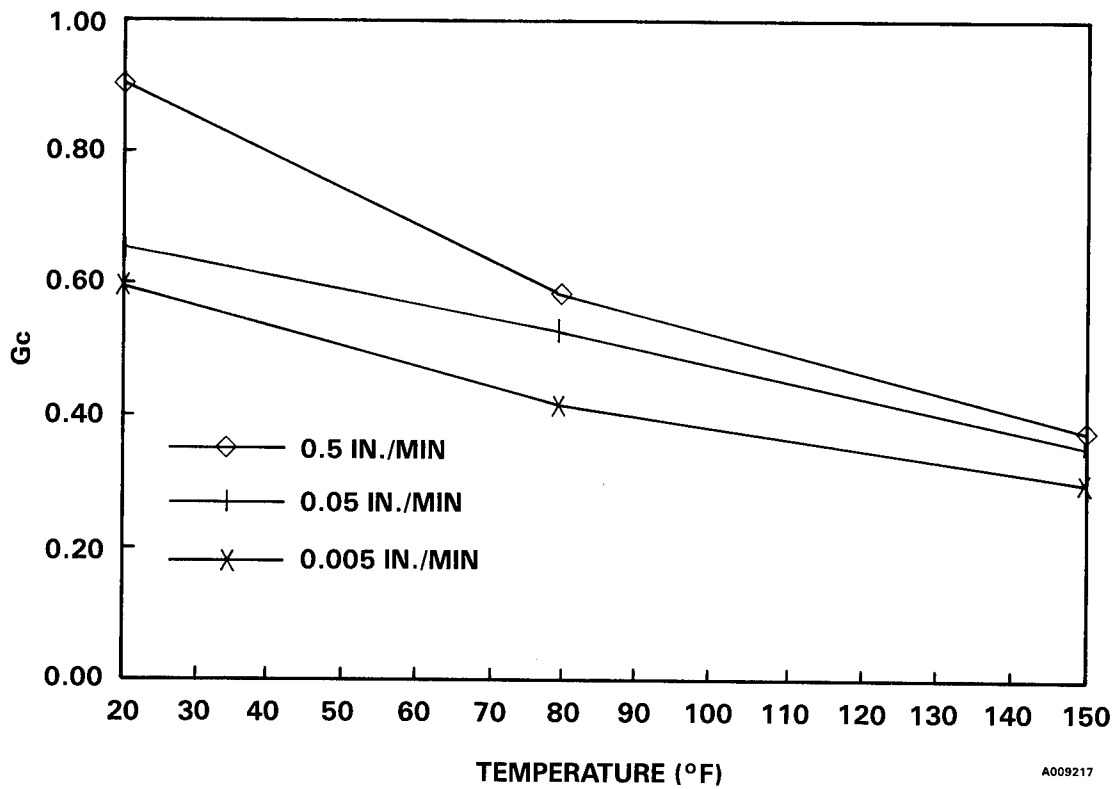
Figure 6. G_c as a Function of Temperature and Load Rate

145
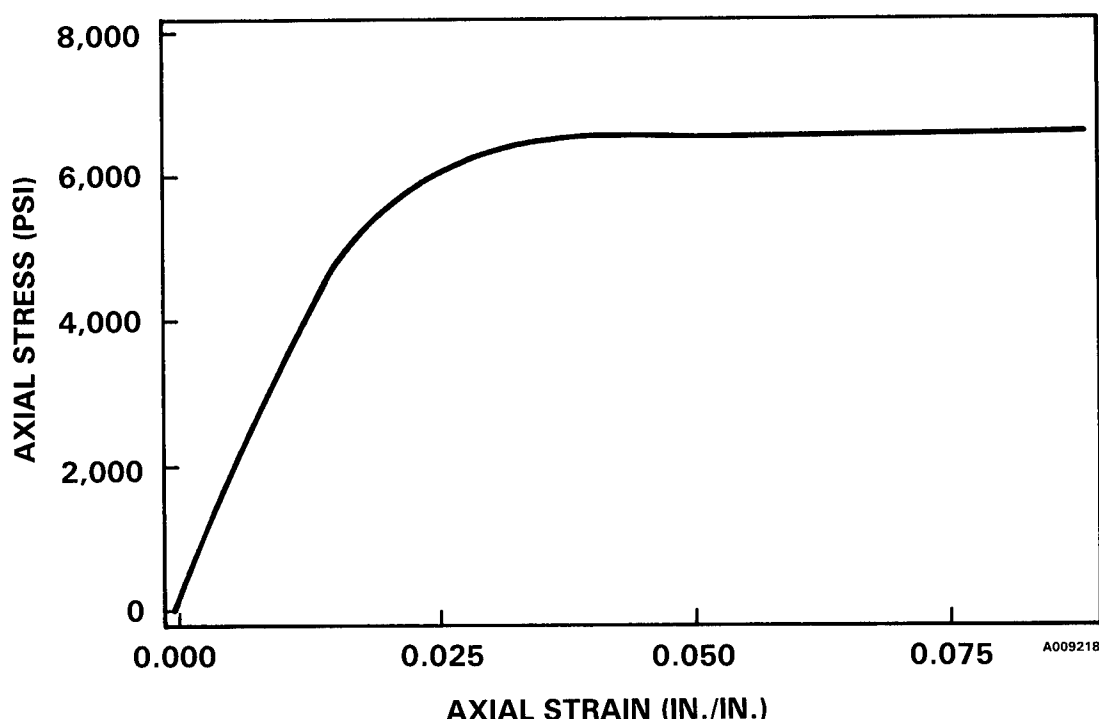
Figure 7. Stress Strain Curve for Nonlinear Epoxy

Three specimen geometries were tested. The specimens differed by the amount of initial debond. Specimens were tested with no intentional debond and with 0.1 and 0.2 inch intentional debonds. As before, the intentionally debonded specimens served to get an independent measure of G_c. The nondebonded buttons allowed assessment of a_o.

Figure 6 shows how G_c varies with both temperature and load rate in the nondebonded buttons. Analysis of these data showed that G_c increases with an increase of load rate and decreases with an increase of temperature. This agrees with the general observation that adhesion strength increases with load rate and decreases with temperature. The inherent flaw size, a_o stayed essentially constant at all temperatures and load rates tested.

Nonlinear Elastic Mode I Testing

A rubber toughened high strength structural epoxy, EA-9309.2NA, a product of Dexter Hysol, Aerospace Division, was used for the nonlinear Mode I testing. This epoxy exhibits a nonlinear stress strain curve as shown in Figure 7. As can be seen, this epoxy has an initial elastic portion with a large plastic portion.

Tensile adhesion buttons were tested with various bond geometries using this nonlinear epoxy. The testing was performed at one temperature and at one load rate. Buttons were tested which had several different thicknesses and bond termination geometries. Groups of buttons with thicknesses of 0.005, 0.030, 0.060, 0.150, and 0.500 in. were tested. Groups of buttons with initial flaws of 0.1 and 0.2 in. were also

146

tested. The different thickness buttons had no intentional debond.

Three failure theories were compared for correctness in analyzing test results. First was the linear fracture mechanics approach which was used with good success for the "linear elastic" approach. This approach proved to be inaccurate which confirmed that a nonlinear approach must be taken to account for plastic deformation. The first nonlinear approach involved the use of the "J"-integral. The "J"-integral is a nonlinear energy release rate which reduces to G in the linear case. This approach was able to predict loads in the 0.2 inch debonded buttons from results obtained in the 0.1 inch debonded buttons within 5 percent. The critical value of the "J"-integral, J_c, obtained was 2.0 in-lb/in^2. Numerical problems arose with the finite element runs to determine a_o. Unreasonably large shear deformations occured for small flaw sizes near a bimaterial interface. Work is continuing to solve the problems.

The second nonlinear approach was the use of a maximum principal strain failure theory.(2) This involves analyzing the localized strain present in a specimen using nonlinear structural analysis. When the strain exceeds a critical level, failure is predicted. This approach worked within 20 percent for the 0.1 and 0.2 inch debonded buttons. The same numerical problems were encountered with the small flaw sizes. The new release of the code promises to have solved the problem.

Mode II (Shear) Testing

One of the problems encountered with specimens thought to be loaded in Mode II (shear) is that most are not purely shear with many being dominated by tension at the failure intiation point. Analysis shows that a thick adherend single lap shear specimen (ASTM 3165) may be up to 90 percent Mode I at the failure initiation point.

Several "Mode II" specimens are being analyzed and tested to determine the ratio of Mode I to Mode II and the Mode II energy release rate, G_{IIc} and a_o.

Three candidate Mode II (shear) specimens which were bonded with the "linear elastic" adhesive were tested. The first specimen tested was the constrained thick adherend lap shear specimen. This consists of a standard thick adherend lap shear specimen which has lateral restraints placed on it at the failure zone. A picture of this specimen is found in Figure 8. The restraints are intended to prevent the Mode I component from becoming large at the crack termination point. This approach had very limited success as the force required to constrain the edge was too great to preclude frictional contribution from the constraints.
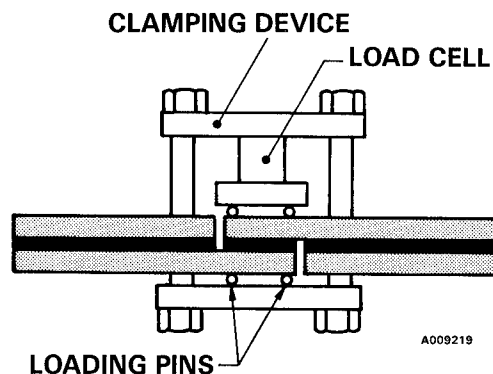
Figure 8. Constrained Lap Shear Test Setup

147

The second specimen is the three point bending beam or edge notched fracture test. This specimen consists of two plates laminated together with adhesive. The assembly is loaded in three point bending so that the adhesive layer is at the neutral axis of the beam. A picture of this specimen is found in Figure 9. Problems have been encountered in this test with detecting the crack growth. Work is continuing with a conductive carbon crack gage. Carbon is vapor deposited on the edge of the specimen and the resistance change is tracked while the crack is propagating.
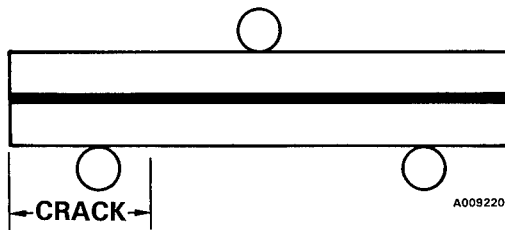
Figure 9. Three Point Bending
Beam Test Setup

The third specimen is the Iosipescu specimen. This specimen consists of two blocks bonded together which are placed in direct shear using fixed grips. A picture of this specimen is found in Figure 10. It is the most promising of all
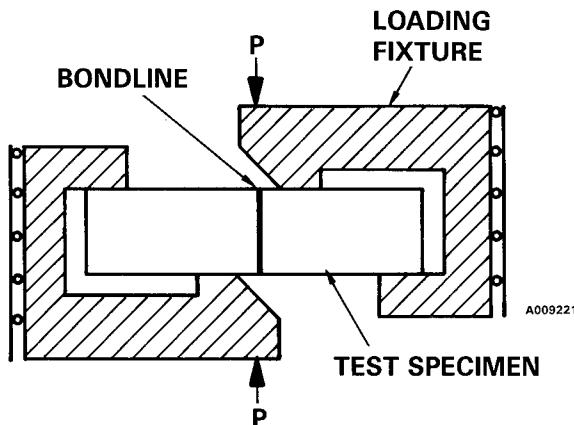
Figure 10. Iosipescu Shear Test
Setup

the Mode II specimens. Fracture mechanics was used to analyze these specimens to assess the relative amounts of Mode I and Mode II present in the failure zone. Analysis showed that the Iosipescu had the highest amount of Mode II present with 96 percent.

A fourth Mode II specimen which is now under construction is the tapered end lap shear specimen. This specimen is derived from a thick adherend lap shear specimen. The only difference is that the cut end of this specimen has been ground to a taper. A picture of this specimen is found in Figure 11. This taper limits the transverse stiffness at the bond termination and should therefore limit transverse force.
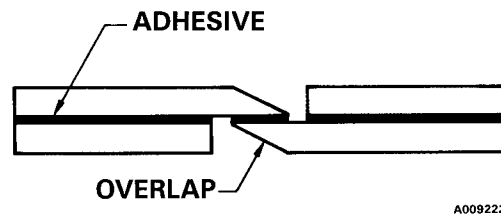
Figure 11. Tapered Lap Shear
Specimen

More analysis work is being done on these Mode II specimens to determine a Mode II energy release rate.

148

Summary

The fracture mechanics approach works well in predicting Mode I failure in nearly linear epoxies. When the theory is extended to nonlinear epoxies, numerical problems are encountered at bi-material interfaces on the current finite element code. Future code improvements promise to solve this problem. Mode II testing involves finding a pure shear specimen and testing it with both linear and nonlinear adhesives. Work is continuing in this area.

References

1. Anderson, G. P. and K. L. DeVries, "Predicting Bond Strength", to appear in Journal of Adhesion, 1987.

2. Harris, J. A., and Adams R. D., "Strength Prediction of Bonded Single Lap Joints by Non-linear Finite Element Methods", Int. J. Adhesion and Adhesives, Vol. 4 No. 2, April 1984

THE POLYMER INTERPHASE AND ADHESION

A THEORY

Charles A. Kumins
Consulting Services, Inc.

RD 4 Box 439
Easton, MD 21601

Numerous theories have been proposed to explain adhesion phenomena. Most involve the sorption and wetting of the substrates to be joined by the adhesive molecules by either physical or chemical interaction between reactive surface sites and specific moieties in the polymer composition of the adhesive. The former may depend on hydrogen bonding, dispersion forces or dipole-dipole interactions whereas the latter comes about by specific chemical interactions (1,2). Early in 1975 (3) and in subsequent papers Fowkes had proposed an acid/base interaction between the adhesive and adherend as the procuser for good structural bonds. A somewhat related electrostatic theory was earlier reported by Derjaquin and Smilger [4]. The special case of polymer to polymer adhesion was considered by Voiyutskii [5] who postulated the interdiffusion of the polymers across the interface into some depth within the bulk.

With this exception, the prevalent theories emphasize the energetics at the <u>interface</u> as the principle, if not the only, factor in production of good adhesive bonds.

It is the purpose of this paper to present an approach to the study of adhesive phenomena associated with macromolecules which is based on restricted polymer segment mobility due to adsorption on the surface of the adherend. The adsorption of a macromolecule on surfaces results in a reduction in the number of configurations the macromolecule can assume when compared to that which exists in the free state. All the bulk polymer molecules are in constant thermal motion. The amplitude of the motion is determined by the amount of available free volume within which they may oscillate, rotate and vibrate. If an adjacent molecule occupies more of its share of the free volume there is less available for the others. Thus if the sorbed molecule is attached to the active sites of a surface it usually occurs via specific moieties which are ordinarily displaced some distance from one another and thus a considerably greater volume is excluded than when it is in the free or unattached state. The result is a surface molecule which is looped and bent. (Figure 1). The movement of the adjacent molecules (those not on the surface) is then restricted. In turn those nearest the adjacent ones are also affected. The initial restriction in polymer segment mobility may be telegraphed through distances as great as 1000-2000 nm. The relatively immobilized segments produce effects similar to that which is observed in cross linked systems. It would appear reasonable at least as a first approximation to expect that the greater extent of hindrance to segmental motion (i.e. like cross linking) the stronger the adhesive bond should be. In other words the thicker the layer of restricted movement the stronger the bond.

In the practical preparation of organically adhered joints experience teaches that the thinnest adhesive layers produce the strongest joints. This may be due to two reasons; one being the lower probability of defects and stress concentration points for propagation of cracks, since the total volume of glue is small as compared with a thicker layer. The other reason may be that the extent of the restricted mobility layers, which may be equal to 1000 nm for the two surfaces, includes the total thick-

ness of the glue region. Bryant and Dukes [6] showed that metal to metal bond strength decreased with increasing thickness of adhesive. As indicated above, this may be the result of the adhesive thickness being greater than the dimension of the restricted mobility layer. It is possible that the extent of the layer of restricted segment mobility and the strength of this region to withstand the ambient environmental effects may be related to the ability of the joined phases to remain together.

The fundamental study of adhesion phenomena is generally hampered by the fact that only limited surface areas are conveniently handled in the laboratory. The condition of surfaces may be studied by electronic or atomic probes such as ESCA, SIMS, IPS, LEED, Auger, etc. But in most cases the surface is examined after the film is removed and this may not represent the actual state of affairs that existed initially.

Experimental evidence that this long range impairment of polymer mobility occurs may be deduced from (1) glass transition measurements, (2) vapor diffusion studies, (3) solubility determinations, (4) mechanical property effects, (5) viscosity measurements, (6) density calculations, and (7) electrical properties. The data obtained from such work may be used to calculate the boundary of the restricted segment mobility region. It is proposed that its extent could possibly be correlated with the capability of the system to remain together under stressing conditions.

The approach taken in some of the experiments to be described was to use particulate material dispersed in a binder. The former could be obtained in small

enough particle size to provide a sufficiently large area for effects to be observed. The experiments described have employed oxides, such as TiO_2, as analogues of the polar or hydrophillic oxides of which most metallic surfaces are composed. For nonpolar or low energy surfaces phthalocyanine blue, whose critical contact angle of 31.3^0 [7] and surface tension of 46.9 dynes/cm [8], qualify it as a low energy surface material, or similar type particles have been used. It should be stressed that these particulate substances are only employed to provide large surface areas whose free energies of formation are similar to those encountered in adhesion technology.

Glass Transition: The glass transition temperature (Tg) divides the rubbery region of a polymer from the glassy phase. On a molecular scale the latter condition postulates restricted vibratory motion with limited amplitude whereas in the former the polymer segments move with greater freedom, amplitude and flexibility.

As mentioned previously, the adsorption of a macromolecule on a surface should restrict the molecules's vibrational modes because it is in a looped configuration and so it would occupy a proportionally greater percentage of the system's free volume. This in turn restrains the neighboring molecules, which restriction could be reflected in glass transition measurements.

Kumins and Roteman [9] determined the Tg of poly (vinyl acetate vinyl chloride) by dilatometry films filled with TiO_2 at varying volume solids. They found several Tg's depending on the total surface area of the TiO_2 present. At about $6\frac{1}{2}$% by volume a new Tg appeared (48^0C

152

as compared with the initial ones; 30° and 77°).

Droste and DeBenedetto [10] using thermo mechanical methods on epoxy filled with either glass beads or clay found the Tg to increase as the surface area of the solids increased as a result of their addition to the composition. They interpreted their result as due to a reduction of polymer molecular mobility due to adsorption. Figure 2 from their publication illustrates this effect.

Price, et al [11] studied a styrene cured polyester filled with potassium perchlorate powder $200 \mu m$ in diameter using NMR and thermo mechanical analysis. They found a range of Tg's depending on the proportions of $KClO_3$ present. Figure 3 from their publication illustrates the results. They attributed their results to the presence of two phases; one arising from the constrained polymer segments and the other to the neat polymer. It is interesting to note that the Tg changes occurred despite the $200 \mu m$ (on small surface area) particle size of the filled system.

Iisaki and Schaboyama [12] using dynamic mechanical analysis and broad line NMR methods found a Tg shift to higher values as the amounts of mica filler in an epoxy system was increased. They attributed the results to the non homogenity of the segmental mobilities of the polymer chains brought about by the addition of the mica (Figure 4).

Beatty [Polymer Composites 5 Oct (1984)] (19) showed that the Tg of polymethyl methacrylate increases as the amount of $CaCO_3$ mixed with it increases. He used dielectric relaxation techniques to detect these changes.

Hahn [J Adh 17 #1 (1984)] (20) showed by strain measurements that considerable differences in residual stress between interfacial and bulk adhesive zones exist in aluminum joined with epoxylite 810.

Theocaris [J. Reinforced Plastics and Composites 3 July (1984)] (21) has reported and mathematically analyzed a thick interphase between a polymer and particles dispersed in it whose properties differ markedly from those of the bulk.

Crowley and Jonath using Rayleigh Scattering and Thermally Induced Dielectric Relaxation techniques on aluminum joints bonded with an epoxy adhesive reported restricted polymer mobility ranging as much as 10,000 nm from the aluminum surface (Adhesion and Adsorption of Polymer Part A 165 and 175 (1980) Plenium Publishing Corp), (22).

These examples using various mensuration methods and different solids of differing surface activity dispersed in different polymers point to a general phenomenon in which there is produced a restricted polymer segment mobility within the volume of polymer between the solid particles. This interparticle volume is of visible dimensions.

Diffusion: The significance of diffusion data in connection with the thesis of this paper rests on the generally accepted model for the transport of gaseous matter through polymer films. This process takes place as a result of the motions of the polymer segments which normally oscillate and vibrate at frequencies of about 10^{12} times per second. At any given point in time there are free spaces formed within the matrix due to the cooperative and simultaneous movement of a number of segments.

153

This "hole" or fluctuation in microscopic local density provides a space within which a diffusing molecule may "jump." Since the glass transition temperature divides the state between restricted mobility of segments i.e. more glass like, and the one in which they move more freely and with greater vibrational amplitudes, it follows that measurements of diffusion rates below and above the Tg vary in a manner which is not proportional to the temperature differences at which the determinations are made. Put another way, the activation energy for diffusion is greater above the Tg than below it because, as stated above, the translation and vibrational movements of segments are greater. The usual way to show this is to plot log D vs 1/T.

The plot for the diffusion of CO_2 through the poly (vinyl acetate, vinyl chloride) TiO_2 film at 12.9 and 19.3 volume % for which the Tg was about 49^0C is shown in (Figure 6). The same results were obtained when H_2O was the diffusant. It should be recalled that the neat polymer exhibited 2 Tg's one at 30^0 and the other at 77^0C. In this system the interparticle distance is calculated to be 1740 nm and 1250 nm respectively.

Since the diffusion data indicate a change in slope of the curve obtained from a plot of Log D vs 1/T which represents an increase in the energy of activation for the diffusion process it follows that the CO_2 or the H_2O must find its way through the maze of the polymer situated between adjacent particles of the solid. Because the process requires more energy due to the restriction of polymer mobility than would obtain in the neat polymer.

Since the change in slope occurs at about 48^0C, the same Tg tem-

perature as found by dilatometric measurements of the same system, further evidence for changes in polymer segment mobility within the material between the particulate matter is obtained.

Solubility: Solubility or swelling data are commonly determined to assess the degree of cross linking of cured polymers. A highly cross linked system swells slightly since the rigid network does not permit the entrance of significant amounts of solvent. The degree of cross linking may be calculated from the Flory-Stannett equation:

$$[\ln (a_1/v_1) - v_2]\, v_2^2 = x + \rho\, (v_1/v_2^2)\, [v_2^{1/3} - (2/f)v_2]\, 1/Mc \tag{1}$$

where a_1=activity of the solvent in the polymer, v_1= volume fraction of solvent, v_2= volume fraction of polymer, x=interaction parameter, f=functionality of the cross linking groups, Mc=mol. wt. between cross links, and p=density of the polymer.

It would be reasonable to assume that restriction of segment mobility would cause the system to act as if it were cross linked to some extent. This would be reflected in a decrease of vapor solubility of the polymer when in contact with a surface.

Figures 7, 8, and 9 do indeed illustrate that the amounts of solvent imbibed by a polymer in contact with a solid surface are considerably less than when the former is in the free film state. The curves also indicate that as the partial pressure of the solvent increases a point is reached where the affected segments are released from their restriction and then the vapor solubility approaches that of the free film.

The curves shown have further relevance in that they contain

154

data obtained from such diverse materials as copper phthalocyanine (a hydrophobic or low energy surface), polyvinylacetate, acetone, chloroform, Epon 828 50% cross linked by hexamethylene diamine and TiO_2, a hydrophillic surface [13,14].

Lipatov and Sergeeva [15] studied the effective cross-linked density by swelling measurements of polyurethane coatings based on polyethers and polyesters in the free film and on an aluminum surface. As illustrated in Table the cross-link densities differed depending upon whether the free film or the surface film was measured. The latter had the lower molecular weight between cross-links. They considered that the chemical reaction was different in each case due to the presence or absence of an interface.

About the same time Lipatov and Sergeeva [16] reported that swelling measurements on a polystyrene/glass fiber system by ethylbenzene vapors showed a decrease in vapor sorption with glass content. This diminution was observed even when the polymer content was 200 wt % of the fibers. In work on polyurethane coatings on solid surfaces they reported "cross linking" effects which only became insignificant at a distance of 200 nm.

Mechanical Properties: Kwei and Galperin [17] studied the mechanical properties of TiO_2 filled polyvinylacetate. If the solid particles were non-reacting with the matrix, the variation of Young's modulus would follow

$$E = E_o (1 + 2.5\phi + 14.1\phi^2) \quad (2)$$

where ϕ is the volume fraction of crystalite and E_o is the Young's modulus at $\phi = 0$. Their data showed that the actual increase of E with TiO_2 content (or surface area) was much greater than

predicted by Equation (2), Figure (10); depending on strain rate the second virial coefficient of the equation was as much as four to six times greater than for the non-interacting value of 2.5.

In addition to the increase in Young's modulus the ultimate elongations were decreased. They state "increases in Young's modulus with higher filler content indicates that the polymer chains as a whole are stiffened. This long range immobilization of polymer chains effectively increases the potential energy for the system. By reducing the degrees of freedom for the polymer chains as a whole, as a result of pigmentation, the close packing of polymer chains could enter into a more ordered state (decrease in total entropy)".

Ziegel and Romanov [18] modified the Kerner equation to take into account the volume of filler and the thickness of the adsorbed layer of polymer surrounding the particulate material.

$$E_f'' / E_o'' = [1 - \phi_f B^n] - 1 \quad (3)$$

where E_f'' / E_o'' is the reduced storage modulus, ϕ_f the volume fraction of filler and B is a correction factor for the interphase (equal to one if no interphasial effects are present), and n is a dimensionless factor. The data for the systems viton/ HiSil® (a fine particle grade of silica) and glass beads of $20 - 60 \mu m$ in size are shown in Figure 11. In both cases the value for B is greater than one (1) indicating the presence of layer of polymer with stiffer properties than in the bulk. It is interesting that even for particulate material whose particle size is as large as the glass bead or conversely such small surface area an interphasial effect occurs.

Fracture mode studies such as reported by DeVries(23) and others [Drzal J. Adh 18 46 (1985)](24) on epoxy systems and other polymer based adhesives show that the fracture front though initially started at the interface moves away from it as the fracture propagates indicating that less energy is required to proceed in the region where the interphase has tapered off.

Summary: There is abundant evidence obtained from studies of many different adhesive/substrate systems to establish the presence of an interphasial region within the polymer matrix whose properties differ from the bulk. This interphacial region is believed to arise originally from the looped configuration of polymers adsorbed initially on the surface. These loops which arise as a result of the lack of registration between the adsorbed polymer moieties and the active sites on the substrate exclude sufficient free volume for the adjacent molecules causing effects that resemble those encountered in chemically cross linked systems.

It is proposed that the extent and dimensions and properties of the interphase determine the ultimate adhesive strength of bonded assemblies. The dimensions of these regions may be calculated by the use of such relationships as the Flory-Stannett equation. In this way a figure of merit may be obtained for systems of interest which will aid in the study of bonded structures and composites.
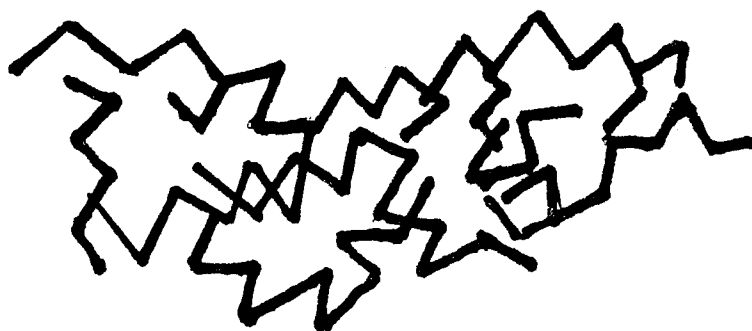
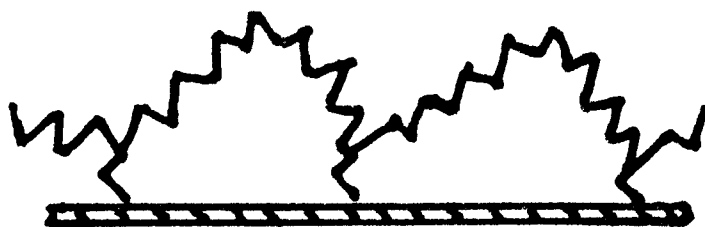This effort has been started at Kent State University in Ohio.

References:

1.   H. Alter and W. Sollar, Ind. Eng. Chem., 50, 922 (1958).

2.   R. H. Sharpe and H. Schonborn, Contact Angle, Wattability and Adhesion, Adv. Chem. Series, 43, ACS, Washington, D.C. (1964).

3.   F. M. Fowkes and J. A. Manson, Presentation at Polymer Solid Interaction Symp., Org. Coatings and Plastics, Chem. Div.,ACS Aug. 1975.

4.   B. V. Derjaquin and V. P. Smilger, J. Appl. Phys., 38, 4609 (1963).

5.   S. S. Voiyutskii, Adhesion and Autohesion of High Polymers, Interscience, New York (1963).

6.   R. W. Bryand and W. A. Dukes, J. Adhesion, 1, 48 (1969).

7.   P. R. Buechler, Conf. on Org., Coatings Technol., University of Detroit, 1970.

8.   S. Wui, and K. J. Brzozowski, J. Colloid Interface Sci.,37,4 (1971).

9.   C. A. Kumins and J. Roteman, J. Polym. Sci., Part A, 1, 527 (1963).

10. O. H. Droste and A. T. DeBenedetto, J. Appl. Polym. Sci., 13, 2149, (1969).

11. E. Price, D. French and A. Tompa, J. Appl. Polym. Sci., 16, 157 (1972).

12. K. Iisaki and K. Schaboyama, J. Appl. Polym. Sci.,22, 1845 (1978).

13. C. A. Kumins and J. Roteman, J. Polym. Sci., Part A, 1, 532 (1963).

14. T. K. Kwei and C. A. Kumins, J. Appl. Polym. Sci., 8, 1483 (1964).

15. Y. S. Lipatov and L. M. Sergeeva, Adsorption of Polymers, John Wiley, New York, p. 162 (1974).

16. Y. S. Lipatov and L. M. Sergeeva, Loc. Cit. p. 148.

156

17. T. K. Kwei and I. Galperan, J. Appl. Polym. Sci., 10, 68 (1966).

18. J. Ziegel and R. Romanov, J. Appl. Polym. Sci., 17, 1119 (1973).

19. Beatty, Polymer Composites 5 Oct (1984).

20. Hahn, J Adh 17 #1 (1984).

21. Theocaris, J. Reinforced Plastics and Composites 3 July (1984).

22. Adhesion and Adsorption of Polymer, Part A, 165 and 175 (1980), Plenium Publishing Corp.

23. J. L. DeVries, University of Utah.

24. Drzal, J. Adh 18 46 (1985).

POLYMER CONFIGURATION

In Bulk

On Surface

FIGURE 1

ADAPTED FROM
DROST & DIBENEDITTO
J. APP. POL. SCI. 13 (1969)

ATTAPULGITE/PHENOXY

GLASS BEADS/PHENOXY

TG (DEG C)

VOL. % FILLER

461510

K·E 10 X 10 TO THE CENTIMETER 18 X 25 CM.
KEUFFEL & ESSER CO. MADE IN U.S.A.

FIGURE 2

159

FIGURE 3

EPOXY RESIN FILLED WITH MICA FLAKES

ADAPTED FROM
ILSAKI & SHIBAYAMA
J. APP. POL. SCI. 22 (1978)

0% MICA
6.2 VOL. %
16.4 VOL. %
28.6 VOL. %
48.9 VOL. %

FIGURE 4

161
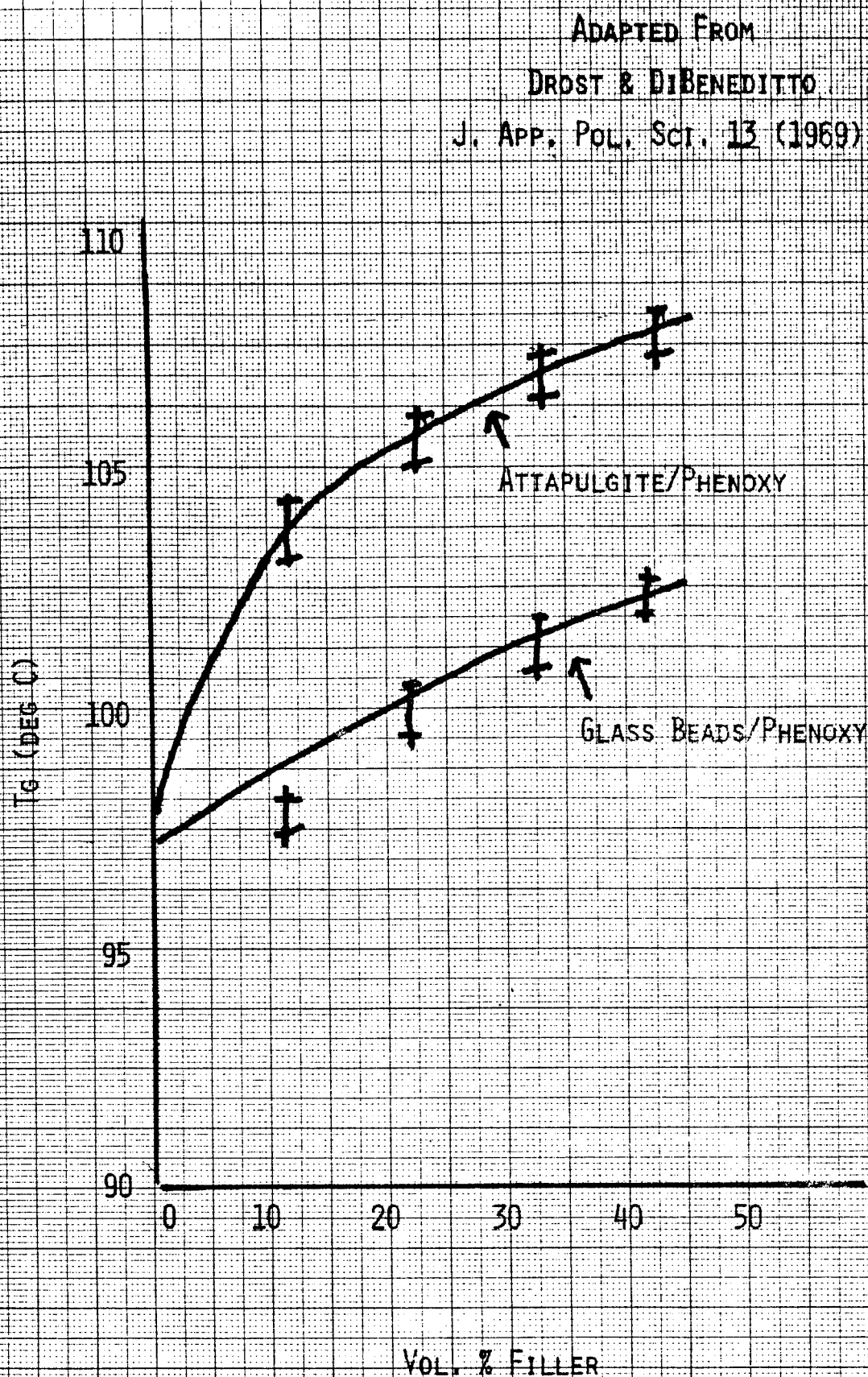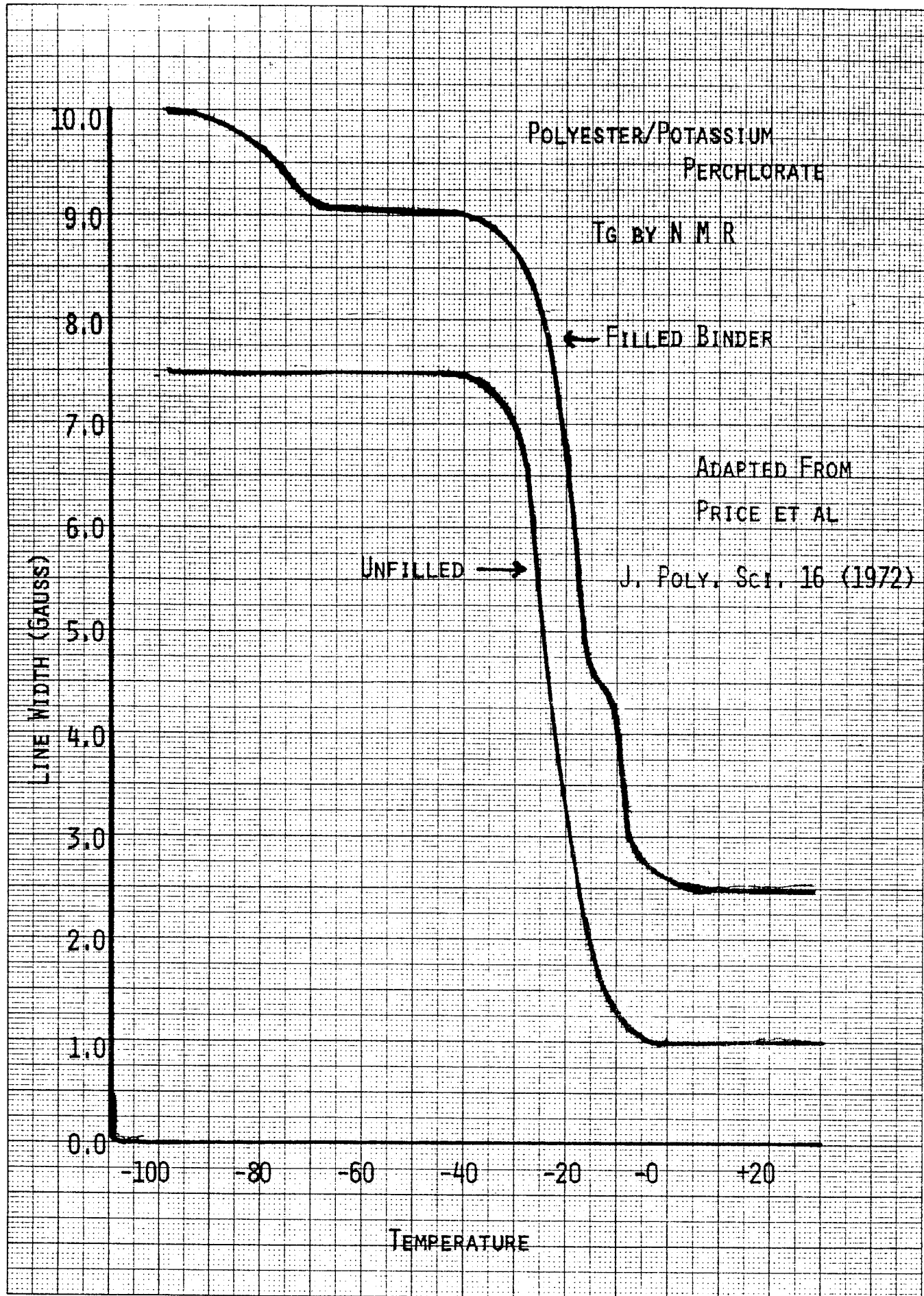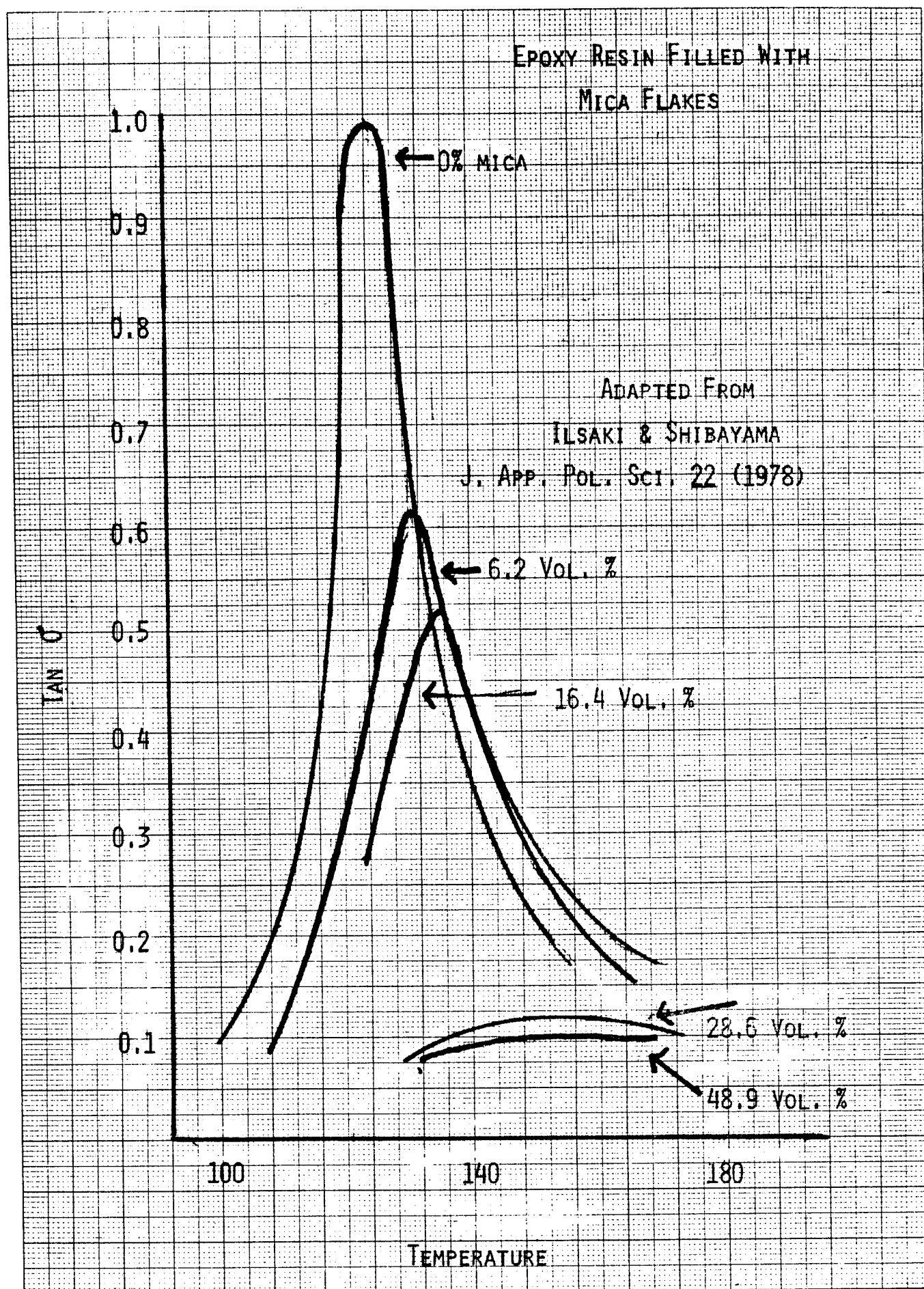
FIGURE 5

Log D vs $\frac{1}{T}$ CO$_2$ – VYHH

X = 19.3 Vol % TiO$_2$

O = 12.9 Vol % TiO$_2$

49°

48°

DIFFUSION COEFFICIENT × 10^9 CM^2/SEC.

$\frac{1}{T}$ × 10^3° K
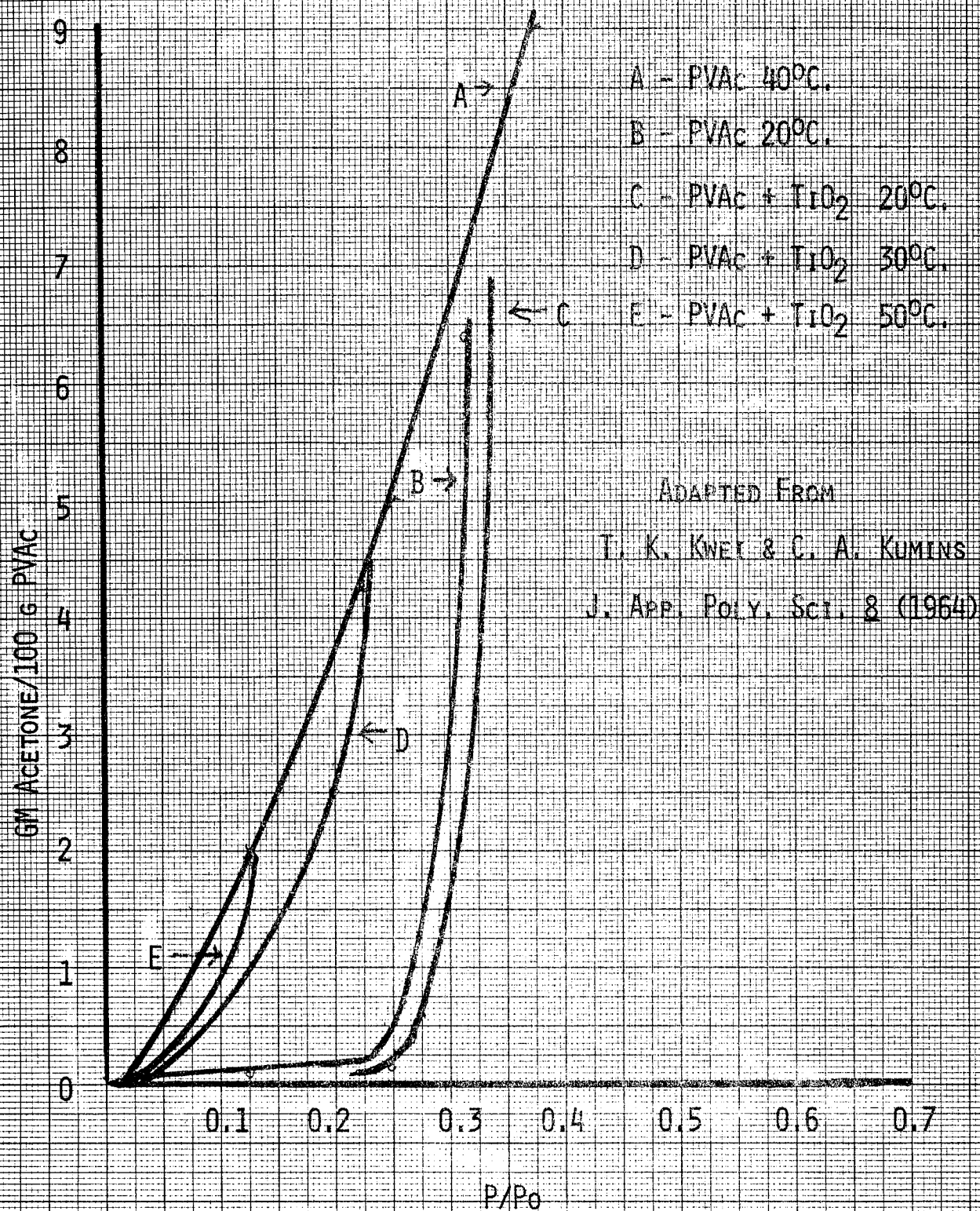
FIG. 8   ACETONE SORPTION OF TiO_2 FILLED PVAc AT DIFFERENT TEMPERATURES
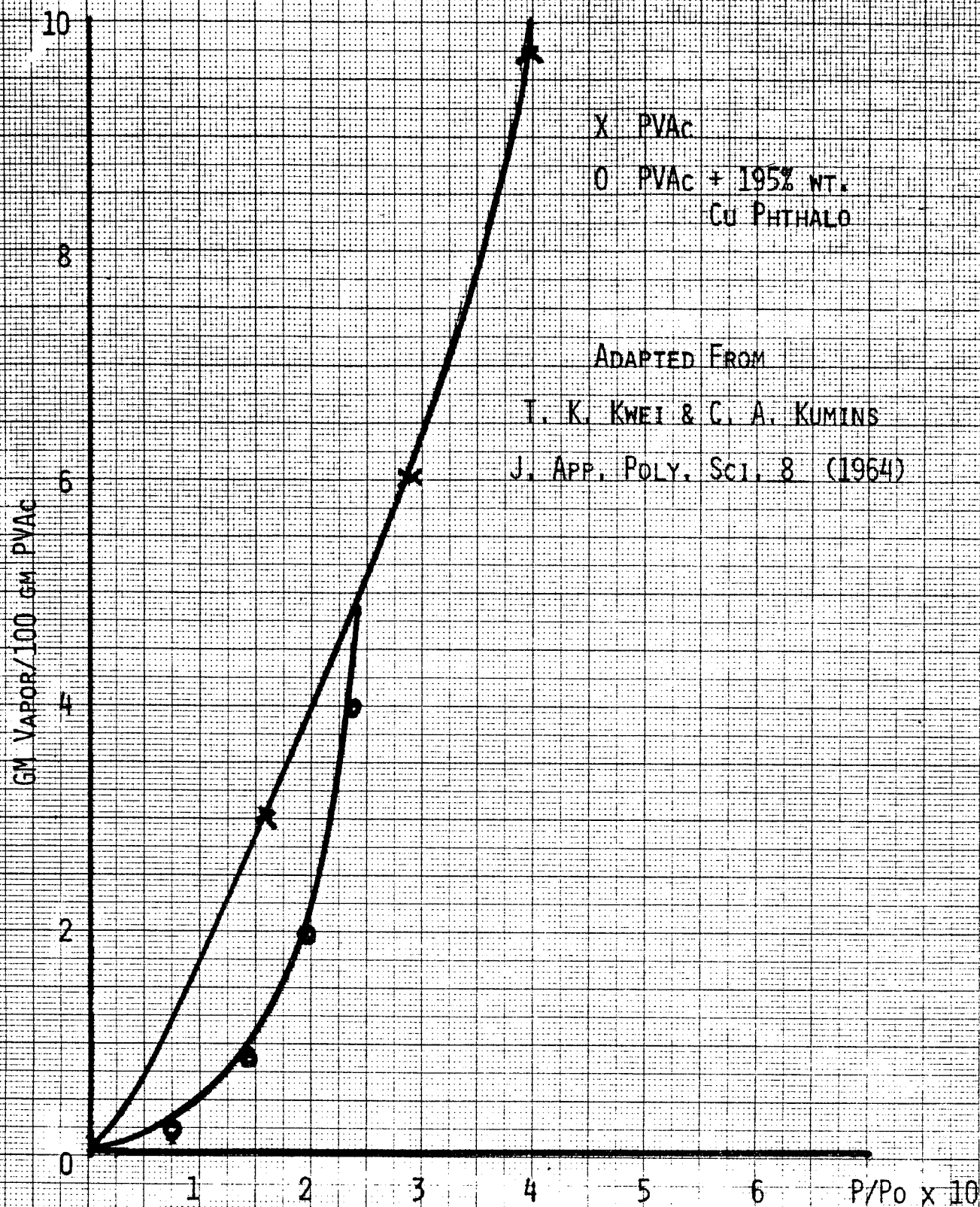
FIG. 7   ACETONE SORPTION PVAC, CUPHTHALOCYANINE

461510

K+E 10 X 10 TO THE CENTIMETER   18 X 25 CM.
KEUFFEL & ESSER CO. MADE IN U.S.A.

164

X Epoxy

O Epoxy + 2.37 wt.% TiO_2

Adapted From

T. K. Kwei & C. A. Kumins

J. App. Poly. Sci. 8 (1964)

P/Po x 10
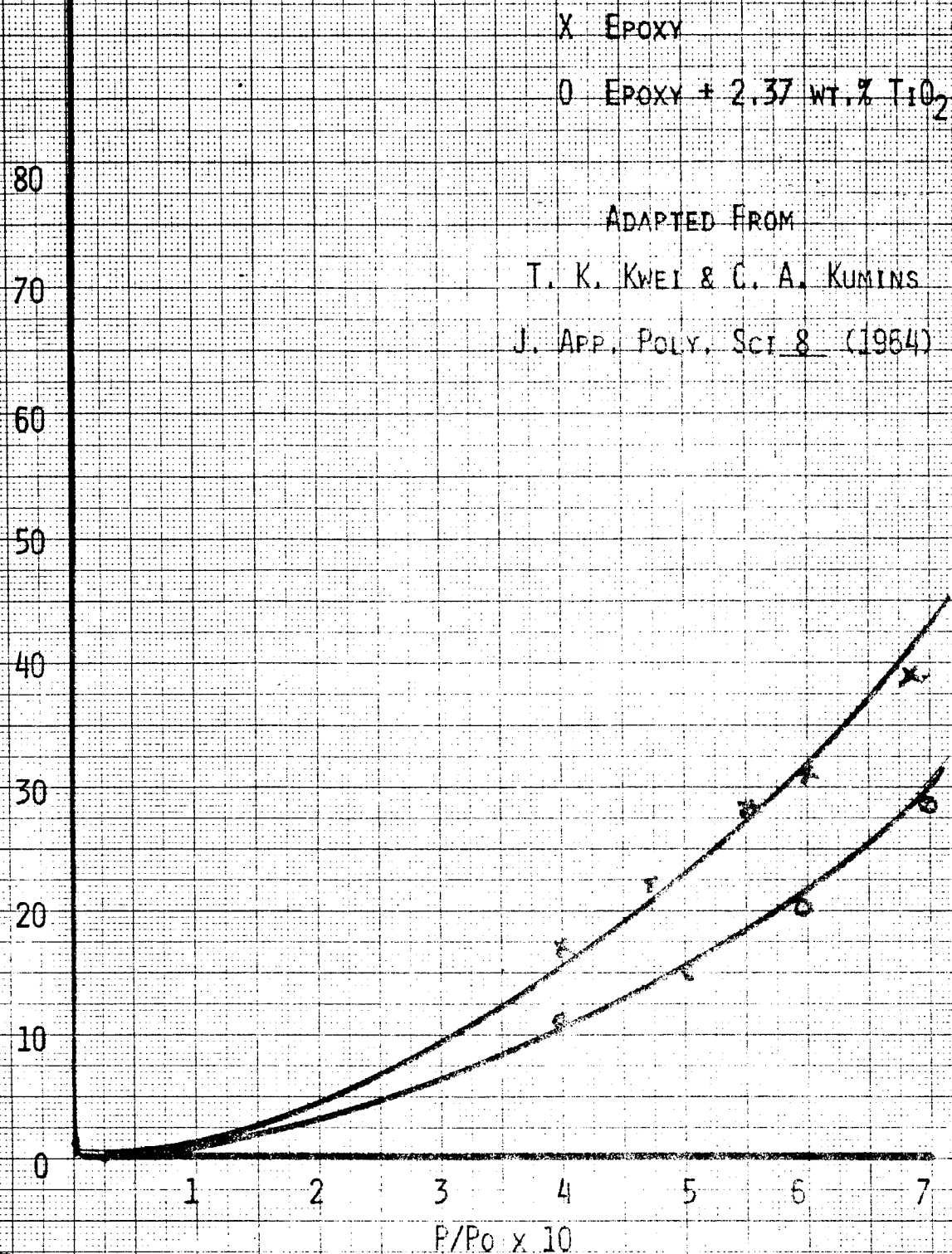
Fig. 8   Sorption of Chloroform by Filled & Unfilled Epoxy

FIGURE 9

ADAPTED FROM
ZIEGEL & ROMANOV
J. APP. POL. SCI. 17 (1973)

KERNER EQ MODIFICATION
REDUCED LOSS MODULUS

$$E''/E_0'' = \left[1 - \phi_F \ B^N\right] - 1$$

B = 3.15

GLASS BEADS

B = 1.1

VITON BINDER

E'/E_0' (REDUCED STORAGE MODULUS)

VOL. FRACTION (ϕ_F)

FIGURE 10

$$E = E_0 \left[1 + 2.5\phi + 14.1\phi^2 \right]$$

$$E = E_0 \left[1 + (2.5 + X)\phi + (14.1 + Y)\phi^2 \right]$$

ADAPTED FROM

GALPERIN & KWEI

J. APP. POLY. SCI 10 (1966)

VOLUME % FILLER × 10^2

SILANE PRIMERS FOR EPOXY ADHESIVES

Dr. Edwin P. Plueddemann
Dow Corning Corporation
3901 S. Saginaw Road
Midland, MI 48640

1. INTRODUCTION

Silane coupling agents are available for improved bonding of mineral fillers and reinforcements to all common thermosetting and thermoplastic polymers(1). A major application for such silanes is as finishes on fiberglass cloth for the production of epoxy laminate circuit boards(2) (Figure 1). The same silanes have been used as additives or primers for structural epoxy adhesives on glass and metals. A study by Andrews(3) shows that silane coupling agents change the rate of deterioration of epoxy-glass bonds by immersion in water, but do not prevent ultimate failure (Figure 2). Rather than to 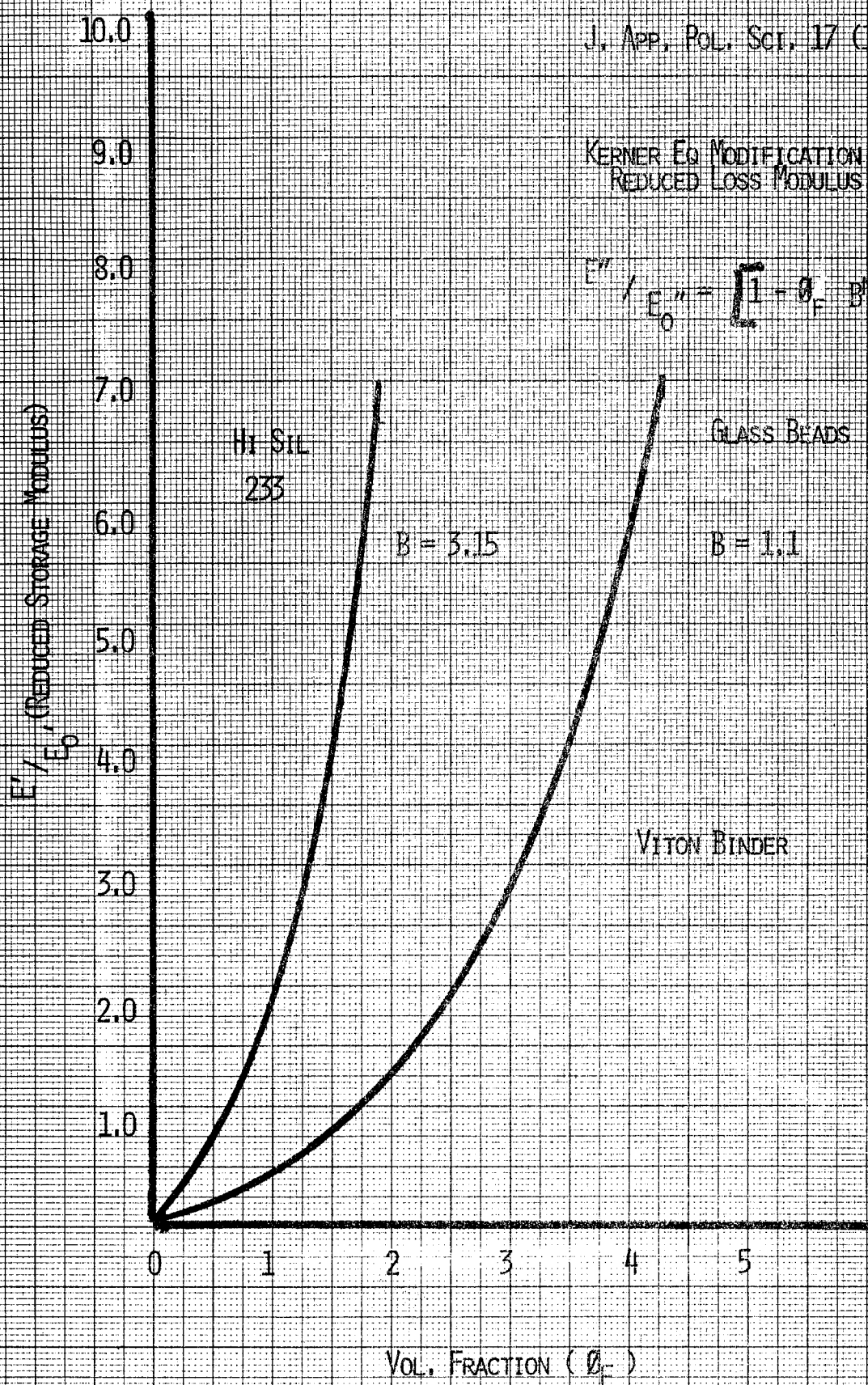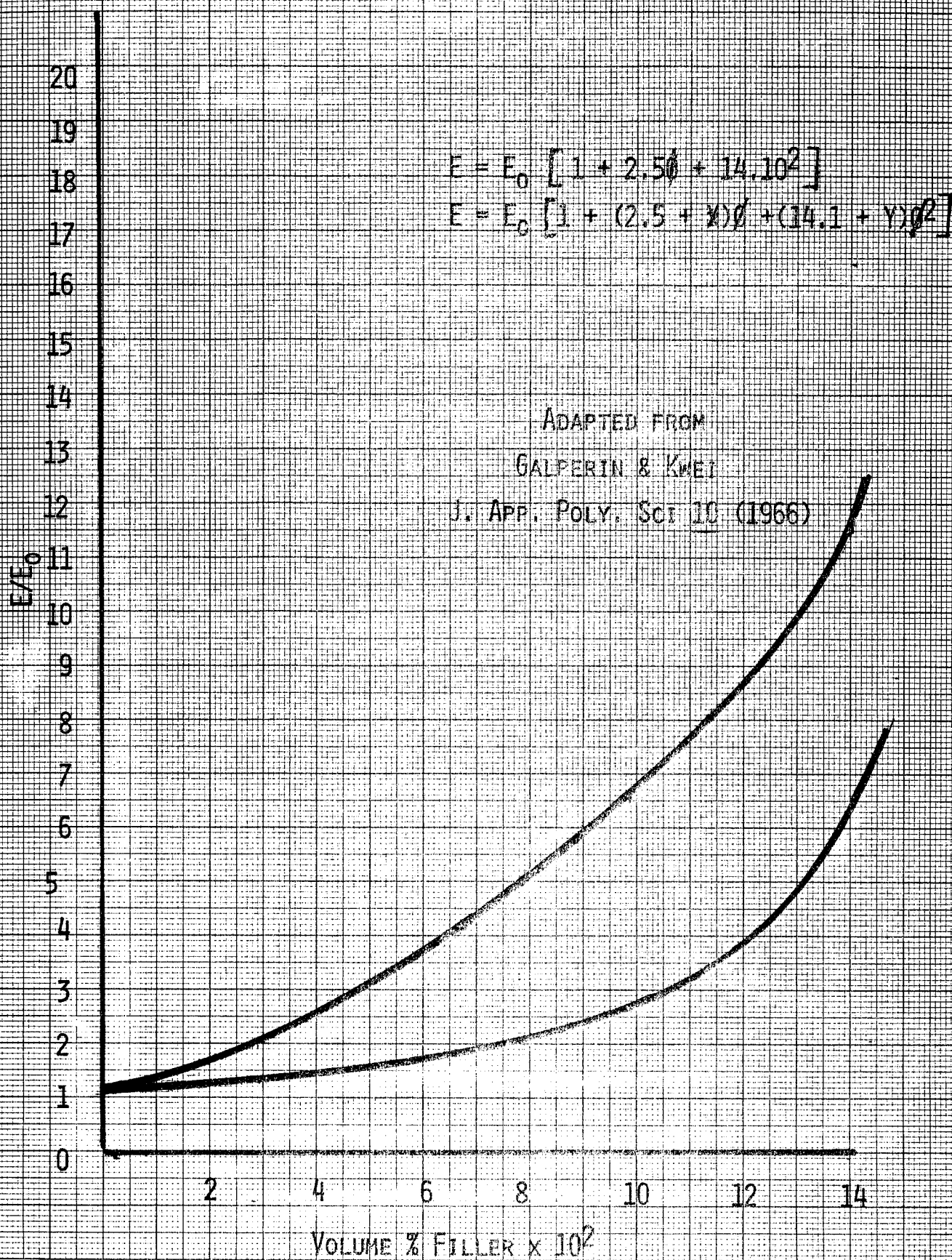attempt to form a perfect bond across a composite interface, it is more practical to design a bond that will be stable under moist conditions for a reasonable time. A goal is set for a bond that is stable for 1000 years under humid conditions at room temperature.

A simple accelerated test for adhesion that is useful for rapid screening of adhesion promoters, is to cure a thin film of polymer on primed glass microscope slides or metal coupons and soak in water until the film can be loosened with a razor blade. Diffusion of water to the interface is almost immediate in this test. Time to failure may differ several thousand-fold between unmodified epoxy adhesives and silane modified epoxies. Further work is planned to correlate results of thin film humidity tests with performance tests under cyclic loading and under conditions of constant creep.

There are a multitude of commercial epoxy formulations using a wide range of curing agents and recommended curing conditions. Each formulation seems to respond differently to silane adhesion promoters so that it is not possible to recommend any silane as 'best' adhesion promoter for epoxies. It is hoped that a series of screening tests with several epoxy formulations might be helpful in suggesting which silanes might be most likely candidates for practical adhesion applications.

2. METHODS

Fisher brand 12-550-11 pre-cleaned microscope slides were used directly from the box. Primers were prepared by diluting commercial silanes to about 20% solids in isopropanol (Table I). Neutral silanes were catalyzed by adding 1% diamino-functional silane (Z-6020) based on total silane. A 2% solution of aluminum secondary butoxide(4) (Chattem Chemical) in toluene was compared with silane primers for some epoxides. Kimwipes tissue paper (Kimberly Clark) were moistened with primers and wiped on the microscope slides or metal coupons to be tested. After 15 minutes at room temperature, an epoxy formulation was troweled on the primed surface with a spatula to give films about 0.2 to 0.5 mm thick. After curing the epoxy, as indicated, the composite was placed in water (70°C or boiling) and tested periodically by attempting to loosen the film with a razor blade. Primers were rated according to the relative length of time the film retained adhesion. Ratings were:

- not recommended, although performance may have been considerably better than a control

+ good, significantly better than the control - as much as a hundred fold increase in time to failure

++ very good, up to a thousand-fold improvement over the control

+++ outstanding, best of the series. When several primers showed no failure they were all rated ++

3. EPOXY FORMULATIONS

A technical grade of diglycidyl ether of bisphenol A, DER 331, (Dow Chemical Co.), epoxy equivalent weight 177-188 was used in all home-made formulations. Curing agents included:

DEH-24 (Dow Chemical Co.)
   Triethylene tetramine
   eq. wt. = 24
DEH-26 (Dow Chemical Co.)
   Tetraethylene pentamine
   eq. wt. = 26
Versamide-125 (General Mills)
   Amine polyamide eq. wt. = 190
DMP-30 (Rohm & Haas)
   tris-dimethylaminophenol used
   at 10 parts per hundred resin
   (phr) for room temperature
   cure
m-phenylenediamine used at 14
   phr
Diaminodiphenylsulfone used at
   33 phr
Dodecenylsuccinic anhydride
   (Humphrey Chemical Co.)
   eq. wt. = 270
Nadicmethylanhydride (Allied
   Chemical) eq. wt. = 180.
   Anhydrides were used in
   stoichiometric amounts

A few commercial epoxy formulations were also tested

Cycom 985   American Cyanimide,
   Wayne, NJ, 60 min, 180°C

EC-2290   3-M, St. Paul,
   Minn., 40 min. at 180°C
Fiberite 976 Fiberite Corp,
   Winona, Minn., 30 min, 180°C
LR 100-713.3 Hysol Div. Dexter
   Corp, Industry, CA, Room
   temp., 14 days
Magnabond 6388.3 Magnolia
   Plastics, Chamblu, GA, room
   temp., 14 days
900000-568 Fenwal Inc.,
   Ashland, MA, room temp., 14
   days
Cyracure Union Carbide Corp.,
   Danbury, CT, U.V. plus 1 hr
   100°C
Gougon Gougon Brothers, Bay
   City, MI, room temp. 4 days
Smooth-on EA-40 Smooth-on,
   Inc., Gillette, NJ, 3 hrs.
   70°C

4. RESULTS

A few typical epoxy formulations with standard curing agents were tested on glass microscope slides as indicated in Table II. Simple amino-functional silanes, which are commonly used as adhesion promoters, are not recommended with most of these formulations. A modified amine functional silane (Z-6032) or a mixture of $PhSi(OMe)_3$, with an aminofunctional silane (X1-6100) are greatly superior for most of the epoxies. Surprisingly good results were obtained with chloropropyl silane (Z-6076) and a silane modified melamine resin (Q1-6106).

Similar tests were run on primed glass and aluminum with six different commercial epoxy formulations with somewhat similar, but better overall results (Table III). High temperature epoxies, in general, gave better bonds than room temperature curing formulations. Rather exceptional adhesion was shown with Fenwal's room temperature curing system on Z-6040 primed glass or aluminum.

After 14 days in boiling water, the aluminum coupon was bent 90" to crack the epoxy coating without loss of adhesion. Hysol, and Magnabond adhesives gave exceptionally good bonds to X1-6100 primer on glass, ceramic or epoxy laminate surfaces. Aluminum butoxide primer was also very good with these epoxies, but not generally useful with other formulations of this series.

Some of the silanes were compared as primers and as additives to Magnabond 6388-3 adhesive on glass (Table IV). Aminosilanes (Z-6020 and Z-6032) were much more effective as additives than as primers. The mixed silane (X1-6100) was very effective as a primer, but not as 1% additive. The major component [$PhSi(OMe)_3$] in X1-6100 would not be expected to be an adhesion promoter unless it was cohydrolyzed with a reactive silane to form mixed siloxane oligomers with reactive sites for bonding.

Silanes were also compared as primers and as additives with Smooth-on EA-40 adhesive cured 3 hours at 70°C on glass (Table V). An aminosilane, Z-6020, was very effective as an additive, but not recommended as a primer. A chloropropyl silane, Z-6076, was very effective as a primer but not as an additive in this system.

Silane additives were studied more extensively in a series of room-temperature curing epoxies supplied by Gougon Brothers (Table VI). Z-6040 seemed to be the best additive, although Z-6020 and Q1-6106 maintained adhesion with two resins to the limit of the test (12 hours in boiling water).

It has recently been disclosed that performance of any silane adhesion promoter can be improved by adding to it a crosslinking silane(5). The compound, bis-trimethoxysilyl-ethane, $(Meo)_3SiCH_2CH_2Si(OMe)_3$, was considered most likely to succeed as a commercial cross-linker and was tested with Z-6020 and with Z-6040 in primers for room-temperature curing epoxies (Table VII). With this crosslinker, it was possible to formulate primers that provided bonds that resisted 70°C water for over a week. Z-6040 required less crosslinker than did Z-6020 to provide water-resistant bonds to glass. The crosslinker, itself, was a creditable adhesion promoter in these systems, although it is not effective alone with some polymers.

Mixtures of crosslinker with diamine-functional silane, Z-6020, were used as sole curing agents for epoxy adhesives bonded to glass and to steel. Z-6020, itself, provided better adhesion than the simple aliphatic amine $C_8H_{17}NHCH_2CH_2NH_2$ of comparable functionality and molecular weight. Water resistance of bonds was improved significantly more by adding crosslinker to Z-6020 curing agent (Table VIII).

Ultraviolet light-cured cyclo-aliphatic epoxide formulations are available from Union Carbide Corp. These materials use arylsulfonium salts as initiators that are stable under normal conditions but release cationic initiators (BF_3 or PF_5) when exposed to ultraviolet light(6). In the presence of generated cationic species, very rapid polymerization takes place.

170

Two formulations were tested with silane adhesion promoters as primers and or additives.

ordinary temperatures and humidities. More severe tests (e.g., pressure cooker,

	Mix A (Hard)	Mix B (Flexible)
Cyracure Resin UVR-6110	96	67
Cyracure Flexibilizer UVR-6351	–	29
Cyracure Initiator UV1 6990	4	4

Thin films (0.1 to 0.5 mm) on glass, aluminum and steel were passed under twin UV lamps (intensity 30.92 Mw/cm^2) through a 61.25 cm path at a rate of 10 feet per minute. Films were tack-free, but were generally given an after cure of one hour at 100°C. Of the standard silanes tested, all amino-functional silanes were completely unsuited since they inhibited the cure. Of the other silanes, several showed significant improvement in adhesion to glass (Table IX). Unprimed adhesion to aluminum was fairly good and further improved by adding 1% silane to the formulation. None of the films retained adhesion very well to steel in 70°C water (Table X). Fluoride ions derived from the initiator may be detrimental for bonding to glass and steel, while they may benefit adhesion to aluminum by producing an insoluble aluminum fluoride surface.

retention of electrical resistivity, etc.) will be needed to establish the limits of some of the better systems.

Adhesion to metals other than aluminum and steel should be studied, although experience suggests that silane adhesion promoters are effective on all structural metals including nickel, magnesium, silver and gold.

5. CONCLUSIONS

Water resistant bonds are possible between epoxy adhesives and glass or metals with the use of proper silane adhesion promoters. Accelerated tests on thin films of adhesive on glass and metal often provide over a thousand-fold improvement over unmodified adhesives. This extrapolates to structural adhesive systems that can be guaranteed to resist delamination by moisture for a thousand-year exposure to

VI.   REFERENCES

1. E. Plueddemann, "Silane Coupling Agents", Plenum Press, New York (1982).
2. E. Plueddemann, Finishing Glass Reinforcements for Epoxy ' Circuit Boards, Moscow Electrochemical Conf., June, 1977.
3. E. Andrews, H. Sheng, H. Majid and C. Vlackos, "Environmental Failure of Adhesive Bonding in Composites", Final Report, U. S. Army Grant No. DAERD/78/G/118, May, 1981.
4. R. Pike and F. Lamm, Proc. ACS Div. Polym. Mater. Sci. and Eng. 56 199 (1987).
5. E. Plueddemann and P. Pape, 42nd Ann. Conf. Comp. Inst., Soc. Plast. Ind. 21-E Feb., 1987.
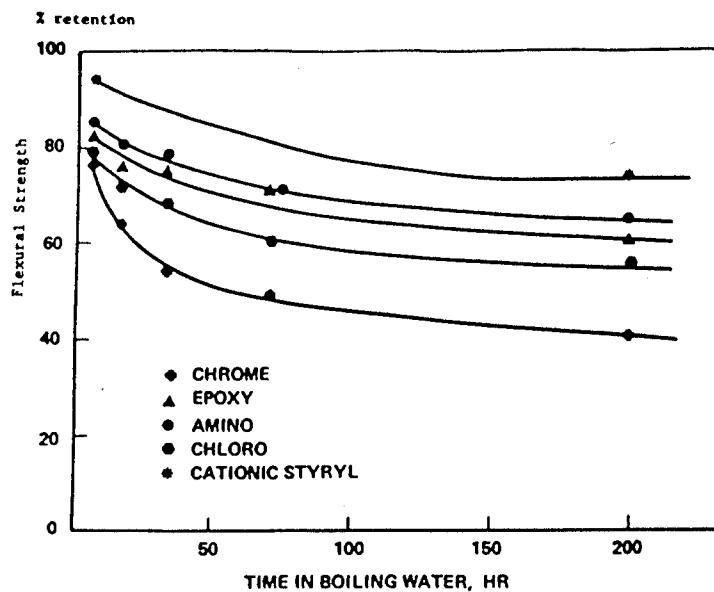6. J. Koleske, Soc. Manuf. Eng., Techn. Paper FG85-798 (1985).

% retention

Figure 1. The effect of boiling water on flexural
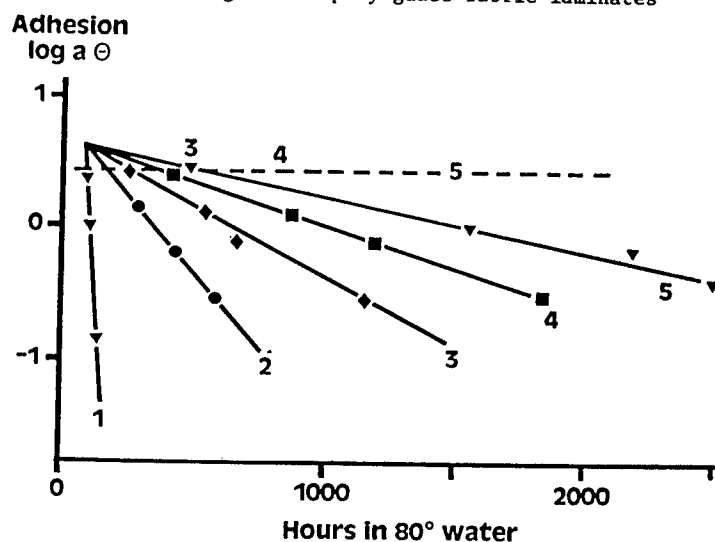strengths of epoxy-glass fabric laminates

Adhesion
log a ⊖

Figure 2. Pyrex blocks bonded with silane-modified epoxy

(1) no silane, (2) 0.05% Z-6040, (3) 0.05% Z-6020

(4) 0.10% Z-6040, (5) 1.0% A-1100

Broken line indicates time for transition from cohesive to
adhesive failure

  a = plasticiztion factor for epoxy saturated with water

  θ = adhesive energy (J m^{-2})

Commercial D. C. Designation	Organofunctional Group on Silicon
Z-6020	Ethylenediamine
Z-6030	Methacrylate
Z-6032	Cationic Styryl
Z-6040	Epoxy
Z-6062	Mercaptopropyl
Z-6076	Chloropropyl
Z-6011	Primary Amine
Q1-6106	Silane-modified Melamine Resin
X1-6100	9/1 mix $PhSi(OMe)_3$/Z-6020
$Al(O-s-Bu)_3$	Non-silane
Q9-6300	Vinyl

TABLE I.
Representative Silane Adhesion Promoters

Primer/Cure	DETA r.t.	TEPA 80°C	DMP-30 r.t.	Versamic r.t.	Nadic-Me Anh. 150°	mPDA 150°	DADPS 180°
Z-6020	-	-	-	+	-	+	-
Z-6030	++	-	+	-	+	++	+
Z-6032	+	++	+++	+	+	++	++
Z-6040	+++	++	+	++	+	++	+
Z-6062	++	+	-	+	-	+	+
Z-6076	++	+++	+	+	+	+++	+++
A-1100	-	-	-	-	-	-	-
X1-6100	++	+	++	-	+	++	+
Q1-6106	++	++	++	+++	+++	-	-
Al(s-BuO)$_3$	+					-	-
Limits of H_2O	-------- 7 days at 70°C ------				14 days	7 days at 70°C	boil

TABLE II.
Silane Primers for Epoxies on Glass

Commercial	Hysol LR 100-713.3	Magnabond 6388-3	Amer. Cy. 985	3-M EC-2290	Fiberite 976	Fenwall 900000-568 to glass	to Al
Cure Conditions	14 days r.t.		150°C	180°C	175°C	r.t. 3 days	
Silane Primer							
Z-6020	+	+	-	++	++	+	-
Z-6030			++	++	++		
Z-6032	++	++	++	++	+	+	-
Z-6040	+	+	++	++	++	+++	+++
Z-6062	+	+	++	++	++		
Z-6076	+	+	++	++	++		
A-1100	-	+	++	+	+		
X1-6100	+++	+++	++	+	++	++	++
Q1-6106	+	+	++	-	+	++	++
Al(OsBu)$_3$	++	++	-	-	+		
Limits of H_2O Test	15 days 70°C	24 days 70°C	14 days boil	14 days boil	14 days boil	24 days boil	

TABLE III Silane Primers for Commercial Epoxy Formulations (on glass)

Silane	Primer	1% Additive
Z-6020	+	+++
Z-6032	+	++
Z-6062	+	−
X1-6100	+++	−
Q1-6106	+	+

TABLE IV.
Compare Silane Primers to Additives
(Magnabond 6388-3 to Glass)

Silane Adhesion Promoter	Primer on Glass	2% Additive to Resin
Z-6011	−	
Z-6020	−	++
Z-6030	+	
Z-6040	++	++
Z-6062	+	
Z-6076	++	−
X1-6100	++	+
Q1-6106	−	−

TABLE V.
Smooth-on EA-40 Cured 3 Hrs. at 70°C
on Glass (Relative Adhesion in
70°C Water)

Epoxy/Hardener[1]	105/205	105/206	XA-3100/XG1A	XA-3134/XG1B
1% Silane Additive	Time to Failure in Boiling Water (Hours)			
None	0.1	0.05	1	1
Z-6020	12	6	c	c
Z-6040	c	c	c	c
X1-6100	1	4	6	12
Q1-6106	6	6	c	c

c = no failure in 12 hours (tests discontinued)
(1) Products of Gougon Brothers, Bay City, Michigan

TABLE VI. Silane Additives to Commercial Epoxies on Glass
(Cure 4 days at Room Temperature)

Primer on Glass	Polyamide	DMP-30	DEH-24
None	<1	<1	<1
Z-6020	1	1	1
9/1 Z-6020-Bis	2	3	1
.8/2 "	2	3	1
6/4 "	3	3	2
1/1 "	4	4	8
1/9 "	c	c	c
Bis-alone	c	6	c
Z-6040	c	8	c
9/1 Z-6040-Bis	c	36	c
8/2 "	c	c	c

Bis = $(CH_3O)_3SiCH_2CH_2Si(OCH_3)_3$
c = No failure after one week in 70°C water

TABLE VII. Room-Temperature-Cured Epoxy Films on Glass
(Hours in 70°C Water to Lose Adhesion)

(Stoichiometric Mix with DER-667 Cured 4 Hrs. at 70°C)

Composition of Curing Agent	Adhesion to coupons in 70°C Water	
	C. R. Steel	Glass
Aliphatic diamine (no Si)	<4 hours	2 hours
Z-6020	2 days	1 day
9/1 Z-6020/crosslinker	3 days	2 days
1/1 " "	5 days	2 days
1/9 " "	>5 days	<5 days

TABLE VIII.
Aminosilane Mixtures as Curing Agents for
Adhesion to Steel and Glass

Silane Primer on Glass	Rigid formulation	Flexible formulation
None	15 min.	15 min.
Z-6030	4 hrs.	30 min.
Z-6040	4 hrs.	2 hrs.
Z-6062	1 hr.	2 hrs.
Z-6076	30 min.	2 hrs.
ViSi(OCH$_3$)$_3$	6 hrs.	4 hrs.
Al(OR)$_3$	30 min.	30 min.

Table IX. Cyacure (UV curable) Epoxies on Glass
(UV Exposure + 1 Hr. 100°C Oven)

Time for loss of adhesion in 70°C water

1% Additive to Formulation	Time for loss of adhesion in 70°C water					
	Rigid formulation			Flexible formulation		
Unprimed	Glass	Aluminum	c.r. Steel	Glass	Aluminum	c.r. Steel
None	15 m.	6 hr.	30 m.	15 m.	4 hr.	15 m.
Z-6030	30 m.	C	1 hr.	1 hr.	1 day	1 hr.
Z-6040	2 hr.	C	1 hr.	30 m.	C	30 m.
Z-6076	2 hr.	C	1 hr.	1 hr.	4 days	1 hr.
ViSi(OCH$_3$)$_3$	2 hr.	C	2 hr.	6 hr.	C	90 m.
(CH$_3$O)$_3$SiCH$_2$CH$_2$Si(OCH$_3$)$_3$	6 hr.	C	1 hr.	2 hr.	C	1 hr.
Q1-6106	1 hr.	4 days	30 m.	45 m.	6 hr.	15 m.

C = adhesion good after 4 days in 70°C water

Table X. Cyacure (UV curable) Epoxy on Glass, Al, and c.r. Steel
(UV exposure + 1 hr. 100°C postcure)

Inorganic Adhesive Primers:
Adhesive Bonding To Titanium

R. A. Pike, F. P. Lamm and J. P. Pinto
United Technologies Research Center
East Hartford, CT 06108

ABSTRACT

The use of inorganic primers in adhesively bonded joints offers an alternate approach to standard resin based organic primers or coupling agents for improving the environmental resistance of bonded structures. The inorganic primers investigated to date, formed by hydrolysis of metal alkoxides on a treated adherend surface are equally effective after room or elevated temperature conversion to the hydrated oxide form indicating potential application for field repair situations. Surface analysis suggests that the resulting primer when formed on aluminum is a stable form of an amorphous Boehmite $[Al(O)OH]x$ which can form on exposure of the alkoxide to limited amounts of moisture. Examples demonstrating the influence of adhesive composition and metal surface treatment for titanium adherends on the effectiveness of inorganic primers are presented and possible causes for use of preferred combinations discussed.

1. INTRODUCTION

As the recognized advantages of adhesively bonded structures, including weight and manufacturing cost benefits, lead to increased use of these systems in the automotive, aircraft, aerospace and marine associated industries the need to achieve improved levels of environmental and temperature resistance is a challenge to both adhesion and surface scientists as well as the manufacturing engineer.

Bond integrity is associated

with the interfacial adhesion in a bonded joint and related to oxide hydrolyic stability, which is generally believed to be the limiting factor in bond durability.[1] Thus, improvements in oxide stability usually result in improved durability as measured by wedge crack tests. Such improvements for aluminum which have been reported to date include coating Forest Products Laboratory (FPL) acid-treated surfaces with phosphorous nitrilo compounds[2] and phosphoric acid dip treatments on chromic acid anodized (CAA)[2] and sulphuric acid anodized (SA)[3] surfaces. These post-anodizing treatments do not alter the rough topography (in fact, they enhance the surface roughness)[3] of the anodized surfaces, in marked contrast to the generation of a relatively smooth oxide surface when the inorganic amorphous primer is employed. Surface treatments for titanium alloys have also been evaluated and ranked in terms of moisture resistance.[4] Those which form micro rough surfaces such as CAA or sodium hydroxide anodizing methods have been found to be superior to acid etching procedures such as phosphate fluoride.

An investigation of the effect of substituting the normally used organic primer in a bonded system with an amorphous aluminum oxide primer was undertaken at UTRC to determine if the application of a relatively smooth pristine oxide coating on a treated surface would effectively function as a primer in an adhesively bonded structure.

The objectives of the investigation are (a) to find an effective primer system which eliminates the use of environmentally undesirable chromium containing compounds (b) improve the environmental resistance of bonded

structures and, (c) define, if possible, the relative roles of mechanical interlocking, chemical bonding and physical forces (acid-base interaction) in adhesion and determine the factors which control these phenomenon in bond formation.

The effect of substituting the normally used organic primer with an amorphous inorganic aluminum oxide primer on the tensile lap shear and T-peel strength of adhesively bonded aluminum was shown to result in equivalent wet and dry strengths for both primer systems.[5] This result was not predictable based on the relatively smooth topography of the inorganic-primed surface since the honeycomb-whisker protrusions related to enhanced bond strength in phosphoric acid anodized (PAA) systems compared to FPL etch treatments, were not available to provide a high degree of mechanical interlocking.[5]

Evidence that the inorganic concept is capable of improving the environmental stability of adhesively bonded titanium adherends has been reported.[6] The extent of improvement over a non-primed adherend was shown to be dependent on the surface treatment employed.

A preliminary hypothesis in the use of inorganic primers on metal oxide surfaces was that the most effective alkoxide would be the material which matched the adherend surface oxide, i.e. titanium alkoxides would be superior to aluminum alkoxide on titanium adherends. In some instances, this has not proven to be the case. Studies at Virginia Tech[6] have shown that the primer generated from aluminum alkoxide was markedly more effective as an inorganic primer than a titanium alkoxide for bonding titanium 6-4 wedge specimens which were treated with phosphate fluoride etch.

This paper presents evidence relating to the effect of one surface treatment, Pasa-Jel 107, on the effectiveness of these same inorganic primers to improve adhesion of epoxy and polyimide bonded titanium joints.

2. EXPERIMENTAL PROCEDURES

Titanium 6-4 alloy was solvent cleaned, grit blasted and etched 20 minutes using Pasa-Jel 107 from SEMCO Div. of Products Research & Chemical Corp. The inorganic primer was formed by applying a one percent toluene solution of E-8385 sec-butyl aluminum alkoxide or n-butyl titanium alkoxide from Stauffer Chemical Co. to the treated surfaces. The alkoxide was converted to oxide primer by heating at 100°C for 30 minutes. Hysol EA-9205, American Cyanamid BR-161 epoxy and LARC-TPI polyimide primers were used for control samples.

Adhesively bonded joints were prepared using scrim supported Hysol EA-9649, American Cyanamid FM300 and FM330 and LARC-TPI prepared as described by Progar.[7] Wedge crack tests were carried out according to ASTM D-3762 at 71°C/95% relative humidity. Exposure times ranged up to 175 hrs. Crack lengths were measured under 20X magnification in millimeters.

Contact angles of each neat resin were measured from enlarged photographs of sessile drops obtained by heating droplets deposited on the metal treated surface up to 177°C with and without inorganic or organic primer coatings.

3. RESULTS AND DISCUSSION

3.1 Epoxy Adhesives

The use of the Pasa-Jel 107 etch treatment with the Hysol EA-9649 adhesive gave a substantial improvement in crack propagation compared to the phosphate/fluoride etch with the aluminum

and titanium based inorganic process. As with aluminum the inorganic primed adherends were superior to the organic epoxy Hysol EA-9205 primer. The results of these tests are shown graphically in Fig. 1. The failure mode of the organic primed specimens was adhesive between adhesive and primer; the inorganic primed specimens failed adhesively with tearing in the scrim cloth.

It was anticipated that since the inorganic primer surface probably consists of a high degree of Al-OH or Ti-OH units compared to the surface generated by the Pasa-Jel treatment that there may be a variation in response of adhesive systems in terms of wetting and spreading which would ultimately affect the level of adhesion as has been reported for aluminum/adhesive systems.[8]

Two other adhesive systems, FM-300 and FM-330 have been evaluated on titanium inorganic primed adherends using BR-161 organic primer as the control. The wedge crack test results are listed in Table I and II respectively.

These results showed that with the FM-300 adhesive the aluminum alkoxide primer was superior to the titanium but slightly poorer than the organic BR-161 system. This suggested that the adhesive wet and spread easier on the acid etched surface than on the alkoxide primed surfaces.

These results showed that the FM-330 adhesive gave improved results with the inorganic primer compared to FM-300 and using 1-2 coats was slightly superior to the organic BR-161. Tests run with EA-9649 adhesive using the aluminum alkoxide primer showed essentially the same difference in crack propagation between 1 and 4 coats of the primer.

181

TABLE I

Wedge Crack Propagation with FM-300 Bonded Titanium[a]

Primer	α_o (mm)	Crack Propagation (mm)[b]
BR-161	27	6.0
Al alkoxide	29	10.0
Ti alkoxide	30.5	18.6

a. Pasa-Jel 107 etched.
b. Values average of 3 tests; in general ±1.0 mm spread; tested at 71°C, 95% RH, 270 hours.

TABLE II

Wedge Crack Propagation with FM-330 Bonded Titanium[a]

Primer	α_o (mm)	Crack Propagation (mm)[b]
BR-161	31.0	5.8
Al alkoxide[c]		
1 coat	34	4.6
2 coats	33	4.6
3 coats	33.6	6.6
4 coats	35	7.2

a. Pasa-Jel 107 etched
b. Values average of two tests, in general ±1.0 mm spread; tested at 71°C, 95% RH for 173 hours.
c. Each coat ≅ 150 nm thickness.

To determine if composition of the two American Cyanamid adhesives might play a role in the ability to wet and spread on titanium treated and primed surfaces a series of sessile drop measurements was carried out. FM-330 is an aluminum filled, dicyandiamide/diaminodiphenyl sulfone cured adhesive which contains a rubber additive which is prereacted with either the

base epoxy resin or the brominated epoxy present in the formulation. FM-300 is a titanium oxide filled adhesive cured with the same catalyst system. Both films are supported on a polyester open net weave scrim cloth. There is more rubber additive in the FM-300 than the FM-330. The two film adhesives were solvent extracted (to separate the filler and support scrim) and taken to dryness under vacuum. Small circular drops of the resulting semi-hard resins were deposited on the respective surfaces. The almost solid drops were heated to 177°C and the resulting angles of the melted resin determined. The results are listed in Table III.

The data indicated that without primer the FM-330 wetted the treated titanium surface better than FM-300. The latter can be considered to be essentially a nonwetting condition. With the organic primer both resins gave the same low contact angle which was slightly less than the three resins on the aluminum alkoxide inorganic primer. Since the results indicated good spreading and wetting capability of the two adhesives on the inorganic primed surfaces the reason for lower crack propagation performance for the FM-330 on inorganic primed titanium remains to be determined. One possible explanation may be that in FM-300 the high level of rubber additive may impede the level of direct chemical or acid/base interaction which may occur between resin and primer. However, in direct contrast it has been found that with inorganic primed 6061 aluminum alloy adherends both resins gave very low cohesive crack propagation (1-2 mm in 160 hours) values. Clearly, additional investigation must be carried out to understand the alloy and adhesive composition,

surface oxide moisture content, and surface treatment effects which control the function of inorganic primers.

3.2 Polyimide Adhesives

LARC-TPI has shown promise as a high temperature adhesive for applications in aircraft and spacecraft.[9,10] It was of interest to determine the wedge crack response of this adhesive to inorganic primers. The unfilled scrim supported adhesive was used to bond Pasa-Jel treated titanium adherends.

The results of several tests are listed in Table IV.

TABLE III

Contact Angles of Epoxy Resin on Titanium Surfaces

Surface Treatment	Adhesive	Sessile Drop[a] Angle,°
Pasa-Jel 107	FM-300	91
Pasa-Jel 107	FM-330	32
PJ-Al alkoxide	FM-300	38.5
	FM-330	34
	EA 9649	38
PJ-BR-161	FM-300	30
	FM-330	29.5

a. Angles measured from photographs of sessile drop.

TABLE IV

Wedge Crack Propagation with LARC-TPI Bonded Titanium[a]

Primer	α_o (mm)[b]	Crack Propagation (mm)[b]	Failure Mode
LARC-TPI	27-30	15-17	adhesive/cohesive
Al-alkoxide	27-29	6.2-9.5	cohesive failure
Al-alkoxide (modified)	28	7.0-9.0	cohesive failure, torn scrim
Ti-alkoxide	27-31	9.5-12.7	cohesive failure

a. Pasa-Jel 107 etched
b. Range of four tests

These results indicate that the inorganic primer approach has the potential to improve the environmental resistance of polyimide adhesive bonded specimens particularly at elevated temperatures due to the demonstrated heat stability of the inorganic primer.

4.0 SUMMARY AND CONCLUSIONS

Preliminary studies have shown that inorganic primers impart environmental resistance to adhesively bonded titanium. There appears to be a greater affect of titanium surface treatment on the performance of the inorganic primer in contrast to aluminum adherends. The application of inorganic primers to polyimide adhesively bonded systems has been demonstrated. Wetting measurements by themselves are not sufficient to explain the difference found between various adhesives when used with the inorganic primer.

REFERENCES

1. Handwick, D. A., Ahearn, J. S., and Venables, J. D., Material Sci., $\underline{19}$, 223 (1984).

2. Poole, P. and Watts, J. F., Int. J. Adhesion and Adhesives, $\underline{5}$, 33 (1985).

3. Arrowsmith, D. J., and Clifford, A. W., Int. J. Adhesion and Adhesives, $\underline{5}$, 40 (1985).

4. Brown, S. R., 27th National SAMPE Sym., May 4-6, 1982, p. 363.

5. Pike, R. A., Int. J. Adhesion and Adhesives, $\underline{5}$, 3 (1985).

6. Filbey, J. A. and Wightman, J. P., Abstract 9th Annual Meeting of the Adhesion Society, Feb. 1986, p. 25a.

7. Progar, D. J., Int. J. Adhesion and Adhesives, $\underline{6}$, 12 (1986).

8. Pike, R. A., Adhesion Sci. Rev., Center for Adhesion Science Virginia Tech, Blacksburg, VA, May 3, 1987.

9. St. Clair, A. K. and St. Clair, T. L., SAMPE Quarterly, 13, 20 (1981).

10. Progar, D. J. and St. Clair, T. L., Proc. 7th Nat. SAMPE Tech. Conf., 7, 53 (1975).

INORGANIC PRIMER ON TITANIUM 6-4

Wedge crack test

Primer		a_0, mm	
⊙	EA 9205	57.2	Etch: Pasa-Jell 107
——	Al alkoxide	31.1	Adhesive: EA 9649
——	Tetra butyl titanate	32.0	Adherend: Titanium 6-4

⊙ (57)

Crack propagation, mm

Time at 71°C, 95% RH, hrs.
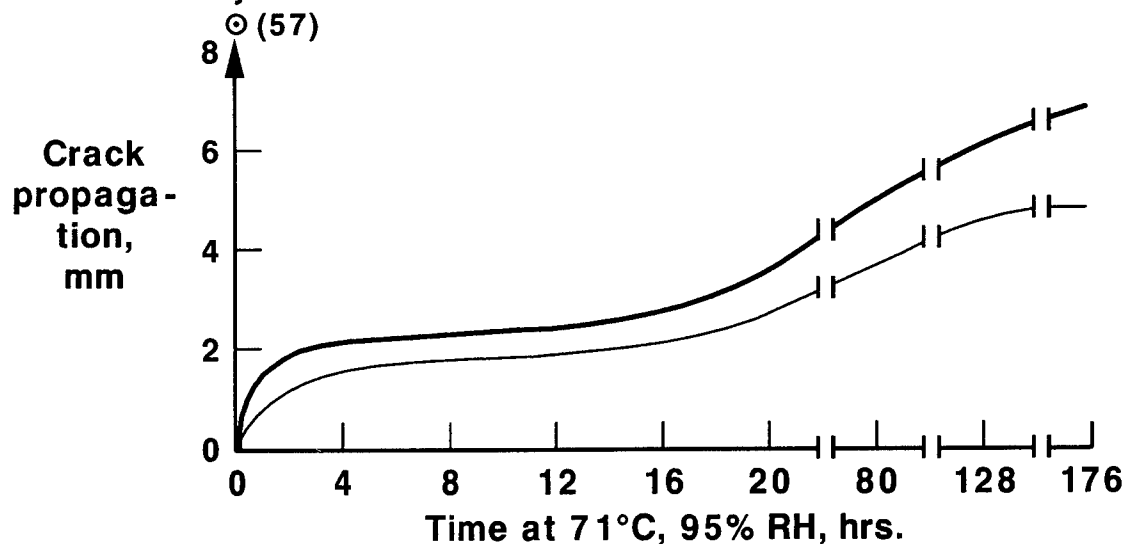
ADHESIVE BONDING OF SiC-REINFORCED ALUMINUM ADHERENDS

D. McNamara, A. Desai and T. Fritz
Martin Marietta Laboratories
1450 South Rolling Road
Baltimore, Maryland 21227

1. INTRODUCTION

Full utilization of the improved stiffness and strength of SiC-reinforced aluminum requires developing effective means of joining pieces together. Welding and brazing techniques are difficult to apply to some geometries,(1) and frequently compromise the properties of the joint. For many applications, adhesive bonding would be an ideal solution; however, no surface perparation treatment has been developed for SiC-reinforced aluminum. Conventional aluminum treatments produce extremely small oxide protusions that serve to "mechanically interlock" the adhesive to the surface. Since the nature of the surface oxides produced by these treatments strongly affects the durability of the structural bonds,(2) the presence of SiC in the aluminum matrix could result in severe bonding problems. Our study compared bonding properties of standard 6061 aluminum substrates with those of both particle- and whisker SiC reinforced 6061 aluminum to determine whether structural adhesive bonds could be made with SiC/Al and which bonding treatments would be most suitable.

2. TEST PROGRAM

A four-phase test program was designed to rapidly assess the potential of a variety of common surface-preparation treatments for aluminum bonding when applied to SiC/Al. In the first phase, electron microscopy was used to study the effect of treatment parameters on surface oxide morphology to rapidly assess which treatments might be suitable for SiC/Al. In the second phase, double-lap-shear specimens were used to measure dry tensile strengths of bondments selected to further evaluate pre-treatment processes. In the third phase, wedge tests were conducted to select the best treatment/adhesive combination for use in phase four, which consisted of extended durability testing using salt-spray-exposure to evaluate retained strength, and stressed-durability test coupons.

3. RESULTS

3.1 Phase I - Morphology Examination

Nine different surface treatments were used to prepare SiC/Al surfaces for morphological examination using the high-resolution scanning mode of a scanning transmission electron microscope. The treatments studied are listed in Table 1. Previous work with ordinary aluminum alloys was used for benchmark comparisons.(2,3) The treated surfaces of the whisker- and particle-reinforced materials generally had similar oxide morphologies. Although both materials exhibited a partial coverage of the surface by SiC residue, the surface of the whisker-reinforced SiC/Al appeared to be covered more completely due to the whiskers' greater surface area per volume.

We varied the processing parameters to reduce the degree of residue coverage and to improve the completeness and depth of the oxide coating. We found that residue coverage was directly related to the degree of chemical etching performed. Unlike chemical cleaning, mechanical removal effectively eliminated SiC residue. Therefore, we used solvent wipe followed by grit-blast cleaning as the initial treatment for all processes listed in Table 1 and did not use any chemical etches before the final treatments.

The treatments studied fall into four categories: mechanical cleaning, chemical cleaning, bonding etches, and anodizations. Grit-blasting is generally regarded as the most effective mechanical cleaning treatment. For SiC/Al surfaces, grit-blasting provided a characteristically rough surface that was indistinguishable from similarly treated ordinary aluminum, or for that matter, steel surfaces (see Fig. 1). The rough furrows and flakes produced with grit-blasting are fairly large-scale features compared to the micro-roughness of oxides that are generally associated with good bonding properties. However, it is an effective method of providing a clean surface for bonding or subsequent treatment.

An alkaline cleaner and two deoxidizers were used for chemical cleaning. All three cleaners left the surfaces very smooth, which is not conducive to good bonding. The Amchem 7-17 surface shown in Fig. 2 also shows the build up of etch residue characteristic of chemical etches. The surfaces produced by chemical treatments were judged to be unsatisfactory for bonding, and no further work was done with them.
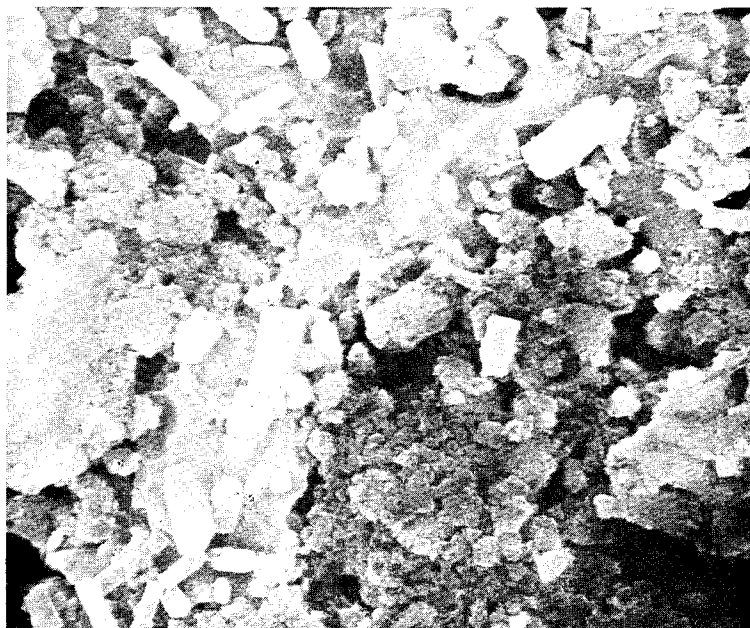
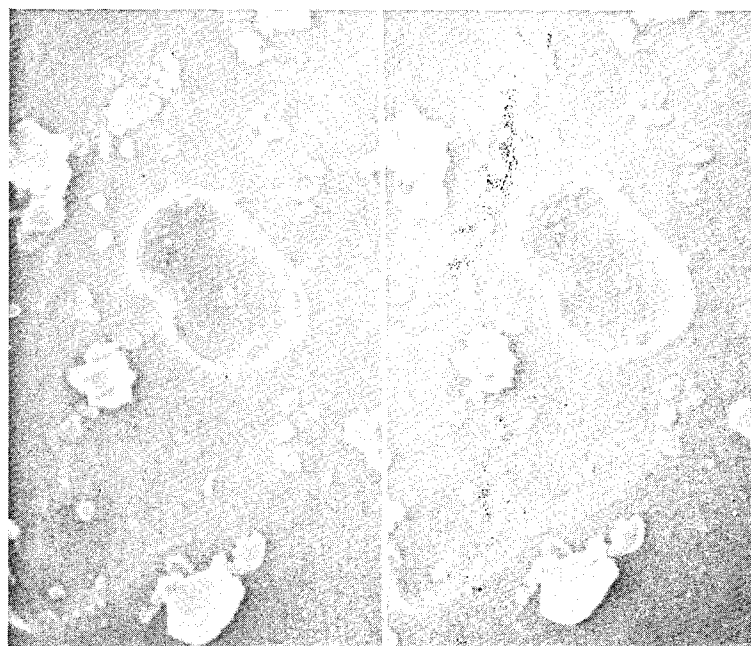188

(a)

1 μm

(b)
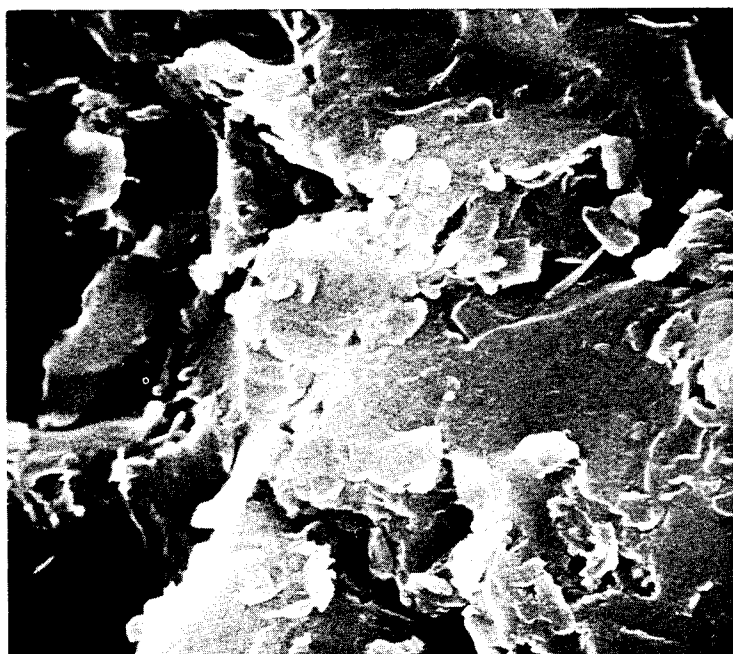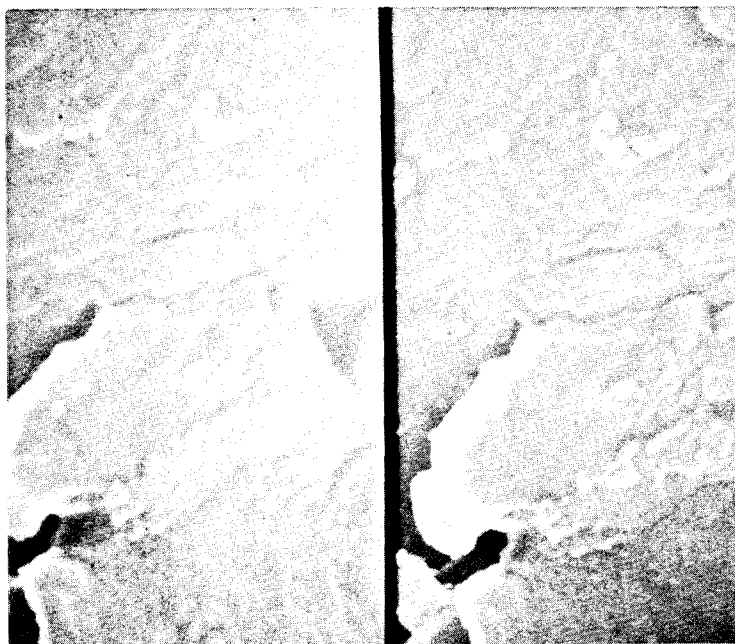
0.5 μm

Figure 1.   (a) Medium- and (b) high-magnification electron
micrographs of SiC/Al particle-reinforced material
after grit-blast cleaning.

(a)

1 μm

(b)

0.5 μm

Figure 2. (a) Medium- and (b) high-magnification electron micrographs
          of SiC/Al whisker-reinforced material after Amchem 7-17 etching.

Table 1

Bonding Treatment Process Specifications

Solution	Solution Makeup	Time (min)	Temperature (°C)
Turco 4125S	160 g/L 4215, 10 ml/L "S" additive	20	R.T.[a]
Amchem 7-17	10 vol% HNO_3, 23 g/L Amchem 7	8	R.T.
Smut-Go #1	140 g/L Smut-Go, 10 vol% HNO_3	15	R.T.
FPL	17 vol% H_2SO_4, 60 g/L $Na_2H_2O_7$ $2H_2O$	15 or 5 or 15 or 4h	65 65 R.T. R.T.
P2	370 g/L H_2SO_4, 150 gm/L $Fe_2(SO_4)3$	20	R.T.
PAA	10 vol% H_3PO_4 at 10V	10 or 5V	R.T.
CAA	30 g/L CrO_3 at 40V (applied in 5V/min steps)	40	35
SAA	10 vol% H_2SO_4 at 15V	20	R.T.

[a] R.T. - room temperature

191

We tried two chemical etches to produce a surface suitable for bonding: the traditional Forest Products Laboratory (FPL) process(4) and the newer P2 etch.(5) The morphology of the oxide grown on the exposed metal areas looked very similar to the shallow-cell and short-whisker morphology normally seen on ordinary aluminum alloys. Figure 3 shows the surface of an FPL-treated particle-reinforced alloy; the P2 surfaces had similar oxide features. Both treatments provided surfaces that appeared to be suitable for bonding.

Three anodizing treatments were studied: phosphoric acid anodization (PAA),(6) chromic acid anodization (CAA),(7) and sulfuric acid anodization (SAA).(8) As Fig. 4 shows, the presence of the SiC during PAA treatments resulted in shallower and more porous oxide structures compared with what we would expect from anodized, unreinforced aluminum alloys. Although this oxide is thinner than normal, it still has considerable micro-roughness, and we expect it would be a very good bonding surface. CAA oxides, which typically have very small pores and, therefore, do not interlock as well with adhesives, also were much more porous on the SiC-reinforced material. SAA treatments, on the other hand, attacked the SiC, causing an exfoliation of

the whiskers, which then increased the surface residue. Thus, only the PAA and CAA treatments appeared to be satisfactory for the SiC-reinforced alloy.

3.2 Lap-Shear Testing

Double-lap-shear specimens were prepared using four surface treatments chosen from the morphology screening. Grit-blast cleaning was used as a benchmark, whereas FPL and P2 etches and PAA were used to judge the effectiveness of these "improved processes" for SiC/Al. Although the oxide morphology of the CAA specimen was good, CAA was not used in this part of the study because it is a relatively difficult treatment to implement and offered no advantage over the simpler PAA treatment, based on experience with ordinary aluminum.(9) The specimen geometry, shown in Fig. 5, was designed to mimic the standard double-lap specimen while using less SiC/Al material. Side plates were made from one of three materials: whisker- or particle-reinforced SiC/Al or plain 6061 Al. Plain 6061 Al was used for the long, center pieces. If a particular problem arose due to surface preparation of the SiC/Al, the specimen would fail at the outer bonding interface at the short overlap end. The SiC/Al alloy did not exhibit any interfacial failures during this test program.

(a)

1 μm

(b)

0.5 μm
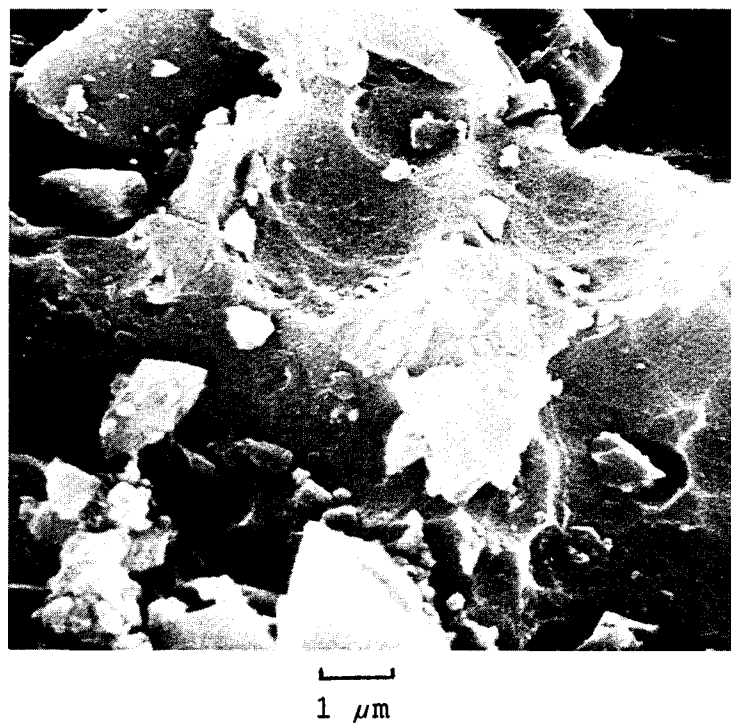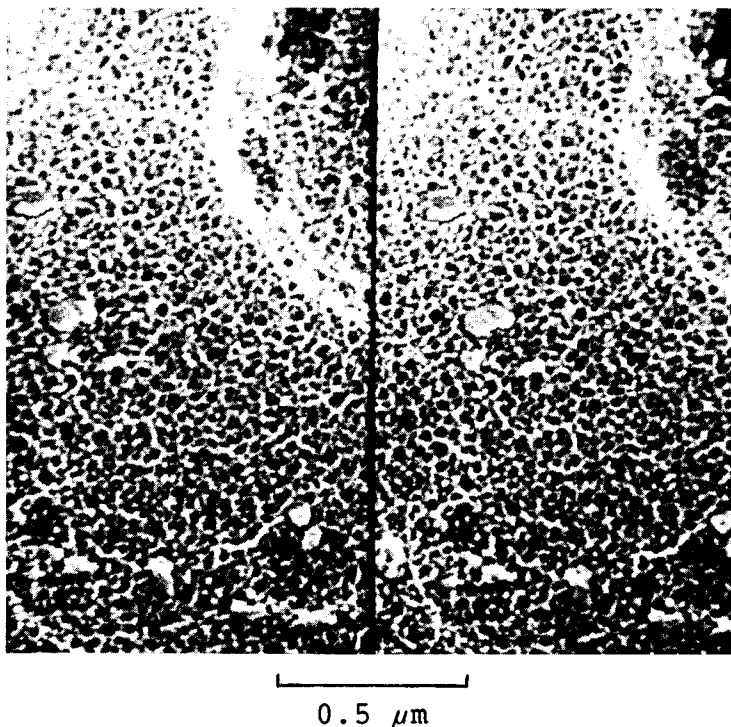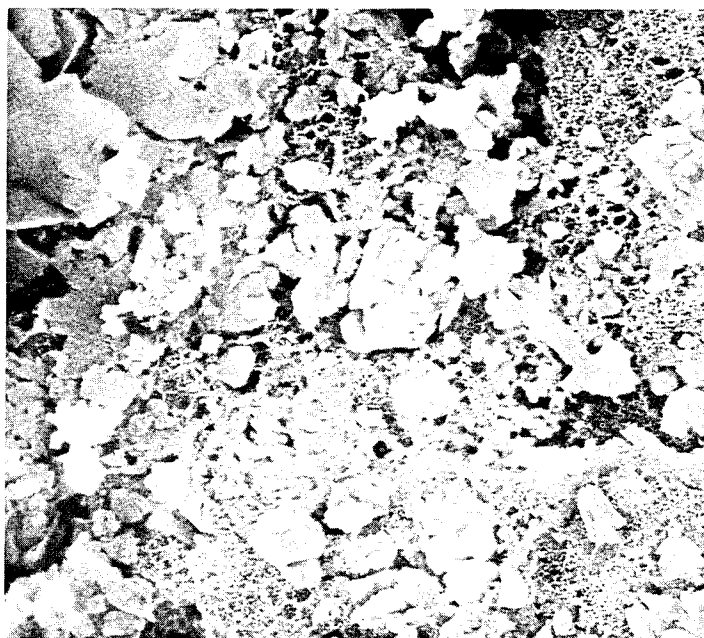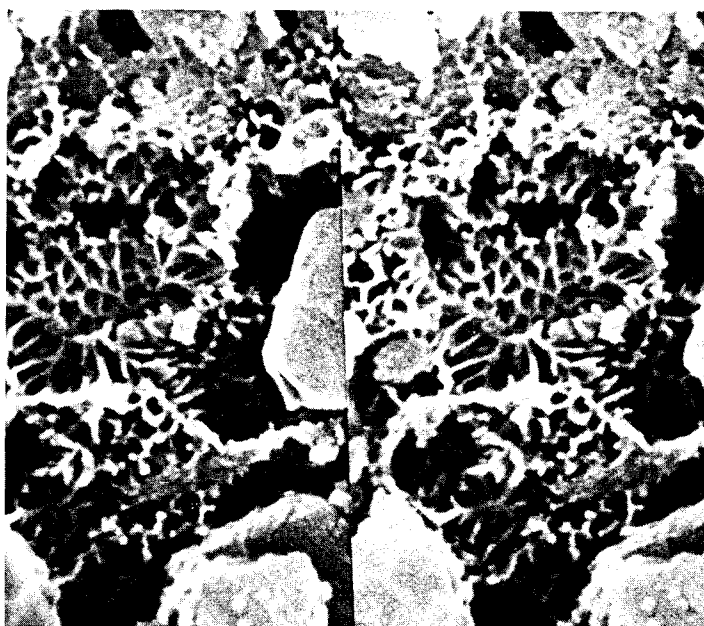
Figure 3. (a) Medium- and (b) high-magnification electron micrographs of SiC/Al particle-reinforced material after FPL etching.

(a)

(b)

Figure 4.   (a) Medium- and (b) high-magnification electron
micrographs of SiC/Al particle-reinforced material
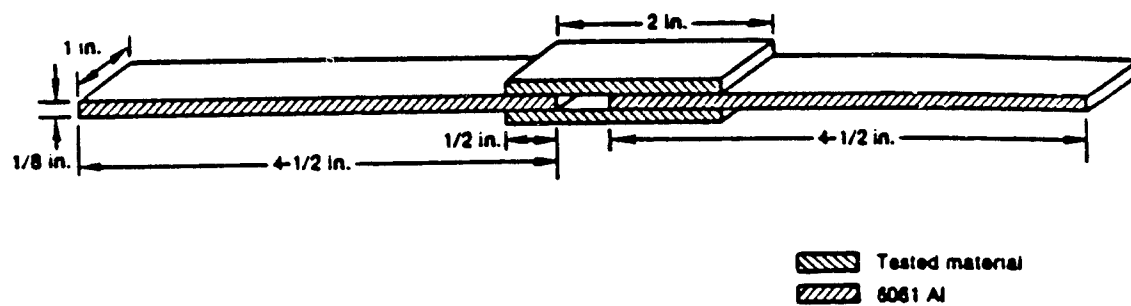after PAA treatment.

Figure 5. Material-conserving double-lap-shear specimen used for Phase I and extended durability mechanical testing.

The average lap shear strength values of the three specimens for each combination of surface preparations and materials are shown in Table 2. Note that the specimens prepared with SiC/Al are similar, and generally slightly stronger, than the control specimens for any given surface treatment. The high strength levels are probably due to the increased stiffness of the SiC/Al plates, which reduces the bending at the edges of the specimen and thereby reduces the degree of stress concentration. The higher strengths of the PAA specimens compared with that of the other specimens may be due to improved sample preparation, more consistent bond line thickness, and uniform pressure, etc., since the PAA samples were the last ones to be prepared. The difference in surface oxide should not explain the strength difference, since none of the specimens failed at or near the metal-adhesive interface.

3.3 Wedge Tests

Whisker- and particle-SiC reinforced 6061 aluminum, and 6061 control strips were prepared to wedge tests according to the ASTM standard.(10) The same four treatments described above for double lap shear specimens were used to prepare the wedge-test sample surfaces. The wedge test was performed to determine which treatment results in the best durability performace, so that two processes could be selected for long-term durability testing.

An interesting result of this test was the very poor performance of grit-blasted surfaces. Figure 6 shows crack-opening stress as a function of exposure time for the three sample substrates after grit-blast surface treatment. The crack-opening stress display (11) was chosen to normalize the stiffness of the samples so that the performance of the reinforced substrates could be compared directly to the control specimens. For this type of data presentation, the higher the number, the better the performance. A rapid drop in stress occurred as the grit-blasted specimens were exposed to the humidity-chamber conditioning. This normally occurs with surfaces that lack microroughness because water molecules at the interface break the epoxy chemical-bonds to the surface oxide. Using the Boeing Corporation criterion as a standard of comparison for properly prepared bonds,(12) which translates to $G_{1c} > 4.4$ after one hour of humidity-chamber exposure, all the grit-blasted specimens failed.

In contrast, the PAA-prepared samples performed very well. As Fig. 7 shows,

Table 2

Double-Lap-Shear Strength as a Function of
Substrate and Surface Treatment

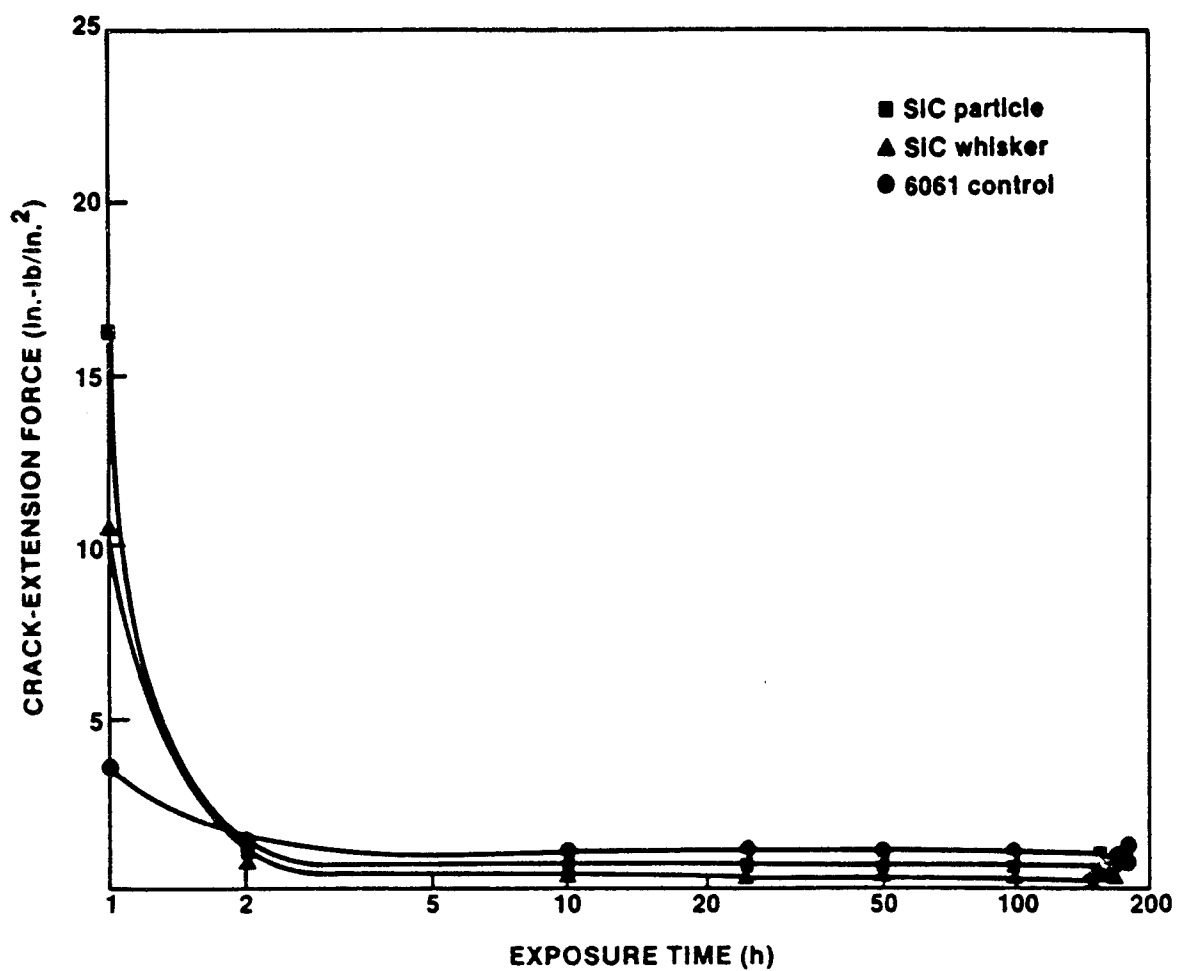| Surface Treatment	6061 Control	SiC Whisker Reinforced	SiC Particle Reinforced
Grit Blast	3490 (270)[a]	4330 (320)	4430 (610)
FPL Etch	3870 (630)	4360 (290)	4210 (190)
P2 Etch	4360 (180)	4250 (410)	4120 (500)
PAA	4680 (380)	5300 (340)	> 5500

---

[a] Standard deviations are in parentheses

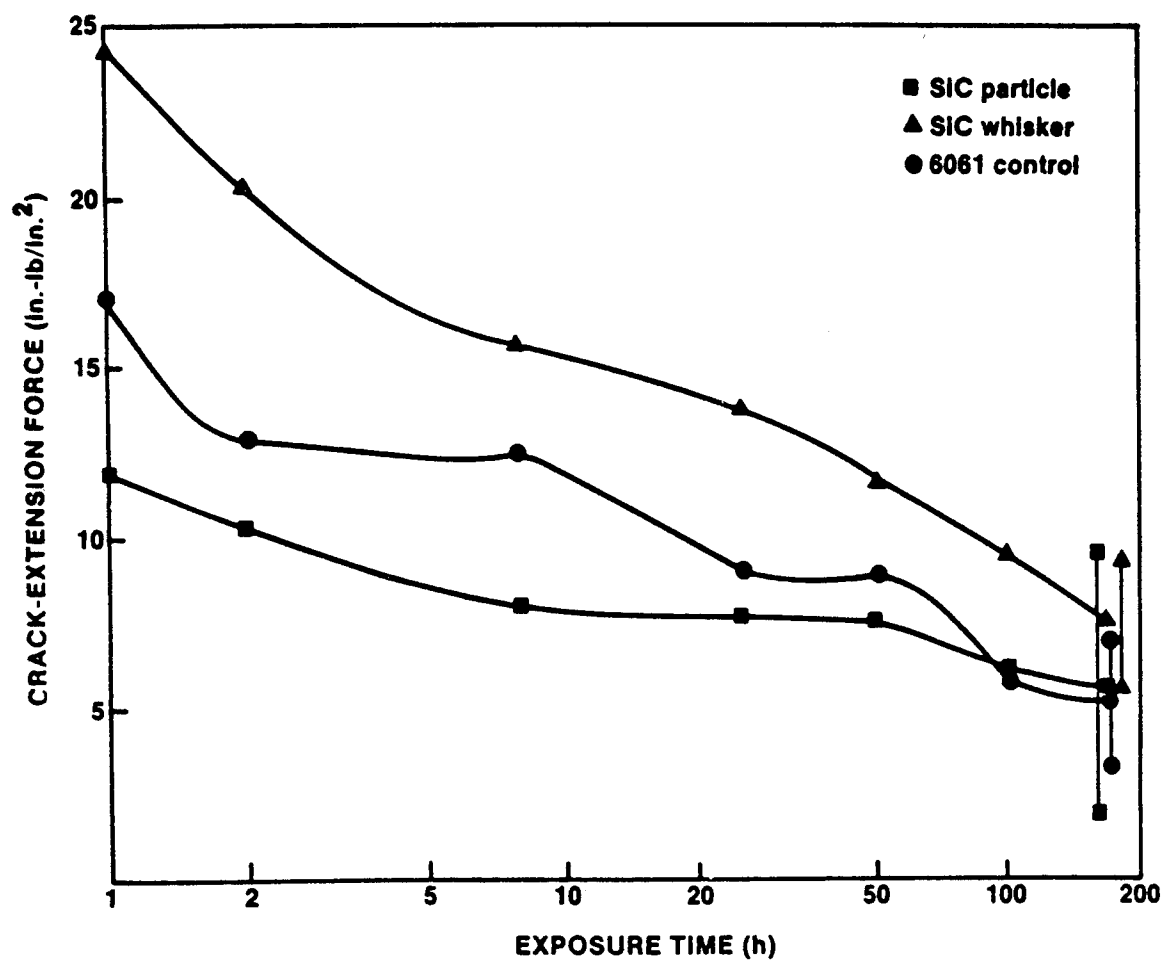Figure 6. Wedge-test results for test substrates grit-blasted prior to bonding.

Figure 7. Wedge-test results for test substrates PAA anodized prior
to bonding.

the PAA samples exhibited a gradual reduction in stress, primarily due to the softening of the adhesive during humidity-chamber exposure.

Wedge results for FPL prepared surfaces are shown in Fig. 8. P2 results were nearly identical. Although both surfaces were much better than grit-blast surfaces, neither was as good as PAA. These results are consistent with our prior experience with wedge tests on normal aluminum substrates. In all cases, the SiC/Al samples performed as well as, or better than control specimens.

A second set of wedge test specimens was used to compare potential adhesives. In these tests, high-temperature-cure (250-350°F) epoxies performed well, whereas room-temperature-cure epoxies did not. The adhesive that performed best in each category was chosen for use in extended durability testing. AF111 (3M Corporation) was chosen from the heat-cure epoxies, and Fusor 304 (Lord Corporation, Hughson Chemical Division) was chosen from the room-temperature-curing epoxy adhesives.

Extended Durability Testing

3.4.1 Salt-Spray Exposure

The same type of double-lap-shear specimens used above in the adhesion tests were prepared and placed in a salt fog chamber to investigate bonding properties in corrosive atmospheres. To prepare the specimens, P2 and

PAA surface treatments were applied, and a chromate-containing, corrosion-inhibiting primer (BR127, American Cyanamid) primer was used with a AF111 heat-curing epoxy film and Fusor 304 two-part room-temperature curing-epoxy paste adhesive. Each specimen remained in the chamber for a specific interval, then it was removed and stored with control specimens in ambient laboratory conditions until the completion of the test. All the specimens were then simultaneously tested in a constant-strain Instron machine. The results are shown in Table 3. The reported values represent the average of all three substrate types, since there was no indication that the values of the two SiC/Al materials differed from those of the control. The only trend in the data is a reduction in adhesive strength as exposure time increases. However, the differences are small, and may be related to changes in the adhesives, since there was no evidence of interfacial failures. Clearly, the bonds to SiC/Al material were no less durable than control material bonds.

3.4.2. Stressed Durability Testing

A limited number of stressed durability tests were run before the expiration of the program. The results are shown in Table 4. Once again, we found no differences between substrates. Substrate type is not shown in the

200
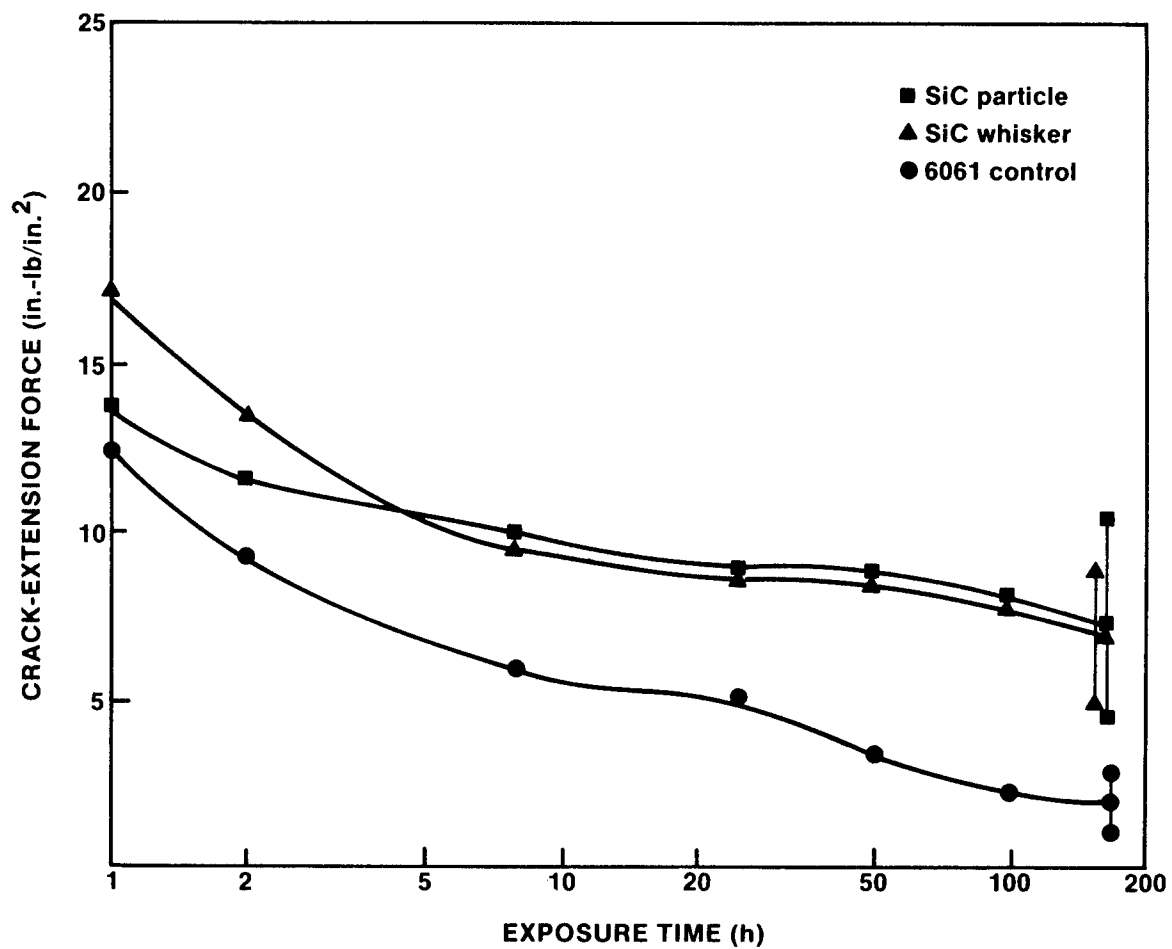
Figure 8. Wedge-test results for test substrates FPL etched prior to bonding.

Table 3

Averaged Double Lap-shear Test Strengths
After Salt-Spray Exposure

Treatment/ Adhesive	0	1 week	2 weeks	4 weeks	8 weeks
PAA/FUSOR	3940(86)	3830(780)	4300(480)	4260(805)	3600(700)
PAA/AF111	5350(320)	5250(265)	5460(150)	5670(190)	5090(370)
P2/FUSOR	4670(270)	4530(380)	4410(350)	4110(420)	3390(400)
P2/AF111	4880(670)	5280(530)	5080(450)	5120(1050)	5340(420)

Table 4

Stressed Durability Test Results

Adhesive	Exposure Conditions	Stress Level (psi)	Time to Failure
FUSOR	80°F, 50% R.H.	480	3 mo
		640	"
		800	"
		960	"
		1120	"
FUSOR	120°F, 90% R.H.	120	4 days, > 2 mo
		160	18 days
		200	> 2 mo, > 3 mo
		240	18 days
		260	4 days
AF111	80°F, 50% R.H.	720	> 3 mo
		960	"
		1200	"
		1440	"
		1680	"
AF111	120°F, 90% R.H.	180	> 3 mo
		240	"
		300	"
		360	"
		420	"

table. The primary result is that room-temperature-cure adhesives are particularly susceptible to moisture degradation. During the relatively short exposure times, the room-temperature-cure (RTC) samples failed. The time to failure was not consistent among all the specimens, possibly due to differences in bond-line thicknesses, and therefore, the moisture diffusion rate. Many failures occurred quickly at stress levels less than 1/10 the stress level supported in "dry" testing.

4. CONCLUSIONS

SiC-reinforced aluminum substrates can be successfully adhesively bonded when surface preparation techniques such as PAA, FPL, or P2 processes are used. The bond properties of these substrates are equal to or better than properties for similarly-processed, normal aluminum alloys. However, the process must be modified by avoiding chemical etching steps before performing the final surface treatment to minimize loose residue on the surface prior to bonding.

Both SiC/Al and ordinary aluminum prepared by grit-blasting perform poorly in durability testing.

Room-temperature-cure epoxies perform poorly under high-humidity exposure conditions.

There is no test evidence of an environmental attack on the SiC/Al alloy surface that would jeopardize adhesive bonds.

5. REFERENCES

1. J.S. Ahearn, C. Cooke, and A.G. Fishman, Fusion welding of SiC-reinforced Al composites, Metal Construction $\underline{14}$(4), 192 (1982).

2. J.D. Venables, D.K. McNamara, J.M. Chen, T.S. Sun, and R.L. Hopping, Oxide morphologies on aluminum prepared for adhesive bonding, Appl. Surf. Sci., $\underline{3}$, 88 (1979).

3. J.D. Venables, Adhesion and durability of metal-polymer bonds, J. Mater. Sci. $\underline{19}$, 2431 (1984).

4. H.W. Eichner and W.E. Schowalter. Report No. 1813, Forest Products Laboratory, Madison, WI, 1950.

5. W.J. Russell, Chromate free process for preparing aluminum for adhesive bonding, Proc. Symposium on Durability of Adhesively Bonded Structures, Picatinny Arsenal, Dover, NJ, 1976.

6. G.S. Kabayashi and D.J. Donnelly. Report No. DG-41517, Boeing Aerospace, Seattle, WA, 1974.

7. N. Rodgers. Bell Heli-
    copter Specification BPS
    4352, 1980.

8. Military Specification
    MIL-A-8625D, 1985.

9. W. Brockmann and O.D.
    Hennemann. Comparison of
    surface treatments of
    aluminum and their
    influence on long term
    strength of metal bonds,
    Proc. 11th National SAMPE
    Technical Conference,
    Boston, MA, 1979, p. 804.

10. Standard D2919, 1985
    Annual Book of ASTM
    Standards (ASTM, Phila-
    delphia, PA, 1985), Vol.
    15,06, p. 241.

11. D.A. Hardwick, J.S.
    Ahearn, and J.D. Venables,
    Environmental Durability
    of Aluminum Adhesive
    Joints Protected with
    Hydration Inhibitors, J.
    Mater. Sci., 19, 1984, p.
    223.

12. R.H. Olsen, Implementation
    of phosphoric acid anodiz-
    ing at Air Force air
    logistics center, Proc.
    11th National SAMPE Tech-
    nical Conference, Boston,
    MA, Nov. 1979, p. 770.

EVALUATION OF SURFACE PREPARATIONS FOR HIGH-SERVICE-TEMPERATURE Ti-6Al-4V ADHERENDS

H.M. Clearfield, D.K. Shaffer,
C.P. Blankenship, Jr. and J.S. Ahearn
Martin Marietta Laboratories
1450 S. Rolling Road
Baltimore, Maryland 21227

ABSTRACT

The structural and bonding properties of Ti-6Al-4V adherends, prepared by chromic acid and sodium hydroxide anodization (CAA and SHA), were studied as a function of exposure in high-temperature environments, such as vacuum, air, boiling and pressurized water, and pressurized steam. Subsequent to the environmental exposures, the adherends were bonded and their adhesive tensile strengths measured. Long-term exposure to high temperature (to 400°C), dry environments did not cause visible structural changes to the adherend oxide, but did result in poor bond strength for CAA adherends. The failure mode in these cases was within the oxide, which was weakened by the exposure. The water- and steam-exposed oxides underwent a transition from amorphous to crystalline TiO_2 (with an accompanying change in oxide morphology); however, bond strength was maintained for moderate exposures at T ~ 250°C. For exposure at T=300°C, the bond strength in CAA adherends was severely degraded due to a lack of porosity in the transformed oxide. In contrast, SHA adherends exhibited little loss in bond strength after identical exposures.

1. INTRODUCTION

Adhesively bonded systems that are stable at high temperatures and in severe environments are becoming increasingly important for military and aerospace applications. Titanium alloy adherends are often used because they have a high strength-to-weight ratio and good mechanical properties under these conditions. As the demands on bonded structures increase, it becomes more important to understand the factors affecting bond strength and durability in very severe environments, as well as the mechanisms of bond degradation. We have investigated some of these factors by studying both the bonded and unbonded surfaces of an alloy used widely throughout the aerospace industry, Ti-6Al-4V.

The long-term durability of titanium adhesive bonds can be correlated with the degree of micro-roughness at the alloy surface.[1] A micro-rough Ti surface, i.e., with features on the order of tens of nm, is generally achieved by anodization in solutions of chromic acid [2-5] (CAA, very common) or sodium hydroxide[6-8] (SHA, less common). Although both treatments result in amorphous, micro-rough oxides, the oxide morphologies are different. The latter treatment also results in a more macroscopic roughness -- mountainous features, with dimensions on the order of microns, interspersed with flat areas. In addition, SHA surfaces have exhibited greater long-term durability in lap-shear tests than CAA surfaces at temperatures over 200°C.[8]

Earlier studies showed that the unbonded CAA oxide underwent a transition from amorphous to crystalline TiO_2 (anatase) when immersed in water at 85°C for as little as 20 hours.[9] The transformation was accompanied by a change in morphology -- from a porous, honeycomb structure to the formation of needle-like crystallites on the surfaces. Although some porosity was retained after this transformation, it was later shown that exposure to humid environments for long times and/or at higher temperatures eventually resulted in a rather smooth, nodular-like oxide that lacked porosity.[5]

The observation that a CAA oxide that was transformed at the lower temperatures retained porosity, suggests that such an oxide might be able to couple mechanically to an adhesive. Because the crystalline Ti oxide phases are more thermodynamically stable than the amorphous phase,[10] we would expect these bonded adherends to retain their strength in severe environments. Thus, by bonding to a crystalline adherend oxide, large-scale morphology changes that normally occur during accelerated testing could presumably be avoided, thereby improving bond durability.

In this study, we have investigated the strength of bonds formed on both CAA and SHA Ti-6Al-4V adherend surfaces after they were subjected to high-temperature environments, such as vacuum, air, boiling water, pressurized water, and steam. Coupons were anodized, exposed, bonded to an Al stud (see below), and tested with an instrument that applies a tensile force normal to the adherend surface. The test was designed to determine the adhesion of the (transformed) oxide to the underlying substrate. Adherends were characterized before and after tensile testing by high-resolution scanning electron microscopy (SEM), x-ray photoelectron spectroscopy (XPS) and scanning Auger microscopy (SAM). These measurements facilitated the identification of the loci of failure in the tensile tests. The failure mechanisms were then correlated with the respective oxide morphologies.

2. EXPERIMENTAL

2.1 Surface Preparation and Environmental Exposure

The anodization procedures are described in detail else-

where.[5a] Briefly, Ti-6Al-4V coupons (2 x 5 x .08 cm) are degreased in dichloroethane, pickled in a solution containing HNO_3 and HF, rinsed, anodized, rinsed again and dried. The CAA solution contains 5% CrO_3 + 0.1% NH_4HF_2 (10 V, 25°C, 20 min) whereas the SHA solution is 5M NaOH (10 V, 30°C, 20 min). No attempt was made to protect the as-anodized or exposed adherends from the laboratory ambient during transfer to the analytical chambers.

Coupons subjected to heat alone were placed in a vacuum furnace for periods of 72 and 160 hr at 400°C, and at a pressure of 3×10^{-4} Pa. Although there was no residual gas analyzer on the furnace, we estimate the partial pressure of oxygen to be less than 5×10^{-5} Pa.[11] Any residual water vapor was pumped away during warmup. Additionally, some coupons were exposed to air in an ordinary laboratory furnace at 330°C. Exposure times varied from 160-1200 hr. The relative humidity in the furnace was not determined.

The boiling water exposures were conducted by immersing the coupons in water maintained at 95-100°C. For higher temperature water exposures, a high-pressure autoclave was used. In this case, a sufficient volume of water was used at each temperature to maintain an equilibrium between liquid and vapor at the saturation vapor pressure. Some coupons were immersed in the liquid; others were exposed only to the vapor. Exposures ranged from 3 to 120 hr at temperatures of 150, 200, 250 and 300°C.

2.2 Adhesion Testing

A pneumatic adhesion tensile testing instrument (SEMicro, Rockville, MD) was used for the adhesion tests. Figure 1 is a schematic drawing of the test geometry. A 1.25 cm-diameter Al stud (that had been etched previously in FPL solution) was bonded to the environmentally-exposed adherend with a two-part epoxy adhesive (3M 1838). The bonding area was defined with a Teflon ring. The adhesive was cured under a pressure of 0.4 MPa for 72 hr at room temperature; the thickness of the bondline was not determined. Prior to testing, the Teflon ring was removed and the specimen was mounted in a jig that prevents the adherend from flexing. The stud was screwed into a pneumatic piston, which applies the tensile force normal to the adherend surface. Thus, the force required to remove the stud provides a relative indication of the bond strength of the oxide.

2.3 Analysis

A JEOL JEM 100-CX STEM, used in the SEM mode, provided the resolution needed to examine the morphologies of the adherend oxides and the bond-failure surfaces. Samples were cut to 1 cm x 2 mm and coated with ~ 5 nm of Pt to eliminate charge buildup on the oxide. The stereo micrographs shown in this study were obtained at ±7 deg tilt.

XPS measurements were made in an SSL SSX-100-03 that was

equipped with a differentially pumped ion gun. The analyzer was operated at 150 eV pass energy with a corresponding full width at half maximum (FWHM) of 1.4 eV for Au $4f^{7/2}$ transition. For compositional analysis, the analyzed area was 600μm in diameter. Depth profiles were obtained from a 300 μm-diameter area at the center of a 3 x 3 mm sputter crater. Both areas were representative of the entire surface. The Auger analysis was conducted in a JEOL JAMP-10SP SAM equipped with a differentially pumped ion gun. To obtain the precise focus needed for some of the analyses, the incident current was kept below 10 nA. The adherend was tilted to expose the flat areas of SHA specimens to the ion beam, which was rastered over an area 1.5 x 1.5 mm. The sputter etch rate was ~ 7.5 nm/min as calibrated by cross-sectional TEM observation of the CAA oxide.

3. RESULTS

3.1 Morphology of Exposed Adherends

The morphology of a typical, as-anodized CAA oxide is shown in Fig. 2. It is characterized by a multilevel, porous structure with cell dimensions of approximately 40 nm. At lower magnifications (Fig. 2a), it is evident that the porous structure covers the entire surface. The multilevel morphology can be attributed to differential etching of the two-phase alloy. Earlier studies show that the

oxide consists of a 30-nm-thick barrier layer covered by 100-nm-thick cells.[5]

Adherends that were exposed to vacuum at 400°C for as long as 160 hr, or to air at 330°C for 1200 hr, showed no apparent change in surface morphology. CAA oxides immersed in boiling water develop crystallites, which is consistent with previous results.[5,9,12] After as little as 3 hr immersion, the honeycomb cell walls begin to thicken. By 24 hr, crystallites can be observed and the cells have nearly closed. By 72 hr, the adherend surface is covered with crystallites, the honeycomb structure has disappeared, and some of the crystallites have fused, as shown in Fig. 3. A dissolution/precipitation mechanism for this change in morphology was proposed earlier.[5a]

The evolution of oxides subjected to high-temperature, aqueous environments depends on whether the coupon is immersed in the liquid or exposed only to vapor. Those immersed in the liquid at 300°C were completely covered by needle-like crystallites after as little as 3 hr. By 24 hr, the crystallites had begun to fuse and the surface appears somewhat flatter. Finally, at 120 hr, the crystallites have become nodular in shape, leaving an oxide that is relatively smooth (compared to the as-anodized oxide). This is shown in Fig 4a. Conversely, vapor-exposed oxides exhibited no needle-like crystallites. Instead, the honeycomb structure

evolved into a more nodular-like oxide. Selected area diffraction (SAD) patterns generated in the TEM show these nodules to be anatase TiO_2. With continued exposure, the nodules began to fuse until, by 120 hr, the oxide surface was again relatively smooth, i.e., lacked porosity, as seen in Fig. 4b. The diameter of the vapor-exposed nodules was approximately one-half that of the corresponding liquid-exposed nodules.

In contrast, the SHA surface does not exhibit the same microporous morphology as the CAA surface. At lower magnification (Fig. 2c), SHA surfaces exhibit rather large, mountainous features, with relatively flat areas between. These flat areas range from 0.5 to 5.0 μm in diameter. At higher magnification (Fig. 2d), some degree of micro-roughness is evident. However, the micro-roughness is not as distinct or as consistent as the microporosity obtained with CAA. Depth profiling by scanning Auger microscopy (SAM) indicates that the flat areas consist of a 40-nm-thick oxide; SAM compositional analysis of the mountainous features has thus far proven inconclusive.

The evolution of the SHA oxide with environmental exposure is nearly identical to that of the CAA oxide. Vacuum and air have no effect on the morphology at the temperatures and times used in this study. Crystallites were observed on surfaces exposed to boiling water. The SHA surfaces developed nodules after exposure to water or steam in the autoclave at 300°C, as seen in Fig. 5.

3.2 Adhesion Tensile Tests

3.2.1 As-Anodized Adherends

The tensile test used in this study measured the relative adhesive strength of the oxide-base metal interface. The results are presented in Table 1. The greatest bond strength was obtained with the respective as-anodized adherends. Upon visual examination, both debonded surfaces had the same appearance -- rough and the same color as the adhesive -- suggesting that the failure mode was cohesive. This was confirmed by SEM and XPS, which showed the characteristic morphology and atomic concentration of the cured adhesive on both failure surfaces.[5b] The actual tensile strength values for the CAA and SHA as-anodized systems, 9.2 MPa (Table 1), represent the cohesive strength of the adhesive in this testing geometry. This value is significantly less than that quoted by the manufacturer, and can be attributed to some flexing of the adherend during testing. Thicker adherends used in the same geometry yield cohesive strengths that approach the manufacturer's reported value.[13]

3.2.2 Vacuum- and Air-Exposed Adherends

Most of the high-temperature vacuum- and air-exposed CAA specimens failed prior to

210

testing as the Teflon ring was being removed. Those that were tested failed at pressures less than 0.7 MPa. In contrast, the SHA adherends retained most of their bond strengths after exposure. The failure mode for the exposed SHA adherends was mixed, i.e., primarily cohesive with some areas of oxide failure.

The debonded CAA surfaces appeared metallic on both the stud and the metal sides, indicating failure entirely within the oxide layer or at the oxide-metal interface. The precise location was determined by SEM and XPS depth profiles. As seen in Fig. 6, the original CAA oxide cell walls are evident on the stud side and have been lifted away from the base metal. The micrograph from the metal side shows a complementary image. XPS survey spectra of both surfaces were identical; however, depth profiles show different oxide-layer thicknesses. On the metal side, Fig. 7a, the oxide-metal interface is abrupt and appears at a depth of less than 10 nm, as indicated by the rapid increase in the Ti signal with depth. (The greatest oxide layer thickness on the metal side of any of these samples was ~ 30 nm.) In Fig. 7b, the stud side, the oxide-adhesive interface is not well defined, due to the penetration of the adhesive into the honeycomb structure.

One feature that is common to both depth profiles is the accumulation of F at both debonded surfaces. Previously, we had observed an accumulation of F near the oxide-metal interface in the as-anodized and air-exposed oxides.[5]

Cross-sectional TEM revealed that the oxide consisted of a 20- to 30-nm-thick barrier layer under the honeycomb structure (~ 100-nm thick). Thus, the depth profile in Fig. 7b can be described in terms of three distinct regions. In the uppermost region, at depths less than 30 nm, the profile is dominated by the steady level of the Ti and O signals, and C is at its background level. This corresponds to the barrier layer. Between 30 and 140 nm, the steady rise in the C concentration indicates that the adhesive penetrated the oxide. At depths greater than 140 nm, the C signal is dominant, which is indicative of the adhesive layer. We conclude from the micrographs and the depth profiles that the debonding occurred within the barrier layer at or very near the oxide-metal interface.

In an effort to understand the differences between air-exposed CAA and SHA adherends, we used SAM to examine both surfaces after environmental exposure, but without bonding. As mentioned above, the CAA oxide was unchanged, both in morphology and composition, as well as in thickness. Although the SHA morphology remained unchanged after exposure, the oxide thickness changed. This is shown for a flat area in Fig. 8. The sputter etch rate was 7 nm/min, and the oxide-metal interface is reached at a depth of 140 nm. A somewhat lower value, 100 nm, was obtained by XPS for the oxide thickness in the flat areas. This discrepancy may be due to the instrumental difficulties in acquiring depth profiles

from rough SHA surfaces.[14] Clearly, there are differences between the as-anodized and the exposed SHA oxide thicknesses. Thus, we conclude that the SHA-treated surface continues to oxidize during environmental exposure.

3.3 Boiling/Pressurized Water- and Steam-Exposed Adherends

CAA and SHA oxides exposed to both liquid and vapor environments at temperatures below 250°C retained almost all of their bond strength, as seen in Table 1. Although these debonded surfaces were not examined by XPS, the appearance of adhesive material on all of them suggests that the failure mode was predominantly cohesive in each case (although small areas of adhesive failure could be delineated). (The tensile strength values listed for water-exposed adherends in Table 1 represent the averages of many samples. Some of the tensile strengths exhibited were comparable to those obtained for the as-anodized adherends.)

CAA adherends exposed to humid environments at 300°C for 24 hr or more failed at low stress levels, whereas corresponding SHA adherends retained most of their initial bond strength. The two debonded CAA adherends were examined using XPS, as shown in Fig. 9. The stud side (Fig. 9a) showed no Ti; only C, O, and Si, which are typical of the adhesive material. In contrast, the metal side (Fig. 9b) contained Ti and O, as well as moderate levels of C

and Si. There are two plausible explanations for these increased concentrations of C and Si on the metal side: Either a very thin adhesive layer (2-4 nm thick) was left after the tensile test, or, more likely, the sample was contaminated during transfer to the XPS vacuum system. Scanning electron micrographs show adhesive on the stud side and the nodular oxide on the metal side of the failure. In contrast, SHA adherends did not exhibit adhesive failures after steam exposure at 300°C. The failure mode for these adherends was predominantly cohesive with small areas of adhesive failure. The unbonded SHA surfaces were examined before and after exposure with SAM and XPS. As seen in Fig. 8c, the SHA adherend continued to oxidize during steam exposure (as with air exposure), which may be responsible for the retained bond strength.

4. DISCUSSION

A possible explanation for the catastrophic failure of CAA adherends is the dissolution of the oxide into the alloy at the exposure temperature. We have observed diffusion of oxygen from the oxide into Ti-6Al-4V alloys after heating in vacuum at temperatures above 450°C. This is shown in Figs. 10a-c, which are Auger sputter-depth profiles of as-anodized (Fig. 10a) CAA surfaces and after heating at 450 and 700°C for 1 hour (Figs. 10b and c). After 1 hour at 450°C, the oxygen has begun diffusing into the alloy, as seen by the degradation of the

original interface (i.e., the "tail" on the O signal). This interfacial degradation becomes more pronounced at longer times or higher temperatures[15] until, at 700°C, there is apparently no oxide left at the surface (Fig. 10c). In this case, the O present at the surface is probably due to adsorbed contaminants. Immediately below the surface, the oxygen concentration is constant and approaches the solubility limit in the alloy. We also observed high carbon levels at the surface that persisted into the alloy. We attribute this to the formation of a carbide phase[15]; the source of the carbon is thus far unknown.

Oxygen dissolved in the alloy at concentrations as low as 0.1% would result in a highly embrittled zone at the oxide-metal interface and defects (i.e., microcracks) in the oxide itself. Both would cause bond failure. We would expect an identical mechanism to be operative for SHA adherends; however, they did not fail catastrophically after similar exposures. Oxide failures have been observed in SHA-treated Ti-6Al-4V bonded structures after long-term exposures (18 months) at 232°C.[16] This suggests that a similar mechanism occurs in SHA adherends, but at a slower rate. We are currently investigating whether the original morphology and/or composition of the oxide affects the kinetics of the microcracking or the oxide dissolution.

Selected area diffraction patterns obtained from water- and vapor-exposed CAA adherends show that the oxide is crystalline (anatase) TiO_2. The tensile test results for temperatures below 250°C indicate that the integrity of the oxide-metal interface is retained despite the amorphous-to-crystalline (structural) transformation in the bare adherend. In contrast, bonded Al adherends that were exposed to aqueous environments during accelerated durability testing underwent chemical changes (i.e., hydration) that resulted in weak bonding to the base metal.[17] It is apparent from the SEM micrographs that porosity exists in water-exposed CAA surfaces even after the transformation; therefore, the adhesive is able to penetrate and interlock mechanically with the oxide. The transformed oxide itself can be bonded with nearly the same strength as the as-anodized oxide.

The reduced bond strength in CAA adherends exposed to humid environments for the longest times and/or at the highest temperatures can be attributed to their lack of porosity. In these instances, the adhesive cannot penetrate the oxide. Since no mechanical coupling can occur, the adhesive merely pulls away from the oxide under very little tensile force. Although the micro-roughness of the SHA adherend was changed to a more fused, nodular structure during steam exposure, bond strength was retained. The remaining macro-roughness of the surface may play a role in retaining the bond strength of the SHA adherends, however further experiments are needed to clarify the issue.

5. SUMMARY

Tensile testing of CAA and SHA Ti-6Al-4V adherends that were exposed to a variety of high-temperature environments prior to testing indicate that the mode of failure depended on the nature of the environmental exposure. The as-anodized adherends all failed cohesively (within the adhesive itself). Although the original morphology was retained on both surfaces after high-temperature exposures in vacuum and air, CAA adherends subjected to these environments at temperatures greater than (or equal to) 330°C degraded severely and failed within the oxide. In constrast, the SHA adherends retained most of their initial bond strength, possibly because of continued oxidation during exposure. Oxides subjected to moderate, humid environments retained almost all of their initial bond strength. Long-term and/or high-temperature aqueous exposures resulted in adhesive failures for CAA adherends, whereas SHA adherends exhibited predominatly cohesive failures after similar exposures.

6. REFERENCES

1. Brown, S.R., Proc. 27th Nat. SAMPE Symp. SAMPE, 1982, p. 363.

2. Moji, Y., and Marceau, J.A., U.S. Patent No. 3,959,091, 1976.

3. a) Ditchek, B.M., et. al., Proc. 25th Natl. SAMPE Symp. SAMPE, 1980, p. 909; b) Venables, J.D. J. Mater Sci. 19, 2431 (1984).

4. Hill, S.G., Peters, P.D., and Hendricks, C.L., NASA contractor Report 165944, contract no. NAS1-15605 (unpublished, 1982).

5. a) Clearfield, H.M., Shaffer, D.K., and Ahearn, J.S., Proc. 18th Natl. SAMPE Tech. Conf. SAMPE, 1986, p. 921; b) Clearfield, H.M. et. al., J. Adhesion, in press.

6. Kennedy, A.C., Kohler, R., and Poole, P., Int. J. Adhesion and Adhesives 3, 133 (1983).

7. Filbey, J.A., Wightman, J.P., and Progar, D.J., J. Adhesion 20, 283 (1987).

8. Progar, D.J., NASA Tech. Mem. 89045 (unpublished, 1986).

9. Natan M., and Venables, J.D., J. Adhesion 15, 125 (1983).

10. Matthews, A., Am. Mineral. 61, 419 (1976).

11. Redhead, P.A., Hobson, J.P., and Kornelsen, E.V., The Physical Basis of Ultrahigh Vacuum (Chapman and Hall, London, 1968).

12. Ditchek, B.M., et al., Proc. 25th Natl. SAMPE Symp. Exhib., Azusa, CA, (SAMPE 1980).

13. Desai, A., private communication.

14. Clearfield, H.M., et al., submitted to Appl. Surf. Sci.

15. Shaffer, D.K., et. al.,
    Martin Marietta Technical
    Report TR87-63c, submitted
    to ONR under contract no.
    N00014-85-C-0804 (unpub-
    lished, 1987).

16. St. Clair, T.L. et. al.,
    private communication.
    Bonded structures from
    this study were analyzed
    by us after testing to
    failure.

17. Venables, J.D., et al.,
    Proc. 12th Natl. SAMPE
    Tech. Conf. Seattle, WA,
    SAMPE, 1980.

7. ACKNOWLEDGEMENTS

8. BIOGRAPHIES

Howard M. Clearfield
obtained his Ph.D. in Mate-
rials Science at the Uni-
versity of Wisconsin in 1984.
Since joining Martin Marietta
Laboratories in 1985, he has
investigated both surface
preparation of Ti alloys for
adhesive bonding applications
and laser annealing of ion-
implanted Si.

D. Kent Shaffer ob-
tained an M.S. in Chemistry at
American University in 1977.
He joined Martin Marietta
Laboratories in 1983, where he
has investigated adhesively-
bonded Ti and Al systems,
organic corrosion inhibitors,
and the analytical character-
ization of the thermal protec-
tion system components of the
Space Shuttle.

C.P. Blankenship is a
co-operative student at Vir-
ginia Polytechnic Institute
and State University. At Mar-
tin Marietta Laboratories, he
has investigated high- temper-
ature adhesive systems, metal
matrix composites, and
rapidly-solidified powder
metallurgy systems. He is
enrolled in the Engineering
Materials Sciences Program at
VPI.

John S. Ahearn is
Senior Manager of the Mate-
rials Science department at
Martin Marietta Laboratories.
He obtained his Ph.D. in Phy-
sics at the University of Vir-
ginia in 1971. Since joining
Martin Marietta Labs in 1975,
he has investigated a variety
of adhesive bonding systems
and defects in electronic
materials. Additionally, he
is a lecturer at the The Johns
Hopkins University.

Table 1. Adhesion Tensile Test Results

Ti-6Al-4V   (CAA 5%)

EXPOSURE	PULL STRENGTH (MPa)
CAA	
As-anodized	9.2 ± 0.5 (cohesive)*
Vacuum (T = 400°C)	0-0.7 (oxide)
Air 330°C, 160 hr	3.5 (mixed)
Air 330°C, 1200 hr	0-0.7 (oxide)
Boiling/pressurized Water, steam (T ≤ 250°C)	6.2-8.3 (mixed)
Pressurized water, steam (T = 300°C)	0-0.7 (adhesive)
SHA	
As - anodized	9.1 (cohesive)
Air 330°C, 165 hr.	6.7 (mixed)
Pressurized Water 300°C	3.9 (mixed)
Pressurized Steam 300°C	7.7 (cohesive)

* Failure mode is indicated in parentheses.
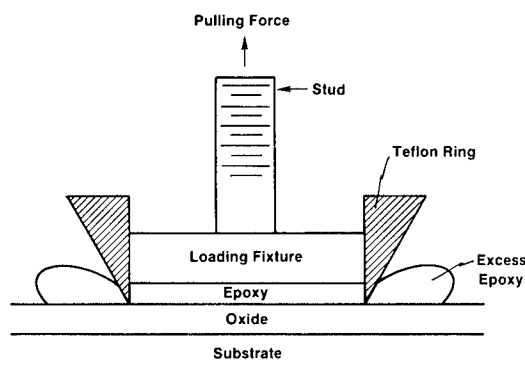
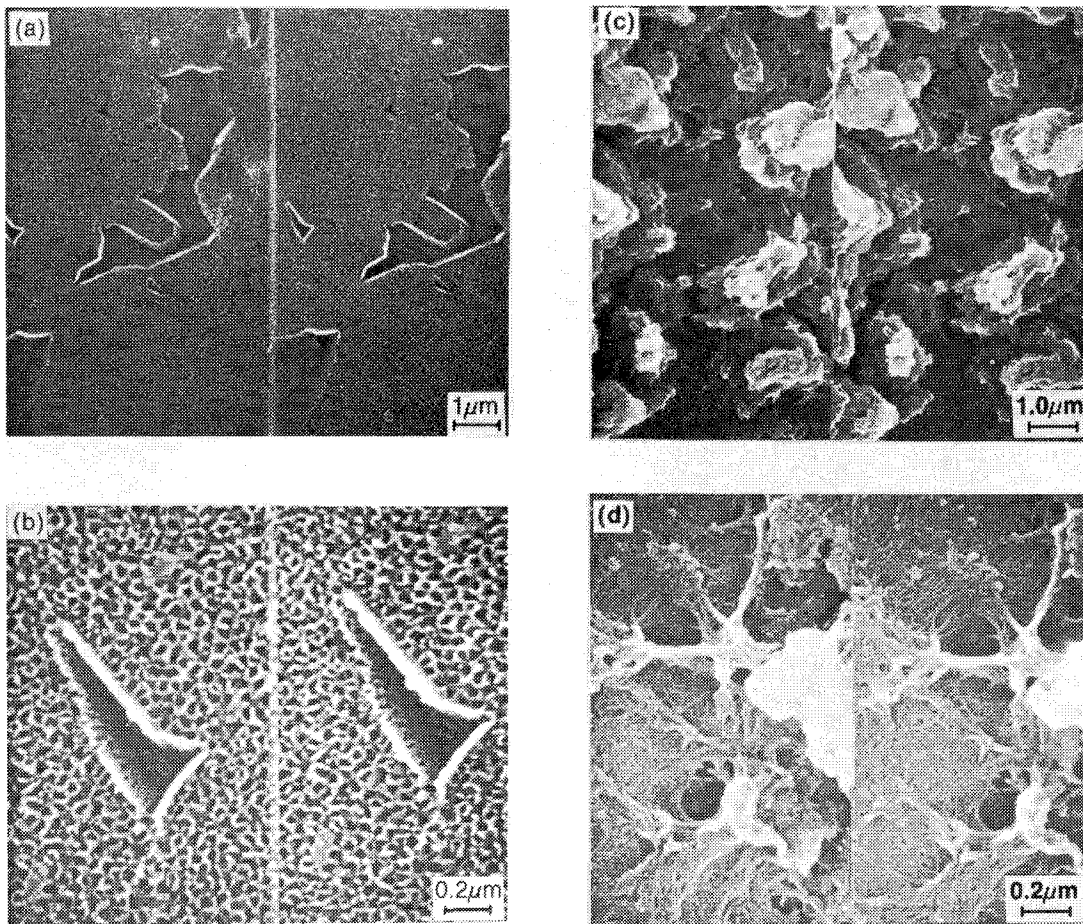Figure 1. Schematic diagram of adhesion tensile testing geometry.

Figure 2. High-resolution, stereo electron micrographs of anodized
Ti-6Al-4V surfaces: a) and b), CAA; c) and d) SHA. Micro
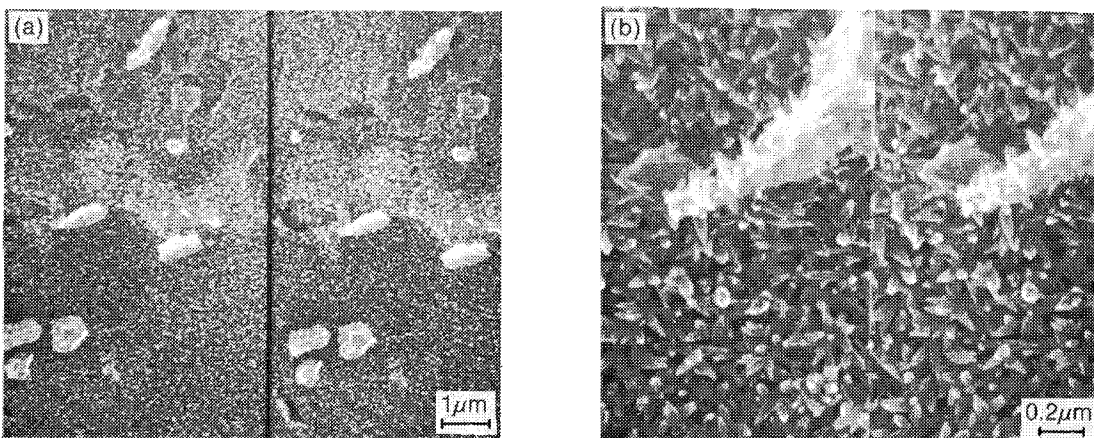roughness is evident in both surfaces.

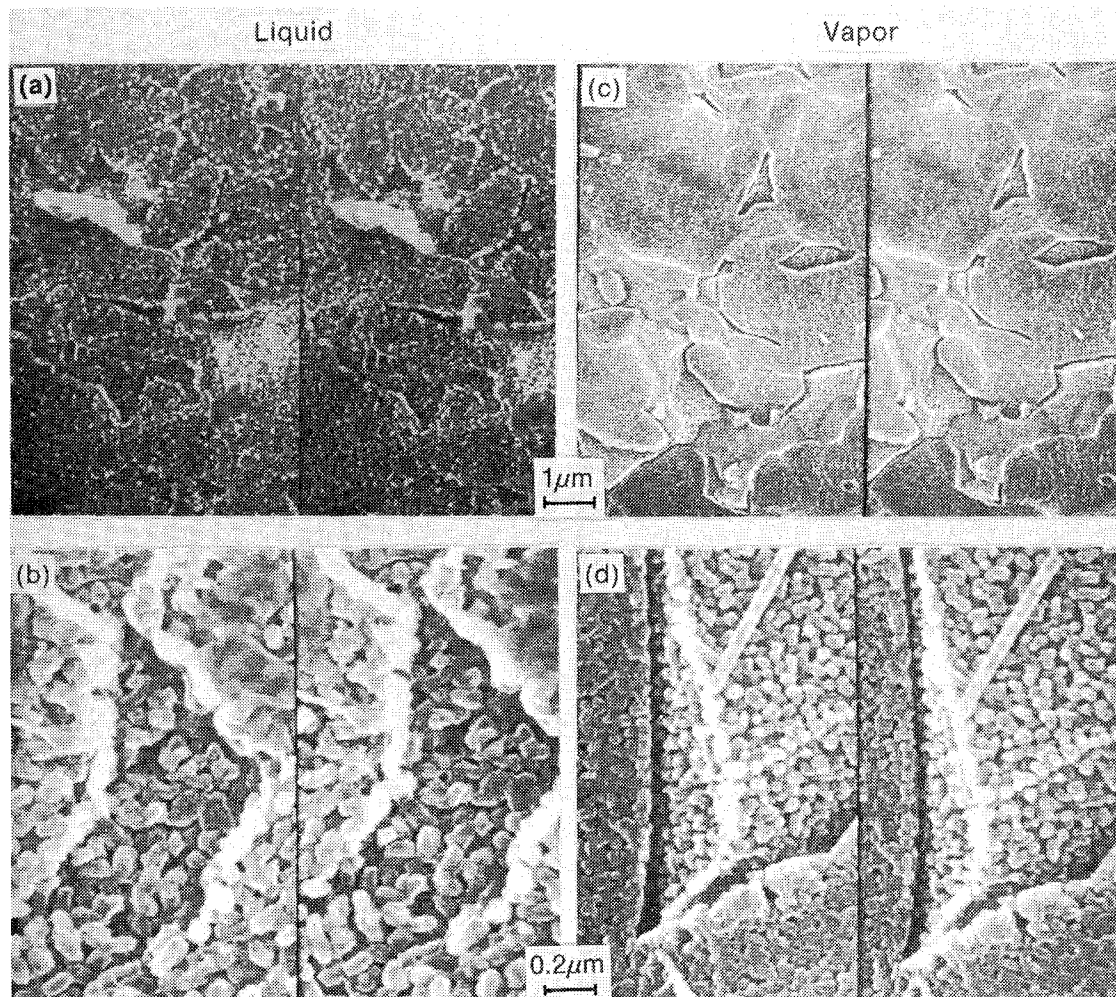Figure 3. CAA oxide after immersion in water at 100°C for 72 hours.

Figure 4. CAA oxide after exposure in an autoclave at 300°C for 120
hours: a) and b) immersed in liquid, and c) and d) exposed
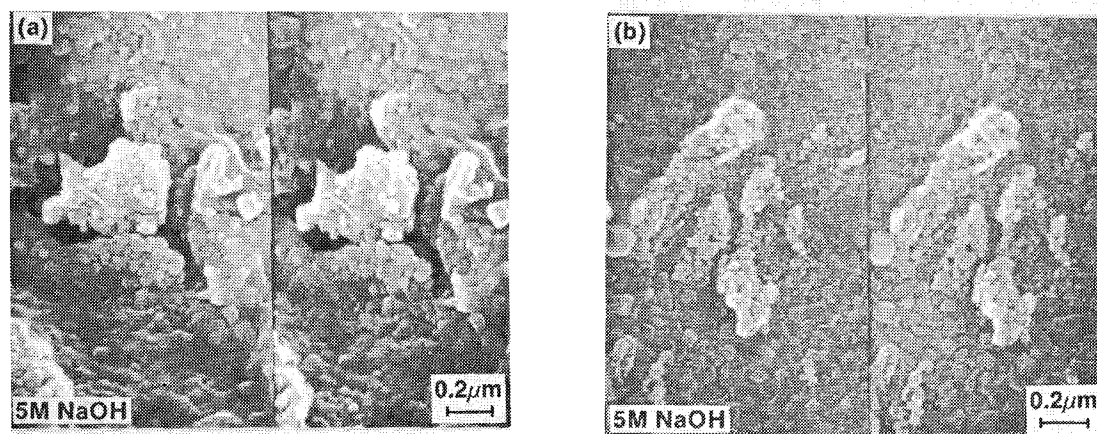to vapor.

Figure 5. SHA oxide after exposure in an autoclave at 300°C for 120
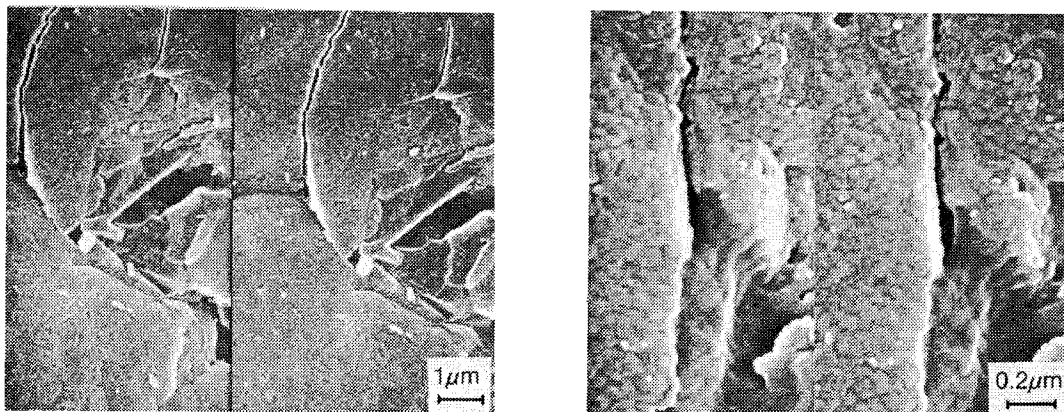hours: a) immersed in liquid, and b) exposed to vapor.

Figure 6. Scanning electron micrograph after tensile testing of the CAA adherend, which had been exposed to air for 1200 hr at 330°C. A replica of a honeycomb structure is evident, indicating that the oxide has been lifted from the adherend.
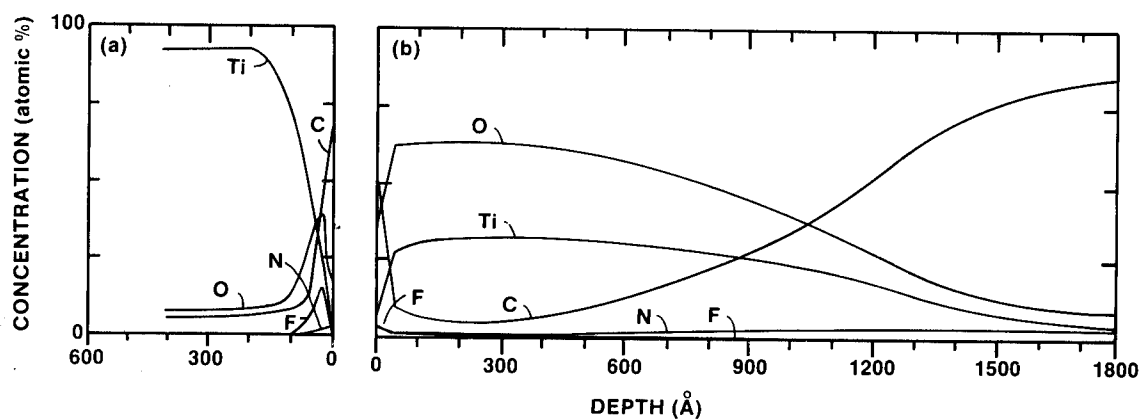

Figure 7. XPS depth profiles after tensile testing of the debonded surface from the a) metal and b) stud side of a Ti-6Al-4V adherend exposed to air for 1200 hr at 330°C. The profiles indicate that failure occurred at the oxide-metal interface.
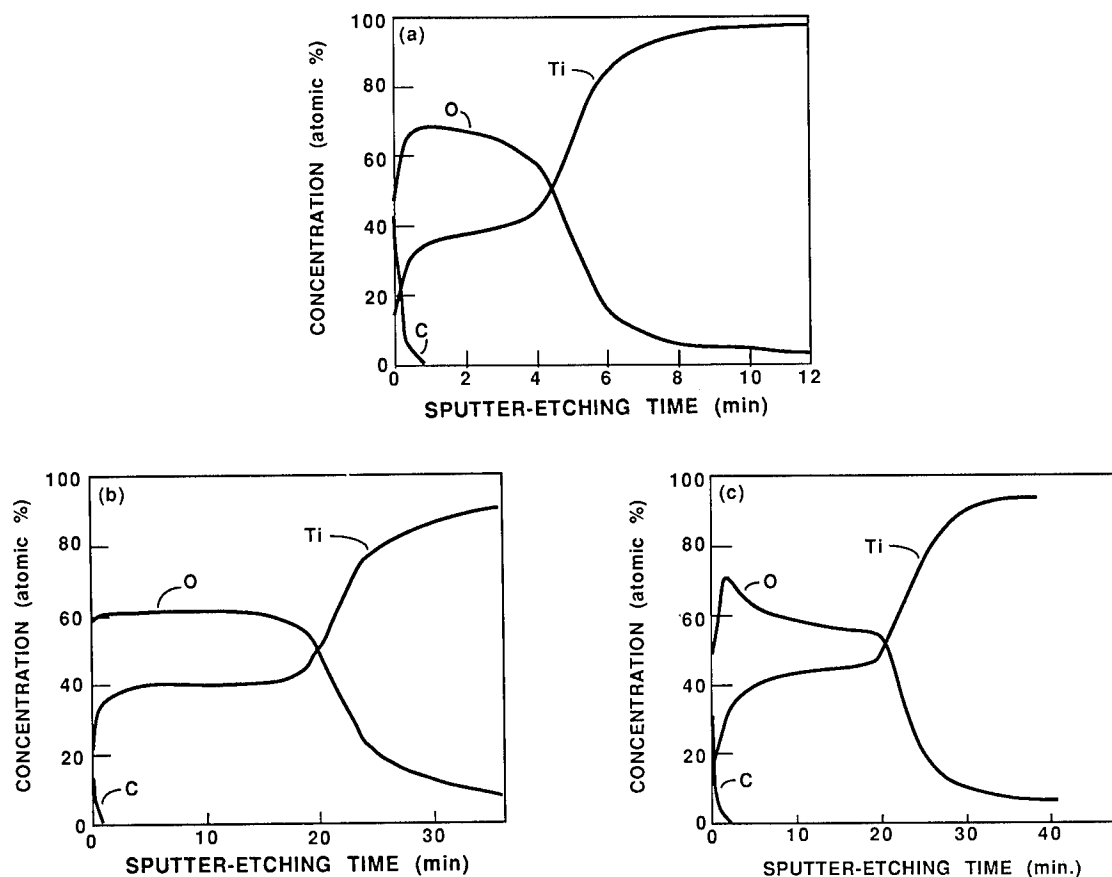
Figure 8. AES depth profiles of the flat areas of unbonded SHA oxides after environmental exposure: a) as-anodized; b) air, 330°C, 165 hr; and c) steam, 300°C, 120 hr.
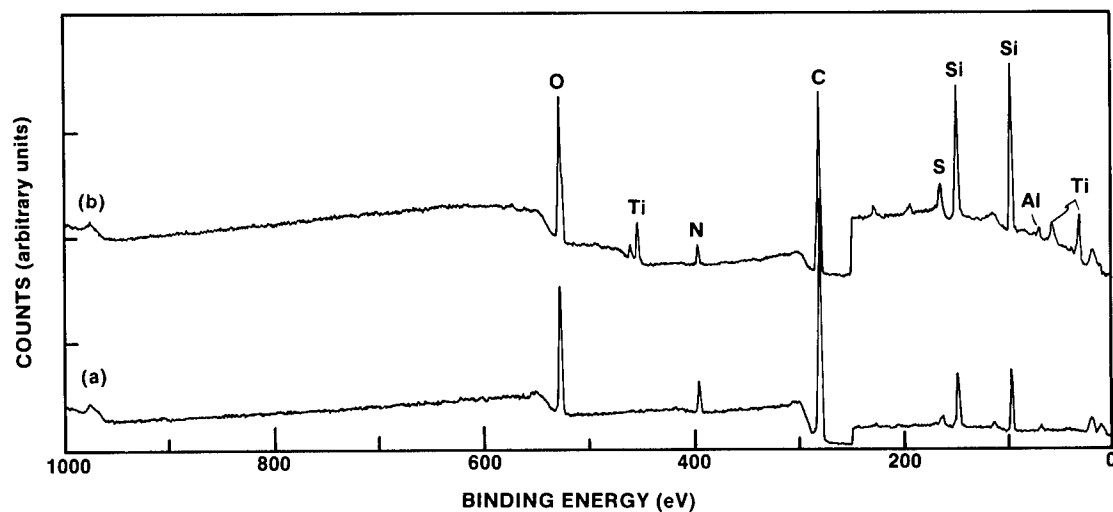

Figure 9. X-ray photoelectron spectra after tensile testing of a) stud and b) metal side of a Ti-6Al-4V adherend exposed to steam in a high-pressure autoclave for 120 hours at 300°C.
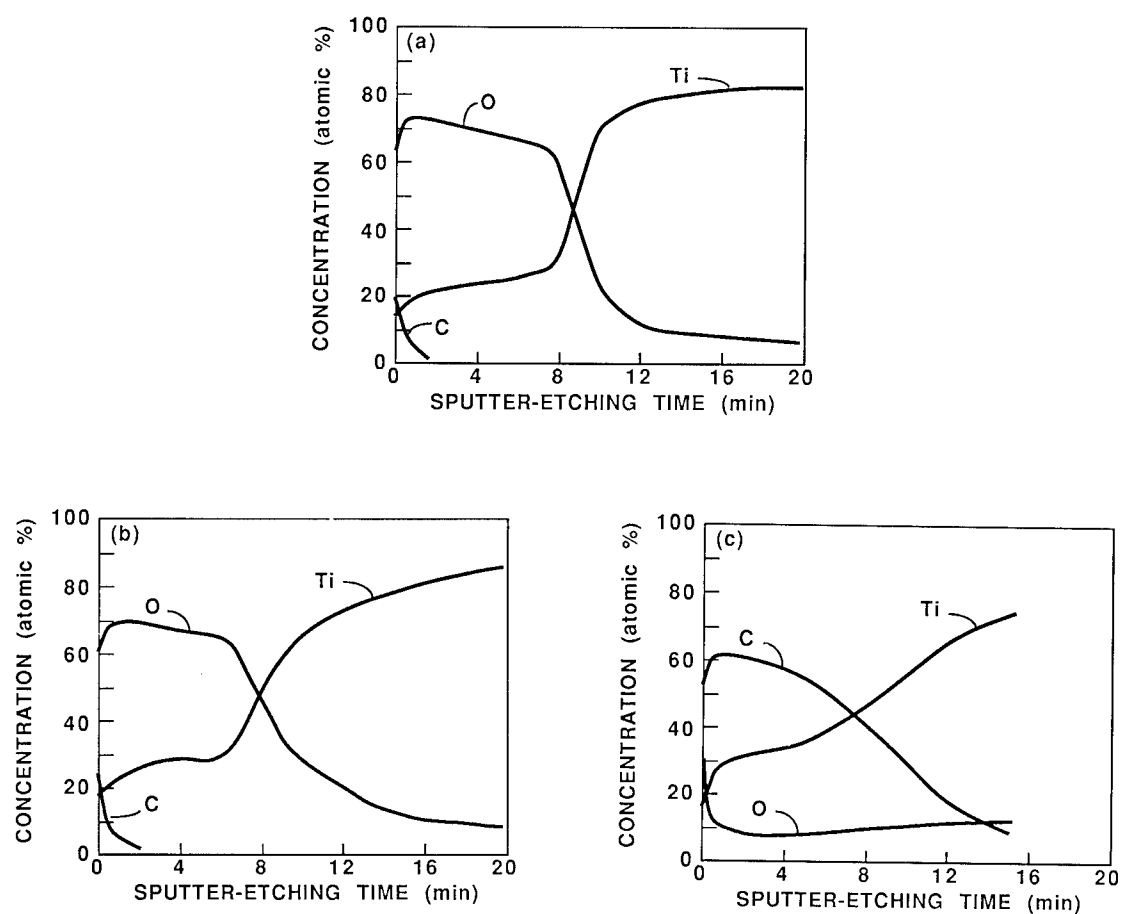
Figure 10. AES sputter-depth profiles of CAA oxides after annealing in
vacuum for 1 hour: a) as-anodized, b) 450°C, and c) 700°C.
The etch rate is ~ 15 nm/min.

3

Conclusion: The chloride concentration generated during the manufacture of sodium bisulfate depends directly on the temperature of the manufacturing process (the higher the manufacturing temperature the lower the concentration of chlorides). Chloride concentrations greater than 50 ppm retards the smut removal process. Smut left on the surface has no appreciable short-term effect on peel strength, but the long-term effect is unknown.

For satisfactory quality control, the smut must be removed prior to bonding (visual evidence of etching should not be masked by the black smut).

MOISTURE EFFECTS AND PEEL TESTING OF POLYMETHACRYLIMIDE FOAM AND HONEYCOMB CORE IN SANDWICH/SKIN STRUCTURES

Dana M. Granville

Materials Engineer – Composites Development Division

U.S. Army Materials Technology Laboratory (MTL)
Watertown, MA

ABSTRACT

One of the greatest concerns of the aerospace materials engineer is how a manufactured final part will change structurally, dimensionally, and weight wise during its lifetime on an aircraft. Polymethacrylimide (PMI) foam has been chosen as a core material for use on the Army's Advanced Composite Airframe Program (ACAP), and is a candidate for use in other current and future Army helicopters (JVX, LXH). The main objective of this paper is to answer a few of the questions concerning structural integrity, dimensional stability, and weight gain of this closed cell thermoplastic structural foam by processing typical sandwich/skin structures, and determining the effects of moisture absorption on peel strength. Results of the PMI foam's exposure to the combined effects of elevated temperature and high humidity conditions were compared directly to identical sandwich/skin constructions using aramid honeycomb core in both 4 and 6 lb/ft^2 densities, used widely by the aerospace industry.

Polymethacrylimide foam cores and honeycomb cores were used both in the "as-is" condition received by the manufacturers, and in an annealed or heat treated condition prior to layup of the sandwich constructions to determine their respective dimensional stability during a standard autoclave curing cycle. Two 350°F cure structural film adhesive prepregs were used for autoclave bonding +45° S-2 glass/epoxy precured facesheets onto both the foam and honeycomb constructions to determine their respective surface bonding ability and relative moisture barrier properties. The cured sandwich panels were then finally machined to ASTM D 1781 climbing drum peel test specimens and subjected to 95% relative humidity at 160°F for exposures up to 720 hours and subsequent redry both with and without RTV-sealed edges to determine comparative moisture weight gains and their effect on peeling torque.

Results showed that water uptake in PMI foam core sandwich structures tested was significantly higher than honeycomb cores of similar density. However, facesheet-to-core peeling torques did not suffer due to this migration of moisture.

INTRODUCTION

Sandwich/skin composite structures have become an increasingly popular structural consideration vs. monoqoque or skin/skeleton designs because of the dramatic strength/stiffness-to-weight improvements that are achievable with organic matrix materials. Applications include use in Army helicopter rotor blades, fuselages, cargo floors, and tail booms, as well as potential use in tactical shelters and high mobility ground vehicles. For aircraft structures in particular, the most commonly used structural core materials have been honeycombs such as "Nomex" a phenolic-coated aramid paper produced by DuPont and manufactured into honeycomb form by Hexcel Corp. Until recently, structural foam cores could not compete on an equal density basis with Nomex, while maintaining acceptably high compressive and peel strengths.[1]

Polymethacrylimide (PMI) foam, manufactured in West Germany by Rohm and Haas, and marketed as "Rohacell" foam, currently offers the highest compressive strength of the low density foam core materials (Figure 1).

Potential advantages of using PMI foam versus honeycomb are listed below:

1. Lower sheet stock cost - aerospace WF grades are presently about 1/3 less than the HRH-10 grades of similar density (Figure 2).

2. Ease of machinability - ability to rough cut foam to approximate shape, then compression mold to final net shape, for complex contour part production without requiring expensive 5-axis machining. Low cost foam mandrels may also be machined, then used for filament winding, braiding, or tape laying operations.[2]

3. When annealed, the isotropic WF grade of PMI foam maintains 0° and 90° compressive strength to 350°F.

4. Thermal expansion of PMI foam at elevated temperatures[3,4] provides internal pressure to help stabilize skins/adhesives during co-curing operations.
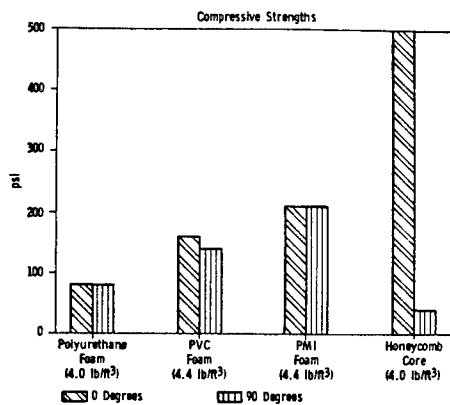
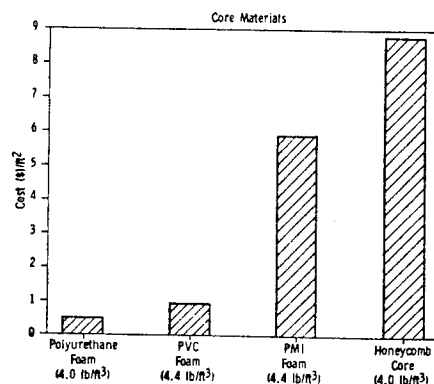Figure 1. 0° & 90° Compressive strengths of aircraft grade core materials.

Figure 2. Cost comparison of aircraft grade core materials.

Three inherent disadvantages of PMI foam are the following:

1. Water absorption is comparatively higher than all of the other aircraft grade foams and honeycomb referenced in this paper.

2. It will burn with a slightly smokey flame.[5]

3. Because of the foam's relatively small cell size, bonding ability to substrates can be difficult.[6,7,8] (Improved bonding can be achieved through the use of needle rollers which are available at the foam supplier).

In this study, aramid honeycomb is compared directly to the PMI foam so that the materials engineer will have a more tangeable understanding of what to expect for dimensional stability during the annealing and autoclave processing, as well as subsequent relative weight gains and peel strengths when these cores are employed as part of an actual sandwich/skin structure.

EXPERIMENTAL

The materials used in the sandwich/skin laminates, along with their manufacturers, are listed in Table 1. 3M's SP-250 S-2 glass/epoxy prepreg, in a two-ply ± 45° orientation, was used for sandwich skin facesheets on all laminates. Forty eight 2 ft. x 2 ft. facesheets were precured in an autoclave using the manufacturer's standard cure cycle, then lightly sanded on one side to improve subsequent bonding to the cores. All 2 ft. x 2 ft. core materials, including two densities of Nomex aramid honeycomb HRH 10-4 and HRH 10-6 (4 and 6 lb. density), were cut down the middle so that one 1 ft. x 2 ft. core half could be dried and annealed while its other half received no treatment. the PMI halves were also needled using a specially built hand needle roller provided by the foam supplier. The "pretreated" heating cycle included 72 hours at 150°F followed by 36 hours of annealing at 350°F in an air circulating oven.[9,10] Even though the annealing acutally takes place only in the PMI foam, the honeycomb was also given the same treatment. These cores were then remated with their untreated other halves, labelled, and placed in polyethylene pouches to await final autoclave processing. It was noted during the rematching of halves that the pretreated foam was a uniform pale yellow compared to the milk white untreated half. The pretreated honeycomb had darkened from a light amber to a brown color. Also noted was an average .11 in./ft. lengthwise contraction or shrinkage of the PMI foam and a corresponding average .12 in./ft. lengthwise expansion of the honeycomb.

With the cores ready for sandwich/skin construction, two structural film adhesive prepregs with scrims were taken out of the freezer for overnight thawing to room temperature in their bags so that condensation would not form on the adhesives. American Cyanamid FM-300K and 3M AF-147, both prepregs approximately .08 lbs/ft.², had been previously identified as having better than average moisture resistance.[11] The layups were done on polyvinylflouride (PVF) release film covered 3/8" T-6 aluminum caul plates, overwrapped with bleeder-release cloth and burlap. Because of the honeycomb core's relatively weak transverse compressive strength, extra metal strips were cut and placed around the perimeters of each construction to prevent "cave-in" of the sides due to autoclave pressure during cure. Nylon vacuum bags with glands were then heat sealed around each layup, and vacuums applied. Since both film adhesives used shared a common cure cycle, all constructions were autoclave cured under the same conditions (Figure 3).

Precured Facesheet:
Scotchply SP-250 S-2
2-Ply ± 45°

Rohacell Rigid Foam:
71 WF (4.4 lb/ft³)
110 WF (6.6 lb/ft³)

Nomex Honeycomb Core:
HRH 10-4 (4.0 lb/ft³)
HRH 10-6 (6.0 lb/ft³).

Structural Film Adhesive Prepreg:
FM-300K or AF-147

Precured Facesheet

Fabricated Sandwich Panel

Autoclave Cure Cycle:
Bonding Pressure - 40 psi + Vacuum Bag
Temperature Rise Rate - 5°F/Minute
Cure - 350°F for 1 hour
Pressure Release - During Cooldown at 100°F

Figure 3. Sandwich/skin constructions.

225

After the cure cycle, the sandwich/skin laminates were removed from their wrappings, marked, and relabelled (Figure 4) for diamond wheel machining into 3" x 12" climbing drum peel test specimens as outlined in ASTM D-1781. When unwrapped, it was observed that the PMI foam sandwiches that had not undergone the redry and annealing pretreatment had compressed in a concave fashion, while their matching pretreated halves appeared unaffected. Average thickness from specimens of the cured laminates are shown in Figure 5. The honeycomb cores, both with and without heat pretreatment, retained very close thickness dimensions (Figure 6).
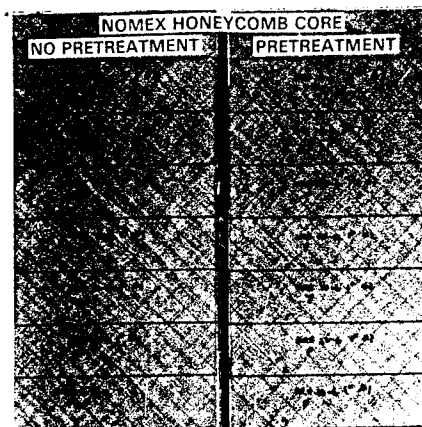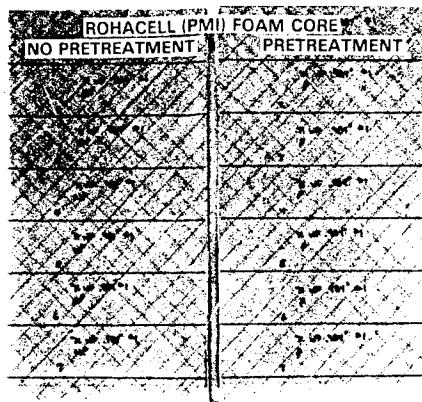
Figure 4. Labelled sandwich/skin laminates prior to machining into climbing drum peel specimens.
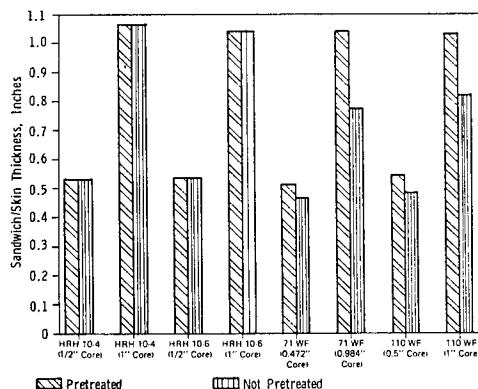
Figure 5. Effect of core pretreatment on thickness of sandwich/skin constructions after autoclave curing.
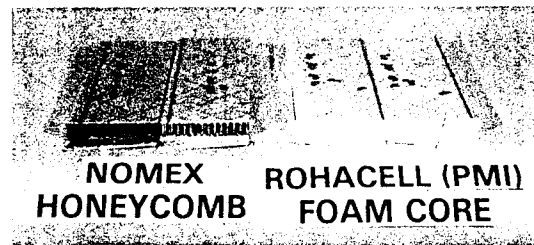
Figure 6. Effect of "Pretreated" versus "Not Pretreated" core materials on final sandwich/skin thickness.

Humidity Conditioning

Each sandwich/skin construction was divided into seven groups with three specimens per group, for humidity conditioning (Table 2). Specimens 1-12 were unsealed along the sides because of the relatively short times of exposure and to help determine water weight gain through the unprotected foam. Specimens 13-21 were sealed with MIL-A46106A type 1 general-purpose RTV silicone adhesive sealant. The sealant was used to help determine water weight gain through the facesheet sides of the specimens over extended exposure times.

Table 2 NUMBERING CLASSIFICATION FOR EACH CORE MATERIAL

A Blue M environmental chamber, model #AC-7602HA, was set at 95% relative humidity and 160°F for all exposures. Except for specimens 1-3, which were baseline specimens that had no exposure in the chamber, each of the 336 specimens tested, both with and without pretreatment, was weighed before and after exposure, and the difference recorded. In addition, one square foot of each separate material used was weighed out and subjected to long-term (90 day) humidity exposure. The prepreg skins and structural film adhesives were precured prior to testing. This testing was carried out to determine the contributing effects of moisture absorption by each component of the composite sandwich/skin laminate.

Climbing Drum Shear Peel Testing

After humidity exposures, each set of specimens was bagged in a polyethylene pouch and transported to ARDEC for climbing drum peel testing. The ASTM D1781 procedure was followed using a Custom Scientific Inc. climbing drum peel apparatus and a standard Instron tensile testing machine (Figure 7). A crosshead speed of 1 inch/minute was used for an effective specimen peel rate of 4 inches/minute on the drum. The chart speed was set at 1 inch/minute. The load required to bend and peel the adherend as well as the load required to overcome the resisting torque of the climbing drum was recorded on the chart paper for each specimen.

RESULTS AND DISCUSSION

Unprotected Core Material Weight Gain

Unprotected 1 ft.^{2} core materials of both Rohacell and Nomex were found to readily accept moisture, but the relative differences in percent weight gain were significant. When they were subjected to long-term humidity exposure, (Figure 8), the Nomex showed a peak weight gain after 30 days of 3.7 - 3.8%, and thereafter a leveling off. The Rohacell varied from 4.4% weight gain after 30 days with the 71 WF .472" core, to as much as 10.9% with the 110 WF 1" core, after which the foam started to lose weight. Because of the 4.4 - 10.9 range in weight gains, it was probable that the lower density foams had reached their saturation point and had started losing weight well before the 30 day weighings. This was confirmed by oven drying (Figure 9) followed by a 72 hour ambient temperature stabilization period, and re-exposure of the core materials, (Figure 10), for a short term under identical humidity conditions but taking data points more often. The Nomex rate of moisture pickup dropped off markedly after 2-4 hours exposure and did not exceed a 3.4% weight increase. The Rohacell weights began to level off only after 24 hours, with weight increases ranging from 7.1 - 7.5%.
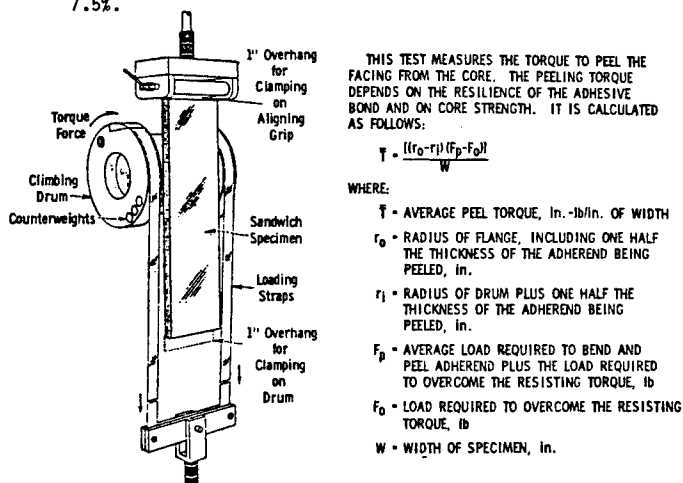
Figure 7. Climbing drum peel test (ASTM D 1781, MIL-STD 401B).

THIS TEST MEASURES THE TORQUE TO PEEL THE FACING FROM THE CORE. THE PEELING TORQUE DEPENDS ON THE RESILIENCE OF THE ADHESIVE BOND AND ON CORE STRENGTH. IT IS CALCULATED AS FOLLOWS:

$$\bar{T} = \frac{[(r_o - r_i)(F_p - F_0)]}{W}$$

WHERE:

$\bar{T}$ = AVERAGE PEEL TORQUE, In.-lb/in. OF WIDTH

r_0 = RADIUS OF FLANGE, INCLUDING ONE HALF THE THICKNESS OF THE ADHEREND BEING PEELED, in.

r_i = RADIUS OF DRUM PLUS ONE HALF THE THICKNESS OF THE ADHEREND BEING PEELED, in.

F_p = AVERAGE LOAD REQUIRED TO BEND AND PEEL ADHEREND PLUS THE LOAD REQUIRED TO OVERCOME THE RESISTING TORQUE, lb

F_0 = LOAD REQUIRED TO OVERCOME THE RESISTING TORQUE, lb

W = WIDTH OF SPECIMEN, in.

Figure 8. Effect of prolonged humidity exposure on 1 ft^2 sandwich/skin components.
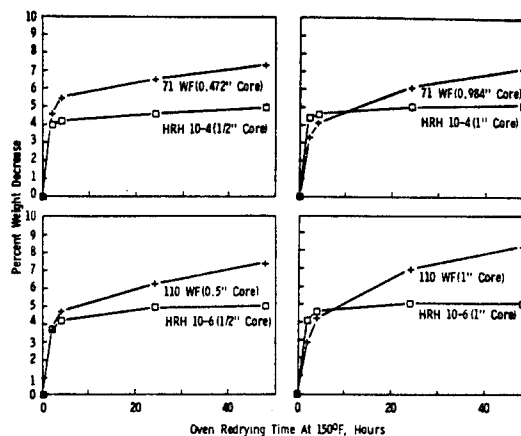
Figure 9. Effect of redry on 1 ft^2 cores after 90-day humidity exposure.
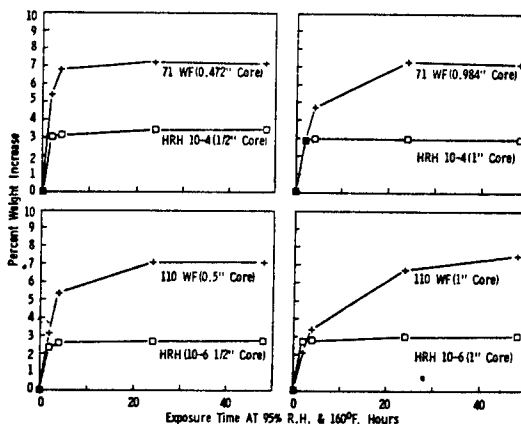
Figure 10. Effect of short-term humidity exposure on 1 ft^2 cores.

Sandwich/Skin Weight Gain - Unsealed Edges

The top halves of Figures 11-14 show the corresponding weight changes of the 3" x 12" climbing drum peel specimens with unsealed edges when exposed to 80 and 160 hours of 95% R.H. and 160°F, and subsequent air circulating oven redry at 140° for 72 hours. The sandwich/skin specimens with pretreated core material registered high weight gains and an equal or higher rate of moisture uptake. At the 160 hour mark, peak percent weight gain for the Nomex was 1.5% for

specimens with pretreated cores and 1.0% for "as-is" or untreated core specimens. There was no significant difference in percent weight gain between the Nomex 1/2" and 1" cores. During the 72 hour redry at 140°F, all specimens returned to or went below their weights as recorded just prior to humidity exposure.

For the Rohacell, peak percent weight gain was 3.2% for specimens with .984" and 1" pretreated cores, double that of the Nomex counterparts, and up to 2.5% for the "as-is" or untreated core specimens. Also, there was a significant difference in the Rohacell thickness-to-percent weight gain relationship, with the thicker cores picking up more moisture. During the subsequent redry, only one specimen returned to its original weight, revealing the foam's greater moisture retention in a sandwich/skin laminate.

Sandwich/Skin Weight Gain-RTV Sealed Edges

The bottom halves of Figures 11-14 show the corresponding weight changes of the climbing drum specimens with RTV-sealed edges when exposed to 360 and 720 hours of 95% R.H. and 160°F, and subsequent redry. Since the edges were sealed off, moisture could only be absorbed through the facings of the sandwich. At the 720 hour mark, peak weight gains for the Nomex were 1.9% for the pretreated HRH 10-4, both 1/2" and 1" core thickness, and up to 2.2% for the HRH 10-6 core. The 72 hour redry took all Nomex specimens back to within .5 grams of the weights before humidity exposure.

For the Rohacell, peak percent weight gain was 4.4% for the pretreated 71 WF .984" core and 6.6% for the 110 WF 1" core. Again, the increase in moisture weight gain due to the thickness of the foam was much more of a factor than with the Nomex. The thicker foams absorbed more moisture and retained it after 72 hour redry than the thinner foams in a sandwich/skin laminate.
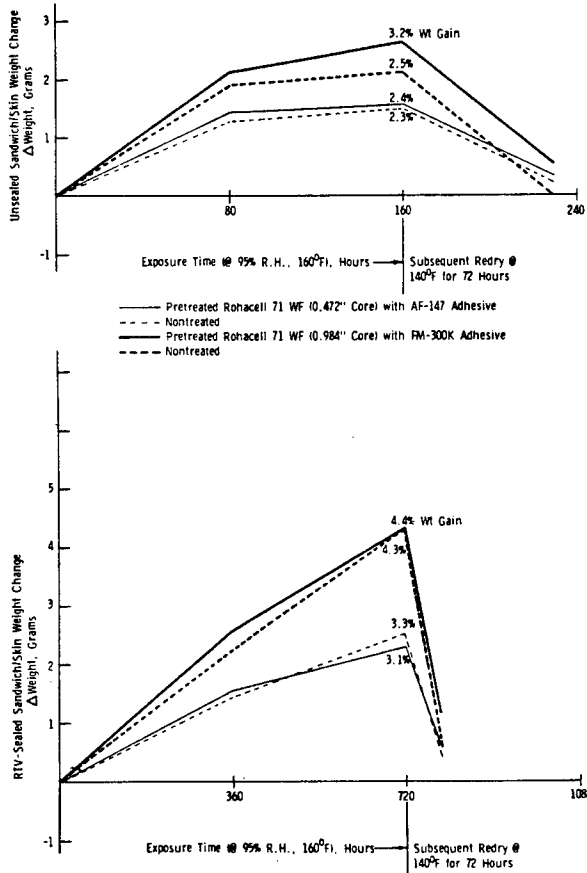
Figure 11. Water weight gain of climbing drum peel specimens - Rohacell 71 WF.
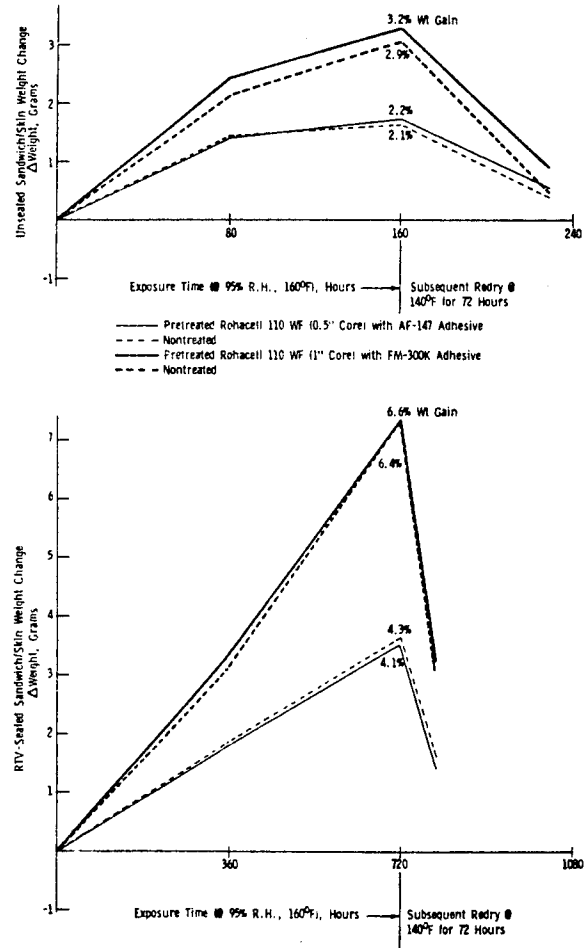
Figure 12. Water weight gain of climbing drum peel specimens - Rohacell 110 WF.
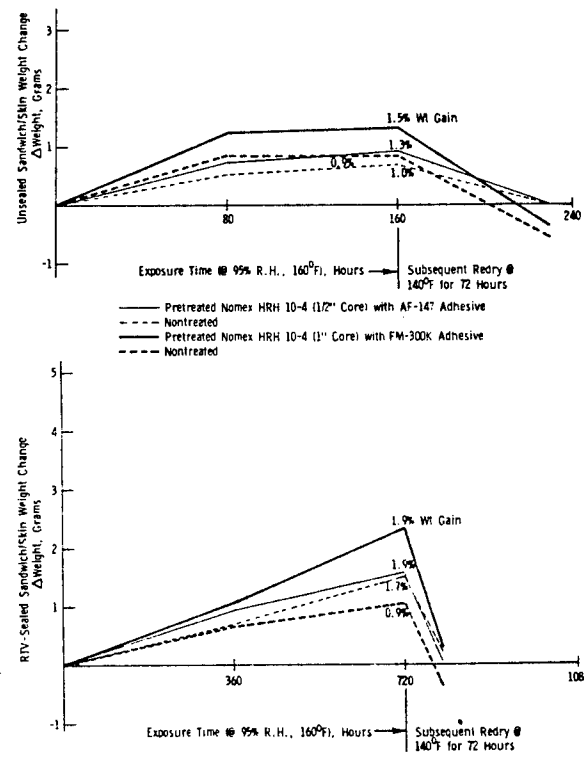
Figure 13. Water weight gain of climbing drum peel specimens - Nomex HRH 10-4.

228
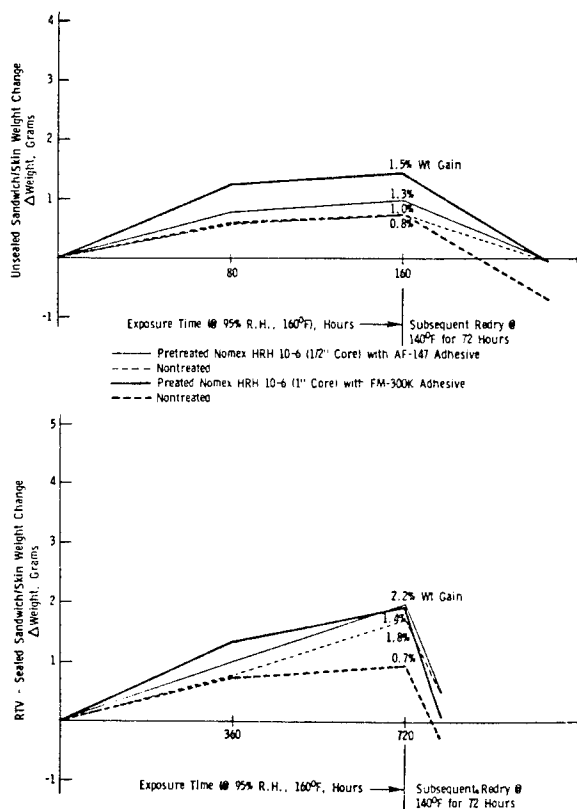
Figure 14. Water weight gain of climbing drum peel specimens - Nomex HRH 10-6.

Average Peel Torque

Since the climbing drum peel test does not discriminate core thickness for determining the peel torque, testing variables were based on core density, core pretreatment, specimen humidity conditioning, and type of structural film adhesive prepreg used.

The type of skin-to-core failures when peeling off skins was significant. Both structural adhesives evaluated bonded better to the Nomex cores than to the Rohacell. For the Rohacell-peeled specimens, the majority of the adhesive was on the skin side rather than on the core. The only evidence of adhesive on the core surface was where small holes were punched through it from the "needling operation", using hand rollers. For the Nomex cores, the adhesive formed a meniscus around each honeycomb cell, which ultimately stayed on the core side.

According to the graphs in Figures 15-18, the trends for the Nomex and Rohacell showed a general increase in peel torque values with humidity exposure time. The AF-147 structural film adhesive performed better for all Nomex specimens, while the FM-300K displayed slightly higher torque values for the Rohacell specimens. The ranges of average peeling torque calculated for the Nomex HRH 10-4 specimens started at 16-20 and spread to 16-29 in. lb/in after exposures. The HRH 10-6 specimens started at 21-23 and fanned out to a range of 16-32 in. lb/in. Rohacell 71 WF average torque values started at a range of 9-13 and changed only slightly to 9-19 in. lb/in. The 110 WF foam values started out at 13-17 and varied only to 13-21 in. lb/in.

From these sandwich/skin test results, the 71 WF specimens averaged about 57% of the HRH 10-4 specimen peel torque, while specimens with 110 WF cores averaged about 67% of the HRH 10-6 core peel torque. There were data points indicating as much as a 3X improvement in average peeling torque with

Figure 15. Average peeling torque of climbing drum specimens - Rohacell 71 WF.
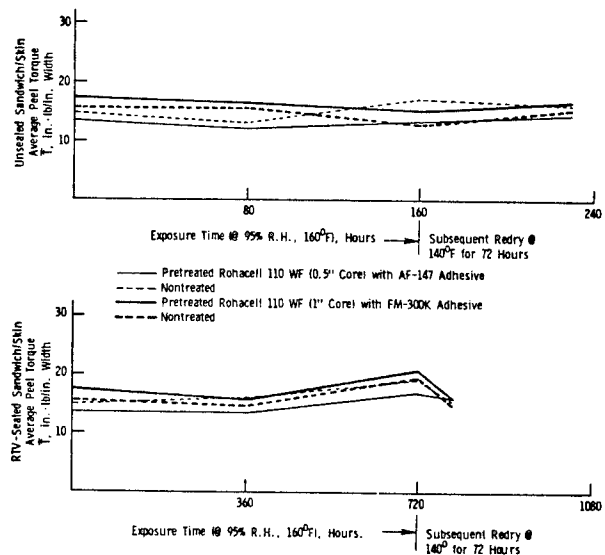
Figure 16. Average peeling torque of climbing drum specimens - Rohacell 110 WF.

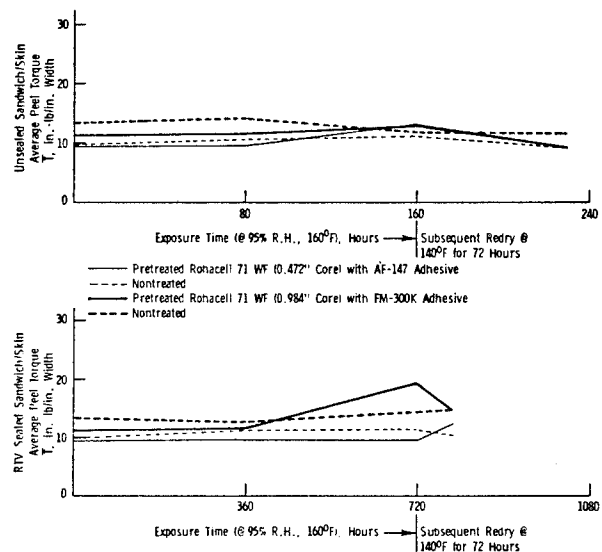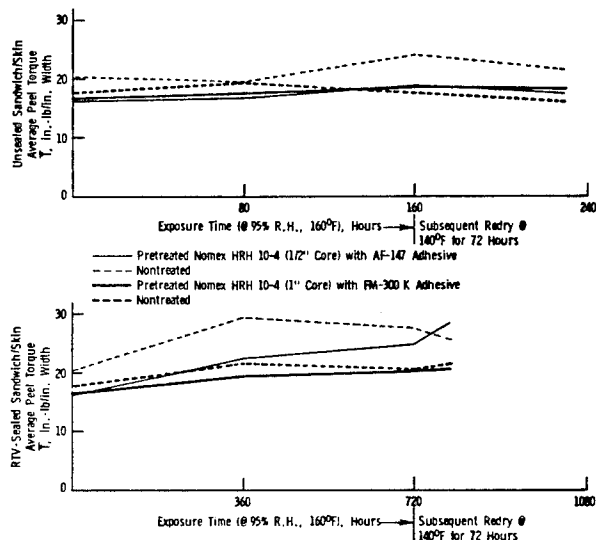Figure 17. Average peeling torque of climbing drum specimens - Nomex HRH 10-4.

229
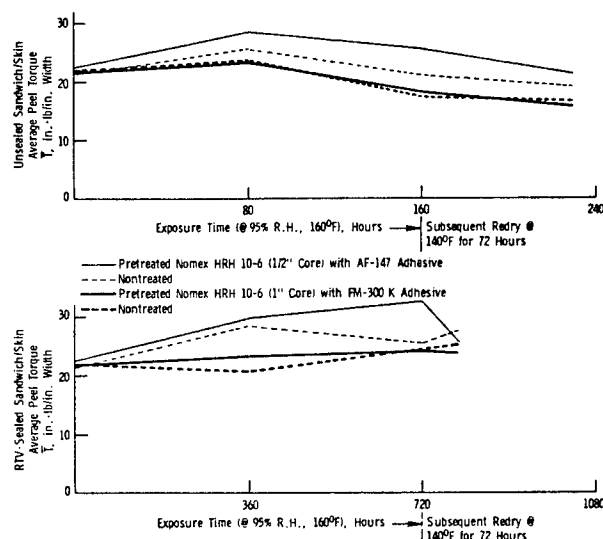
Figure 18. Average peeling torque of climbing drum specimens - Nomex HRH 10-6.

the honeycomb specimens over the structural foam counterparts, but the honeycomb core values fluctuated because of a more complex tearing of skin and honeycomb, while the foam sandwiches peeled much more cleanly.

CONCLUSIONS AND RECOMMENDATIONS

The comparison of moisture weight gains using unprotected core materials only, as well as unsealed and sealed sandwich/skin laminates typical of candidate composite aircraft structures, provided a more realistic guide for understanding how the moisture is absorbed, how much moisture is absorbed and released for given exposures, and its effect on structural integrity.

The results of this study showed that moisture absorption did not effectively decrease the peel torques on the sandwich/skin specimens but actually increased them. A reason for his behavior may be a plasticizing effect or reduced brittleness that the moisture imparted to the sandwich/skin laminates.[12] The moisture also acts to relieve stress concentrations that may be present at the skin/adhesive/core interface.

Since moisture uptake was substantial for the unprotected foam in particular, the need for increased moisture resistance in the skin adhesive bonding film became more significant. The two film adhesives used had very similar weight gains with respect to exposure time, and were found to be compatible with both cores. In the foam specimens, the AF-147 film adhesive was better able to flow into the cell structure and needled holes of the foam core than the FM-300K, but the FM-300K resultant peel torques were marginally higher.

The Nomex honeycomb proved to be superior in moisture weight gain and peeling torque for both densities tested. For Rohacell applications where weight stability is critical and high humidity exposure is significant, it is recommended that lower density and thinner cores be used to minimize weight gain. Also recommended is further study in improved moisture barrier resins and prepregs compatible with the PMI foam. For most applications, however, where a hot wet environment is not a concern, or where the skin thicknesses are greater, the ease to machine and form heat treated PMI foam into complex contour and tapered shapes will continue to be an asset.

REFERENCES

1. Hollman, Martin, "Which Sandwich?", Homebuilt Aircraft, Werner and Werner Publishing Co. Encino, CA, February 1984.

2. Koski, K. J., et al, "Manufacturing Technology for Complex Composite Fuselage Structures", Report IR-469-9 (XV),Contract F33615-81-C-5122 General Dynamics, Ft. Worth, TX, April 1985.

3. Maass, David P. and Hoon, Douglas M., "Low-Cost Thermal Expansion Molding (TEM) Process for Composite Structure Fabrication", The 28th National SAMPE Symposium, April 1983.

4. Ware, M., private communication, Thermal Expansion Resin Transfer Molding (TERTM) Process, We no nah/Maxcraft, Winona, MN, August 1984.

5. Rohacell Technical Information Handbook, CYRO Ind., Orange, CT.

6. "Home Study Course on Sandwich Panels - Part 2", M. C. Gill Corp., El Monte, CA, v. 21, Fall 1984.

7. "Home Study Course on Sandwich Panels - Part 3", M. C. Gill Corp., El Monte, CA, v. 22, Winter 1985.

8. Lubin, George, ed, Handbook of Composites, Van Nostrand Reinhold Co., New York, 1982, ch. 21.

9. Blake, E. E., and Bladwin, J., private communication, PMI foam compressive testing, Bell Helicopter Textron, Ft. Worth, TX, October 1983.

10. Dorf, M., and Caruso, R., private communication, CYRO Ind., Orange, CT, August 1984.

11. Labor, J. D., "Depot Level Repair for Composite Structures", Report NADC-79171-60, Contract N622269-80-C-0232, Northrup Corp., Hawthorne, CA, October 1981.

12. Douglas, C. D., and Pattie, E. R., "Effects of Moisture on the Mechanical Properties of Glass/Epoxy Composites", in Advances in Aerospace Structures and Materials, AD-01, The American Society of Mechanical Engineers, 1981 Winter Annual Meeting.

PROCESS CONSIDERATIONS FOR ROOM TEMPERATURE CURING
STRUCTURAL ADHESIVES

R. D. Hermansen, K. Yeh, S. R. Felstein, D. T. Chow
ELECTRO-OPTICAL & DATA SYSTEMS GROUP - HUGHES AIRCRAFT COMPANY
EL SEGUNDO, CA

1. INTRODUCTION

The assembly of large structures can be accomplished by adhesive bonding using room temperature (RT) curing adhesives. Such a joining technique is routinely utilized for the structural assembly of Hughes Aircraft Company's communication satellites. The large size of these structures makes oven or autoclave cures impractical. Where such adhesive bonds join the primary structure of the spacecraft, special controls must be administered to assure high reliability. The need for reliability is compounded by the tendency to design ultra-light weight assemblies and by the non-repairability of orbiting spacecraft. Thus, a technology of optimizing RT-cured adhesive bonding has evolved at Hughes over more than two decades.

2. COMPARING RT-AND HEAT-CURING STRUCTURAL ADHESIVES

Heat-curing adhesives are most commonly procured in film form, whereas RT-curing adhesives are most commonly procured in paste form. Film adhesives generally consist of a mixture of reactive polymeric ingredients applied to a carrier fabric and sandwiched between removal release films. The task of weighing and blending these ingredients is performed by and proved correct by the adhesive manufacturer prior to leaving their factory. In contrast, paste adhesives are commonly sold as two component kits, which are measured and mixed by the user.

Generally, heat-cured adhesives develop higher bond strengths and may have a higher useful temperature range than do RT-cured adhesives. The process of heat-curing the adhesive drives the polymerization reaction to completion and maximizes the glass transition temperature (Tg) of the polymer. Higher TG's are associated with higher useful temperature limits.

Autoclave processing of the assembly is often employed to apply additional pressure to the bondline and mazimize wettine and adhesion. For these reasons, heat-cured adhesives are preferred over RT-cured adhesives in the absence of other considerations.

Some of the reasons for selecting an RT-cure bonding process include: 1) getting around the size limitations (or non-availability) of autoclaves or ovens, 2) getting faster production rates and less-costly processing, and 3) minimizing the residual stress in the bondline at RT. The last point can be explained as follows: The difference between coefficients of thermal expansion of adherend #1, adherend #2, and the adhesive give rise to a state of residual shear stress in the adhesive as the assembly cools from the cure temperature down to room temperature. It

231

a. Configuration at cure temperature.

b. Same structure after cooling.
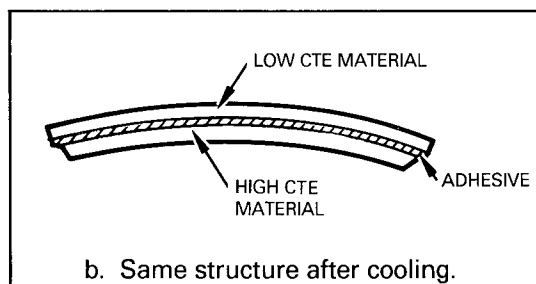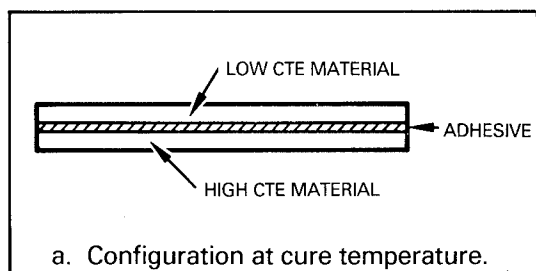
HEAT-CURING OF ADHESIVES MAY WARP OR BREAK
ASSEMBLED HARDWARE DUE TO EXCESSIVE STRESS IN
BONDLINE DURING COOL DOWN

Figure 1. Mismatch of coefficients of
thermal expansion.

Figure 2. INTELSAT VI.

is possible that the stress can be large enough to rupture the adhesive or warp the assembly. This is illustrated in Figure 1. Ideally, the zero-stress state should be the mid-point of the service temperature range. For many applications, RT is the midpoint. If the cure temperature is RT then stress is nearly zero at RT.

3.   APPLICATIONS FOR RT-CURING
     ADHESIVES

There are a variety of applications where the cure of the adhesive is best done at ambient conditions. Assembly of space-craft structures is one case, as mentioned earlier. The size of communication satellites have been getting steadily ever larger. The latest of the Hughes satellites, Intelsat VI, has a fully deployed size of 12 feet diameter x 39 feet long. Figure 2 shows the satellite's size relative to the assembly crew. Such large
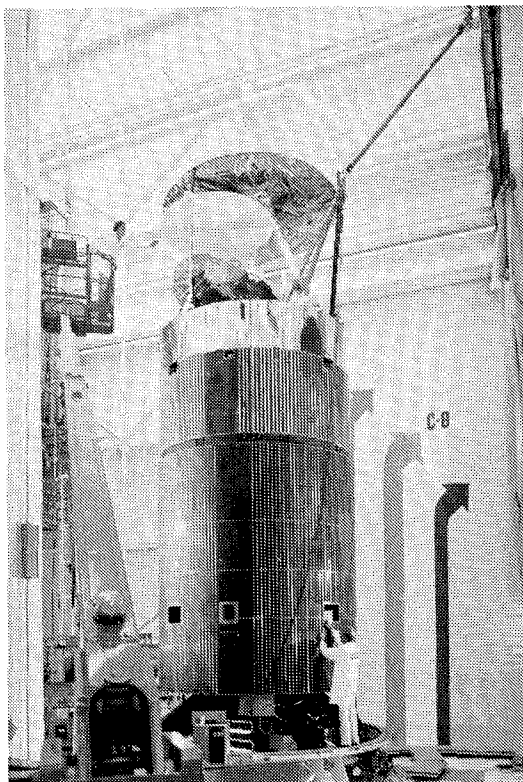
structures, especially when held in their related assembly fixtures, are not readily moved into ovens or autoclaves.

Another application for RT-curing adhesives is the bonding of optical assemblies. Glass is a very low expansion material, but is often joined to higher expansion materials such as aluminum or stainless steel. The brittle nature of glass can easily lead to fractures from the stresses of CTE mismatch. Another problem is distortion of the optics caused by heat cures and stresses formed from cooling. For these reasons, RT cures are used for optical bonding.

Another application, which the authors recently have been involved with, is the assembly of mobile army bridge members. Figure 3 shows the deployment of these tri-arch bridges.

232

Here, due to large size, the army engineers are primarily interested in RT-curing structural adhesives for this application. Cost reduction resulting from open room assembly and avoidance of bondline stress from CTE mismatch are the reasons.

TRI-ARCH BRIDGE CONCEPT
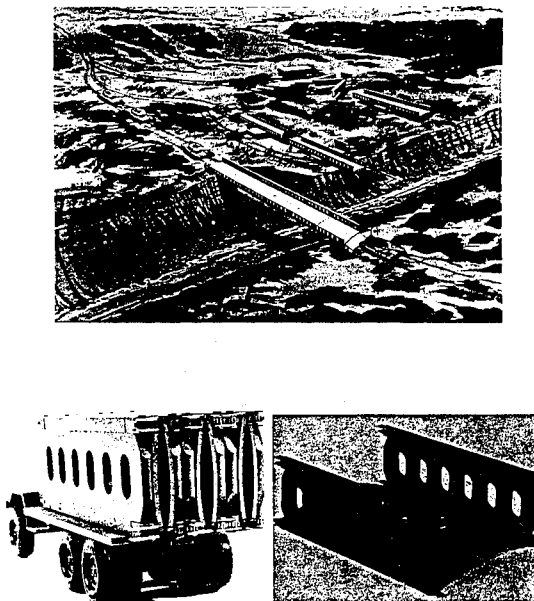
Figure 3. Tri-arch bridge.

Field repair of damaged military equipment and/or structures, especially during combat conditions, is another area for RT-curing structural adhesives. It may be impossible to operate an autoclave process in the field during battle conditions. RT cures with simple, even make-shift tooling is more feasible.

4. SPECIAL PROCEDURES FOR RT-CURING ADHESIVES

Due to the differences between heat-cure and RT-cure bonding processes, a special technology for RT-curing adhesives is really necessary to attain reliable structural bonds. Some of the special considerations are:

4.1 Adherend Preparation

One of the advantages of heat cures is the increased solubility of the adhesive at elevated temperatures. This characteristic allows the adhesive to dissolve and penetrate surface contaminates on the adherend. Lacking this, the RT-curing adhesives require a better level of surface cleanliness and wettability.

The commonly-bonded materials for satellite assemblies include: aluminum, beryllium, titanium, Kevlar/epoxy, graphite-fiber/epoxy composites. Hughes has conducted numerous studies of surface preparation methods for these materials using both film adhesives and RT-curing paste adhesives in the evaluations. There is a greater sensitivity to quality of surface preparation for the RT-curing adhesives. Tank-etching of metallic adherends yields higher bond strengths than paste-etch techniques. The process specifications, which define the acceptable methods of surface preparation, reflect the differences in required lap shear strength by different processes. Fiber-reinforced composite materials require abrasive treatments to remove residual release agents from previous processing and to break the glaze of the epoxy surfaces. However, techniques must not be deleterious to the composites' properties. Table 1 summarizes the preferred methods of surface preparation for various materials.

Use of primers is primarily a convenience to manufacturing. Prepared metal surfaces deteri-

233

TABLE 1. METHODS OF SURFACE PREPARATION FOR STRUCTURAL BONDING

MATERIAL	SURFACE PREPARATION METHOD
ALUMINUM	IMPROVED FPL ETCH METHOD (ALKALINE CLEAN, SULFURIC ACID/ SODIUM DICHROMATE ETCH)
BERYLLIUM	AJAX CLEAN, NITRIC ACID/HYDROFLUORIC ACID ETCH
TITANIUM	ALKALINE HYDROGEN PEROXIDE METHOD
FIBER-REINFORCED PLASTICS	AJAX CLEANING OR SANDPAPER

orate with time and therefore bonding must be performed within hours if the adhesive joint is to develop optimal properties. However, if a primer is applied to the etched metallic surface instead of the adhesive, the prepared adherend may be stored for months. Manufacturing has more leeway in scheduling operations as a result of using primers.

If corrosion-resistant primers are required for sensitive substrates such as beryllium, the primer is serving two functions. The first function is as a protective coating. The protective mechanism is due to corrosion inhibitors, such as zinc chromate being incorporated in the primer formulation. The second function is as a convenience to manufacturing as stated above.

4.2 Adhesive Preparation

The accurate weighing and propper mixing of adhesive components is a skill-dependent process. Weighing errors, under-mixed adhesive, or air-bubble-laden adhesive could cause a structural failure to occur in the adhesive if the strength is inadequate. Film adhesives do not have this problem because the weighing and mixing have been done beforehand and the properties of the resultant adhesive verified. However, paste adhesives require special verification for each in-house preparation of adhesive. Special training of bonding technicians is utilized to assure that the proper techniques are learned. Furthermore, representative lap shear specimens are made and tested.

To assure even greater reliability, frozen premix cartridges are prepared of the most commonly-used adhesives to relieve the technicians of the weighing/mixing operation. Freezing the adhesive immediately after mixing ingredients and storing at -40 °F suspends the curing reactions until thawed for use. Small samplings are taken from each frozen cartridge. The samples are used to verify that lap shear strength is acceptable. Some drawbacks to frozen premixes are: some delay to manufacturing in allowing for the thawing of the adhesive, loss of freezer electrical power which can endanger the stock of frozen premix, and processing characteristics of frozen premixes change with storage time. Figure 4 illustrates that the work life of frozen premixed adhesive RTC-1 diminishes with freezer storage time. Freshly frozen adhesive can be applied even 150 minutes after thawing without appreciable loss of lap shear strength. Five month old adhesive must be applied quickly after thawing to avoid a loss of lap shear strength.

234
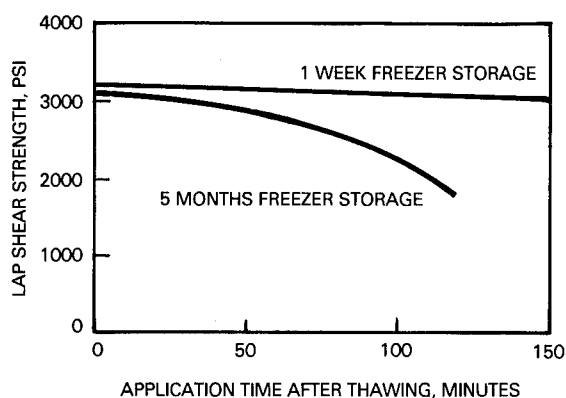
Figure 4. Lap shear strength dependence on adhesive application time versus freezer storage age for frozen premixed adhesive.

Figure 5. SEMKIT mixing machine.

Another approach to the reliability question is the use of preweighed kits in their own mixing container. The Semkit concept is an example. (Semkit is a tradename of Semco Division, Products Research Corp.) The reactive components are preweighed into the Semkit, but are separated by a foil barrier (Barrier Kit) or by an injector valve (Injector Kit). Semkit mixing machines are used to mix the adhesive when it is needed. Figure 5 illustrates the use of a Semkit mixing machine. The pre-packaged approach avoids thaw time delays and freezer malfunction concerns.

4.3 Adhesive Application - Timing Considerations

RT-curing paste adhesives must be reactive enough to polymerize under such adverse conditions as in thin layers adjacent to thermally-conducting heat sinks like aluminum. On the other hand, the pot of mixed adhesive, where the heat of reaction is well retained, must NOT polymerize too rapidly so the work life of the adhesive is impractically short.

Work life can be defined as the time interval from start-of-mixing to end-of-spreadibility. Many of the paste adhesives exhibit shorter work lives for larger quantities being mixed. Therefore, work life test methods generally specify a defined quantity of adhesive and a defined final viscosity.

Once the adhesive is spread to the thickness of a typical bondline (e.g., ten mils), the viscosity changes in the adhesive are much slower than for the same adhesive in the pot. The additional time may be vitally needed to position and close tooling for complex assemblies. The time interval from application-of-adhesive to safe-closing-of-tooling is called the "open assembly time." The open assembly time for an adhesive can be determined by spreading adhesive simultaneously to lap shear

235

specimens and assembling the
specimens and closing the fix-
tures at increasing time inter-
vals. The resultant lap shear
strengths can be plotted
against closure time and the
open assembly time determined
by what is deemed to be safe.
Figure 6 shows the change in
lap shear strength of frozen
premixed adhesive RTC-1 versus
fixture closure time. Both
freshly frozen and 5 month old
adhesives are plotted in this
figure. The open assembly time
can be determined by engineer-
ing judgement from this data.

Figure 7. Rheometrics analyzer.

Figure 6. Lap shear strength dependence on
fixture closure time versus freezer
storage age for frozen premixed
adhesive.

Laboratory methods of evalu-
ating the behavior of the re-
acting liquid adhesive have
been getting more sophisticated
in recent years. In the past,
viscosity changes were measured
with a Brookfield Viscometer.
This instrument requires a bulk
amount of liquid (preferably
400 cc), some external control
of the liquid temperature, and
frequency readings by the tech-
nician. A newer method, which
is more applicable to studying
adhesives, involves the use of
a Rheometrics Analyzer as shown
in Figure 7. This latter in-
strument measures a thin layer
of sample, has programmable

temperature/monitoring control,
automatically measures changes
in the polymerizing liquid, and
computes values for different
properties. Thus, viscosity
versus time versus temperature
determinations are measurable
on thin cross-sections similar
to a bondline. Timing of gela-
tion and cross-linking can also
be determined. Table 2 shows
that Rhoemetrics obtained the
same work life for Adhesive
RTC-1 in a simple determination
as was obtained by extensive
mechanical testing.

TABLE 2. COMPARISON OF METHODS
FOR DETERMINING WORK LIFE OF A
FROZEN PREMIXED ADHESIVE

TEST METHOD	WORK LIFE, MINUTES	
	FRESHLY FROZEN ADHESIVE	TWO MONTH OLD FROZEN ADHESIVE
RHEOMETRICS (ONSET OF GELLATION)	115	80
CHANGE IN LAP SHEAR FAILURE MODE (FROM COHESIVE TO ADHESIVE)	BETWEEN 120 AND 150	BETWEEN 75 AND 90

Having adequate work life and
adequate open assembly time is
not the last of the require-
ments for a good paste adhe-
sive. It must also cure fast
enough to allow the tooling/

fixturing to be used for the next unit in a reasonable time. Thus, a trade-off between long work life/open assembly time and cure-to-handling-time usually must be made. Figure 8 shows the development of lap shear strength over the first 20 hours after application for Adhesive RTC-1. Cure-to-handling-time can be defined in in terms of the corresponding time to attain some minimum lap lap shear strength.

surface. In other cases, the best fit may cause larger bondlines at one location than at another. Figure 9 shows the relationship between lap shear strength and bondline thickness for Adhesive RTC-1. The strength is optimal for the smallest bondline (2 mil) and gradually decreases with increasing bondline thickness.
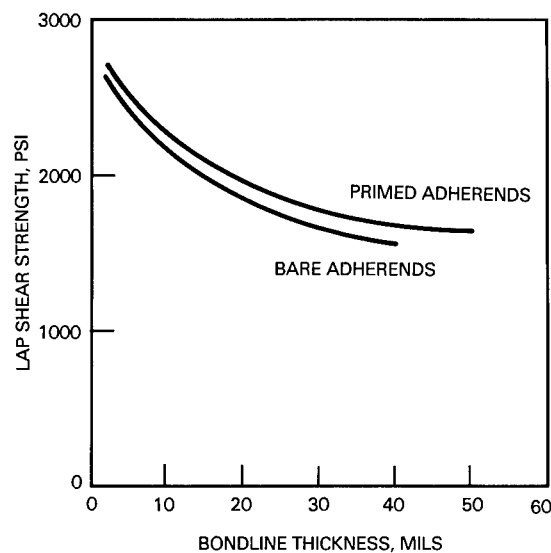
Figure 9. Lap shear strength of aluminum-aluminum specimens bonded with adhesive RTC-1 versus bondline thickness.

Figure 8. Lap shear strength of adhesive RTC-1 versus room temperature cure hours.

4.4 Adhesive Application - Geometric Considerations

In assembly of spacecraft structures, the configuration of the bondline gap may or may not be a uniform dimension. A commonly encountered irregular gap occurs when a flat component is bonded to the circular exterior of the structure. This exterior, being a large radius, is nearly flat. However, the bondline may vary from 5 mils to 60 mils due to the deviation from a truly flat

surface. Where bondlines are wedge-shaped, the paste adhesive may tend to run out of the gap. This is particularly true for vertical bondlines. For such assemblies, the adhesive should have a non-sag consistency. This characteristic is called thixotropy and is a time-dependent, non-newtonian phenomenon. That is, the resistance of the paste to shear forces becomes disproportionately high at low shear rates and even increases further when undisturbed. Small additions of fumed silica powder to the paste adhesive causes thixotropy to develop.

237

The opposite kind of problem can develop with injection bonding processes. That is, the sag resistance of the paste adhesive may be too high to allow good wetting of adherends, complete air bubble release, and knitting of adhesive. Injection bonding is a process, where the liquid adhesive is pumped into a cavity between two parts. A common application is the joining of tubular beams to socket clevises. The dimensions of these parts must be precise in order to fit into later assemblies. The fixturing determines the distance between pin points. Hughes has developed tests to compare adhesives for injection bond processing. One simple test that worked particularly well was to determine the distance an adhesive can travel in small diameter Tygon tubing under a fixed air pressure.

4.5 Cure Conditions

Do RT-curing adhesives fully cure at room temperature? One of the most effective instruments for answering this question is a Differential Scanning Calorimeter (DSC) as shown in Figure 10. This device can detect exotherms (i.e., heat of reaction in an adhesive) if the previous cure had not driven

the polymerization reaction to completion. Table 3 shows the residual exothermic heat released from Adhesive RTC-2, which has been subjected to a variety of cure schedules. The heat energies were compared by determining the area under the exothermic peak on the graphical output from the tests. It is interesting to note that the cure is not complete even after 22 days at room temperature. However, one hour at 180 °F essentially completed the cure.

TABLE 3. CURE STATE OF RT-CURING ADHESIVE USING DIFFERENTIAL SCANNING CALORIMETRY

CURE	POSTCURE	EXOTHERMIC HEAT UNRELEASED*
18 HOURS AT 75°F	NONE	100 UNITS
5 DAYS AT 75°F	NONE	76 UNITS
22 DAYS AT 75°F	NONE	59 UNITS
18 HOURS AT 75°F	4 HOURS AT 125°F	39 UNITS
18 HOURS AT 75°F	6 HOURS AT 125°F	31 UNITS
18 HOURS AT 75°F	8 HOURS AT 125°F	31 UNITS
2 HOURS AT 160°F	NONE	10 UNITS
1 HOUR AT 180°	NONE	5 UNITS

*1 UNIT IS ARBITRARILY DEFINED AS 2.42×10^{-3} IN^2 AREA UNDER DSC EXOTHERM CURVE PER mg OF SAMPLE.

Rheometrics also is an excellent technique for measuring changes in the adhesive during cure or after different kinds of cures. The shear modulus of the cured adhesive can be measured and reported as a function of temperature, the glass transition temperature determined, and even the cross-link density of the adhesive polymer can be inferred from the data.

Designers should be warned that some adhesives drastically lose strength during their first climb to higher temperatures. Although a gradual temperature

R90 SYSTEM MODULES

910 DIFFERENTIAL SCANNING CALORIMETER (DSC)
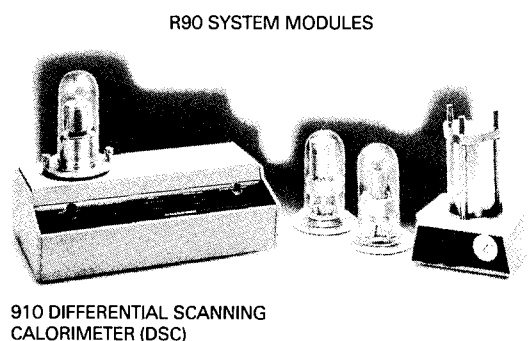
Figure 10. Differential scanning calorimeter.

238

rise may be safe, a rapid temperature rise of the adhesive if under load may be catastrophic. The difference is that with the slower temperature rise, additional curing and development of elevated temperature strength is taking place. Whereas, with the rapid temperature rise, there is little available elevated temperature strength. Figure 11 shows the rapid loss of modulus of an RT-cured adhesive upon first exposure to elevated temperatures. The data was obtained using a Rheometrics instrument oscillating at 11 Hz. Note that the same adhesive postcured one hour at 180 °F did not have the sudden drop in modulus. Adhesive formulators can circumvent these problems by using high functionality resins and curing agents.

cal applications are large-sized structures. Successful use of RT-curing adhesives depends upon: optimal surface preparation of adherends, reliable mixing/packaging techniques, proper trade-offs between work life and quick curing, proper selection of bondline thickness and tooling orientations, and adequate cures.
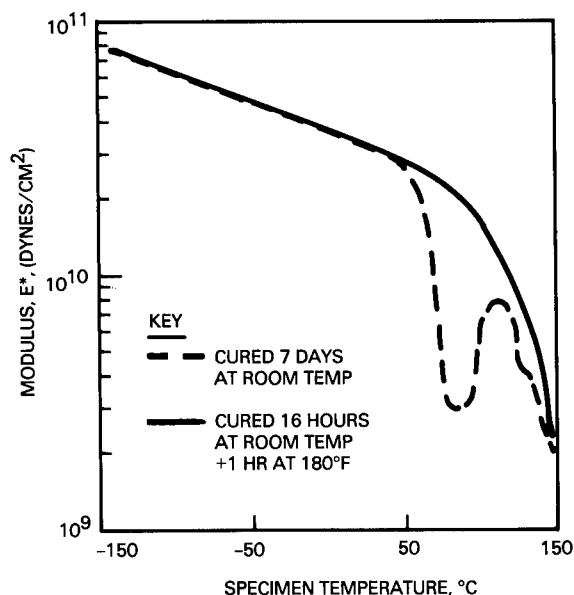
Figure 11. Modulus versus temperature for adhesive RTC-2 for two different cure conditions.

5. SUMMARY

There are applications where RT-curing adhesives are preferred to heat-curing adhesives for structural bonding. Typi-

239

HIGH TEMPERATURE ADHESIVES

Ronald J. Kuhbander
University of Dayton
300 College Park Avenue
Dayton, Ohio 45469

ABSTRACT

With the development of new air-to-air missile technology, which may utilize graphite/polyimide composites as body and/or control surfaces, it was discovered there was a lack of data available on structural adhesive systems suitable for use at temperatures in excess of 1,000°F. A program was conducted to evaluate several adhesives in tensile lap shear at temperatures of -65°F to 1,000°F. The tensile lap shear properties were also determined after exposure to temperature and high humidity. The adhesive systems include the following polyimides: Thermid LR-600, LaRC-13, PMR-15, FM-34, FM-34B-18, FM-36, IP-600, NR-150, FA-7001, and LaRC-TPI. Data are also given for PBI and PBI paper. Most of the data presented were obtained using titanium to titanium lap shear specimens. Some discussion of surface preparation is included. Special attention is given cure and postcure cycles so each adhesive would be suitable for bonding to graphite/polyimide composite structures.

1. BACKGROUND AND INTRODUCTION

The University of Dayton Research Institute under an Air Force contract at Wright-Patterson Air Force Base, Ohio, has fabricated and tested structural elements representative of a missile control surface utilizing high temperature reinforced plastic laminates. The design of these structural elements required adhesive bonding of individual components into the final missile control surface. The structural element assembly was subjected to windtunnel tests in which the air temperature exceeded 1000°F (538°C). During the tests the structural elements were subjected to this high temperature until failure. However, the failure did not occur in the reinforced plastic laminates, but rather in the adhesive used to bond the elements together. Although improvements could be made in the integrity of the element by changes in design, a search was made to determine what structural adhesives would perform best at temperatures up to 1000°F (538°C). It was discovered that for most candidate adhesives little or no data existed above 600°F (316°C). Therefore, an investigation was undertaken to generate data on some candidate adhesives at high temperatures for short time periods.

In performing this investigation it was necessary to choose adhesives that were readily available to the laboratory at UDRI. The adhesive or adhesives which maintained the highest structural integrity would be used to fabricate additional windtunnel structural elements. Another consideration in choosing an adhesive for element fabrication would be processing conditions. However, all readily available candidates would be evaluated. In the fabrication of elements, the adhesives would be bonding composites to composites; however, due to both cost and time considerations the adherends in this evaluation would be 6-4 titanium and to a lesser degree 17-7 PH stainless steel. Close observation would be made of the failure modes to

ensure that the results would reflect adhesive properties and not the metal to adhesive interface.

2. ADHESIVE SELECTION AND PREPARATION

An inventory was taken of the readily available candidate adhesives and were as follows: Thermid LR-600, LaRC-13, PBI (polybenzimidazole), PMR-15, and FM-34. Later in the program two additional adhesives were selected: FM-34B-18 and FM-36. After this evaluation was completed it became apparent that an excellent data base was being accumulated. Additional adhesives were then selected for the purpose of expanding that data base and include: IP-600, FA-7001, LaRC-TPI, NR-150, and PBI paper.

Some of the adhesives in the inventory were in the form of films and were supplied by commercial sources. Other adhesives were in the form of "neat" resin and the adhesive films were processed at UDRI. Table 1 lists the adhesives, resin source, and adhesive film source.

All of the adhesive films that were processed at UDRI were supported with heat cleaned 112 style glass cloth. The adhesive was applied to the glass cloth from a solution of solvent and dissolved resin. It was then necessary to remove most of the solvent using heat which resulted in a film that could be easily handled, cut into desired sizes, and fabricated into adhesive bonds. Also, during the drying cycle some chamical reaction may have taken place known as imidization. Table 2 lists the adhesives processed at UDRI and the drying and/or

imidizing cycle. In some cases the adhesive film required more than one application to obtain the desired resin content.

3. ADHERENDS AND SURFACE PREPARATION

Initially, the intended use for the adhesives evaluated in this program was to bond graphite/polyimide composite to composite. However, due to the relative cost, and in particular, to the short time required to have sufficient data to choose an adhesive for the wind-tunnel test specimens, 6Al-4V titanium and to a lesser degree, 17-7 PH stainless steel were chosen for adherends. Similar considerations were given the candidate surface preparations as were the candidate adherends. The choice for titanium was an acidic gelatin known as Pasa-Jel 107. The gelatin was applied for 10-15 minutes, rinsed thoroughly with deionized water, and immediately dried at 160°F (71°C). Surface preparations for titanium do exist which may be superior to Pasa-Jel 107; however, these are primarily known for their long term durability. None of the data generated in this program was considered long term. Regardless, special attention was given to the failure modes to ensure the results would reflect adhesive properties and not interface properties. The choice for stainless steel is known as the phosphate etch. It consists of hydrochloric acid (841 ml), phosphoric acid (89 ml), and hydrofluoric acid (43 ml). Application was at 180°F (82°C) for 2 minutes, then the specimens were thoroughly rinsed in deionized water and dried at 160°F (71°C).

241

Nearly all the specimens, titanium and steel, were primed immediately after the surface preparation. The primers for PMR-15, FM-34, FM-34B-18, and FM-36 were supplied by the adhesive manufacturers. The primers for LR-600, LaRC-13, PBI, IP-600, FA-7001, LaRC-TPI, and NR-150 were prepared at UDRI by diluting the adhesive neat resin with solvent to about a 10% solids solution. The primers were then dried and the specimens were placed in a dessicated cabinet until fabrication.

3.1 Specimen Geometry

The type specimen used in this investigation was a single overlap specimen as recommended in ASTM D1002. The titanium specimens were fabricated from five finger panels. The stainless steel specimens were fabricated individually with five specimens in the curing fixture at a time. All specimens had an overlap of 1 inch (2.54 cm) in width and 0.5 inch (1.27 cm) in length. The thickness of both the titanium and stainless steel adherends was 0.050 inch (0.13 cm). No control was given the thickness of the glueline other than that supplied by the adhesive film and the curing process.

3.2 Cure and Postcure Cycles

The cure and postcure cycles for the adhesives used are not necessarily well established, in particular for use temperatures in excess of 600°F (316°C). The cure and postcure cycles selected were based on information from the manufacturer and/or the developer of the adhesive. Time did not allow for optimization of cure and postcure cycles. The selected cycles reflect the choice of the author based on what information was available. One of the prime considerations in the selection was that the adhesive chosen would have cure and postcure cycles compatible with the fabrication of the structural elements for windtunnel testing. Some of the candidates added later to the program do not necessarily meet this requirement.

4. TEST CONDITIONS AND PROCEDURES

The test condition of most interest was that at 1000°F (538°C) after short time periods at that temperature. Intermediate temperatures, between 600°F (316°C) and 1000°F (538°C) would also be helpful to obtain a good baseline for all adhesives investigated. It also seemed appropriate to determine what effect hot-humid aging would have on shear properties. Since these adhesive materials are candidates to be used in the construction of air-launched missile systems, it was also of interest to determine shear properties at higher test speeds than that normally used for tensile lap shear, in particular at low test temperatures. The speeds selected were 20 times the normal rate and then 20 times the intermediate rate. Table 3 lists all the test conditions used in this program. The lap shear tests were conducted in accordance with ASTM methods D1002 and D2295. Prior to each series of tests, a dummy specimen was used to preset the test chamber to the desired test temperature. Temperature control was maintained at ±1 percent of the desired temperature.

5. DISCUSSION OF RESULTS

Most of the data discussed here is from the initial seven adhesives selected: LR-600,

242

LaRC-13, PMR-15, FM-34, FM-34B-18, PBI, and FM-36. These seven adhesives were readily available to UDRI and each seemed to be a suitable candidate for the construction of windtunnel test elements. Currently the data base is being expanded to include: IP-600, FA-7001, LaRC-TPI, NR-150, and PBI paper. This is work in progress and only a small amount of data is available here, but more is expected during the presentation at the symposium on "Structural Adhesive Bonding".

5.1 Titanium to Titanium Lap Shear Strengths

Results were obtained from specimens fabricated using 6-4 titanium at dry conditions from -65°F (-54°C) to 1000°F (538°C), wet conditions from R.T. to 600°F (316°C), and at accelerated test speeds from -65°F (-54°C) to R.T. Usually one, five finger panel was fabricated for each data point. On occasion individual specimens were fabricated but even then five were placed in the fabrication fixture.

Table 4 lists the data obtained for the original seven adhesives and a limited amount for the additional five adhesives at normal test speeds and dry aging conditions. Examination of the data indicates several interesting items. All the adhesives maintain a substantial % of the room temperature lap shear strength after 0.1 hour at 1000°F (538°C). Five adhesives maintain about 20% of the R.T. strength: LR-600, PMR-15, FM-34, FM-34B-18, and FM-36. One adhesive, PBI, maintained about 30% and one adhesive, LaRC-13, about 35%. PBI appears to withstand both 600°F (316°C) and 800°F (427°C) better than the other six adhesives, which

all have similar properties at those test temperatures. Also, most of the adhesives appear to have higher lap shear strengths at any given temperature with increased time at that temperature. This may be caused by insufficient postcure, at least for the conditions tested in this program. No postcure study was undertaken because it was not the intent of this effort to optimize the cure or postcure cycle of any of the adhesives.

5.2 Lap Shear Strengths After Humidity Aging

Adhesive bonded panels were prepared and humidity aged at 160°F (71°C) and 95-100% relative humidity for two weeks and then tested at room temperature and at 600°F (316°C) after 3 minutes exposure at 600°F (316°C). At room temperature the adhesives maintained from 65% (PMR-15) to 85% (LaRC-13) of their dry room temperature strength. The wet lap shear strengths at 600°F (316°C) after 3 minutes are almost identical to those obtained for dry specimens at 600°F (316°C) after 10 minutes, indicating that the heat soak probably dried the lap joint. If so, at least the lap shear strength does recover after removal of absorbed moisture. When tested at elevated temperature the adhesives appear to be affected more by that temperature than by absorbed moisture. The results for the original seven adhesives and what limited data obtained for the additional five are shown in Table 5.

5.3 Lap Shear Strengths At High Test Speeds

Upon completion of the initial adhesive investigation, a candidate would be selected to

243

adhesively bond structural elements representative of missile control surfaces for windtunnel testing. Although not necessarily pertinent here, some question arose to how these candidates would perform under high load rates, in particular at reduced temperatures. Tensile lap shear tests were then obtained at 20 times the normal test speed and then 20 times that speed at both R.T. and at -65°F (-54°C). The results obtained at the first accelerated test speed were not significantly different than those at normal rates. However, at the fastest test speed, which is 400 times the normal, there is a significant reduction in tensile lap shear strength. At room temperature all of the adhesives evaluated were reduced in strength by 50%. At -65°F (-54°C) some of the adhesives (PMR-15, FM-34B-18, PBI, and FM-36) were about 80% to 90% of that obtained at the normal test rate. Two adhesives, LR-600 and LaRC-13, were about the same at R.T. and -65°F (-54°C). Perhaps this is an indication of the toughness of the adhesives; if so, the latter two may indeed be much tougher than those others evaluated in the investigation.

5.4 Stainless Steel to Stainless Steel Lap Shear Strengths

A very limited amount of data was obtained from specimens fabricated using 17-7 PH stainless steel. The results obtained are shown in Table 7 and are not significantly different than those obtained for the same adhesives using titanium adherends. Since much of this paper is presenting work in progress, some additional data may be obtained. If no change in lap shear strength is observed due to adherend type, the amount of data obtained will be limited.

6. SUMMARY

The initial work on this program was initiated because there was a lack of engineering data on structural adhesives above 600°F (316°C). At least 12 adhesives have now been included in the data base. Other adhesives may be added at some later date and possibly other tests could be included, in particular tests which may reflect adhesive toughness.

Upon completion of the testing for the original seven adhesives, two were selected for use in the fabrication of structural elements for windtunnel tests, LR-600 and LaRC-13. Although many of the adhesives evaluated maintained a significant % of strength at 1000°F (538°C), these two appeared to have the best properties at all conditions tested. Elements were fabricated and successfully windtunnel tested at temperatures well in excess of 1000°F (538°C).

7. ACKNOWLEDGEMENTS

TABLE 1

LIST OF ADHESIVE, RESIN, AND ADHESIVE FILM SOURCES

Adhesives	Neat Resin	Adhesive Film
LR-600	Gulf[1]	UDRI
LaRC-13	UDRI[2]	UDRI
PBI	Acurex	UDRI
PMR-15	Ferro	Ferro
FM-34	American Cyanamid	American Cyanamid
FM-34B-18	American Cyanamid	American Cyanamid
FM-36	American Cyanamid	American Cyanamid
IP-600	National Starch	UDRI
FA-7001	National Starch	UDRI
LaRC-TPI	Rogers	UDRI
NR-150	DuPont	UDRI
PBI Paper	Celanese	Celanese

[1]No longer available from Gulf, currently available from National Starch.

[2]Formulated at UDRI with instructions from NASA Langley.

TABLE 2

DRYING AND/OR IMIDIZING CYCLES FOR
PREPARATION OF ADHESIVE FILMS

Adhesive	Drying and/or Imidizing Cycle
LR-600	45 mins. @ 250°F (121°C) plus 30 mins. @ 375°F (191°C)
LaRC-13	60 mins. @ 275°F (135°C)
PBI	30 mins. @ 175°F (80°C) @ 15 in. Hg Vac. plus 30 mins. @ 175°F (80°C) @ 30 in. Hg Vac.
IP-600	45 mins. @ 250°F (121°C)
FA-7001	45 mins. @ 250°F (121°C)
LaRC-TPI	4 mins. @ 375°F (191°C)
NR-150	40 mins. @ 185°F (80°C) plus (1st application) 20 mins. @ 212°F (100°C) plus 20 mins. @ 248°F (120°C) 40 mins. @ 185°F (80°C) plus (2nd application) 20 mins. @ 212°F (100°C)

TABLE 3

TEST CONDITIONS FOR HIGH TEMPERATURE
ADHESIVES STUDY

6 Al-4V Titanium

10 min. @ -65°F (-54°C)	humidity aged[1]
72°F (22°C)	72°F (22°C)
10 min. @ 600°F (316°C)	0.05 hr. @ 600°F (316°C)
0.5 hr. @ 600°F (316°C)	test @ 1 in./min. (2.54 cm/min.)[2]
24 hr. @ 600°F (316°C)	
0.1 hr. @ 800°F (427°C)	10 min. @ -65°F (-54°C)
0.5 hr. @ 800°F (427°C)	72°F (22°C)
0.1 hr. @ 1000°F (538°C)	test @ 20 in./min. (50 cm/min.)[2]
	10 min. @ -65°F (-54°C)
	72°F (22°C)

17-7 PH Stainless Steel

72°F (22°C)

0.5 hr. @ 600°F (316°C)

0.5 hr. @ 800°F (427°C)

0.1 hr. @ 1000°F (538°C)

---

[1] 2 weeks @ 160°F (71°C) and 95-100% relative humidity.

[2] Higher test speeds, all others were 0.05 in/min. (0.13 cm/min.).

TABLE 4

LAP SHEAR STRENGTH OF HIGH TEMPERATURE
ADHESIVES ON TITANIUM ADHERENDS

Test Condition	LR-600		LaRC-13		PMR-15		FM-34		FM-34B-18		PBI		FM-36	
	(psi)	[MPa]	(psi)	[MPa]	(psi)	[MPa]	(psi)	[MPa]	(psi)	[MPa]	(psi)	[MPa]	(psi)	[MPa]
0.17 hr. @ -65°F(-54°C)	2270	[15.6]	2530	[17.4]	2020	[13.9]	---	---	2600	[17.9]	1140	[7.9]	3320	[22.9]
72°F (22°C)	2830	[19.5]	2270	[15.6]	2290	[15.8]	3480	[24.0]	2880	[19.8]	2690	[18.5]	3080	[21.2]
0.17 hr. @ 600°F(316°C)	1270	[8.8]	1355	[9.3]	1240	[8.5]	1280	[8.8]	1220	[8.4]	1725	[11.9]	1400	[9.6]
0.5 hr. @ 600°F (316°C)	1250	[8.6]	1370	[9.4]	1770	[12.2]	1350	[9.3]	1285	[8.8]	1800	[12.4]	1280	[8.8]
24 hrs. @ 600°F(316°C)	1710	[11.8]	1330	[9.2]	1340	[9.2]	1730	[11.9]	1370	[9.4]	1960	[13.5]	1550	[10.7]
0.1 hr. @ 800°F(427°C)	575	[4.0]	555	[3.8]	485	[3.3]	860	[5.9]	700	[4.8]	915	[6.3]	560	[3.9]
0.5 hr. @ 800°F(427°C)	740	[5.1]	920	[6.3]	860	[5.9]	1065	[7.3]	785	[5.4]	950	[6.5]	880	[6.1]
0.1 hr. @ 1000°F(538°C)	580	[4.0]	810	[5.6]	480	[3.3]	775	[5.3]	635	[4.4]	760	[5.2]	615	[4.2]

247

TABLE 4 (Continued)

LAP SHEAR STRENGTH OF HIGH TEMPERATURE
ADHESIVES ON TITANIUM ADHERENDS

Test Condition	NR-150		IP-600		FA-7001		LaRC-TPI		PBI Paper	
	(psi)	[MPa]	(psi)	[MPa]	(psi)	[MPa]	(psi)	[MPa]	(psi)	[MPa]
0.17 hr. @ -65°F (-54°C)										
72°F (22°C)	2275	[15.7]	2425	[16.7]	1865	[12.8]	2060	[14.2]		
0.17 hr. @ 600°F (316°C)										
0.5 hr. @ 600°F (316°C)										
24 hrs. @ 600°F (316°C)										
0.1 hr. @ 800°F (427°C)										
0.5 hr. @ 800°F (427°C)										
0.1 hr. @ 1000°F (538°C)										

248

TABLE 5

LAP SHEAR STRENGTH OF HIGH TEMPERATURE
ADHESIVES ON TITANIUM ADHERENDS

After 2 Weeks @ 160°F (71°C) and 95-100% R.H.

Test Condition	LR-600 (psi) [MPa]		LaRC-13 (psi) [MPa]		PMR-15 (psi) [MPa]		FM-34 (psi) [MPa]		FM-34B-18 (psi) [MPa]		PBI (psi) [MPa]		FM-36 (psi) [MPa]	
Wet														
72°F (22°C)	2330	[16.1]	1930	[13.3]	1430	[9.9]	2410	[16.6]	1900	[13.1]	2040	[14.1]	2250	[15.5]
0.05 hr. @ 600°F(316°C)	1450	[10.1]	1320	[9.1]	1280	[8.8]	1110	[7.6]	1165	[8.0]	2130	[14.7]	1020	[7.0]
Dry														
72°F (22°C)	2830	[19.5]	2270	[15.6]	2290	[15.8]	3480	[24.0]	2880	[19.8]	2690	[18.5]	3080	[21.2]
0.17 hr. @ 600°F(316°C)	1270	[8.8]	1355	[9.3]	1270	[8.5]	1280	[8.8]	1220	[8.4]	1725	[11.9]	1400	[9.6]

TABLE 5 (Continued)

LAP SHEAR STRENGTH OF HIGH TEMPERATURE
ADHESIVES ON TITANIUM ADHERENDS

After 2 Weeks @ 160°F (71°C) and 95-100% R.H.

Test Condition	NR-150 (psi)	[MPa]	IP-600 (psi)	[MPa]	FA-7001 (psi)	[MPa]	LaRC-TPI (psi)	[MPa]	PBI Paper (psi)	[MPa]
Wet										
72°F (22°C)										
0.05 hr. @ 600°F (316°C)										
Dry										
72°F (22°C)	2275	[15.7]	2425	[16.7]	1865	[12.8]	2060	[14.2]		
0.17 hr. @ 600°F (316°C)										

250

TABLE 6

LAP SHEAR STRENGTH OF HIGH TEMPERATURE
ADHESIVES ON TITANIUM ADHERENDS
AT HIGH TEST SPEEDS

Test Condition	LR-600		LaRC-13		PMR-15		FM-34		FM-34B-18		PBI		FM-36	
	(psi)	[MPa]	(psi)	[MPa]	(psi)	[MPa]	(psi)	[MPa]	(psi)	[MPa]	(psi)	[MPa]	(psi)	[MPa]
0.05 inch/min. (0.13 cm/min.)														
0.17 hr. @ -65°F (-54°C)	2270	[15.6]	2530	[17.4]	2020	[13.9]	---	---	2600	[17.9]	1140	[7.9]	3320	[22.9]
72°F (22°C)	2830	[19.5]	2270	[15.6]	2290	[15.8]	3480	[24.0]	2880	[19.8]	2690	[18.5]	3080	[21.9]
1 inch/min. (2.54 cm/min.)														
0.17 hr. @ -65°F (-54°C)	1940	[13.4]	2290	[15.8]	1970	[13.6]			3220	[22.2]	2250	[15.5]	3200	[22.0]
72°F (22°C)	2200	[15.2]	2100	[14.5]	1670	[11.5]			2260	[15.6]	2100	[14.5]	2880	[19.8]
20 inch/min. (50.8 cm/min.)														
0.17 hr. @ -65°F (-54°C)	1130	[7.8]	1320	[9.1]	380	[2.7]			490	[3.4]	480	[3.3]	290	[2.0]
72°F (22°C)	1120	[7.7]	1400	[9.6]	1180	[8.1]			1120	[7.7]	1250	[8.6]	1720	[11.9]

TABLE 6 (Continued)

LAP SHEAR STRENGTH OF HIGH TEMPERATURE
ADHESIVES ON TITANIUM ADHERENDS
AT HIGH TEST SPEEDS

Test Condition	NR-150 (psi) [MPa]	IP-600 (psi) [MPa]	FA-7001 (psi) [MPa]	LaRC-TPI (psi) [MPa]	PBI Paper (psi) [MPa]
0.05 inch/min. (0.13 cm/min.)					
0.17 hr. @ -65°F (-54°C) 72°F (22°C)	2275 [15.7]	2425 [16.7]	1865 [12.8]	2060 [14.2]	
1 inch/min. (2.54 cm/min.)					
0.17 hr. @ -65°F (-54°C) 72°F (22°C)					
20 inch/min. (50.8 cm/min.)					
0.17 hr. @ -65°F (-54°C) 72°F (22°C)					

252

TABLE 7

LAP SHEAR STRENGTH OF HIGH TEMPERATURE
ADHESIVES ON STAINLESS STEEL ADHERENDS

Test Condition	LR-600		LaRC-13		PMR-15		IP-600		LaRC-TPI		NR-150	
	(psi)	[MPa]	(psi)	[MPa]	(psi)	[MPa]	(psi)	[MPa]	(psi)	[MPa]	(psi)	[MPa]
72°F (22°C)	2066	[14.2]	2486	[17.0]	2240	[15.3]						
0.5 hr. @ 600°F (316°C)	1207	[8.3]	1562	[10.7]	2179	[14.9]						
0.5 hr. @ 800°F (427°C)	652	[4.5]										
0.1 hr. @ 1000°F (538°C)	616	[4.2]										

SELECTION OF STRUCTURAL ADHESIVES FOR 180° F AND MINIMAL SURFACE PRETREATMENT APPLICATIONS

Loretta Peters
FMC
Central Engineering Laboratories
1205 Coleman Avenue
Santa Clara, CA 95052

BACKGROUND

To obtain maximum performance, military tracked vehicle components must be lightweight, but they must also retain adequate strength and structural rigidity. Because of this, thin-gauge aluminum sheet is often used for making various components. Conventional welding processes cause distortion of thin sheet due to the heat input. In addition, several high-strength aluminum alloys are unweldable and cannot be used.

Cost is also a significant factor in many lightweight component installations. Frequently, there is extra care and effort required to weld lightweight items to a heavy vehicle hull without distortion. Adhesive bonding is often a more efficient attachment.

In order to take advantage of the weight reduction, cost savings and stiffer joints without distortion offered by adhesive bonding, a study was undertaken to identify and select structural adhesives for possible implementation on FMC Ordnance Vehicles in the following areas:

(1) As a supplement to or replacement for mechanical fasteners and welds for the assembly of ammo storage rack.

(2) As an attachment for lightweight brackets, decals, and instrument panel windows.

These adhesives will have to perform at 180°F with minimal surface preparation in order to fit production and end-use requirements. Production requirements are minimal surface preparation on bare aluminum in a normal shop environment and a bondline thickness of 5 to 10 mils. Adhesives whose strengths were very sensitive to bondline thickness and reproducibility could not be utilized in a common shop environment. End-use requirement mandated finding adhesives that were temperature resistant to 180°F.

TESTS PERFORMED

A preliminary evaluation of 33 adhesives from 10 manufacturers was undertaken using tensile lap shear test (ASTM D1002). The results are in Table I. Adhesives with the best tensile lap shear strengths were further evaluated by the following tests:

o Tensile Shear (ASTM D1002), -67°F, 70°F (dry), 70°F (wet), 180°F

o Cleavage Strength (ASTM D1062), -67°F, 70°F (dry), 70°F (wet), 180°F

o Tensile Strength (ASTM D2095), -67°F, 70°F (dry), 70°F (wet), 180°F

o Impact (ASTM D950), -67°F, 70°F (wet)

o T-Peel (ASTM D1876), -67°F, 70°F (dry), 70°F (wet), 180°F

The results are summarized in Table II and graphically presented in Figure 1. Five adhesives, two acrylics, and three epoxies, were identified to have good properties.

In order to assuage the concerns about the long-term durability of adhesive bonds, the following durability tests were performed on the three non-Hysol adhesives

255

(the Hysol adhesives had deteriorated significantly after six months).

o Tensile Lap Shear Strength (ASTM D1002) retention after dipping in the four Bradley hull cleaning solutions (all lap joints were oriented vertically to facilitate drainage) using a scheme of soak as follows:

1. Load all the test panels in the container.

   - 20 panels total
   - 5 panels/adhesive

2. Dip all 25 panels in Ridoline 53, soak for a maximum of 10 minutes, remove, and subject to two water rinses.

3. Remove one panel of each adhesive.

4. Dip the remaining panels (20 -5 = 15) in Deoxidizer 310, soak for a maximum of 5 minutes, remove, and subject to two water rinses.

5. Remove one panel of each adhesive.

6. Dip the remaining panels (15 -5 = 10) in Alodine 1200-S, soak for a maximum of 3 minutes, drain, and rinse.

7. Remove one panel of each adhesive.

8. Dip the remaining panels (10 -5 = 5) in Deoxylite 10, soak for a maximum of 3 minutes, remove, and rinse.

Test results are in Table III.

o Adhesion Measurement by Tape Test (ASTM D3359)

o Ambient Temperature Creep Deformation Evaluation (MMM-A-132, Section 4.6.8). Results are in Table IV.

o Vibration testing of rectangular specimens with final dimensions of 6" x 6" 4" where the four joints have 1/2" overlap using the following test procedure:

1. Subject assembled rectangular test specimens to a varying vibration cycle from 20-40 Hertz for one hour.

2. Heat to 160°F.

3. Shake for another hour.

4. Cool to -40°F.

5. Shake for another hour.

DISCUSSION

The effect of surface pretreatment on the aluminum oxide surface is critical and intimately related to the bond permanence/durability of aluminum joints (Refs. a., b., c., d.). J. Dean Minford of Alcoa evaluated the effects of different surface treatment on stressed epoxy bonded aluminum joints under varying weathering conditions. These conditions included: immersion in room temperature water, soaking in continuously-condensing humidity at 52°C (125°F), hot water soak/freeze/thaw cycling; as well as, exposure in an industrial-type atmosphere and a seacoast atmosphere. The surface preparations employed were: vapor degreasing, belt sand

abrasion, blasting, chromic-sulfuric acid etching, alodining, and sulfuric acid anodizing.

The one conclusion from Minford's study of import to this program states that most etching, anodizing, or conversion coating surface preparations will likely produce superior-durability epoxy-bonded aluminum joints under stress and corrosive, salt water exposure conditions. Simply degreasing or sanding the substrate prior to bonding produces joints that performed poorly in comparison, regardless of alloy choice.

For adhesives whose performances were not as sensitive to unprepared substrate surfaces, the adhesives of choice are the acrylics whose documented advantages (refs. e. and f.) are their simple no-mix method of application, rapid cure at room temperature, tolerance to uncleaned surfaces, and good structural properties.

The epoxy adhesives (Permabond 110, Epibond 1543, Hysol 9410) had above average tensile, cleavage, tensile, and impact strengths. The acrylic adhesives (Versilok 204, Hysol 9446) held up better to peel loads than the epoxy adhesives. None of the five tested adhesives had good 180°F cleavage strength. Overall, the cleaning baths did not adversely affect the tensile lap joints. After a 1,600 psi stress had been applied for 192 hours, neither the acrylic nor the epoxies showed appreciable creep. The acrylic and the epoxies survived the hot-cold cycle plus three hours of vibration testing and showed a generally adequate level of adhesion to paint.

CONCLUSION

Although the epoxies have higher strengths, durability of epoxy-bonded aluminum joints are more sensitive to surface pretreatment than acrylic-bonded aluminum joints (refs. a. to f.). Limited durability information obtained from published sources (Table V), as well as experimental data, showed the acrylic-bonded aluminum joints to be equivalent to the epoxy-bonded aluminum joints in this respect.

ACKNOWLEDGEMENTS

REFERENCES

a. J. Dean Minford, "Aluminum Adhesive Bond Permanence," Treatise on Adhesion and Adhesives, Volume 5, 1981.

b. J. Dean Minford, "Effect of Surface Preparation on Stressed Aluminum Joints in Corrosive Salt Water Exposure," Adhesives Age, October 1980.

c. J. Dean Minford, "Effect of Surface Preparations on Adhesive Bonding of Aluminum," Adhesives Age, July 1974.

d. J. Dean Minford, "Comparison
    of Aluminum Adhesive Joint
    Durability As Influenced by
    Etching and Anodizing
    Pretreatments of Bonded
    Surfaces," Journal of Applied
    Polymer Science: Applied
    Polymer Symposium 32,
    pp 91-103, 1977.

e. Thomas L. Wilkinson and Diana
    P. Tyler, "Acrylics Improve
    for Bonding Automotive
    Aluminum Alloys," Adhesives
    Age, December 1981.

f. Thomas L. Wilkinson, "Acrylic
    Adhesives: New Way to Bond
    Aluminum Auto Parts,"
    Adhesives Age, June 1978.

g. Definitions of Terms Relating
    to Adhesives and Sealants,
    Adhesives Age, May 31, 1983,
    pp 35-46.

TABLE IA. ADHESIVES SCREENED FOR ROOM TEMPERATURE LAP SHEAR STRENGTH

Manufacturer	Adhesive	Type/Form	R.T. Tensile Lap Shear Strength, psi
Hysol	9309	2-part epoxy paste	2,522
	9330	2-part epoxy paste	2,270
	9446	2-part acrylic	3,737*
	9649	Epoxy film	2,846
	9410	2-part epoxy paste	3,000*
	940	Epoxy tape	Broke in hand
	3CI-1000	Cyanoacrylate liquid	460
	3CI-500	Cyanoacrylate liquid	Broke in hand/jaws
	911F	2-part epoxy paste	850
3M	2216	2-part epoxy paste	390
	1838	2-part epoxy	Broke in hand
	2214	Epoxy paste	2,780
	Y-9473	Acrylic tape	74
	Y-4945	Acrylic tape	86
	Y-9469	Acrylic tape	104

TABLE IB. ADHESIVES SCREENED FOR 180° LAP SHEAR STRENGTH

Manufacturer	Adhesive	Type/Form	180°F Tensile Lap Shear Strength, psi
H. B. Fuller	FE 004	2-part epoxy	1,417
	FE 086	2-part epoxy	1,400
	RA 0018	2-part acrylic	271
Ablestick	342-13 Acc	1-part epoxy	300
	342-3	2-part epoxy	300
Crest	2225	2-part modified epoxy	300
Thiokol	--	Polysulfide sealant	200
Hysol	934	2-part epoxy	726
3M	3525	Polyurethane paste	1,000
	3549	Isocyanate polyol	300
Loctite	324	Acrylic	602
	326	Modified acrylic	600
	12876	Modified cyanoacrylate	901
	Assemble	Modified acrylic	640
Permabond	ESP 110	1-part toughened epoxy	2,633*
	612	Acrylic	1,000
Epibond	1543B	2-part modified epoxy	2,496*
Hysol	9446	Separate application acrylic	1,576*
Versalok	204A	Separate application acrylic	1,651*

*Adhesives with good properties.

259

TABLE II. SUMMARY OF TEST RESULTS

MATERIAL	TENSILE LAP SHEAR x1000 psi				CLEAVAGE x1000 psi				TENSILE x1000 psi				IMPACT x10 ft-lbs/in²		T-PEEL x10 lb/in of width			
Room Temp. Cure	-67°F	70°F Dry	70°F Wet	180°F	-67°F	70°F Dry	70°F Wet	180°F	-67°F	70°F Dry	70°F Wet	180°F	-67°F	70°F,Wet	-67°F	70°F Dry	70°F Wet	180°F
Hysol 9410	2.6	3.8	2.9	0.2	2.0	2.0	1.8	0.2	8.7	4.7	2.9	0.6	0.3	0.7	2.8	2.8	2.6	9.1
Hysol 9446	1.4	3.7	2.5	1.6	0.8	0.8	0.7	0.5	6.0	3.3	2.7	1.1	0.2	1.0	1.2	3.6	3.7	2.4
Versalok 204	1.4	3.2	3.2	1.7	1.2	1.0	1.0	0.6	4.0	2.6	2.8	1.4	1.0	0.2	1.0	3.2	4.8	3.1
High Temp. Cure																		
Permabond 110	2.3	2.9	2.7	2.6	1.2	2.0	1.6	0.7	9.6	8.2	6.1	4.0	1.0	1.0	1.7	1.7	2.1	1.4
Epibond 1543	1.1	1.2	1.4	2.4	1.7	1.1	1.2	0.8	5.0	3.8	2.8	3.9	0.7	0.4	0.6	1.2	1.2	0.7

TABLE III. % TENSILE LAP SHEAR (TLS) STRENGTH RETENTION AT 75°F

Environment	Versilok 204	Permabond 110	Epibond 1543
Control	3200 psi	2800 psi	1500 psi
(TLS Data from Task 320)	(3229 psi)	(2893 psi)	(1200 psi)
Ridoline 53	28%	77%	88%
Deoxidizer 310	100%	71%	88%
Alodine 1200-S	111%	74%	85%
Deoxylite 10	115%	69%	97%

TABLE IV. CREEP TEST DATA (Amount of Creep in Inches)

Time/Date	Versilok 204	Permabond 110	Epibond 1543
1530/11-17	0	0	0
0730/11-18	0	.0001	.00015
1130/11-18	0	.0001	.00022
1600/11-18	0	.00025	.00035
0830/11-21	.00069	.00158	.00212
1600/11-21	.00069	.00158	.00220
0720/11-22	.00640	.00158	.00215
1530/11-22	.00100	.00230	.00249
0725/11-23	.00100	.00183	.00292
1600/11-23	.00247	.00189	.00306
0730/11-24	.00249	.00191	.00305
1115/11-24	.00249	.00190	.00307
1422/11-24	.00249	.00190	.00307
945/11-25	.00249	.00192	.00302
1215/11-25	.00249	.00191	.00306
1530/11-25	.00249	.00191	.00308
800/11-26	.00249	.00192	.00302

TABLE V. DURABILITY TEST: PUBLISHED INFORMATION

Environment	Time (Days)	Tensile Lap Shear at 75° Fahrenheit (psi)				
		Versilok 204	Hysol 9446	Permabond 110	Epibond 1543	Hysol 9410
None (Control)		3229	4000	5800	2500	4750
77°F, Tap Water	14/30	-/2760	-/3880	-	-/2500	-/4200
212°F, Water	7/30	Bond Broke/-	2900/-	-	-	-/4300
120°F, 100% RH	14/30	-	-/3785	-	-/3100	-/3800
105°F, 5% Salt Spray	14/30	-/2960	-/4065	5336/5220	-/2300	-
Air @ 180°F/300°F	40	-	-	4900/1000	-	5600/-
Anti-icing Fluid @ 77°F	7	3000	-	-	3100	4800
Hyd-Oil/JP A 77°F	7	3000	2695/4000	-	2700	5500/5200
Room Temperature Fatigue Test Data (Cycles to Failure)		3,618,000	-	1,956,000	1,705,500	-

NOTE: "-" signifies no published data available.

262

FIGURE IA. BAR CHARTS OF TENSILE LAP SHEAR DATA

Room Temperature Wet

Adhesives Qualified Under Task 320 Activities

180 degrees F

Adhesives Qualified Under Task 320 Activities

263
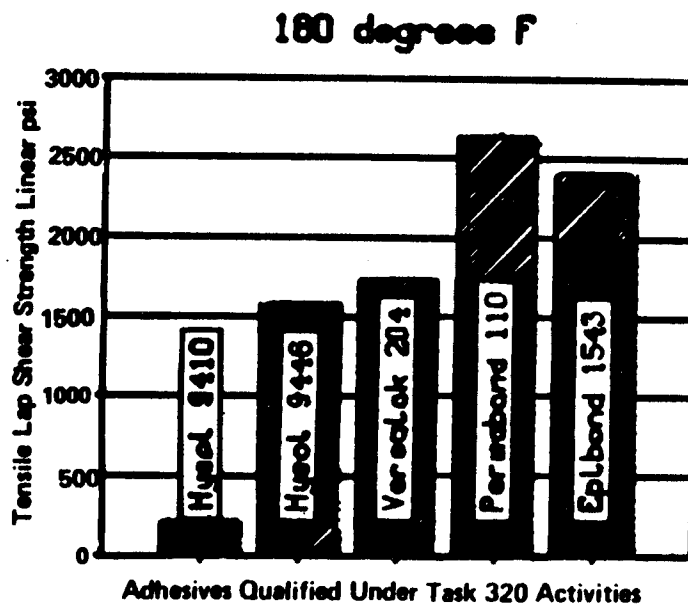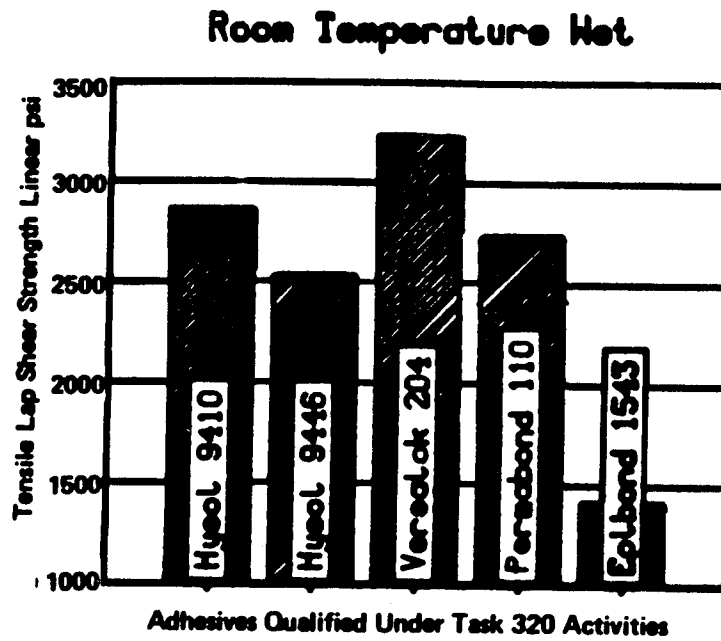
FIGURE IA. BAR CHARTS OF TENSILE LAP SHEAR DATA (Cont'd)

Room Temperature

-67 degrees F

FIGURE IB. BAR CHARTS OF CLEAVAGE STRENGTH DATA
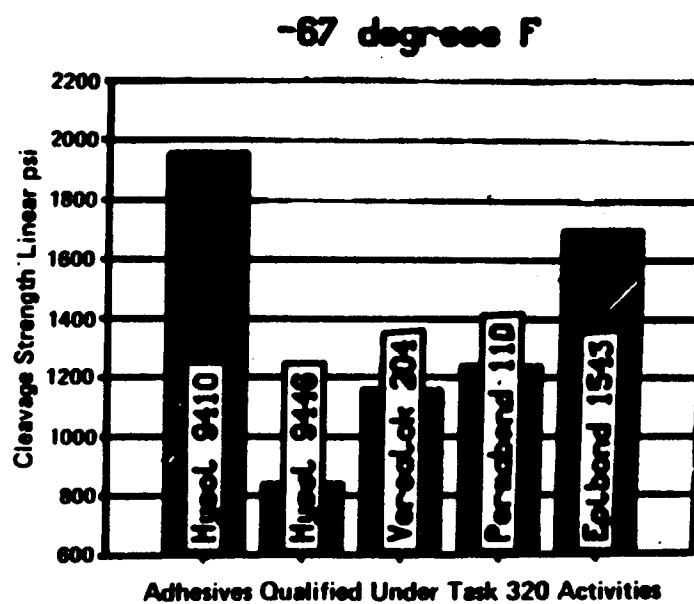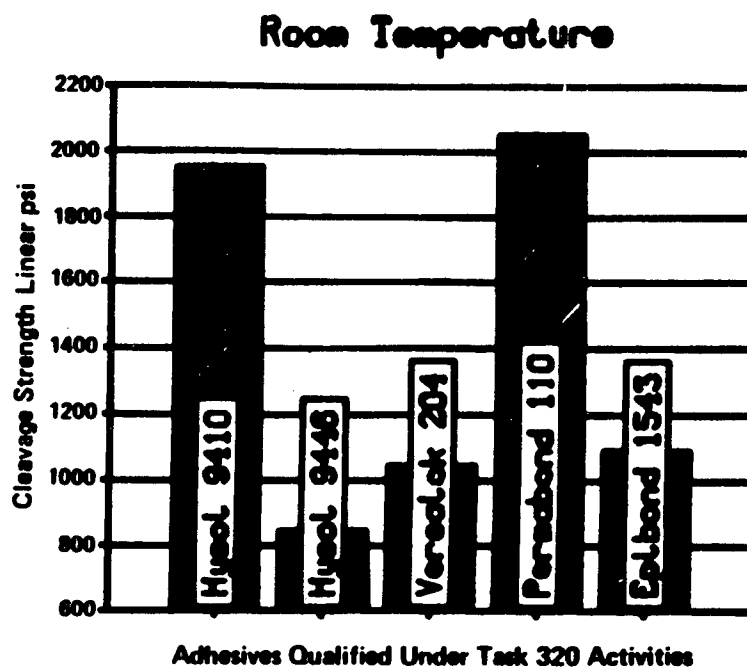
Room Temperature Wet

180 degrees F

FIGURE 1B. BAR CHARTS OF CLEAVAGE STRENGTH DATA (Cont'd)

Room Temperature

-67 degrees F

FIGURE IC.   BAR CHARTS OF TENSILE STRENGTH DATA

24 hour Water Immersion - W

180 degrees F

267

FIGURE IC.   BAR CHARTS OF TENSILE STRENGTH DATA (Cont'd)

Room Temperature

-67 degrees F

268
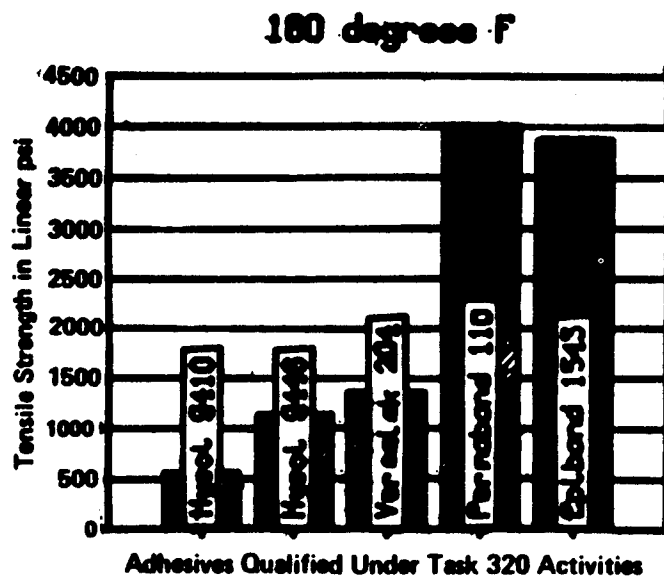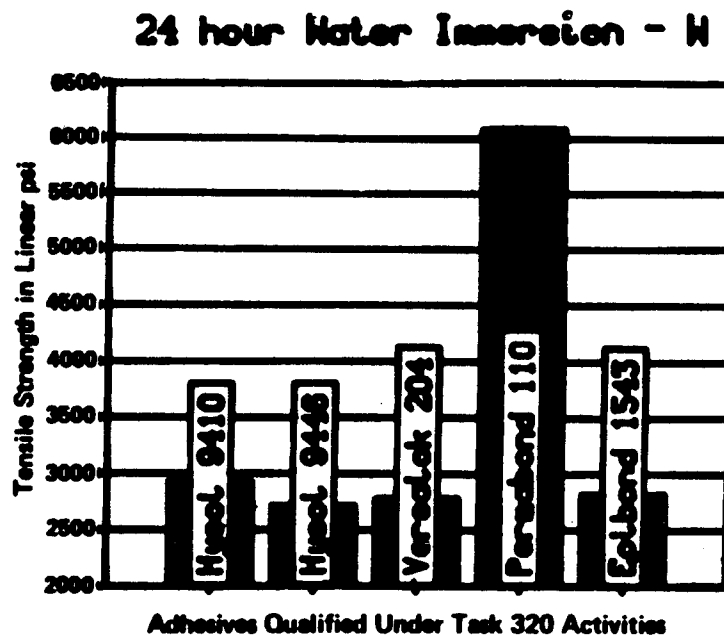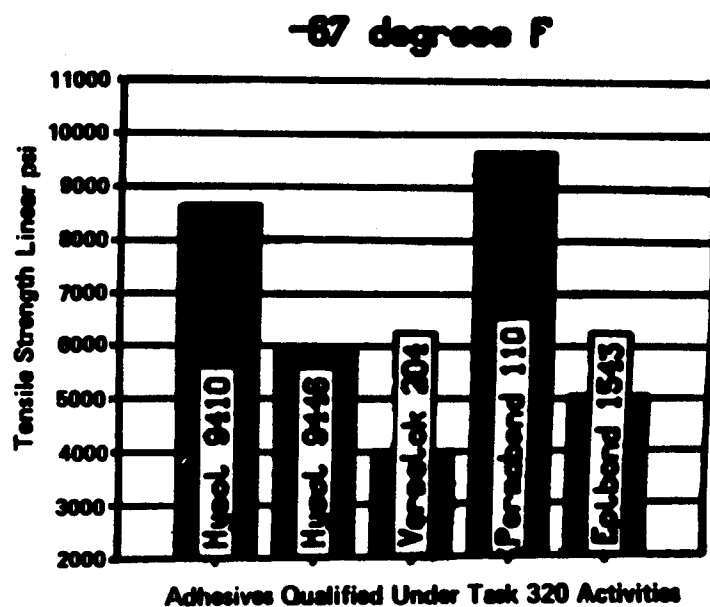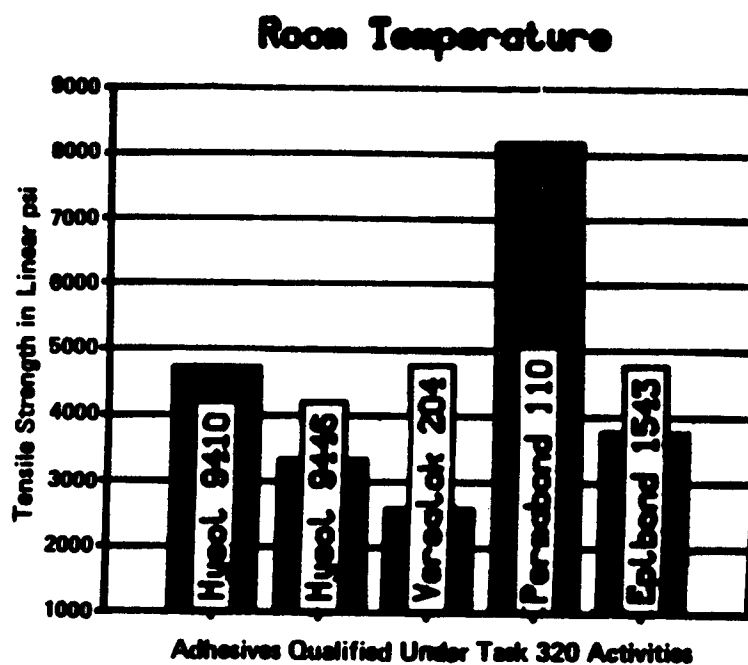
FIGURE ID.   BAR CHARTS OF IMPACT STRENGTH DATA

WET

Adhesives Qualified Under Task 320 Activities

−67°F Dry

Adhesives Qualified Under Task 320 Activities
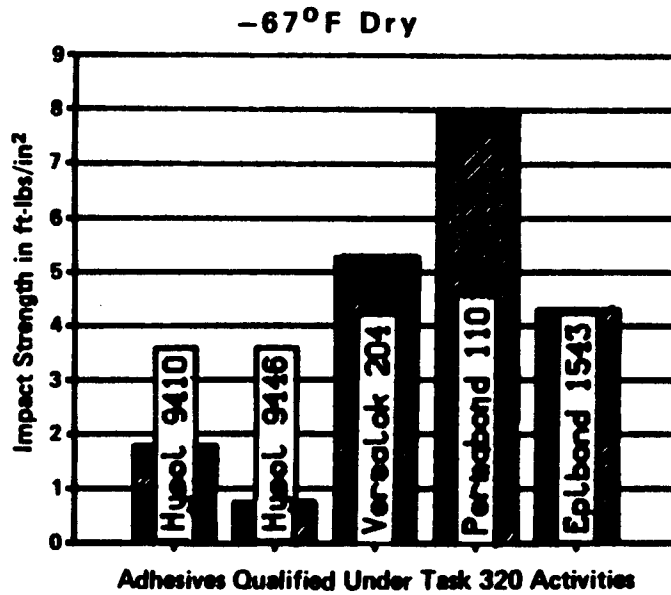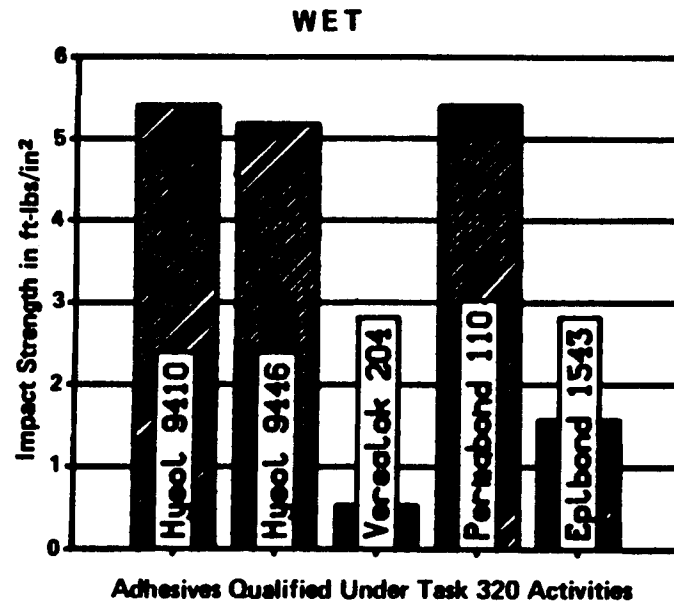
FIGURE IE.   BAR CHARTS OF T-PEEL STRENGTH DATA

24 hour Water Immersion - W

Adhesives Qualified Under Task 320 Activities

180 degree F

Adhesives Qualified Under Task 320 Activities

Room Temperature

-67 degrees F

271
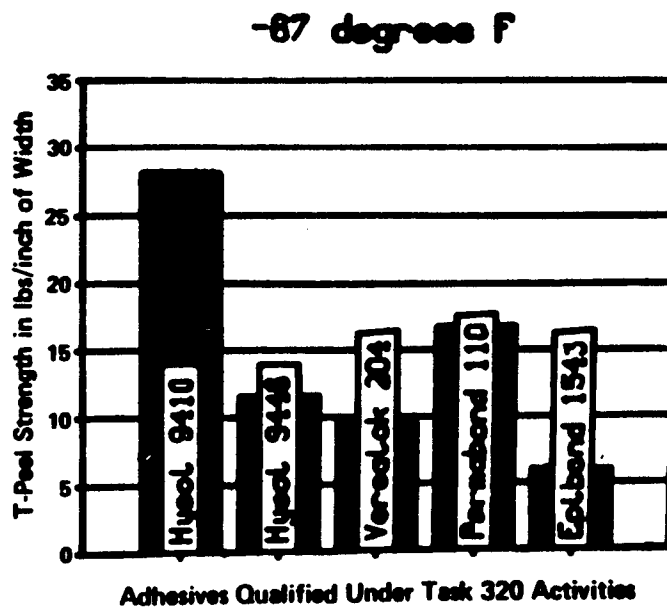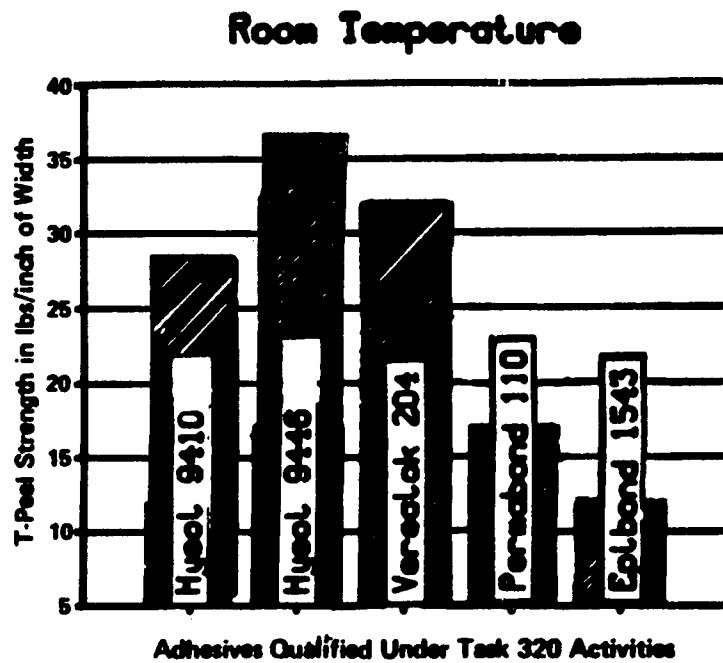
DEVELOPMENT OF EPOXY ADHESIVES
FOR FIELD REPAIR OF MILITARY EQUIPMENT

Gregory A. Luoma
Defense Research Establishment Pacific
DND Canada
Bldg. 199, CFB Esquimalt
B.C., Canada VOS 1BO

INTRODUCTION

Battle damage or in-field repair of military equipment is gaining increasing importance worldwide. The potential for extensive damage to military equipment requires that repairs be achievable quickly in the field to avoid unacceptable down times.

Adhesives have a clear advantage for fast repair. If the appropriate formulations are available, turnaround times can be on the order of hours compared to the days required for more conventional techniques such as welding and riveting. Further, adhesive repairs generally require less skilled personnel and far less equipment, thereby making remote repairs more feasible.

The acceptance of adhesive repair has been slowed, however, by a number of problems associated with available commercial formulations. First, most formulations will not bond adequately to sanded metal surfaces. Since more elaborate surface preparations cannot be performed in the field, this problem has severely limited the use of adhesives. Second, most adhesives (especially epoxies) are brittle, and lack the toughness necessary to withstand impact damage, differential thermal expansions, and peel forces. Again this problem severely limits their use in repair scenarios. Third, most adhesives which cure at room temperature will not provide adequate high temperature properties for use in military aircraft. This problem has resulted in the development of elaborate heating blanket systems which may be too bulky for field repairs. Finally, many adhesives lack the environmental durability necessary for longer term repairs.

The program at DREP was originally designed to select suitable commercial adhesives for Aircraft Battle Damage Repair (ABDR) applications. However, after the aforementioned problems were uncovered, it was decided to attempt to formulate improved epoxy adhesives and primers. The results to date indicate that a large improvement in bonding to poorly prepared metal surfaces is achievable, while at the same time dramatically increasing toughness without decreasing the shear strength. The adhesives also display good environmental durability, and retain acceptable higher

273

temperature properties when cured at moderate temperatures.
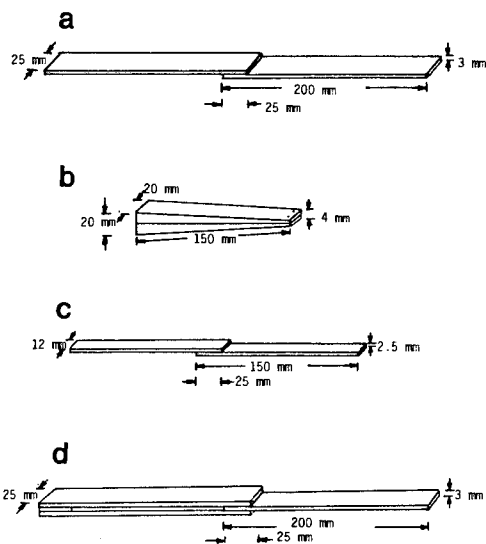
Figure 1. Geometries of the specimens used to test adhesive strength (a) single lap shear specimen for aluminum; (b) cleavage specimen; (c) single lap shear specimen for titanium; (d) double lap shear specimen.

EXPERIMENTAL

1. Specimens Types

Three types of aluminum specimens were used in the present studies: a single lap shear specimen, a double lap shear specimen, and a cleavage specimen. The exact dimensions of these specimens are given in Figure 1. The single lap shear specimen is a mixed mode of shear and peel forces. The double lap shear specimen is designed to measure absolute strength (mode 2) while the cleavage specimen is designated to measure toughness (mode 1). For single lap and cleavage specimens Al 6061-T6 was used, while for double lap specimens the higher strength Al 7075-T6 was employed. Titanium specimens were tested in single lap shear only using the geometry shown. The titanium alloy used was aircraft grade and contained 6% aluminum and 4% vanadium.

2. Surface Preparations for Bonding

For aluminum specimens two different surface preparation procedures were employed. In the first, specimens were degreased by immersion in 1,1,1,-trichloro-ethane. They were then etched for ten minutes at 68°C in chromic acid solution (34 g sodium dichromate, 304 g sulphuric acid per liter), washed with ultrapure water, and dried and stored in absolute ethanol. In the second, the degreased specimens·were hand-sanded with 100-grit sandpaper and immersed in absolute ethanol. For primed samples the primer was applied after the sample was removed from the ethanol.

For titanium specimens, similar procedures were followed. The major difference is that the etching solution was a standard peroxide etch solution (0.5 M

sodium hydroxide, 0.2 M hydrogen peroxide) and the etching time was one hour at 60°C.

3. Bond Testing

Specimens were broken using an MTS 312.21 servohydraulic testing apparatus. For temperature studies the grips were enclosed in an oven, and all specimens were equilibrated at each temperature for ten minutes.

4. Environmental Studies

To determine environmental durability of adhesive bonds, accelerated aging tests were employed. Bonds were subjected to 100% condensing humidity and UV light at 60°C for periods up to three months in a WeatherOmeter environmental chamber. All specimens were allowed to dry before testing after removal from the environmental chamber.

RESULTS AND DISCUSSION

1. Effects of Additives on Shear and Cleavage Strength

Figures 2 and 3 show the effect of adding carboxyl terminated butyl nitrile rubber (CTBN) on the single lap shear strength and cleavage strength of a basic epoxy adhesive. They also show the effect of the addition of a further toughening agent, designated additive A. The important observation is the synergism exhibited by the two additives to produce a doubling in cleavage strength over conventional systems. Figure 4 demonstrates that different rubber additives have different abilities to toughen the basic epoxy adhesive. In general, a solid rubber is preferrable for the production of tough bonds, but the concentration is limited by viscosity. The use of rubber tougheners also tends to decrease the operational temperature and the shear strength of the adhesive. Therefore, the choice of combinations of additives is critical to the production
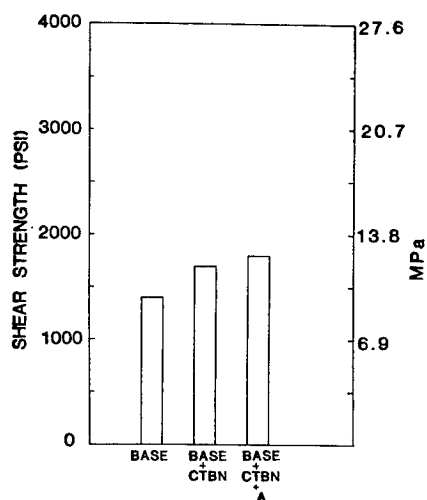
Figure 2. Comparison of the single lap shear strengths of standard and toughened epoxy systems on etched aluminum adherends.
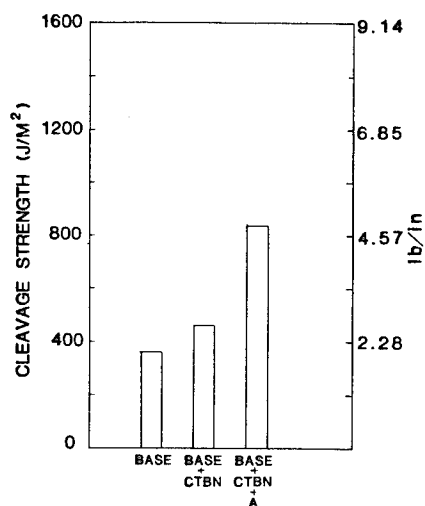
Figure 3. Comparison of the cleavage strengths of standard and toughened epoxy systems on etched aluminum adherends.
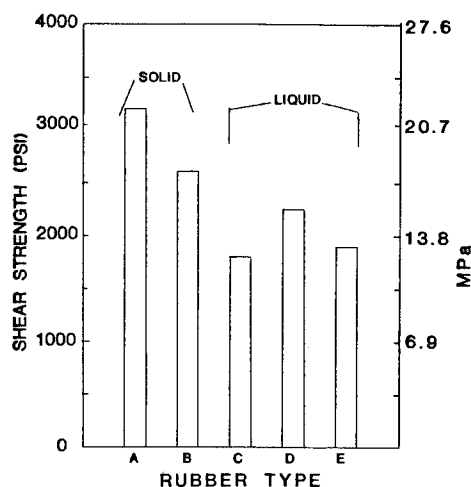
Figure 4. Comparison of the ability of various rubber formulations to increase the single lap shear strength on etched aluminum adherends. All rubber concentrations were 5 phr.

of a strong, tough adhesive which will retain strength at the desired temperature.

Similarly, the choice of additives, primers, and curing agents can have a marked effect on the ability of the adhesive to bond to poorly prepared surfaces. Figure 5 shows how various additives and primers can affect bond strength to sanded aluminum, while Figure 6 shows the varying shear strengths of adhesives made with different curing agents on a sanded titanium surface. All of these effects centre around the ability of the adhesive to wet the metal surface, and are intimately related to the chemistry of the "interphase" region between metal and adhesive. The use of primers, additives, or other components which either improve compatibility of the metal and adhesive or cause chemical bonding between the metal and the adhesive are necessary when bonding to sanded metal surfaces. The DREP-formulated adhesives, therefore, contain additives to promote bonding to sanded surfaces, and a special primer which has been developed to specifically promote adhesion to poorly prepared aluminum surfaces.

For longer term repairs, environmental durability of the bond is important. In this case both the selection of adhesive and surface treatment are of major concern. Assuming that no more extensive surface pretreatment than sanding is possible, the production of durable bonds is largely dependent on formulating an adhesive which does not absorb water and on preventing water ingress at the adhesive-metal interphase. Figure 7 shows the good environmental durability obtained using a DREP-formulated adhesive. These results indicate that the service life of these adhesive bonds is in excess of three years under normal operating conditions.

Figure 6. The effect of different curing agents on the ability of an epoxy adhesive to bond to sanded and etched titanium adherends. In each of the adhesives only the curing agent is varied.

Figure 5. Demonstration of the abilities of additives and primers to increase the single lap shear strength of base epoxy and a commercial adhesive on sanded aluminum adherends.
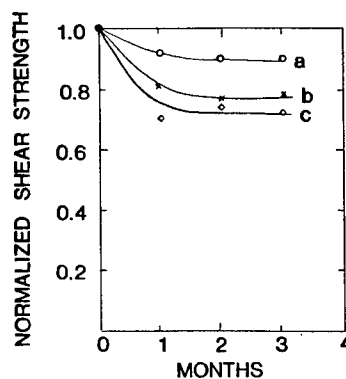
Figure 7. Effect of surface pretreatment on the environmental durability of epoxy adhesive bonds to aluminum adherends. (a) chromic acid etched; (b) sanded and primed; (c) sanded. All bonds were aged under ultraviolet lights at 60°C with 100% relative humidity.

277

Another consideration for epoxy adhesive formulations to be used in field repairs is their ability to function over a broad range of temperatures without requiring a high temperature cure. Figure 8 indicates that the choice of curing agent affects the operational temperature, and that the adhesives which retain strength at high temperatures generally have poorer shear strengths and toughness at room temperature. Therefore, several formulations have been created to cover the normal temperature range of interest.
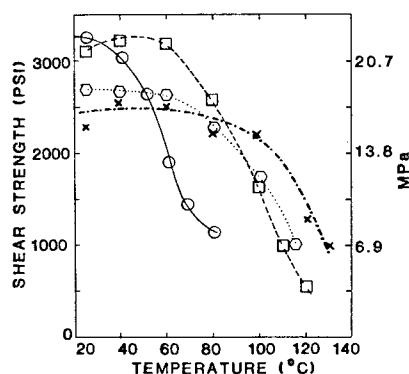
Figure 8. Comparison of the single lap shear strengths of DREP-formulated adhesives on etched aluminum as a function of temperature. (O—O) LP#1; (O···O) LP#3; (□--□) LP#5; (X--X) LP#6.

A final important feature of epoxy adhesives is the speed with which cure is obtained. Our experiments indicate that accelerators can be used to speed up cure times, but they also severely limit pot life. The only effective compromise is to use heat blankets and moderate cure temperatures to affect the cure in one to two hours while retaining a reasonable pot life at room temperatures for applying the adhesive.

2. Comparison of DREP-Formulations and Commercial Adhesives

Having considered the requirements of a good repair adhesive, adhesive formulations were prepared using additives to improve toughness and bonding to poorly prepared surfaces. A number of adhesives were formulated to cover all operational temperature ranges.

Figure 9 compares the double lap shear strength on aluminum of DREP-formulations with two widely used commercial products: Cyanamid FM300 (K) which is a high temperature epoxy film adhesive used in bonding skin to honeycomb on fighter aircraft, and Hysol EA9321 which is the approved room-temperature-curing adhesive for repairing CF-18 aircraft. As is apparent from the Figure, all of

278

the DREP-formulated adhesives have strengths equal to FM300 while curing at a much lower temperature. In particular, LP #1 which cures at room temperature, has exceptional strength when compared to EA9321 and even exceeds FM300 in overall strength. Both LP #2 and LP #3 (with higher operational temperature capabilities) also have very high strengths.

Figure 10 compares the cleavage strengths (G_{Ic}) or toughness of the same adhesives. Again, LP #1 has exceptional toughness, exceeding the values for EA9321 by a factor of three, and equalling the value for FM300. The highest temperature formulation (LP #3) has a much lower toughness, but recent results using different curing agents indicate that the toughness can be restored without decreasing the operational temperature or the shear strength of the adhesive.

Figure 11 compares the single lap shear strength of LP #1 with various aluminum surface preparations to the same tests using EA9321. In this case LP #1 bonded with more than 90% of full strength on sanded aluminum, as opposed to 50% for EA9321. When a DREP-formulated primer is used on sanded aluminum, both adhesive formulations bond with greater than 90% of maximum strength. This finding verifies the ability of specially formulated primers to improve bonding to aluminum surfaces. However. when the correct adhesive formulation is used, primers may not be necessary for efficient bonding to sanded aluminum. Figure 7 confirms the bond quality of the DREP-formulated adhesives on sanded aluminum, since the differences in environmental durability of bonds using the three different surface preparations is small.

Figure 12 compares bonding of LP #1 and LP #2 to EA9321 on sanded and etched titanium. In this case, both LP #1 and LP #2 formed exceptionally strong bonds on both sanded and peroxide-etched titanium, indicating that no special surface treatment is necessary when bonding to titanium.

Finally, to obtain strength at temperatures above 100°C for aircraft repairs, specialized curing agents must be employed. These curing agents tend to lower the overall strength of the adhesive by making it more brittle.
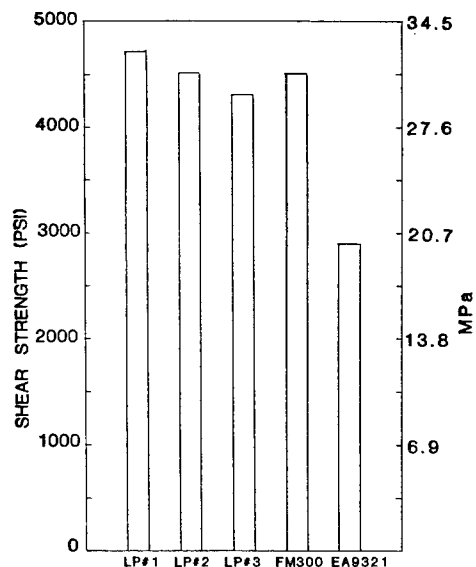
Figure 9. Comparison of the double lap shear strengths of DREP-formulated adhesives and selected commercial adhesives on etched aluminum adherends.

Figure 11. Comparison of the abilities of a DREP-formulated adhesive and a selected commercial adhesive to bond to aluminum adherends with various surface preparations.

Figure 10. Comparison of the cleavage strengths of DREP-formulated adhesives and selected commercial adhesives on etched aluminum adherends.
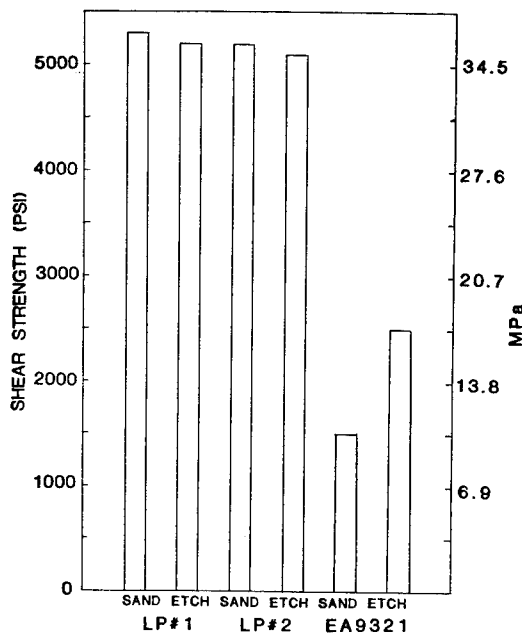
Figure 12. Comparison of the single lap shear strengths of DREP-formulated epoxy adhesives and a selected commercial adhesive on sanded and etched titanium surfaces.

Therefore, a range of adhesives has been produced to provide the best formulations for specific needs. For lower temperature applications LP #1 provides extremely good properties for all kinds of surface preparations. For higher temperature applications LP #3 and the newer formulations LP #5 and LP #6 have good properties, although they do not form as tough bonds as LP #1 and do not bond as well to poorly prepared metal surfaces. These problems are presently being addressed.

CONCLUSIONS

1. The use of formulation additives can have a dramatic effect on the overall strength and toughness of epoxy adhesives.

2. Adhesives can be formulated which will bond with high strength to sanded metal surfaces while retaining good environmental durability.

3. DREP has formulated a number of two-part epoxy adhesives with properties exceeding commercial products. Shear values are up to 50% higher than other room-temperature-curing adhesives, and toughness values are up to 300% higher. These adhesives bond with up to 90% of maximum strength on sanded aluminum and have excellent environmental durability.

The AH-1S Cobra K747 Polyurethane Erosion Guard: A Review of the Materials of Construction and Associated Adhesive Bonding Processes

Joseph A. Brescia
J. Richard Hall
Robert B. Bonk

U.S. Army Armament Research, Development and Engineering Center
Armament Engineering Directorate
Armaments Technology Division
Organic Materials Branch, Adhesives Section
Picatinny Arsenal, New Jersey 07806-5000

1. Introduction

The AH-1S Cobra K747 main rotor blade is an all-composite state-of-the-art assembly comprised of a filament-wound S-2 glass spar, basket weave S-2 glass skin, Kevlar® wet filament-wound spline, and a Nomex honeycomb core (fig. 1). The spar section of the rotor blade is protected from sand and rain damage by a polyurethane erosion guard which is attached to the spar in a one-step adhesive bonding operation.

Four models of the K747 blade have been developed over several years. The earliest version, the 205, possesses a full-length Estane polyurethane erosion guard. A field maintenance problem developed when it was found that the Estane became unstable (soft) at temperatures in the range of +180°F to +200°F--temperatures that the blade normally undergoes in hot, sunny environments. In this condition, the Estane would tend to pick up a large amount of debris. For this reason, an intermediate blade design (the 205+) was developed, having an Estane guard along the majority of the leading edge except for the tip section, at which a P0655 polyurethane strip was used. This type of polyurethane had similar properties in resistance to sand erosion and slightly less in rain than

Estane, but had improved temperature stability. Subsequent K747 models included the 209 and the 303 series, both possessing a full-length P0655 erosion guard with the exception that the 303 has a replaceable steel leading edge guard at the blade tip area.

In the recent past, the U.S. Army has experienced debonding of P0655 erosion guards on blades in the 209 series. An investigation conducted in 1985-86 by a special U.S. Army panel identified a number of factors which may have contributed to the debonding incidents (ref 1). These included: (1) an overly operator-dependent adhesive bonding process and void-detection method (tactile); (2) possible presence or migration of silicones (from mold releases) to the bondline, and (3) the presence of a metallic coating (used to reduce the overall radar cross-section of the blade) in the joint. The latter factor was seen by both the Army and the blade's manufacturer to be the principal reason for the debonding of the erosion guard in light of its apparent lack of cohesive strength. It was the manufacturer's contention at that time that the radar-absorbing layer should be removed from subsequent blade design specifications.

Based on the conclusions and recom-

mendations of the panel, the U.S. Army Research, Development and Engineering Center (ARDEC) was tasked by the U.S. Army Materials Technology Laboratory (MTL) to develop a test program to (1) evaluate the adhesive bonding procedures (i.e., surface preparation of adherends and actual bonding) for erosion guards which currently exist; (2) conduct accelerated tests representing long-term environmental exposures on the materials of construction and their effect on joint performance (specifically in shear), and finally (3) to perform surface studies to detect possible silicone contamination on "as-received" erosion guard materials and determine whether the standard surface preparation methods presently being followed by the blade manufacturer are sufficient to remove it.

2. Approach

Long-term environmental aging effects on the erosion guard adhesive bond were determined by accelerated tests on single sandwich lap shear joints fabricated according to the surface preparation methods and adhesive bonding procedures listed in the manufacturer's process specification.

Accelerated tests representing long-term exposure of the P0655 polyurethane material to harsh environments, particularly under high heat/humidity conditions were also performed. Past studies (ref 2) have shown that ester-based polyurethane elastomers are susceptible to reversion under those conditions. To investigate this possibility, periodic durometer hardness readings were recorded on specimens conditioned under a variety of elevated temperature/humidity environments.

Material studies also included Electron Spectrometer Chemical Analysis (ESCA) of "as-received" P0655 as well as P0655 surfaces prepared according to the manufacturer's adhesive bonding process specification. The goal of this endeavor was to detect the possible presence of silicones (from either mold release or contaminants in the plant) and determine whether those silicones would be removed following the blade manufacturer's process specification. The impact of unremoved silicones is very serious from an adhesive bonding standpoint in that the chances of obtaining strong, durable bonds are made difficult at best.

3. Materials

Epon 826 resin--an unmodified bisphenol. An epoxy resin with a weight per epoxide rating between 180 and 188 and a viscosity in the range of 65 to 95 poises at 77°F.

Versamid 125--a polyamide-based curing agent which provides a modest degree of flexibility to the cured polymer.

DTA (diethylenetriamine)--an aliphatic amine curing agent used to cure epoxy resins at room temperature. They afford relatively short working lives (approximately 30 minutes) and require 4 to 7 days for complete cure at room temperature.

E/S2 glass-epoxy laminate--±45° basket-woven S2 glass backed by a ±90° E-glass scrim cloth reinforcement. Matrix epoxy resin is Ciba-Geigy R920, a proprietary formulation. Total laminate thickness is about 0.025 inch.

Orange P0655 polyurethane—an ester-based polyurethane elastomer with a manufacturer-reported Shore A durometer reading of 60. This type of P0655 is orange in color due to pigment added and was supplied as 0.125-inch thick skived sheet stock.

Black P0655 polyurethane—reported by manufacturer to have identical chemical/physical properties to orange P0655 with the exception that black pigment has been added to meet U.S. Army requirements. The black P0655 utilized in this study was supplied in the form of an actual pre-molded erosion guard, rather than skived material.

RAC (radar-absorbing compound)—a combination of specially processed carbon particles in a fluoroelastomer resin system designed to provide high resistance values. Diluent/carrier is methyl ethyl ketone. The RAC is used to reduce the radar cross-section of the K747 blade.

4. Experimental

4.1 Durometer Studies

Black P0655 erosion boot sections were cut from the leading edge area so that 15 specimens approximately 0.125-inch thick were obtained for aging at 140°F/97% RH, 150°F/97% RH, and 160°F/97%RH.

Orange P0655 sections were cut from skived sheet stock 0.125-inch thick for aging at 140°F/97% RH, 150°F/97% RH, and 160°F/97% RH.

Both types of P0655 were tested according to ASTM-D2240 Standard Method for Rubber Property Durometer Hardness (ref 3).

Calibration of heat/humidity chambers was done with an external thermocouple/digital thermometer.

A type A durometer was used to obtain readings on all specimens, with the specimen being tested stacked on top of the other four in its respective test group.

4.2 Preparation of the Adhesive

All lap shear joint systems were adhesively bonded using the following adhesive mixture:

Epon 826	100 parts by wt.
Versamid 125	10 parts by wt.
DTA	6 parts by wt.

Handling strength develops after 24 hours at room temperature with full cure obtainable in 7 days (ref 4).

4.3 Surface Preparation of Adherends*

4.3.1 P0655 Polyurethane

- 0.50-in. wide strips cut from erosion guard leading edge area in span direction.

- P0655 strips solvent-wiped with MEK (3 times).

- P0655 strips mechanically abraded with #60 grit oxide (Al_2O_3) on a horizontal circular sander.

- P0655 strips solvent-wiped with MEK (3 times).

4.3.2 ±90 E-glass

- E-glass surface solvent-wiped with MEK (3 times).

- Hand abraded with #120 grit Al_2O_3.

- Solvent-wiped with MEK (3 times).

---

*According to the contractor's adhesive bonding process specification for the erosion guard.

4.3.3 Application of RAC

- #120 grit Al_2O_3 sanded E-glass solvent-wiped with MEK (3 times).

- E-glass surface (backed by 0.063-in. aluminum doubler) dip-coated in an agitated container of RAC.

- RAC-coated E-glass adherends allowed to air dry in a rack at room temperature, then placed in an air circulating oven at +150°F for 2 hours.

- Final RAC thickness 0.45 to 0.6 mils.

4.4 Lap Shear Systems

4.4.1 The following lap shear systems were constructed:

E-glass/RAC/*/P0655/*/RAC/E-glass

E-glass/*/P0655/*/E-glass

E-glass/RAC/*/RAC/E-glass

E-glass/*/E-glass

*Epon 826-V125-DTA adhesive

All lap shear joints incorporated 0.063 aluminum doublers for added stiffness and were fabricated using a bonding template (fig. 3). The entire bonding assembly was vacuum-bagged and a pump was used to create the necessary 20-inch Hg vacuum and maintain it for the 24-hour RT cure.

4.4.2 Environmental Conditioning/Testing of Lap Shears

Lap shear systems were environmentally conditioned according to table 1. Testing was performed in accordance with ASTM-D1002 Standard Method for Strength Properties of Adhesives in Shear by Tension Loading (ref 5).

4.5 Electron Spectrometer Chemical Analysis Runs (ESCA)

ESCA runs were made on the following types of black P0655: (1) "as-received" material; (2) 3-time MEK solvent-wiped samples, and (3) 3-time MEK-wiped/60 grit abraded/3-time MEK-wiped samples.

Black P0655 specimens were removed from the erosion guard supplied by the manufacturer. Spectrometer runs for all black P0655 samples were performed on the inside surface of the boot material.

The ESCA plots in this study represent data obtained from surface scans in which the samples were orientated so that the surfaces to be analyzed were 60° to the analyzer slit. In this way, electrons would escape out from depth of about 12 angstroms (Å) within sample being scanned.

5. Discussion of Results

5.1 Durometer Studies

Black P0655

The black P0655 was not noticeably affected by the 140°F/97% RH conditioning through 3 weeks of exposure, with average durometer readings of 57, 56, and 58 for 7, 12, and 19 days, respectively.

Figure 4 shows, however, that aging at 150°F/97% RH did prove deleterious, reducing the average durometer reading to 55 after 1 week of exposure. Aging an additional 10 days reduced that average to 49; and after a 21-day exposure, the average fell to 40. Figure 4 also illustrates that the deterioration of the black P0655 was greatly accelerated when aged in the 160°F/97% RH environment. After only a 10-day exposure, the average

durometer reading was determined to be 43; after 12 days 40, and finally, after 14 days it had decreased to 34. The last durometer readings obtained after 18 days of exposure yielded an average of 21. Aging the PO655 beyond that point made subsequent readings impossible to obtain due to the degradation observed.

From the durometer data obtained at 150°F/97% RH and 160°F/87% RH, it appears that an extensive amount of reversion took place in a relatively short time (up to 21 days) under those conditions. Reversion of an ester-based polyurethane, like PO655, occurs when its ester linkages are attacked by water molecules resulting in a hydrolysis reaction. The net result of this action, given enough time, is the conversion of the urethane rubber into a shapeless blob [ref 6 (such a condition was observed in this study for black PO655 polyurethane erosion guard specimens aged for a period of 25 days at 160°F/97% RH as shown in fig. 5)]. In addition, the durometer readings also seem to indicate that the conditions necessary for the onset of significant black PO655 reversion were in the range of 150°F to 160°F/97% RH, with an expected increase in the rate of reversion accompanying a rise in conditioning temperature at a given humidity level.

Orange PO655

Considering the orange PO655, aging at 140°F/97% RH also did very little to affect durometer hardness of the material for exposure times as long as 7 weeks. Data obtained for aging 1 week at 150°F also indicated no noticeable change from the control average of 65. After an elapsed time of 17 days at 150°F, however, a slight decrease to an average of 62 was observed, and an additional 4 days aging reduced that figure to 61. Going further, aging at 160°F/97% RH did result in minute, yet significant decreases in durometer readings: after a 10-day exposure period, durometer readings fell to 60; after 12 days 58; after 14 days the average durometer reading fell to 57, and finally, after 18 days, it was 55.

The data presented for orange PO655 indicates that some limited reversion of that material took place, but to nowhere near the extent previously described for the black PO655. Figures 4 and 6 reveal the relatively high reversion resistance of the orange PO655 as compared to the black PO655. There are a number of possible reasons for this phenomenon. Although claimed by the manufacturer to be chemically identical (except for the addition of black pigment) to orange PO655, this particular erosion boot may not have been prepared with the proper stoichiometric ratios of resin to curing agent. Differences in stoichiometric ratios for the same material have been shown in the past studies (ref 2) to affect a material's reversion characteristics. Another explanation is related to the physical processing of the two types of PO655. The black PO655 is die-molded, a material which has a relatively large surface area due to the microporosity of its surface. The orange PO655 is a skived material, sliced off a billet of PO655 polyurethane, which has a relatively smooth surface. Consequently then, given the difference in the amount of reacting surface, one would expect to find a higher reversion rate for the black PO655 material. A third and more likely possibility is that the two types used different polyol resins to form the polyurethane.

5.2 Lap Shear Results

5.2.1 General Observations

The testing of the E-glass/ E-glass and the RAC/RAC adhesively bonded systems exhibited very little tendency to bend under tension loading, thus greatly minimizing the effects of peel and yielding accurate shear strength values with little scatter for the adhesive and/or the RAC.

The lap shear specimens incorporating P0655 polyurethane as an adherend, on the other hand, cannot be classified strictly as "lap shear" joints; rather, these specimens, when loaded in tension, exhibited failure characteristics representing a complex combination of shear and peel forces.

Figure 7 shows a typical sandwich lap shear under tension. As the joint elongates, peel forces must develop at the free surface edge to maintain equilibrium (ref 7). These peel forces represent a small percentage of the total joint stresses for a very rigid system. In the case where P0655 is used as a sandwich member, however, its tendency to elongate magnifies this edge peel effect. Consequently, the ultimate performance of this type of joint, in a so-called "shear" situation, becomes directly dependent on the bond condition at the free surface edge, i.e., if it is good, then the failure would be expected to be largely the result of shear forces. If, however, a poor edge bond exists, the concentration of peel forces at the free edge would cause a joint failure to be initiated there first, propagating under a complex combination of peel and shear stresses, thus yielding lower than expected lap shear values. This scenario could serve as an explanation for the

apparent discrepancy in lap shear strengths reported for those E-glass/E-glass and P0655/E-glass joints reported to fail with high degrees of cohesive failure in the Epon 826 adhesive system. Ideally, if the latter joint system was rigid with failures occurring cohesively in the adhesive, the two systems should have yielded similar shear strengths, which they did not. In a similar sense, failure in the P0655/RAC joints may have been 100% cohesive in the RAC layer, but that average was significantly lower than the shear strength average reported when RAC/RAC lap shears were tested. Therefore, it is evident that the RAC in the P0655/RAC joint system must have failed under stresses other than pure shear in view of the relatively low shear strengths obtained.

It must be concluded then, that the lap shear results obtained in this study for the systems incorporating P0655 as an adherend, although they may be compared to each other, may not be compared to results obtained for rigid systems (i.e., the E-glass/ E-glass and RAC/RAC systems).

5.2.2 Room Temperature and Aged Lap Shear Results

E-glass/E-glass Joints

The room temperature average obtained when E-glass/E-glass adhesively bonded joints were tested in tension was 1,455 psi. Aging this lap shear system at 150°F/97% RH for 0 to 2 weeks resulted in a substantial increase in average lap shear strength as shown in figure 8, possibly due to a post-curing effect. Additional aging in this environment, however, served to decrease lap shear strength by 25% after 21 days total exposure time to 1,640 psi. Although its performance on a residual strength basis exceeded expectations, this fact does not necessarily imply that

287

this adhesive system would be equally resistant to the effects of a high heat/high humidity environment under a stressed condition.

Conditioning for 1 hour and testing at 180°F reduced the average lap shear strength to 30% of the room temperature average. Although this figure is not good from an adhesive bond standpoint, it was still about 300 psi higher than the shear strength of the RAC tested under the same conditions and 350 psi higher than the shear strength requirement of 30 psi in the contractor's process specification.

RAC/RAC Joints

From lap shear data presented in figure 9, it is evident that this RAC does not possess an optimum weathering capability when exposed to hot, humid environments. In less than 16 days in a 150°F/97% RH environment, RAC/RAC lap shears lost an average of 80% of their room temperature lap shear strength of 572. Although a K747 blade is rarely subjected on a constant basis to such conditions while in service, similar conditions could possibly be met in depot storage containers in hot, humid areas, as reported in past studies with the UH-1 blade (ref 8).

Conditioning for 1 hour and testing at 185°F (dry) would, however, be representative of normal operating conditions of the blade in hot, sunny locations. The results at 185°F showed a rapid deterioration of lap shear performance with an average of 85 psi and the principal mode as being 100% cohesive in the RAC layer. Although this figure is still

above the shear requirement (30 psi), it by no means qualifies this RAC material as a constituent in most adhesive bonding applications requiring strength and durability.

From the lap shear data obtained in this study, it is clear that this particular RAC is not a desirable material to be incorporated into any adhesive bonding application due to its poor weatherability, as well as its susceptibility to catastrophic failure in complex loading situations involving peel, as well as shear forces.

Black P0655 Sandwich Lap Shears

Figure 10 shows two curves representing the effect of a 160°F/97% RH environment on the lap shear strength of P0655 joints containing the RAC layer and those in which the P0655 is bonded to E-glass surfaces.

P0655 joints containing no RAC possessed, on average, room temperature lap shear strengths 400 psi higher than joints in which the RAC layer was incorporated. This figure, however, had a very large standard deviation associated with it, as seen in table 4. The observed scatter in P0655 lap shear data may have been, in part, due to the complex loading described earlier for P0655 sandwich lap joints. Still another explanation could be that the relatively large deviations were due to the presence of unremoved silicones from the P0655 surface. In either case, room temperature lap shear values can be expected to range anywhere from 300 to 1,000 psi based on the lap shear data obtained for this type of joint.

Aged non-RAC joints displayed significant losses in lap shear strength in the 1- to 3-week period of exposure, dropping an average of 300 psi in that time. Failure modes for early periods of exposure were a mixed combination of adhesive-to-E-glass/ failures in the adhesive/or cohesive in the P0655. Successive conditioning periods were marked, however, by complete failure in the P0655 at very low stress levels (27 psi after 5 weeks). The condition of the P0655 material for the latter exposure period (3 to 5 weeks) was so deteriorated that typical elongations of the P0655 lap shear joints obtained prior to failure were almost ten times those for the unaged control lap shears (1.5 inches versus 0.15 inch to total Instron crosshead travel). This deterioration of the black P0655 after 2 to 5 weeks of exposure is further proof of what limited durometer studies indicated earlier: that some type of reversion of the material must have taken place. Consequently then, from the aged black P0655 lap shear data available, it is not inconceivable that the instability of the black P0655 in hot, humid conditions eventually could reduce the bond strength to minimum acceptance levels over the long-term.

Lap shear joints in which the black P0655 was bonded to RAC-coated E-glass were also exposed to the 160°F/97% RH environment. The results of prolonged exposures to this environment are also graphically depicted in figure 14. Note that for initial periods of exposure (through 8 days), lap shear values obtained for aged joints did not deviate from the control average. Upon additional aging, however, there appeared to be a

rapid decrease in shear strength in the period between 14 and 21 days (almost 55%). Subsequent aging (21 to 33 days) produced a deterioration trend in that region identical to that of the P0655/E-glass joint described earlier; also affected in exactly the same manner was the P0655 material which, again, showed signs of significant reversion.

Table 4 also shows the effects of conditioning for 1 hour and testing both types of black P0655 lap shears at 185°F. The figures show drastic reductions in average shear strengths for joints containing the RAC and those which do not. Those specimens which did not have the RAC layer as an adherend experienced, on average, an 80% drop in lap shear strength as compared to the control group. Joints in which the P0655 was bonded to the RAC underwent a similar loss in lap shear strength (64%). Failure modes in the latter group were 100% cohesive in the RAC layer. On the other hand, for joints not incorporating the RAC the failure modes were mixed, having varying degrees of P0655 cohesive failure. Conditioning for only 1 hour at 185%F, it seems, also served to measurably soften the black P0655, allowing it to stretch much more as the lap shear was being pulled.

5.3 ESCA Studies

Figures 11 through 13 report the results for ESCA runs performed on "as-received" and surface-prepared samples of black P0655 erosion guard material. Each figure contains three plots superimposed for comparative purposes and are graphs of the counts registered by the ESCA versus the binding energy in electron volts (eV).

Figure 11: Shown is the spectra for the carbon 1s region of the black P0655 materials with different surface treatments: (a) "as-received"; (b) following three MEK wipes; and (c) after three MEK wipes, abrasion with #60 grit Al_2O_3, and three MEK wipes. Spectra was taken with high resolution.

Figure 12: Nitrogen 1s region of black P0655 polyurethane with different surface preparations: (a), (b), and (c) as above.

Figure 13: Energy region showing silicon 2s and 2p lines for black P0655 with different surface preparations: (a), (b), and (c) as above.

Interpretation of ESCA Results

The basic structural unit for a urethane can be written as follows:

$$
\begin{array}{cc}
H & O \\
| & \| \\
R - N - C - OR &
\end{array}
$$
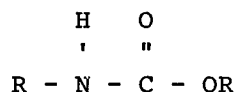
Figure 11 shows the carbon 1s energy region for black P0655 specimens with three different surface preparations. As can be seen when the "as-received" curve is compared with the three-MEK wipe trace, there is a noticeable carbonyl peak ($-\overset{|}{C}=O$) present for the latter specimen. The carbonyl group, as seen above, is indicative of the polyurethane material itself, and since there was not any carbonyl spectra observed in the "as-received" scan, it can be surmised that something on the "as-received" surface must have prevented the detection of the urethane carbonyl group. This was the first indication that a mold release may have been on the "as-received"

specimens. This data also indicated that the three MEK wipes significantly reduced the amount of the unknown surface film based on the appearance of the carbonyl peak.

Figure 12, in a similar way, shows that in a scan in the nitrogen 1s region for the "as-received" specimen, the spectra obtained was basically noise with no nitrogen (also indicative of polyurethane as seen above) peak detected. After the three MEK wipes, however, a nitrogen 1s peak does appear lending further proof to the existence of some type of masking film on the surface of the black P0655 "as-received" specimens.

Figure 13 represents the 2s and 2p lines for silicon. It is immediately apparent that a high intensity peak for silicon was obtained for the "as-received" black P0655 sample. Although the ESCA instrumentation could not distinguish between silica and silicone spectra, the possibility of silicone surface contamination could not be ruled out for a number of reasons. First of all, the silicon counts for the three-MEK-wiped black P0655 was noticeably lower than for the "as-received" black P0655 (15.7 counts versus 24 counts, respectively). This would indicate that the three MEK wipes served to remove significant amounts of some type of compound containing silicon in its structure, most likely a mold release. The silicon 2p line was further reduced by surface preparation (c) to an eight count level.

From the evidence provided by the carbon, nitrogen, and silicon ESCA spectra for black P0655 specimens, there is a strong indication that a relatively thick silicone layer prevented scanning of the polyurethane

material itself in the case of "as-received" samples. It was also indicated that the three MEK wipes significantly reduced the amount of this silicone layer, but its total removal could not be confirmed. This is due, in part, to the possibility that silica-containing fillers or flow control agents in the P0655 may be responsible for the Si lines in the cases for samples prepared by methods (b) and (c).

6. Summary and Conclusions

Durometer studies on black and orange P0655 polyurethane indicated that reversion of this ester-based urethane occurred for specimens exposed to 150°F and 160°F/97% RH environments, with the rate of reversion of the black molded P0655 significantly higher than that of orange skived P0655 material, for reasons related to differences either in the chemical constituents (polyol resins, etc.) and/or processing of the two materials. Further, the observed reversion rate was found to be proportional to increases in temperature for a singular high humidity environment. To rectify this situation, it may be necessary to replace the current P0655 material with one possessing a lower reversion susceptibility, possibly a polyether-based urethane.

Lap shear results for specimens incorporating P0655 and the metallized RAC indicate that this particular RAC is a very poor substrate to bond to in any adhesive bonding application. The RAC was also shown to have extremely poor weathering capabilities under high heat/humidity environments such as those a helicopter blade

may typically be exposed to in storage containers located in hot, humid areas.

From the ESCA results obtained, it can be stated that the "as-received" samples of black P0655 contained a surface film of a silicone-based product, possibly a mold release. Further, it was shown that the surface preparation procedures listed in the contractor's process specification seemed to significantly reduce the amount of silicone contamination, but the total elimination of the silicones could not be confirmed. The presence of unremoved silicones on any material to be adhesively bonded, as previously stated, will most likely result in a very poor adhesive bond. This may, in part, serve to explain the varying degree of P0655 bondability observed in this study.

Taken in their entirety, the black P0655's susceptibility to reversion, the RAC's poor adhesive bond performance, the possible presence of unremoved silicones from the erosion guard, as well as the observed variance in P0655 bondability, all serve to emphasize the need for (1) thorough and proper testing and qualification of materials in the design/selection phase; (2) strict compliance on the assembly line to surface preparation and adhesive bonding procedures listed in the contractor's process specification, and (3) stringent controls on the formulation and acceptance of any material to be adhesively bonded. Lack of control over any one of these factors will inevitably lead to costly production delays, time consuming overhauls, and/or expensive retesting of replacement materials, as shown in this adhesive bonding study.

291

7. References

1. Carlson, R., et al, "Bonding Problems in Army Aircraft," Final Report, October 1985.

2. Meadows, P., Sheth, S., Delmonte, J., "Reversion Resistant Urethanes," SAMPE Journal, Vol. 15, pp 773-780, 1969.

3. American Society for Testing Materials, Standard Test Method for Rubber Property: Durometer Hardness, ASTM D2240, 1981.

4. Epon Resins for Casting, Shell Chemical Company, 1967.

5. American Society for Testing Materials, Standard Test Method for Strength Properties of Adhesive in Shear by Tension Loading, ASTM D1002, Reapproved 1983.

6. Delmont, J., Electrotechnology, July 1967.

7. Kedward, Dr. K. T., "Design and Analysis of Adhesive Joints," Adhesion, Adhesives, and Adhesive Joints, UCLA Extension, March 1985.

8. Wegman, R. F., Levi, D. W., "Aging and Environmental Effects on the UH-1 Main Rotor Blade Adhesives," Technical Report ARSCD-TR-84016, ARRADCOM, Dover, NJ, June 1984.

8. Biographies

Joseph A. Brescia is a materials engineer with the Adhesives Section of the Organic Materials Branch at ARDEC. He is active in many adhesive bonding projects which include the bonding of metals, glasses, and composites, with particular emphasis on their relation to aircraft structural bonding. He received his Bachelor of Engineering degree at Stevens Institute of Technology and is presently pursuing a Masters degree in Materials Science at Stevens.

J. Richard Hall received his B.S. in Polymer Chemistry from the University of Maryland and his Ph.D. from Brooklyn Polytechnic Institute. He did post-doctoral work at Columbia University.

Robert B. Bonk received his B.S. degree in Science in 1972 from Fairleigh Dickinson University. He served in the U.S. Army working for the Surgeon General as a chemical laboratory specialist. For the past 20 years he has been employed at Picatinny Arsenal. He is presently a materials engineer working in the areas of adhesives and adhesion, polymers, and elastomers, and has published over 20 papers in these areas. Mr. Bonk is a member of SAMPE, SME, and ARDEC representative for ASTM D-14 on Adhesives.

Table 1. Test program for lap shear specimens

Rigid lap shear systems	Test environment(s)
E-glass/E-glass	Room temperature controls
	1 hour at 185°F
	1, 2, 3 weeks at 150°F/97% RH
RAC/RAC	Room temperature controls
	1 hour at 185°F
	1, 2, 3 weeks at 150°F/97% RH

P0655 lap shear systems	
Black P0655 - no RAC	Room temperature controls
	1 hour at 185°F
	1, 3, 5 weeks at 160°F/97% RH
Black P0655 - with RAC	Room temperature controls
	1 hour at 185°F
	1, 3, 5 weeks at 160°F/97% RH

Table 2. E-glass/E-glass lap shear results.

Lap shear number	Type	Exposure time	Lap shear strength (psi)	Failure mode % cohesive in 826 system	% adhesive to E-glass	% adherend failure
1	RT	-	1360	100%	-	-
2	control	-	1240	100%	-	-
3		-	1800	100%	-	-
4		-	1420	100%	-	-
Average			1460			
Std Dev			241.8			
5	150°F/	4 days	1480	40%	60%	-
6	97% RH	4 days	1780	50%	50%	-
7		4 days	1620	45%	55%	-
Average			1630			
Std Dev			150.2			
8	150°F/	13 days	1800	50%	50%	-
9	97% RH	13 days	2000	20%	80%	-
10		13 days	1980	40%	60%	-
Average			1930			
Std Dev			110.2			
11	150°F/	15 days	1880	-	-	100%
12	97% RH	15 days	1840	-	-	100%
13		15 days	2320	10%	90%	-
Average			2010			
Std Dev			266.3			
14	150°F/	21 days	1600	60%	40%	-
15	97% RH	21 days	1560	50%	50%	-
16		21 days	1740	50%	25%	25%
Average			1630			
Std Dev			94.5			
17	185°F	1 hour	480	100%	-	-
18		1 hour	410	100%	-	-
19		1 hour	380	100%	-	-
20		1 hour	300	100%	-	-
Average			390			
Std Dev			74.5			

293

Table 4. Environmental aging of black P0655 sandwich lap shears[1]

Lap shear type	Exposure time	Lap shear strength (psi) Avg.	Lap shear strength (psi) Std. Dev.	Average failure mode type observed % cohesive in 826 system	Average failure mode type observed % P0655 failure	Average failure mode type observed % cohesive in RAC
No RAC in joint						
RT - Controls	-	535	244.9	80%	20%	-
160°F/97% RH	4 days	320	44.2	70%	25%	-
160°F/97% RH	8 days	342	112.6	80%	20%	-
160°F/97% RH	16 days	105	6.2	-	100%	-
160°F/97% RH	22 days	62	8.7	-	100%	-
160°F/97% RH	33 days	25[2]	11.6	-	100%	-
185°F	1 hour	112	23.8	60%	40%	-
RAC in joint						
RT - Controls	-	147	22.8	-	-	100%
160°F/97% RH	4 days	140	42.6	-	-	100%
160°F/97% RH	8 days	145	31.9	-	-	100%
160°F/97% RH	22 days	57	7.2	-	100%	-
160°F/97% RH	33 days	27[2]	8.3	-	100%	-
185°F	1 hour	53	16.3	-	-	-

[1] Minimum number of specimens per test group was 6.

[2] Fails to meet contractor's shear strength specifications.

Table 3. RAC/RAC lap shear results

Lap shear #	Type	Exposure time	Lap shear strength (psi)	Failure mode % cohesive in 826 system	Failure mode % cohesive in RAC	Failure mode % RAC to E-glass
1	RT ctl	-	540	-	100%	-
2		-	600	-	100%	-
3		-	530	-	100%	-
4		-	620	-	100%	-
Average			572			
Std Dev			44.3			
5	150°F/97% RH	7 days	300	-	10%	90%
6		7 days	360	-	70%	30%
7		7 days	300	-	25%	75%
Average			320			
Std Dev			30.3			
8	150°F/97% RH	14 days	120	-	10%	90%
9		14 days	140	-	25%	90%
10		14 days	200	-	25%	75%
Average			154			
Std Dev			41.6			
11	150°F/97% RH	21 days	228	-	30%	70%
12		21 days	120	-	10%	90%
13		21 days	170	-	20%	80%
Average			172			
Std Dev			54.0			
14	185°F	1 hour	70	-	100%	-
15		1 hour	82	-	100%	-
16		1 hour	88	-	100%	-
17		1 hour	100	-	100%	-
Average			85			
Std Dev			12.4			
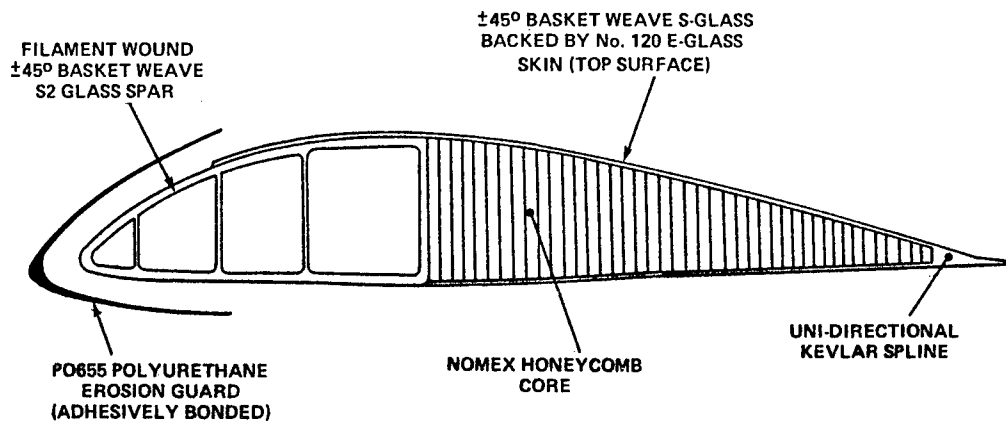
Figure 1. AH-1S main rotor blade section
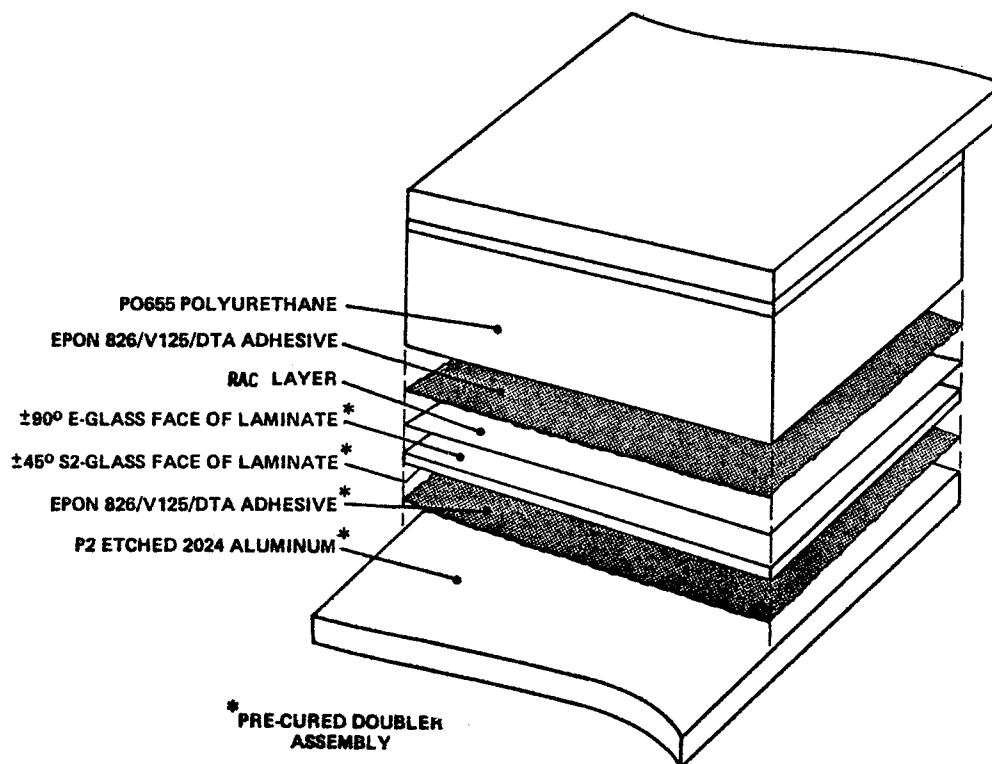
Figure 2. Typical lap shear test specimen
(includes P0655 polyurethane and RAC).

295
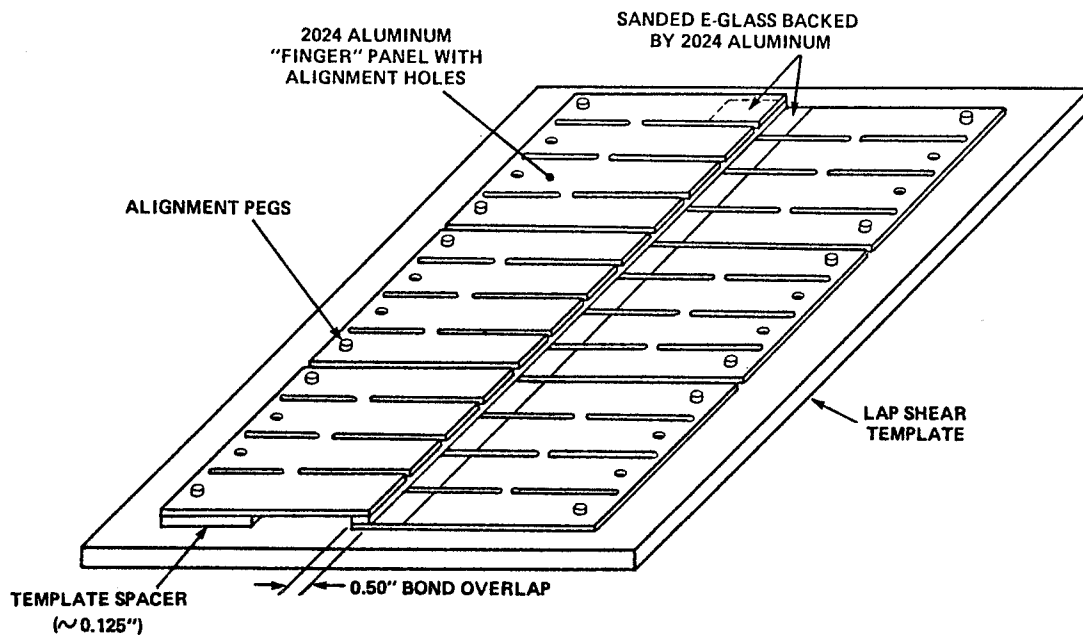
Figure 3.   Fixture used in fabrication of lap shear specimens (vacuum bagging not shown)
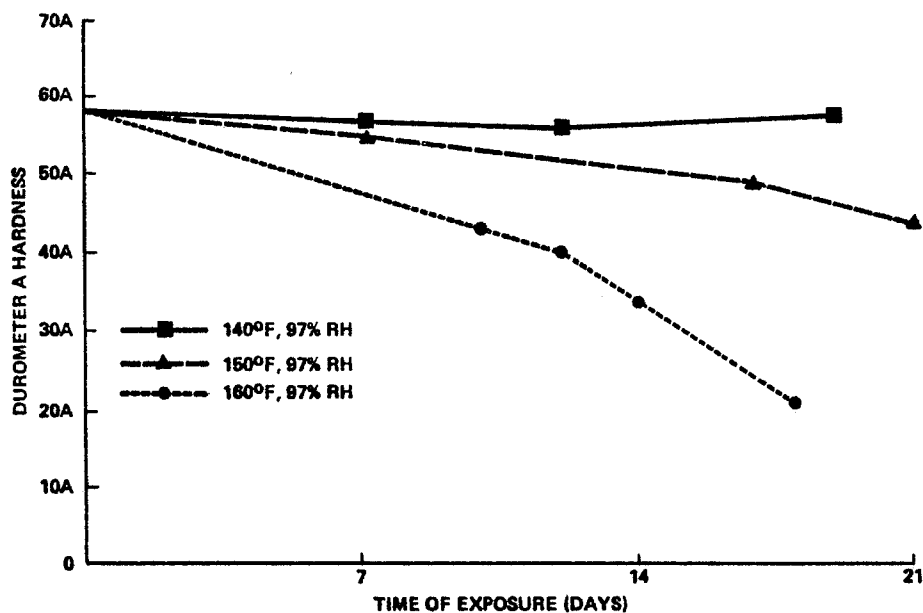
Figure 4.   Effect of various high heat/high humidity environments on durometer A hardness of black PO655

296

BLACK & ORANGE
PO655 POLYURETHANE

AGED 35 DAYS
AT
150 ± 5°F , 97 % R.H.

AGED 25 DAYS
AT
160 ± 5°F , 97 % R.H.
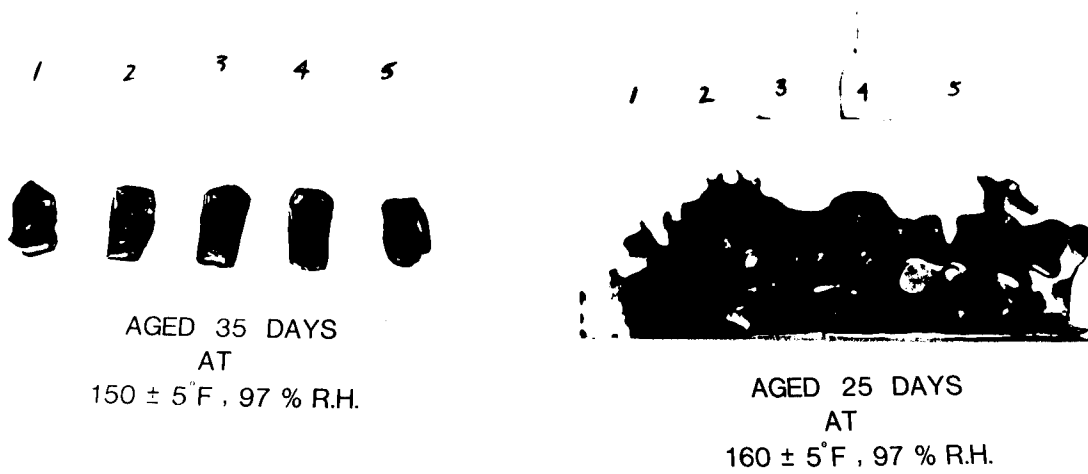
Figure 5.   PO655 polyurethane aged under high heat/
high humidity environments
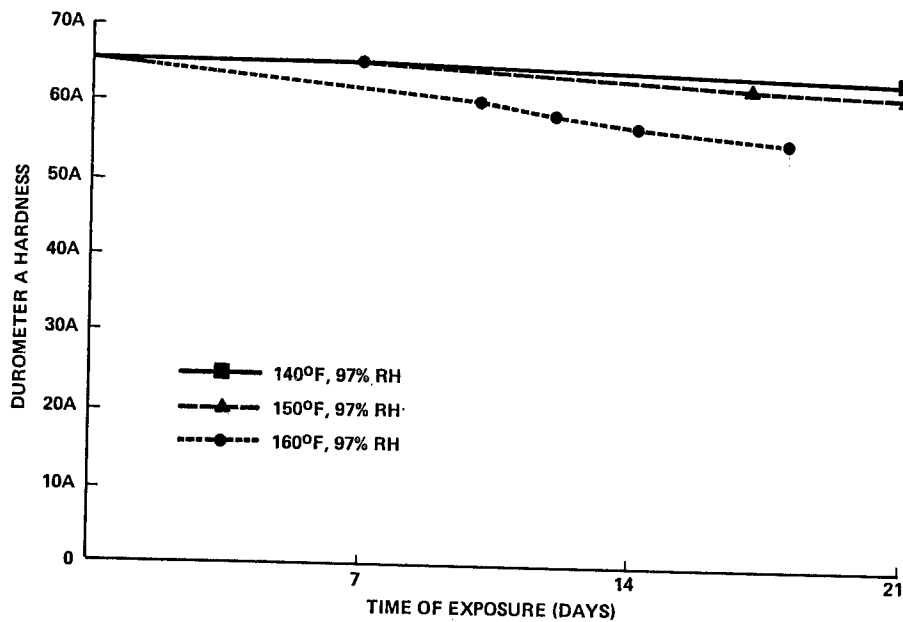
Figure 6.   High heat/humidity environments on durometer A
hardness of orange PO655

297
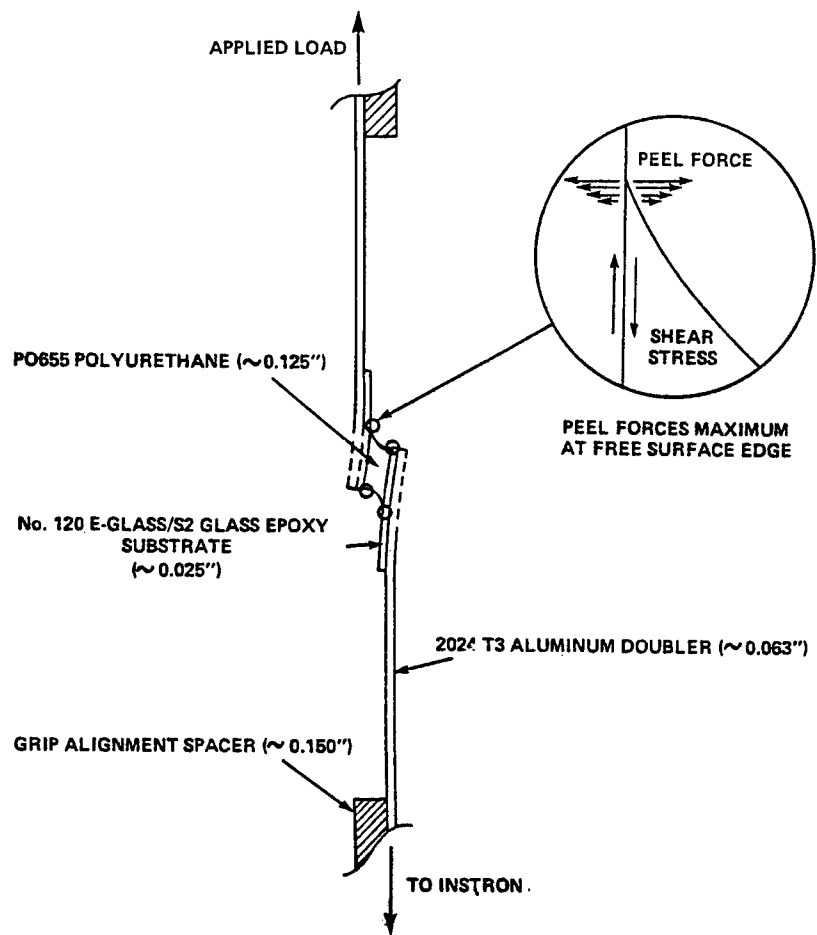
Figure 7. Development of peel forces in PO655 sandwich lap joint
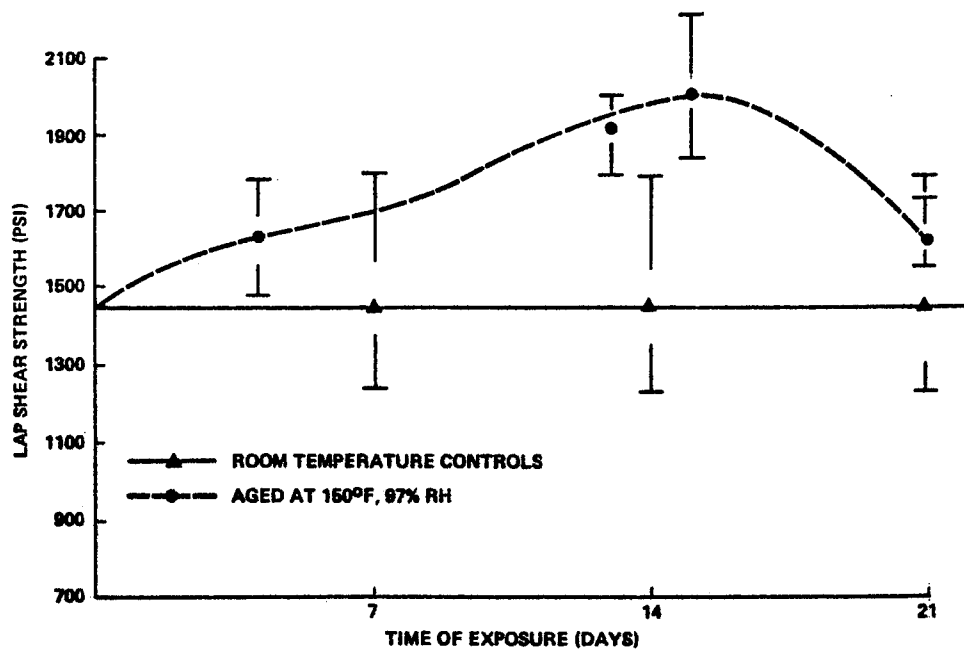
Figure 8. Effect of high heat/humidity aging on lap shear
strength E-glass/E-glass joint
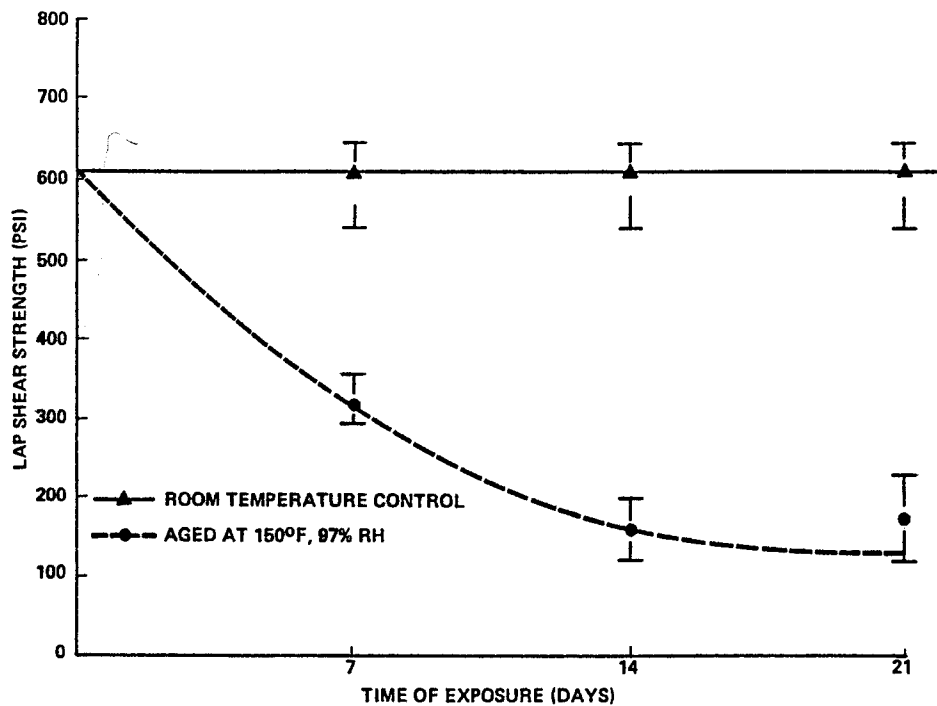
Figure 9.   Effect of high heat/humidity aging on lap
            shear strength RAC/RAC joint
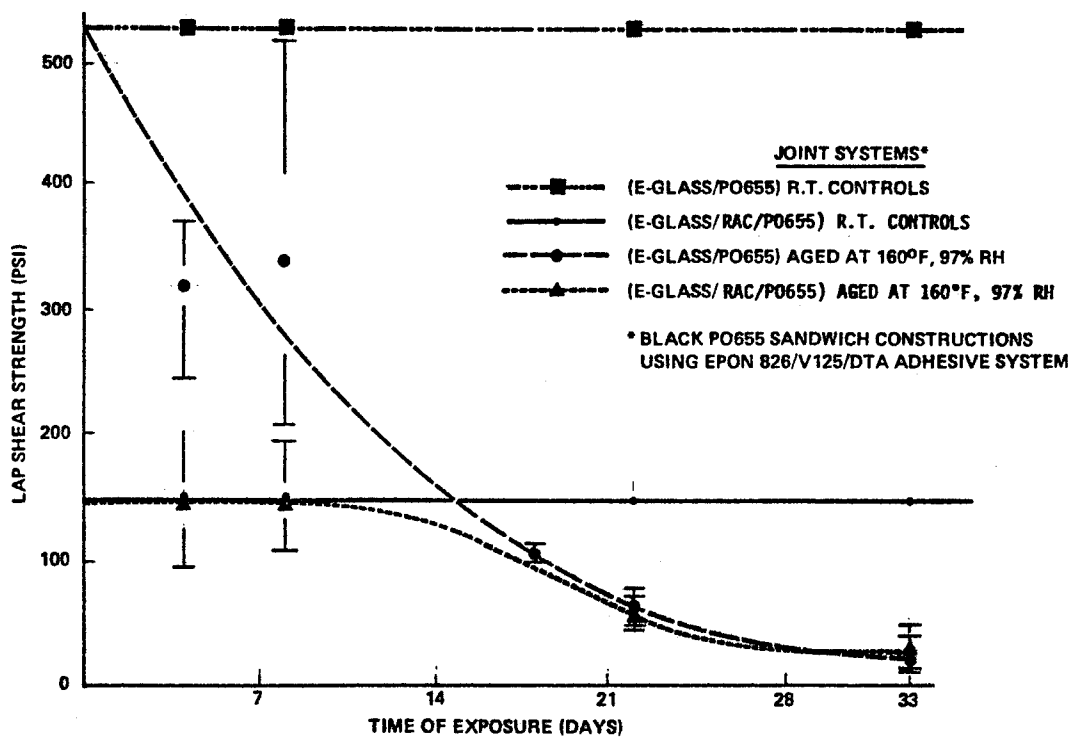
Figure 10.   Effect of high heat/humidity aging on lap shear
             strength black PO655 sandwich lap shears
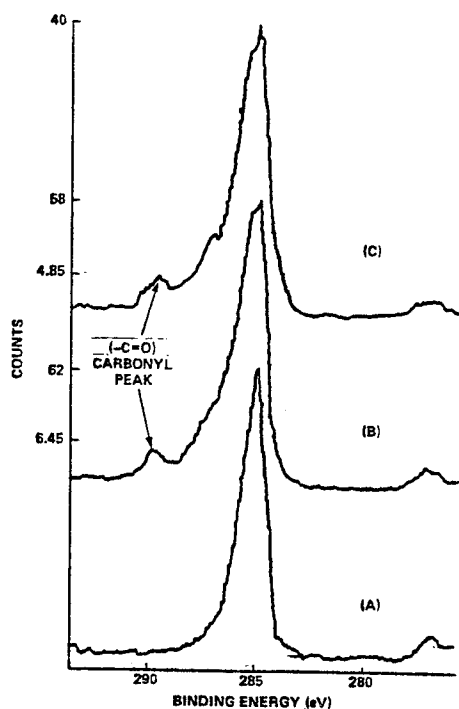
Figure 11. ESCA scan of carbon 1s region black P0655 specimens
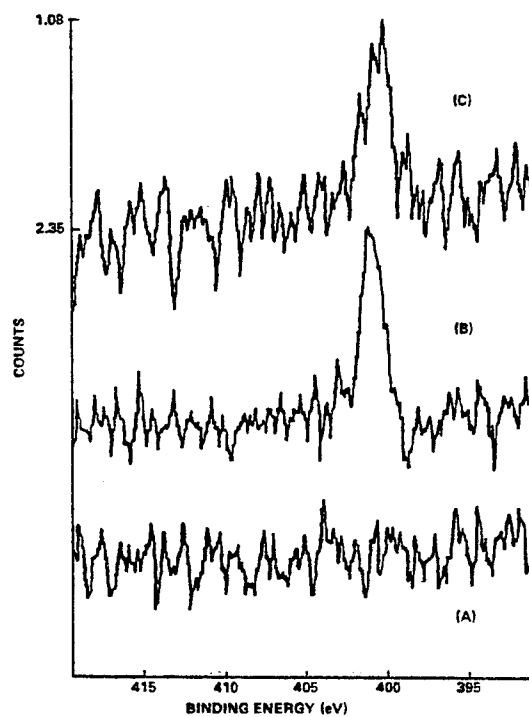
Figure 12. ESCA scan of nitrogen 1s region black P0655 specimens
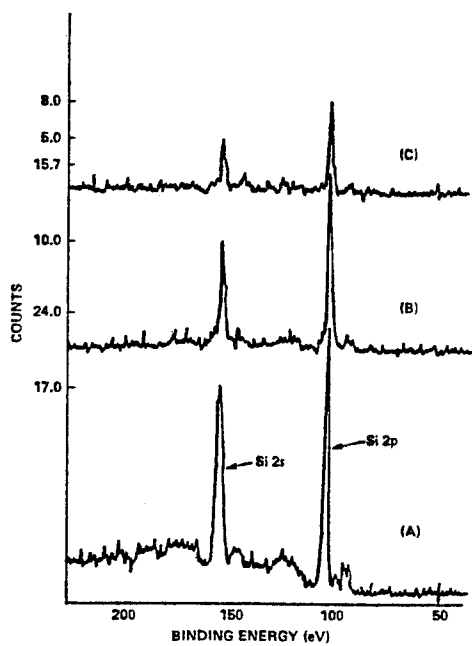
Figure 13. ESCA scan of Si 2s and Si 2p regions black P0655 specimens

COMPUTERIZED ADHESIVE TECHNOLOGY

by
John Nardone

US Army Armament, Research, Development, & Engineering Center
Picatinny Arsenal, NJ

INTRODUCTION

The Army's technology for adhesive bonding is being compiled for retrieval using the computer technology at the U.S. Army Armament Research, Development and Engineering Center (ARDEC), Picatinny Arsenal, New Jersey. This initiative, sponsored by the Army Materiel Command (AMC), will consolidate the command's activities in support of the application of adhesives for structural bonding.

What is unique about this effort is that engineering data will be centralized in a main computer file and accessible from remote locations using conventional telephonic means enabling individuals to assess the most current research and methodology. The technical information will help to minimize duplication of effort, disseminate results of materials assessments, and expedite problem solving. ARDEC was tasked to develop an AMC oriented data file since it had previously developed a specialized adhesives data base for Aviation Systems Command (AVSCOM). This file concentrated on engineering data for bonding and repair of aircraft structures. It was a limited file but provided the foundation for a more all encompassing data base. The requirements for tough, lightweight, high-performance structures are relying on adhesive bonding as the means of joining, thus a need was seen for a more comprehensive file of numerical data as well as pertinent information connected with design, manufacture, and function.

The adhesives data base was developed in a joint effort of ARDEC's Adhesives Section and the Plastics Technical Evaluation Center (PLASTEC), located within the Armaments Technology Division, bringing together the technical expertise in adhesives and the developed data base technology at PLASTEC. The staff of the Adhesives Section is the largest and most experienced group of scientists and engineers in the Department of the Army whose primary interests and work are devoted

to the science of adhesion and engineering with adhesives for bonding applications. PLASTEC on the other hand is an Information Analysis Center (IAC) and maintains expertise in plastics, adhesives, and organic-matrix composite materials and has developed a number of numerical, data bases using the latest computer technology.

The adhesive data base developed in FY87 represents the initial effort toward the goal of providing data for engineering use. The program is currently being used in support of ARDEC but will be optimized in FY88 and will be available for remote access by other defense personnel and contractors in the fourth quarter of FY88. It is expected that use by the many segments of government and industry will foster comments and suggestions to make it an invaluable user oriented data base.

DATA BASE TECHNOLOGY

The evolution of the mini and the micro-computer over the last 20 years has opened a new vista in the field of information handling. It has enveloped numerous lives even though many are not directly involved. For engineering materials technology much is being done. Most work is independent and serves a limited need. Initiatives by organizations such as the National Bureau of Standards (NBS), and the American Society for Testing and Materials (ASTM) are directed at sharing and standardization of data, a

task that is certainly challenging.

Some of the concerns given to computerized data center around the user, the computer itself, and the data. Computer programs must consider the intended users, generally those having limited familiarity with the program. Programs should require user friendly access routines to allow usage by the broadest possible audience. Programs which are difficult to use or require extensive training result in disinterest. For instance, computer aided design routines are sophisticated and their use is limited to those few skilled in design analysis only. The use of a program will be directly proportional to its complexity. A useful program should consider user interest and needs provided as input to subsequent program developments.

Computer programs may be written for mini-computers or for the ever present micro or personal computer. The advantages and disadvantages vary and are dependent on the available hardware and software, storage capacity, and peripheral equipment. Certainly, the capabilities of a mini-computer are more extensive than a micro-computer, but are not easily accessible since they require a networking feature or a direct-dial-modem hookup. A program written for a personal computer has the immediacy of use, yet the program may not have the sophistication of the mini-computer and the data may require periodic update.

Developers of programs for engineering use will generate

data formats based on their individual capabilities and experiences. Most data provided lacks credibility, that is, it is not supported by documentation or does not provide test method details. In essence, most program developers direct their activities to suit their own needs. Engineering property data must be such that it services a broad community and is provided in a standardized format. The establishment of a centralized file of credible data is an invaluable tool in engineering applications developments.

Neophytes to the computer work expect total capability; e.g. they expect to have all conceivable types of information to answer any question at will. They do not recognize the complexity of marrying materials technology with computer technology and the associated cost. The technologies are available but an all encompassing program remains a challenge.

ADHESIVE DATA BASE

The adhesives data base represents an initial effort in meeting the AMC Adhesive Bonding Initiative. The directions have been established to meet the basic goals established by PLASTEC in computer technology. The data base, although developed for the Army, will be useful by the other services, government organizations, and their contractors.

The adhesive data and information has been categorized into three areas; properties, lessons learned, and design/manufacturing. Each area has been developed to provide data and information to support military bonding applications.

The data base is a menu driven program which is very easy to operate. Access within ARDEC is made using the local area network (LAN), however, remote access is made using a standard VT100 compatible terminal and modem, dialing through commercial telephone lines. Access is also available through the military telephone network. A section of data or information is obtained by making a choice available at the screen. A series of responses will result in the information desired. Although the program is self explanatory, a user guide is to be provided to describe data access, content, and sources.

One might expect that the adhesive data base is a complete encyclopedia of information. This is not the case. Although the potential is there, consider it as an index to technical information most of which may be used directly with other data requiring further review and assessment. The data base is a first step in satisfying user needs. A greater exchange of ideas is necessary to develop the utmost in a computerized program. The program developers welcome critique and comment to optimize the program.

Behind the scenes of the adhesive data base is a sophisticated data base management system (DBMS). It has an automated data base builder for initializing and

303

modifying the data base and a versatile information processor (VIP) program which enables the creation of data entry and maintenance screens. The VIP program is also used in the generation of sophisticated user access menus which enables the user to query the data base and retrieve data. The entire program is stored in one of the ARDEC disks and accessed through a VAX 11/780 computer.

To reiterate the adhesive data base has been segregated into three distinct areas; adhesive property, lessons learned, and design/manufacture. The user may easily browse through each type of information by returning back to the master menu. Although distinct areas, all are to a degree interrelated. The property data contains all the basic materials information while the lessons learned file is a materials and systems or end item digest. The design/manufacture portion is a qualitative approach to adhesive materials selection and utilization. The specific type of data and information contained in each is described in the following paragraphs.

ADHESIVE PROPERTY DATA

The main focus of the data base is the basic adhesive technology. This has been included in the menu selection for properties. Although specific engineering properties are of greatest interest the data base contains several blocks of records containing supportive information. These will be

presented in the menu listing as follows:

- Adhesives
- Adherends
- Surface Preparations
- Test Methods
- Trade Designations
- Documents
- Test Data

Each subject area contains pertinent data and/or information to give the user as much information at the screen as practical. Upon selecting a subject area the user will be led through a series of menus to provide the respective information.

"Adhesives" selection provides data on generic adhesives in broad classifications such as epoxy, acrylic, etc. A listing of materials and their codes; e.g., EP for epoxy, and detailed information for each can be obtained.

"Adherends" selection provides for a list of adherends and codes contained in the data base with appropriate critical comments related to their use in adhesive bonding applications.

"Surface preparations" provides a list of the types and codes contained in the data base with appropriate critical comments related to their use in adhesive bonding applications.

"Test methods" provides a list of adhesive related methods used in the evaluating of materials. A list of codes and a description of each is provided as a ready reference to test methodology.

"Trade designations" are

provided since they represent a key element in the identification of materials used in adhesive bonding applications. A ready reference to their source and the generic form are provided.

"Documents" represent the source of all data. All engineering test data must be limited to a credible document for inclusion in the data base. A main feature of the document search is the keyword index. It will enable the review of document listings based on terms representing the interest of the user. Each document has been abstracted and contains all pertinent data for subsequent acquisition if desired.

"Test data" describing the properties of adhesive systems in numerical form is the main thrust of the properties data base. Test data generated from the many material evaluations is reviewed, assessed for adequacy, and input into the data base. The test data includes residual lap shear, roller peel, wedge, climbing drum peel, creep, fatigue, flexure, wedge, T-peel, and stressed durability.

The selection process involves the input of adhesive and/or adherend codes for data retrieval. Codes are used to simplify the process of data selection. When the input is provided, a summary or listing of the available data is provided from which the user selects one of the listings to review the technical data compiled.

The advantage of a centralized data base is that all available data is provided such that the user may compare materials, assuming like specimen preparation from various investigators. Or the data may reflect the variation in test results based on different parameters employed.

Test data provided in material evaluations are not generally useful in design applications since they are based on coupon specimens. However, they are extremely valuable since they provide the first and most fundamental technical information for engineering design. The data will provide substantial insight into the performance as influenced by both process variables and environmental influence, particularly temperature and humidity.

To reiterate, this is a first effort at a comprehensive, engineering oriented data base for adhesives. When used by command wide personnel it is hoped that their needs have been served. It is expected that constructive comment over the next two years will result in an enhanced program of great value to the technical community.

LESSONS LEARNED DATA

One of the most valuable forms of information is the historical data or experience factors on problems otherwise known as "lessons learned." As the name implies, we hope to learn from the lessons of the past. They are compiled for one specific purpose, i.e., not to repeat mistakes. Unfortunately, many deficiencies are not well

documented since they would rather be forgotten than remembered.

Lessons learned are compiled in various forms throughout the AMC. The most notable is the Corrosion Data Base available through the Materials Technology Laboratory (MTL), Watertown, MA, in which adhesive deficiencies reported are few in number. The adhesives lessons learned, available from the MTL file as other command sources, are being solicited for the adhesive data base. Although some duplication will result, there is an advantage to having all the adhesive problems within one file.

Lessons learned for adhesives center on the failure of the adhesive, the adherend, or the joint configuration. Failure may be related to improper design/manufacturing practices or due to exposure to unanticipated end use conditions. The data base has been structured to acquire comprehensive data related to the adhesive/adherend system, the surface preparation, manufacturing procedure, the problem encountered, corrective action, and the product details. Basically the lessons learned file is directed at what was used, what happened, and what was learned.

To query the lessons learned file the master menu selection is made. The next menu will direct the user into two directions: one is the adhesive/adherend system and the second is the hardware orientation. The

menu is addressing two points: the first is if one is contemplating use of a generic/specific adhesive and/or adherend, what experience is available on performance. The second is obvious, raising the question of what problems have been experienced with aircraft, fuses, missiles, or other form of materiel.

The selection for the adhesive/adherend of interest will require the entry of material codes or the area of interest. The coding is identical to that provided in the selection property data. Keyword search capability will also be included, hopefully to allow access using a broad range of words.

A key aspect of the lessons learned file is the acquisition of adequately documented records. The cooperation of all interested parties will assure that this vital type of information is obtained.

DESIGN/MANUFACTURE DATA

The third major part of the adhesives data base centers on the aspects of designing with adhesives to include the associated manufacturing aspects so critical to performance. The approach taken in this initial effort is qualitative, in that the parameters pertinent to design and manufacture are enumerated. No attempt has been made to enter the world of computer aided design/computer aided manufacture (CAD/CAM), a highly sophisticated arena which employs expensive equipment with three dimensional graphics capability, design analysis routines, and highly skilled

personnel. If only the basic parameters of design/manufacture are included in the adhesives data base in a user friendly manner, the effective use of adhesives will be enhanced.

The factors to be considered in designing with adhesives include: joint geometry and design, materials selection, surface treatment, compatibility issues, use of primers, cure conditions, environmental and durability requirements, and validation of design and process requirements. The data base will contain a digest of all these factors to assist the designer in assuring that proper consideration has been given for effective use.

Manufacturing parameters to be provided deal with the production process and include manufacturing facilities and equipment, processing conditions, process controls, quality control and testing. Again each area will contain a digest to assure the proper use of materials and equipment.

To obtain the stored information, a selection is made from the master menu. the next menu that appears will lead the user step by step through a series of submenus, each providing more detailed information as required. The program will provide the user with a digest of all parameters describing what they are, how they are used, precautions to be given, and a critical review. Also to be included in each digest is reference to design guides, technical

publications, and references containing further guidance.

What has not been included in this current effort is a logical procedure where a specific adhesive system is selected for an application. Such a program requires more extensive assessment and development. It is planned to address this issue in the next fiscal year. Computer capability exists to develop this procedure and it will focus on the use of an "expert system". This term is in vogue today and is a branch of artificial intelligence that answers questions in a specific manner to provide advice at a level surpassing that of a human expert in that field. Expert systems can combine the expertise of several experts and can be continuously modified and expanded.

FUTURE DIRECTIONS

Current plans are to make the data base available for remote use in the fourth-quarter FY88. The data base will have sufficient information to make it credible and enable the user to query the information at will.

The question now remains, where do we go from here? Efforts should be directed at the concerns established earlier; i.e., the user, the computer, and the data. Certainly, as the developers, limitations in adhesive technology will be identified, but only from our perspective. But what about other command needs and interests? Once available, developer-user dialogue is essential.

The availability of the data

base for use will result in
that necessary critique of
the automated mode of access.
Do user friendly screens
enable easy and rapid access
to data? A dialogue with
users is essential to deliver
the best product.

What type of improvements
could be made? Perhaps the
presentation at the screen in
a different format or the
capability to present
graphical presentations of
numerical data. Improvements
of this type will be the base
of user needs.

Now that we have a
centralized data base which
requires telephonic
communications for access,
what about those who do not
have the capability? Do we
exclude them from our user
list? The answer of course
is no. Can the mainframe
orientation be adapted to the
PC? The answer is Yes!
However, by doing so, the
sophisticated capability of
the mini-computer and its
sophisitcated DBMS is lost.
Although capability is lost,
it is apparent that
downloading to the PC
environment is almost a
necessity. Although computer
technology is available, what
and how remains the tasks to
consider.

Although consideration has
been given to those users
with PC's, what about those
without any equipment? There
remains the next avenue and
that is hard copy. The
capability exists to download
data into report format for
ready reference. Although
both the PC-diskette or the
hard-copy route suffer from
being outdated, they are

forms of the data base which
will maximize data base use.

What about integration with
CAD-CAM systems? This is
certainly feasible but it is
complicated by hardware-
software interface. This
remains a future task of a
long-term nature.

The most important part of the
data base is the data itself.
What has to be assured is that
what property data or
information reported is of such
quality that it is acceptable
for general use. Does all
reported data follow ASTM
formats? Do all the data
generators provide sufficient
details? Is the data reported
sufficient to meet user needs?
These questions need be
addressed to assure the maximum
utilization of resources; both
in data generation and in
computerization.

Another aspect of high interest
for the future is the
electronic reporting of data
for computerization. How
standardization is to be
achieved requires coordination
between the government,
industry, and the technical
societies. To reiterate, the
data base developed represents
an initial effort in digesting
adhesive technology for the
military. In the months and
years to come, it is hoped that
our accomplishments will
greatly aid the community at
large; a goal that can only be
achieved by the cooperation of
all responsible and interested
organizations.

DEVELOPMENT OF AN ALTERNATE ADHESIVE
SYSTEM FOR A TACTICAL
MISSILE RADOME JOINT

by

Donald Paterson and Duncan Boyce

Raytheon Company, Bedford, MA

Summary

The Patriot Missile Radome base joint is comprised of a Slip-Cast Fused Silica ceramic bonded to a Kevlar/epoxy composite thread ring. The current production adhesive used to bond the joint is Hysol EA-934. This adhesive contains an aluminum and asbestos filler in order to meet certain physical and thermal properties. In December 1986 Hysol discontinued the manufacture of EA-934 because of the hazards of asbestos. A program to select and qualify an alternate adhesive system commenced in March 1986. The alternate adhesive system which consists of Dow Corning X1-6132 Silane primer for the ceramic and Magnolia Plastics Inc. Magnobond 6388-3 adhesive successfully completed the Qualification test program in January 1987.

The engineering program implemented to select and qualify the alternate adhesive system started in March 1986 and was completed in January 1987. The first four months of the program were dedicated to the identification of candidate adhesives, the screening of compatible and durable primer/adhesive systems, and the development of a bonding process which utilized the existing manufacturing facilities, tooling, and procedures with minimum impact.

The complexity of the radome joint configuration and the adherend material required that an adhesive substitution alone was not sufficient. In order to insure a structurally adequate bond joint with good durability in the presence of storage humidity, a ceramic primer material selection and process development was also necessary. Comparative evaluation of epoxy primers, silane coupling agents, and numerous high strength adhesives was performed leading to two primary candidate systems.

The final selection of the alternate adhesive system for the two primary candidate systems was made by testing full scale radomes under identical conditions. This engineering test program consisted of subjecting six radomes of each bond system to

the worst case environmental conditions required for qualification and comparing the ultimate strength, failure mechanisms and resistance to humidity.

The Magnolia 6388-3 adhesive and Dow Corning X1-6132 silane coupling agent bond system was superior under all test conditions than was the follow up system comprised of Magnolia 6388-3 adhesive and American Cyanamid HT-424 epoxy primer.

Baseline Design Description

The baseline radome design consists of a slip-cast fused silica tangent ogive radome bonded to a filament wound Kevlar/epoxy composite thread ring. The ceramic billet is cast and rough ground by Brunswick Corp., Raytheon finish grinds the inside diameter to a conical bond surface at the base, a tangent ogive constant forward wall thickness, and special tip configuration.

The Kevlar/epoxy ring is filament wound by Hercules on a two unit mandrel. The winding is cured on the mandrel to the finish inside diameter dimensions including the buttress thread which attaches the radome to the missile airframe bulkhead. The outside diameter is machined to finish dimension on a templet controlled lathe. The forward portion outside diameter of the thread ring is conical to provide a matching bond surface with the radome ceramic.

The bondline is tapered at a scarf angle of 10° to minimize stress concentrations at the edges of the joint. The ceramic is spray primed with American Cyanamid HT-424 to a maximum thickness of two mils (.002 in.) and cured at 350°F for 72 hours prior to bonding to the ceramic billet. The bond surface of the thread ring is grit blasted with a 180 grit aluminum oxide abrading media to remove any glossy resin rich surface area. These areas result from machining the shallow scarf angle across the longitudinal laminates of the composite construction.

The Hysol EA-934 adhesive is applied to both surfaces and the joint is mated within 40 minutes of mixing the adhesive. A room temperature cure of the bond joint is required for five days minimum prior to final grinding of the outside diameter of the ceramic. The alignment of the ceramic billet and thread ring during the first sixteen hours of curing is accomplished with a specialized bonding fixture which supports the billet on two inside spring loaded disks concentric with a male thread which supports the thread ring. The fixture is designed to produce a controlled and repeatable bondline thickness radome to radome.

After removal of the radome the bonding fixture, excess adhesive is trimmed from the leading edge of the thread ring-to-billet interface and a smooth tapered adhesive fillet formed on the ceramic.

Figure 1 illustrates the physical characteristics of the baseline radome design.

The forward end of the radome is machined to accommodate a metal protective tip.

Radome Design Requirements

There are four major requirements for the radome design which include the dimensional configuration, the functional performance, the environmental tolerance, and the producibility.

The dimensional configuration as described in Figure 1 is dictated by the missile system requirements for airframe size, shape, and mechanical interface. The missile is radar guided and flies supersonic trajectories with large maneuvering acceleration capability. Therefore, the radome functional performance entails electromagnetic compatibility with the missile seeker, thermo-structural and aerodynamic compatibility with the missile airframe. The
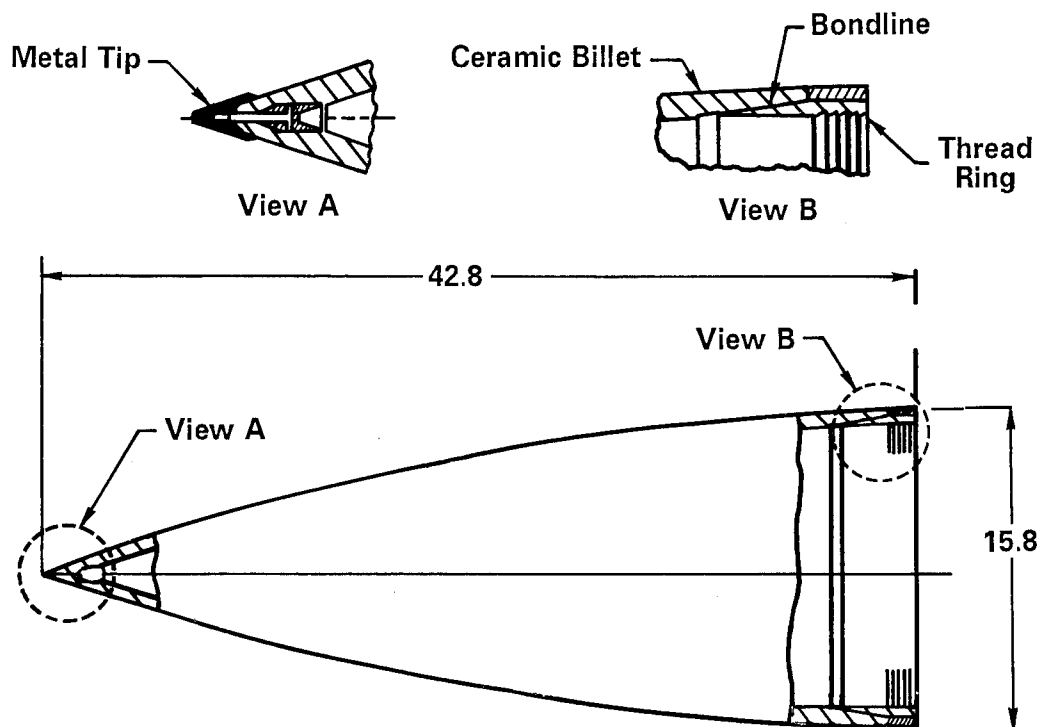
Figure 1 - Radome Physical Configuration

materials selected for the baseline design were dictated by these functional requirements.

The critical environmental conditions that the radome must be tolerant of are one, high temperatures and thermal gradients due to aerodynamic heating, two, surface erosions due to supersonic flight in rain fields, and three, stable dielectric and bond strength in the presence of long term storage at field deployment temperature and humidity.

The engineering design and development of the radome considered all of these requirements in the selection of materials, design configuration, processing of radome components, and adhesive bond system. Slip-cast, fused silica was selected as the radome billet material. The fundamental reasons were stable dielectric constant over wide temperature range and high thermal shock resistance due to very low thermal coefficient of expansion. Slip-cast fused silica is a porous material with exceptionally low tensile strength. Since porous materials absorb moisture and variable moisture content results in undesirable dielectric constant variation, the billet ceramic required sealing by impregnation with a silicone compound. The low tensile strength of the ceramic dictated thermal expansion and

stiffness compatibility with the thread ring requiring Kevlar/epoxy composite. Kevlar was the only fiber available for tailoring the thermal and mechanical properties of the ring because the ring had to be non conductive in order to permit electromagnetic transmission.

In addition, the low tensile strength of the ceramic requires that the bond joint configuration be optimized for load transfer and minimum stress concentration factor. This is classically accomplished by the use of a scarf joint as indicated in the radome base configuration. However, a scarf angle at the base of the billet reduces the ceramic thickness at the base of the radome and increases the bondline temperature of the adhesive during flight at the point of maximum peel stress. The high temperature strength of the adhesive can be increased by curing at elevated temperature but this is not an acceptable procedure for this radome design because the low temperature residual stress in the ceramic becomes critical when superimposed on radome shrinkage which further aggravates the apparent strength of the radome at low temperature.

The baseline radome structural capability is determined by each of the three joint components depending on the temperature regime under which mechanical shear and

bending loads are applied to the base joint. The failure modes are one, tensile failure of the ceramic at low temperature, two, interlaminar shear failure of the thread ring at room temperature, and bondline shear failure at elevated temperature. Each of these failure modes exhibit broad statistical variations which result in strength overlap at intermediate temperature. The thermostructural design of the baseline radome is well balanced with respect to the strength of each component of the bond joint. This is indicated in Figure 2. Therefore, the program to select and qualify a new adhesive had to insure that the interaction between the bond joint adherents and the alternate adhesive system would not upset this balance within the radome structure.

Alternate Bond System Requirements

The alternate bond system requirements are dictated by the uniqueness of the radome joint design, adherend materials and operational structural requirements. The alternate adhesive system had to have
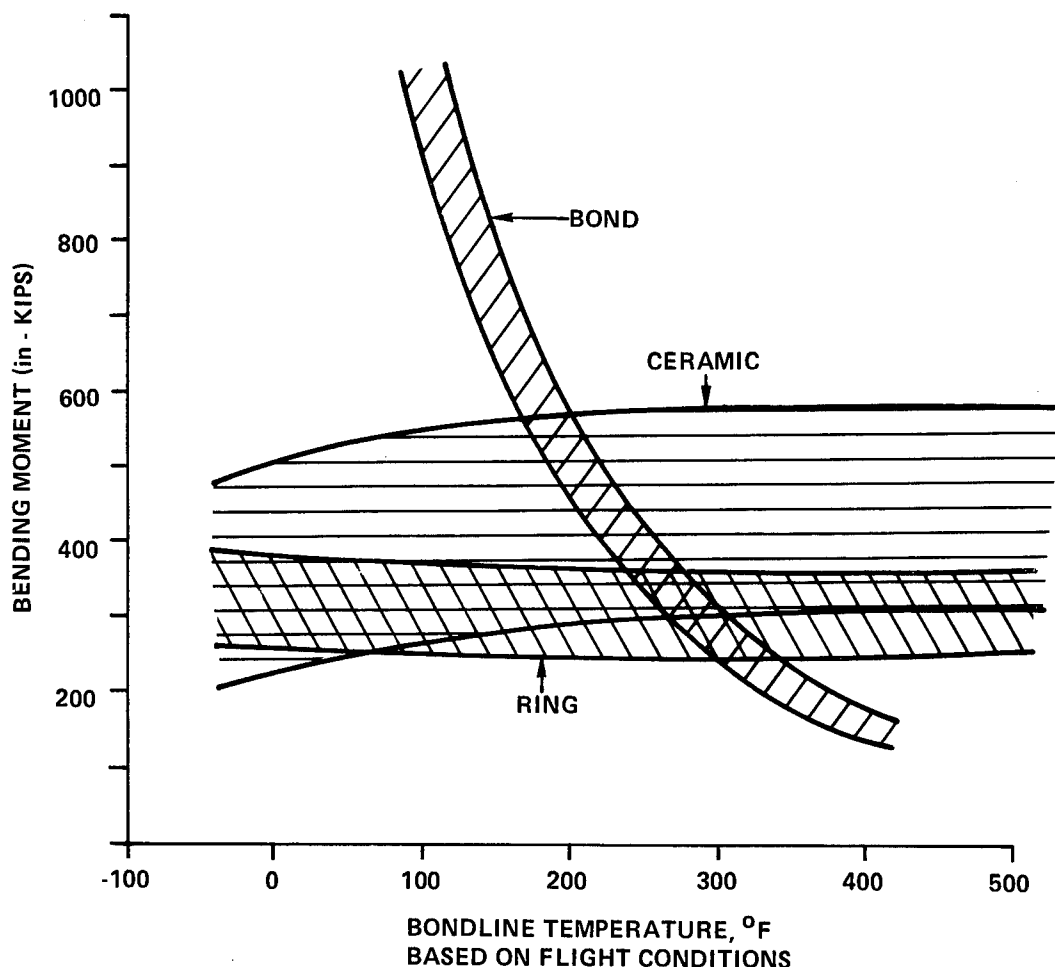
Figure 2 - Schematic Of Joint Failure Modes

313

properties comparable to the existing adhesive system in order to satisfy all the mechanical, electrical, and manufacturing requirements of the radome assembly. In order to meet the requirements of the radome assembly the following material properties are necessary in the bond system.

1. The adhesive must cure at room temperature.
2. Adhesive strength as measured by lap shear specimens must be equal to or greater than Hysol EA-934 adhesive when tested at temperature up to 450°F.
3. The shear modulus of the adhesive must be comparable to Hysol EA-934.
4. The adhesive cure shrinkage and coefficient of thermal expansion must be comparable to EA-934.
5. The pot life of the adhesive after mixing must be at least on hour.
6. The adhesive A and B components must have reasonable shelf life without deterioration.
7. The mixed adhesive must be thixotropic to permit application to the radome joint adherends without excessive running or sag.
8. The adhesive and primer must be compatible with each other as well as the adherends.

Many other requirements exist which are necessary so that the alternate adhesive system will be useable in the existing radome production facility with a similar bonding process to the existing process. These requirements were provided to many manufacturers as preliminary requirements.

Initial Screening Tests

It was clear at the onset that the selection of an adhesive that would satisfy all the requirements would not be a trivial task. It was anticipated that many potential materials would have to be evaluated in order to identify a suitable substitution adhesive. Practical time limitations required that a preliminary screening process be defined in order to reduce the candidate materials to a manageable number in the shortest possible time. This was confirmed after direct or indirect contact of fifteen adhesive manufacturers and ten aerospace structural adhesive users leading to thirty-six adhesive samples being provided to Raytheon for evaluation. A list of the Adhesive and Manufacturers is given in Table 1.

A preliminary screening program was defined which measured three critical adhesive properties and evaluated and compared the results against the requirements. These properties included the double lap

314

TABLE 1 - CANDIDATE ADHESIVES

AND MANUFACTURERS

No.	Adhesive Part No.	Manufacturer
1	6388-3	Magnolia
2	EA934	Hysol
3	EA934NA	Hysol
4	EA9321	Hysol
5	LR100-713	Hysol
6	LR100-713.3 (XEA9381)	Hysol
7	LR100-809	Hysol
8	LR100-810	Hysol
9	LR100-819.0	Hysol
10	LR100-819.1	Hysol
11	LR100-819.2	Hysol
12	LR100-820.0	Hysol
13	LR100-820.1	Hysol
14	LR100-820.2	Hysol
15	LR100-821.0	Hysol
16	LR100-821.1	Hysol
17	LR100-821.2	Hysol
18	EP35	Master Bond
19	EP35P	Master Bond
20	EP35R	Master Bond
21	FE7614	H.B. Fuller
22	FE004	H.B. Fuller
23	FE6026	H.B. Fuller
24	FE0037	H.B. Fuller
25	1543	Furane
26	88842	Furane
27	2800	Crest
28	2154	Crest
29	4086	Crest
30	FR7010	Fiber Resin
31	1XB3578	3M
32	A661	Armstrong
33	A38	Amicon
34	BR95 (3 mixes)	American Cyanamid

shear strength of the adhesive at room temperature, 350°F and 440°F, the pot life of the adhesive as mixed in the existing production process, and the thixotropy of the adhesive as qualitatively measured on an 75° incline.

The double lap shear tests were performed at room temperature, 350°F and 440°F. Adherends used for these tests were phosphoric acid anodized aluminum coated with corrosion inhibiting primer American Cyanamid BR-127 per ASTM D 3933. The specimen configuration for all preliminary screening tests at temperature were double lap shear. This type of specimen minimized the amount of bending in the sample during testing and was an efficient and simple sample to make. The results of preliminary screening for lap shear strength are shown in Table 2.

Initial tests for establishing the sag/flow resistance of the adhesive were conducted quite simplistically yet very effectively. A controlled amount of adhesive was mixed, a ten-gram sample was removed and applied to an aluminum plate which was mounted at a 75° angle to the horizontal. A criteria of a total sag/flow of four inches maximum was established as acceptable. The results of these tests are shown in Table 3. Fourteen adhesive were eliminated for failing the sag/flow tests. This requirement was fundamental to the ability to apply the adhesive to the Kevlar/epoxy thread ring and radome billet conical surface during the bonding operation without excessive sag or flow.

TABLE 2 - DOUBLE LAP SHEAR STRENGTH (AVERAGE OF SIX COUPONS)

Shear Strength (PSI)/Std. Deviation			
Adhesive Part No.	Test Temperature		
	75°F	350°F	440°F
1. Magnolia 6388-3	2889/127	1484/119	599/34
2. Hysol EA 934	3626/97	714/77	523/52
3. Hysol EA 934 NA	3648/62	715/27	449/31
4. Hysol LR100-713	3877/136	527/57	430/36
5. Hysol XEA 9381	3187/147	1028/121	601/83
6. Hysol LR100-809	4031/63	562/40	649/28
7. Hysol LR100-810	3630/236	560/33	351/22
8. Hysol LR100-819.0	3551/273	975/35	621/20
9. Hysol LR100-819.1	3401/157	503/100	606/95
10. Hysol LR100-819.2	3524/175	1404/105	676/33
11. Hysol LR100-820.0	3550/379	827/46	570/50
12. Hysol LR100-820.1	3992/105	418/110	385/31
13. Hysol LR100-820.2	2944/443	699/79	422/25
14. Hysol LR100-821.0	2824/321	745/27	644/35
15. Hysol LR100-821.1	3507/271	1007/31	731/40
16. Hysol LR100-821.2	1651/134	516/134	417/17
17. Masterbond EP 35P	--	411/26	--
18. Masterbond EP 35R	--	384/5	--
19. Fuller FE 0037	3314/64	259/12	226/24
20. Fuller FE 6026	2703/393	421/38	344/36
21. Am. Cyanamid BR-95(3/1)	3538/69	719/36	502/58
22. Am. Cyanamid BR-95(6/1)	2516/137	510/45	452/53
23. Am. Cyanamid BR-95(10/1)	1692/165	385/29	473/47
24. Crest 2800	3179/616	251/54	112/5
25. Crest 2154	3931/17	140/32	92/9
26. Furane Epibond 1543	2517/105	592/41	479/36
27. Armstrong A661	3029/699	258/35	286/14
28. Amicon A38	1348/176	512/41	374/71
29. Fiber Resin FR 7010	1617/112	804/23	644/59
30. Furane 88842	--	743/46	--

Initial screening pot life testing was a purely subjective test. More sophisticated, accepted standard engineering tests would eventually be used for Quality Control procedures. Expensive testing of these preliminary candidate adhesive was unreasonable at the time since a great deal of insight into pot life could be obtained by merely mixing 50 grams of adhesive and periodically checking its flow in the container. It is quite interesting to note that these results reflect exceedingly well the pot life results subsequently obtained by more sophisticated engineering methods. Three adhesives were eliminated because their pot life was too short and did not meet the required criteria. These are indicated in Table 3.

Based on the initial screening tests a major down selection was possible in an effective and efficient test program. As indicated fourteen adhesives did not pass sag/flow tests and were eliminated. Three adhe-

316

TABLE 3 - SAG/FLOW TEST RESULTS

	Pass			Fail	
No.	Adhesive Part No.	Manufacturer	No.	Adhesive Part No.	Manufacturer
1	6388-3	Magnolia	1	EA934NA	Hysol
2	(XEA9381)	Hysol	2	EA9321	Hysol
3	LR100-809	Hysol	3	LR100-713	Hysol
4	LR100-810	Hysol	4	BR95 3/1	American Cyanamid
5	LR100-819.0	Hysol			
6	LR100-819.1	Hysol	5	2154	Crest
7	LR100-819.2	Hysol	6*	4086	Crest
8	LR100-820.0	Hysol	7*	EP35	Master Bond
9	LR100-820.1	Hysol	8	EP35P	Master Bond
10	LR100-820.2	Hysol	91	FE7614	H.B. Fuller
11	LR100-821.0	Hysol	10	FE004	H.B. Fuller
12	LR100-821.1	Hysol	11	FE0037	H.B. Fuller
13	LR100-821.2	Hysol	12	A661	Armstrong
14	BR95 6/1	American Cyanamid	13*	A38	Amicon
15	BR95 10/1	American Cyanamid	14	1XB3578	3M
16	2800	Crest			
17	FE6026	H.B. Fuller			
18	88842	Furane			
19	EP35R	MasterBond			
20	FR7010	Fiber Resin			

*Failed Pot Life

sives were eliminated for failing to pass the pot life tests. The results of lap shear testing indicated that only seven of the adhesives met the requirements of the lap shear tests, while still meeting the other requirements. A summary of lap shear results for those adhesives is listed in Table 4.

From Table 4, the only candidate adhesive in full scale production was Magnobond 6388-3. The Hysol materials, while possessing exceptional strength, only one was in pilot-plant production, XEA9381, and the others were experimental.

It was considered that the risks associated with using an experimental adhesive were too great. Therefore, a decision was made to cease further investigation of the five experimental adhesives from Hysol and direct all efforts of secondary screening to studying Magnobond 6388-3 and Hysol XEA-9381. The latter adhesive was in pilot plant production while Magnobond adhesive had been in production for three years.

Primer/Adhesive Compatibility

The current bond surface of the ceramic radome is primed with American Cya-

TABLE 4 - SUMMARY OF PRIME CANDIDATES

Adhesive	Vendor	Lap Shear, PSI			Manufacturing Status	Comments
		R.T.	350°F	440°F		
Magnabond 6388-3	Magnolia Plastics	2889	1484	599	Full Production for 3 Years	Low Viscosity version tested by Kaman shows superior moisture resistance
LR100-713.3 (XEA-9381)	Hysol	3187	1028	601	Developmental to Pilot Plant	Developed for Grumman - not fully accepted yet
LR100-819.0		3551	975	621	Experimental	Developed for Raytheon Patriot Radome Bonding
LR100-819.2		3524	1404	676		
LR100-820.0		3550	827	570		
LR100-821.0		2824	745	644		
LR100-821.1		3507	1007	731		
EA934	Hysol	3626	714	523		To be Discontinued

318

namid HT-424 epoxy which is applied in a spraying operation and cured at elevated temperature. The cured primer is lightly sanded, prior to bonding the radome to the thread ring, in order to improve the adhesive interface. This surface has been the failure site for high temperature radome tests in the past. In addition, under severe temperature and humidity conditions there was evidence that the primer to ceramic interface degraded reducing the bond strength. Therefore, primer/adhesive compatibility was an important consideration in the alternate adhesive system selection process. The evaluation of primer/adhesive compatibility involved the testing of 19 epoxy primer/adhesive combinations and 18 silane primer/adhesive combinations. There were four different test specimens used to evaluate primer/adhesive compatibiity which are shown in Figure 3. These consist of peel test (P), wedge test(W) quad-lap test (Q), and ceramic/ceramic peel test (T) configurations. The test specimens were bonded with the primer adhesive combination shown in Figure 4. Over 250 test specimens were fabricated and tested during the compatibility evaluation. The approach to assessing primer/adhesive compatibility required testing after coupons had been subjected to an accelerated aging environ-

ment. Each specimen was conditioned, prior to testing for its mode of failure, by either boiling in water for 24 hours or pressure cooking at 250°F for 24 or 48 hours. The results of the primer/adhesive compatibility evaluation demonstrated that all silane coupling agents are more durable than the epoxy primers and that the current HT-424 primer is equal or better than all other epoxy primers.

Screening Peel Test

The large number of primer/adhesive combinations made it necessary to devise a coupon that was relatively easy to fabricate, condition, and test. The screening peel coupon consisted of a ceramic block primed and bonded with the candidate primer/adhesive combination to a Kevlar/epoxy strip. After the adhesive had cured, coupons were subjected to one of the following:

1. 24 hours in boiling water.
2. 24 hours in a 250°F (15 psig) pressure cooker.
3. 48 hours in a 250°F (15 psig) pressure cooker.

The test results indicated that the silane primers provided greater resistance to the aging environments than the epoxy primers. The epoxy primed coupons all failed at the primer-to-ceramic interface.

Kevlar

Ceramic

Screening
Peel Test

Kevlar

Kevlar

Ceramic

Quadlap Shear Test

Kevlar

Ceramic

Wedge Test

Ceramic

Ceramic/Ceramic
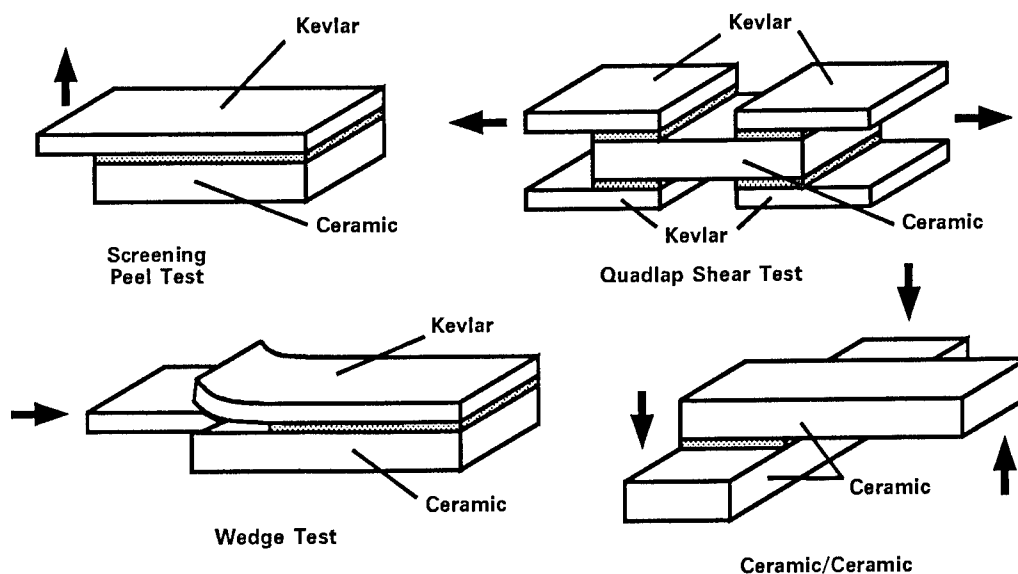
Figure 3 - Adhesive/Primer Compatibility Test Coupons

Quadlap Shear Test

The results of the screening peel test led to using both the quadlap shear coupon and the wedge coupon. The quadlap coupon would demonstrate the resistance of the candidate primer/adhesive system to shear loading and the wedge coupon would evaluate the resistance to peel loading. Both of these loading types are present in the radome bondline and both contribute to its failure. The quadlap coupon consists of 4 Kevlar/epoxy strips each separately bonded to the strips. As shown in Figure 4, the quadlaps were bonded using a significantly reduced number of primer/adhesive combinations. Essentially only the 2 most promising adhesives were selectively combined

with the most promising silanes. The coupons were tested in 2 conditions as follows.

1. As-cured, i.e., after the adhesive manufacturer's recommended cure time.
2. Aged, i.e., after 48 hours in a 250°F (30 psia) pressure cooker.

The coupons, after cure or cure and aging were placed in a tensile test machine, heated such that the bondline reached 350°F in 3 minutes, then tested in tension to produce a shear failure in the bond.

The quadlap shear strengths, averaged for 5 coupons, are shown for each of the adhesives in Tables 5 and 6 and as can be seen the primers with the exception of Magnolia 750 all combined well with the two adhesives when tested in the as-cured state.

320

Adhesive	Primer									
		Silane				Epoxy					No Primer
		DC X1-6132	Hysol 9203	Furane 88060	3M EC 2333	AM CY HT 424F	Magnolia 750	AM CY BR-127	Hysol 9205R	3M EC 3917	No Primer
Hysol EA 934		P	P	P	P	PQW	P	P	P	P	P
Magnolia 6388-3		PQWT	PQWT	PQW	P	PQW	PQWT	P	P	PQW	P
Hysol XEA-9381		PQWT	PQWT	PQWT	PQW	PQW	P	PQW	PQW	PQW	P
Fiber Resin 7010		P	P	P		P				P	P
Furane Epibond 1543		P	P	P		P		P			P

Specimen Code: P – Screening Peel Q – Quadlap Shear W – Wedge T – Ceramic Peel

Figure 4 - Adhesive/Primer Compatibility Test Matrix

The effect of the accelerated aging environment on all the epoxy primers was substantial, they only retained between 11 percent and 27 percent of their as cured strength. The silane primed quadlaps showed a strength retention between 60 percent and 100 percent. Though it was evident that the silanes provided better durability than the epoxies, it was difficult to differentiate among the silanes.

Wedge Test

As stated in the previous section, the wedge testing was conducted simultaneously with the quadlap testing to measure the

TABLE 5 - MAGNOBOND 6388-3/ PRIMER COMPATABILITY - QUADLAP STRENGTH (PSI)

	Primer	As-Cured	Aged
Epoxy	Am. Cyanamid HT-424	1119	123
Epoxy	Magnolia 750	475	118
Epoxy	3M PA 3917	738	201
Silane	Dow Corning X1-6132	812	501
Silane	Furane 88060	738	444

peel resistance of the candidate systems under accelerated aging environments. The wedge coupon, consisted of a Kevlar/epoxy strip bonded with the candidate primer/ adhesive system to a ceramic block. To fa-

TABLE 6 - HYSOL XEA 9381/PRIMER COMPATABILITY - QUADLAP STRENGTH (PSI)

	Primer	As-Cured	Aged
Epoxy	Am. Cyanamid HT-424	733	128
Epoxy	Am. Cyanamid BR-127	591	161
Epoxy	Hysol 9205R	671	161
Silane	Dow Corning X1-6132	674	542
Silane	Furane 88060	635	653
Silane	3M EC 2333	612	443

cilitate inserting the aluminum wedge between the ceramic and Kevlar, a one-half inch section at one end of the coupon was left unbonded. The test matrix is indicated by the W's in Figure 4. After curing the adhesive, an aluminum wedge was driven between the ceramic and Kevlar/epoxy initiating a crack in the bond. The coupons were then placed in a pressure cooker at 250°F and 30 psia for 48 hours, after which the wedge was driven completely through the bondline and the failure mode examined. The failure mode results, averaged for 5 coupons, are shown in Table 7. The epoxy primer combinations, with both adhesives, all showed the primer-to-ceramic failure mode which is less desirable than other possible failure modes since it is generally indicative of reduced bond strength. The wedges of the coupons that failed in the primer-to ceramic mode were easy to drive through the bondline whereas, the ones with the Kevlar-to-adhesive failure modes proved extremely difficult to drive the wedge. The silane primed wedges were more resistant to the accelerated aging environment, however, it was still difficult to differentiate among the silanes.

Ceramic/Ceramic Peel Test

Since the silane primed wedge coupons has been failing primarily at the Kevlar to adhesive interface, the ceramic/ceramic

TABLE 7 - ADHESIVE/PRIMER COMPATIBILITY - WEDGE COUPONS

Primer	Failure Mode	
	Magnolia 6388-3	Hysol XEA 9381
Am. Cyanamid HT-424	Primer-to-Ceramic	Primer-to-Ceramic
Am. Cyanamid BR127	-----	Primer-to-Ceramic
Hysol 9205R	-----	Primer-to-Ceramic
Magnolia 750	Primer-to-Ceramic	-----
3M PA 3917	Primer-to-Ceramic	-----
Dow Corning X1-6132	Kevlar-to-Adhesive	Kevlar-to-Adhesive
Hysol 9203	-----	Primer-to-Adhesive
Furane 88060	Primer-to-Adhesive	Primer-to-Adhesive
3M EC 2333	-----	Kevlar-to-Adhesive

peel coupon, was designed, eliminating the Kevlar strip, thus differentiating among the silanes would be possible. Two ceramic blocks were primed and bonded to each other forming a T. The test matrix for this coupon included the 2 adhesive candidates and the 3 remainidd silane primers, Dow Corning X1-6132, Hysol 9203 and Furane 88060. The coupons were either tested in the as-cured state or conditioned in a pressure cooker at 250°F, 30 psia for 24 hours. The peel test consisted of placing the coupon in tensile test machine such that one of the blocks was restrained, heating the coupon to bring the bondline to 350°F in 3 minutes, then applying a tensile load to the unrestrained ceramic block.

Test results, shown in Table 8, indicate that the aging did result in a substantial de-

crease in peel strength, however no silane showed a clear advantage over the others. The Furane 88060 was eliminated because it was colorless and would not be suitable for production process without being dyed for visibility on primed ceramic surface.

Radome Subscale Coupon

In a final attempt to distinguish between the two remaining silane primers, radomes bonded with the Magnolia 6388-3 adhesive and the two remaining silane primers were machined into 1-inch wide strips along the bondline as shown in Figure 5. The coupon consisted of a piece of the Kevlar/epoxy ring bonded to a piece of the radome. After machining from the radomes, these subscales, four Magnolia 6388-3/Dow Corning X1-6132 and eight

TABLE 8 - ADHESIVE/PRIMER COMPATIBILITY - CERAMIC PEEL COUPONS

Primer	Conditioning	Magnolia 6388-3		Hysol XEA 9381	
		Failure Load (lbs)	Failure Mode	Failure Load (lbs)	Failure Mode
DC X1-6132	As-Cured	76	Primer-to-Adhesive	70	Primer-to-Adhesive
DC X1-6132	24 hr at 250°F; 15 psig	32	Primer-to-Adhesive	12	Cohesive
Hysol 9203	As-Cured	75	Primer-to-Adhesive	62	Primer-to-Adhesive
Hysol 9203	24 hr at 250°F; 15 psig	24	Primer-to-Adhesive	15	Cohesive
Furane 88060	As-Cured	100	Cohesive	82	Primer-to-Adhesive
Furane 88060	24 hr at 250°F; 15 psig	35	Cohesive	18	Cohensive

Magnolia 6388-3/Hysol 9203, were placed in a pressure cooker and maintained at 250°F and 30 psia. After 24 hours of conditioning five of the eight Hysol 9203 primed specimens had fallen apart. After 40 hours of conditioning two additional specimens had also failed. After 48 hours one Hysol specimen was tested at room temperature and failed at 345 psi. All four of the X1-6132 primed coupons survived the pressure cooker environment. Two were tested at room temperature and failed at loads ranging from 1072 psi to 1300 psi. The two other specimens were tested at 350°F and failed at 285 psi and 350 psi. The Dow Corning X1-6132 primed radome subscales showed substantially greater resistance to the aging environment and X1-6132 was selected as the silane primer best suited for this application.

The Dow X1-6132 silane was the best coupling agent based on the discrimination tests. The HT-424 was equal to or better than any other epoxy primer based on primer/adhesive compatibility test. The Magnobond 6388-3 and Hysol XEA-9381 adhesives met all the bonding process requirements and were stronger than EA-934 at elevated temperature.

The four combinations of adhesive and primer were reduced to two bond systems for the Engineering Test Program which was designed to select the final adhesive system for qualification. The Hysol XEA-
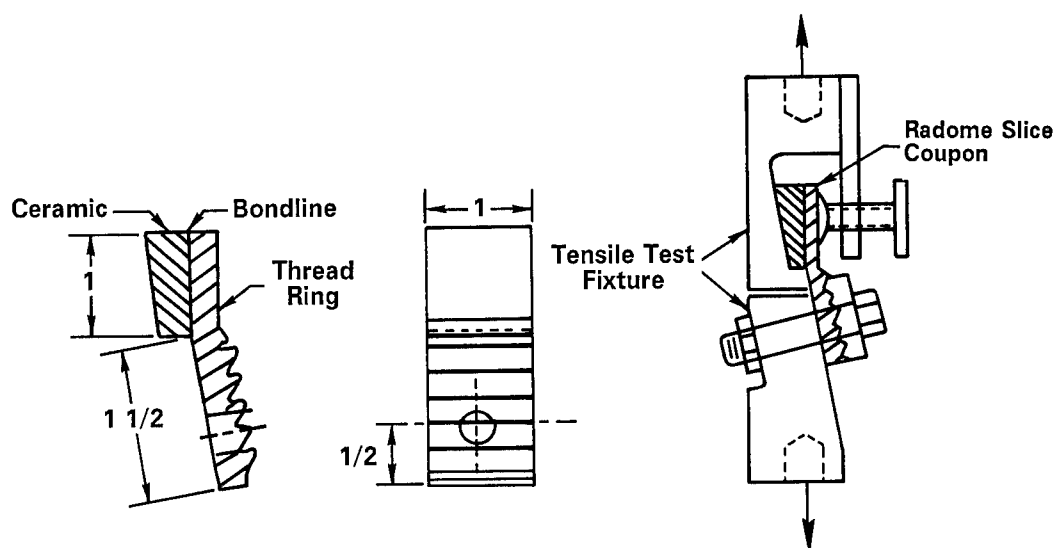
Figure 5 - Radome Slice and Test Fixture

324

9381 adhesive was eliminated for two reasons. Principally the product was in pilot production and Hysol could not define when transition to full production would occur and the XEA-9381 was more viscous requiring some modification of the radome bonding process, thus Hysol XEA-9381 was eliminated as an adhesive. Therefore the two primary candidates became Magnobond 6388-3 adhesive with Dow Corning X1-6132 silane and American Cyanamid HT-424 epoxy for primers.

Exploratory Radome Test

During the development of the process for applying the silane primer to the ceramic, several scrap radome billets were bonded using identical bond fixtures and simulated production bond room conditions. The scrap radomes were rejected for other than structural reasons and, therefore, provide excellent and cost effective exploratory test hardware.

The slip-cast fused silica ceramic is an extremely fragile material. The use of a new silane primer for the ceramic billet was of concern despite the superior moisture resistance demonstrated during the primer adhesive compatibility study. In addition, there had been some indication that the subscale specimens primed with silane ex-

hibited spalling of the ceramic several days after the initial test failures. For example, some of the peel test specimens which failed at the adhesive Kevlar interface after boiling and pressure cooker exposure spalled after several days at the ceramic surface. A possible explanation for this secondary failure mode is that as the adhesive dries it shrinks inducing stress in the ceramic. Since the Kevlar adherend has separated from the specimen, the constraint at one surface of the adhesive is removed permitting an increase in adhesive strain inducing stress in the ceramic. Such a condition could exist in a full scale radome at the fillet, a point of maximum ceramic stress during flight.

Another explanation could be that silane somehow acts on the ceramic causing surface damage and inherent material weakness.

In order to evaluate this potential problem two of the development radomes were subjected to a test. The test consisted of soaking both radomes at 130°F for 16 hours. This preconditioning would result in post curing the adhesive and inducing the maximum shrinkage expected under storage conditions in the life of a fielded radome. The stresses due to postcure shrinkage would be superposed on the thermal stress-

325

es due to cooldown to -30°F, resulting in reduced loading carrying capability for the radome. One radome was to be structurally tested at -30°F, and the other at +440°F. The test plan and results are illustrated in Figure 6.

The low temperature test failed at 70 percent of design load. The high temperature test failed at nearly 200 percent of design load. Both failures occurred in the ceramic. A failure analysis was performed to identify the cause of the low temperature failure.

Failure Analysis

The failure analysis involved three separate activities which included visual inspection of the failure, a stress analysis and material property tests.

The visual inspection of the ceramic failure identified the failure site. Based on the visual inspection an analysis was performed of the stress field surrounding the failure site.

Experimental measurements of the cure and thermal shrinkage of adhesive were conducted to determine if the Magnolia 6388-3 adhesive would induce higher stresses than the existing adhesive and contribute to the low temperature failure.

The visual inspection of the ceramic first involves the piecing together of all of the ceramic fragments. A first order evaluation of the failure initiation site can be
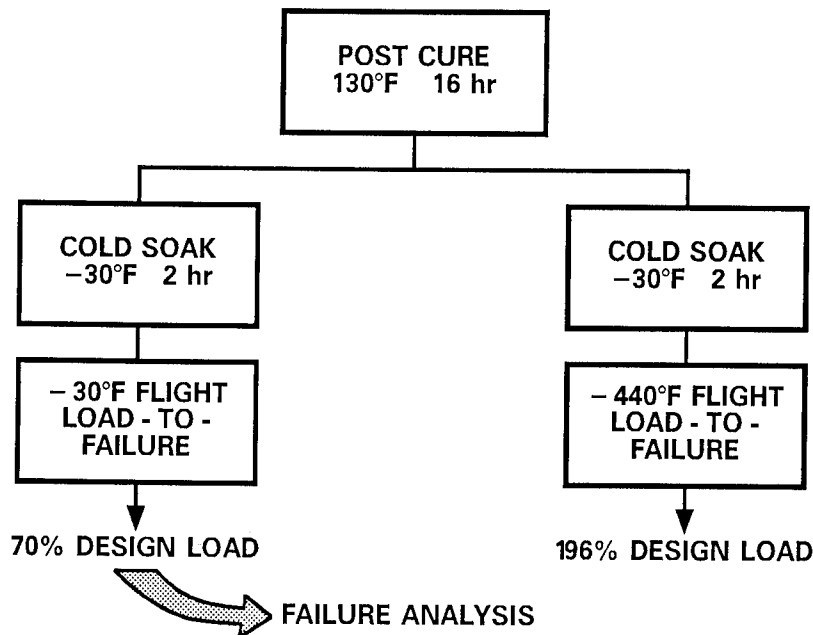
Figure 6 - Exploratory Radome Test - Low Temperature Sensitivity

made by observing the pattern and inspection of fracture surfaces. Radome ceramic failures involve high energy release rates which frequently results in major secondary damage complicating the evaluation. If the primary fracture surface is identified, a more intense surface inspection is performed with indirect lighting and often magnification. This inspection occasionally will identify the precise failure initiation site in the ceramic. More often, the surface inspection will only approximate the failure site based on the change in texture of the facture surface. The evaluation procedure was applied to the failed radome and the conclusion was that failure initiated on the tension side of the radome below the adhesive fillet. An inspection of the adhesive fillet revealed that large variations in geometry of the fillet existed around the inside circumference of the radome.

The adhesive fillet is a critical component of the radome joint. The function of the fillet is to reduce the stress concentration at the leading edge of the thread ring in the ceramic. The tapered cross section of the fillet reduces the maximum stress and shifts the location forward to the tip of the fillet. The inspection of the fillet cross section revealed that the tip of the fillet near the failure site was thicker than the base.

By observing the fracture surface which intersected the fillet a cross section geometry was defined for modeling purposes.

A detailed finite element model was generated of the radome joint in the local area of the fillet. An analysis was performed to predict the effect on the ceramic stress of adhesive cure shrinkage due to 130°F post cure, thermal stress due to -30°F soak, stress concentrations due to the anomalous fillet geometry. The post cure shrinkage of the adhesive had been experimentally determined by embedded strain gage measurements of cast adhesive samples.

The effect of post cure shrinkage increases the ceramic tensile stress at the tip of the fillet by 16 percent. The effect of the geometry deviation of the fillet increases the ceramic tensile stress by a factor of 2. Figure 7 illustrates the principal tensile stress in the ceramic for a normal and defective fillet. The combined effect would cause an otherwise normal radome with an average low temperature strength of 220 percent of design load to fail at 95 percent. Therefore, the low temperature radome failure at 70 percent is not unexpected based on the failure analysis.

The cure shrinkage and coefficient of thermal expansion (CTE) for three adhesives are shown in Table 9. A comparison
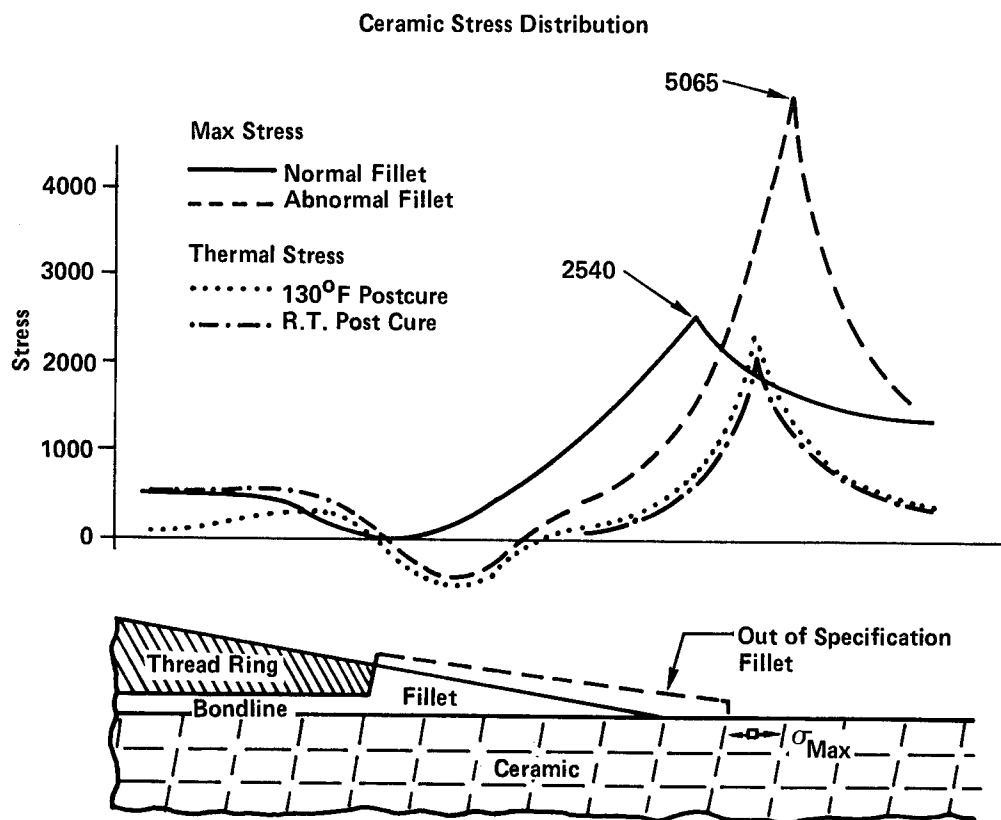
Figure 7 - Radome Joint Finite Element Analysis Results

of Magnolia 6388-3 to Hysol EA-934 indicates a 50 percent increase in cure shrinkage and an 8 percent decrease in CTE for the Magnolia adhesive. The effect of simulated high/low storage temperature on the residual strain in the adhesive was evaluated to determine if the alternate adhesive could induce greater ceramic damage than the existing production adhesive.

TABLE 9 - RADOME ALTERNATE ADHESIVE PROPERTIES

Strength (psi)	Magnolia 6388-3	Hysol XEA 9381	Hysol EA934
- at 75°F - at 350°F - at 440°F	2889 1484 599	3187 1028 601	3626 714 523
30 min. pot life strength (psi) at 350°F	1276	911	--
Room temp strength 130°F cure - 16 hrs	2416	2004	--
CTE (-30°C -60°C)	48.6	53.3	53.1
Cure shrinkage (10^{-6} in/in) (after 7-day RT cure)	-940	-1080	-580

The results of this experiment are illustrated in Figure 8. The strain gaged adhesive specimens were temperature cycled as follows: room temperature for 7 days, 130°F for sixteen hours, -50°F for two hours and back to room temperature. The strain history represents the combined effects of cure shrinkage and thermal contraction. The Hysol EA-934 has the lowest room temperature cure shrinkage but the largest post cure shrinkage. Consequently at the completion of the post cure cycle all three adhesives have approximately the same residual strain which is small. At room temperature the post cure shrinkage strains are 75 percent larger for all samples than after the room temperature cure and Magnolia has the least residual strain. Both at -50°F, and at the completion of the temperature test profile, Magnolia continues to have the least net shrinkage.

The conclusion resulting from the failure analysis and adhesive shrinkage test is that the 70 percent radome failure was caused by the improper fillet geometry and the primary adhesive candidate contributed insignificantly to the premature failure. The predicted ceramic stress is equal to the expected failing stress and therefore it was concluded that the silane did not reduce the ceramic strength. This evaluation clearly emphasizes the critical nature of the adhesive fillet and its proper processing inspection and control to insure adequate low temperature strength of the radome.
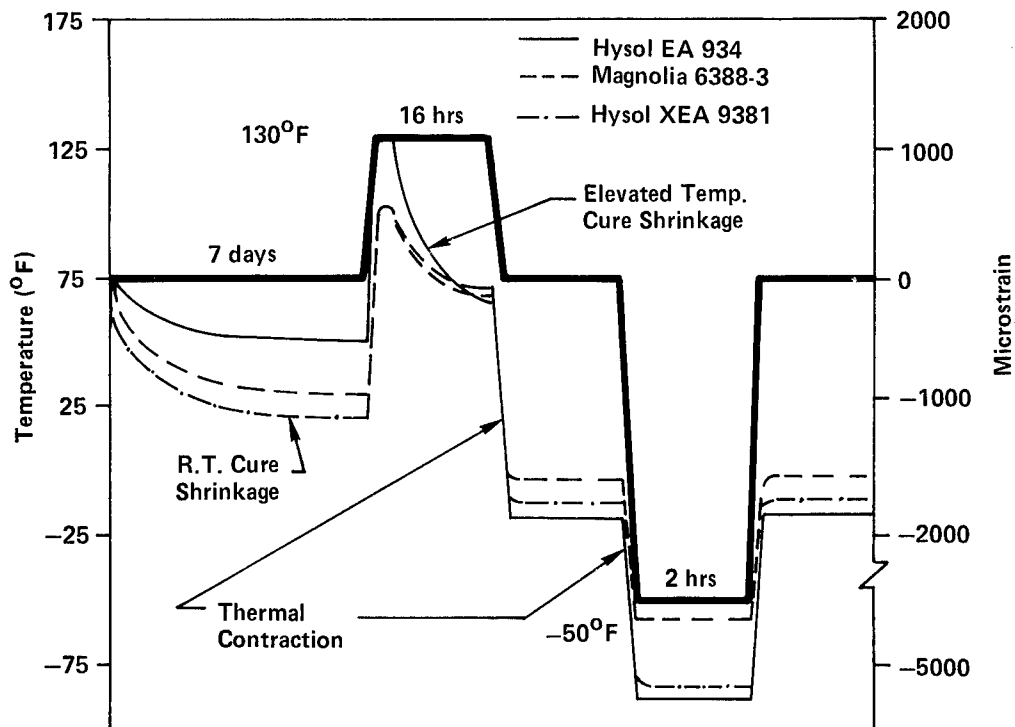
Figure 8 - Patriot Radome Alternate Bond System Adhesive Strain Response

Engineering Test and Evaluation

The purpose of the engineering test and evaluation was to provide full scale radome assembly data to insure the best selection of the final adhesive system. The test plan consisted of bonding six epoxy primed and six silane primed radomes with Magnolia 6388-3 adhesive. The bonding operation was performed in the production facility. Preliminary process sheets and inspection procedures were employed with the bonding done by production bond room person-nel under Production and Engineering supervision.

The tests were designed to evaluate the worst case conditions at the maximum bon-dline temperature possible within current Patriot mission capability and at minimum temperature under worst case pre-flight storage conditions. Figure 9 illustrates the preconditioning and thermo-structural test conditions imposed on the twelve engineer-ing test radomes. One radome of each bond system was tested to failure at each of the six conditions. As a basis of comparison,

one production radome was tested at 440°F after baseline preconditioning environments.

The shock and vibration tests were conducted to verify that no ceramic strength degradation occurs due to low temperature dynamic stress representative of transportation and free flight dynamic loads. One each of the 130°F/16 hr post cured radomes was subjected to the dynamic conditioning prior to the low temperature (-30°F) test to failure. Figure 10 summarizes the shock and vibration test conditions and results.

The accelerated aging pressure cooker test was conducted on one of each radome prior to testing to failure at 440°F. This test was conducted in a large industrial Hydroclave at Ideal Roller Co., in Marlboro, Mass. The two radomes were supported on a pallet within the Hydroclave and stored for 72 hours at 250°F/30 psia saturation condition. After 72 hours the radomes were shipped to Raytheon Spencer Laboratory and tested at 440°F. Figure 11 summarizes the pressure cooker test conditions and results. This test condition is extreme and did cause unrealistic damage to the adhesive bondline and fillet. However, the silane primed radome sustained nearly 100 percent of design load at 440°F, whereas the epoxy primed radome failed at 28 percent.

The comparison of test results between the epoxy primer and the silane primer
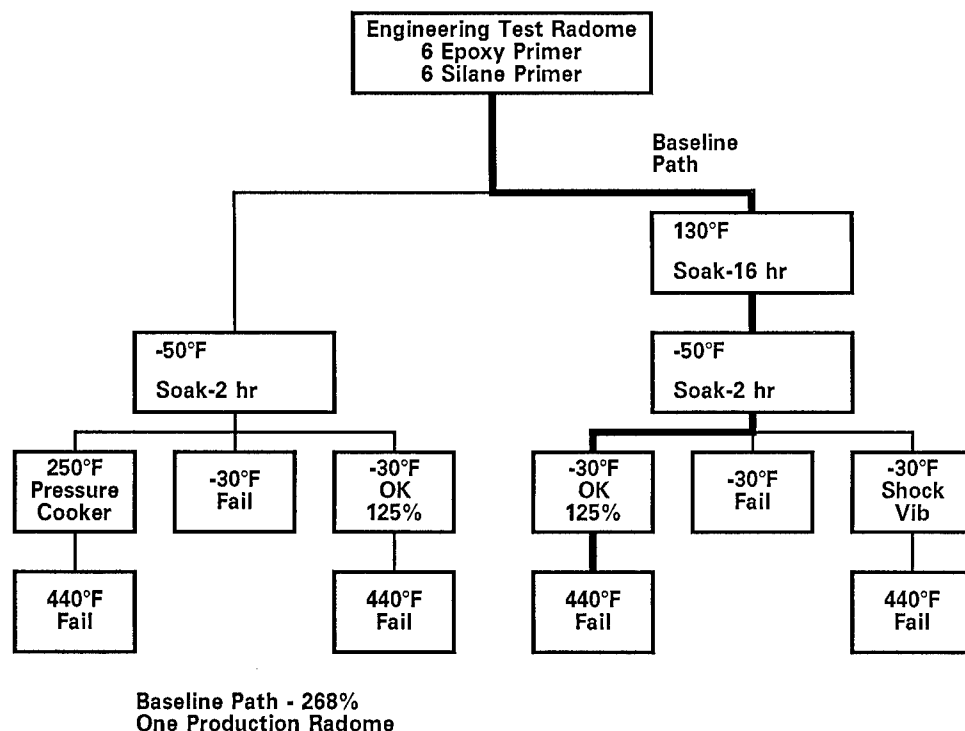
Figure 9 - Engineering Test and Evaluation Plan Alternative Bond System

Shock & Vibration Test

- Purpose
  - Verify No Ceramic Strength Degradation Due to Low Temp. Dynamic
  - Stress for Maximum Residual Stress Condition
- Dynamic Conditioning Profile
  - Shock at -30°F
    - Prelaunch - Three 20 g 11 msec 0.5 Sine
    - Flight - Three 90 g Peak SRS
  - Vibration at -30°F
    - Prelaunch - 5 g Peak Sine Sweep 5 - 500 Hz
    - Flight - Random 50 - 3000 Hz 3.8 grms - 2.5 min.
- Structural Test in Plane of Dynamic Loads
  - 125% Load at -30°F
  - 440°F Flight Condition
    - HT - 424 Failed at 241%
    - X1 - 6132 Failed at 262%

Figure 10 - Shock and Vibration Test

Aging/Pressure Cooker Test
Primer Tie Breaker

- Purpose
  - Repeat Subscale Pressure Cooker Test Conditions on Full Scale Radome
    - Relative Comparison Between HT424 & X1-6132
    - Four X1-6132 Subscales for Controls
- Full Scale Test
  - Ideal Roller Company, Marlboro, MA
  - Bonding Process Hydroclave
  - Conditions 30 PSIA< 250°F, 100: RH
  - Duration 72 Hours
- Test Results
  - Subscales – Zero Strength
  - Full Scale – Silane 3.4 Times Epoxy Strength
  - Silane 94% of 440°F Design Load

Figure 11 - Aging/Pressure Cooker Test Primer Tie Breaker

332

shows the radomes bonded with silane to have superior strength for all cases. The summary of the test results is given in Figure 12. The final selection for the alternate adhesive system is based on these results which concluded that Dow X1-6132 silane primer and Magnolia Magnobond 6388-3 adhesive is the best replacement bond system for the Patriot radome base joint.

Qualification Test Program

The structural Qualification test program is designed to demonstrate high margins of safety for the following four specific conditions:

1. The high and low temperature strength of the radome subjected to low temperature (-50°F) storage conditions followed by both high and low temperature shock and vibration environments.

2. The high and low temperature strength of the radome subjected to high temperature (130°F) and low temperature (-50°F) storage conditions followed by both high and low temperature shock and vibration environments.

3. The baseline audit test strength of the radome, 30°F soak and test to failure at 350°F, for comparison with current production.

4. The effect of rebonding with the alternate adhesive system on cur-

Patriot Radome Alternative Bond System
Engineering Radome Test Results

Test Sequence						Radome Primer			
Radome No.	130°F Soak	-50°F Soak	-30°F 125%	-30°F Fail	440°F Fail	HT-424		X1-6132	
1	X	X	X		X	189610	226%	228210	272%
2	X	X		X		316710	207%	No Failure	235%
3		X	X		X	207230	247%	222340	265%
4		X		X		347310	227%	No Failure	226%
5*	X	X	X		X	202570	241%	219600	262%
6**		X			X	23120	28%	78930	94%

* Low Temperature Shock & Vibration Preconditioning
** Hydroclave at 250°F/100% RH
    for 72 Hours – 50% RT Proof

Conclusion: Silane > Epoxy

Figure 12 - Patriot Radome Alternative Bond System Eng'g Radome Test Results

rent production, HT-424 primer, and future production,X1-6132 silane primer, radomes.

The qualification test plan is illustrated in Figure 13 and the rebond demonstration test plan is illustrated in Figure 14. The total of twenty-two radomes were tested per the plan. All of the Qualification Test Program objectives were met successfully.

Qualification Test Objectives

The objective of the Structural Qualification test was to demonstrate that the radome base joint design when fabricated to a specific process with the alternate adhesive bond system has sufficient strength to sustain with high margins-of-safety the worst case loads under pre-launch and missile flight conditions. The strength of the radome base joint is dependent on the strength of the Kevlar/epoxy thread ring, the fused silica ceramic, and the bond system. The thread ring and ceramic are the weakest elements in the joint at low temperature and in general the room temperature cured adhesive bond is the weakest element at high temperature.

The thread ring failure mode at room temperature is tearing out of the molded threads due to interlaminar shear at the aft end of the structure. This failure mode and strength is not influenced by the adhesive system used to bond the radome. Therefore
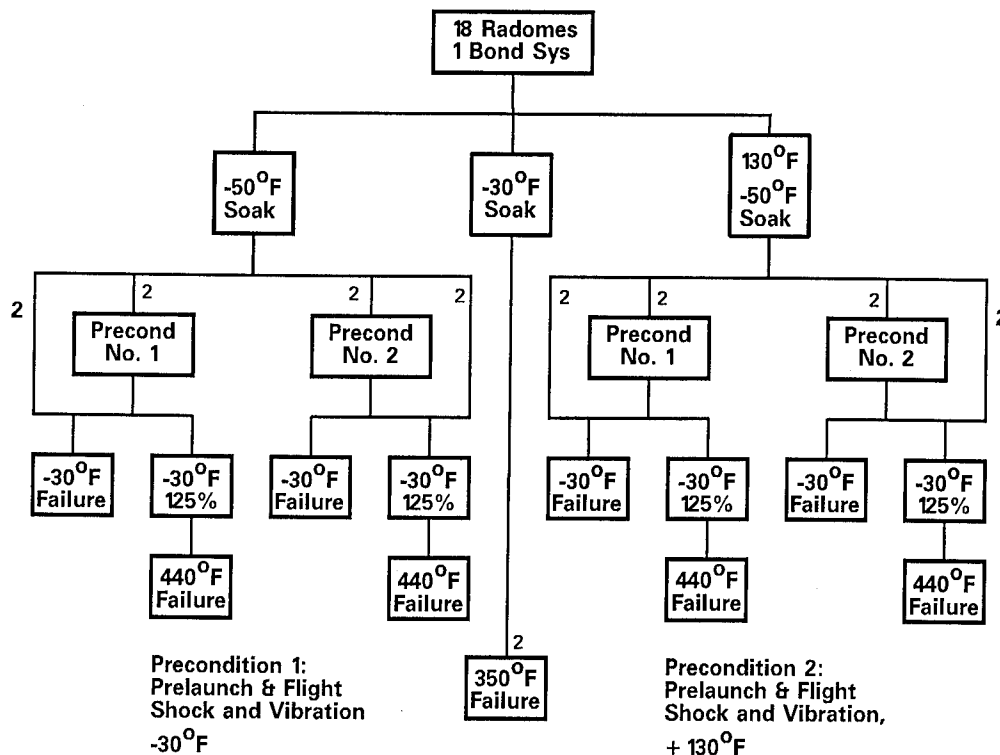
Figure 13 - Patriot Radome Alternative Bond System Qual Test Plan

Rebond Radomes

		424/Hysol	424/Mag	6132/Mag
Initial Bond	424/Hysol	N.A.	N.A.	X
	424/Mag			
	6132/Mag	N.A.	N.A.	X

• Test Plan

```
        ┌─────────────┐
        │   130°F     │
        │ Soak - 16 hr│
        └─────────────┘
               │
        ┌─────────────┐
        │   -50°F     │
        │ Soak - 2 hr │
        └─────────────┘
        2              2
  ┌─────────┐      ┌─────────┐
  │  -30°F  │      │  -30°F  │
  │ Failure │      │  125%   │
  └─────────┘      └─────────┘
                        │
                   ┌─────────┐
                   │  440°F  │
                   │ Failure │
                   └─────────┘
```
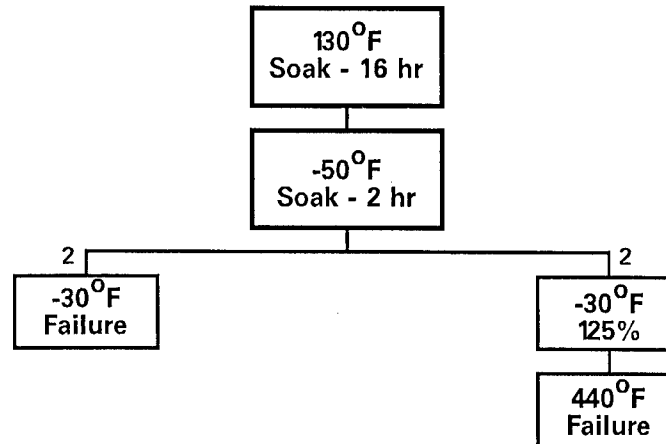
Figure 14 - Patriot Radome Alternative Bond System Rebond Demonstration

room temperature tests were not included in the Qualification Test Plan.

The low temperature failure mode of the ceramic is a tensile fracture of the radome initiating at approximately the leading edge of the thread ring. This failure mode and strength is strongly influenced by the adhesive fillet formed during the post bond beading operation as well as certain material properties of the adhesive such as cure shrinkage and coefficient of thermal expansion.

The high temperature failure mode of the bondline is a shear failure which can occur on either the tensile or compressive side of the radome, but is most common on the tensile side. The primary failure mode of

the current production audit tests at 350°F is a bondline shear failure. The Magnolia 6388-3 adhesive is nearly twice as strong as the current EA-934 adhesive at 350°F and, as such would shift the 350°F failure mode to the ceramic. Therefore, in order to adequately demonstrate the strength capability of the bondline, the high temperature tests were conducted at the 440°F maximum flight temperature. For the alternate adhesive this is the critical test condition for the bondline because the margin-of-safety for an adhesive failure is minimum at 440°F.

Qualification Test Results

The results of the qualification test program demonstrates that the radome has

more than adequate strength for the worst case high and low temperature conditions. The evaluation of the rebond processing indicates no problem in the bondline strength at high temperature or in the ceramic at low temperature. The two baseline 350°F audit test radomes failed at design margins well above the average for the current production radomes. A summary of the test results is shown in Tables 10, 11, and 12.

The average strength of ten radomes tested at the maximum bondline flight temperature (440°F) is equal to 282 percent including rebond radomes. The average strength of three radomes tested at 440°F which were not subjected to 130°F storage or 130°F shock/vibration conditions is equal to 225 percent of design load. The seven radomes subjected to the 130°F storage soak and/or the 130°F shock/vibration conditions had an average 440°F strength of 293 percent of design load. This difference in average strength is due to the effect of elevated temperature postcuring of the adhesive. The failure mode for all high temperature tests is a tensile failure of the ceramic at the forward edge of the thread ring and secondary bond separation on the compression side of the radome.

The average strength of ten radomes tested at minimum bondline flight temperature (-30°F) is equal to 232 percent of design load. The average strength of three radomes test at -30°F and not subjected to 130°F storage or 130°F shock/vibration conditions is equal to 235 percent of design load. The seven radomes subjected to 130°F soak or 130°F shock/vibration conditioning had an average -30°F strength of 231 percent. The difference in strength for these two conditions is insignificant. This is an important result because it demonstrates that post curing the adhesive does not produce substantial cure shrinkage which would adversely affect the ceramic strength after -50°F storage and at -30°F flight load conditions. The low temperature failure modes are combinations of ceramic and thread ring failures. Two radomes survived the maximum load capacity of the test apparatus without failure. Two radomes failed in the ceramic only without any indication of thread ring damage. One radome failure involved only thread ring damage. One radome failure involved only the thread ring shear out with no damage to the ceramic. Five radomes had primary failures in the thread ring and secondary failure in the ceramic.

TABLE 10 - QUALIFICATION TEST RESULTS - 440°F RADOME STRENGTHS

Radome S/N	Preconditioning Environment					Test Results				
	+130°F Soak 16 hrs	-50°F Soak 2 hrs	-30°F Shock Vib	+130°F Shock Vib	-30°F 125° Preload	Test Temp °F	Shear Load lbs	Bending Moment in/lbs	% Design Load	Comments
670075	X	X	X		X	440	14268	250260	298	Ceramic tensile failure; bond separation comp. side
670131	X	X		X	X	440	13667	239720	286	Same as above
670101	X	X			X	440	13872	243310	290	Same as above
670197	X	X	X		X	440	13604	238610	284	Same as above
670043		X			X	440	11100	194690	232	Same as above
670027		X		X	X	440	14258	250080	298	Same as above
670028		X			X	440	12652	221920	265	Same as above
670001		X			X	440	12709	223970	267	Same as above

TABLE 11 - QUALIFICATION TEST RESULTS - -30°F RADOME STRENGTHS

Radome S/N	Preconditioning Environment					Test Results				Comments
	+130°F Soak 16 hrs	-50°F Soak 2 hrs	-30°F Shock Vib	+130°F Shock Vib	-30°F 125° Preload	Test Temp °F	Shear Load lbs	Bending Moment in/lbs	% Design Load	
670110	X	X	X			-30	17416	342220	222	Ceramic tensile failure
670118	X	X		X		-30	18739	368220	235	No failure
670135	X	X				-30	16889	331870	215	Thread ring failure, secondary ceramic failure
670111	X	X				-30	18158	356800	232	Thread ring failure
670031		X	X			-30	18578	365060	237	Ceramic tensile failure
670040		X		X		-30	18187	357370	232	No failure
670020		X				-30	18724	367930	239	Thread ring failure, secondary ceramic failure
670081		X				-30	17890	351540	228	Thread ring failure, secondary ceramic failure

TABLE 12 - QUALIFICATION TEST RESULTS - REBOND/350°F RADOME STRENGTHS

Radome S/N	Preconditioning Environment					Test Results				Comments
	+130°F Soak 16 hrs	-50°F Soak 2 hrs	-30°F Shock Vib	+130°F Shock Vib	-30°F 125° Preload	Test Temp °F	Shear Load lbs	Bending Moment in/lbs	% Design Load	
670013*	X	X			X	440	15415	270380	322	Ceramic tensile failure; bond separation comp. side
670115*	X	X				-30	18807	369560	240	Thread ring failure, secondary ceramic failure
650257**	X	X			X	440	13130	230300	274	Ceramic tensile failure; bond separation comp. side
615029**	X	X				-30	18407	361700	235	Thread ring failure, secondary ceramic failure
670007						350 Audit	14868	260780	270	Ceramic tensile failure; bond separation comp. side
670103						350 Audit	14297	250770	260	Ceramic tensile failure; bond separation comp. side

* Rebond - Silane on Silane
** Rebond - Silane on HT-424

The Magnolia Plastic Inc. Magnobond 6388-3 adhesive in conjunction with Dow Corning X1-6132 silane primer provide a bond system qualified to replace the existing Hysol EA-934 adhesive and American Cyanamid HT-424 primer for Patriot radome production. The alternate bond system is superior in strength at elevated temperature and severe engineering tests under extreme temperature humidity conditions indicate substantially better durability.

NAVAL AIR DEVELOPMENT CENTER
AIR VEHICLE AND CREW SYSTEMS TECHNOLOGY DEPARTMENT
WARMINSTER, PENNSYLVANIA 18974-5000

CHARACTERIZATION OF VINYL-PHENOLIC ADHESIVE USED
IN BONDING SELF-LUBRICATING BEARING LINERS

By

Michael F. DiBerardino, Alan E. Ankeny
and Stanley R. Brown

Prepared for Presentation

at

Joint Government-Industry Symposium on
Structural Adhesive Bonding

Sponsored By

American Defense Preparedness Association

Army Armament Research, Development and Engineering Center
Dover, New Jersey

November 1987

CHARACTERIZATION OF VINYL-PHENOLIC ADHESIVE USED IN BONDING SELF-LUBRICATED BEARING LINERS

Michael F. DiBerardino, Alan E. Ankeny
and Stanley R. Brown

Naval Air Development Center
Air Vehicle and Crew Systems Technology Department
Warminster, Pennsylvania 18974-5000

ABSTRACT

A program was undertaken to evaluate and approve a new source of FE-7119 vinyl-phenolic adhesive since the manufacturer, H. B. Fuller Company, is discontinuing production of this thermosetting material. FE-7119 is used both as an adhesive and an impregnating resin for in place bonding of self-lubricating anti-friction/anti-wear liner material between the inner and outer races of bearings. These bearings have numerous applications on aircraft, helicopters and other vehicles.

This study included physical and chemical analyses, mechanical joint evaluations, and thermal analyses of both the resin and the cured adhesive material. Tests were performed on uncured samples before and after aging, and on cured adhesive as bonded and after environmental exposures.

Samples of FE-7119 from five different production lots evaluated within six months of manufacture provided test results that yielded the basis for establishing new manufacturing limits. Sample preparation methods were developed for thermal analysis and stress-strain testing of FE-7119. Even though the uncured samples were stored at $-18°C$ ($0°F$), there was a deterioration of some adhesive properties as the samples aged for six to twelve months. Preliminary tests on samples after twelve months indicate significant changes in performance, especially loss of ultimate shear and strain values

1. INTRODUCTION

Practical self-lubricating bearings were developed because of the need for bearings that function under conditions of oscillatory motion with high loads where elastohydrodynamic lubrication could not occur. The development of these bearings was made possible by of the invention of polytetrafluoroethylene

342

(Teflon). PTFE is an ideal candidate for use as a dry lubricant because it is "slippery", inert and has a low coefficient of friction. However, PTFE sheet is difficult to work with because it has low structural strength, exhibits permanent set under load and is difficult to bond to other materials. A 1957 invention overcame these problems and made practical self-lubricating bearings for use in the aircraft and automotive industries.[1] This patented concept used a fabric made of PTFE fibers combined with a second bondable reinforcing fiber to overcome the problems of PTFE sheet. A weave style was selected that produced a fabric with one side predominatly PTFE threads and the other side predominately the reinforcement threads. Using an appropriate adhesive, the structural side of the fabric is bonded to one raceway of a bearing with the PTFE side of the fabric facing the other race. Adhesive requirements for use with self-lubricating liners include: (1) structural strength to withstand compressive and shear forces developed in the bearing, (2) ability to bond to the fiber and metal surfaces, (3) resistance to degradation by water and operational fluids, and (4) ease of application during bearing production. The adhesive resin must have good flow and wetting properties since it is also the prepreg resin for the fabric.

FE-7119 is a vinyl-phenolic thermosetting adhesive used to bond anti-friction/anti-wear liner in many high performance applications. The phenolic groups provide high temperature resistance while the vinyl groups impart toughness to the liner system.[2,3] FE-7119 is superior to other adhesives in certain applications where the bearing experiences cyclicly reversing loads. In some cases FE-7119 is the only adhesive qualified for the manufacture and refurbishment of these bearings.

H. B. Fuller Company is discontinuing manufacture of this product FE-7119 adhesive. Because FE-7119 is the only adhesive used in the qualification of many bearing systems, a program was established to fully characterize the adhesive properties, establish shelf life and qualify another production source.

2. TEST PROGRAM

Five samples of FE-7119 adhesive manufactured by the H. B. Fuller Company were obtained from various sources and evaluated to determine properties and expected limits.

Mechanical joint and thermal analysis tests were conducted to fully characterize the adhesive in the as-received condition, after bonding, and after severe environmental exposures. Statistical methods were used to tabulate results and establish FE-7119

343

performance test limits for the bearing adhesive.

Viscosity measurements and Fourier Transform Infrared Spectroscopy (FTIR) analysis were performed on all five batches of the vinyl-phenolic adhesive prior to testing to insure material uniformity.

An additional study was conducted to determine effects of aging in the uncured state. Upon completion of the initial characterization, a single batch was selected and aged for testing six months beyond the recommended shelf life of the adhesive. Mechanical and thermal analysis were repeated on the aged adhesive sample. In addition, sets of mechanical and thermal analysis test specimens of the aged adhesive were exposed to a one-hour postcure at 191°C (375°F) before testing.

Lap Shear Tensile Strength: Lap shear strength of the adhesive was determined according to ASTM method D1002-72 (Test for Strength Properties of Adhesives in Shear by Tension Loading [Metal-to-Metal]). Single lap shear specimens were fabricated using 1 inch wide, 0.063 inch thick 2024-T3 bare aluminum adherends bonded with a 0.5 inch overlap. Tests were conducted at 25, 163 and -55 °C (77, 325 and -67°F).

Peel Resistance: The peel resistance of the adhesive was determined by ASTM method D3167-76 (Test for Floating Roller Peel Resistance of Adhesives). Floating roller peel

specimens were fabricated using 1 inch wide, 0.063 inch thick rigid member and 0.025 inch thick flexible member 2024-T3 bare aluminum adherends. Peel tests were conducted at 25°C (77°F) after no exposure and after 1 week at 77°C (170°F), 95% relative humidity.

Thick Adherend: As part of the aging study, thick adherend lap shear test specimens were prepared and tested. A clip-on extensometer and a computer modeling program were used to develop stress-strain curves from three separate batches of adhesive: new (as received), aged six months, and aged twelve months. Stress-strain curves were developed at 25°C (77°F) for as bonded conditions and after a one-hour postcure at 191°C (375°F).

Thermal Analysis: The dynamic mechanical analyzer, DuPont model 982 DMA, uses a freely oscillating resonant technique combining flexure, shear, tension, and compression to obtain the dynamic shear storage and loss moduli as a function of temperature. DMA test were performed on samples of adhesive after curing, after 24 hours at 163°C (325°F), after 1 week at 77°C (170°F) and 95% relative humidity, and after 24 hours immersed in MIL-H-83282 hydraulic fluid at 82°C (180°F).

DSC After Aging: In order to determine the extent of adhesive advancement during aging, differential scanning calorimetry (DSC)

measurements were made on three batches of adhesive: new (as received), aged six months, and aged one year. The corresponding heats of reaction were calculated. Calorimetric measurements were made with the DuPont model 910 DSC using a pressure cell.

Specimen Preparation:
Prior to bonding both lap shear and peel mechanical test specimens, the aluminum adherends were pretreated according to ASTM method D3933-80 (Practice for Preparation of Aluminum Surfaces for Structural Adhesive Bonding [Phosphoric Acid Anodizing]). The specimens were cured at 177°C (350°F) in a specially designed laboratory autoclave for 30 minutes with 150 pounds per square inch nitrogen atmosphere.

The thermal analysis bulk adhesive cured specimens were prepared by flashing off the solvent from the paste to form a thin film of adhesive. Several layers of the solvent free film were used to fill a 0.25 inch thick release mold. The release mold was made from a five inch square sheet of teflon with a 3 inch by 3 inch opening. The adhesive was cured at 177°C (350°F) for 30 minutes with 150 pounds per square inch nitrogen atmosphere. The 3 inch by 3 inch, 0.25 inch thick cured adhesive was cut down to appropriate DMA test specimens.

3. RESULTS AND DISCUSSION

Single lap shear results at various test temperatures are given in Table III. All five batches averaged between 4350 and 4940 pounds per square inch (psi) when tested at ambient conditions.

The mechanical test results for the characterization of the five batches were within the acceptable performance test limits. Specimen averages as well as minimum and maximum values for the five batches are given in Table I (single lap shear strength) and Table II (floating roller peel strength). On samples bonded within the six-month shelf life period the adhesive exhibited a 92 percent retention of room temperature lap shear strength when tested at −55°C (−67°F), but only a 14 percent strength retention when tested at 163°C (325°F). The floating roller peel results indicate only a 5 percent loss of the room temperature peel resistance after a short term humidity exposure. The narrow ranges of both lap shear and peel test results illustrate the uniformity among the five batches tested.
The fundamental bulk adhesive properties obtained by DMA are useful in predicting changes in adhesive properties as a result of environmental exposure.[4] In this study the adhesive glass transition temperature (Tg), shear storage modulus (G') are reported from DMA results. The Tg has been determined for the as-

received adhesive at the conditions investigated (Table III) by locating the point of downward concavity of the G' curve as a function of temperature (the intersection of the lines tangent to the G' curve). The G' shows the imposed shear energy stored and recovered by the adhesive and as such is an indication of the rigidity of the material.

Table III shows the Tg values obtained from the G' curves for the various conditions tested. As can be seen from this table, the post cured sample displays an elevated Tg over the unexposed sample as does the sample immersed in $82^{\circ}C$ ($180^{\circ}F$) hydraulic fluid. This indicates a higher useful temperature range for the adhesive after exposure to heat (it is believed that the elevated temperature and not the hydraulic fluid caused the increase in the Tg). The sample exposed to humidity conditions, however, shows a slightly decreased Tg due to the absorption of moisture into the adhesive.

The effects of aging the adhesive in the uncured state on the mechanical joint properties can be seen in Table IV for single lap shear strength and in Table V for floating roller peel resistance. The aged adhesive had a slightly increased lap shear strength over the as received material when tested at room temperature, $163^{\circ}C$ and $-55^{\circ}C$. The post cure of the aged material increased the high temperature lap shear strength by 74 percent over the aged adhesive and 150

percent over the as-received material. The post cure, however, decreased the low temperature lap shear strength of 95 percent of the unaged adhesive. The aged adhesive showed a slight decrease in peel resistance form the unaged values and a further decrease after the post cure when tested at room temperature and after short term humidity exposure. In either case the humidity exposure showed only a very slight decrease from the room temperature value.

The glass transition temperatures (Tg's) were obtained by DMA for the neat adhesive samples cured after aging in the uncured state. The Tg values after environmental exposures are shown in Table VI. The aged material exhibited a higher Tg for the as-cured, short term humidity exposure and immersion in hydraulic fluid then the unaged samples. Post curing the aged adhesive also exhibited higher Tg's for the as-cured and hydraulic fluid immersion, but showed a significant drop after short term humidity exposure. The Tg's after 24 hour exposure to $163^{\circ}C$ were very close for the as=received, aged and aged post cured. After aging six months the adhesive showed the similar behavior to the unaged adhesive; no significant loss die to humidity exposure and a slight increase after elevated immersion in hydraulic fluid. The post cured sample, however, showed a significantly lower Tg after humidity exposure

than in the as-cured state due primarily to the susceptibility to moisture absorption.

Ultimate shear strain and stress values obtained from thick adherend specimens are shown in Table VII. The effect of aging is illustrated by the formation of a more brittle, cured adhesive structure that results in decreased strain values. There is also a loss of ultimate shear stress as the material ages. Post curing the six months aged sample did increase the ultimate stress close to the values for the as-received material, but there was a reduction in strain due to the loss of toughness. The sample aged twelve months exhibited low ultimate values and duplicate specimens that were post cured failed while loading in the test grips.

In order to determine the extent of adhesive advancement during storage in the uncured state, DSC scans were performed and corresponding heats of reaction were calculated. Due to entrapped water from the vinyl-phenolic condensation reaction, it was necessary to conduct the calorimetric measurements under nitrogen pressure.[5,6] Figure 1 is a composite scan of uncured adhesive prior to, and following aging. The reported heats of reaction indicate some advancement is taking place during storage.

4. CONCLUSIONS

The following conclusions can be drawn from this program:

1) The adhesive is consistent in characteristics and properties as shown by this study using samples tested from five different production lots.

2) Extreme care must be taken during the bonding process to prevent retaining solvent or water in the bondline and neat adhesive specimens. Otherwise, test results could be invalid.

3) Acceptance values determined for quality assurance are:
a. Viscosity of 2500 +/- 500 centipoise at 25°C(77°F).
b. Single lap shear minimum tensile strengths of 3900 psi at 25°C(77°F).
c. Floating roller minimum peel strengths of 55 piw at 25°C(77°)F.
d. DMA glass transition temperature (Tg) range of 59-70°C(138-158°F) for as cured neat adhesive.
e. DMA glass transition temperature (Tg) range of 111-118°C(231-245°F) for cured neat adhesive post cured at 163°C(325°)F for 24 hours.

4) Advancement of the uncured adhesive takes place even during storage at -18°C(0°F) limiting shelf life to six months.

5. ACKNOLWEDGEMENT

The authors would like to thank G. J. Pilla and K. A. Burger for assistance in preparing and testing the mechanical and thermal analysis specimens.

6. REFERENCES

(1) White, C., U.S. Patent 2,804,886 (Sept. 3, 1957). U.S. Patent RE 24,765 (Jan. 12, 1960).

(2) Robins, J., Structural Adhesives: Chemistry and Technology, ed. S. R. Hartshorn, Plenum Press, New York (1986), pp.97-9.

(3) Minford, J. D., Durability of Structural Adhesives, ed. A. J. Kinloch, Applied Science Publishers, London (1983), pp.174-8.

(4) Pitrone, L. R. and Brown S. R., Adhesively Bonded Joints: Testing, Analysis and Design, ed. W. S. Johnson, ASTM STP (1987), To Be Published.

(5) Koutsky, J. A. and Ebewele R., Chemistry and Properties of Crosslinked Polymers, ed. S. S. Labana, Academic Press Inc., New York (1977), p.521.

(6) Levy, P. F., Nieuweboer, G. and Semanski, L. C., Thermochin. Acta, 1, (1970), pp.429-39.

TABLE I
Single Lap Shear Strength for Five Batch Characterizations

Test Temperature	Average (psi)*	Minimum (psi)**	Maximum (psi)**
-25°C (77°F)	4750	4355	4940
163°C (325°F)	640	580	680
-55°C (-67°F)	4495	4295	4670

* Average of all batches
** Minimum and maximum batch averages

TABLE II
Floating Roller Peel Strength for Five Batch
Characterizations

Test Temperature	Average (piw)*	Minimum (piw)**	Maximum (piw)**
25°C (77°F)	67.0	63.7	70.6
25°C (77°F) 1 week at 170°F /95% RH	63.4	59.5	67.8

* Average of all batches
** Minimum and maximum batch averages

TABLE III
DMA Glass Transition Temperatures Obtained
for Five Batch Characterizations

Exposure Conditions	Average Tg*	Minimum Tg**	Maximum Tg**
As Cured	63°C	59°C	70°C
24 hrs @ 325°F	113°C	111°C	115°C
1week @ 170°F 95% RH	61°C	58°C	65°C
24 hrs @ 180°F MIL-H-83282 Hydraulic Fluid	81°C	75°C	85°C

* Average for all batches
** Minimum and maximum batch values

TABLE IV
Single Lap Shear Strength Before and After Aging

Test Temperature	Cured as Received (psi)	Cured After 6 Months (psi)	Cured and Post Cured After 6 Months (psi)*
25°C (71°F)	4750	5290	5345
163°C (325°F)	640	930	1615
-55°C (-67°F)	4495	5215	4230

* Post cured 1 hr @ 375°F

TABLE V
Floating Roller Peel Strength Before and After Aging

Test Temperature	Cured as Received (piw)	Cured After 6 Months (piw)	Cured and Post Cured After 6 Months (piw)*
25°C (77°F)	67	64	47
25°C (77°F) After 1 week @ 170°F 95%RH	63	50	45

* Post cured 1 hr @ 375°F

TABLE VI
DMA Glass Transition Temperatures Before
and After Aging

Exposure Conditions	Cured as Received (Tg)	Cured After 6 Months (Tg)	Cured and Post Cured After 6 Months* (Tg)
No exposure	63°C	85°C	109°C
After 24 hrs @ 325°F	113°C	119°C	118°C
After 1 wk @ 170°F/95% RH	61°C	87°C	78°C
After 24 hrs @ at 180°F in MIL-H-83282 Hydraulic Fluid	81°C	100°C	110°C

* Post cured 1 hr @ 375°F

TABLE VII
Thick Adherend Lap Shear Stress-Strain
Results Before and After Aging

Condition	Ultimate Shear Strain in./in	Ultimate Shear Stress (psi)
As Received	1.13	7110
As Received and Post Cured*	.56	7850
After 6 Months Storage	.90	5923
After 6 Months Storage and Post Cured*	.69	7270
After 12 Months Storage	.73	3170
After 12 Months Storage and Post Cured	**	**

* Post cured 1 hr @ 375°F
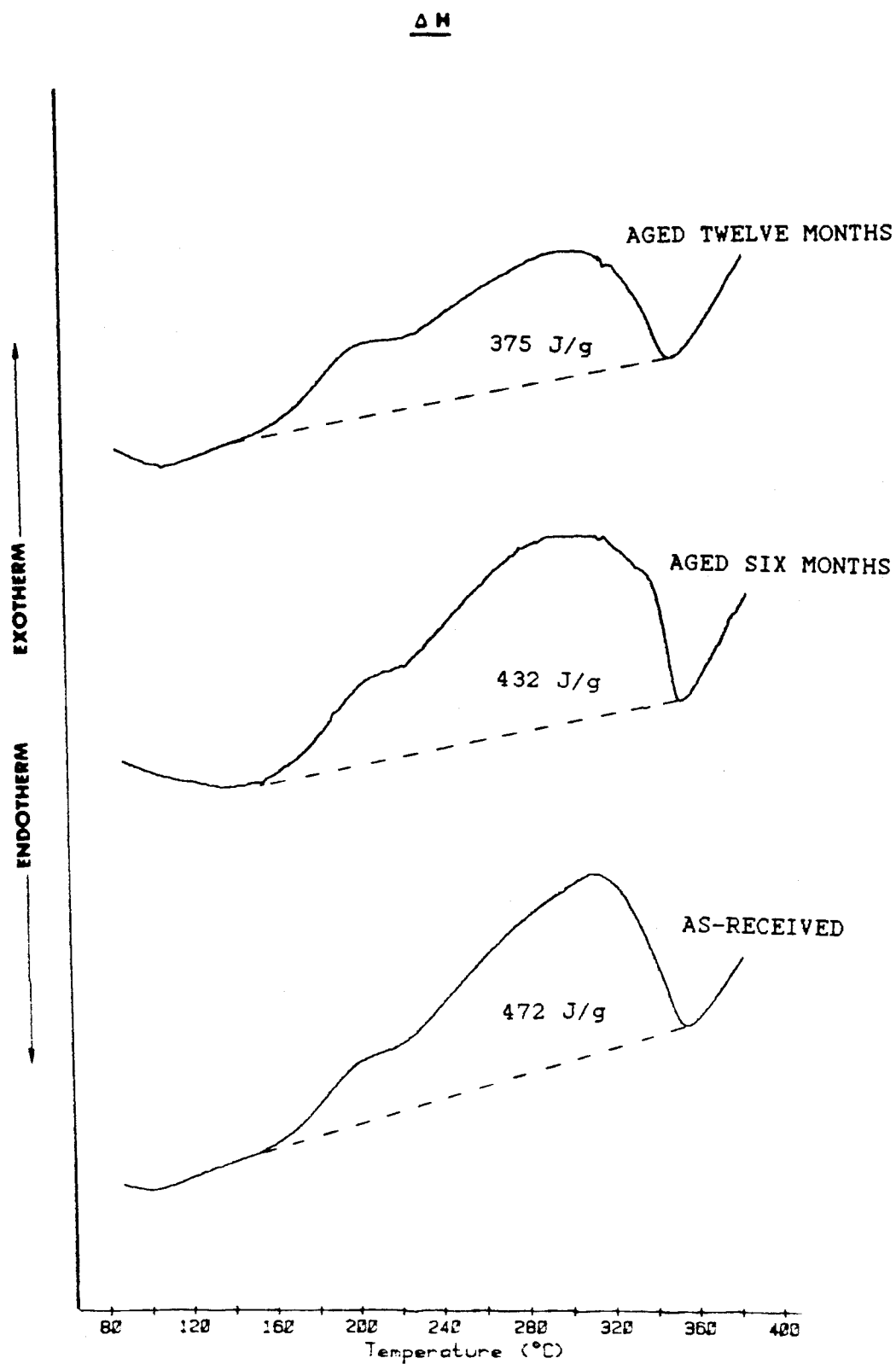** Specimens failed on loading

Figure 1. FE-7119 adhesive PDSC scans before and after aging in the uncured state.

Durability of Adhesive Bonding to Steel and Copper

James P. Bell and
Randall G. Schmidt
Polymer Science Program
Institute of Materials Science
U-136
University of Connecticut
Storrs, CT 06268

Introduction

Adhesives and primers in general do not form covalent chemical bonds with metal surfaces, but most often form hydrogen bonds with the surface metal oxide. These hydrogen bonds are ultimately broken by moisture which diffuses from the surrounding air, with larger surface areas requiring longer time to debond than small areas. Retardation of moisture diffusion to the interface of course helps, but only by delaying the debonding. The durability problem is particularly great when the bond experiences stress.

Incomplete and non-reproducible cure are additional, separate, problems of room temperature cure systems.

There is no magic chemical coupling agent that forms chemical bonds to all substrates. Silane coupling agents, when properly applied, provide very effective bonds to glass. As one would expect from their structure, they are less effective with metals.

We have developed a polymeric coupling agent system which chemically bonds to iron and copper oxides as well as to epoxy type adhesives. Resulting bonds retain most of their strength after long exposure to hot or boiling water. Normal systems debond completely in a few hours. The coupling agent is applied to the metal surface before application of the adhesive.

Proper wetting of the surface by the adhesive and proper hydrophobicity and hydryolysis resistance are of course also very important. Mechanical interlocking is much less important except when special etching treatments are used, as with aluminum (1). A more detailed discussion of these effects in relation to steel can be found elsewhere (1).

Results and Discussion

1. Coupling agents

After consideration of several types of bonding reactions to steel and copper, two types were investigated more extensively. The first type consists of multifunctional mercapto esters such as hexanetriol trithioglycolate (HTTHG) and pentaerithrytol mecaptopropionate* (PETMP) these compounds, shown below, have the capability to bond to steel, copper, and epoxy resins.
They must be present in a very thin ' layer however, since multiple layers of the low molecular weight compounds are mechanically weak. Also, there is a relatively high concentration of polar groups, making the coupling agent rather hydrophilic.

The second type of coupling agents, shown in Fig. 2., involves attaching functional groups, such as mercapto esters, onto a less polar,

*Purchased from Evans Chemetics Co.

354

relatively strong polymer backbone. This results in a less hydrophilic, stronger coupling agent region.

2. Joint strength results.

The torsional shear strength method used in our earlier studies (2-4) was also used in this work. The adhesive bond is tested in pure shear; the method gives far better reproducibility than lap shear and similar methods, and is much easier to interpret.

The durability in 57°C water of joints containing 10 mil thick Epon 828-methylene dianiline adhesive are shown in figure 3. Exact preparation conditions are described elsewhere (3). The prior metal treatment resulted in significantly improved durability.

3. Peel Strength Tests

Peel tests of treated and untreated raw copper foil show similar results (Table 1). When the control sample was exposed to boiling water, the peel strength became too low to measure.

Peel strength tests on thinly coated HTTHG treated steel gave negligible improvement relative to control samples. We believe this was because of the rapid diffusion of water perpendicular to the coating that occurs in the peel samples. Results with steel and polymeric coupling agents are given in Table 2. The different EME contents represent different weight percentages of mercapto ester groups along the polyethylene backbone. One observes that, prior to water exposure, the greatest concentration of mercaptoester groups gives the greatest peel strength, far superior to the controls. Upon exposure to 57°C water, the strength of all samples decreases dramatically. We have shown elsewhere (5) that this is because of loss of the epoxy properties in water, not because of the coupling agent. The numbers in parentheses are peel strengths that were obtained when the samples were redried.

The last column in the table is indicative of the relative rates of corrosion of the samples. It represents the time in hours for an average of three visible pits to form under the coating. In this instance an optimum value is found somewhere in the vicinity of 23 weight percent mercaptoester groups. Apparently at higher mercaptoester concentrations the increased polarity and hydrophilicity associated with the ME groups facilitates transport of water, O_2 and ionic species to the interface, causing corrosion to occur, even though bonding to the metal remains relatively strong. The optimum coupling agent mercaptoester concentration for peel strength improvement is thus different from the optimum for corrosion resistance.

In conclusion, the mercaptoester family of coupling agents shows promise for greatly improving the durability of epoxy-steel and epoxy-copper joints and coatings, although much work remains to be done.

References

1. Schmidt, R. G. and J. P. Bell, Epoxy Adhesion to Metals, Chapter Two in Epoxy Resins and Composites II, Vol. 75, in Advances in Polymer Science Series, K. Dusek, Ed. Springer-Verlag, Berlin. Review Paper.

2. Bell, J. P. and W. T. McCarvill, Torsional test method for adhesive joints, J. Adhesion, 6 (3), 185.

3. DeNicola, A. and J. P. Bell, Polyfunctional chelating agents for bonding of epoxy resins to steel, Chapter 6 in Epoxy Resins, R. Bauer, Ed., ACS Advances in Chemistry Series Vol. 221, American Chemical Society, Washington, DC, 1983.

4. Park, J. and J. P. Bell, Epoxy adhesion to copper, Part II. Electrochemical Pretreatment. Adhesive Joints, K. Mittal, Ed., Plenum Press, New York, pp. 523-541.

5. R. G. Schmidt and J. P. Bell, Investigation of Steel-/Epoxy Wet Adhesion Durability Using Polymeric Coupling Agents, Proceedings of the ACS Division of Polymeric Materials: Science and Engineering 56, 309, 1987.

Pentaerithritol tetramercaptopropionate(PETMP)

Fig. 1b HTTHG and PETMP structures

Hexanetriol trithioglycolate(HTTHG)

Fig. 1 HTTHG and PETMP structures
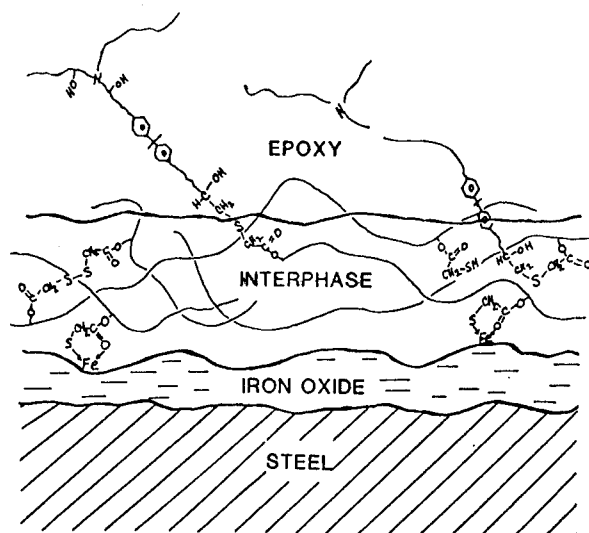
Fig. 2 Schematic of interface showing polymer structure
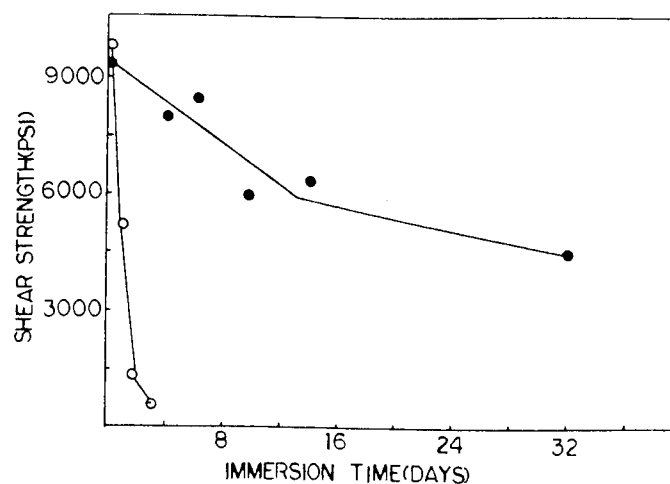
Figure 3 Effect of HTTHG treatment on bond durability (57°C) of methylene dianiline cured adhesive joints: (O) HTTHG, (•) Control.

Table 1. 180° Peel Tests with Untreated Raw Copper Foil

Treatment	Peel Strength, lbs/in	Standard Deviation, lbs/in
Control	3.42	0.18
Control after 24 hrs in 100°C water	very low	---
5-aminobenzotriagole (5ABTA) treatment followed by NaOH wash	6.49	0.67
5ABTA treatment followed by NaOH wash after 24 hrs in 100°C water	3.80	0.36

5ABTA treatment: 10 min. in a 1×10^{-3} m Aq 5ABTA soln. at room temperature, NaOH wash: dipped in a 0.1% Aq. NaOH solution for one minute.

WET AND (REDRIED)* 90 PEEL STRENGTHS (G/IN) FOLLOWING SPECIFIED 57C WATER IMMERSION

TREATMENT	PEEL STRENGTH (G/IN) IMMERSION TIME (HRS 57C WATER)					CORROSION PROTECTION (HRS)
	0	1	5	11	24	
CONTROL	78	69 (57)	9 (24)	4 (16)	2 (5)	14
EME 23	47	26 (40)	11 (26)	10 (23)	9 (19)	46
EME 47	284	139 (196)	36 (71)	16 (57)	13 (44)	32
EME 90	729	319 (543)	24 (187)	16 (66)	11 (30)	20

*SAMPLES DRIED 1 HR UNDER VACUUM AT 50C

TABLE 2

THERMAL ANALYTICAL TECHNIQUES FOR THE DETERMINATION OF STRUCTURAL ADHESIVE CURE STATE AND BONDED JOINT PERFORMANCE

Larry R. Pitrone
Naval Air Development Center
Air Vehicle and Crew Systems Technology Department
Warminster, Pennsylvania 18974-5000

ABSTRACT

Premature structural adhesive failure of a propeller blade trailing edge joint required the cure state of the failed adhesive be determined to confirm that complete cure had been achieved upon repair. Only a small fillet was available for this evaluation. DSC was the selected method of analysis. It successfully determined that the adhesive was completely cured yet had realized the consequences of aging which were more effectively elucidated by DMA.

Effects of the bonding process on the molecular structure of a modified epoxy adhesive and the resultant interfacial quality of the bonded joint were successfully established by DMA, using small-scale laminate joints. Tan δ served to trace changes in the adhesive and the subtle interfacial alterations resulting from application of various organofunctional silane primers. Interfacial adhesion quality as determined by DMA correlated with floating roller peel mechanical test results.

1. INTRODUCTION

The proper cure state of adhesives employed in aerospace structural joining is paramount to successful performance. The present capability of sophisticated thermal analytical techniques to determine cure state enables confirmation that appropriate cure has been realized. It also permits the resolution of associated cure schedules for advanced developmental adhesives such that projected performance gains may be achieved. Differential Scanning Calorimetry (DSC) was the technique employed in this adhesive failure analysis study to determine if complete cure was the cause of a propeller blade trailing edge debond, realized during aircraft service.

The propeller blade trailing edge bonded joint

in question realized premature fracture which necessitated repair. Several factors of the repair procedure were analyzed to determine the cause of failure. Proper cure state prior to deployment was the consideration of this investigation. A very small adhesive fillet was all the failed material available for this study. Consequently, DSC was selected for this analysis as it requires a minimal amount of material, can be conducted rapidly, traces cure advancement, and reveals other important polymer properties, e.g. T_g.

Successful performance of a structural bonded joint strongly depends upon the specific adhesive properties within that bonded configuration and the adhesive-adherend interfacial characteristics[1,2,3,4]. It is well documented that both the incorporation of a rigid filler within a polymer matrix and the filler-polymer adhesion play crucial roles in the performance properties of filled polymers and organic matrix composites[5]. As a result of the similarity of adhesive joints to these systems, comparable phenomena effecting performance should be expected, e.g. adhesion of adherend to adhesive and alteration of adhesive polymer network as a result of adhesion. In the past, dynamic mechanical methods have successfully elucidated these phenomena in filled polymers and composites[5,6].

The viscoelastic nature of both the adhesive and interface encourage the application of Dynamic Mechanical Analysis (DMA) to characterize the effects of bonding on the adhesive and the interfacial adhesion quality resulting from various adherend pretreatments. In this study, DMA was conducted on neat adhesive and bonded aluminum laminates, before and after hygrothermal exposure. The objective was to ascertain effects of bonding on the adhesive molecular structure through evaluating primary and secondary transitions by Tan δ peaks and transition temperatures.

Organofunctional silanes have been evaluated as metal adherend prebond primers in an attempt to maintain joint adhesion in aggressive environments of heat and humidity[7,8,9]. Solution pH of silane primers has been observed to effect joint durability performance[10]. The interfacial adhesion quality resulting from the application of these primers at two pH levels in a bonded laminate was another objective to be determined by DMA. Subtle differences in surface characteristics were detected and correlated with mechanical performance by the Floating Roller Peel (FRP) test.

360

2. EXPERIMENTAL PROCEDURE

2.1 ADHESIVE CURE STATE EVALUATION

The structural adhesive film employed in fabricating the propeller blade trailing edge joint is 3M Co. AF-111; a 121°C (250°F) cure system subjected to 15 psi during the one hour cure cycle of bond formation. The adhesive is supported with a random mat scrim and is based on an epichlorohydrin/ bisphenol-A epoxy resin cured with dicyandiamide and modified with nitrile latex.

As a result of the failure mode, a 20 mg adhesive fillet represented the entire amount of AF-111 available for cure state evaluation. Three DSC specimens of 4 mg each were carefully prepared from the failed sample. In order to determine whether the adhesive had realized a complete cure, neat AF-111 samples were prepared in the laboratory at various cure temperatures (uncured, 93°C (200°F), 107°C (225°F), and 121°C (250°F)) such that a spectrum of DSC traces could be obtained to "fingerprint" the AF-111 cure advancement. These DSC specimens were cut from castings of adhesive prepared in a release mold and cured in a small-scale laboratory autoclave. DSC was conducted using a DuPont 910 Differential Scanning Calorimeter with associated 1090 thermal analyzer/controller at a heat-up rate of 10°C (18°F)/min from room temperature to 210°C (410°F).

Diffuse Reflectance Infrared Fourier Transform Spectroscopy (DRIFT) was conducted to augment the DSC spectrum on the remaining 8 mg sample received from the failed joint, as well as on 20 mg laboratory samples cured at 121°C (250°F) and 93°C (200°F) respectively. As the name implies, DRIFT spectra result from the detection of weak, diffusely reflected radiation from the sample, now attainable in the mid-infrared region by the advent of FTIR[11].

2.2 BONDED JOINT ADHESIVE AND INTERFACIAL PROPERTY EVALUATION

The adhesive selected for this study, 3M Co. AF-163-2K, is an aerospace structural film which is supported on a nylon knit carrier. The adhesive formulation incorporates both brominated and bisphenol-A based epoxy resins for moisture resistance and a rubber modifier for increased toughness. Two cure cycles of one hour at 45 psi and 121°C (250°F) and 177°C (350°F) respectively were effected in preparing both neat and bonded test specimens. Adherends of selected joints were primed prior to bonding with either one of two organofunctional silane solutions or an epoxy phenolic primer (American Cyanamid Co. BR-127). The organofunctional silane used was a τ-amino-propyltriethoxy silane

(Union Carbide A-1100) applied to the adherends by immersion as a 1% solution at a pH of 10 and 4, obtained by addition of hydrochloric acid.

Neat adhesive DMA specimens were cut to size (50.8 mm (2.0") x 6.4 mm (0.25") x 1.9 mm (0.075")) from larger castings after realizing appropriate cure cycles in the small-sale laboratory autoclave (Figure 1). Bonded laminates were prepared for DMA (50.8 mm (2.0") x 5.1 mm (0.2") x 3.5 mm (0.135")) from laminate overlap shear specimens (ASTM D-3165) of 2024-T3 bare aluminum, phosphoric acid anodized (PAA) and primed with BR-127 prior to bonding (Figure 1). Small-scale overlap shear joints comparable in size to the DMA laminates (Figure 1) were also prepared from ASTM D-3165 specimens. These were mechanically tested to failure along with their full-scale counterparts as confirmation that they were representative of the full-scale joints, i.e. inherent material impurities or processing flaws did not dominate the characteristic joint performance as a result of specimen size reduction. Single adherend DMA laminate adhesive specimens (50.8 mm (2.0") x 5.1 mm (0.2") x 1.9 mm (0.075")) were fabricated by selective removal of one adherend from the standard DMA laminates (Figure 1).

As a means of elucidating silane primer effectiveness, FRP tests (ASTM D-3167) were conducted on PAA, 2024-T3 bare aluminum prepared without primer and with two A-1100 silane solutions, pH 10 and 4 respectively. DMA was also conducted on selected small-scale laminates prepared from these FRP specimens (Figure 1).

Prior to DMA, selected neat and bonded laminates were exposed to 82°C (180°F) and 100% R.H. for 2 weeks to evaluate hygrothermal effects on the adhesive and interface respectively.

DMA was conducted using a DuPont 982 Dynamic Mechanical Analyzer with associated 1090 thermal analyzer/ controller over the temperature range -100°C (-148°F) to 230°C (446°F) at a heat-up rate of 5°C (9°F)/min.

3. RESULTS AND DISCUSSION

3.1 ADHESIVE CURE STATE DETERMINATION

Among other approaches, the adhesive cure state can be characterized in two different ways[12]:

(1) By measuring a transition temperature such as a glass rubber transition (T_g).

(2) By measuring the residual heat of reaction in the sample.

Calorimetric techniques enable DSC to detect both polymer molecular transitions, i.e. T_g, and heat of reaction. Thus, DSC traces of AF-111 specimens after exposure to

362

various cure temperatures were produced to characterize the cure advancement (Figure 2). The exotherm of the fresh adhesive is 523 Jg^{-1} in comparison to a complete cure of 121°C (250°F) in which the exotherm has vanished and the T_g at 113°C (232°F) is indicated by the change in baseline. The sample cured at 93°C (200°F) demonstrated an exotherm of 93 Jg^{-1} preceded by a small endotherm corresponding to melting of the adhesive. As the cure proceeds, indicated by DSC at higher cure temperatures, the exotherm disappears and the endotherm diminishes in size revealing the primary transition at the T_g, the position of which as obtained by DSC is independent of specimen size. Upon analysis of the failed AF-111 adhesive (Figure 2), the absence of an exotherm indicated complete cure had been realized. Yet, the definitiveness of the primary transition was absent, and it was shifted to a lower temperature (105°C (215°F)) in comparison to the fully cured sample prepared in the laboratory. As a result, a specimen from the laboratory sample was allowed to age for six months in the laboratory environment and then tested by DSC. The trace as shown in Figure 2 is similar to that of the failed AF-111, i.e. decreased Tg and diminished transition definitiveness. To further elucidate the effects of aging, DMA was conducted on neat, laboratory aged AF-

111. The results of this analysis are shown in Figure 3; reduction of T_g, increased tensile storage and loss moduli (E', E''), and increased transition region breadth are revealed by the aged material. These changes are indicative of moisture ingression and the general process of chemical crosslinking that network polymers manifest upon aging[13,14]. Note the T_g differences indicated by DMA and DSC. This is due to the time dependency of the glass-rubber transition which effects these test methods differently[15,16].

DSC analysis was augmented by DRIFT to assure complete cure advancement of the failed AF-111 adhesive. DRIFT spectra were obtained from the failed adhesive as well as laboratory prepared and aged specimens (Figure 4), after complete and partial cures of 121°C (250°F) and 93°C (200°F) respectively. As a consequence of varied sample sizes, cure advancement was determined by obtaining the baseline-peak height ratios of epoxy ring to aromatic ether spectral lines. Table 1 lists these ratios for each cure condition analyzed and clearly indicates the complete cure of the failed adhesive by the close proximity of ratios of fully cured and failed adhesive, 0.77 and 0.82 respectively. Although DRIFT is not able to reveal essential material performance characteristics as thermal analysis, i.e. T_g, moisture plasticization, and

363

modulus, it successfully verified the failed adhesive cure state.

Established by analytical support from DRIFT and DMA of cure advancement and aging effects respectively, DSC has independently and successfully confirmed the failed AF-111 as having realized complete cure, with a minimal amount of material. This eliminated incomplete cure as a primary cause of joint failure. It has also enabled the detection of aging effects and the resulting impact on adhesive performance.

3.2 ADHESIVE AND INTERFACIAL CHARACTERISTICS WITHIN A BONDED JOINT

As an effective technique for quantifying polymer viscoelastic properties, DMA is extremely sensitive to subtle second order epoxy transitions, second phase rubber T_g in modified epoxies, and interfacial adhesion quality[17,18,19,20]. It thus provides a powerful tool in analyzing the characteristics of the modified epoxy adhesive AF-163-2K within a structural bonded joint and the associated integrity of interfacial adhesion following various adherend prebond treatments.

Prior to conducting DMA of small-scale bonded laminates (Figure 1), mechanical tests were performed on laminate joints for tensile shear strength (ASTM D-3165) and their small-scale counterparts (Figure 1)

comparable in size to the DMA specimens. This served as a basic evaluation of small-scale joint performance. Table 2 lists the room temperature laminate tensile shear strengths for all specimen sizes. The comparable strengths resulting for full- and small-scale joints serves as a basic indicator that inherent processing flaws and adhesive impurities did not adversely effect performance as a result of size reduction. Thus, the DMA laminates secured from the same large panels as the full-and small-scale joints tested appear to be representative of adhesive and interfacial properties within a structural bond.

DMA was initially conducted on neat AF-163-2K cured at 121°C (250°F) and 177°C (350°F) both before and after hygrothermal exposure (Figures 5 and 6) in order to establish fundamental adhesive properties in a non-bonded configuration. Table 3 indicates the transition temperatures, as determined by location of Tan δ peaks, and associated Tan δ peak values. Tan δ is defined as the ratio between the energy loss, due to molecular motion and phase transition, and the maximum energy stored in the material upon oscillation[21]. The anomalous behavior of AF-163-2K cured at 121°C (250°F) in comparison to 177°C (350°F), as demonstrated by the higher T_g and lower Tan $δ_{Tg}$ values, indicates the dependency of molecular network formation on the

cure schedule. The higher T_{mec} and lower Tan δ_{mec} of 177°C (350°F) cure versus 121°C (250°F) indicate that the rubber phase may be more tightly bound to the matrix as a result of the elevated cure temperature[18]. This secondary AF-163-2K peak revealed in Figures 5 and 6 is predominantly assigned to the rubber phase T_g and dominates the epoxy β peak otherwise expected in the same low temperature region[22].

After equilibrium moisture absorption was obtained during hygrothermal exposure, the T_g values of specimens cured at both high and low temperatures were essentially equal, as were Tan δ_{Tg} and Tan δ_{mec} values (Table 3). T_{mec} values were the exception, with the elevated cure demonstrating a higher value as was the case prior to exposure. A Tan δ transition specifically related to moisture, Tan δ_{H2O}, appeared after cure at 121°C (250°F) and exposure (Figure 5). This is not present in the exposed neat elevated cure AF-163-2K (Figure 6). The low temperature cure also realized an increase in weight over the elevated cure by 43% due to moisture ingression, which parallels the emergence of Tan δ_{H2O}, and indicates the dependency of molecular network formation on cure schedule. These results parallel those obtained with other epoxy systems[23,24]. Comparison of neat adhesive properties before and after exposure following both cure

temperatures (Table 3) indicate decreased T_g and Tan δ_{Tg} due to plasticization and the deleterious effects of heat and moisture in combination.

DMA was also conducted on bonded laminate and single adherend specimens cured at 121°C (250°F) and 177°C (350°F) (Figures 7 and 8), both before and after hygrothermal exposure, in order to determine the effects on the adhesive of curing within bondline constraints and of interfacial adhesion. Table 4 specifies the transition temperatures and associated Tan δ peak values of bonded and single adherend DMA laminates. Trends in T_g, Tan δ_{Tg}, T_{mec}, and Tan δ_{mec} for the various cure and exposure conditions of bonded laminates and single adherends were similar to the neat adhesive as expected. The exceptions were Tan δ_{Tg} of the low temperature cure after exposure, which was less than that of the elevated cure, T_{mec} of both cure temperatures after exposure which was greater than that prior to exposure, and Tan δ_{mec} which was greater prior to exposure than after for the 121°C (250°F) condition.

In demonstrating the effect on fundamental adhesive properties as a result of curing within a bonded laminate configuration and in elucidating interfacial adhesion characteristics, DMA of neat adhesive, bonded laminate, and single adherend proved

advantageous. Evaluation of Figures 5, 6, 7, and 8 and Tables 3 and 4 indicate the T_g of the bonded laminate in all cases is greater than the single adherend, which in turn is greater than the neat adhesive. Similar trends have been reported with filled polymer systems indicating the T_g to be a measure of the change in polymer matrix properties due to addition of a rigid second phase (filler), this phenomenon being independent of mechanical reinforcement by the filler[25,26]. Such increases in T_g have been attributed to filler surface area effects, restriction of polymer molecular motion, packing density changes of polymer chains, and modification of conformation and orientation of polymer chain segments as a result of strong interfacial filler-polymer adhesion.[27,28]. With respect to a strongly bonded laminate configuration, similar phenomena should result at the adherend-adhesive interface. This was in fact indicated by the T_g trends noted above. In other studies, Ultrasonic Rayleigh Wave measurements conducted on aluminum adherend-epoxy adhesive laminates[29] revealed a shear modulus gradient through the bondline region of the adhesive, higher near the interface for certain adherend prebond treatments. This correlates with the observed increase in T_g due to laminate bonding and indicates the altering of adhesive properties near the interface by strong interfacial adhesion. The Tan δ_{Tg} peak values also demonstrate the effects of adhesion as the neat adhesive Tan δ_{Tg} was greater than that of the laminate, which was greater than the single adherend. This illustrates the restriction of damping enforced by bonding and also the capability of the interface to dissipate inputted mechanical energy. These results also demonstrate that the rubber phase transition is made considerably broad and shifted to higher temperatures as a result of the bonding process, perhaps reflecting altered adhesion with the matrix as a consequence of polymer matrix alteration by virtue of bonding with the adherend[18,25]. As was illustrated with Tan δ_{Tg}, a similar trend follows with Tan δ_{sec}. Thus, the process of bonding/adhesion is seen to effect both the polymer matrix structure and the rubber-matrix adhesion.

Various primer pre-treatments were applied with the intent of altering the adhesive-adherend interface for correlation of mechanical analysis with Tan δ interfacial adhesion characterization. FRP specimens, from which DMA specimens were secured (Figure 1), were prepared both unprimed and with a τ-aminopropyltriethoxy silane (A-1100) solution applied at pH 10 and 4 respectively. Peel strengths, Tan δ peak values, and corresponding

transition temperatures are listed for each prebond treatment in Table 5. Specimens prepared with A-1100 solution at pH 4 yielded an average peel strength similar to that obtained when no primer was applied. In both cases, failure modes were cohesive as shown in Figure 9. The A-1100 prebond treatment applied at pH 10 resulted in lower peel strengths and exhibited an adhesive failure mode (Figure 9). Corresponding Tan δ_{Tg} traces obtained from DMA laminates of FRP specimens revealed a higher Tan δ_{Tg} value for the A-1100 pH 10 pretreatment as compared with the other pretreatments. Thus, an inverse correlation was exhibited between Tan δ_{Tg} and peel strengths for the various prebond primer treatments. Viewing the interface as viscoelastic in nature[20], this indicates the A-1100 pH 10 pretreatment absorbed more inputted energy, because the primer is the only variable in this comparative study. Thus, a structurally weaker interface is indicated as was well demonstrated by the respective peel strengths. Similar phenomena have been reported for adhesion of a glass fiber reinforced polyester composite in which Tan δ, as a measure of interfacial adhesion quality, was correlated with interfacial shear strength after treatment of the glass reinforcement with various primers[20]. Glass transition temperatures also reflect the varied interfacial quality of the bonded laminates. The T_g of unprimed laminates was greater than those pretreated with A-1100 at pH 4 and 10, both of which were similar. Analogous T_g trends have also been observed with treated fillers in polymer matrices[25].

4. CONCLUSIONS

DSC has successfully determined the cure state of a structural adhesive obtained from an in-service joint failure and effectively distinguished the results of aging on this adhesive. DMA of fully cured laboratory aged adhesive of the type failed served to augment the DSC study and confirm moisture plasticization and molecular structural effects on the adhesive polymer. The cure state was also validated by conducting DRIFT on the failed adhesive as well as laboratory prepared fully and partially cured specimens.

DMA of bonded and single adherend laminates permitted exclusive elucidation of effects on the adhesive resulting from cure within a bonded joint and interfacial adhesion quality within a bonded configuration. Tan δ comparisons of neat adhesive and bonded laminates revealed that adhesive polymer matrix and rubber-matrix adhesion of the rubber modified epoxy adhesive were effected by the bonding procedure. The T_g was also shifted to

elevated temperatures as a result of subjecting the adhesive to bonding. This phenomenon is analogous to similar trends exhibited by filled polymer systems and correlates with Ultrasonic Rayleigh Wave studies of shear gradients within epoxy adhesive bondlines. Hygrothermal effects of plasticization on the neat adhesive and bonded laminates were also demonstrated by DMA. The interfacial adhesion quality of epoxy-aluminum bonded laminates was also successfully determined by DMA. This was accomplished by comparison of peel performance with Tan δ_{Tg} values of corresponding laminates. It was determined that Tan δ_{Tg} was inversely related to peel strengths for the primer pretreatments applied. As such, DMA proved a powerful tool for evaluating the viscoelastic nature of adherend pretreatments and mechanical performance of the joint interface respectively.

5. ACKNOWLEDGEMENT

6. REFERENCES

(1) "Reliability of Adhesive Bonds Under Severe Environments", Publication NMAB-422, Report of the Committee on Reliability of Adhesive Bonds Under Severe Environments, National Materials Advisory Board, Washington, D. C., 1984.

(2) Smith, T. and Kaelbe, D. H., Treatise on Adhesion and Adhesives, Vol. 5, ed. R. L. Patrick, Marcel Dekker, Inc., New York (1981), p.139.

(3) Minford, J. D., Durability of Structural Adhesives, ed. A. J. Kinloch, Applied Science Publishers, London (1983), p.135.

(4) Millard, E. C., Adhesive Bonding of Aluminum Alloys, eds. E. W. Thrall and R. W. Shannon, Marcel Dekker, Inc., New York (1985), p.89.

(5) Manson, J. A. and Sperling, L. H., Polymer Blends and Composites, Plenum Press, New York (1976), p.373.

(6) Nielsen, L. E., Mechanical Properties of Polymers and Composites, Vol. 2, Marcel Dekker, Inc., New York (1974), p.422.

(7) Kinloch, A. J., Durability of Structural Adhesives. ed. A. J. Kinloch, Applied Science Publishers, London (1983), p. 1.

(8) Hewlett, P. C. and Pollard, C. A., Adhesion, Vol. 1, ed. K. W. Allen, Applied Science Publishers, London (1977), p. 33.

(9) Gettings, M. and Kinloch, A. J., J. Mat. Sci., 12, (1977), p. 2511.

(10) Theidman, W., Tolan, F. C., Pearce, P. J., and Morris, C. E. M., Proceedings of the International Meeting of the Adhesion Society, Feb. 1987, To Be Published.

(11) Ferraro, J. R. and Basile, L. J., Fourier Transform Infrared Spectroscopy, Techniques Using FTIR, Vol. 3, Academic Press, New York (1982), p.152.

(12) Brett, C. L., Adhesion, Vol. 3, ed. K. W. Allen, Applied Science Publishers, London (1979), p. 53.

(13) Clarke, J. A., Polymer Communications, 26, (1985), p.15.

(14) Peng, S. T. J., NASA Technical Brief, 9, (4), (1985), Item #90.

(15) Sichina, B., TA Hotline, Fall 1986, DuPont Co., Wilmington, DE.

(16) Gill, P. S., Thermal Analysis Application Brief, No. 81, DuPont Co., Wilmington, DE.

(17) Blaine, R. L. and Lofthouse, M. G., Thermal Analysis Application Brief, No. 65, DuPont Co., Wilmington, DE.

(18) Shah, D. N., Attalla, G., Manson J. A, Connelley, G. M., and Hertzberg, R. W, Rubber Modified Thermoset Resins, ACS Advances in Chemistry Series, No. 208, eds. C. K. Riew and J. K. Gillham, American Chemical Society, Washington, D. C., (1984), p.117.

(19) Murayama, T., Dynamic Mechanical Analysis of Polymeric Materials, Elsevier Scientific Publishing Co., New York (1978), p.111.

(20) Chua, P. S., SAMPE Qtly., 18, (3), (1987), p.10.

(21) Nielsen, L. E., Mechanical Properties of Polymers and Composites, Vol. 1, Marcell Dekker, Inc., New York (1974), p.12.

(22) Almer, C. J. and Pocius, A. V., Proceedings of the 12th National SAMPE Technical Conference, Oct. 1980, p.924.

(23) Manson, J. A. and Sperling, L. H., Polymer Blends and Composites, Plenum Press, New York (1976), p.450.

(24) Gillham, J. K. and Glandt, C. A., Chemistry and Properties of Crosslinked Polymers, ed. S. S. Labana, Academic Press, New York (1976), p.491.

(25) Lewis, T. B. and Nielsen, L. E., J. Appl. Poly. Sci., 14, (1970), p.1449

(26) Droste, D. H. and
DiBennedetto, A. T., J.
Appl. Poly. Sci., 13,
(1969), p.2149.

(27) Nielsen, L. E.,
Mechanical Properties of
Polymers and Composites,
Vol. 2, Marcel Dekker,
Inc., New York (1974), p.
425.

(28) Murayama, T.,Dynamic
Mechanical Analysis of
Polymeric Materials,
Elsevier Scientific
Publishers, New York
(1978), p.131.

(29) Knollman, G. C. and
Hartog, J. J., J. Appl.
Phys., 53, (8),(1982),
p.5514.

TABLE 1-DRIFT peak height values and ratios of certain chemical functional groups for various AF-111 cure conditions.

Cure Condition	Epoxy Ring (830 cm^{-1})	Aromatic Ether (1250 cm^{-1})	Epoxy Ring/ Aromatic Ether
Full Cure 121°C(250°F)	0.035	0.046	0.77
Partial Cure 93°C(200°F)	0.15	0.093	1.61
Failed Adhesive	0.007	0.009	0.82

TABLE 2-Laminate tensile shear strengths of various specimen sizes at room temperature.

Cure Temperature	Full-Scale Tensile Shear Strength ASTM D-3165 kg/cm^2 (PSI)*	Small-Scale Tensile Shear Strength kg/cm^2 (PSI)*
121°C(250°F)	332 (4720)	356 (5063)
177°C(350°F)	390 (5543)	371 (5270)

*Average values of five specimens.

TABLE 3—Transition temperatures and associated Tan δ peak values for neat AF-163-2K adhesive.

Pre-Test Exposure	Cure Temperature	T_g °C (°F)	Tan δ_{T_g}	T_{sec} °C (°F)	Tan δ_{sec}
Unexposed	121°C (250°F)	147 (297)	0.55	-42 (-44)	0.045
	177°C (350°F)	134 (273)	0.65	-39 (-38)	0.039
2wks/82°C (180°F)/ 100% R.H.	121°C (250°F)	105 (221)	0.42	-44 (-47)	0.053
	177°C (350°F)	106 (223)	0.41	-40 (-40)	0.056

TABLE 4—Transition temperatures and associated Tan δ peak values for bonded and single adherend laminates.

Joint Type (Pre-Test Exposure)	Cure Temperature	T_g °C (°F)	Tan δ_{T_g}	T_{sec} °C (°F)	Tan δ_{sec}
Bonded Laminate (unexposed)	121°C (250°F)	174 (345)	0.197	2 (36)	0.023
	177°C (350°F)	166 (331)	0.260	4 (39)	0.012
Bonded Laminate (2wks/82°C (180°F)/ 100% R.H.)	121°C (250°F)	136 (277)	0.176	8 (46)	0.017
	177°C (350°F)	134 (273)	0.220	10 (50)	0.015
Single Adherend (unexposed)	121°C (250°F)	166 (331)	0.037	-36 (-33)	0.004
	177°C (350°F)	161 (322)	0.040	-27 (-17)	0.003

TABLE 5-Transiton temperatures, Tan δ peak values, and peel strengths of bonded laminates with various prebond primer treatments.

Primer	Cure Temperature	T_g°C (°F)	Tan δ_{T_g}	T_{sec}°C (°F)	Tan δ_{sec}	Peel kg/cm wd (PIW)*
None	121°C (250°F)	168 (334)	0.140	-32 (-27)	0.002	17.5 (98)
A-1100 pH=4	121°C (250°F)	166 (330)	0.146	-34 (-29)	0.002	17.3 (97)
A-1100 pH=10	121°C (250°F)	166 (330)	0.160	-35 (-31)	0.002	15.7 (88)

*Average values of five specimens.
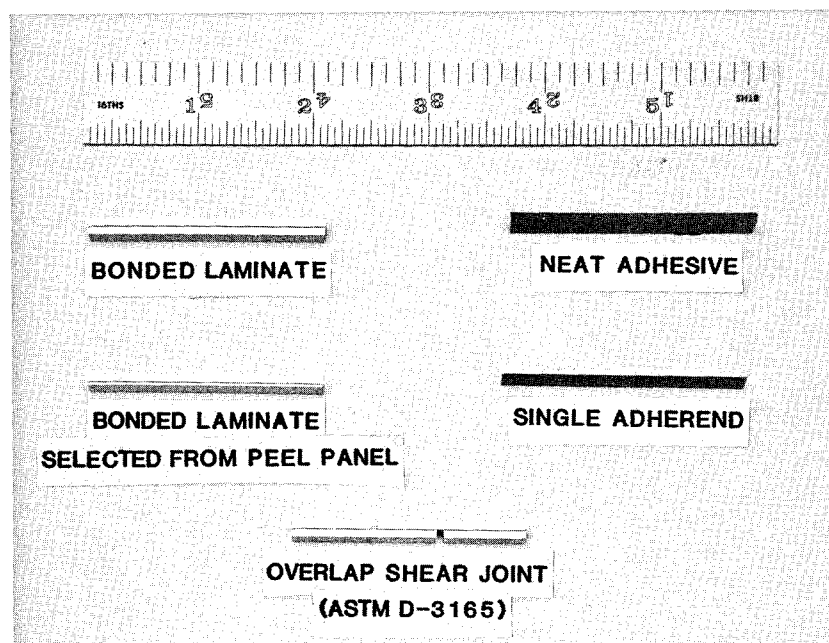
FIGURE 1-Small scale DMA laminates, joint, and neat adhesive.
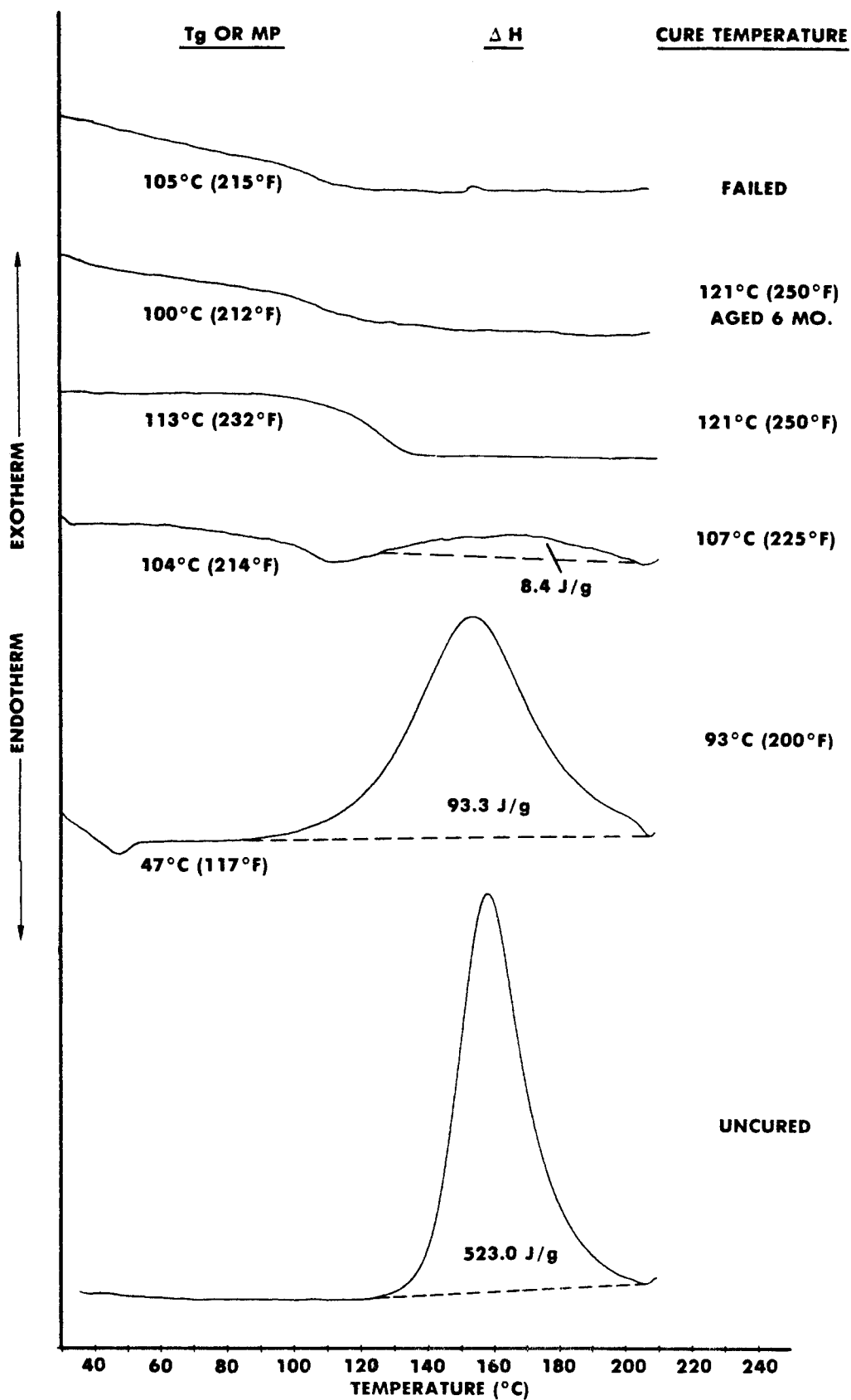
FIGURE 2-AF-111 adhesive DSC scans following various cure temperatures and aging.
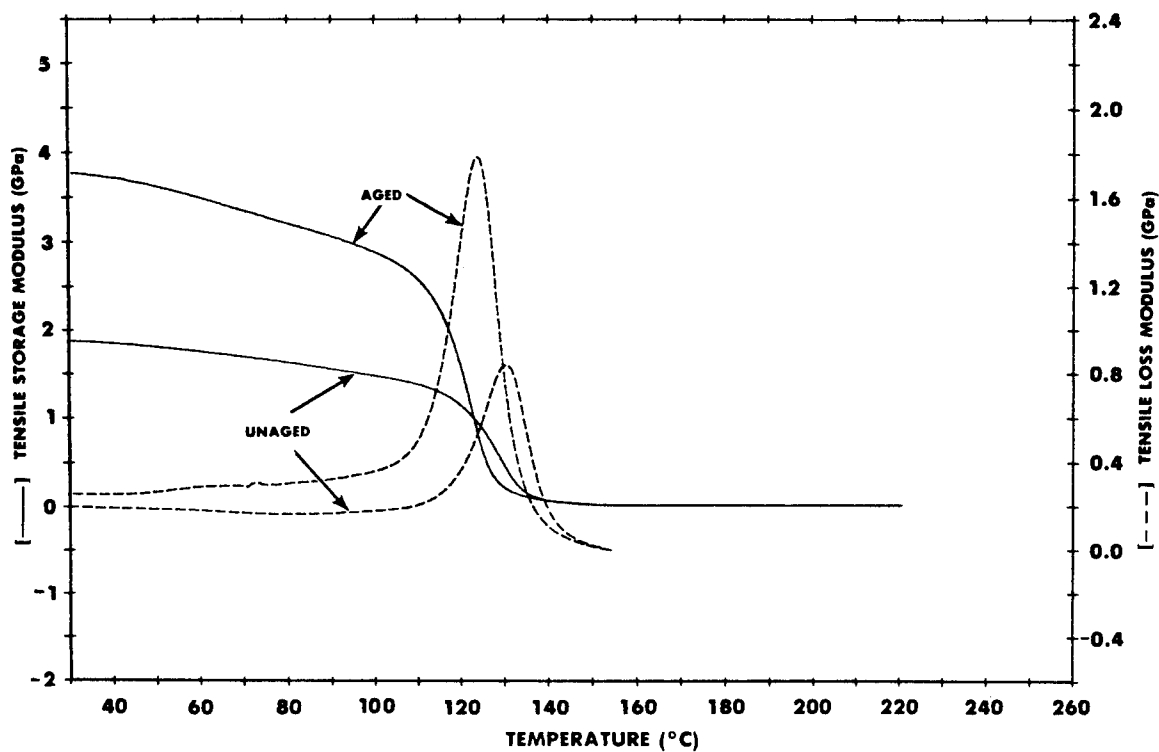
FIGURE 3-DMA of AF-111 adhesive immediately following and
six months after a complete 121°C (250°F)
cure cycle.
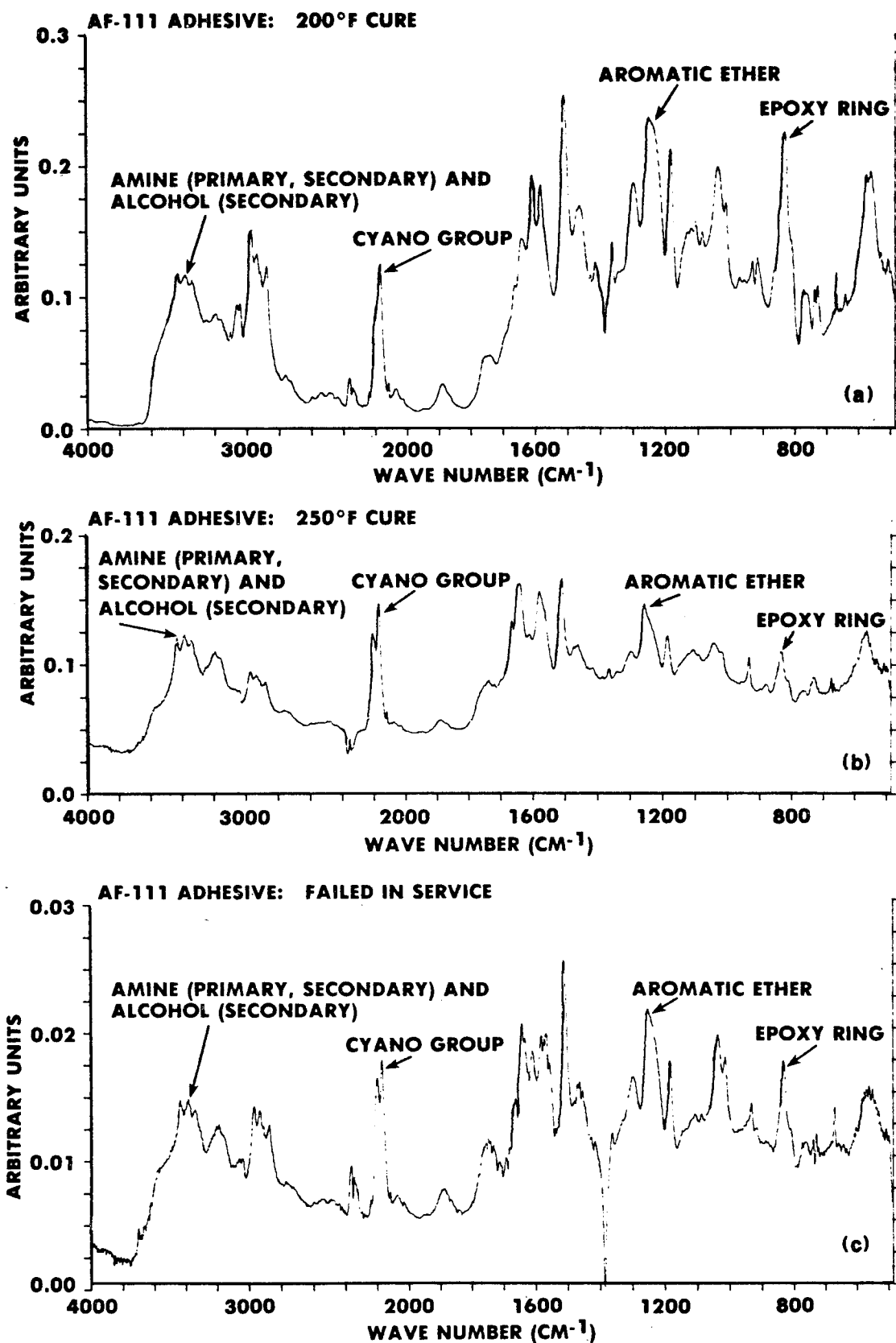
FIGURE 4—DRIFT spectra of AF-111 adhesive after various cure conditions and failure; (a) 93°C (200°F) cure (b) complete cure 121°C (250°F) (c) failed.
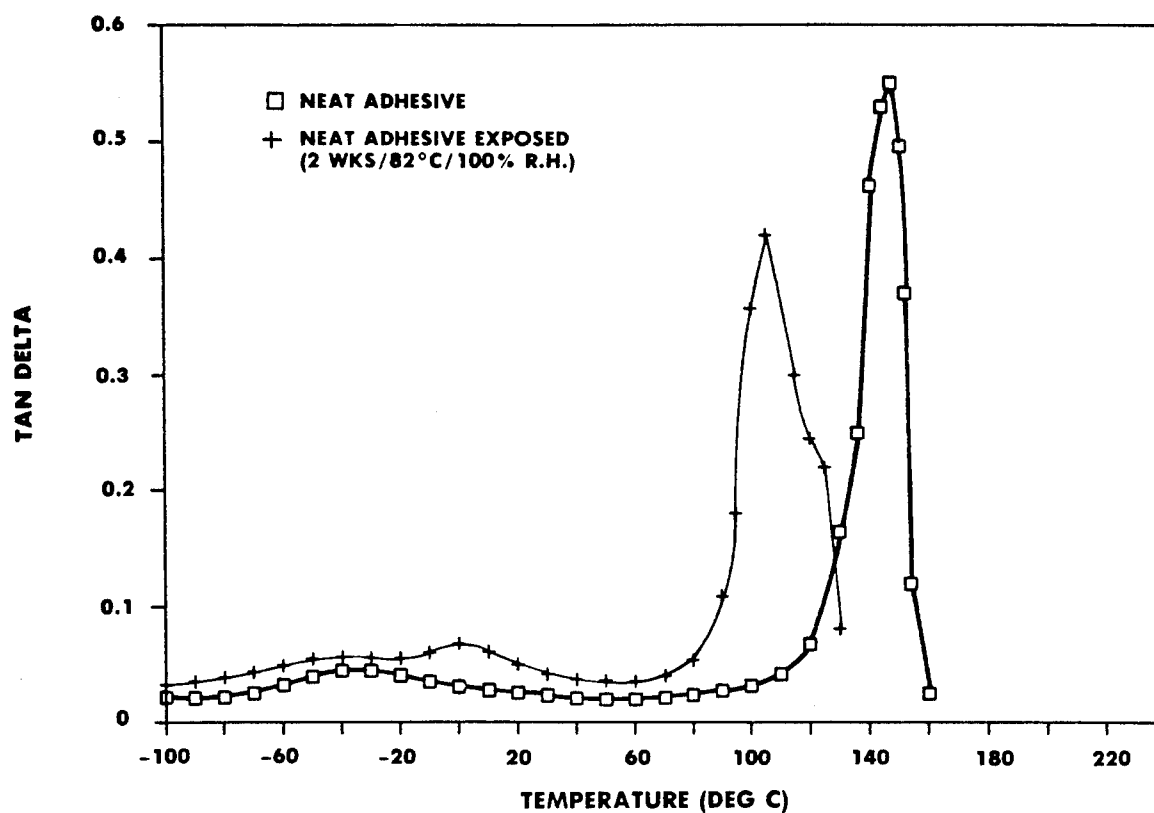
FIGURE 5-DMA of neat adhesive after 121°C (250°F) cure.
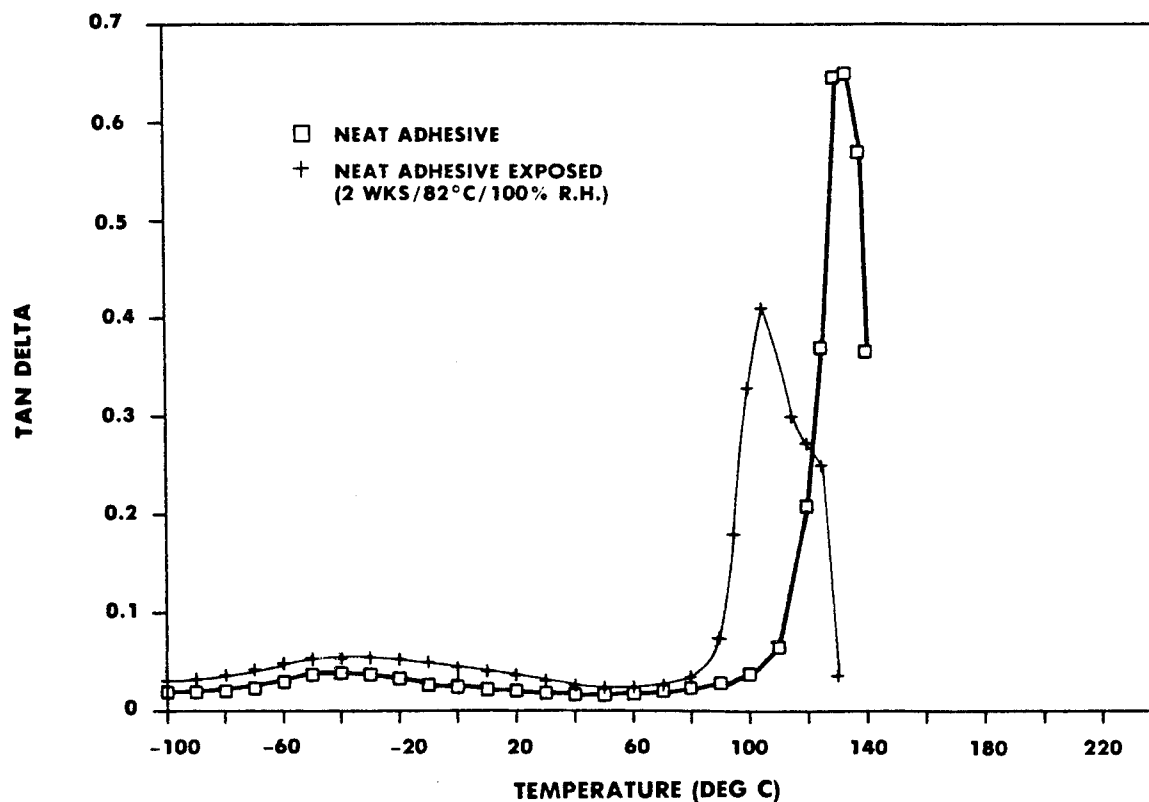
FIGURE 6-DMA of neat adhesive after 177°C (350°F) cure.

FIGURE 7-DMA of adhesive laminates after 121°C (250°F)
cure.

FIGURE 8-DMA of adhesive laminates after 177°C (350°F)
cure.

378

PRIMER:ORGANOFUNCTIONAL SILANE (A-1100) pH 10

PRIMER: ORGANOFUNCTIONAL SILANE (A-1100) pH 4

PRIMER: NONE

FIGURE 9-Peel specimens of various prebond primer
treatments after failure.

DURABILITY OF STRUCTURAL ADHESIVE BONDS IN A HOSTILE ENVIRONMENT

J.P. Wightman, H.F. Brinson, D.A. Dillard, D.J.D. Moyer and T.C. Ward
Center for Adhesion Science
Virginia Tech
Blacksburg, VA 24061

Abstract

Three surface chemistry aspects of the bonding of Ti-6Al-4V alloy with FM-300U epoxy adhesive were studied. First, x-ray photoelectron spectroscopy (XPS) was used to follow s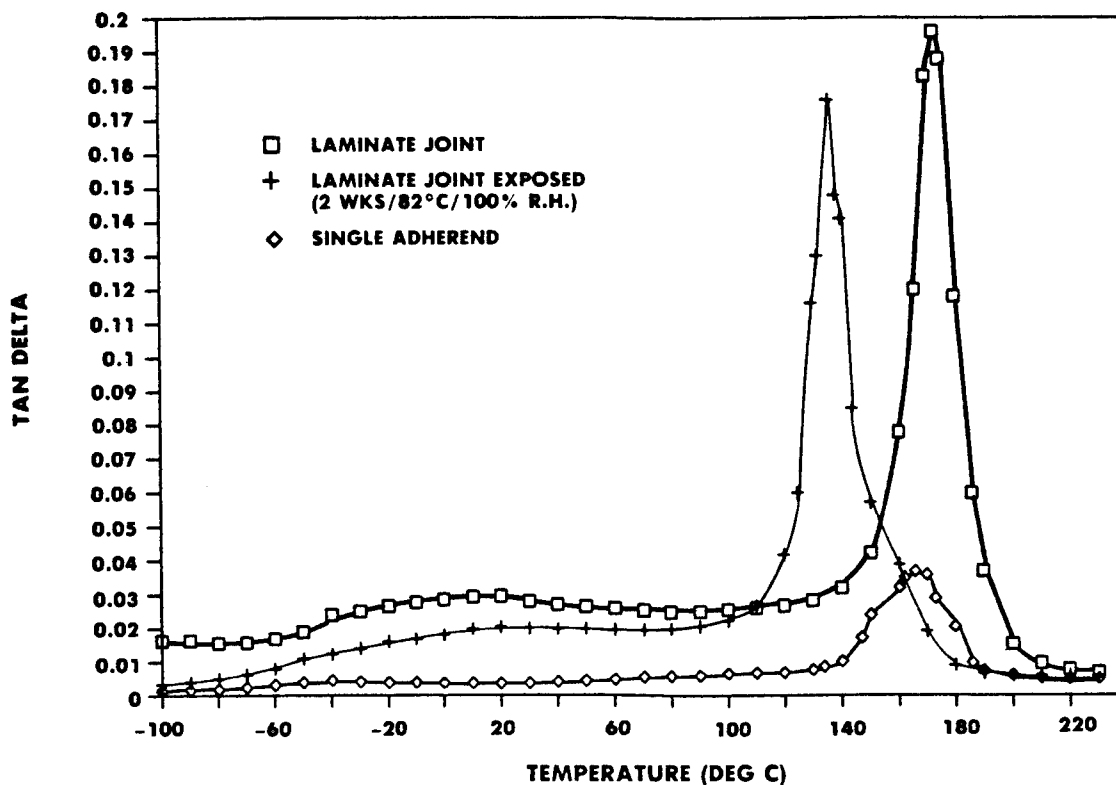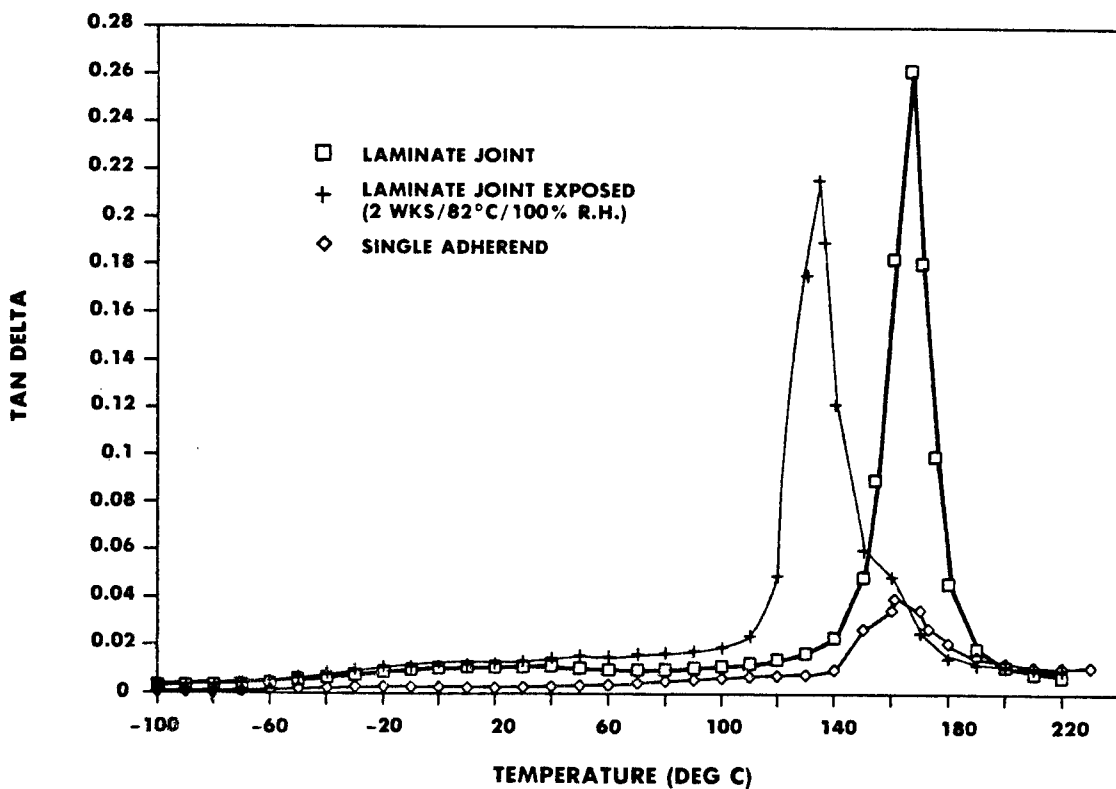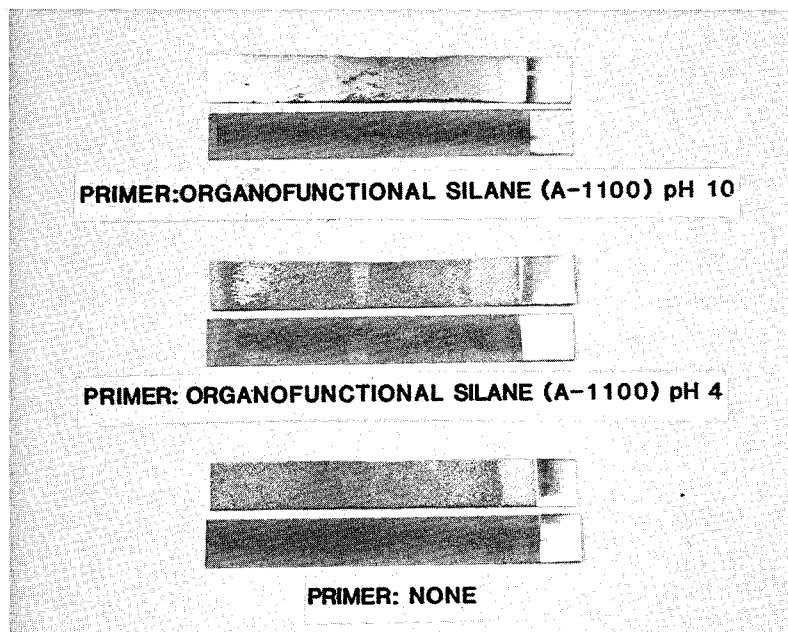urface contamination of pretreated Ti 6-4 adherends prior to adhesive bonding. Second, the determination of G_{Ic} values for adhesively bonded Ti 6-4 wedge samples which failed cohesively in one case and interfacially in another case was attempted. Third, moisture intrusion into adhesively bonded wedge samples was monitored by quantitative image analysis and by XPS. Failure became more interfacial as the samples were exposed to longer periods of immersion in water. The results suggest non-Fickian diffusion of water into the bondline.

1. INTRODUCTION

The durability of structural adhesive bonds in hostile environments is an area of continuing research (1-3).

The main advantage in using adhesives for structural applications is the high strength to weight ratio of the bonded components. There is also an increase in design flexibility. However with the use of structural adhesives, a severe limitation commonly observed is the detrimental effect of moisture on the bond strength (4). Some studies have dealt with the behavior of water in cured epoxy resin from the point of water absorption and diffusion. The behavior of water at the interface in an adhesive bond has not yet been clarified quantitatively (5). The loss of bond strength and the mechanisms involved in environmental failure of structural adhesive joints are not well understood. The work presented in this paper was done to quantify the effect of a contaminating environment on the surface composition of pretreated Ti 6-4 adherends and to study moisture intrusion into an epoxy/Ti 6-4 wedge sample.

2. EXPERIMENTAL

The materials, procedures and techniques used in this study are described below.

2.1 Contamination Study

Coupons of Ti 6-4 alloy were pretreated using a phosphate-fluoride etch (6). The samples were placed immediately after pretreatment in a Perkin-Elmer 5300 XPS spectrometer. After obtaining the initial spectrum, the sample was cleaned in situ using an argon ion beam. A second spectrum was obtained on the cleaned sample. The sample was then removed from the spectrometer and exposed to air for a specified period of time.

The sample was reinserted in the
spectrometer and a third spectrum
was obtained followed by ion
bombardment. This process was
repeated several times. XPS
angle studies (90°, 30° and 10°)
were also performed.

2.2 Directed Failure Study

Wedge samples were prepared from
pretreated Ti 6-4 coupons bonded
with FM-300U epoxy. Precracks
were initiated in separate
samples with the use of Teflon
film placed in the center of the
bondline and at the adhesive/
adherend interface. A wedge was
inserted and driven manually into
the sample.

2.3 Moisture Intrusion

Moisture intrusion into wedge
samples was studied by placing
the wedge samples described in
Section 2.2 above in deionized
water at 98°C for varying times.
The samples were removed from the
water. One set of samples were
opened by a wedge driven manually
into the samples. The other set
of samples had a precrack of
about 6 cm made in the bondline.
The samples were then opened and
the critical load (P_c) was
determined using an Instron model
1123. Values of G_{Ic}, the
critical strain energy release
rate, were calculated using the
equation

$$G_{Ic} = 12\ P_c^2 a^2 / B^2\ Eh^3$$

where a is the length of the pre-
crack [6 cm], B is the adherend
width [2.54 cm], E is the modulus
of the adherend [1.14×10^{11}
Pascals] and h is the adherend
thickness [0.38 cm]. The failure
surfaces were analyzed by
quantitative image analysis and
by XPS.

3. RESULTS AND DISCUSSION

The results of the three
phases of this work are presented
and discussed below.

3.1 Contamination Study

It is well known that pretreated
solid surfaces contaminate
readily upon exposure to
laboratory conditions. However,
the type, extent, and speed of
contamination is not often
documented (7) particularly in
adhesion studies. Ti 6-4 samples
were pretreated with a phosphate-
fluoride etch and then exposed to
the lab atmosphere for varying
amounts of time. Careful
attention was paid to the
reference binding energy of the
carbon 1s photopeak in order to
give an unambiguous assignment of
the bonding state of carbon on
the pretreated surface. The
results are summarized in Table
I. Contamination is rapid and is
limited to the topmost surface of
the pretreated Ti 6-4 adherend.

3.2 Directed Failure Study

This study is an initial attempt
to measure a material property of
the interphase region critical in
the modeling of adhesive bonding.
Cohesive failure was easy to
initiate and measure
reproducibly. On the other hand,
although failure could be
initiated nominally at the
interface, the crack would
immediately jump into the
adhesive precluding measurement
of the interfacial strain energy
release rate at the interface.

3.3 Moisture intrusion

The initial study here was
concerned with the quantitative
image analysis of wedge samples

opened after varying periods of exposure in hot water. Sketches of the appearance of the failure surfaces after different exposure times are shown in Fig. 1. The percentage of adhesive area on the failure surface is plotted as a function of exposure time in Fig. 2. It is assumed that diffusion of water into the bondline produces delamination. A linear decrease is noted in Fig. 2 consistent with non-Fickian diffusion of water into the bondline.

The critical strain energy release rate was determined in a more extensive study. Values of G_{Ic} are plotted against exposure time in Fig. 3. Again, a linear decrease was observed consistent with the results seen in Fig. 2. The zero day sample is taken as the control. The failure surfaces in the more extended study were also analyzed by XPS and the results are shown in Table II. The C/Ti ratio decreased with increasing exposure times indicating decreasing amounts of residual adhesive left on the failure surface. Nitrogen is a tag element contained in the epoxy and the N/Ti ratio parallels the trend seen for the C/Ti ratio. The oxygen photopeak for the four failure surfaces shown in Fig. 4 support the decreasing amount of residual epoxy adhesive with increasing exposure time. A doublet is clearly seen for the 7 day sample. The higher binding energy peak at about 533 eV is associated with oxygen in the epoxy and is seen to decrease in intensity with increasing exposure time. Conversely, the lower binding energy peak at about 531 eV associated with oxygen in the surface oxide on the Ti 6-4 adherend is seen to increase in intensity with increasing exposure time.

4. SUMMARY

The contamination of pretreated Ti 6-4 adherend surfaces is rapid and is due to partially reversible, multilayer adsorption of organic vapors from the lab environment. Crack propogation in wedge samples is not controlled simply by location of the precrack. Critical strain energy release rates can be obtained as a function of time for environmentally exposed wedge samples and the values decrease as exposure time in hot water increases. Failure becomes more interfacial as the wedge samples are exposed for longer times and the diffusion of moisture is non-Fickian.

5. ACKNOWLEDGEMENT

6. REFERENCES

1. P. J. Boerio and C. H. Ho, J. Adhesion, 21, 25(1987).
2. P. Commercon and J. P. Wightman, J. Adhesion, 22, 13 (1987).
3. V. T. Kreibich and A. F. Marcontonio, J. Adhesion, 22, 153 (1987).
4. R. A. Gledhill and A. J. Kinloch, J. Adhesion, 6, 315 (1974).
5. K. Nakamura, T. Maruno and S. Sasaki, Int. J. Adhesion and Adhesives, 7, 97 (1987).
6. J. G. Mason, R. Siriwardane and J. P. Wightman, J. Adhesion, 11, 315 (1981).
7. G. Koranyi and T. M. Acs, Acta Chim. Hung., 24, 3337 (1960).

TABLE I

XPS ANALYSIS OF P/F ETCHED TI 6-4

Time Interval	Take-Off Angle	Atomic Fraction C/Ti	O/Ti	Ar Sputtered C/Ti	O/Ti
30 sec	90	1.5	4.1	0.68	4.1
60 sec	90	1.2	4.0	0.59	3.8
150 sec	90	1.3	4.1	0.68	3.8
300 sec	90	1.2	4.2	0.47	3.9
13 hrs	90	1.3	3.4		
13 hrs	30	1.8	3.5		
13 hrs	10	3.3	3.9		

TABLE II

XPS ANALYSIS OF FAILURE SURFACES

Time Immersed (98°C H_2O)	Visual Appearance	C/Ti	N/Ti
0 days	Adhesive	190	1.6
7 days	Film	13	0.47
28 days	Metal	6.4	0.18
P/F only	Metal	1.3	0
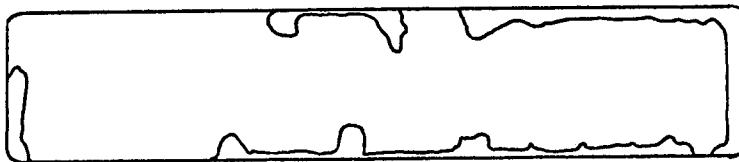
Figure 1. Sketch of failure surfaces after opening experimentally aged samples.

Figure 2. Quantitative image analysis of failure surfaces after opening environmentally aged samples.

Figure 3. Values of G_{Ic} determined for environmentally aged samples.

Figure 4. XPS 01s photopeaks from failure surfaces for environmentally aged samples.

DURABILITY PREDICTIONS FOR ADHESIVE JOINTS

David A Dillard, Assistant Professor
Ramzi Hamadeh, Graduate Research Assistant
H F Brinson, Professor

Engineering Science and Mechanics Department

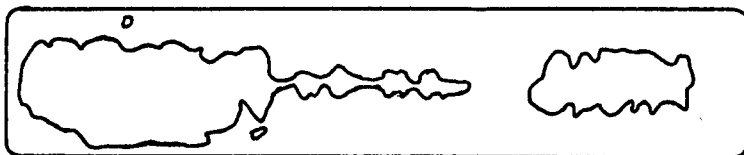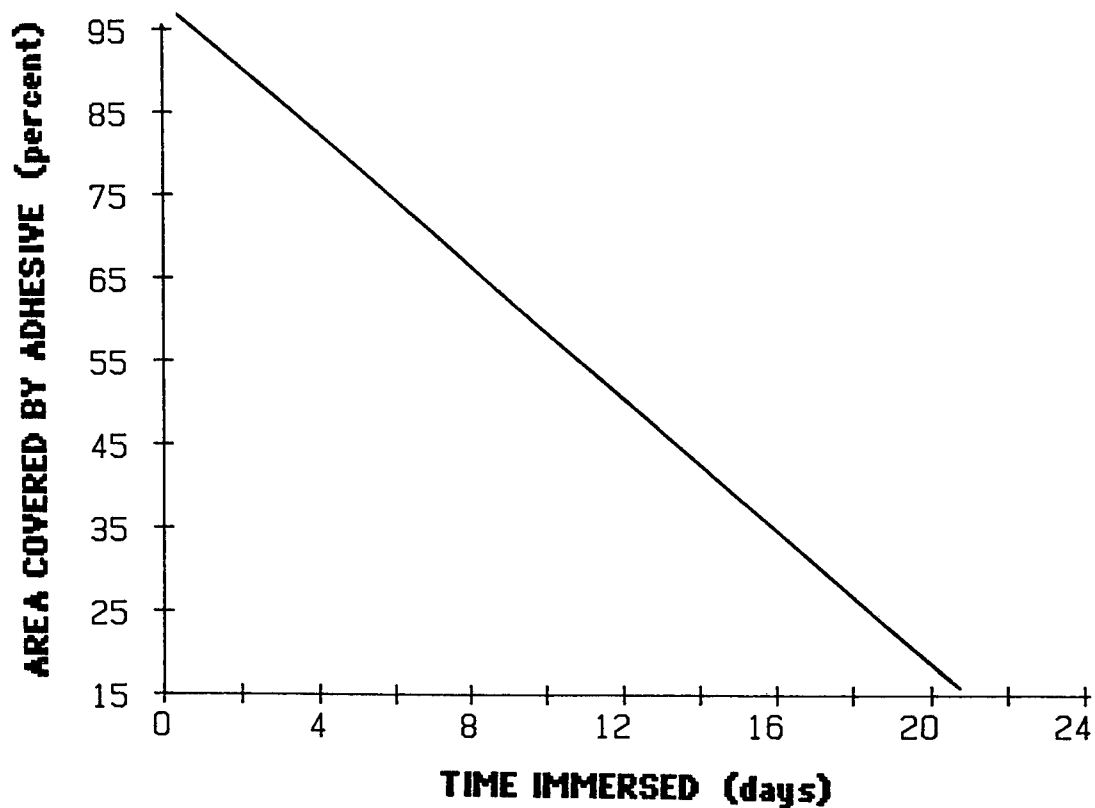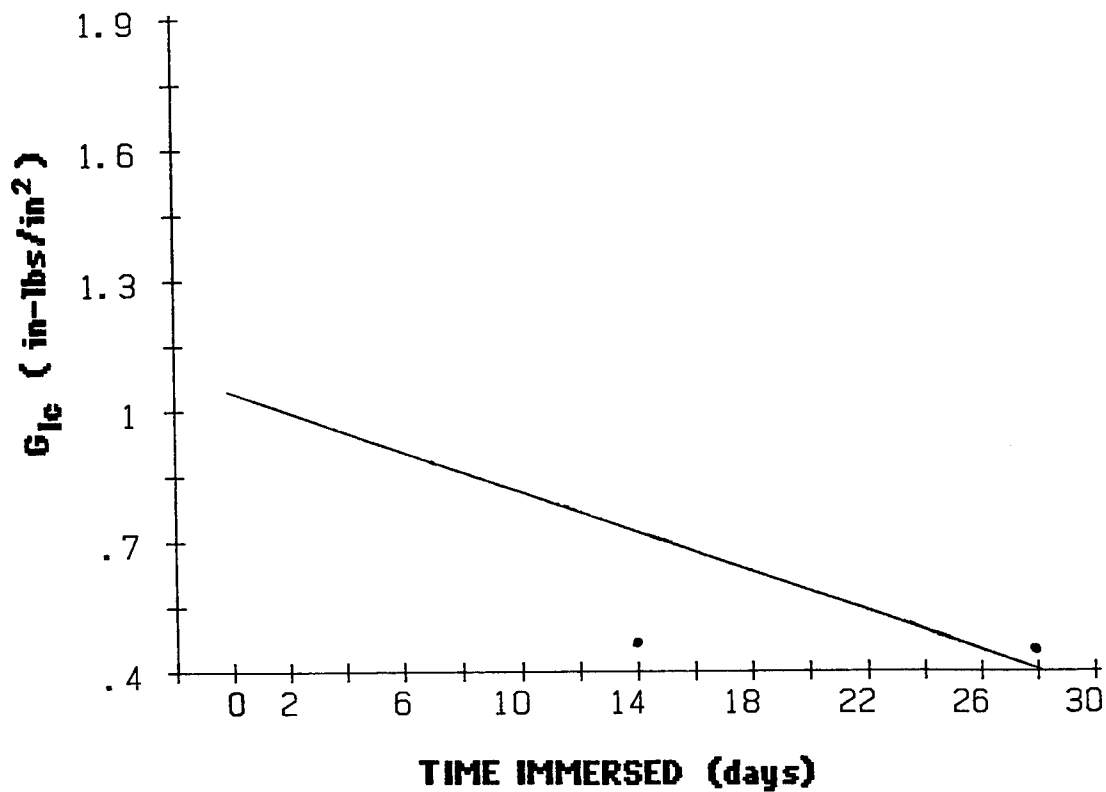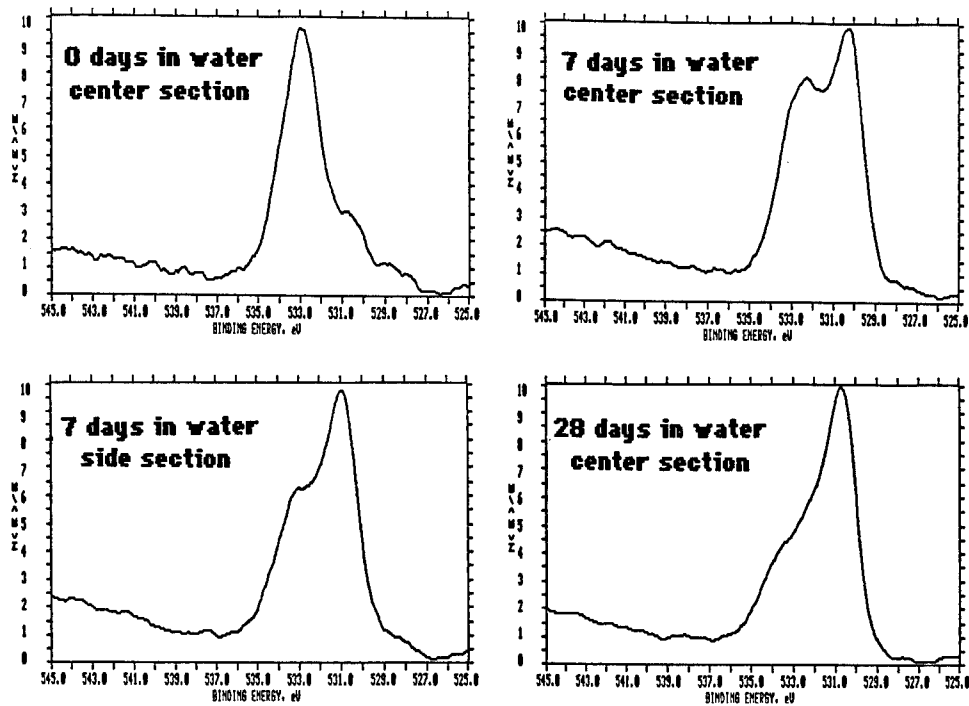Virginia Polytechnic Institute

Blacksburg, Virginia

ABSTRACT

The degradation of rubber to metal bonds exposed to marine environments is discussed. The primary cause of bond deterioration is found to be a cathodic delamination mechanism similar to that observed with thin organic coatings. A model for debonding is presented, along with observations which may suggest design modifications to improve reliability.

INTRODUCTION

Elastomer to metal bonding is an important adhesion problem for a variety of modern structures and components. Major applications include the automotive, tire, shipbuilding, and off-shore drilling industries. In these applications, the rubber may serve to inhibit corrosion, to seal the component from intrusion of unwanted substances, or as a load bearing structure. Although acceptable bonds are routinely produced for many of these functions, bond durability can be a problem upon exposure to certain environments. This paper will address the durability of rubber to metal bonds for marine applications.

Under favorable conditions, rubber to metal bonds are quite stable in seawater environments, but the presence of small amounts of cathodic potential can rapidly deteriorate the adhesive bond. Cathodic potential may be provided by the galvanic action of dissimilar metals. This situation is intentionally created on many marine structures by the use of sacrificial anodes. Ironically, these anodes serve to protect the steel hull, but degrade the performance of rubber bonds, paint, and other organic coatings. Even if the metal substrates are initially electrically insulated from the anodes, corrosion products and sediment can build up on the components

to permit the flow of electrons. Evidence is even pointing to the possibility of localized anodic and cathodic regions on the metal substrate which may provide an electron supply under certain circumstances. Cathodic debonding processes have been widely studied by researchers in the area of thin organic coatings [2-4]. When metallic substrates are exposed to aqueous salt solutions and supplied with free electrons, reduction of dissolved oxygen or water at the adhesive to metal oxide interface occurs according to the following formulae:

$$O_2 + 2H_2O + 4e^- = 4OH^-$$

or

$$2H_2O + 2e^- = 2OH^- + H_2$$
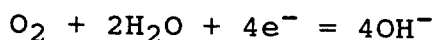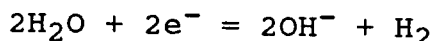
In seawater, oxygen reduction is favored at low cathodic potentials and hydrogen reduction is favored at higher potentials. Note that either reaction increases the pH around the metal substrate. When these reaction products are sequestered inside a small debonded region, an extremely high pH can result. Several mechanisms have been proposed to explain the relatively rapid debonding that results from the alkaline environment. Leidheiser and co-workers [2,3] feel that the high pH may cause the oxide layer to deteriorate. Koehler [4] maintains that the high pH may cause the polymer to have more attraction for water molecules than for the metal oxide. This causes the polymer to metal oxide bond to be displaced by a water layer, greatly reducing the strength of adhesion. Other investigators [5] have indicated that the probable mode of failure is hydrolysis or saponification of the polymer by the high pH environment induced in the coating near the interface.

The actual mechanism of bond weakening and failure is not clearly understood. Each of the mechanisms are supported by certain experimental results, but each method also has problems associated with it. Indeed, it is possible that the actual failure process may depend on a combination of these methods, and it is possible that the mechanism may change as one goes from one metal substrate, organic coating, and environment system to another. For the case of neoprene bonded to ANSI 1026 steel with a vulcanizing primer and topcoat of interest in the present study, further tests are being performed to better understand the actual mechanism. The purpose of this paper, however, is to discuss some of the mechanics issues which influence debonding rate.

A variety of tests have been advocated for evaluating the adhesion of a flexible layer bonded to a rigid substrate. The cone test (ASTM D-429) has been widely used for measuring the adhesion of rubber to metal substrates. The design of this test causes debonding to initiate at the interior of the specimen, however, making it inappropriate for tests

subjected to environmental exposure. A number of different specimens have been based around the peel concept. These include the climbing drum peel test (ASTM D-1781), the floating roller peel test (ASTM D-3167), and the simple peel test, using 180° peel (ASTM D-903) or other angles. Unfortunately, most of these tests are quite cumbersome to use in a harsh liquid environment. In an effort to avoid some of the problems associated with these specimens for our application, several alternate techniques have been developed.

A blister specimen was utilized for testing, but it required rather large amounts of rubber to achieve high enough strain energy release rates. It was also difficult to accurately monitor the debond radius on this type of specimen. Liechti [6] developed a strip blister specimen which involved a 25 mm. wide strip of steel with rubber bonded to one side. By inserting a dowel into an initial debond in the specimen, the specimen could be loaded to various strain energy release rates. The open design of the specimen permitted measurement of debond distance with specially shaped calipers. This specimen has proved to be quite useful for the systems being studied and is being used extensively at the present time. By bonding a thin layer of the neoprene between steel adherends, a double cantilever sandwich beam was produced [7]. Using the analysis of a beam on an elastic foundation, strain energy release rates could be estimated.

The tests reported herein were conducted on a commercially available primer and topcoat of a vulcanizing adhesive. Boerio [8] has studied several of the currently available vulcanizing adhesives for bonding rubber to metals and has found that several of these products are quite similar in composition. The primers normally consist of a phenol formaldehyde base perhaps blended with a chlorinated rubber and containing a variety of fillers which may include carbon black, rutile titanium oxide, zinc oxide, and aluminum silicate. The topcoats showed more variability, but appear to consist primarily of a chlorinated rubber base. Actual tests conducted on several different adhesive systems have also revealed similar failure modes and rates of debonding. Thus the information presented herein should be typical of several of these closely related systems.

In order to learn more about the components of the selected adhesive system and the role each played in the failure process, it became desirable to fabricate neat specimens of the components. Because of the high solvent content of the primer and the very brittle nature of the residual solid, these specimens were difficult to cast. Several techniques were tried including drawing thin layers of film on glass or Teflon plates and casting films on mercury. The

quality of the films produced on the mercury was quite good because there was no resistance to shrinkage as the solvent evaporated. This produced films without significant cracking. In an effort to avoid the mercury exposure hazard, thin films were then cast directly onto a woven glass cloth. Again the cloth appeared to be flexible enough to minimize the shrinkage cracking.

These films were separated from the cloth, stacked together, and molded at vulcanizing temperature and pressure into solid specimens large enough for mechanical characterization. The quality of these specimens seemed acceptable for conducting mechanical tests and moisture ingression tests. Specimens of the topcoat material were difficult to fabricate because of apparent outgassing of the specimens during cure. The void content of these specimens was high, but the ductile nature of the material permitted mechanical tests to be performed without premature fracture. Figure 1 gives the stress strain diagrams of topcoat and primer specimens illustrating the ductile and brittle natures, respectively. A 50%/50% blend of the two components was molded into a specimen to simulate the interdiffusion which might occur between the relatively thin layers within an actual bond. The blend shows good stiffness and toughness properties, although we do not presume that this material is necessarily representative of the polymer in the actual bond.

Neat primer specimens were subjected to exposure in various environments and evaluated in terms of mass uptake and residual mechanical properties. DMA analysis revealed that the exposure did reduce the glass transition temperature of the cured primer material and there was also a drop in the mechanical properties. Exposure seemed to reduce the modulus by roughly 50%, although there was quite a bit of scatter between specimens.

The mass uptake studies revealed some interesting data as shown in Fig. 2. The neat primer samples all showed significant moisture uptake in NaOH environments. Although the uptake occurred slower at lower concentrations, it appears that the total mass uptake at various concentrations is quite comparable. It is not clear why the mass uptake at 3.0 N NaOH is faster than for the 10.0 N solution.

When the specimens were dried in an oven at the same temperature as the conditioning bath, moisture came out of the specimens much more rapidly than it had gone in. This suggests that a chemical reaction had taken place which significantly changed the properties of the material. After drying, the specimens were returned to their respective environments. Again the mass uptake occurred very rapidly. Interestingly, the specimens returned to there respective mass levels. For these thin specimens, it is believed that the initial mass uptake in the high pH environments

is controlled by the rate at which the polymer degrades. This produces mass uptake curves which are linear in time space rather than square root of time space as would be the case for Fickian diffusion.

Figure 3 gives a clue as to the probable amount of NaOH which entered the specimen conditioned in 1N NaOH showing the mass uptake curve for a specimen which was initially exposed to 1N NaOH, dried, and then exposed to deionized water (DIW), and finally redried again. The mass uptake in the specimen in DIW was quite fast, but the equilibrium amount was less than would have been achieved in the original alkaline bath. Upon redrying, a very large amount of mass was lost, suggesting that NaOH within the specimen had leached out. One might speculate that a substantial amount of the specimen may have leached out during the first exposure, only to be replaced by NaOH, thus resulting in a very small mass change between the original sample mass and the mass of the redried samples in Figure 2.

Surface analysis of these neat primer samples also revealed that there has been a break down of the polymer. ESCA results revealed that carbon linkages were being broken to form carboxylates and carbonates. The chlorine in the chlorinated rubber component appeared to show some signs of deterioration as evidenced by the rise of an inorganic chlorine peak.

Similar analyses conducted on the steel and rubber sides of failed bonds also revealed similar results.

An important question is the role which stress plays on the rate at which bond degradation and failure occurs. It has been observed that by applying a sufficient opening mode stress to the debond, the rate of debonding is increased. One possible explanation is that the tensile stress increases the free volume of the polymer and hence the diffusion rate. An examination of the stresses required to affect such a change, however, suggests that this does not account for the significant effects which are observed. It does appear that the peel stresses can accelerate the physical separation of the rubber from the steel. This shortens the diffusion distance and therefore can speed up the diffusion process.

Figure 4 illustrates a bonded diffusion specimen which was utilized to investigate diffusion rates along an actual bond. Specimens were exposed to a given environment and removed after various exposure times. The bonds were pulled open and the amount of bond degradation could be measured easily because the failure was interfacial where bond degradation had occurred, but cohesive in the rubber where the bond had not been degraded. The figure also shows a darker region where the bond has regained some strength upon drying judging by the increase in number of

rubber ligament pull-outs that often coincide with grit-blast crater tops. Figure 5 shows the distances which the bond degradation had progresses compared to the square root of time. The data strongly suggests that in the absence of applied stresses, the bond degradation is limited by a diffusion process that resembles Fickian. The non-Fickian behavior observed in the neat primer specimens were probably due to the fact that these specimens were thin enough that the chemical reaction provided more limitation to penetration that the diffusion process. For longer diffusion distances, however, the diffusion process limits the rate as is the case for the bonded diffusion specimens.

Tests on specimens loaded with peeling stresses show that the rate of debonding is relatively constant. A possible scenario is that the bond degradation results in a weakened region which can not maintain the tensile stresses and fails. This shortens the diffusion path and the process continues as long as the stress is maintained. Over at least some range of stress levels, the rate of debonding is only moderately affected by the stress level.

Tests were also conducted with the bond in compression. Initial results showed that the compressive stresses slowed down the diffusion rate in proportion to the amount of stress applied. More recent tests have failed to repeat this behavior and further testing is underway to evaluate this effect.

Several types of specimens were tested with a shear load applied. Shear stresses large enough to produce as much as 160% shear strain in the neoprene did not appear to affect the debond rate at all. The only exception to this is on the leading edge of the bond where peel stresses are also induced.

At this time it appears that the peel stresses can significantly affect the debonding rate, largely due to the changing boundary conditions for the diffusion process. Compression stresses may have some beneficial effect, but this is not entirely clear at the present time. In order improve the durability of these joints in service, it is advantageous to minimize any possible peel stresses and to increase the length of the bond as long as possible to increase the amount of time for penetration to occur.

In summary, the debonding process of neoprene to steel in a marine environment in the presence of cathodic potential is closely tied to the diffusion process of water into the adhesive layer. Initially a small amount of moisture diffuses into the adhesive layer and forms an electrolyte for the reduction process to begin. Either reduction process will begin to generate hydroxide ions. The presence of hydroxide ions in the

adhesive appears to increase the saturation level as well as increase the diffusion rate of moisture into the adhesive layer. The significance of this is that the weakened layer left behind by the advancing diffusion front appears to be quite uniform in behavior. If the diffusion rate were not affected, one would expect a gradual change in the bond strength corresponding with the moisture gradient. The effects of stress and temperature (within the service range for transducer applications) seem to be very small compared to the effects of cathodic action and pH. By making measurements of the diffusion rates, it is anticipated that one can make predictions of the expected lifetime of rubber to metal bonds.

ACKNOWLEDGEMENTS

REFERENCES

1   Stevenson, A.,"On the Durability of Rubber/Metal Bonds in Seawater", International Journal of Adhesion and Adhesives, V 5, N 2, April 1985, pp.81-91.

2   Leidheiser, H, W Wang, and L Igetoft, "The Mechanism for the Cathodic Delamination of Organic Coatings from a Metal Surface", Progress in Organic Coatings, V 11, 1983, pp 19-40.

3   Wang, W, and H Leidheiser, "A Model for the Quantitative Interpretation of Cathodic Delamination", Pourbaix Symposium Volume of the Electrochemical Society, New Orleans, October 1984.

4   Koehler, E L, "The Mechanism of Cathodic Disbondment of Protective Organic Coatings - Aqueous Displacement at Elevated pH", Corrosion - NACE, V 40, N 1, January 1984, pp 5-8.

5   Hammond, J S, J W Holubka, and R A Dickie, Journal of Coatings Technology, V 51, 1979, p 45.

6   Dillard, D A, K Liechti, D R Lefebvre, C Lin, J S Thornton, and H F Brinson, "The Development of Alternative Techniques for Measuring the Fracture Toughness of Rubber to Metal Bonds in Harsh Environments," ASTM Symposium on Adhesively Bonded Joints: Testing,

Analysis, and Design, Baltimore, 1986.

7   Lefebvre, D R, D A Dillard, and H R Brinson, "The Development of a Modified Double Cantilever Beam Specimen for Measuring the Fracture Energy of Rubber to Metal Bonds," <u>Experimental Mechanics</u>, V 27, 1987, (in press).

8   Boerio, F J, STRIP Quarterly, work unit II.A.3a, 2nd Quarter, 1985.
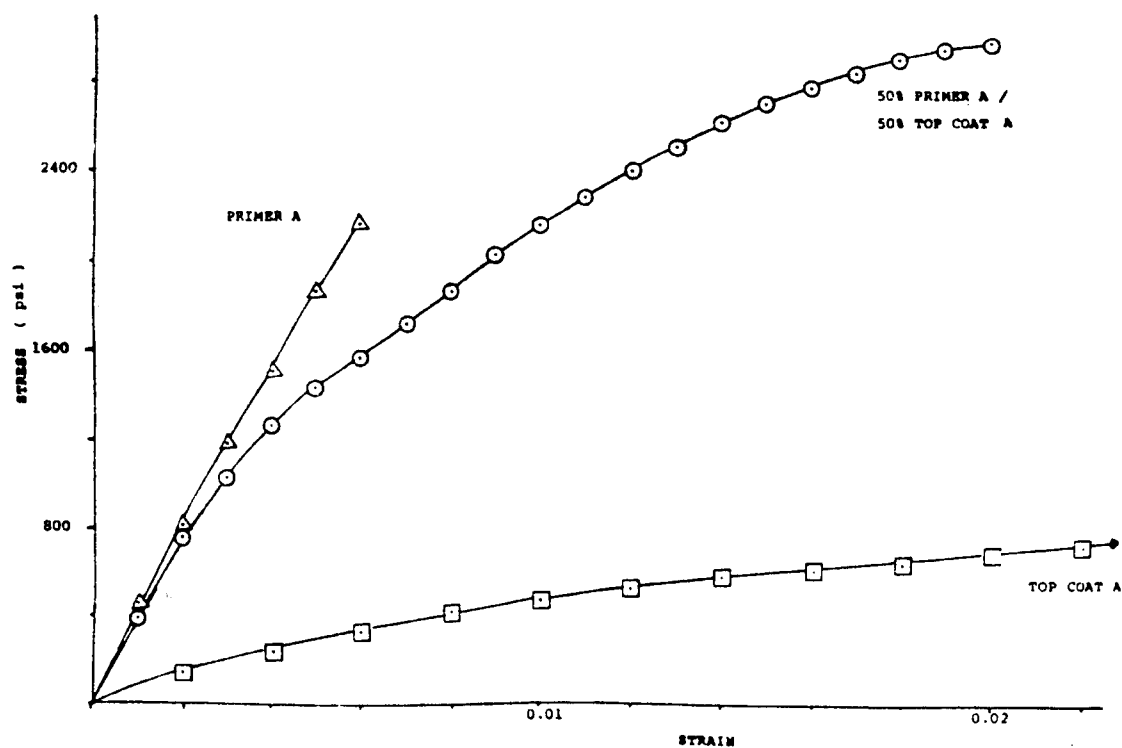
Figure 1. Stress-strain plot of neat adhesive specimens.

SORPTION CURVES
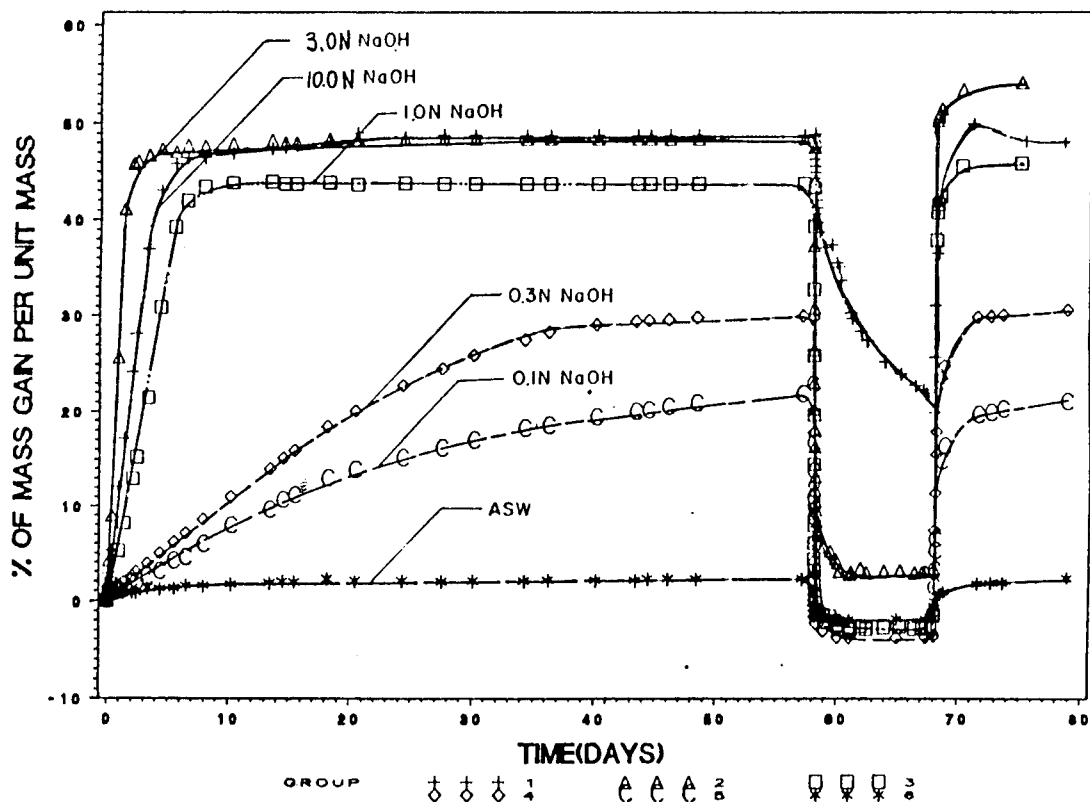
Figure 2. Sorption curves for neat primer A specimens at 33° C
showing exposure, drying, and resorption response.
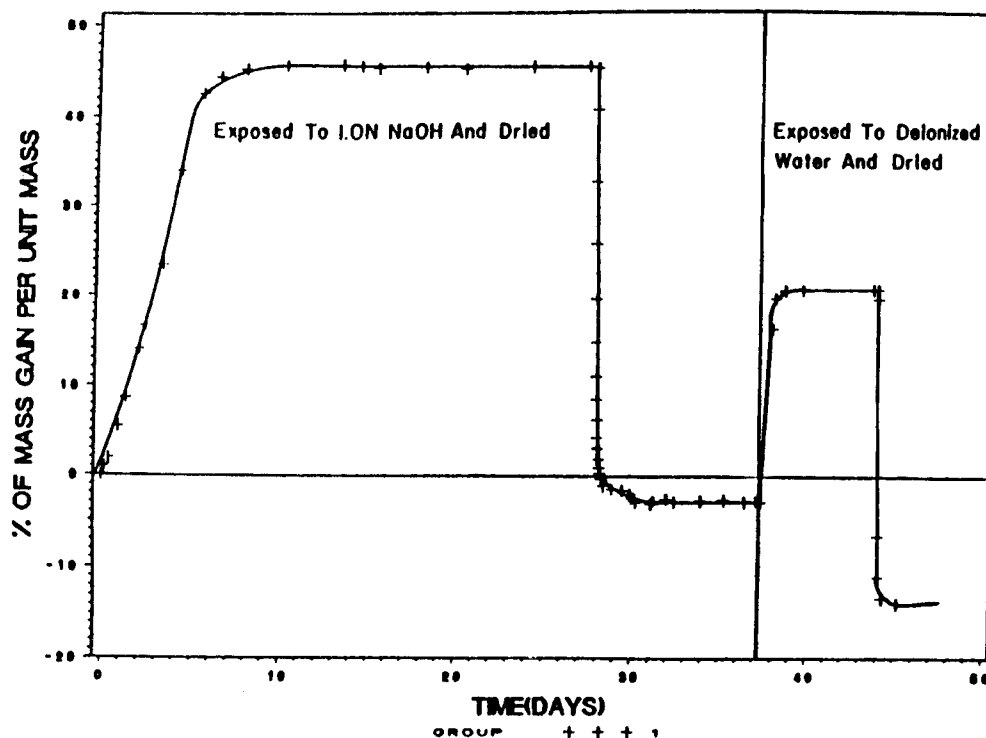
Figure 3. Sorption curve for a primer A specimen conditioned in NaOH, dried, conditioned in water, and redried.
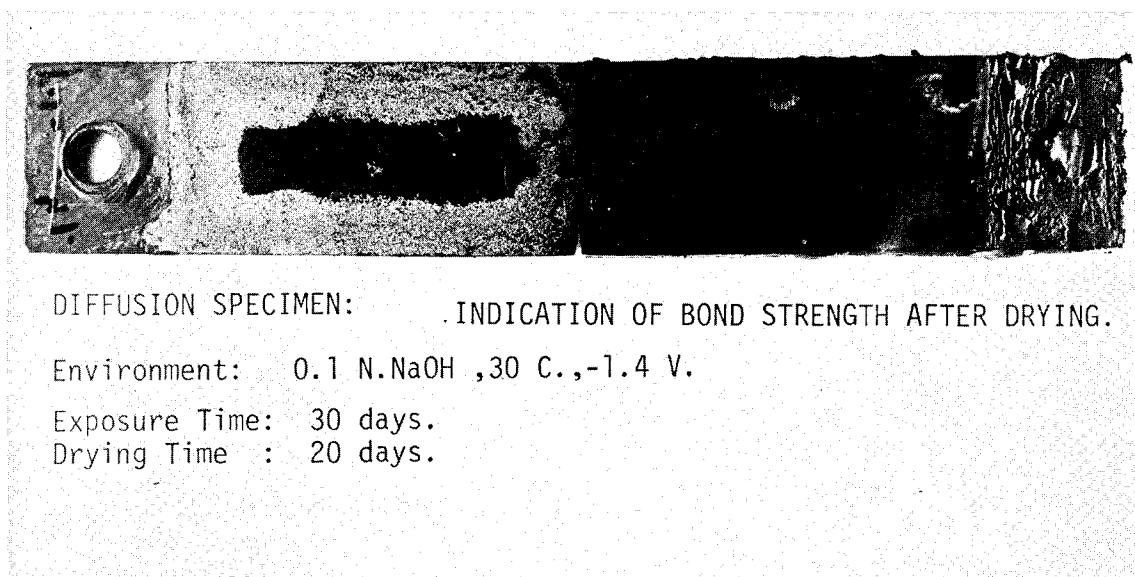
Figure 4. Photograph of bonded diffusion specimen showing the "diffusion window" and drying effect on durability.

EFFECT OF ENVIRONMENT
TEMP=30 C.
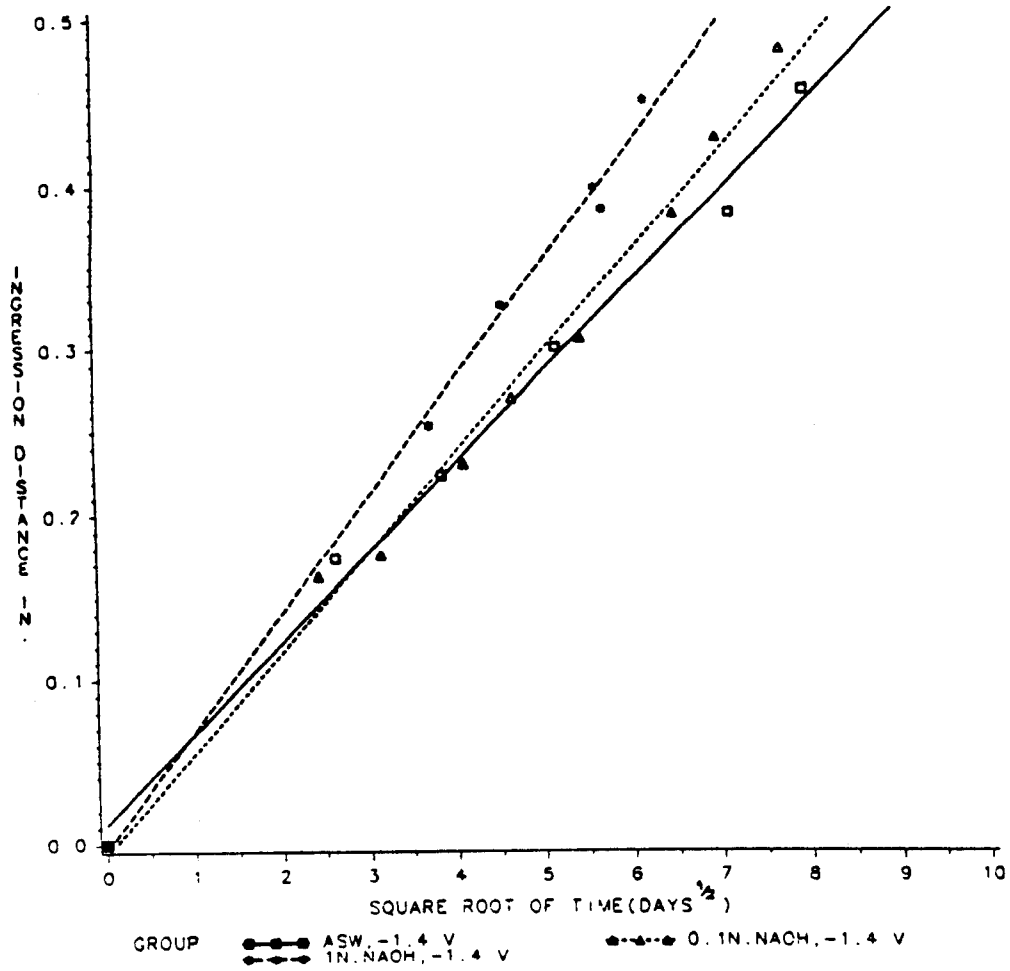
Figure 5. Ingression distance vs. square root of exposure time of the bonded diffusion specimen for different environments.

NONDESTRUCTIVE EVALUATION OF ADHESIVE BONDS
USING NUCLEAR MAGNETIC RESONANCE

George A. Matzkanin, A. De Los Santos and J.D. King
Southwest Research Institute
San Antonio, Texas

INTRODUCTION

Nuclear Magnetic Resonance (NMR) is currently being investigated and developed for the nondestructive evaluation (NDE) and characterization of polymer-based adhesively bonded structures such as organic matrix composites. NMR is sensitive to molecular motions and structural changes and can be used to obtain both qualitative and quantitative information on the dynamic environment in which molecules are located. In particular, certain characteristics of NMR signals can provide information on 1) the presence of atoms in different physical states; 2) the type and strengths of interactions between atoms of both the same species and different species; 3) changes in molecular structure and intermolecular binding; and 4) transport (diffusion) phenomena. For application to adhesives and adhesively bonded structures, NMR has been used to measure absorbed moisture and distinguish moisture in different binding states, determine aging and environmental degradation, and characterize degree of cure and modulus variations[1]. Instrumentation approaches have been developed for practical application of NMR to the nondestructive inspection of structures, such as composites. These approaches are based on the use of U-shaped magnets and flat detection coils to allow measurements to be made from a single surface. With suitable control of the magnetic field gradients, these one-sided NMR approaches allow localized measurements which can be used to map out spatially varying quantities such as moisture gradients and material inhomogeneities.

In the next section, a brief discussion will be presented of the NMR technique, followed by experimental results obtained on several adhesives, and descriptions of NMR instrumentation systems which have been developed for practical NDE applications.

TECHNICAL BACKGROUND OF NMR

Nuclear magnetic resonance (NMR) is a branch of spectroscopy based on the interaction between nuclear magnetic dipole moments and a magnetic field. The term "resonance" is used because a natural frequency of the magnetic system, namely, the frequency of gyroscopic precession of the magnetic moment in an applied static magnetic field, is the quantity detected. Typically, the resonance frequency falls in the radio-frequency (RF) region of the electromagnetic spectrum. To implement the NMR method, a static magnetic field is applied to the specimen to polarize the magnetic dipole system and resonance detection is accomplished by coupling a suitable electromagnetic field to the specimen by means of an

RF induction coil. A block diagram of a typical pulsed NMR measurement system is shown in Figure 1. RF pulses of the proper frequency and intensity to produce NMR are applied to the sample coil through the coupling network. The sample coil also senses the NMR response which is connected through the coupling network to the receiver where it is amplified and demodulated. Although NMR has been utilized as an investigative tool for many years in physics and chemistry laboratories, only recently has it been seriously considered for NDE of materials[2].
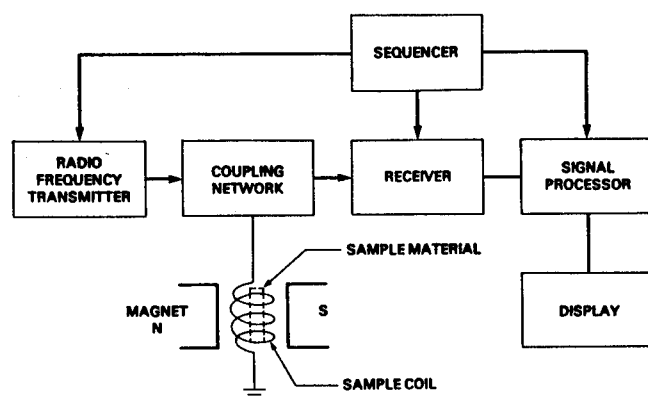
Figure 1. Block Diagram of a Typical Pulsed NMR System

Application of NMR to polymers involves measurement of the hydrogen nucleus (proton) NMR signal. Fortunately, the proton NMR signal is very strong and easily measured. Much of the physical and chemical information available through the use of NMR is associated with the relaxation characteristics of the nuclear magnetic moments, which can be measured using pulsed NMR techniques. The energy exchange between nuclear moments and the surrounding lattice is characterized by the spin-lattice relaxation time, T_1, while the energy exchange among nuclear magnetic moments is described by the spin-spin relaxation time, T_2. These relaxation times are very sensitive to molecular motions and structural changes and can be used to provide both qualitative and quantitative information on the dynamic environment in which the nuclei are located.

Although the majority of work thus far on composites and polymers has involved application of NMR to the measurement and characterization of moisture, other NDE problem areas which NMR is capable of addressing include:

o Environmental degradation and aging

o Incomplete cure

o Modulus variations

o Process control - degree of cure; validation of materials; resin impregnation; plasticizers

EXPERIMENTAL APPROACH

NMR measurements on adhesives were made using a laboratory NMR system operating at a frequency of 27 MHz. The samples were put

into 5 cm (2 in.)-diameter glass vials and placed into a detection coil in the gap of an electromagnet. Parameters measured for the various samples included the free induction decay (FID), the spin-lattice relaxation time, T_1, and the spin-spin relaxation time, T_2. For most of the samples, multiple relaxation times were observed. Processing of the data to obtain the various time constant components and other parameters of interest was done on an HP1000 computer. For measuring the amount of moisture absorbed into hydrogen-bearing materials, such as composites and polymers, a common NMR method utilized is based on determining the voltage amplitude of the hydrogen FID signal at two selected points along the decay curve. A ratio of these amplitudes generally correlates well with moisture for solid materials. However, for viscous materials, such as uncured resins and adhesives, the spin-spin relaxation time, T_2, is relatively long so that an FID ratio measurement as described above would have low sensitivity

to moisture variations. In this case, an NMR pulse sequence which produces a spin echo proves useful since the ratio of the echo amplitude to the peak of the FID signal correlates well with moisture.

RESULTS

Adhesive Scrim

NMR measurements were made on five samples of adhesive scrim. The samples all had the same manufacture date but three underwent moisture conditioning prior to NMR measurement. One sample (AD) was dried in a desicant for 24 hours, and two samples (A24 and A48) were exposed to approximately 100 percent relative humidity at room temperature for 24 hours and 48 hours, respectively. Of the two unconditioned samples, (AR) was allowed to age at room temperature for 30 days, and the fifth sample (AC) was an unconditioned control. NMR results obtained are summarized in Table 1.

TABLE 1

ADHESIVE SCRIM-NMR TEST RESULTS

SAMPLE	CONDITION	T_{11}(msec)	T_{12}(msec)
AC	Control	121	243
AD	Dried 24 hours with Dririte	138	399
A24	Exposed to $\approx$ 100 percent RH, RT for 24 hours	136	399
A48	Exposed to $\approx$ 100 percent RH, RT for 48 hours	118	370
AR	As received	109	292
AR30	After 30 day aging	140	481

As can be seen, the long
components of the spin-lattice
relaxation times, T_{12}, for the
conditioned samples (AD, A24,
and A48) were considerably
longer than the comparable times
for the samples not exposed to
moisture conditioning (AR and
AC). Also, the T_{12} time
constant component increased
substantially with aging time
for sample AR.

Film Adhesives

NMR measurements were performed
on three samples of each of two
film adhesives, FA-1 and FA-2.
One sample of each adhesive type
was measured at room temperature
upon removal of the material
from a sealed container. Two
samples of FA-1 were humidified
for periods of 15 and 40 hours
at 80% R.H. to provide absorbed
moisture levels of 0.23% and
0.82%, respectively. Two
samples of FA-2 were humidified
for periods of 22 and 118 hours
at 80% R.H. to provide moisture
levels of 0.98% and 1.28%,
respectively. Because of the
relatively long T_2 relaxation
time for the film adhesives (T_2
$\approx$300 µs), a two-pulse sequence
was used to produce spin echoes
and the echo-to-FID amplitude
ratios were obtained. Results
obtained for the two film
adhesives are shown in Figures 2
and 3. As can be seen, for both
adhesives, the NMR measurements
correlate well with moisture
content and provide a potential
approach for nondestructive
determination of the water
content.

Resin

Neat resin samples for NMR
measurement were prepared by
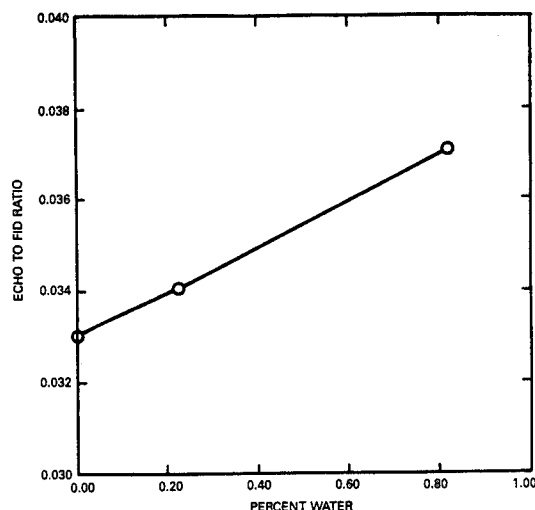adding water directly to the

Figure 2. FA-1 Film Adhesive
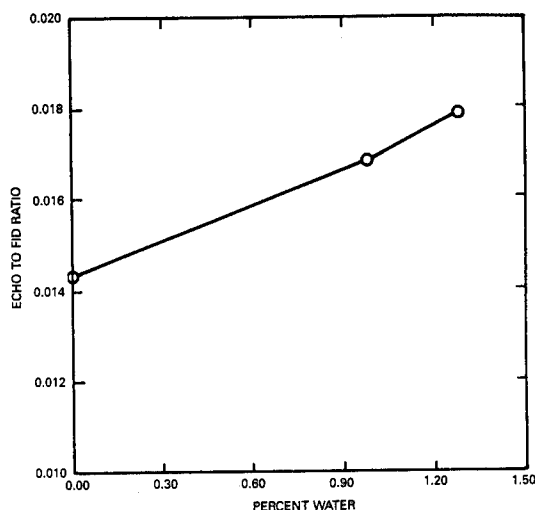Echo to FID Ratio vs Percent
Water

Figure 3. FA-2 Film Adhesive
Echo to FID Ratio vs Percent
Water

resin to produce moisture percentage levels ranging from 1% to 10%.

In the case of the uncured resin, a distinct moisture component is not observed in the free induction decay because of the long spin-spin relaxation time for this viscous material. However, it was found that the spin-lattice relaxation time, T_1, for the neat resin with no added water was about 50 ms compared with resin containing added water which had a T_1 component of about 50 ms for the resin plus a T_1 component of approximately 1-2 s for the water in the resin. Therefore, the free induction decay difference signal obtained for two different pulse repetition rates contains a substantial water signal component whereas the resin contribution cancels out. A plot of the FID difference signal versus percent water in uncured resin is given in Figure 4.

After the resin samples were cured, it was noticed that the resin with increased water added before cure became considerably more brittle. Although the NMR free induction decay signal did not show a distinct moisture component for the cured resin, relative measurement of the signal amplitude at various times during the free induction decay can be used as a determination of the amount of amorphous to crystalline character. The free induction decay ratio measured at times of 23.5 µs and 70 µs vs percent water added before cure is shown in Figure 5. The decrease in this ratio which implies decreasing amorphous character correlates well with the increased brittleness observed for the cured resin samples with greater amounts of added water.

Figure 5. Free Induction Decay Ratio vs Percent Water Added Before Cure for Cured Resin

ONE-SIDED NMR DETECTION
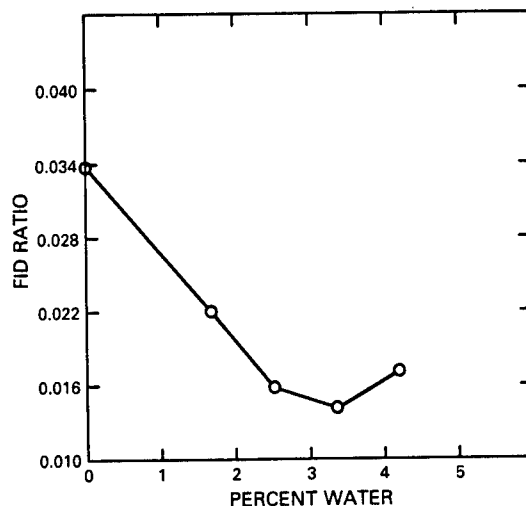
Developments pioneered at Southwest Research Institute have demonstrated the feasibil-

Figure 4. Free Induction Decay Difference vs Percent Water in Uncured Resin

401

ity of NMR measurements on materials external to the RF coil and the magnet structure. The basic configuration utilizes a U-shaped magnet and a flat spiral-coaxial RF coil as shown schematically in Figure 6. The U-shaped magnet provides a static magnetic field H_0 which extends from one pole to the other as shown by the dashed lines. The RF coil provides a field H_1 which is perpendicular to the plane of the coil. In that region where the frequency and static field intensity have the proper relationship an NMR response will be detected by the coil. By varying the magnetic field strength, the sensitive region can be moved closer to, or farther away from, the magnet, thus providing a means for obtaining NMR information as a function of depth. Based on this approach a fieldworthy NMR moisture measurement system for nondestructively measuring the amount of moisture in reinforced concrete bridge decks was designed and fabricated[3]. This system utilizes a U-shaped magnet and a flat RF coil to obtain NMR signals at depths down to 9.5 cm from the top surface of a bridge deck. Profiles of the moisture gradient in bridge decks have been measured by using magnetic field gradients to obtain spatially localized NMR measurements with a resolution of approximately 3mm[4].
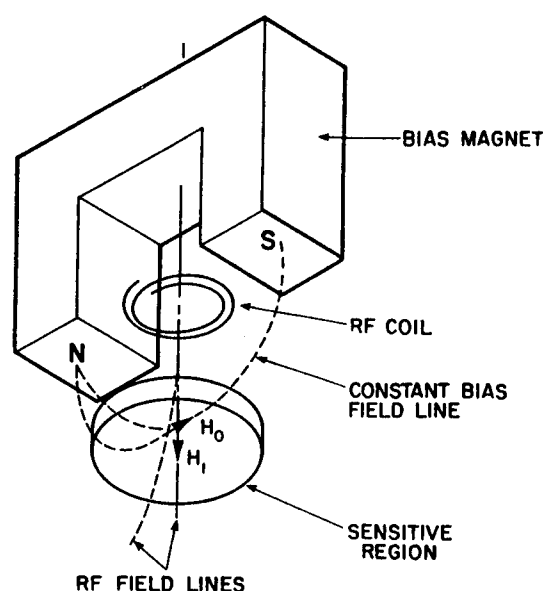
Figure 6. Schematic Illustration of One-Sided NMR Detection for a Specimen External to the RF Coil and Magnet Structure

To achieve the measurement depth required for measuring moisture in concrete bridge decks, the NMR sensor for the inspection system described above needed to be rather large (about 272 kg). However, by using recently developed rare-earth material permanent magnet technology, a considerably smaller, hand-portable NMR sensor (about 7 kg) has been designed for near-surface (e.g. depths of 3 mm) measurements on composite or plastic materials and structures.

CONCLUSIONS

Nuclear magnetic resonance methods provide the opportunity for making important NDE measurements in polymer based materials such as adhesives and composites that are difficult and many time impossible by other sensory techniques.

Laboratory studies have demonstrated the capability of NMR to quantitatively determine the amount of absorbed moisture in adhesives and resins, both cured and uncured. In addition, certain features of the NMR signals may be useful in providing information on moisture in different physical states within the material. While the measurement of moisture is the most obvious application of NMR for NDE of adhesives and adhesively bonded composites, other areas which NMR is capable of addressing, and for which limited results have been obtained, include: environmental degradation and aging, incomplete cure, modulus variations, and process control. Although most available NMR apparatus has been intended for use in a laboratory environment, recent instrumentation developments at Southwest Research Institute, in particular one-sided NMR detection, have removed limitations on sample size and configuration, operational restraints and apparatus size, and expanded the capability of NMR for practical NDE applications outside the laboratory.

REFERENCES

1. Matzkanin, G.A., "Applications of Nuclear Magnetic Resonance to the NDE of Composites," Proc. 14th Symposium on NDE, pp. 270-286, San Antonio, Texas, April 19-21, 1983.

2. King, J.D., Rollwitz, W.L., and Matzkanin, G.A., "Magnetic Resonance Methods for NDE," Proc. 12th Symposium on NDE, pp. 138-149, San Antonio, Texas, April 24-26, 1979.

3. Matzkanin, G.A., De Los Santos, A., and Whiting, D.A., "Determination of Moisture Levels in Structural Concrete Using Pulsed NMR," FHWA/RD-82/008, April 1982.

4. Matzkanin, G.A., "Application of Spatially Localized NMR to Nondestructive Evaluation," Proc. of the 11th World Conference on NDT, pp. 1607-1614, Las Vegas, Nevada, November 1985.

PROGRESS IN THE QUANTITATIVE NONDESTRUCTIVE EVALUATION
OF ADHESIVE BOND PERFORMANCE

Jonathan H. Gosse
Materials and Processes
Boeing Aerospace Company

Robert L. Hause
Quality Assurance
Boeing Aerospace Company

Paul B.Y. Mori
Materials and Processes
Boeing Aerospace Company

INTRODUCTION

Performance determination of adhesively bonded systems is a subject of intense interest to both researchers and designers. Attempts to predict adhesive bond performance have mainly focused on nondestructively identifying gross anomalies such as voids or unbonded regions and either correlating these features with destructively determined mechanical performance or using these features in an analytical analysis using concepts such as fracture mechanics or stress concentration. Recently, unpublished work has been conducted at the University of Idaho involving the correlation of damped acoustic responses to mechanical performance. An instrumented hammer is used to impart an impulse to the adhesively bonded joint and the fourier transform of the reflected (or trans- mitted) acoustic signal is used to determine global damping as a function of a given frequency or frequencies. The damping characteristics are correlated to destructively determined strength.

It is well known that adhesively bonded systems can exhibit variability in mechanical performance even when the systems under evaluation are fabricated identically and appear to lack major anomalies such as those determined by through-transmission ultrasonics (voids, disbonds, etc.). Obviously, the ability to nondestructively determine adhesive bond performance is needed if these systems are to be utilized in a load bearing capacity.

The nondestructive evaluation of any materials system is most successful when the physics of

the materials in the system are understood in terms of their interaction with each other during fabrication and under service loading conditions. The anatomy of a bonded system consists of several material subsystems. The work described in this paper involves a single lap shear bonded configuration (Figure 1a). The anatomy of the bonded system (Figure 1b) consists of the metal adherends, the surface treatment (metal oxide), the low viscosity primer, and finally the adhesive itself (in this paper scrim supported). The metal adherend surface is surface treated to develop an oxide on the surface of the metal. The low viscosity primer (of similar chemical composition to the adhesive) is applied and allowed to penetrate the porous oxide. Finally, the higher viscosity adhesive chemically bonds to the primer. Stress is theoretically transferred from one adherend to another through mechanical interlock mechanisms and chemical bonds.

The approach used in the work presented in this paper was first to select an adhesively bonded system for evaluation and understand the anatomy of the bonded region. Once the system was selected only the specimens lacking major anomalies (as determined by through-transmission ultrasonics) were saved for evaluation. Once selected, the bonded systems were scanned with an applicable instrumental nondestructive evaluation (NDE) technique. The instrumental NDE technique identifies a material parameter which can be utilized in analytical analysis to determine mechanical performance. The instrumental NDE technique used in this study was high frequency (MHz) ultrasonic resonance. The resonant response of the bonded area is mapped through the thickness over the surface of the bonded area (normal to the load axis) with a focused ultrasonic transducer. The scanning was continuous with a resolution of approximately 0.02-0.05 square inches.

Once scanned and analyzed, the NDE output is used in closed form analytical expressions which determine the shear and normal stress distributions in the adhesive, along with the bond length (1) in the direction of the loading axis.

EXPERIMENTAL

SINGLE LAP SHEAR SPECIMEN FABRICATION

Referring to Figure 1, the single lap shear assembly consisted of Ti-6-4 adherends with a nominal thickness of 0.05 inches. The adherends were chromic acid anodized to develop the surface oxide. The low viscosity primer used was an epoxy based system (EC 3917, from 3M). The adhesive was a scrim reinforced toughened epoxy (AF-191, from 3M). The toughening of the brittle epoxy is accomplished through the addition of an elastomeric phase. The lap shear assemblies are fabricated in sheets so that five single lap shear specimens are fabricated simultaneously (see Figure 2). The sheet assembly is layed up on a steel tool to insure proper bondline geometry. The tool with the assembly is then vacuum bagged for autoclave cure per Boeing Materials Specifications (BMS 5-104). It should be noted that the process yields slightly different heating and cooling rates for each side of the bonded joint. In other words, the top face of the bonded region will see a thermal history slightly different than the opposite side residing against the steel tool.

After fabrication, the single lap shear specimens are separated, scanned, and subsequently failed in tension in accordance with Boeing Support Specifications (BSS 7202).

ULTRASONIC RESONANCE SCANNING

The technique employed for ultrasonic resonance examination involves the application of an incident burst of sine wave ultrasonic energy to a test part such that the burst width, or time duration, exceeds the round trip transit time of sound through the test part. Methods of extracting material properties information then may be carried out in various ways. One method employed is to sweep the acoustic frequency through a wide range of frequencies (such as 2-10 MHz) and observe the results of constructive/destructive interference as established between the material's parallel surfaces. Another method, especially suited to "ringing" metallic materials, is to apply the sine wave burst around the materials thickness resonance point, and observing the ring-down signal after the drive energy has ceased. This method is well suited to observing the damping effects of energy absorbing materials which are acoustically coupled to the

test materials back surface.

The test equipment employed is a modified Holosonics 200 acoustic holography unit, which is designed specifically for sine burst operation. The original fixed frequency tunable signal source was replaced with a Hewlett Packard 3312A function generator.

The pulse-echo output signal is recorded and processed by a Dynacon Systems Ultrasonic Data Recording and Processing System (UDRPS) which digitizes and records the signal along with C-scan coordinate information. The UDRPS, which consists primarily of a Hewlett Packard computer, an ANALOGIC Array processor and a Ramtek 9465 color display system, then reconstructs a high resolution color video display of the recorded C-scan using a rainbow color format with 255 level color resolution.

In addition to amplitude information, point-by-point x-y plots of amplitude vs. frequency may be made to observe frequency shifts resulting from material properties variations.

DISCUSSION OF RESULTS

The justification for choosing the Ultrasonic Resonant technique for the instrumental NDE of the bonded systems lies in the technique's potential capability to detect changes in adhesive bond stiffness, through-the-thickness, anywhere over the area of the bonded region. Provided that nondestructively determined information regarding the changes in the elastic modulus of the adhesive is available, then it was hypothesized that an approximate closed form solution for adhesive stress distribution could be utilized (such as those available in the literature (1)) to predict the mechanical performance of these "flawless" bonded assemblies.

Five single lap shear specimens were fabricated as described previously. The specimens were scanned at approximately 3 MHz in a continuous mode. Both sides of the bonded region were scanned and examples of the results are shown in Figures 3 through 5. Upon inspection of the five specimens (both sides) it was observed that one side of each specimen was significantly more acoustically attenuative than the opposite

side. For each specimen, the same side was consistently more attenuative than the other. Recalling the fact that each face of the bonded area saw a slightly different thermal history during fabrication suggests the possibility of a nonuniform distribution of the phases within the cured adhesive system. If this assumption is realistic, then it may be possible that micro-regions within the adhesive in contact with the primed adherend could demonstrate variable acoustic impedances. For example, an elastomeric rich micro-region would most likely produce a relatively high interfacial acoustic impedance with respect to an elastomeric poor micro-region. Taking into account the relatively low power used to impart the resonant response through-the-thickness of the bonded area, it is likely that the order in which the imparting signal sees the various acoustic impedance interfaces may well determine the strength of the resonant response. Using techniques available from the field of Theoretical Acoustics (2), it can be shown that the above assumptions are reasonable.

It is well established that the shear and normal (peel) stresses in a single lap shear configuration exist at the joint edges (1). With this in mind, the Ultrasonic Resonant scans of each specimen were assessed with respect to the joint edges. With our current hypothesis to describe signal attenuation, it was felt that only the lightly attenuated face need be considered since it is this face which will bear a majority of the load (due to stiffness considerations). At this point in time it was desired only to determine whether or not the approach used in this paper should be continued. If so, then a more complete assessment of the entire bonded assembly would be warranted. It should be noted that nearly all five specimens failed in such a manner that the lightly attenuated face failed in the oxide, giving preliminary credence to our earlier assumptions. By examining the acoustic response of the joint edge regions only, we assumed a redistribution of stress at the edge as a function of the degree of attenuation and percent area covered of each section of the acoustic response. The response was roughly divided into three levels, blue (lightly attenuated), yellow (attenuated),

and red (highly attenuated). Figure 3 shows the Resonant response over the bonded region of sample #1. Although the photograph shown is not in color, the highly attenuated region toward the center of the edge of the joint is evident. Figure 4 illustrates the same type of information for sample #4 only with a center region lightly damped. Figure 5 shows very little, if any, attentuation across the joint edge (sample #3). By determining the failure stresses at the joint edge for a well bonded system (as determined by 3M) knockdowns from these levels can be established by measuring the percent attenuated area at the joint edge and assigning a relative modulus factor as a function of the attenuation. Blue required no knockdown, yellow resulted in reduction in load carrying capacity of 1/3. Red resulted in a reduc-

tion in load carrying capacity of 2/3. Using either the principal maximum shear stress or the principal normal stress (3) for the well bonded case as the condition to knockdown, the following allowables were determined.

For a nominal adherend thickness of 0.05 inches and a failure load of 2500 lbs (and all other elastic constants of the components available from 3M) the maximum principal shear stress was determined to be 17,595 psi at the joint edge. The principal normal stress at the edge was found to be 26,665 psi.

In this paper the average adherend thickness along with the destructively determined failure loads were used to determine the average joint edge principal failure stresses. These values were compared to the knockdown values from the Resonant scans. The results are shown in Table 1.

TABLE 1. RESULTS

Sample Number	Calculated Principal Maximum Shear Stress (psi)	Maximum Principal Shear Stress (NDE Knockdown) (psi)	Calculated Principal Normal Stress (psi)	Principal Normal Stress (NDE Knockdown) (psi)
1	13,306	10,711	20,323	16,244
2	14,550	14,548	22,184	22,064
3	15,096	17,582	23,003	26,665
4	14,923	14,197	22,752	21,598
5	14,919	17,582	22,747	26,665

CONCLUSIONS

As can be seen from Table 1, there appears to be some agreement between both the calculated and knockdown stress values using the approach presented in this paper. Much remains to be accomplished to conduct a complete analysis, however the results of this paper are encouraging. With reliable knockdown values for the pricipal stresses it may well be possible to calculate the failure load reliably. Most likely a finite element analysis for stress determination will be necessary for better results.

REFERENCES

1. "The Stresses in Cemented Joints", by M. Goland and E. Reissner, Journal of Applied Mechanics, dated March, 1944.
2. "Stress Waves in Solids", by H. Kolsky, Dover Publications, dated 1963.
3. "Introduction to Mechanics of Solids", by Egor P. Popov, Prentice-Hall Inc., dated 1968.
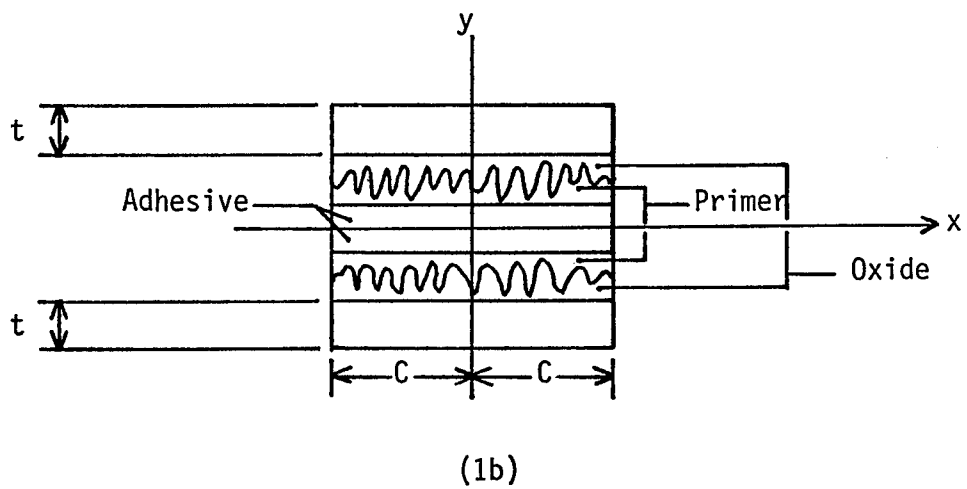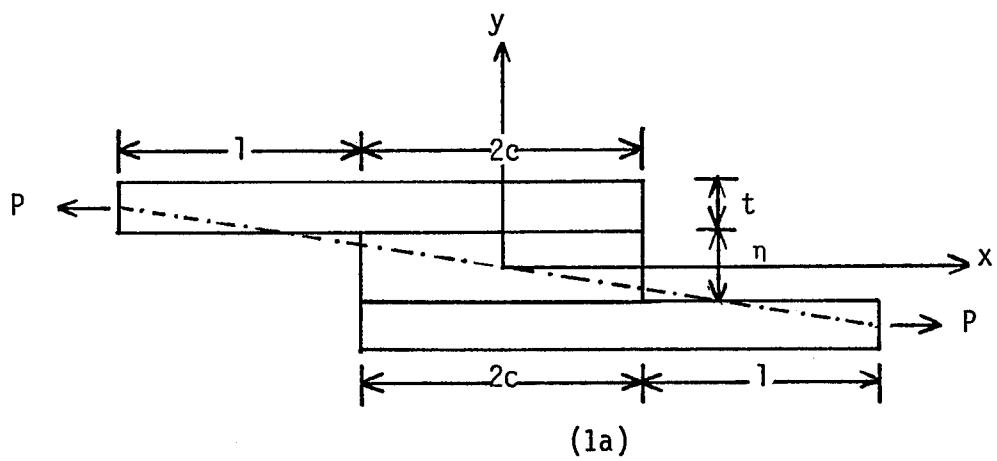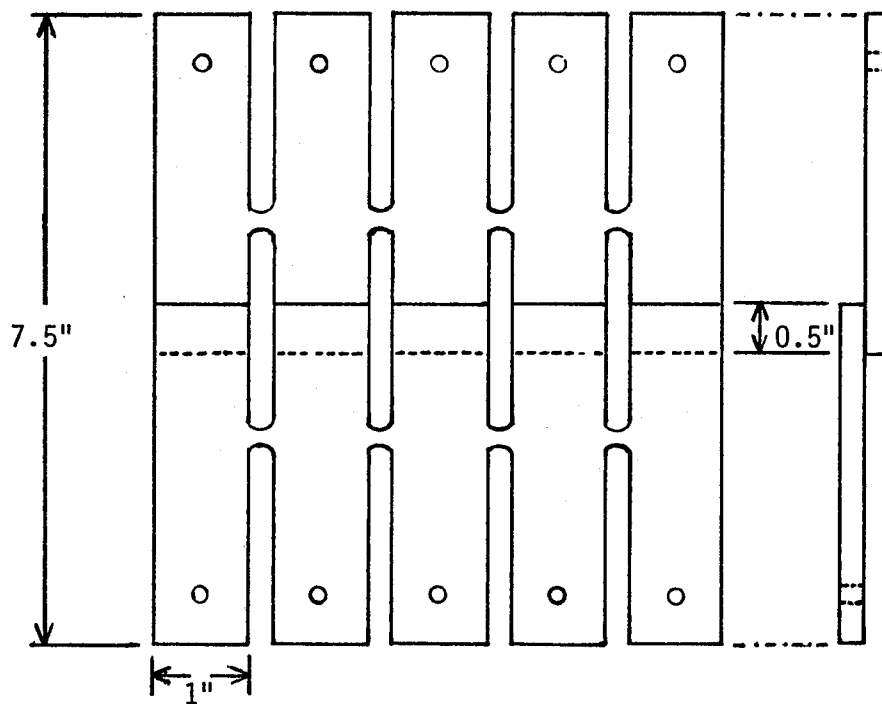
Figure 1. Single Cap Shear Configuration
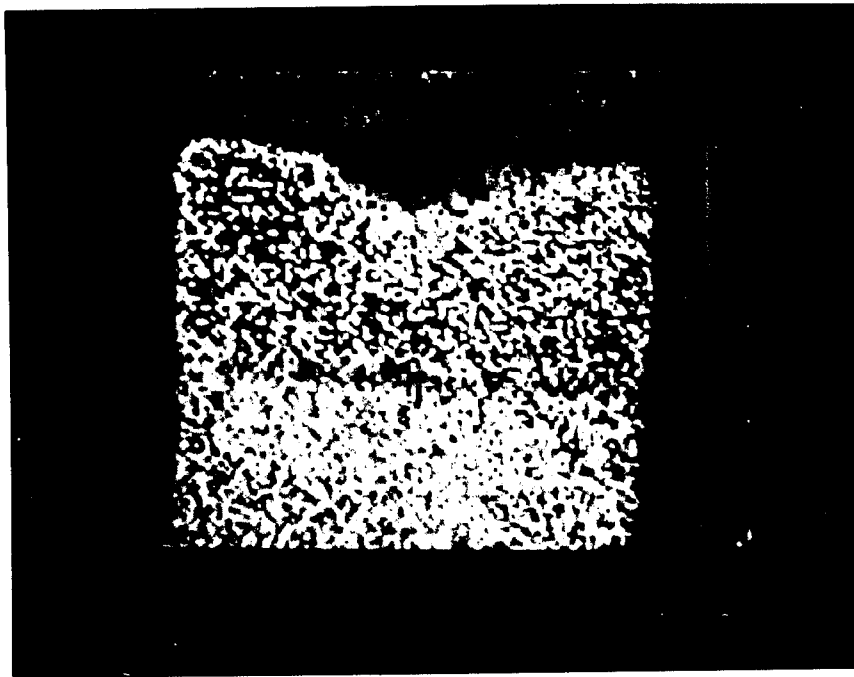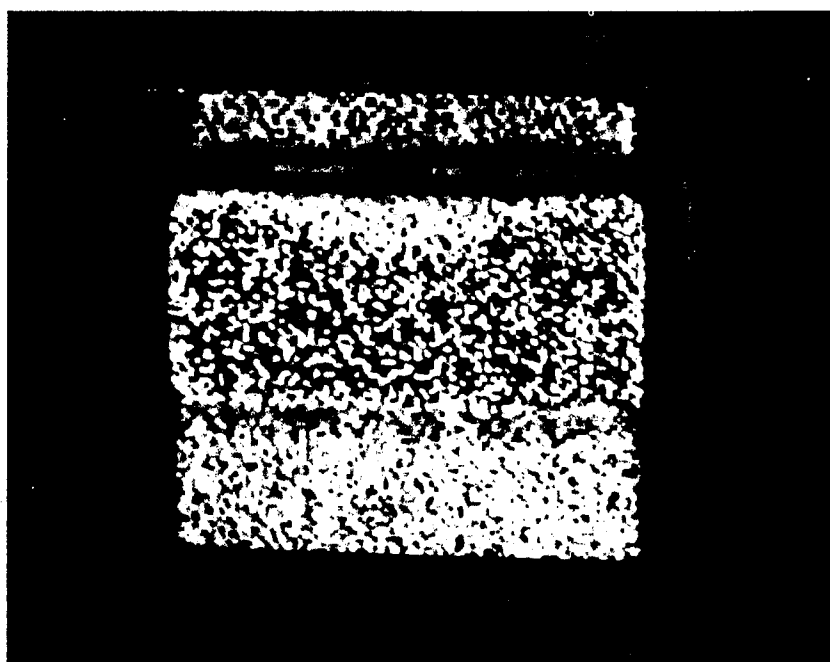
Figure 2. Finger Panel Assembly

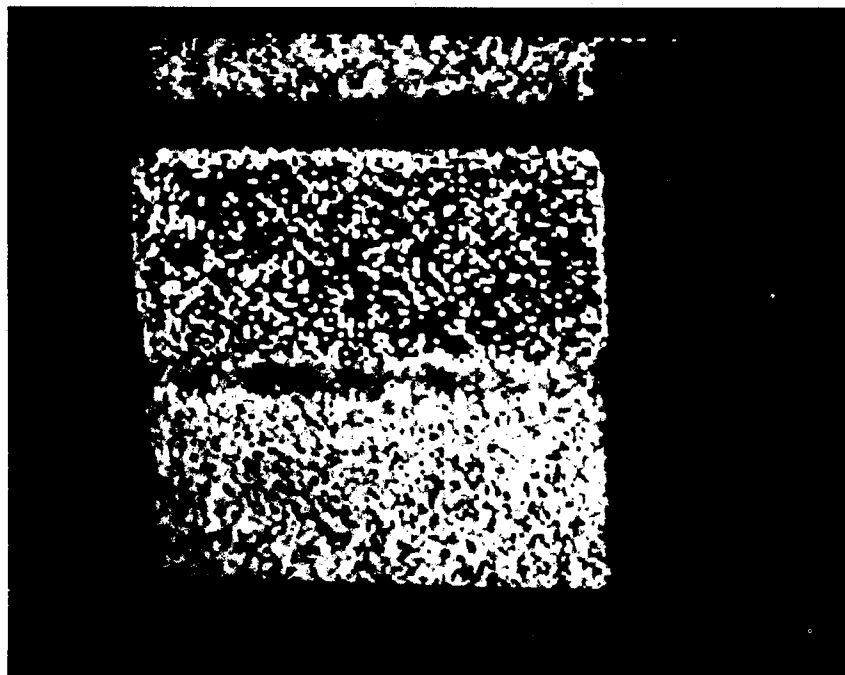Figure 3. Sample #1

413

Figure 4. Sample #4

Figure 5.   Sample #3

THE MTL BOND INTEGRITY NDE PROGRAM

PAUL G. KENNY
MATERIALS TECHNOLOGY LABORATORY
ATTN: SLCMT-MSI-NE
WATERTOWN, MA. 02172-0001
(617) 923-5241

ABSTRACT

This paper discusses the Bond Integrity NDE (Nondestructive Evaluation) Program being implemented by the NDE Branch of the Materials Technology Laboratory (MTL) located in Watertown, MA. After a brief introduction, the role of NDE in the adhesive bonding process will be described. The program plan and the status of it's various elements will then be discussed, followed by brief comments regarding future thrusts.

INTRODUCTION

There is an increased emphasis on structural adhesive bonding in the Army. The stimulus occured when General Thompson in 1986 recommended a technology thrust in the area. As a result, MTL has been designated lead laboratory for the overall effort to address adhesive bonding problems in the Army, and the NDE Branch at MTL has developed a Bond Integrity NDE Program to support this effort.

One of the root causes of adhesive bonding problems is the failure to perform bonding operations properly. To address this, the program goal is to develop NDE techniques to assure adhesive bond integrity.

The approach is two-fold. Existing technology must be better implemented and the state-of-the-art must be improved.

There are a number of project elements which are being undertaken in the program. These elements will be performed both in-house and under contract. Some of the work being performed includes:
- bibliographic searches and a state-of-the-art report
- evaluating currently available bond testing equipment
- bondline characterization
- ultrasonic signal processing
- a Workshop on Bond Integrity NDE

This paper will describe these and other projects and how they fit together in a coherent study on the NDE of adhesives.

DISCUSSION

Background

The successful application of adhesive bonding for joining materials in the aerospace and aircraft industries has resulted in adhesively bonded structures being utilized in the Army as primary and secondary components where strength and performance are

critical. The application of adhesive bonding has resulted in new designs that improve fatigue characteristics and change the failure modes of these structures.

The use of structural adhesives require the adoption of intricate process control measures which include the careful selection of materials and adhesives and strict control of bonding conditions to insure high integrity of bonded structures. Faulty execution of the bonding process is a distinct possibility because the human element is more involved than in other metal fabrication methods. This necessitates that the user apply stringent acceptance tests that can only be accomplished through the nondestructive testing of all bonded areas.

Adhesive Bonding and NDE

The ultimate aim of any nondestructive test is the correlation of some parameter measurable by nondestructive methods with the failure property of interest. This requires a decision as to what is the critical failure property. The answer is complex in the case of bonded joints. Bond quality is affected by both the cohesion of the cured adhesive layer and by the quality of adhesion between the adhesive and bonding surface. Low adhesive layer cohesion may be attributed to deteriation of the adhesive, stress concentrations, shrinkage and serious flaws in the adhesive. Poor adhesion between adhesive and bonding surface may result from air, incorrect adhesive concentration, inadequate adhesive concentration and chemical reactions.

No nondestructive test parameter has yet been found that will correlate with the intermolecular forces between the adhesive layer and the bonded surface after the bond has been created. It appears the quality control of adhesion is then only possible prior to the application of uncured adhesive materials. Efforts are thus being concentrated on characterizing a surface as suitable or unsuitable for bonding. This is because after an optimum surface treatment, the adhesion is much stronger than the strongest cured adhesive layer. If the adhesive quality is kept under control, measurement of the cohesive quality of the adhesive should yield an indication of bond strength. In fact, some cohesive quality variations can be related to physical properties measurable by nondestructive test methods.

Another issue is in-service degradation. Conventional NDT has been relatively successful if voids and disbonds are generated and the bond layer is accessible for examination. It is very important then that NDT be considered during the component design phase.

To address these issues, the program objectives include (1) to establish and improve NDE techniques to assure adhesive bond

integrity in Army structures, (2) to provide more effective production control over process variables and product uniformity associated with adhesively bonded structures and (3) to implement the above via the generation of procedural documentation for quality verification.

Program Plan

Existing technology will be exploited and implemented to obtain more reliable detection and definition of disbonds and delaminations in Army structures. The Nondestructive Testing Information Analysis Center (NTIAC) and Plastics Technical Evaluation Center (PLASTEC) will be used to achieve this.

Several efforts will be conducted to develop NDE techniques to quantitatively measure the adhesive quality of the cured adhesive layer and quality of adhesion between the adhesive and bonding surfaces. Work to achieve this end will be performed both in-house and under contract.

What follows is a brief discussion of each of the projects currently being undertaken and the status of each. Following that, a description of future thrusts will occur. Special attention should be given to the workshop, which is a direct follow-on to the present conference.

PROJECTS/STATUS

WORKSHOP ON NDE OF ADHESIVE BOND INTEGRITY-The proposed workshop on NDE will extend the topic of NDE beyond the present symposium and will focus on summarizing the current state-of-the-art regarding NDE of adhesive bond integrity and determining what needs to be done to expand the state-of-the-art for practical applications. The proposed Workshop is scheduled for April of 1988 in Orlando, FL. It will be run in conjunction with the American Society for Nondestructive Testing (ASNT) spring Conference during the week of 11-15 April. Several sessions of the ASNT conference will address topics relevant to the Workshop. These sessions will compliment the Workshop by providing added input to Workshop participants. The Workshop, however, will operate separately from the ASNT Conference.

Specifically, the Workshop objectives are to:
-identify, summarize and document current state-of-the-art on the NDE of adhesive bond integrity.
-identify present and future requirements for the NDE of adhesive bond integrity
-identify new and emerging scientific and engineering opportunities for NDE of adhesive bond integrity
-endeavor to agree on approaches to improve NDE technology for adhesive bond integrity (i.e. develop a plan of attack)
- foster communication

among workshop participants.

Any inquiries regarding the Workshop may be addressed to the author.

EVALUATION OF BOND TESTING EQUIPMENT FOR INSPECTION OF ARMY ADVANCED COMPOSITE AIRFRAME STRUCTURES-The objective of this project is to evaluate bond testing equipment presently existing and to obtain more reliable detection of disbonds and delaminations in Army adhesively bonded composite airframe structures. This project expands the scope of of an Air Force project which evaluates bond testing equipment, but uses as specimens standard reference samples. The present project uses real specimens taken from aircraft components.

Preliminary results of the Air Force effort indicate that one type of bond testing equipment may be better than another, depending on the type of bonded specimen. It is hoped that these results will carry over to the adhesive bonds encountered on Army materiel.

NDE OF ADHESIVE BOND INTEGRITY: STATE-OF-THE-ART-REPORT-Several failures of critical parts in aircraft and other applications have raised concerns that current technology may not have been used properly in design, manufacture and quality control or that new technology may be needed. In order to insure the reliability and integrity of bonded joints, nondestructive evaluation is required to determine the quality of bonded joints. The state-of-the-art-report will review and document the present status of nondestructive evaluation of adhesive bonds in a variety of structures, including organic matrix composites, metal matrix composites, thermoplastic composites and metal-metal joints. The report will include information on characteristics of adhesive bonds, bonding processes and bond quality, failure mechanisms, inspection needs during fabrication and in-service, currently available NDE methods and the status of quantitative NDE.

Various databases will be searched and the literature will be reviewed and the most relevant documents will be obtained. The report will be written from this and from information obtained from persons currently working in the field of NDE of adhesives.

Since the timing of this report is concurrent with the Workshop, it is expected that the report and Workshop will compliment one another and information will be shared between the two efforts.

USING LOW VELOCITY IMPACT FOR QUALITY ASSURANCE OF ADHESIVELY BONDED JOINTS-The principle goal of this research effort is the development of a reliable method for assessing the structural integrity of bonded composite structures. The approach includes a thorough investigation of

interface properties with particular emphasis on structures where there is limited adhesion between adhesive and adherend.

While many nondestructive testing techniques have proven useful for a wide variety of cohesive defects, there is not now available a reliable method for inspecting bonded joints for defects in adhesion. Surface cleanliness is critical to bond strength. Even in minute quantities, the presence of contaminants on the surface of a part can adversely affect bond integrity. Conventional nondestructive test methods are not capable of detecting these weak bonds.

The novel approach to this project is based on the propagation of a high amplitude tensile stress wave across the adhesive-adherend interface. The approach is not totally nondestructive, but rather functions along the lines of a localized proof test. Tensile stresses will be generated at the adhesive-adherend interface with an impact sufficient enough to produce failure in a weak joint while, it is hoped, not affect the integrity of a well bonded structure. This includes the avoidance of impact damage. If successful, the test procedure would be to impact a bonded structure at several points along it's surface with sufficient amplitude to produce a local tensile proof stress at the bondline. Since debonds would be created in the weakly bonded regions while well bonded regions would be

left intact, an ultrasonic C-scan could then be used to detect the debond regions. The main task is then to determine the appropriate stress levels, if they exist, for various bonding scenarios (metal-metal, metal-honeycomb etc.).

NDE OF ADHESIVE BONDS-This is a general project at this point. The objective of this work will be to evaluate various NDE techniques applied to adhesive bond inspection. The effort will be centered on laser based techniques and perhaps high frequency ultrasound.

TEST SPECIMENS-Aluminum-aluminum lap shear specimens are being procured for ultrasonic evaluation of surface finish variations. These variations include (1) using as-recieved aluminum, (2) using the prescribed cleaning and etching, (3) over-etching and (4) deliberate contamination. These specimens will be evaluated using ultrasonic methods described below, followed by tensile tests which will be monitored by acoustic emission.

ULTRASONIC DATA AQUISITION EQUIPMENT PROCURED-Digital analyzers have been procured which are capable of capturing, storing and manipulating the short duration signals associated with thin bondlines. An array processor is being procured which will allow many more calculations to be done in real-time. This will be very powerful in extracting more information

which can then be displayed via the NDE methods to be described next.

DEVELOP NDE TECHNIQUES- Available in-house are systems for ultrasonic velocity and defect scans (both in C-scan format). Development work has led to a B-scan capability. By having the B-scan capability, which shows a slice through a specimen (cross-section), a visualization of the bondline is arrived at. Combining these capabilities with the equipment being procured will allow more feature scans to be displayed. In other words, more information will be able to be extracted from the bondline.

FUTURE THRUSTS

Many of the efforts discussed are multi-year taskings. Other programs will be used to broaden the scope of the present one. The Small Business Innovative Research (SBIR) program is an excellent mechanism for encouraging innovative and imaginative research. The Army Research Office (ARO) Summer Faculty Program allows for the hire of faculty from universities while the schools are on summer break. Topics for these programs will probably center on spectroscopic and/or X-ray methods to evaluate bond integrity.

It might be noted at this time that the Sagamore 1988 summer conference will focus on adhesive bonding. The role the present program has

in the Sagamore conference is unknown at this time, but it will be significant.

CONCLUSION

Two approaches will be investigated to improve Army bonding:

(1) implement existing technology
(2) develop a bond strength measurement technique.

existing technology will be exploited and implemented to obtain more reliable detection of disbonds and delaminations. A special task will be conducted to evaluate commercially available NDT equipment on aircraft specimens. This task will augment an ongoing Air Force special task with the same goal. A State-of-the-Art-Report on NDE of adhesive bonding will be prepared and a Workshop will be devoted to the subject.

Several efforts will be conducted to develop NDE techniques to quantitatively measure the adhesive quality of the cured adhesive layer and quality of the adhesion between adhesive layer and bonded surfaces. Specimens will be made and several promising ultrasonic spectroscopy and signal analysis techniques for examining the quality of the adhesive will be investigated in-house. A contract has been let to investigate NDE bondline characterization techniques. The Small Business Innovative Research and Army Research Office Summer

Faculty programs will also
be utilized to address the
issue of NDE of adhesive
bonding.

IMPULSE FREQUENCY RESPONSE TECHNIQUE FOR MEASUREMENT

OF DYNAMIC MECHANICAL PROPERTIES OF

ADHESIVELY BONDED JOINTS

T. S. Srivatsan[*]
Department of Mechanical Engineering
University of Akron
Akron, Ohio 44325

Raju Mantena, R. F. Gibson and T. A. Place
Department of Mechanical Engineering
University of Idaho
Moscow, Idaho 83843

T. S. Sudarshan
Materials Modifications Inc.
Falls Church, Virginia 22044

ABSTRACT

Non-destructive analysis through damping capacity measurements were performed to analyze contributions from intrinsic defects caused by improper curing of the adhesive and induced porosity on the performance of adhesively bonded joints. The damping measurements were made using an impulse-frequency response technique. Double-lap adhesively joined specimens were excited in flexural vibration. The specimen response was measured with an eddy current probe. A fast fourier transform analyzer was used for rapid acquisition of data and computation of damping (loss factor) by curve fitting to the frequency response function. Strength of the adhesive joint was determined for the two different types and levels (size and volume) of defects. The damping characteristics was found to correlate well with strength, with strength decreasing and damping increasing with increasing severity of the defect. The micro-mechanisms governing the performance and durability of bonded joints are discussed in terms of the specific role of several concurrent and mutually competitive factors involving curing time, curing temperature, adhesive degassing time, adhesive chemistry and specimen geometry.

1. INTRODUCTION

In recent years, adhesive bonding of metals has engendered considerable interest in the aerospace, transportation and other high technology industries, and has great potential for replacing traditional joining techniques in a growing number of applications. There are several reasons for the application of adhesive bonding:
(1) separation of dissimilar metals to prevent galvanic corrosion,
(2) absorption of vibration from one component to another, and
(3) joining cold rolled or heat sensitive materials.

* formerly with Materials Modifications Inc.

In addition to providing savings in weight, reduced part count, manufacturing cost effectiveness and aerodynamically smooth surfaces adhesive bonding is attractive primarily because it offers considerable advantages that often outweigh their higher cost (1). For example, the transfer of stress occurs over an entire bond area, thereby avoiding stress concentrations that occur with welding, riveting and fastening with screws (2).

Use of adhesive bonding simplifies construction and obviates the harmful effects of elevated temperatures associated with welding and brazing, resulting in improved appearance and reduced weight. In spite of the advantages being manifold, progress in the use of adhesive bonding in primary structures (3) has been painfully slow and hampered by:
  (a) an inability to guarantee that the completed joint is of adequate strength, and
  (b) lack of adequate non-destructive testing procedures without which the reliability of a structure cannot be guaranteed.

An important consideration in the acceptance of an adhesive joint for a particular end use is its durability or permanence. Ideally, the most reliable information on the durability characteristics of a given adhesive and/or adherend-adhesive system need to be developed by subjecting the test sample to conditions comparable to those of the glued product in service. However, such long term tests are impractical. Consequently, greater reliance is being placed on results obtained from short term accelerated tests. Non-destructive test techniques could predict the strength of an adhesive bond. However, this is difficult to achieve, partly because a direct measurement of strength cannot be non-destructive. Hence, it is advantageous to correlate strength with properties such as stiffness, damping and bond area. Recent studies have found the impulse-frequency response technique to be an effective non-destructive test technique for evaluating dynamic mechanical properties (4-6). Since the stress distribution in a typical adhesive joint is far from uniform, the strength is sensitive to the integrity of some areas of the joint than to the others (7). The basic premise of the work reported here was that measurements of the dynamic mechanical properties of an adhesively bonded member could be used to indicate the structural integrity of the adhesive joint.

In this paper the contributions from intrinsic defects of varying level (size and volume) and degree of severity caused by improper curing and induced porosity on the performance of double-lap adhesive joint bonded with a structural epoxy adhesive is analyzed. The defects were created through careful control of processing variables and the analysis was performed non-destructively using the impulse-frequency response technique. The micromechanisms governing the performance and durability of bonded joints are discussed in terms of the specific role of several competing and mutually concurrent factors involving cure time, curing temperature, adhesive degassing time, adhesive chemistry and specimen geometry.

2. EXPERIMENTAL PROCEDURES
   AND TECHNIQUE

A double-lap specimen configuration with provisions for clevis pins was chosen (Figure 1). The clevis pins facilitates loading of the test specimen in a servo-hydraulic structural test machine. The material chosen for the adherend

424

was a hot rolled structural steel having a fine grain size, while the adhesive was a mixture of EPON 815 epoxy and Hardener V-40. Details of the specimen design and configuration can be found elsewhere (8).

The surface layer of the adherend in its original state has a deleterious effect on adhesive bond strength and needs to be removed by suitable treatment before bonding (9). In order to render the steel adherends receptive to bonding, the ASTM Standard Practice for preparation of metal surfaces for adhesive bonding, D26510-798 was used. The suggested ten minute etch with strong sulfuric acid-sodium dichromate solution was replaced by polishing the surfaces with 400-grit silicon carbide paper wetted with dilute sulfuric acid. The residue was washed with warm water and the adherends stored in acetone until use. This procedure enhances bond strength by:

   (a) removing the rust and exposing the bare steel surface, and

   (b) roughening the surface, therebym increasing the area for bonding.

The adhesive was prepared in accordance with manufacturers specifications. Epon 815, a plasticised liquid epoxy resin was mixed with Hardener V-40 in the proportion of 100 parts of Epon and 80 parts of Hardener by weight. The adhesive was prepared at ambient-room temperature (23 C) in laboratory air environment, using weight proportioning. The resin and hardener were thoroughly mixed for 20 seconds to ensure a uniform mixture. Following mixing, the adhesive was degassed under vacuum at a temperature of 100 C for a period of seven minutes. The viscous adhesive was then poured into the 'female' adherend positioned in the jig. The 'male' adherend was lowered into the double-lap female adherend to form the required joint. The assembled jig with adherends in position was placed in a furnace for curing at an elevated temperature of 100 C. The elevated temperature facilitates acceleration of the cure process. The cured composite specimens were then stored for 48 hours in a low humidity environment in order to minimize any environmental effect on bond stability.

In the Fast Fourier Transform (FFT) based impulse technique (5,6), excitation of flexural modes (Figure 2) of vibration in the specimen is obtained by tapping the specimen with an electromagnetic hammer which has a piezoelectric force transducer attached to its tip. The specimen response is sensed by a non-contacting eddy current proximity detector positioned at a desired location away from the nodal points. The input signal from the force transducer and the response signal from the motion transducer, are fed into the FFT analyzer, and the desired frequency response function on the desired frequency span is displayed on the analyzer screen in real time.

A computer program written in BASIC for the HP-85 computer was used for data acquisition and reduction. The program reads binary values from the memory of the FFT analyzer, makes the corresponding transformations to the current scale, locates the points on either side of the half-power points, and finds the half-power points by interpolation. The resonant frequency, f_n, and the half-power bandwidth are used in Equation (1) to find the loss factor

$$\eta = \frac{\Delta f}{f_n} \quad . \quad . \quad . \quad . \quad (1)$$

425

where

Δf = bandwidth at the half-power points of resonant frequency.

f_n = resonant frequency of the n th mode.

In the flexural test technique, the adhesive end of the composite specimen (two steel adherends held together by a double-lap adhesive joint) was clamped to a depth of one inch (25 mm), while the adhesive and the other end of the composite specimen were free, giving a fixed-free end condition. The non-contacting eddy current probe was positioned at the free end. The advantages of using an electromagnetic hammer having a piezoelectric force transducer at its tip is outlined in detail by Suarez and Gibson (6). Details of the test technique are described elsewhere (8).

3. RESULTS AND DISCUSSION

3.1 Effect of Curing on Adhesive Joint Response

Improper curing, that is, too low a curing temperature or inadequate time at the required curing temperature or improper mixing of the components of the adhesive are factors responsible for variation in physical properties of an adhesive due to insufficient cross-linking of the polymer. Composite specimens with the adhesive cured over a range spanning the under-cured (low stiffness and strength) to fully cured condition (high stiffness and strength) were obtained by varying the cure time. Cure time is the amount of time the specimen is in the oven. Cure schedules with cure time settings of 60 minutes,

120 minutes, 180 minutes and 240 minutes (complete cure) at the cure temperature were chosen.

Dynamic tests in the flexural mode were conducted on the composite specimens using an impulse-frequency response technique. The tests were performed at ambient, room temperature (23 C). Prolonged delay in testing following accelerated curing for different time periods was avoided since it could result in self-correction of poor cure, i.e., the chemical reaction could continue at the ambient temperature, albeit slowly. On the other hand, tests showed that properties changed significantly within the first few hours after curing, as the material reached equilibrium. Thus, in order to minimize contributions from prolonged delay or non-equilibrium conditions, the dynamic tests were conducted following a 48 hour delay period for the different cured conditions.

The effect of cure time (at constant cure temperature of 100 C) on dynamic mechanical properties is summarized in Table 2. From this Table, it is observed that undercuring, i.e., curing for time periods less than the prescribed time period (240 minutes) results in an increase in damping (loss factor). The increase is as high as 35 percent for the specimens cured for only 60 minutes. At cure time of 120 minutes the increase in damping was only marginal. The marginal increase in damping suggests that the adhesive achieves a stable and favorable molecular network structure at time periods beyond 120 minutes. As a result, there occurs a complete bonding of the adhesive to the steel adherend. The variation of loss factor with cure time is exemplified in Figure 4.

Several mechanistic explanations can be put forth to account for the the transient change in damping. The high temperature, short cure

time schedule represents a highly unsteady condition favoring the build-up of large thermal stresses. However, these stresses are most likely relieved during the slow cool-down rate and is an appealing rationale for the adhesive developing a more stable and favorable molecular structure (10).

Variation in the degree of shrinkage of the adhesive is a plausible reason for the observed change in damping and stiffness. A study on the effect of glue-line thickness on bonded steel-to-steel joints revealed that the shrinkage of the adhesive is a function of its thickness (11). For joint thickness greater than 0.06 inch the adhesive shrinkage was observed not to degrade strength. Since the thickness of the adhesive in the adhesively joined composite steel specimen used in this study is 0.04 inch, contributions to damping from shrinkage if any, cannot be ruled out.

The other reason for the observed change in damping (loss factor) could be due to a combination of:
    (a) the chemical nature, and
    (b) the physical characteristics of the adhesive in relation to the adherend.
Controlled wetting and penetration are two important prerequisites which need to be satisfied for the formation of a joint of sound integrity. For these two conditions to be fulfilled, an appropriate viscosity level is imperative (12). Attainment of this viscosity level is contingent upon:
    (1) components of the adhesive
    (2) cure temperature, and
    (3) cure time.
The first two factors were held as constant as possible in this experiment. Thus, the over-riding or controlling factor is the cure time and it was observed to have only a marginal influence on joint performance.

Results of the dynamic tests reveal only a marginal change in resonant frequency with cure time (Table 2). While the different degrees of cure do not cause any dramatic change in the 1st mode resonant frequency (Figure 5), the corresponding change in loss factor is significant for the 60 minute cure (Figure 4).

The shear strength of the adhesive joint was determined by uniaxial loading of the composite specimen in a servohydraulic testing machine. Failure was taken to be the point at which the 'male' adherend separates from the 'female' adherend due to failure of the adhesive layer. Provision was made at the adhesive end of the composite specimen to accommodate a clip-gage type extensometer which measures the relative movement of the adhesive layer during deformation of the composite specimen under a uniaxial (tensile) load. A load-displacement curve was obtained on an X-Y recorder. From the load-displacement curve, the shear stress (τ) and the shear strain (γ) at failure were determined.

The adhesive cured for 60 minutes at the temperature of 100 C will henceforth be referred to as an under-cured condition. It is observed that the shear strength is lowest for the under cured condition. When compared with the strength of the completely cured adhesive joint, a degradation in shear strength is observed for the under-cured adhesive (Figure 6). The severity of the under-cured condition is responsible for the degradation in strength which is as high as 55 percent (Table 2). A decrease in strength of the adhesive joint results in a concomitant increase in damping of 35 percent (Table 2). For the specimens cured for 120 minutes and 180 minutes, the adhesive

joints are observed to be stronger than the perfectly cured specimen. This trend confirms the observation that the adhesive achieves a stable molecular structure at times beyond 120 minutes. A comparison of the shear stress-shear strain curves for the different cure times is made in Figure 7.

3.2 Effect of Porosity on Joint Performance

Voids or large gas bubbles are caused by a lack of adhesive or by the presence of foreign matter on the adherends, or even in, the adhesive. Porosity of the adhesive is similar to voiding except that the size of the bubbles are much smaller. It is usually caused by volatiles or gases trapped in the adhesive. Porosity is a major problem in composite adherends and occurs when the absorbed moisture vaporizes during the cure cycle to produce bubbles in the adhesive.

The degree of porosity in the adhesive was controlled by varying the degassing time of the liquid adhesive. By degassing the adhesive under vacuum for times less than the time prescribed for complete degassing, air and product gas resulting from the reaction between the epoxy and hardener are trapped in the adhesive mixture. Thus, the volume of air and reaction gas pockets (pores) are likely to be greater when the adhesive mixture was not degassed.

Preliminary tests revealed a migration of pores to the top portion of the double-lap adhesive joint and eventual breakdown of these pores and voids during curing at an elevated temperature ($100^{\circ}C$). Therefore, to minimize the depletion of induced pores and voids by the elevated temperature cure, the porosity specimens were allowed to cure at ambient temperature ($25^{\circ}C$) for a period of 7 days.

When compared with a totally degassed mixture (7 minutes), the adhesive mixture which was not degassed (referred to as 0 minutes in Table 3 and in Figures 8-11) prior to pouring, caused a drastic change in dynamic properties of the adhesive joint. The loss factor for the different degassing times (0, 2 and 7 minutes), reveals an increase as high as 445 percent for the composite specimen whose adhesive mixture was not degassed (Case: 0 minutes) (Figure 8). The change in first mode resonant frequency caused by the presence of fine microscopic pores and voids was only marginal as shown in Table 3 and exemplified in Figure 9.

The impulse-frequency response technique successfully detects and magnifies the presence of pores and/or voids as is evident by a large change in damping (loss factor). The volume fraction of flaws caused by the entrapped air and product/reaction gases, i.e., pores and voids, results in a marked degradation in the shear strength of the adhesive joint as summarized in Table 3. The volume fraction of pores and/or voids in the undegassed adhesive mixture coupled with contributions from adhesive chemistry and changes in reaction kinetics, results in the adhesive joint having inferior strength (Figure 10) and exhibiting increased damping. While the degradation in strength is 75 percent, the concomitant change in damping is as high as 445 percent. It seems likely that the pores at an adhesive-adherend interface, act as debond area and consequently, degrade the strength of an adhesive joint. From Figure 8, Figure 10 and Table 3, it is evident that degassing the adhesive mixture for even short periods of time, say 2 minutes, is adequate to

to reduce the total amount of entrapped air in the adhesive mixture, and complete the reaction kinetics of the adhesive mixture thus, minimizing contribution from these factors and resulting in only a marginal change in damping and frequency.

Since the joints were observed to fail primarily by interface separation, it is expected that the pores at an interface would affect the strength (8). Damping is influenced by pores both at the surface and those embedded in the adhesive. This hypothesis was born out by the results obtained in this intensive study. It seems plausible that the reaction kinetics between the EPON 815 epoxy and the hardener is different when the adhesive mixture is not degassed under vacuum when compared to the strong reaction accompanied by the evolution of gas bubbles that occurs when degassed under vacuum. The change in reaction kinetics could be an additional factor contributing to the observed differences in damping and strength.

The strength and damping of the adhesive joint are very sensitive to: (1) porosity, (2) changes in reaction kinetics of the adhesive mixture, and (3) chemistry of the adhesive. The impulse-frequency response techniques gives a sensitive measure of the presence of fine microscopic defecrs such as pores, changes in reaction kinetics and adhesive chemistry.

4. CONCLUDING REMARKS

While specific results have been presented in the discussions, the major conclusions of this study can be summarized as follows:
(a) The impulse-frequency response technique based on the use electromagnetic hammer in conjunction with a FFT analyzer and a microcomputer successfully detects the presence of intrinsic flaws as is reflected by a pronounced change in damping (loss factor) with an increase in size, number density and severity of the flaws.
(b) The observed change in damping with cure time at the accelerated cure temperature is attributed to several competing mechanistic processes involving: (i) shrinkage of the adhesive, (ii) chemical and physical characteristics of the adhesive relative to the adherend, and (iii) thermal stresses.
(c) Fine pores and microscopic voids induced by not degassing the adhesive in conjunction with changes in reaction kinetics of the adhesive mixture causes a large change in damping which is detected by the impulse technique. The internal pores affect damping while those at an interface contribute to degradation in strength besides causing change in dynamic response.

REFERENCES:

1. E. M. Petric: Adhesives
    Age, Vol. 23, 1980, p. 14.

2. M. M. Villalobos and
    P. Czarnock: Journal of
    Adhesion, Vol. 19, 1986,
    pp. 79-87.

3. R. W. Shannon: "Primary
    Adhesively Bonded Structure
    Technology," AFFDL-TR-77-107,
    Air Force Flight Development
    Laboratory, Dayton, Ohio,
    September 1977.

4. R. Mantena, T. A. Place
    and R. F. Gibson: "Character-
    ization of Matrix Cracking
    in Composite Laminates by the
    use of Damping Capacity
    Measurements," Symposium
    on Role of Interfaces in
    Material Damping, TMS-AIME
    Fall Meeting, Toronto, Canada,
    October 1985, ASM Paper No:
    8522-002.

5. S. A. Suarez and R. F. Gibson:
    "Computer Aided Dynamic
    Testing of Composite
    Materials," Proceedings of the
    Fall 1984 Meeting of the
    Society of Experimental
    Mechanics, Milwaukee,
    Wisconsin, 1984.

6. S. A. Suarez and R. F. Gobson:
    Journal of Testing and Evalua-
    tion, Vol. 15(2), 1987, pp. 114-
    121.

7. R. D. Adams and N. A. Peppiatt:
    Journal of Strain Analysis,
    Vol. 9, 1974, pp. 185-196.

8. T. S. Srivatsan: "Portable
    Impulse Measurements to Non-
    Destructively Predict the
    Integrity of Adhesive Joints,"
    Final Report, Naval Surface
    Weapons Center, Contract
    No. N60921-86-C-0210, April 87.

9. K. W. Allen and H. S. Alsalim:
    Journal of Adhesion, Vol.8,
    1977, pp. 183-194.

10. E. Sancaktar, H. JoZavi and
    R. M. Klein: Journal of
    Adhesion, Vol. 15, 1983,
    pp. 241-251.

11. R. W. Hylands and E. H. Sidwell:
    Journal of Adhesion, Vol. 11,
    1980, pp. 203-218.

12. R. O. Ebewele, B. H. River
    and J. A. Koutsky: Journal
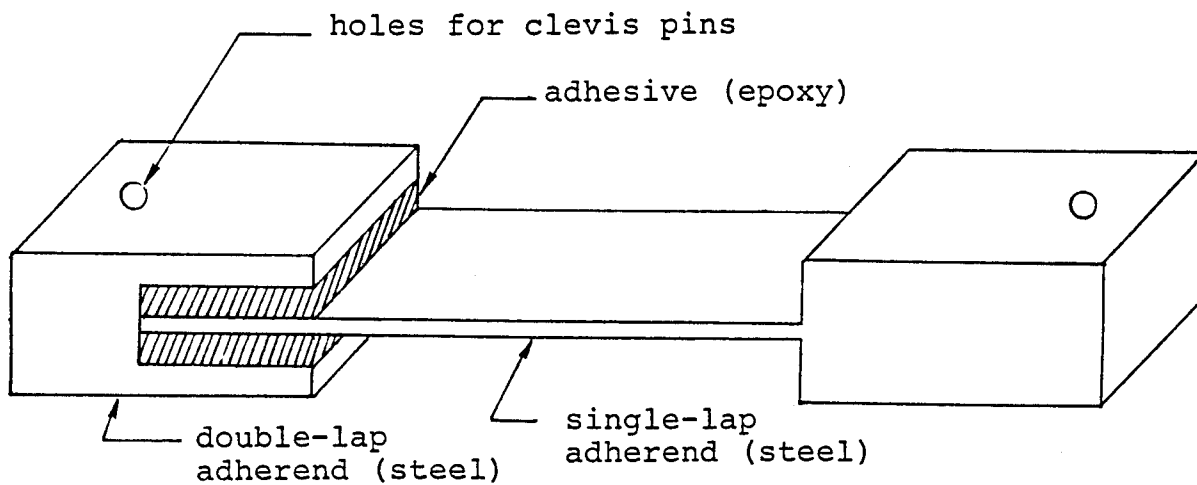   of Adhesion, Vol. 14, 1982,
    pp. 189-217.

Figure 1. Schematic showing configuration of the composite test specimen.

TABLE 1. Dimensions of the Composite Test Specimen and Test Conditions.

(a)	Length of composite specimen	= 127.0 mm
(b)	Width of composite specimen	= 19.05 mm
(c)	Adherend thickness	= 1.524 mm
(d)	Adhesive thickness	= 1.016 mm
(e)	Density of Steel	= 7.76 g/cm^3
(f)	Yield strength of steel	= 379.0 MPa
(g)	Tensile strength of steel	= 571.0 MPa
(h)	Density of Epoxy (EPON 815)	= 1.085 g/cm^3
(i)	Test temperature	= 70-80 F
(j)	Humidity	= 55-65 percent
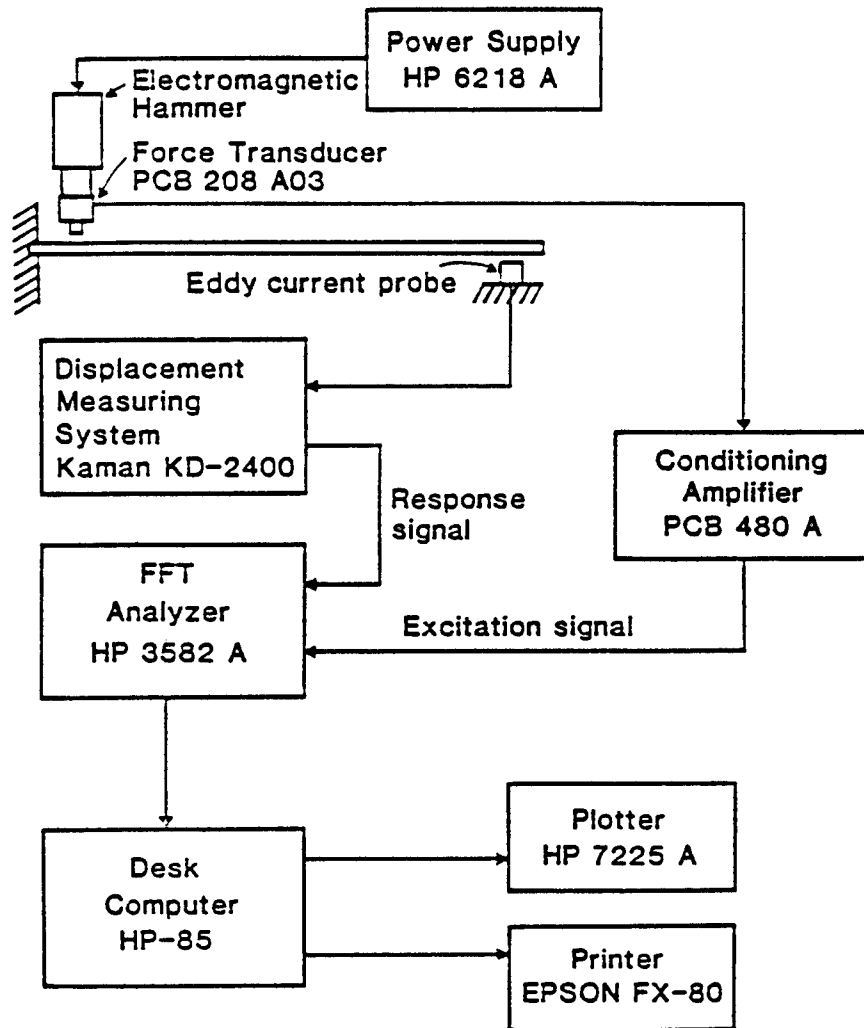
Figure 2. Block diagram showing the flexural vibration
apparatus (Ref. 6).
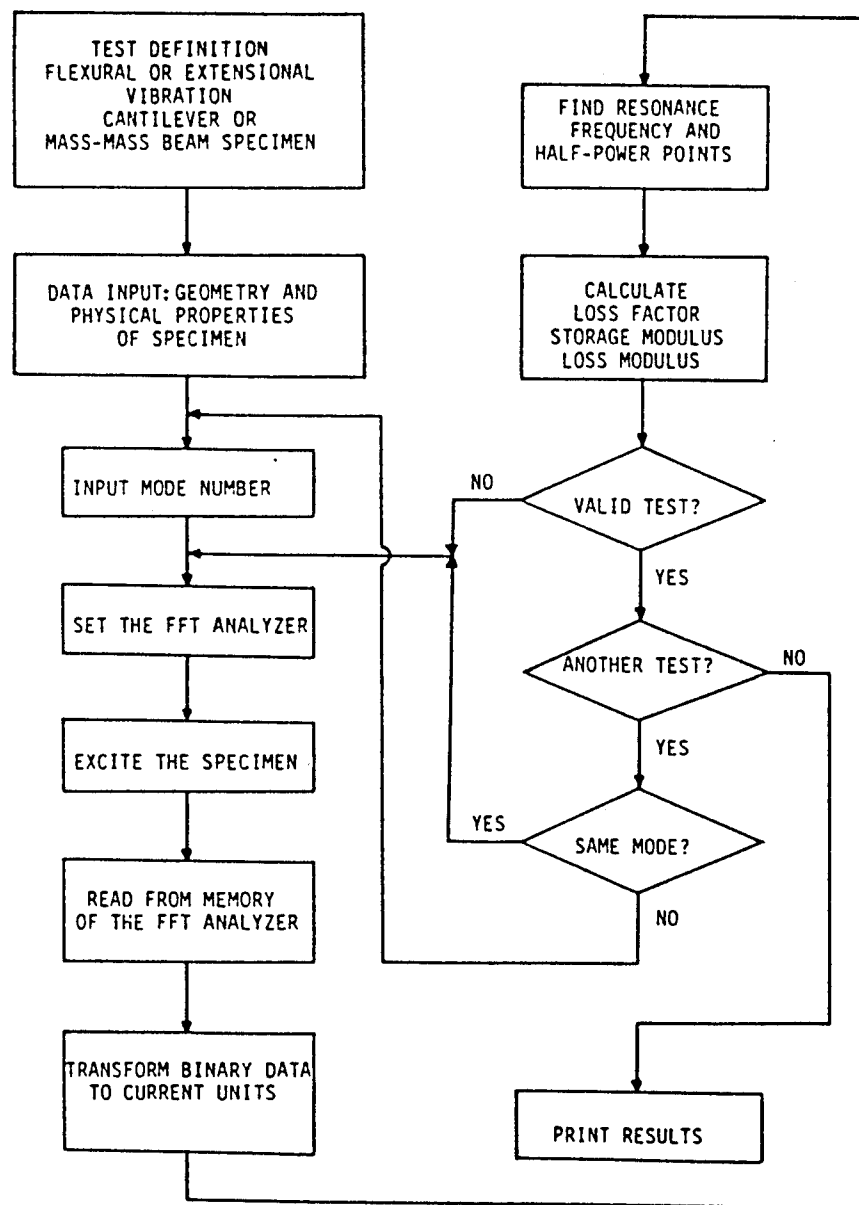
Figure 3. Flow chart for data acquisition and reduction
program (Ref. 6).

TABLE – 2.

Effect of Curing Time on Loss Factor[●], Resonant Frequency[□], and Strength[▲]

Cure-time (minutes)	Loss Factor	Percentage change in loss factor	Resonant Frequency (Hz)	Percentage change in Resonant Frequency	Shear Strength (psi)	Percentage change in shear strength
240	0.0192	–	261.70	–	2167	–
180	0.0197	+2.60	268.40	+2.56	2800	+29.20
120	0.0184	-4.10	268.90	+2.75	2767	+27.68
60	0.0259	+35.00	261.50	-0.08	967	-55.30

[□] results are the mean based on three tests, and each test is the average of four trials.

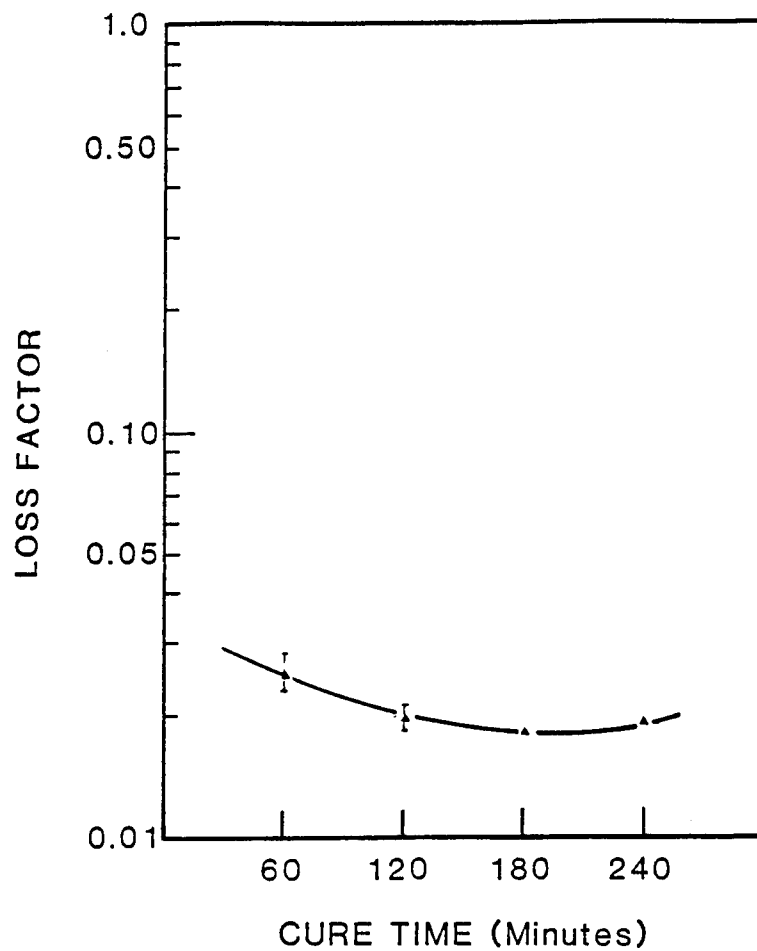[▲] results are the mean of two tests.

434

Figure 4. Effect of accelerated cure time on damping (loss factor) of adhesive joint.
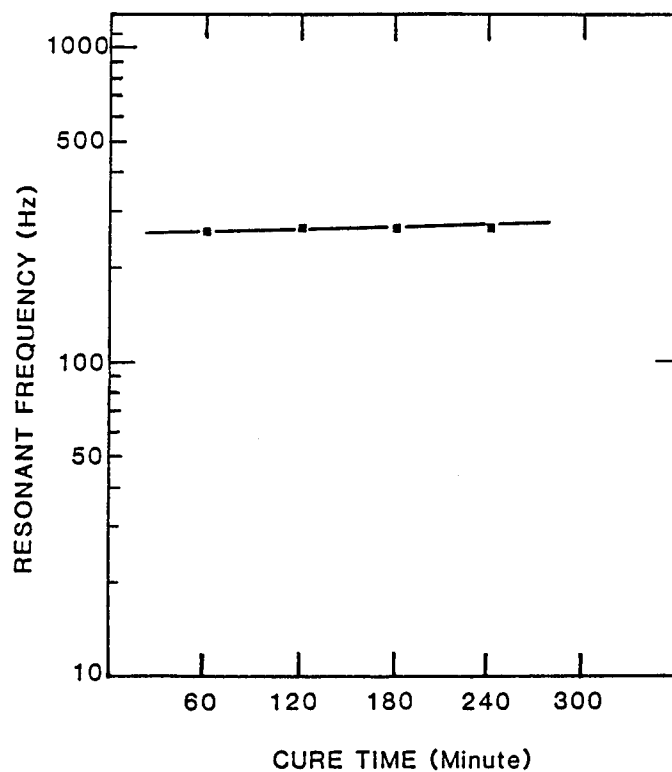

Figure 5. Variation of 1st Mode resonant frequency (Hz) of adhesive joint with cure time (minutes).
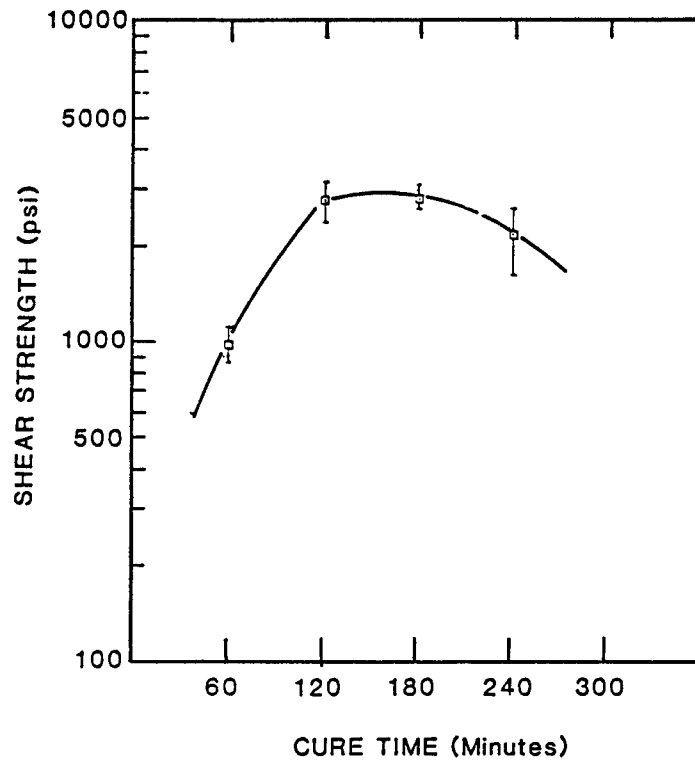
435

Figure 6. Variation of joint shear strength (psi) with cure
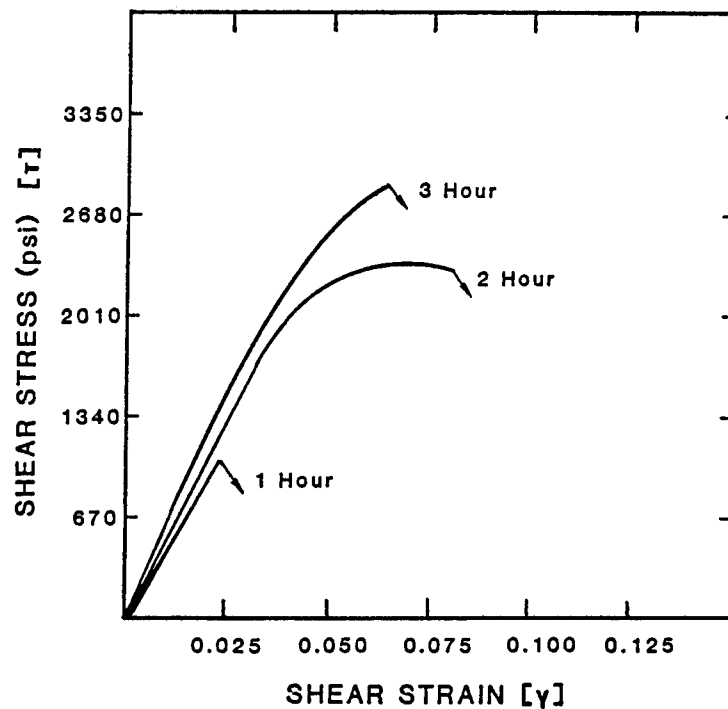time (minutes).

Figure 7. Comparison of representative shear stress-shear
strain curves for the different cure times.

TABLE - 3

Effect of Degassing Time on Loss Factor●, Resonant Frequency□, and Strength▲

Adhesive Degassing Time (minutes)	Loss Factor (η)	Percentage change in Loss Factor	Resonant Frequency (Hz)	Percentage change in Resonant Frequency	Shear Strength (psi)	Percentage change in shear strength
7	0.02531	-	267.028	-	1517.0	-
2	0.0225	-10.90	265.256	-0.66	2566.5	+69.20
0	0.1380	+445.00	191.515	-28.28	373.5	-75.37

● □ results are the mean based on three tests, and each test is the average of four trials
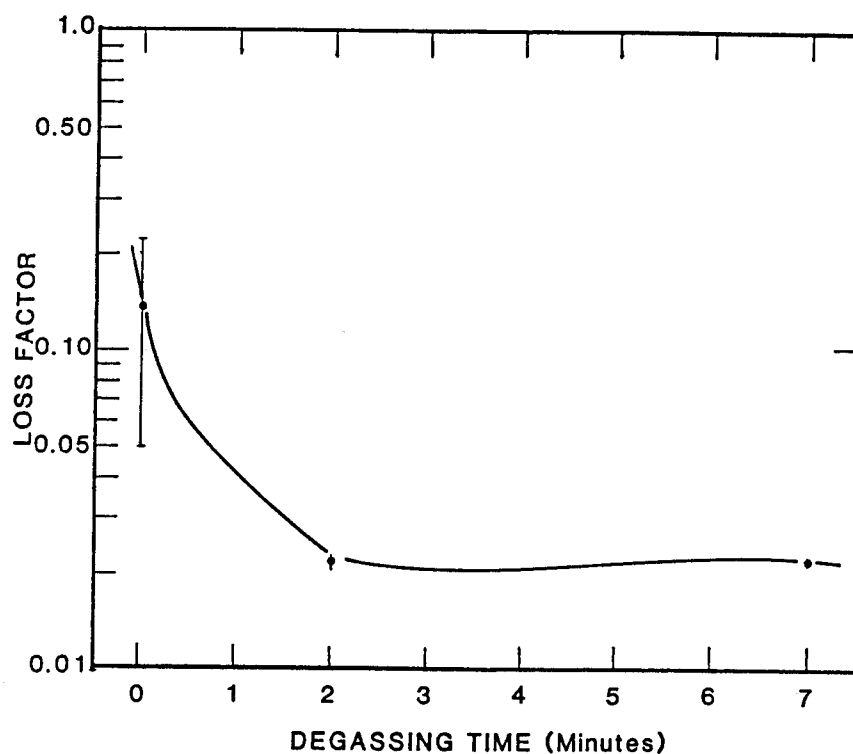
▲ results are the mean of two tests.

Figure 8. Effect of adhesive degassing time (minutes) on
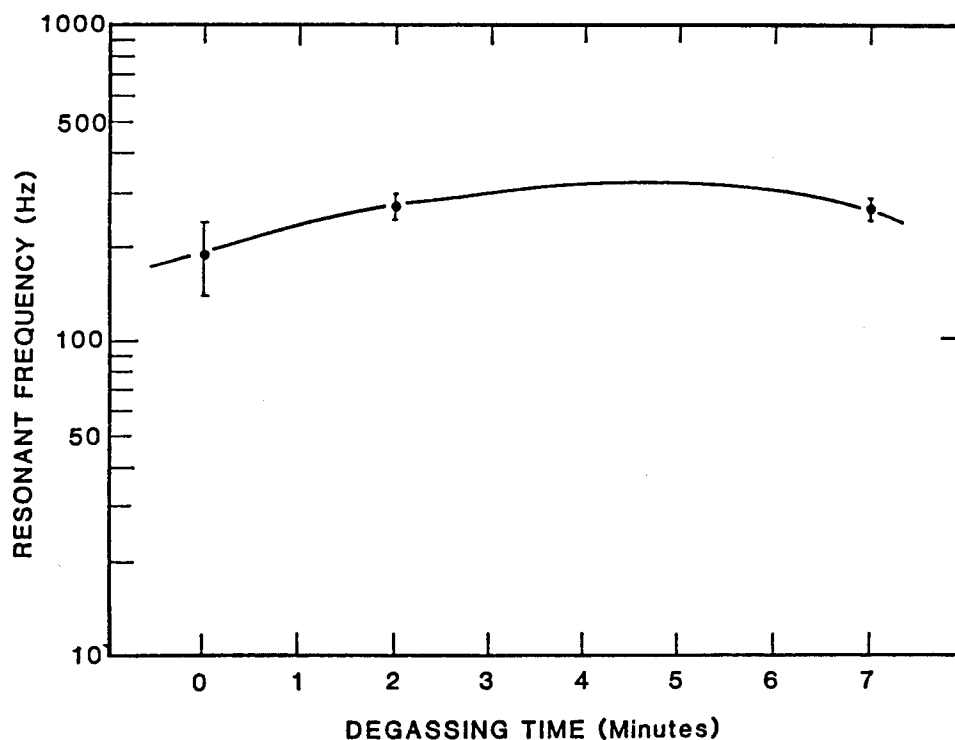adhesive joint damping (loss factor).

Figure 9. Variation of 1st mode resonant frequency (Hz) of
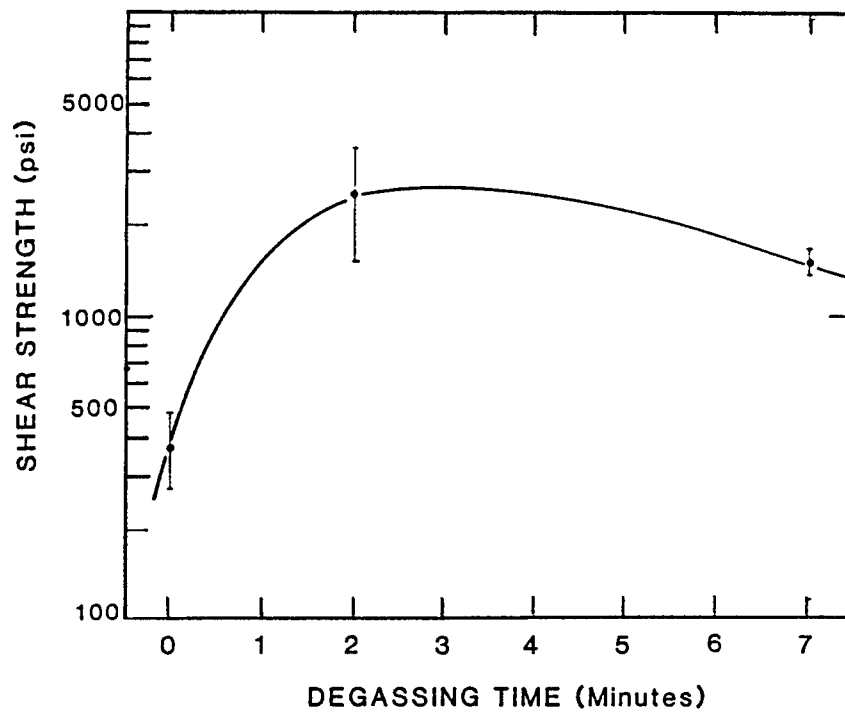adhesive joint with adhesive degassing time (minutes).

Figure 10.   Variation of joint shear strength (psi) with
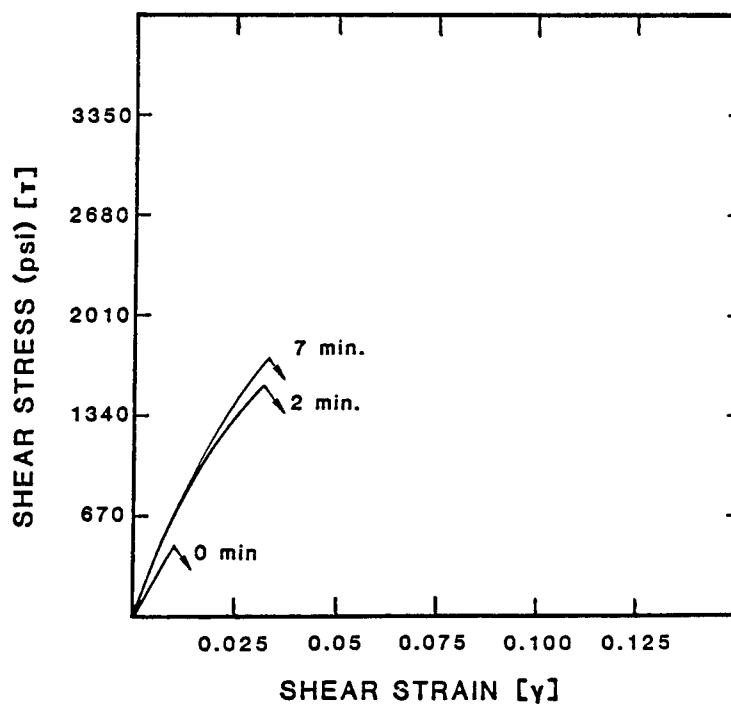adhesive degassing time (minutes).

Figure 11.   Comparison of representative shear stress-shear
strain curves for the different degassing times.

439

MOISTURE-RESISTANT LOW-TEMPERATURE-CURING ADHESIVES

C. Arah, J. Vogin, D. McNamara, J. Ahearn,
A. Berrier, and G. Davis
Martin Marietta Laboratories
1450 South Rolling Road
Baltimore, Maryland 21227

ABSTRACT

The need for light-weight materials for a variety of needs has led to the fabrication of bonded composite-metal prototype structures. For bridge applications or high-humidity environments, the bonding system must overcome two fundamental problems affecting bond strength and durability: 1) the thermal expansion mismatch between metal alloys produced at the conventional bonding temperatures of 250° - 350°F, which leads to delaminations at use temperatures (-50° to +160°F); and 2) the strength loss upon exposure to high-moisture environments.

To respond to these critical needs, we have been working to develop adhesives that are practically insensitive to moisture effects and can achieve high bond strengths upon curing at or around use temperature. In this effort, supported by the U.S. Army Troop Support Command's Belvoir RD&E Center, we are formulating adhesives with strength-improving and moisture-resistant additives and then screening/selecting the most promising compositions. To date, we have achieved durable bulk compositions curing at temperatures below 70°C (158°F) by advancing epoxy compositions to epoxy-equivalent weights of approximately 300 with stiff, hydrophobic chain extenders containing azo and fluoro groups.

While studing the effects of chemical modifications on adhesive embrittlement, we concluded that the elastic energy release rate, G, alone does not adequately characterize the fracture resistance of these adhesives. However, a useful measure of total fracture resistance was derived when an unload compliance test was

applied to 1/2-CT-plan (B=0.25 in.) bulk-adhesive specimens. This measure of total fracture resistance was shown to better characterize adhesive resistance to crack propagation than the elastic energy release rate, and can thus be used to evaluate improvements in adhesive formulation.

1. INTRODUCTION

Systematic evaluation of structural adhesives, such as epoxies and acrylics, has shown that these materials are extremely likely to lose initial mechanical properties (strength, modulus, etc.) when subjected to adverse environments.[1] In fact, the degradation of these adhesives is so pronounced in high-relative-humidity (RH) and high-temperature environments that almost none of them can be considered for long-term outdoor applications, such as bonding structural components for bridges. Under high-RH conditions, moisture infuses into the polymer, separating polymer molecules and reducing their secondary bond attraction, so that it is easier for the

molecules to slide past each other. A high degree of crosslinking is therefore necessary to minimize these effects of moisture. But, in most thermosetting adhesive systems, the development of a high crosslink density requires elevated-temperature curing, conditions difficult to achieve in the field. What is needed, therefore, is a strong, durable, moisture-resistant adhesive that cures at ambient temperatures. In an effort to address this issue, we have been trying to modify low-temperature-curing commercial adhesives for improved performance. Our research has resulted in several promising formulations, as well as a unique approach to evaluating the fracture resistance of these rather brittle materials.

2. BACKGROUND

The greatest limitation associated with ambient-temperature-curing adhesives is the low degree of cure. Isothermal cure at a temperature, T_{cure}, that is below the ultimate glass transition tempera-

ture (Tg_∞) leads to $Tg = T_{cure}$. Hence, for thermoset adhesive resins, which generally have a Tg_∞ above 70°C, curing at ambient temperature results in vitrification below Tg_∞ and, eventually, gelation.

The problem becomes evident when the gelled material is heated: devitrification (i.e., increased chain mobility) takes place at a temperature T_{soft}, and is immediately followed by a curing exotherm (see Fig. 1).[2] Thus, ambient-temperature-cured adhesives never attain full cure nor full mechanical properties until cured at elevated temperatures. Because isothermal reactions proceed slowly after vitrification, the low-temperature-cured adhesives tend to age, i.e., display a time-dependent character. For instance, T_{soft} increases with time because the devitrification or softening temperature approaches the ultimate glass temperature, Tg_∞, as cross-linking occurs in the glassy state (see Fig. 2).[2]

Brittleness in the adhesives is the result of high crosslink density, which is necessary to impart rigidity and moisture resistance. Brittle materials usually fail by unstable crack propagation at applied loads well below those expected from materials strength or limit load analysis (the crack is usually initiated from processing- and/or fabrication-induced flaws and microvoids in the material). The addition of reactive liquid elastomers to adhesive formulations can substantially increase their resistance to fracture without sacrifice of stiffness.[3,4]

Pure linear elastic fracture mechanics[5] (LEFM) fully describe adhesive performance for brittle materials but not for tougher and less brittle ones. Indeed, if ductility (plastic deformation) is sufficiently high, a fracture mechanics-type analysis holds little meaning and simple limit load analysis is sufficient. The question then arises of how to analyze performance in moderately brittle adhesives. To solve this problem, we drew on the work of Rice[6] who recognized that

in materials where limit load analysis is not useful, ductility represents a "plastic" resistance to crack growth; accordingly, he introduced the J-type fracture parameter to evaluate both "elastic and plastic" crack growth resistance.

3. METHODOLOGY

Our approach to developing moisture-resistant, low-temperature-curing adhesives is to screen and evaluate off-the-shelf adhesives, use the best commercially available adhesives as a performance baseline, and test the effects of additives on these formulations. We selected the additives by matching a desired property with a plausible modification procedure that will achieve it (see Table 1). This methodology, however, exposes the contradictory nature of some of the desired goals. For instance, 1) a high-temperature cure is usually necessary for good environmental durability; 2) chemical structures that provide the best resistance against adverse environments also yield rigid and brittle adhesives with low peel and impact strengths; and 3) functionalities (e.g., hydroxyl) that promote cure and adhesion to high-energy surfaces are also hydrophilic. Thus, we have combined and permuted the various resin modification procedures to minimize their deleterious effects and maximize the attainable goals.

Environmentally sensitive formulations were screened out based on tensile tests performed on bulk-adhesive strips conditioned at 120°F and 80% RH. Single lap-shear measurements were then conducted on selected specimens passing the bulk tensile tests to both augment the tensile results and test the compatibility of the formulations with the standard FPL (Forest Products Laboratory) surface pretreatment for aluminum adherends. The need for fracture testing became evident when some of these "durable" formulations fell apart with little or no applied force during the lap-shear measurements. We adopted the unload

Table 1. Approach

Desired Property	Resin Modification
Ambient-temperature curing	Reactive RT curing agents Low-viscosity resins
Toughness	Increase in molecular weight between crosslinks (EEW 250-300) Reactive elastomers
Environmental durability	Hydrophobic chain extenders Non-ring-opening reactions Hydration inhibitors
High modulus and shear strength	Stiff advancement agents Modifiers, fortifiers, and coupling agents

compliance test for this purpose for several reasons: it is commonly used to examine the fracture properties of materials undergoing stable crack growth; samples are easy to prepare; and with digital data acquisition, a single specimen can be used to develop a great deal of information about the contemporaneous fracture mechanics parameters K, G, and J.

4. EXPERIMENTAL PROCEDURE

Our formulation procedure is summarized in Scheme 1. The epoxide ring-opening reaction of the resin (diglycidyl ether of bisphenol A) and a diol or a diacid is usually conducted at elevated temperatures (100-150°C for about 1-2 hours) using triphenylphosphine or tertiary amines as catalysts, according to known procedures (see Scheme 2).[7] The advanced resin, though of higher viscosity than the base resin, still has reasonably good flow properties at ambient conditions, allowing mixing with diluents and curative before casting. The commercially available adhesives were mixed according to the manufacturer's specifications.

To cast adhesive specimens for tensile measurement,

we poured the thoroughly mixed adhesive composition onto an aluminum block (12 in. x 5 in. x 1 in.) covered with a silicone release sheet, placed another sheet on top, and rolled the adhesive pool with a rolling pin to remove entrapped air. Another aluminum block, with four 10-mil shims glued to its corners was then placed on top of the sheet, the entire assembly was clamped, and the adhesive was allowed to cure. Curing was allowed to proceed for 2 - 7 days at ambient temperatures or for 7 hours at slightly elevated temperatures. Thin strips cut from the cured film with an Exacto knife (sometimes hot) were then conditioned and tested in an environmental chamber at 120°F and 80% RH. Unconditioned strips were also tested at ambient laboratory conditions.

The bulk compact tension specimens were cast in aluminum molds treated with mold release agents. The dimensions of the 20% side-grooved specimen are shown in Fig. 3. A razor blade was used to initiate a sharp starting crack prior to tests of the specimens in the Instron tensile testing machine using the standard unload compliance methodology.[8]

The cured materials were also characterized by thermal and mechanical

Scheme 1: Formulation Procedure

Chain Advancement

Resin (EEW ~ 189) + Advancement Agent Catalyst --------> Advanced Resin (EEW 250 - 300)

Advancement agents: cyanates, diols, diacids
Catalysts: phosphines, cobalt naphthenate, amines

Curing Reaction

Advanced Resin (EEW 250 - 300) + Diluent Curative --------> Cured Adhesive

Diluents: functional reagents, modifiers, coupling agents, rubber tougheners
Curatives: amines, cobalt naphthenate/MEK peroxide

Table 2. Formulation Data

Formulation	Additive (phr)	Rubber[a] (phr)	Calculated E.E.W. (approx.)	Curative[b] (phr)	T_{soft}[c] (°C)
BPA-250	5.7	12	250	9.76	56
BPA-300	6.8	12	300	8.27	56
DZD-250	7.6	10	250	9.85	55
6F-DCA	8.1	10	250	9.96	58

[a] Hycar CTBN 1300 X 13.
[b] phr triethylenetetramine (TETA) of advanced resin.
[c] Peak height of DSC endotherm.

analysis. Thermal analysis was used to follow the softening and curing transitions in the adhesive. Most of the epoxy-based adhesive systems studied showed a characteristic softening point at 50-60°C and a curing exotherm immediately after (Fig. 1).

Mechanical analysis consisted of tests on specimens mounted in a tensile testing device enclosed in a controllable environment.[1] Tests were conducted at ambient conditions and after the specimens had been conditioned for 48 hr at 120°F and 80% RH. Since these tests were to be used primarily for screening and for guiding the formulation effort, we focused on properties such as ultimate tensile strength (UTS), elongation (as an estimate of toughness), modulus for dry specimens, and retained tensile strength and sustainable stress for conditioned samples.

Fracture toughness, in terms of K, G, and J, and a new method of energy separation (ENSEP) were evaluated using the standard unload compliance test method with an interactive computer program. A qualitative measure of resistance to crack propagation was obtained by correctly partitioning the area under the load versus load-line displacement record into its elastic and plastic energy components.

5. RESULTS AND DISCUSSION

5.1 Formulation

The chain advancement reaction involving the epoxy resin, the diacid, and/or diol proceeds readily at high temperatures (100-150°C) with triphenylphosphine as catalysts.[7] The additive (diacid and/or diol) is slowly stirred into excess resin to ensure uniform incorporation into the network, and the reaction is complete (1-2 hr) when infrared analysis indicates complete disappearance of absorption due to the additive. Further details can be obtained from Ref. 7. The formulation information is tabulated in Table 2.

Advancing the basic diglycidyl ether of bisphenol A from an EEW of 189 to 250-300 increases the molecular weight of the chain between the epoxy groups and, hence, between crosslinks in the cured resin. The result is a reduction in "tightness" of the network and consequently, its degree of brittleness and stiffness. However, since these advancement molecules were intrinsically stiff, the offset in the reduction in stiffness and brittleness, which often translates into increased toughness, was not enough to produce a durable adhesive. A reactive liquid elastomer, Hycar CTBN 1300 X 13, was then used to further toughen the adhesives. Further information on rubber-modified epoxy resins and their toughening mechanisms, can be found in Refs. 3,4,7, and 9-11.

5.2 Thermal Analysis

Differential scanning calorimetry (DSC) was used to determine the degree of cure, softening temperature, T_{soft}, and curing exotherm for partially cured adhesives, and the glass transition temperature, T_g, for fully cured systems. Figure 4 shows the characteristic softening of the uncured adhesive, followed by the curing exotherm, as well as the glass transition temperature, T_g, of the adhesive cured (fully) at a slightly elevated temperature. The softening temperature, T_{soft}, of the epoxy-based adhesives ranged from 50°-60°C depending on curing time, and

Table 3. Mechanical Testing Data for Adhesives

Specimen	Dry (Ambient Conditions)[a]			Conditioned (120°F, 80%RH)[b]		
	UTS (psi)	Modulus (ksi)	Elongation (%)	UTS (psi)	Modulus (ksi)	Elongation (%)
M1[c]	7651	395	3.1	5853	238	2.9
M3[c]	6663	343	3.2	2648	180	5.7
V1[c]	2166	112	10.6	1846	87	12.6
D1[c]	11556	685	2.8	8082	512	2.2
H1[c]	10938	1080	4.0	7708	740	2.2
H2[c]	6752	416	4.3	6061	320	3.3
BPA-250[d]	10653	519	5.4	9188	515	3.0
BPA-300[d]	10868	570	3.2	8810	565	2.7
DZD-250[d]	12150	599	3.5	8879	465	3.1
6F-DCA[d]	12560	655	6.3	9262	500	3.2

a) Average of 5 tests.
b) Average of 3 tests.
c) Commercial composition.
d) In-house formulation.

tended to shift to higher temperatures with time, as the adhesive continued to cure. The primary questions raised by these results are: what is the influence of this phenomenon on mechanical properties, and -- even more important -- is it more desirable to have an adhesive with a low T_{soft} or a high T_{soft} after 1 to 2 days at ambient conditions?

The presence of a softening temperature, of course, makes it difficult to evaluate the effects of chemical modification on these adhesives

since optimum mechanical properties are not rapidly achieved with ambient- temperature cure. To avoid these problems, we cured all the tensile test specimens at 70°C for 7 hr. The glass transition temperature of the cured system is taken as the intersection of the lines drawn adjacent to the point where the baseline begins to shift (see Fig. 4). The T_g of the cured adhesives studied ranged from 80°C to 110°C.

5.3 Mechanical Evaluation

The mechanical test data (see Table 3) suggest that several adhesive compositions are quite durable and retain their properties after exposure to a simulated adverse environment. The following trends in the data are significant:

1. Adhesive compositions with high elongations generally have low values for modulus and ultimate tensile strength. Exceptions are the BPA-250 and 6F-DCA systems, which have modulus and UTS values of 519 ksi and 10,653 psi, and 655 ksi and 12,560 psi, respectively, for corresponding elongations of 5.4 and 6.3%.

2. The compositions obtained using intrinsically stiff advancement agents have quite high modulus values.

3. There is an obvious anomalous effect of environmental exposure on elongation. Although elongation is expected to increase after conditioning in the humidity chamber, due to the plasticizing effect of moisture on the network, it actually decreases. The significance of this result is not known and cannot be attributed to further curing of the adhesives since they were fully cured (70°C for 7 hr) before being placed in the 120°F (50°C) and 80% RH chamber.

4. The high elongation of the 6F-DCA system is consistent with the known chemistry of the 6F group, which seems to influence chain dilations without reducing the stiffness and strength of the network.

Based on these bulk tensile results, we concluded that the incorporation of intrinsically stiff molecules into epoxy adhesive formulations generally produces durable adhesives, which are also slightly susceptible to moisture effects and somewhat brittle. Our formulations generally performed better in these tests than did commercially available materials,

but we do not know to what degree strength and modulus values will have to be compromised to reduce the brittleness to acceptable levels.

5.4 Fracture Testing

Since the unload compliance test provides a load versus load-line displacement (LLD) record of the test specimen, the area under the plot represents the total energy a fracture specimen stores, releases, or dissipates during an increment of displacement between consecutive loadings. The work, W, done by the external load, P, can be related to the internal energy, U, by

$$dW = dU_s + dU_e + dU_p \qquad (1)$$

where

W = work done by the external load

U_s = stored elastic strain (potential) energy

U_e = elastic energy released during crack extension

U_p = plastic energy dissipated during crack extension.

Figure 5 shows the LLD record of the adhesive specimen M2A with the energy partitioned between adjacent unloadings. As is noted in the figure:

Area OAA'O' = ΔU_p

Area O'A'B = ΔU_e

Area OAC = U_s prior to new crack extension (U_{si})

Area O'BD = U_s after crack extension (U_{si+1}).

The total energy resisting a crack growth increment, aΔ, is then the sum of the dissipated plastic energy represented by the area OAA'O' and the released elastic energy O'A'B. Expressed mathematically, this relation becomes:

$$J_{ENSEP} = G + I$$

$$= \frac{1}{B_n} \frac{dU_e}{da} + \frac{1}{B_n} \frac{dU_p}{da} \qquad (2)$$

where

J_{ENSEP} = the total rate of energy release to the specimen

G = the elastic energy release rate

I = the plastic energy dissipation rate

B_n = the net specimen width between side grooves.

The increment of crack extension Δa is determined from the unload-load compliance slopes, as discussed in Ref. 8. The cumulative values of U_p, U_e, and a (crack extension) are the simple summations:

$$\frac{U_p}{B_n} = \frac{1}{B_n} \sum_{i=1}^{n} \Delta U_{p_i}$$

(3)

$$\frac{U_e}{B_n} = \frac{1}{B_n} \sum_{i=1}^{n} \Delta U_{e_i}$$

$$a = \sum_{i=1}^{n} \Delta a \quad .$$

These energies and the instantaneous value of U_s/B_n are plotted against crack extension in Fig. 6. The slopes of the lines for U_e/B_n and U_p/B_n versus crack extension at any point provide the elastic and plastic energy release rates, G and I, respectively, where

$$G = \frac{1}{B_n} \frac{dU_e}{da}$$

and   (4)

$$I = \frac{1}{B_n} \frac{dU_p}{da} \quad .$$

The values of G and I versus crack extension are plotted in Fig. 7, which also shows the average value of I.

The scatter in the test results is due in large part to our use of test apparatus designed for steel specimens under greater loads. Adjustments to accommodate very low-load specimens (i.e., 50-lb maximum load) will reduce the scatter.

Interestingly, both G and I decrease with crack extension, reflecting their dependence on specimen geometry rather than materials properties. If specimen dimensions are kept constant, however, relative values can then be compared. For instance, for a crack extension of 0.03 in. and an initial crack length of 0.509 in., G and I are given as

$$G_{(0.03)} = 5.5 \frac{in-lb}{in^2}$$

$$I_{(0.03)} = 9.2 \frac{in-lb}{in^2} \quad .$$

It should be reiterated that values of G and I are the <u>absolute</u> energy rates, i.e., represent energy flowing through the specimen in general, with no specific reference to the crack tip.

The values of G, I, J and P_{max} for the adhesives

451

tested are tabulated in Table 4. Note that the G, I, and J values are for a 0.03-in. crack extension.

As is seen from Table 4, the G values for an arbitrarily chosen crack extension (0.03 in.) of the adhesives tested vary between 5 and 9 in-lb/in^2, and are similar to G values obtained for Plexiglas® (6.0 in-lb/in^2)[11] and other epoxy adhesives studied by Ting and Cottington[5] in similar tests. Since these specimens differ widely in toughness, these results imply that G alone does not fully characterize fracture toughness, as has been widely assumed. The absolute plastic energy dissipation rate, however, fully characterizes the ability of these materials to propagate cracks.

The material that best resists crack growth is specimen V1, while the worst is specimen D1. Interestingly, the UTS and modulus values for specimens V1 and D1 are, respectively, 2166 psi and 112 ksi, and 11556 psi and 685 ksi. While this observation supports the conclusion drawn from bulk mechanical analysis (i.e., adhesives with high elongations tend to be"weak"), it is possible to have an adhesive that is both "strong" and relatively tough. A good example is specimen H1, which has UTS and modulus values of 10938 psi and 1080 ksi, respectively, and also has an I value of 25 in-lb/in^2. The ideal adhesive for the intended application would have high values of G, I, J, and P_{max}.

6. CONCLUSION

Durable bulk-adhesive compositions curing at temperatures below 70°C have been achieved by advancing relatively low-viscosity epoxy resins to materials of epoxy-equivalent weights of approximately 300 with intrinsically stiff, hydrophobic chain extenders containing azo and fluoro groups. While investigating the effects of chemical modifications on the embrittlement that accompanies increased durability in these adhesives, we concluded that the elastic energy release rate, G, alone does not adequately characterize their fracture resistance. By using

Table 4. <u>Comparative Data for the Adhesives from LLD Records</u>

Specimen	Crosshead Displacement Rate (in/min)	G^c (in-lb/in^2)	I^c (in-lb/in^2)	J^c (in-lb/in^2)	P_{max} (lb)
M1[a]	0.02	8.0	9	10.0	27
M2A[a]	0.01	5.5	9	6.6	26
M3[a]	0.01	6.0	15	9.0	27
V1[a]	0.01	7.0	60	16.2	16
H1[a]	0.01	7.0	25	15.0	45
H2[a]	0.01	4.5	9	6.0	31
D1[b]	0.005	9.0	0	9.0	35

a) Stable fracture (crack arrest was possible).
b) Unstable fracture.
c) At 0.03-in. crack extension.

unload compliance analysis, we were able to evaluate the elastic and plastic energy components in terms of current elastic-plastic parameters and provide a useful measure of total specimen fracture resistance.

7. REFERENCES

1. Albrecht, P., M.F. Mecklenburg, J. Wang, and W. Hong, "Effect of Environment on Mechanical Properties of Adhesives," Final Report, Office of Research, Development, and Technology, Federal Highway Administration, Contract #DTFH-61-84C-00027, February 1987.

2. Arah, C.O., and J.M. Vogin, Martin Marietta Laboratories, Baltimore, MD, unpublished results.

3. Rowe, E.H., and C.K. Riew, "What Failure Mechanisms Tell about Toughened Epoxy

Resins," Plastics Engineering, 45 (March 1976).

4. Pocius, A.V., "Elastomer Modification of Structural Adhesives," Rubber Chem. and Technol., 58, 622 (1985).

5. Ting, R.Y., and R.L. Cottington, "Comparison of Laboratory Techniques for Evaluating the Fracture Toughness of Glassy Polymers," J. Appl. Polym. Sci., 25, 1815 (1980).

6. Rice, J.R., "A Path Independent Integral and the Approximate Analysis of Strain Concentration by Notches and Cracks," J. Appl. Mech., 35, 379 (1968).

7. Drake, R.S., "Elastomer Modified Solid Epoxy Resins," Goodrich Technical Literature (RSD-824-81), B.F. Goodrich Chemical Group, Cleveland, Ohio, November 1981.

8. Joyce, J.A., and J.P. Gudas, "Elastic-Plastic Fracture," ASTM STP 668, American Society for Testing and Materials, 1979, p. 451.

9. Riew, C.K., E.M. Rowe, and A.R. Siebert, "Toughness and Brittleness of Plastics," R.D. Deanin and A.H. Grugnala, eds., Adv. Chem. Series, 154, Am. Chem. Soc., Washington, DC, 1976, p. 326.

10. Drake, R.S., and A.R. Siebert, "Elastomer-Modified Epoxy Resin for Structure Applications," SAMPE Quarterly, 6 (July 1975).

11. Drake, R.S., and A.R. Siebert, "Reactive Butadiene/Acrylonitrile Liquid and Solid Elastomers: A Bibliography for Formulating Epoxy Structural Adhesives," in Adhesives Chemistry, L. Lee, ed., Plenum, New York, 1984, p. 643.

12. Albrecht, P., W.R. Andrews, J.P. Gudas, J.A. Joyce, F.J. Loss, D.E. McCabe, D.W. Schmidt, and W.A. VanderSluys, "Tentative Test Procedure for Determining the Plane Strain J_1-Curve," J. Testing and Evaluation, 10 (6), 245 (November 1982).

13. Rice, J.R., P.C. Paris, and J.G. Merkle, "Progress in Flaw Growth and Fracture Toughness Testing," ASTM STP 536, American Society for Testing and Materials.

14. Mecklenburg, M.F., The Smithsonian Institution, Washington, DC, private communication.
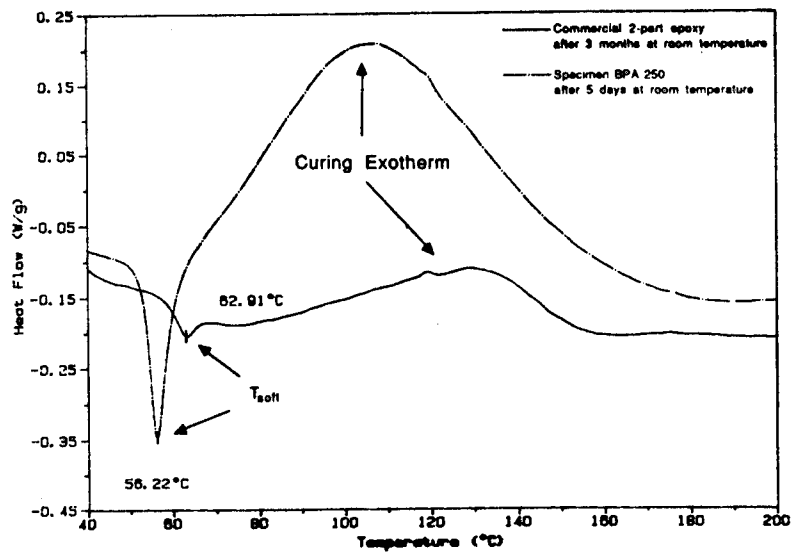
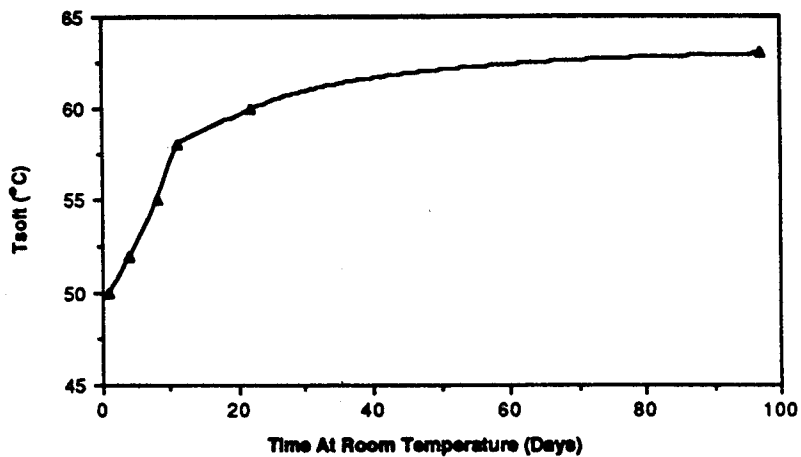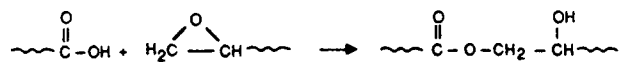Figure 1: DSC scans of ambient-temperature-cured
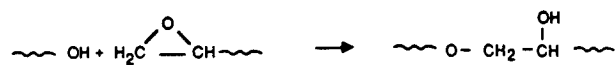   adhesives.

Figure 2: T_{soft} as a function of time for an
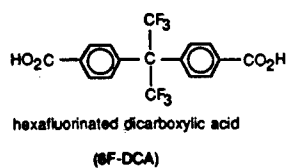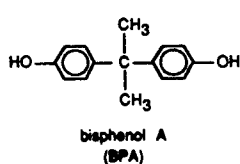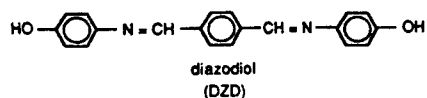   ambient-temperature-curing epoxy adhesive.
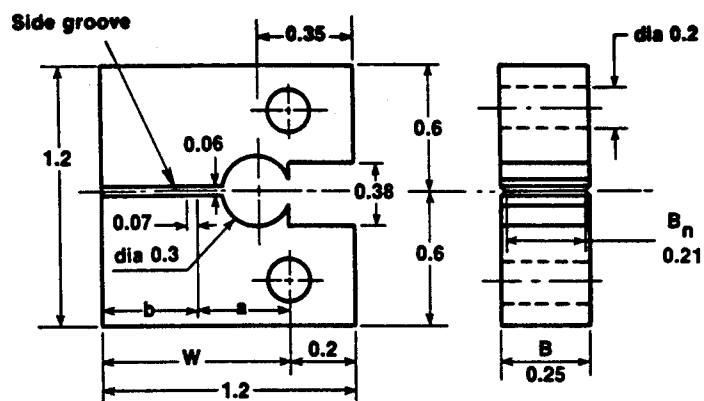
Esterification

Etherification

Advancement Agents

diazodiol
(DZD)

bisphenol A
(BPA)

hexafluorinated dicarboxylic acid
(6F-DCA)

Scheme 2: Epoxy advancement reaction.

(dimensions in inches) $a_o \simeq 0.509$

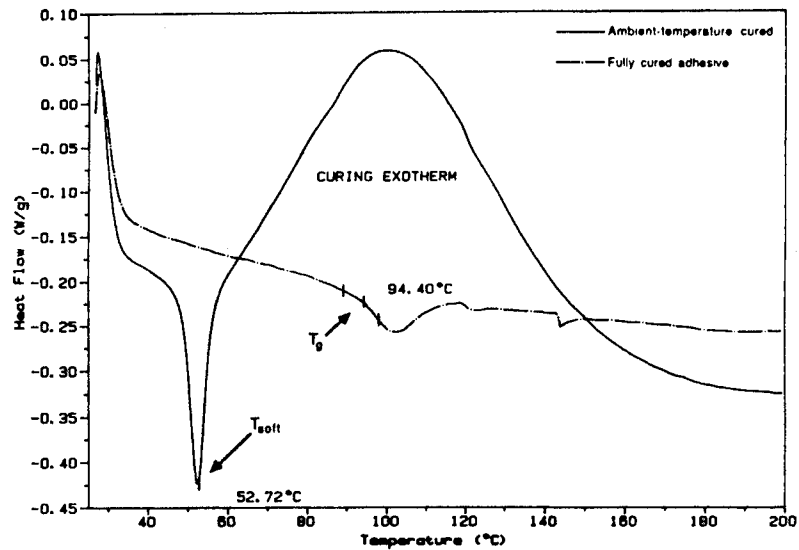**Figure 3: Dimensional diagram of 1/2-CT-plan specimen.**

Figure 4: DSC scans of ambient-temperature-cured and elevated-temperature-cured adhesives.
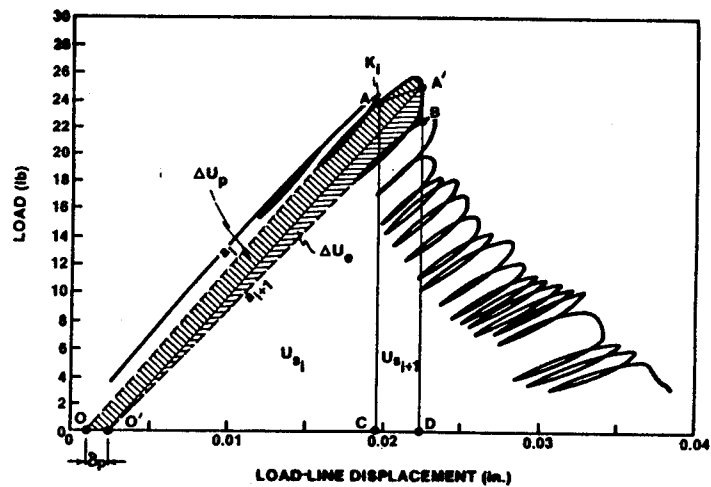

Figure 5: Partitioned load versus load-line displacement record for specimen M2A.
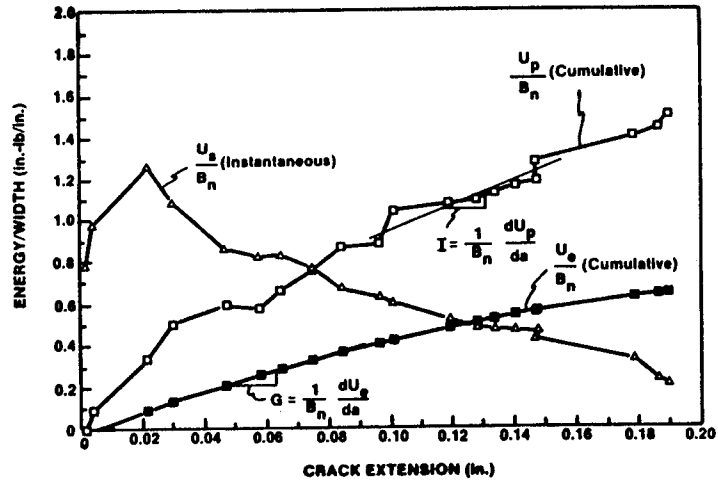
Figure 6: Cumulative energy released (elastic) and dissipated (plastic) and the instantaneous energy stored versus crack extension for specimen M2A.
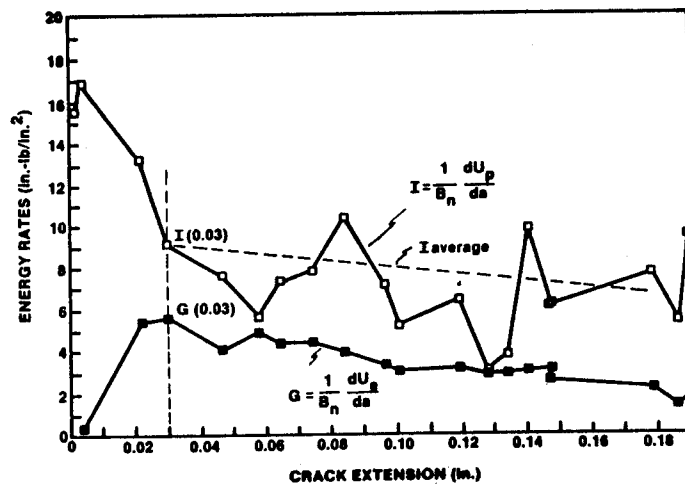

Figure 7: Elastic energy release rate and absolute plastic energy dissipation rate versus crack extension for specimen M2A.

SHELF LIFE WORK ON STRUCTURAL ADHESIVE BONDS IN ORDNANCE MATERIALS AT AB BOFORS

Christer K. Forsgren
AB Bofors, Sweden. Department of
Explosives Technology
S-691 80 Bofors, Sweden
Telephone +46586 83461

At AB Bofors all new projects of development include shelf life work on the complete system. The purpose of shelf life work is:

-To secure the fulfilment of shelf life requirements of a product when developed

-To estimate the shelf life of a product

-To give ideas for maintenance routines

Some of our shelf life specialists are experts in polymers, including adhesives. A coaxial bond between an aluminium ring and a kevlar/ epoxy tube, used as the missile body in Rbs 56, Bill will be used as an example. See fig 1.
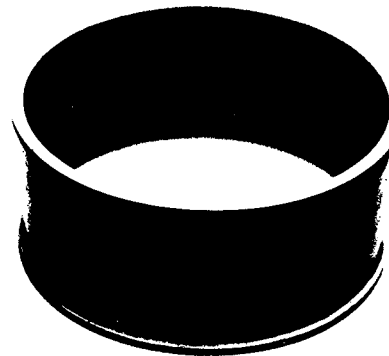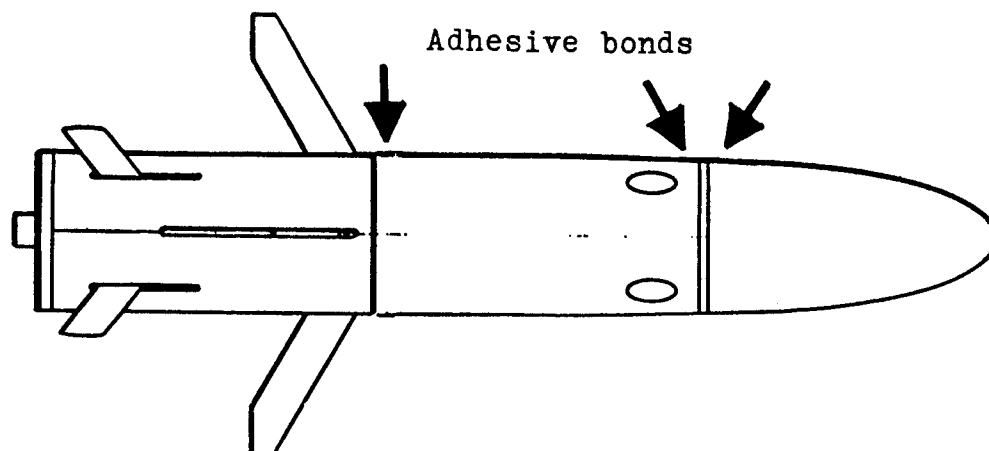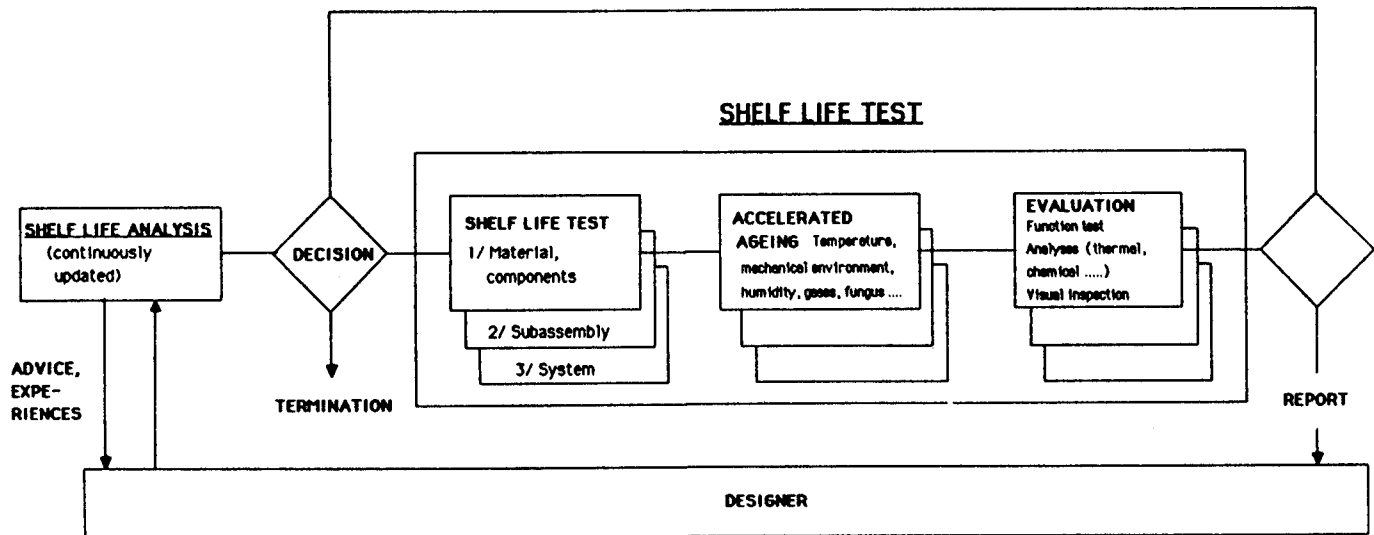

Figure 2

Adhesive bonds

Figure 1

During the environmental testing
of the Bill-antitank system there
has been a number of sub-units and
missiles thermally aged and tested
for function (go or no - go). The
aim of shelf life work is to
analyze how much longer and in what
type of environment the reliability
still remains high.

SHELF LIFE TEST

SHELF LIFE ANALYSIS (continuously updated)	

DECISION

SHELF LIFE TEST 1/ Material, components

2/ Subassembly

3/ System

ACCELERATED AGEING Temperature, mechanical environment, humidity, gases, fungus ....

EVALUATION Function test Analyses (thermal, chemical .....) Visual Inspection

ADVICE, EXPE-RIENCES

TERMINATION

REPORT

DESIGNER

1   SHELF LIFE ANALYSIS

All components including function
and requirements are listed, a
classification of the need for
further work on each component
has been carried out.

In this case there will be
discussions about the selection
of materials, joint design, surface
treatment, environmental effects,
producibility and non-destructive
testing with the designer and
manufacturer.

The preliminary design included a
chromated aluminium ring cleaned
with a solvent in an ultrasonic
bath. An epoxy (AW 106/HV 953U)
cured at 70°C for 2 h was used.
Tests were conducted using ultra-
sonic non-destructive equipment to
assure good gapfilling of the bond.

2   SHELF LIFE TESTS

Test 1   Materials/components

(Time: The beginning of the
         design work of the missile)

Accelerated test at 60°C/60 % RH
and volatile components from rocket
motor and gasgenerator propellants,
often in a higher concentration than
obtained in the missile under real
storage conditions.

Evaluation by visual inspection,
gravimetry and shore hardness
measurements. Compatibility tests
using microcalorimetry will,
depending on the application, be
performed on at least one adhesive.

More than one adhesive is normally
tested to get alternatives, if the
chosen adhesive would not pass the
test.

460

In this case five adhesives were chosen. From CIBA-GEIGY: Araldit AW136/HY994, AW144/HY994 and AW106/HV953U. From Permabond: ESP110 (one comp. epoxy) and E31. Test items consisted of solid aluminium cylinders with ∅ 40 mm for shear strength testing. A gap of 0.14 mm was used. The two-component epoxies were cured for 3 days at +60°C and the one-component for 1.5 h at +140°C. Evaluation was carried out at 60°C.

·The different adhesives were simultaneously tested in the production plant. The high curing temperature of the one-component epoxy eliminated Permabond ESP110. The thin kevlar/epoxytube could perhaps change some dimensions during high temperature curing, which would be critical. The viscosity of AW136/HY994 was too low during curing and ran out of the gap. Filler sedimentation of Permabond E31 eliminated another alternative. Araldit AW144/HY994

RESULTS
Shear strenght
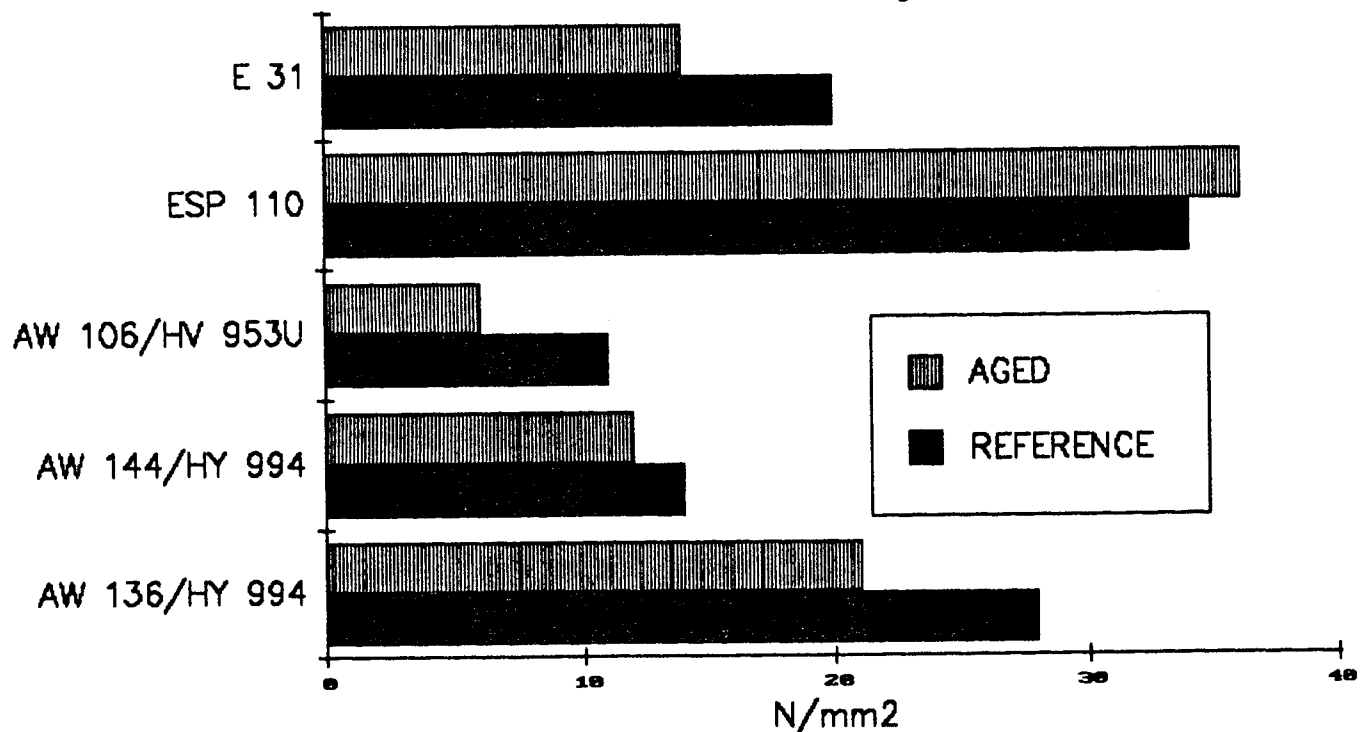
Fungus test

A Bonded test part (see fig 2) was together with other Bill-materials tested according to MIL-STD 810D method 508.3 fungus. The Bonding-preparations were the same as in the production plant. No growth of fungus could be detected (Grade 0).

has a suitable viscosity (Gap approximally 0.2 mm), good temperature characteristics and is not too much affected by this type of aging.

Short parts of the missile body were then bonded to aluminium rings and tested axially, see fig 2. Calculations showed that at 500 g (acceleration during firing) a maximum force of 15000 N would be obtained. All test items bonded with Araldit AW144/HY994 could

withstand more than 30000 N. This indicates a tensile shear strength of 3 N/mm² at 60°C in this application. One of the limiting factors is the strength of the epoxy matrix in the composite.

Test 2   Sub-assembly

(Time: At the end of the design period)

Accelerated test in a humidity/temperature chamber with temperatures between 30-70°C and relative humidity of 15-95 % RH.

Aging simulating 3-5 years of tropical storage.

Test-items: Bonded aluminium ring and epoxy/kevlar tube. Bonded test-pieces of aluminium for falling weight impact testing at different temperature.

Evaluation test: Acceleration test (axial) simulating firing of the missile.

Result: No displacement between ring and tube.

Test 3   System

(Time: During qualification)

Accelerated test in humidity/temperature chamber (see test 2) simulating 15 years of tropical storage followed by mechanical environmental tests.

Evaluation test: Acceleration test (axial) simulating firing of the missile.

Result: The first test will be performed in November 1987.

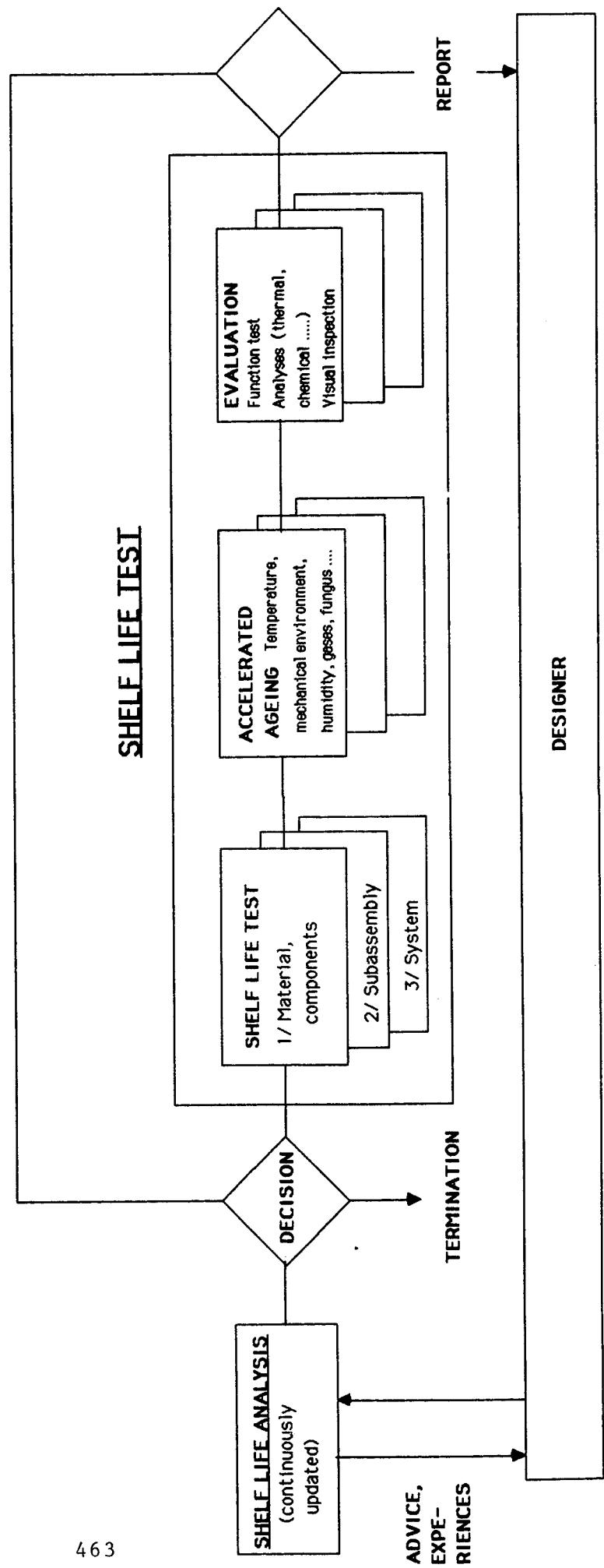There has been a continuing discussion concerning the quality of adhesive and the final joint. Ultrasonic non-destructive testing has been used occasionally during the development of the missile body to verify the manufacturing method. The correlation between ultrasonic testing and strength has not been too good. The fact that the margin of safety is quite high (more than three times), work is now concentrated to quality control in the production. Samples for destructive testing are taken from the production line at specified time intervalls.
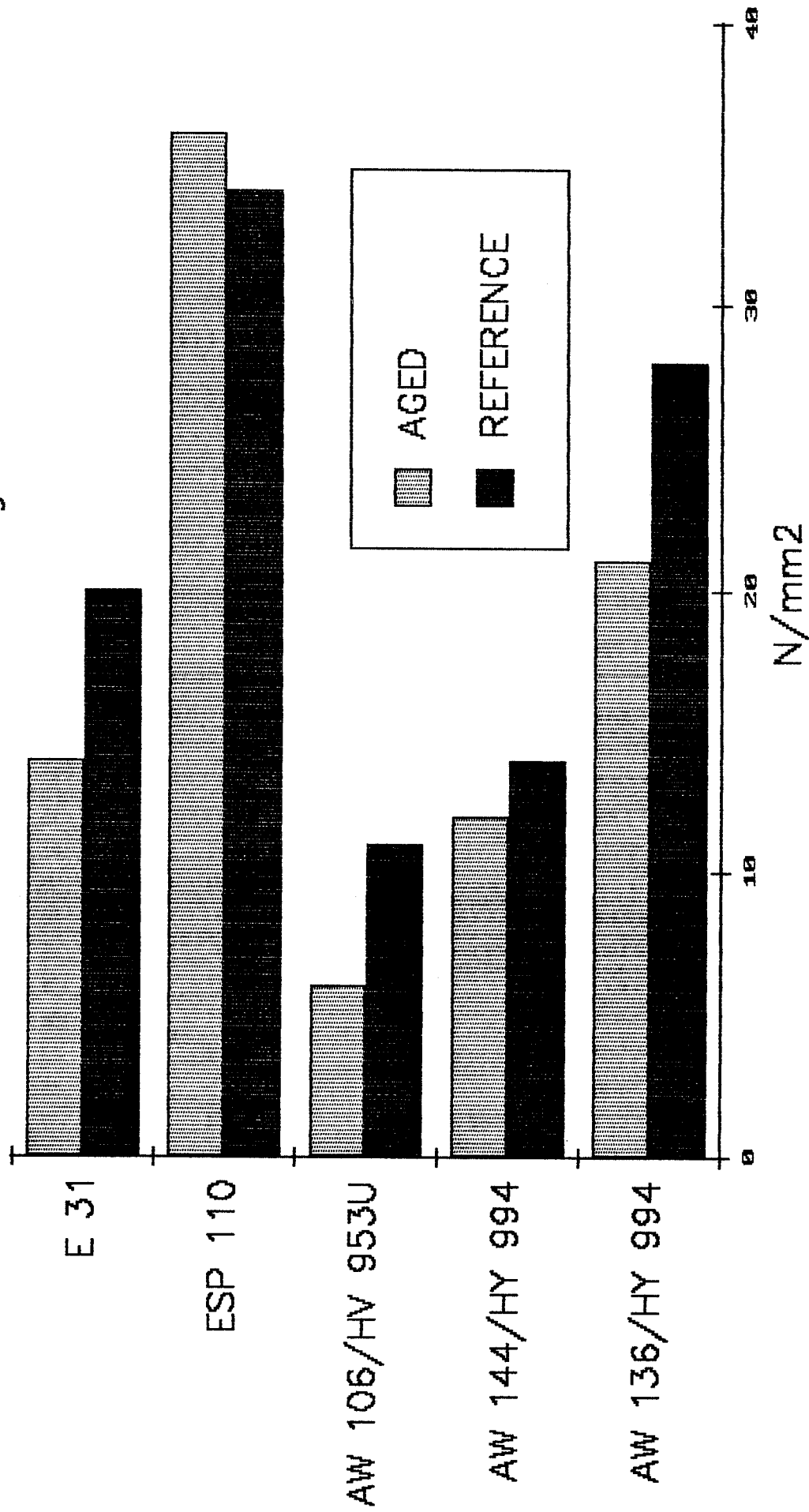
SUMMARY CONCLUSIONS

-Shelf life work establishes high reliability and safety also after long term storage and handling

-The realization of shelf life work has made designers and production personnel aware of the importance of the long-term aspects on selection of adhesives, surface treatment compability, production parameters and test procedures.

SHELF LIFE TECHNOLOGY AT AB BOFORS

SHELF LIFE TEST

SHELF LIFE TEST
1/ Material, components
2/ Subassembly
3/ System

ACCELERATED AGEING Temperature, mechanical environment, humidity, gases, fungus ....

EVALUATION
Function test
Analyses (thermal, chemical .....)
Visual inspection

REPORT

DECISION

TERMINATION

SHELF LIFE ANALYSIS (continuously updated)

ADVICE, EXPE-RIENCES

DESIGNER

RESULTS
Shear strenght

E 31

ESP 110

AW 106/HV 953U

AW 144/HY 994

AW 136/HY 994

AGED

REFERENCE

N/mm2

0   10   20   30   40

464

OPTICAL BONDING TECHNOLOGY

K. Yeh, R.D. Hermansen, S.R. Felstein, D.T. Chow
Electro-Optical and Data Systems Group
Hughes Aircraft Company
El Segundo • California

1. ABSTRACT

Ready access to reliable engineering properties data of materials is essential to effective material selection and application. Since adhesives are often used for the attachment of optical elements, it is critical that the proper adhesive be selected for a particular design to ensure the performance reliability of the system. In this study, various bond joint configurations were examined and the material properties of some commonly used adhesives in optical bonding applications were characterized and reported.

2. INTRODUCTION

Adhesives are used extensively for bonding optical elements which are used to provide electronic boresight in an electro-optical system. Adhesives tend to shrink slightly during cure which leads to distortion of the optical elements. Mismatch in the coefficient of thermal expansion between the adhesive, optics, and metal mount also introduces stresses when the operating temperature changes, creating more distortion. In order to preserve system aiming accuracy over the operating temperature range, it is critical that the proper adhesive be selected for a particular design. Proper adhesive selection also assures the performance reliability of the system. The deficiencies of the adhesive can only be circumvented by design alternatives if the material properties of the adhesive are available. The objective of this study is to optimize an adhesive bond joint design using finite element analysis techniques and to establish a reliable material properties database which is essential to effective adhesive selection and application.

3. ADHESIVE CHARACTERIZATION

Table 1 lists the adhesive characterized and the cure schedule used for each material. The material properties generated and corresponding test methods are shown in Table 2. The shear

TABLE 1. ADHESIVES CHARACTERIZED

ADHESIVE	GENERIC TYPE	CURE SCHEDULE
A-12 (1:1)	EPOXY	24 HRS/RT PLUS 2 HRS/160°F
A-12 (2:3)	EPOXY	24 HRS/RT PLUS 2 HRS/160°F
A-12 (1:2)	EPOXY	24 HRS/RT PLUS 2 HRS/160°F
EC2216	EPOXY	16 HRS/RT PLUS 16 HRS/160°F
PR 1440B2	POLYSULFIDE	7 DAYS/RT
URALANE 5753LV	POLYURETHANE	7 DAYS/RT
DC 93-500	SILICONE	7 DAYS/RT

TABLE 2. MATERIAL PROPERTIES AND CORRESPONDING TEST METHODS

MATERIAL PROPERTY	TEST METHOD
SHEAR STRENGTH	ASTM D1002
SHEAR MODULUS	RHEOMETRICS
TENSILE PROPERTIS	ASTM D412
LINEAR CURE SHRINKAGE	ASTM D2566
SPECIFIC HEAT	ASTM D2766
THERMAL CONDUCTIVITY	COLORA THERMOCONDUCTOMETER
GLASS TRANSITION TEMPERATURE (Tg)	RHEOMETRICS
COEFFICIENT OF THERMAL EXPANSION	THERMOMECHANICAL ANALYSIS (TMA)

strength data requires definition of substrate surface preparation. The 2024-T3 alclad aluminum was Ajax scrubbed followed by FPL acid etch. Bondline thickness was maintained at 10 mils for all lap shear specimens. The shear modulus, and glass transition temperature (Tg) were measured using an RDS (Rheometric Dynamic Spectrometer) 7700 with an automatic torsional strain adjust feature. Testing at 1 Hz on a 2.5 by 0.5 by 0.125-in specimen was performed.

The thermal conductivity of the adhesives was measured at 93°C only using a Colora Thermoconductometer. The sample thickness was controlled at 0.125 inch. It is important to control the sample thickness in order to obtain a comparable value for different adhesives because this technique is sensitive to the thickness of the material being tested. Thermomechanical analysis (TMA), used to determine the coefficient of thermal expansion, was performed using a Dupont 990 thermal controller in conjunction with a Dupont 941 Thermomechanical analyzer. Testing was performed on a 0.25-in. cube specimen under a 5 gm load and a heating rate of 10°C per minute. All other testing was performed per the applicable ASTM method listed in Table 2.

4. FINITE ELEMENT ANALYSIS

A non-linear, NASTRAN finite element analysis program was used to model the glass to metal bond. The model was established to determine in what way the bond geometry and adhesive properties could be changed to minimize the cure and thermally induced strain in the optical element. Such parameters as bondline thickness, adhesive modulus, cure shrinkage,

coefficient of thermal expansion, and temperature were varied to determined their relative contribution to the overall distortion of the optics, Specific material property data and joint dimensions were input to the program. These materials include BK-7 borosilicate glass, 416 stainless steel mount, and EC2216 adhesive. EC2216 adhesive was selected in the study because its glass transition temperature (91°F) is right in the middle of the operating temperature range for most electro-optical systems which make the problem more interesting. Three different bond joint configurations were modeled: (1) a circular bond spot (Figure 1a), (2) an annular bond area (Figure 1b), and (3) a post-bond (Figure 1c).
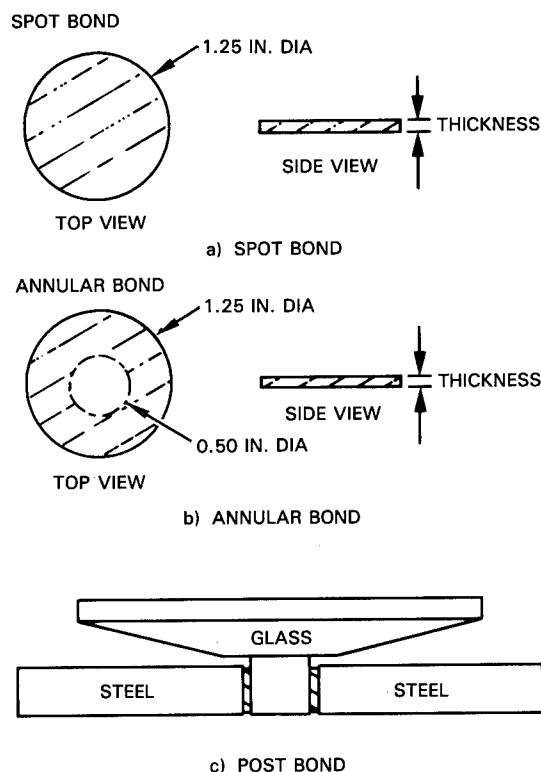

Figure 1. The annular spot and post bond configurations modeled by the Nastran analysis.

466

In all cases, the model translates the stresses caused by volume shrinkage during cure to thermally induced stresses. Simply by lowering the reference (stress-free) temperature for room and elevated temperature calculation and by increasing the reference temperature for induced strain prediction below room temperature. Normally the EC2216 adhesive is cured at room temperature for 16 hours followed by a 16 hours post-cure at 160°F. To simplify the analysis, the post-cure effect was not simulated. Instead, the cure shrinkage was assumed to occur entirely at room temperature. Any cure induced strain during post-cure was ignored by the model. This is not an unreasonable assumption since the majority of shrinkage occurs at the initial cure and not during the post-cure. A later experiment validates the assumption in this case.

The analysis also did not model any time-dependent (viscoelastic) effects because of the lack of data on the adhesive creep characteristic at the time of analysis.

5. BONDING STUDY

Mirrors were bonded using adhesives with different characteristics (i.e., glass transition temperature and modulus). Room temperature distortion measurements (see Table 3) showed that the mirror bonded with EA9323 (Tg = 220°F, E (160°F) = $3.63.10^5$ psi) was distorted completely. The mirror surface changed from concave to convex shape after an elevated temperature (160°F) post-cure. This contradicted the assumption made in the model that the thermally induced stresses during post-

TABLE 3. THE R.T. MIRROR DISTORTION MEASUREMENT FOR ANNULAR BONDED MIRROR WITH DIFFERENT ADHESIVES

ADHESIVE	R.T. MIRROR DISTORTION (NO. OF FRINGES)	
	EA 9323	EC 2216
BEFORE BONDING	0.02	0.084
AFTER INITIAL R.T. CURING	0.105	0.101
AFTER 16 HRS POST CURE AT 160°F	CX*	0.083

*CX — THE SHAPE OF MIRROR CHANGED FROM CONCAVE TO CONVEX

cure could be ignored. The large volume change at the initial stage of cure had less significant effect than the thermal stresses created during post-cure when the adhesive was much harder. However, the assumption is still valid if the adhesive is rubber-like at the post-cure temperature as in the case of the second mirror which was bonded with EC2216 (Tg = 91°F, E (160°F) = $5.8.10^3$ psi). Elevated temperature post-cure actually relieved some of the residual stress created in the initial stage of curing.

Three more BK-7 mirrors were bonded to 416 stainless steel mount with different bond geometries (spot, annular and post) using EC2216 adhesive. The bondline thickness was controlled at 10 mils and all three assemblies were room temperature cured for 16 hours followed by a 16 hour post-cure at 160°F. The interferometry pattern for each assembly was then taken at -65°F, 0°F, 68°F and 160°F. The results are then compared to the analysis.

6. RESULTS

The material properties data for some commonly used adhesives in the optical bonding application

are given in Table 4 through Table 9. The material properties data are provided in this report for reference and should not be mistaken as design allowable. Only limited samples have been

TABLE 4. LAP SHEAR STRENGTH OF VARIOUS ADHESIVES

ADHESIVE	SINGLE LAP SHEAR STRENGTH (PSI)*		
	−65°F	77°F	160°F
A-12 (1:1)	2500	3500	1300
A-12 (2:3)	2100	3100	850
A-12 (1:2)	1600	3120	325
EC2216	2310	3020	.715
PR1440B2	2607	359	240
URALANE 5753LV	3400	750	250
DC 93-500			

*THE BOND STRENGTH VALUES REPORTED ARE FOR ALUMINUM SUBSTRATES TESTED IN ACCORDANCE WITH ASTMD 1002

TABLE 5. THERMAL PROPERTIES OF DIFFERENT ADHESIVES

ADHESIVE	CTE BELOW Tg (IN/IN/°F)	Tg (°F)	CTE ABOVE Tg (IN/IN/°F)	THERMAL CONDUCTIVITY (BTU/FT HR°F)
A-12 (1:1)	$42 \cdot 10^{-6}$	158	$179 \cdot 10^{-6}$	0.21
A-12 (2:3)	$46 \cdot 10^{-6}$	120	$138 \cdot 10^{-6}$	0.20
A-12 (1:2)	$44 \cdot 10^{-6}$	95	$114 \cdot 10^{-6}$	0.20
EC2216	$37 \cdot 10^{-6}$	91	$65 \cdot 10^{-6}$	0.20
PR1440B2	$33 \cdot 10^{-6}$	−42	$111 \cdot 10^{-6}$	0.15
URALANE 5753LV	$41 \cdot 10^{-6}$	−85	$114 \cdot 10^{-6}$	0.14
DC 93-500	$44 \cdot 10^{-6}$	−175	$158 \cdot 10^{-6}$	0.10

TABLE 6. SHEAR MODULUS OF DIFFERENT ADHESIVE AS FUNCTION °F TEMPERATURES

ADHESIVE TEMP (°F)	SHEAR MODULUS (×10⁵ PSI)								
	−80	−65	−40	0	40	75	110	150	180
A-12 (1:1)	2.9	2.8	2.7	2.4	2.2	1.9	1.5	0.36	0.23
A-12 (2:3)	−	2.5	2.3	2.1	1.9	1.7	0.96	0.018	0.0075
A-12 (1:2)	−	2.6	2.3	2.0	1:7	1.1	0.023	0.0045	0.0036
EC2216	−	3.3	3.1	2.7	1.8	0.21	0.026	0.016	0.015
PR1440B2	1.6	0.76	0.019	0.0037	0.0022	0.0016	0.0012	0.0011	−
URALANE 5753LV	1.1	0.21	0.067	0.032	0.021	0.015	0.011	0.0078	−
DC 93-500	0.02	0.015	0.012	0.0076	0.0063	0.0056	0.0051	0.0049	0.0047

TABLE 7. TENSILE PROPERTIES OF SEVERAL ADHESIVES AT DIFFERENT TEMPERATURES

ADHESIVE	TEST TEMP (°F)	TENSILE STRENGTH (PST)	TENSILE MODULUS (PST)
A-12 (1:1)	−65	$7.2 \cdot 10^{3}$	$5.4 \cdot 10^{5}$
	77	$5.9 \cdot 10^{3}$	$3.9 \cdot 10^{5}$
	180	$3.4 \cdot 10^{2}$	$3.5 \cdot 10^{3}$
A-12 (2:3)	−65	$5.8 \cdot 10^{3}$	$5.3 \cdot 10^{5}$
	77	$2.5 \cdot 10^{3}$	$1.6 \cdot 10^{5}$
	180	$1.5 \cdot 10^{2}$	$1.7 \cdot 10^{3}$
A-12 (1:2)	−65	$5.0 \cdot 10^{3}$	$4.6 \cdot 10^{5}$
	77	$1.3 \cdot 10^{3}$	$5.4 \cdot 10^{4}$
	180	−	−
EC2216	−65	$6.5 \cdot 10^{3}$	$8.9 \cdot 10^{5}$
	77	$2.7 \cdot 10^{3}$	$2.7 \cdot 10^{5}$
	180	$5.2 \cdot 10^{2}$	$1.4 \cdot 10^{3}$
PR1440B2	−65	$2.2 \cdot 10^{3}$	$7.7 \cdot 10^{5}$
	77	$3.6 \cdot 10^{2}$	$5 \cdot 10^{2}$
	180	$3.4 \cdot 10^{2}$	$4 \cdot 10^{2}$

TABLE 8. SPECIFIC HEAT OF VARIOUS ADHESIVES AT DIFFERENT TEMPERATURES

ADHESIVE TEMP (°F)	SPECIFIC HEAT (BTU/LB °F)							
	−117	−81	−45	−9	77	117	153	189
A-12 (1:1)	0.21	0.24	0.27	0.29	0.32	0.35	0.38	0.40
A-12 (2:3)	0.18	0.20	0.22	0.25	−	0.38	0.41	0.43
A-12 (1:2)	0.27	0.29	0.31	0.34	−	0.50	0.53	0.55
EC2216	0.66	0.69	0.73	0.78	0.90	0.94	0.96	0.98
PR1440B2	0.10	0.12	0.20	0.21	0.25	0.26	0.27	0.28
URALANE 5753LV	0.19	−	0.32	0.35	0.41	0.43	0.45	0.46
DC 93-500	0.16	0.17	0.19	0.20	0.22	0.23	0.24	0.25

TABLE 9. LINEAR CURE SHRINKAGE OF DIFFERENT ADHESIVES

ADHESIVE	LINEAR CURE SHRINKAGE (%)
A-12 (1:1)	0.33
A-12 (2:3)	0.18
A-12 (1:2)	0.22
EC2216	0.21
PR1440B2	0.15
URALANE 5753LV	0.24
DC 93-500	

TABLE 10. MIRROR DISTORTION
PREDICTED BY NASTRAN NONLINEAR
ANALYSIS. FOR "SPOT", "ANNULAR"
AND "POST" BOND GEOMETRIES AS
COMPARED TO THE EXPERIMENTAL
RESULTS. THE ADHESIVE BONDLINE
THICKNESS IS CONTROLLED AT
10 MILS

TEMP (°F)	TYPICAL ELASTIC MODULUS (PSI)	MIRROR DISTORTION (NO. OF FRINGES)					
		SPOT		ANNULAR		POST	
		PREDIC-TION	EXPERI-MENT	PREDIC-TION	EXPERI-MENT	PREDIC-TION	EXPERI-MENT
-65	$8.5 \cdot 10^5$	16.3	10^+	15.8	10^+	12.6	10^+
0	$4.1 \cdot 10^5$	5.8	5-10	5.4	5-10	10	5-10
68	$1.8-8.8 \cdot 10^4$	0.096-0.463	0.275	0.060-0.298	0.254	0.823	0.534
160	$3.7 \cdot 10^3$	0.19	12	0.12	12	1.98	7-8

tested. The shear strength values provided are only the adhesion strength to the aluminum substrate, the actual adhesion to other adherends may vary. Some physical properties of the adhesives depend greatly on the type of test specimen and test method used. The shear moduli calculated from the measured tensile moduli and poisson's ratio are not in total agreement with the shear moduli measured in torsional mode. The thermal conductivity of the material also varies as the sample thickness changes.

The amount of distortion predicted (number of fringes) in the optical element by the analysis in given in Table 10. The data presented is based on 68°F as being the stress free temperature. The distortion predicted at 68°F is caused by the curing shrinkage only. The values at other temperatures were obtained by adding the distortion at reference temperature with those predicted due to temperature change. It is observed that the number of fringes increases significantly with decreasing temperature. This is due primarily to the increase in modulus and not the mismatch in the thermal expansion coefficient. Since both the adhesive modulus and coefficient of thermal expansion affect the amount of distortion predicted by the analysis, these parameters were specifically investigated to determine the relative contribution of each. By decreasing the modulus by a factor of two an average of 34% reduction in the number of fringes is seen. This compares to an 8% change in distortion when the coefficient of expansion is lowered by a factor of two. Furthermore, the modulus of an adhesive is much more sensitive to temperature change than its thermal expansion characteristic. The modulus may vary by several orders of magnitude going through the glass transition region whereas the thermal expansion coefficient is significantly less sensitive to temperature variations.

In addition, a thicker bondline seemed to have a negative influence on the predicted distortion. This is true at room temperature and below, but not so at the higher temperature. This result is not unusual since the net volume change due to cure will be greater as the volume of the adhesive increases. Thus, as the temperature is lowered, more shrinkage is expected with a thicker bondline and distortion is greater. When the temperature is raised, however, the increased volume expansion of the adhesive combined with the cure shrinkage results in lower distortion.

In all cases, the analysis shows that the annular bond yields lower distortion for the mirror than the spot bond. Thus, any decrease in the lateral bond area seems to have benefit on the overall distortion.

469

One technique which may further reduce the distortion is to use a series of smaller bond spots in an annular distribution. For the post-bond geometry, predicted distortion at or above room temperature is greater than either of the other two geometries. The axial contraction of the adhesive due to cure induces bending moments on the mirror which are "in the plane" of the mirror. Whereas, bending moments induced by the spot or annular geometry are perpendicular to the plane of the mirror. Therefore, the post-bond is more sensitive to cure shrinkage. When the temperature is lowered, both the adhesive and the metal mount contract which creates more distortion in the mirror. For the spot or annular geometry, both contractions contribute to the distortion of the mirror. For the post-geometry, this is not the case. Further axial contraction due to a lowering of temperature is offset by the radial contraction of the metal mount. Thus, while the mirror is more sensitive to axial adhesive contraction this effect is reduced by the contraction of the metal mount.

Although the NASTRAN model predictions for all three bond geometries with EC2216 adhesive are in agreement with the experimental results, for temperatures below the glass transition temperature (91°F), the model fails to predict the mirror distortion accurately at 160°F. This is probably due to the inaccurate material properties data input at 160°F. The behavior of the adhesive in thin-layer form may be different than that in the bulk form. The tensile properties (stress-strain curve) of the EC2216 adhesive used in this analysis were generated in bulk form with dog-bone specimens. While the adhesive remains rigid below its glass transition temperature, the difference in thin-layer form may not be significant. However, the adhesive may not behave as an elastomer in thin-layer form above its glass transition temperature as expected.

7. CONCLUSION

The finite element analysis appears to predict, with reasonable accuracy, the behavior of a glass mirror bonded to a metallic mount. It should be noted that these results are predicted by a static analysis and any changes in residual stress through relaxation or creep with time will change the predicted distortion.

The analysis is only accurate if the material properties data of the adhesives are reliable. Since the behavior of the adhesive in thin-layer form appears different to that in bulk form; and the accuracy of the mechanical properties of the adhesive also depends on the type of specimen and test method used, it is suggested that specimens for determining mechanical properties should be of thin-layer configuration. Furthermore, the specimen joint configuration and specimen substrate should be as close to those used in the real application as possible.

SORPTION AND TRANSPORT PROPERTIES
OF MY 720/DDS EPOXY REACTED WITH
BLOCKING REAGENTS

by
B. K. Kelly, R.D. Gilbert, R.E. Fornes, S. Lonikar,
and N. Rungsimuntakul

Fiber and Polymer Science Program
North Carolina State University
Raleigh, NC 27695

Introduction

Fisher et al(1) and Hu, Fornes and Gilbert (2) showed that the equilibrium moisture absorption of the epoxy system tetraglycidyl 4,4'-diamino-diphenylmethane (TGDDM) cured with 4,4'-diaminodiphenyl-sulfoxide (DDS) is lowered as much as 75 percent if the residual functional groups (e.g. -OH, -NH$_2$, -CH - CH$_2$) are blocked by silylation, cyanoethylation or carbanila-tion. The optimum results were obtained if the blocking reagents contained fluorine.

Here we report the sorption and transport behaviour of several reactants using thin films of the epoxy and the effect of blocking the epoxy functional groups on the sorption and transport properties of water in the epoxy at 30° and 70°.

Some preliminary data on masked isocyanates incorporat-ed into the epoxy resin prior to cure are also reported.

Experimental

MY720 composed primary of TGDDM and DDS were kindly supplied by Ciba-Geigy. Acetonilrile, dimethyl sulfoxide (DMSO) were Fisher reagent grade and were dried over CaH$_2$ and molecular sieves, respectively. Trimethylsilylisocyanate (TMSI) (85%), α,α,α -trifluoro-m-tolyl isocyanate (MTPI),α,α,α -trifluoro-o-t-olyl isocyanate (OTPI) (97%) and benzyltrimethylammonium hydroxide (Triton B), 40% in CH$_3$OH, were obtained from Aldrich and were used without further purification. Acrylonitrile (ACN) from Polyscience, was used as received.

Thin films of cured epoxy resin were prepared using a 73/27 w % ratio of MY720 and DDS. The two components were agitated at 110° for 4-6 min. to obtain a uniform mixture which was deareated for 30-40 min. in a heated vacuum desiccator, allowed to cool under reduced pressure for 10-15 hour and then stored at 5° until further use. This prepolymer was finely ground and placed between two smooth teflon sheets and heated to 70°. The telfon sheets were backed with aluminum plates, the assembly clamped, placed in an oven preheated to 150°, the oven flushed with N$_2$ and evacuated. The epoxy samples were cured at 150° for 1 h and at 177° for 5 h. Then the samples were placed in glass vials and stored in a desic-cator at ambient temperature.

The sorption of distilled water by the epoxy films was determined at 30°, 45°, 55° and 70° using two sets of films (for each temperature) prepared at different times and each set consisting of at least 5 samples. The two sets had different film thicknesses. Film thicknesses were measured and grouped so that the thicknesses matched as closely as possible. Each set was immersed in water for 5 days at the particular temperature to remove water-soluble species. The films were dried at 100° under vacuum for 5 days, weighed, placed in sealed vials containing water (10ML) and heated to the desired temperature. The films were removed at various time intervals, padded dry and weighed to the nearest microgram until the weights remained constant for three successive weighings. The weight obtained one week later was used as the infinite absorption weight (Woo). The films were then heated at 100° under vacuum for 5 days and then reweighed (Wo).

Other sets of films were extracted with water to remove oligomeric species. Clean, dry vials were cooled to 0° and Triton B(0.25ML) and acrylonitrile (9.5 ML) added. The mixture was agitated during the addition and cooling was continued for 5 min. after the addition of ACN was completed. The vials were sealed and heated to either 30° or 70° and a dry, preheated epoxy film added to each vial. Periodically, the films were removed, wiped and weighed. This was repeated until equilibrium was reached or the ACN polymerized. Each film was rinsed in CH_3CN to remove unreacted ACN, heated to 100° under vacuum for 5 days to remove any CH_3CN, and then immersed in distilled H_2O and the equilibrium moisture determined as described above.

Similarly, sets of films were reacted with TMSI, OTPI and MTPI but the films were first extracted with dimethyl sulfoxide (DMSO) to remove low molecular weight species and then preswollen with DMSO to permit better penetration of the reactants. The equilibrium moisture absorption was determined after the reaction was terminated and DMSO and excess reactant removed with CH_3CN.

Masked isocyanates were prepared by reacting an isocyanate and a masking reagent in stoichiometric amounts. Proof of structure was by elemental analyses and NMR spectroscopy. Their unblocking temperatures were determined by the procedure of Griffin and Willworth (8). A desired amount of the masked isocyanate was added to the mixture of MY 720 and DDS prior to the curing step and the mixture cured as above.

Results and Discussion

Unmodified Resin

The equilibrium sorption values for water in the epoxy resin at four temperatures are given in Table I. The samples were immersed in distilled

water a minimum of 500 h to achieve approximate equilibrium. Figures 1-4 are plots of relative weight gain, M_t/M_{00}, vs $t^{1/2}/1$ (1 = film thickness) at the different temperatures. At each temperature the epoxy exhibits Case I or Fickian behavior. For water sorption, that is, the rate of diffusion is much slower than the rate of relaxation. The overlap of the curves for different film thicknesses at each temperature confirms Case I behavior. Diffusion coefficients (D) calculated (3.4) using equation (1) and Figures 1-4 are in Table II

$$D = \frac{0.0499}{(t/1^2)} \quad - - - (1)$$

where t is the time when M_t/M_{00} = 0.5, D increases with increasing temperature from 30° to 45° and decreases at 70°. Generally, the diffusion coefficient of a penetrant in a system increases monotonically with temperature unless chemical changes are occurring. Netraveli et al (5) report that absorbed water reacts with residual oxirane groups in the epoxy at 70°c resulting in an increased concentration of hydroxy groups while very little reaction occurs at R.T. This would, in turn, lead to increased hydrogen bonding with water in the resin, thereby lowering D since a significant reaction occurs at higher temperatures, i.e., D = D_{IR} (diffusion accompanied by reaction). In the simplest case where the reaction is essentially instantaneous compared with diffusion D_{IR} = D/(1+R) resulting in a lower value of the measured diffusivity. R is the ratio of the concentrations of reacting and diffusing penetrants and is usually 70. These data also suggest that the reaction of H_2O with oxirane groups is insignificant at 55°.

Modification of the Epoxy Films

The diffusion accompanied by reaction of acrylonitrile was monitored gravitrically at 30_0 and 70°C. It is known that the quarternary base, Triton B causes some polymerization of acrylonitrile (1) and consequently equilibrium could not be reached. Typical plots are presented in Figure 5 for the 2.5 mil. samples at 30° and 70°. At the lower temperature the increase in weight essentially levels off. At 70°, however, when more homopolymerization is taking place, the weight continues to increase. An arbitrary time of 169 hours was taken as the equilibrium value. The two curves are somewhat different in shape. Since relaxations, diffusion with reaction and homopolymerization are all occurring, it is not possible to analyse such complex curves in any detail. Assuming that all the ACN has resulted in cyanoethylation, a maximum of 34 and 39% (Table III) of the residual functional group (OH, NH, NH_2, C - C) have reacted at 30° and 70° respectively (assuming no poly acrylonitrile formed insitu).

Percent equilibrium weight gains for TMSI, OTPI and MTPI are also in Table III. The epoxy films were taken to equilibrium with DMSO

prior to addition of the reactants. MTPT reacted to a greater extent than the other isocyanates, presumably due to differences in mobility and steric interference. At 30° MTPI reacts to about the same extent as ACN but the reaction with ACN at 70° is significantly greater. Details of sorption behavior of the isocyanates and acetonitorle in DMSO will be discussed in a separate paper (2).

Plots of M_t/M_{00} vs $t^{1/2}/1$ show the sorption of the isocyanates essentially follow Case I or Fickian behaviour except at 70° TMSI shows Pseudo-Fickian behavior. Diffusion coefficients were calculated using the instantaneous reaction procedure or equations (1) and (2)

$$\frac{dc}{dt} = \left(\frac{D}{Rt\lambda}\right)\left(\frac{d^2 C}{dX^2}\right) - - -(2)$$

where C is the concentration of the penetrate, at a distance x from the surface. The values are given in Table IV. The D_{IR} values are in the order MTPI > TMSI > OTPI at 30° and MTPI > OTPI > TMSI at 70° and are higher for each reactant at 70°. The differences at the two temperatures is presumably due to the temperature coefficients for diffusion of the reactants.

Equilibrium weight gains after immersion in distilled water for the epoxy resin before and after reaction with the various blocking reagents are in Tables V and VI. As low molecular weight species had been pre-extracted from

the films, it was assumed no loss occurred during the water absorption tests. Reductions in equilibrium moisture absorption of 63 and 68% at 30° and 70°, respectively, were obtained by cynoethylation and 62 and 54% after carbanilation with MTPI (Table V). The equilibrium moisture absorptions show a decrease with an increase in the number of blocked functional groups (Figure 6) at both 30° and 70°. The reductions in equilibrium moisture values at 70° are lower than those at 30° at equivalent degrees of reaction, when an isocyanate is the blocking reagent. Presumably at the higher temperature there is a larger unoccupied volume in the resin which is not fully compensated for by blocking the unreacted functional groups. Johncock and Tudgey (6) showed that halogen substituents on the phenyl ring of an epoxide decreases the equilibrium moisture uptake. The present results indicate there is a correspondence between the reduction of moisture absorption and the number of blocked functional groups regardless of the nature of the blocking group (Figure 6). This is somewhat surprising and contrary to the data of Hu et al (2) which indicate perfluorinated blocking groups provide the largest decrease in moisture absorption. However, a swelling agent for the epoxy resin was used in the case of the reactions with the isocyanates which may have resulted in an increase in unoccupied volume compared to the case for the reactions with ACN.

474

In Tables V and VI the equilibrium moisture absorption values are compared based on the reacted and unreacted dry weights. The latter values reflect the effect of the blocking reagent molecular weight and show the importance of employing blocking reagents of low molecular weight.

M_t/M_∞ vs. $t^{1/2}/l$ plots for moisture uptake at both $30°$ and $70°$ indicated moisture diffusion exhibits Case I or Fickian diffusion for the films after blocking with the various reactants. A typical plot is in Figure 7. Diffusion coefficients calculated employing equation (1) are in Tables VII and VIII. At $30°$ (Table VII), the diffusion coefficients are significantly higher for the resins after reaction with the blocking reagents. Johncock and Tudgey (3) noted an increase in diffusion coefficient for an aniline-based epoxy having a $-OCH_2 (CF_2)_6H$ group attached to the phenyl ring, which may indicate bulky substitutents alter the unoccupied volume of the resin. In addition, blocking of hydroxyl and amine groups reduces the possibility for hydrogen bonding which hinders water penetration.

At $70°$ the diffusion coefficient is unchanged compared to the value at $30°$ for the films reacted with ACN. However, the diffusion coefficients for the films reacted with the isocyanate blocking reagents are significantly reduced compared to the epoxy resin. This may be of significance regarding the effect of hygrothermal history on water absorption.

Masked Isocyanates

The melting points and unblocking temperatures of several masked isocyanated are shown in Table IX and their elemental analyses are in Table X. Their structure were confirmed by both ^{13}C and ^{19}F - NMR spectroscopy. These data will be reported elsewhere.

Reductions in the equilibrium moisture absorptions of cured films containing several of the masked isocyanates are in Table XI. As shown, reductions as high as 67 per cent were obtained .

Dynamic mechanical analysis data for a control and an epoxy containing Ph. HUMDI are in Figures 8 and 9 respectively. It is gratifying that the incorporation of the masked isocyanate has no significant effect on the complex modulus (C) until Tg is reached. There is a reduction in Tg (from $280°$ to $176°C$), but probably this can be adjusted by altering the cure regime.

REFERENCES

1. Fisher, C.M., R.D. Gilbert, R.E. Fornes and J.D. Memory, J. Poly. Sci., Poly. Chem Ed., 23, 2931 (1985).

2. Hu, H.P., R.D. Gilbert and R.E. Fornes, J. Polym. Sci., Polym. Chem Ed., Accepted for publication.

J.D. Memory, J. Poly. Sci., Poly. Chem Ed., 23, 2931 (1985).

2. Hu, H.P., R.D. Gilbert and R.E. Fornes, J. Polym. Sci., Polym. Chem Ed., Accepted for publication.

3. Crank, J., The Mathematics of Diffusion, 2nd Ed., Oxford Press, London, 1975.

4. Stannett, V. and H. Yasudo, " The Measurement of Gas and Vapor Permeation and Diffusion in Polymers", Ch. 3 in Testing of Polymers, J.V. Schmitz d., Interscience N.Y, 1965.

5. Netravali, A.N., R.E. Fornes, J.D. Memory and R.D. Gilbert, J. Appl. Polym. Sci., 31, 1531 (1986).

6. Johncock, P. and G.F. Tudgey, Brit. Polym. J. 15, 14(1983).

7. B.K. Kelly, R.D. Gilbert, R.E. Fornes and V.J. Stannett, to be published.

8. G. R. Griffin and L. J. Willworth, Ind. Eng. Chem. Prod. Res. Develop., 1, 265 (1962).
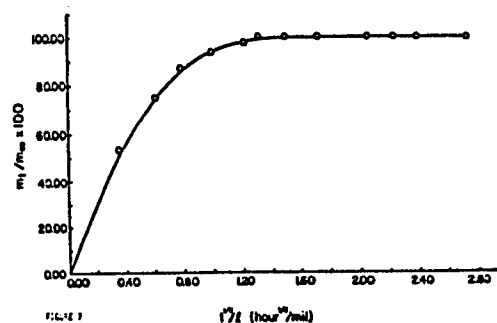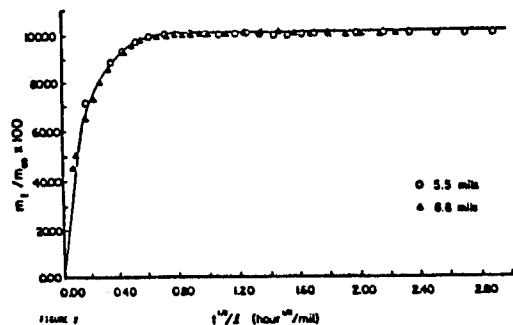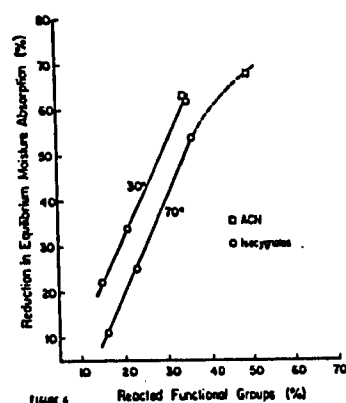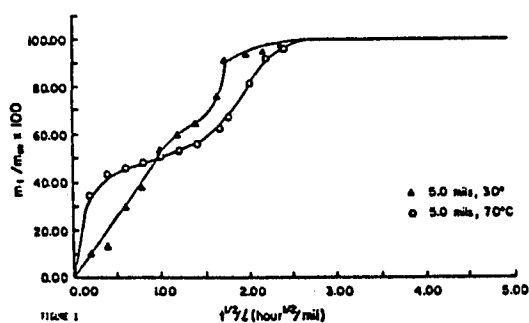
List of Figures

Table I. Percent equilibrium weight gain values of untreated water soaked MY720/DDS cured epoxy films

Temperature (°C)	Thickness (mils)	M_t/M_0 x 100
30	2.5	6.12 ± 0.65
	1.6	6.40 ± 0.20
Average	2.0	6.26 ± 0.42
45	8.0	6.67 ± 0.26
	5.4	7.37 ± 0.23
Average	6.7	7.02 ± 0.26
55	8.0	6.36 ± 0.46
	4.7	6.51 ± 0.36
Average	6.4	6.43 ± 0.24
70	8.8	6.89 ± 0.27
	5.3	7.07 ± 0.15
Average	7.0	6.98 ± 0.14

Table II. Diffusion coefficients for diffusion of distilled water in untreated MY720/DDS cured epoxy films

Temperature (°C)	D (cm^2/sec) x 10^9
30	0.083
45	5.64
55	10.3
70	6.12

Table III. Percent equilibrium weight gain values of reactant and number of blocked sites after reaction in MY720/DDS cured epoxy film

Reactant	Temperature (°C)	M_r/M_0 x 100^{a}	% Blocked^{b} Site
ACN^{c}	30	16.32 ± 0.74	34
	70	23.54 ± 3.52	49
THSI	30	21.84 ± 0.52	21
	70	23.80 ± 0.60	23
HTPI	30	59.77 ± 0.43	35
	70	61.56 ± 0.48	36
OTPI	30	26.29 ± 0.38	15
	70	27.53 ± 0.46	16

a/ These values are based on dried weights.

b/ These values were calculated assuming one molecule reacted creates one blocked site, and all weight gain is due to reacted reactant. (See Appendix 8.2 for sample calculation.)

c/ All ACN values are averages of two sets of samples of different thicknesses at 169 hours rather than equilibrium.

Table IV. Diffusion accompanied by reaction values, D_{IR}, for reactants in MY720/DDS cured epoxy films

Reactant	Temperature (°C)	D_{IR} (cm^2/sec) x 10^{10}
OTPI	30	0.66
	70	2.28
HTPI	30	0.86
	70	2.38
THSI	30	0.86
	70	1.01

Table V. Percent equilibrium moisture absorption values of water soaked MY720/DDS cured epoxy films at 30°C

Reactant	M_w/M_0 x 100^{a}	% Change	M_w/M_0 x 100^{b}	% Change
Untreated^{c}	6.12 ± 0.65	---	6.12 ± 0.65	---
ACN^{d}	2.31 ± 0.15	-63	2.69 ± 0.15	-56
OTPI^{e}	4.89 ± 0.10	-22	6.14 ± 0.10	+ 0.4
HTPI^{e}	2.40 ± 0.08	-62	3.81 ± 0.08	-37
THSI^{e}	4.11 ± 0.07	-34	5.01 ± 0.07	-18

a/ Percent gain and change in water sorption based on the reacted dry weight.

b/ Percent gain and change in water sorption based on the unreacted dry weight.

c/ Average film thickness = 1.8 mils

d/ Average film thickness = 3.0 mils

e/ Average film thickness = 2.0 mils

NOTE: The percent weight gain of the reactants can be found in Table III. All reactions were conducted at 30°C.

Table VI. Percent equilibrium moisture absorption values of water soaked MY720/DDS cured epoxy films at 70°C

Reactant	M_w/M_0 x 100^{a}	% Change	M_w/M_0 x 100^{b}	% Change
Untreated^{c}	7.00 ± 0.14	---	7.00 ± 0.14	---
ACN^{d}	2.24 ± 0.17	-68	2.77 ± 0.18	-60
OTPI^{e}	6.20 ± 0.04	-11	7.91 ± 0.04	+13
HTPI^{e}	3.22 ± 0.30	-54	5.20 ± 0.30	+26
THSI^{e}	5.23 ± 0.26	-25	6.47 ± 0.26	- 8

a/ Percent gain and change in water sorption based on the reacted dry weight.

b/ Percent gain and change in water sorption based on the unreacted dry weight.

c/ Average film thickness = 6.2 mils

d/ Average film thickness = 3.8 mils

e/ Average film thickness = 2.0 mils

NOTE: The percent weight gain of the reactants can be found in Table III. All reactions were conducted at 70°C.

Table VII. Diffusion coefficients for diffusion of distilled water in MY720/DDS cured epoxy films at 30°C

Reactant	D (cm^2/sec) x 10^{10}	% Change
Untreated	0.82	---
ACN	455.40	55400
OTPI	6.51	694
MTPI	7.63	830
THSI	6.51	694

NOTE: All reactions were carried out at 30°C.

Table VIII. Diffusion coefficients for diffusion of distilled water in MY720/DDS cured epoxy films at 70°C

Reactant	D (cm^2/sec) x 10^{10}	% Change
Untreated	61.22	---
ACN	455.40	643
OTPI	21.18	-65
MTPI	22.04	-64
THSI	15.30	-75

NOTE: All reactions were carried out at 70°C.

Table IX

Masked Isocyanates Synthesized

	Isocyanate	Masking Agent	Code Name	M.P.°C	Unblocking Temp. °C
1.	α,α,α-Trifluoro-o-tolyl isocyanate	Pentafluorophenol	PhF$_5$.F$_3$oTI	73	
2.	Phenyl isocyanate	FC-10*	FC-10.Ph	88	130
3.	Hexamethylene diisocyanate	FC-10*	FC-10.HD4.MDI	105	185
4.	Hexamethylene diisocyanate	n-Butanol	Bu.HMDI	88	120
5.	Hexamethylene diisocyanate	Pentafluorophenol	PhF$_5$.HMDI	169	170
6.	Hexamethylene diisocyanate	Phenol	Ph.HMDI	136	180
7.	Cyclohexyl isocyanate	Phenol	Ph.CyHex	137	130
8.	Cyclohexyl isocyanate	Pentafluoro-thiophenol	PhF$_5$SH.CyHex	148	130
9.	Cyclohexyl isocyanate	2,4-Difluorobenzyl alcohol	F$_2$Bz.CyHex	83	120

*FC-10 = C$_7$F$_{16}$SO$_2$N(C$_2$H$_5$)C$_2$H$_4$OH

Table X

Elemental Analyses of Masked Isocyanates

	Masked Isocyanate		%C	%H	%N	%F	%S
1.	PhF$_5$.F$_3$oTI	Calc.	45.3	1.34	3.27	48.9	
		Found	44.96	1.33	3.95	48.71	
2.	FC-10.Ph	Calc.	33.38	2.25	4.21	45.71	
		Found	33.53	2.01	4.46	45.63	
3.	FC-10.HMDI	Calc.	29.83	2.63	4.44	48.38	
		Found	30.43	2.48	5.19	47.90	
4.	Bu.HMDI	Calc.	60.76	10.13	8.86		
		Found	60.81	10.18	8.79		
5.	Ph.HMDI	Calc.	67.41	6.74	7.85		
		Found	67.33	6.83	7.83		
6.	PhF$_5$.HMDI	Calc.	44.77	2.61	5.23	35.44	
		Found	44.60	2.63	5.34	35.25	
7.	Ph.CyHex	Calc.	71.23	7.76	6.39		
		Found	70.99	7.67	6.52		
8.	PhF$_5$SH.CyHex	Calc.	48.00	3.69	4.30	29.23	9.84
		Found	47.75	3.60	4.36	28.86	9.85
9.	F$_2$Bz.CyHex	Calc.	62.45	6.31	5.20	14.12	
		Found	62.34	6.14	5.44	14.01	

Table XI

Water Absorption Data for the Masked Isocyanate Incorporated epoxy Films

Masked Isocyanate	Mole % * Masked Isocyanate	Wt %	Maximum Water Uptake (wt %)	Reduction in Water Absorption (%)
None ("Control Epoxy")		0	6.1	0
Bu.HMDI	26	29	4.1	33
Ph.HMDI	49	44	2.6	55
PhF$_5$.SH.CyHex	20	37	1.9	65
Bu.Ph	20	26	2.1	62
Ph.CyHex	20	28	3.9	29
Ph.CyHex	30	37	2.8	46
F$_2$Bz.CyHex	20	32	3.42	38

*Based upon the total number of functional groups in epoxy prepolymer.

EFFECTS OF ENVIRONMENTAL EXPOSURE ON FIBER/RESIN INTERFACIAL SHEAR STRENGTH

Bernard Miller and Umesh Gaur

Textile Research Institute (TRI), Princeton, New Jersey 08542

INTRODUCTION

Mechanical properties of some fiber-reinforced polymers are known to degrade upon exposure to various environmental factors including hydrothermal (immersion in water) and hygrothermal (contact with water vapor) exposures. Moisture can affect each of the three phases in a composite, namely, the fiber, the matrix, and the interfacial zone. The changes induced in fiber and matrix polymers can be determined by separate studies on each component by itself, but the effect of moisture on the interface must be determined by studies on the composite system. It is generally accepted that the principal cause of composite shear strength reduction upon exposure to moisture is debonding or weakening of the interfacial bond.

Fiber-reinforced composites are generally characterized and evaluated by means of various standard tensile, flexural, and fatique tests performed on actual composite specimens. Although these tests provide valuable information about the overall or macroscopic properties of the composite, their results are strongly dependent on such factors as specimen geometry, fiber/matrix volume ratio, and fiber aspect ratio. Direct information about the fiber/matrix interface cannot be obtained by such means. In addition, macroscopic methods are not sensitive to heterogeneities in fiber surface, strength, and diameter.

A new experimental technique for direct measurement of the interfacial adhesion between a fiber and a resin matrix has been developed at TRI (1). The technique involves application of microdroplets of resin onto a single fiber, followed by measurement of the force required to pull out or debond the fiber from each droplet. The main advantage of this modified pull-out technique is that small diameter (about 10 μm) fibers, commonly used in fiber-reinforced composites, can be evaluated successfully.

The dimensions involved in the microbond method lead to several advantages with regard to environmental studies. First, uniform environmental exposure is simplified by the small droplet size. Also, any diffusion-controlled processes proceed on a shorter time scale than with the typical bulk composite. Thus, environmental studies may be conducted at lower temperatures and over shorter time periods using the microbond technique. Finally, the method allows localized fiber heterogeneity (on a scale of about 100 μm fiber lengths) to be considered in evaluating the effect of environmental exposures.

TRI MICROBOND TECHNIQUE

Background

The commonly used single fiber pull-out test involves measuring the force, in a direction parallel to the fiber axis, to "pull out" a single fiber which is partially embedded in a pool of cured resin. However, if the embedded length is greater than a critical value, ℓ_c, tensile failure will occur in the nonembedded portion of the fiber. This critical fiber length is given by

$$\ell_c = \frac{\sigma_f d}{4\tau}$$

where d = fiber diameter,

σ_f = ultimate fiber tensile stress at break , and

τ = interfacial bond strength (shear stress).

For very fine fibers such as those associated with engineering composites (glass, carbon, and aramids), the critical fiber length becomes extremely small. These fibers can be expected to have diameters of about 10 μm, tensile strengths ranging from 2,000-4000 MPa, and average interfacial shear strengths with typical resins of 10-70 MPa. Therefore, their critical fiber lengths fall in the range of 0.07-1.0 mm. Such very short embedded lengths are difficult to obtain experimentally, and are hard to handle and process. In addition, meniscus rise around the circumference due to wetting can increase the embedded length enough so that the critical fiber length is exceeded and the fiber fails prior to pull-out. Another potential problem is that the thinner resin coating in the meniscus region may rupture prior to debonding, leaving behind a crown or resin cone on the surface of the fiber. Although this complex failure process does not invalidate the subsequent shear strength measurement, it does require the inspection of every specimen after debonding to determine the true embedded length.

The TRI Microbond Test

The TRI microbond pull-out test involves the deposition of a small amount of resin onto the surface of a fiber in the form of one or more droplets which form concentrically around the fiber in the shape of ellipsoids. After appropriate hardening or curing, the fiber diameter and the droplet dimensions are measured with the aid of an optical microscope, the size of the droplet along the fiber axis determining the embedded length.

The fiber specimen is pulled out of the droplet using a special device to grip the droplet bonded to the fiber (Figure 1). This device consists of two adjustable plates that form a slit or micro-vise that is attached to a vertical drive system. The plates are positioned just above the droplet and the slit is narrowed symmetrically until the plates just make contact with the fiber (see Figure 1). As the plates move downward, an initial frictional force between the fiber and the shearing plates is registered, indicating that the slit is just touching the fiber and the droplet has little chance of slipping through; this frictional force is reproducible and can be adjusted to the same value for each specimen. As the shearing plates continue to move downward, they encounter the droplet and exert a downward force on it, which is recorded.
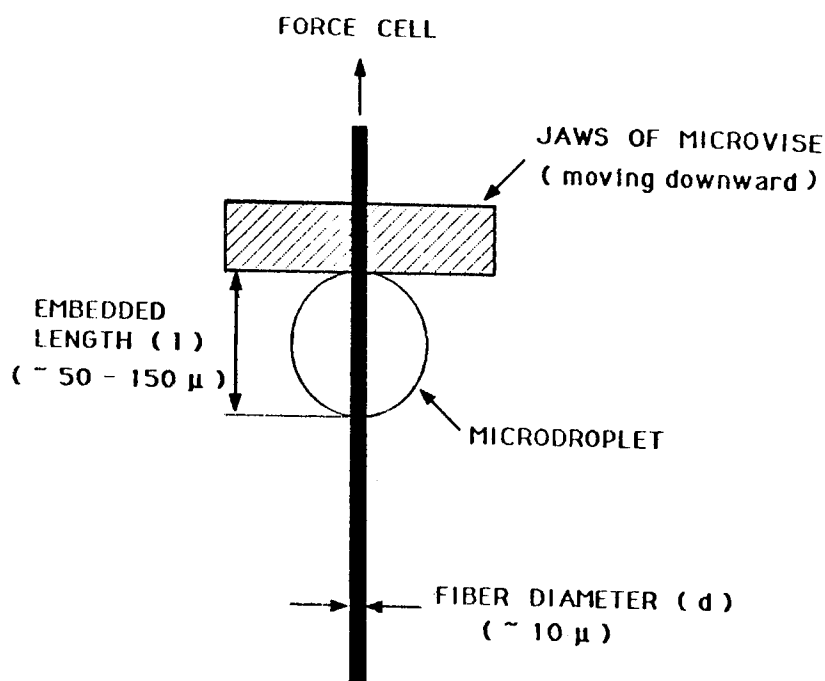

Figure 1. Arrangement for fiber/microdroplet debonding.

The interfacial shear stress, τ, is calculated using the equation:

$$\tau = \frac{F}{A} = \frac{F}{\pi d \ell} , \qquad (1)$$

where   F = measured debonding force,
        A = interfacial area,
        d = fiber diameter, and
        ℓ = embedded length.

Complete details of the microbond technique are given in reference (1).

Effect of Droplet Size

The general relationship used in shear strength measurement implies that the applied force is distributed uniformly and equally to all elements of the interface. This is not likely to be happening during microbond shearing nor, for that matter, in any other type of pull-out test. Force applied to a small portion (the area of contact between the micro-vise and the droplet) of a finite elastic body (the droplet) would not be evenly distributed but should decrease with distance from the point of application (Saint-Venant's principle).

Since the droplets in these experiments are very small, the variation in applied stress along the embedded length might be expected to have only a minor effect on the bond strength measurement. However, because of this small size, embedment length can be varied by a factor of five for some fiber/resin systems. Figure 2 shows pull-out load versus embedded area (proportional to embedded length) data collected for a large set of Kevlar 49/ Epon 828 specimens. (Because of the high tenacity of the fiber, it was possible to use large drops without having the bond shearing process pre-empted by fiber rupture.) The points in Figure 2 show a distinct trend away from linearity and toward a reduced slope (i.e., apparently lower bond strengths) as embedded area is increased. Figure 3 shows the same data divided into subsets according to embedded area; each bar represents areas within a $500 \ \mu m^2$ (14 μm length) range. The average shear strengths, as calculated using Equation 1, are shown for each subset. There is an obvious trend toward decreasing bond strength as the embedment area increases.

The results in Figures 2 and 3 suggest that the applied shearing force is not being distributed uniformly over the entire interface but is concentrated at the upper part. Thus, when a certain amount of force produces pull-out, more of it has been applied to that location to produce initial bond rupture which propagates down the interface. As
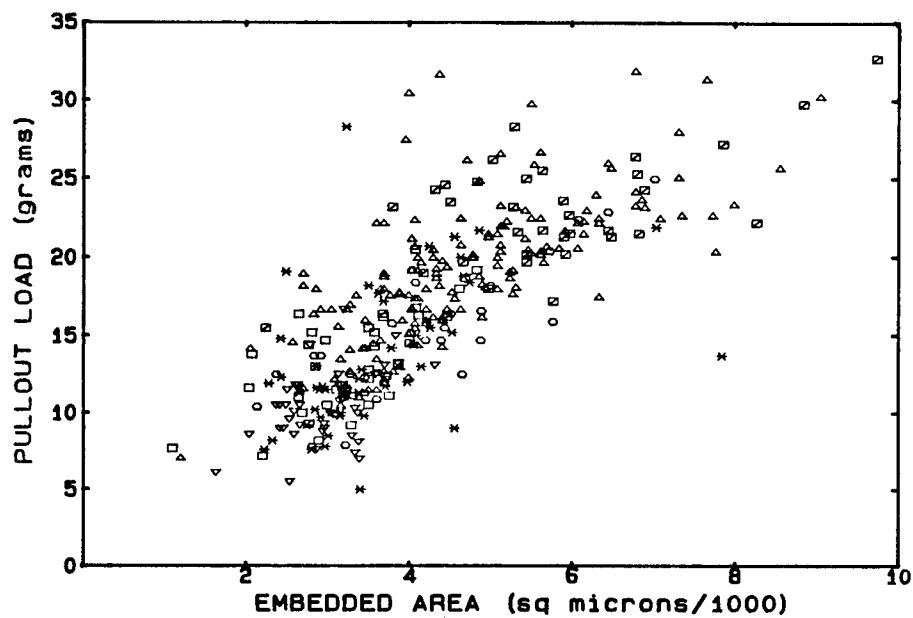
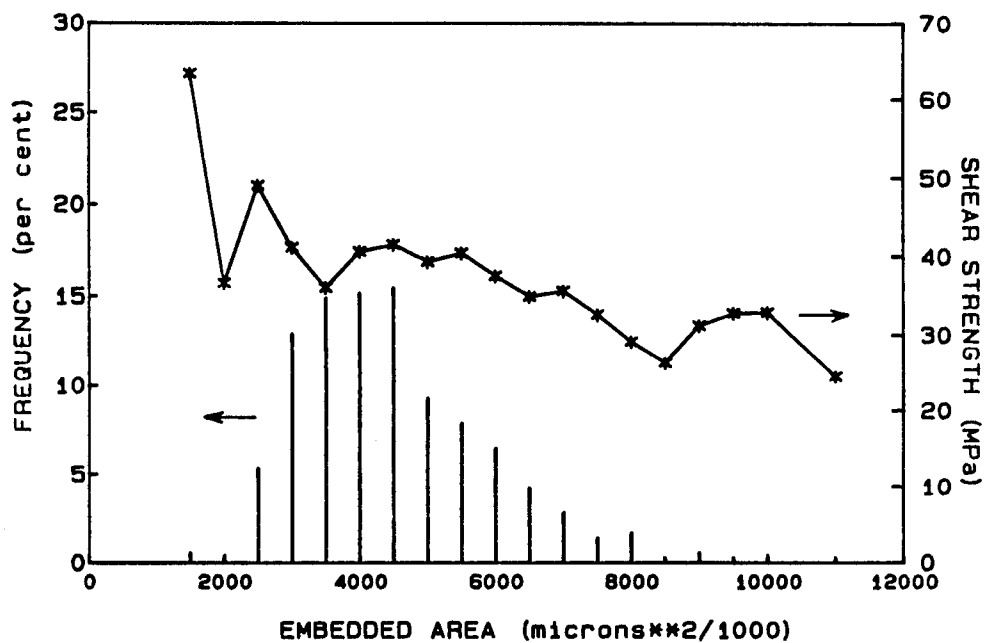Figure 2. Pull-out data for six different experiments with Kevlar 49/Epon 828.

Figure 3. Frequency distribution of average embedded areas for 500 μm^2 ranges (data of Figure 2). Average shear strengths are shown for each subset.

embedded length increases, the proportion of the applied force that is concentrated at the top of the interface increases, leading to premature rupture and an apparent reduced bond strength when Equation 1 is used. This interpretation makes it necessary either to keep drop sizes and size distribution as small as possible, which may not always be practical, or to compare results for different systems only within narrow embedment length ranges.

EFFECTS OF HYDROTHERMAL & HYGROTHERMAL EXPOSURES

Materials
Kevlar® 49 (Du Pont). Average filament diameter 11.4 μm, washed in methanol, rinsed in acetone, and air dried.

E-glass (Owens-Corning Fiberglas). Pristine E-glass, average filament diameter 11.3 μm, used without further treatment.

Resin: Epon 828 (Shell) and 4,4'-methylene diamiline (Aldrich Chemicals), 4:1 weight ratio, cured 2 hours at 80°C and 2 hours at 150°C.

Results and Discussion
The microbond technique has been used to investigate the response of Kevlar 49 / Epon 828 and E-glass / Epon 828 interfaces to a number of environments. The basic procedure involves exposure of a set of 15-40 cured fiber/resin microdroplet assemblies to the environmental factors of choice for a specified period of time and shearing the microdroplets promptly following exposure. A control experiment is conducted in parallel with each set of environmental exposures. Embedment lengths of control and aged microdroplets are similar, so that measured average shear strengths are directly comparable.

Typical responses to environmental stress are shown in Figures 4 , 5, and 6. In Figure 4, the shear strength distribution of Kevlar 49/ Epon 828 control specimens are compared with those of the specimens held at 0% relative humidity for 480 hours (20 days). Not only are the shear strength values equivalent, but the strength distributions are almost identical. Figure 5 shows a significant shift in shear strength distribution towards lower values as a result of refluxing in water at 88°C for 70 hours. Figure 6 shows a similar shift in shear strength distribution for E-glass/Epon 828 specimens after refluxing in water 0.5 hour at 88°C.
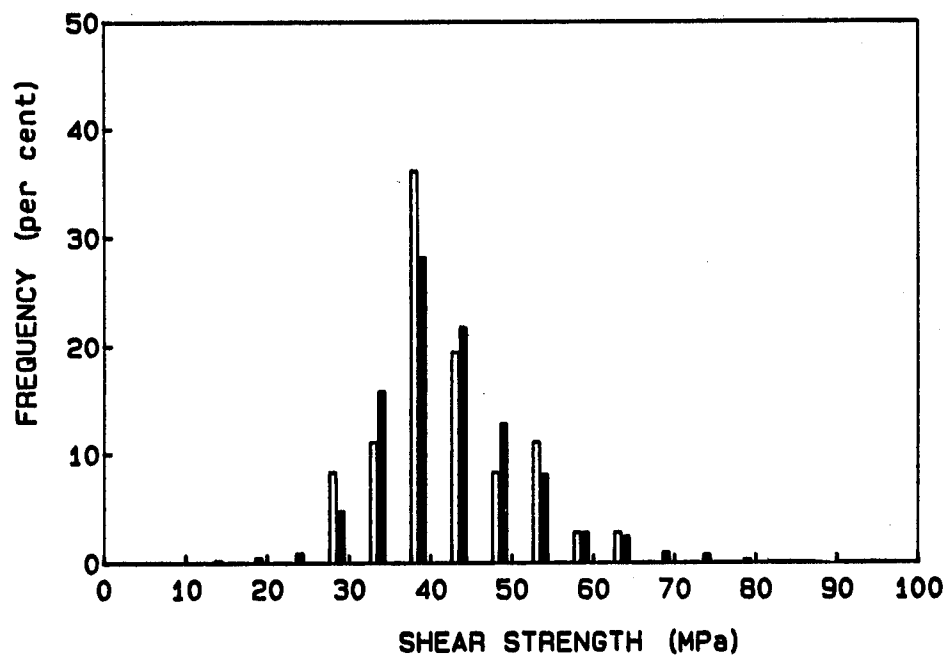
Figure 4. Shear strength distributions for Kevlar 49/Epon 828 before (filled bars) and after 480 hours of aging at 0% RH (open bars).
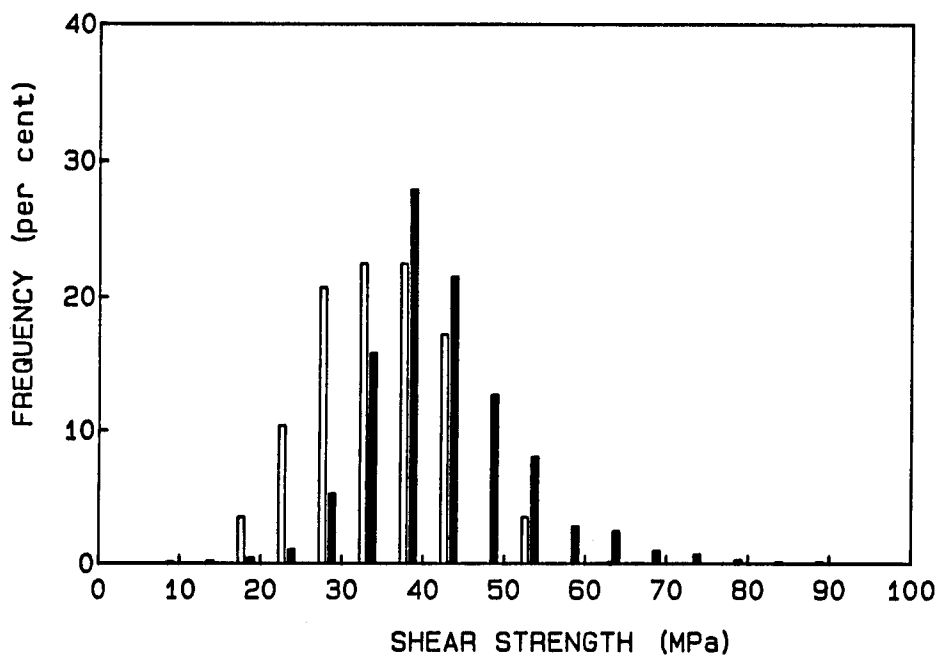

Figure 5. Shear strength distributions for Kevlar 49/Epon 828 before (filled bars) and after 70 hours exposure to water at 88°C (open bars).
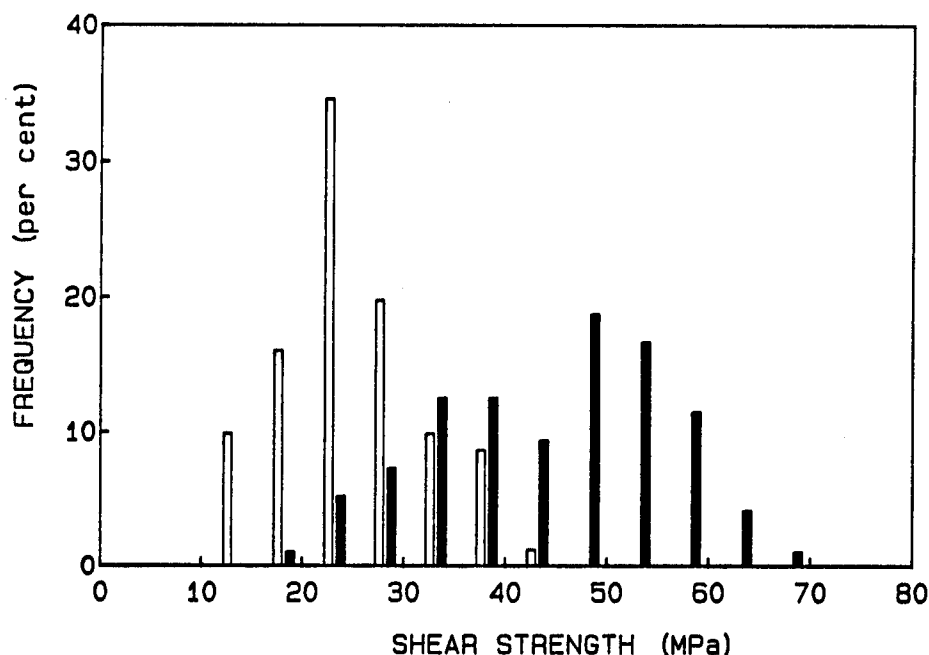
Figure 6. Shear strength distributions for E-glass/Epon 828 before (filled bars) and after 0.5 hour exposure to water at 88°C (open bars).

Effects of environmental exposures on average shear strength for Kevlar 49/Epon 828 and E-glass/Epon 828 are summarized in Tables I and II. The results in Table I indicate that significant bond strength reductions for Kevlar 49/Epon 828 were obtained only upon exposure to steam and upon refluxing in water at 88°C. The results in Table I also imply that reduction does not go beyond a loss of about 40% of the initial shear strength value. Similarly, Table II indicates a plateau in bond strength reduction for E-glass/Epon 828 after a loss of about 40% of the initial shear strength value.

The most reasonable explanation for this lower limit is that interfacial shear strength comes from a number of contributions to fiber/resin interaction, possibly including chemical bonding, van der Waals forces, electrical attraction, friction, and residual thermal compression forces. The shear strength degradation produced by exposure to water would not be expected to degrade all of these forces.

Table I

Effect of Hydrothermal and Hygrothermal Exposure on Shear Strength of Kevlar 49/Epon 828

Control shear strength: 39-45 MPa

Environment	Exposure time, hours	Shear strength, % of control value
Dry (0% RH), 22°C	40	0.97
	144	1.09
	480	1.03
85% RH, 22°C	16	1.00
	576	0.90
Water, 22°C	168	1.02
HCl (pH 2), 22°C	2	0.95
	26	1.02
	168	0.88
HCl (pH 1), 22°C	168	1.03
Water, 88°C	20	0.80
	40	0.77
	70	0.77
	88	0.76
	240	0.85
	600	0.69
Steam	2	0.62
	8	0.73
	20	0.59

Table II

Effect of Hydrothermal Exposure on Shear Strength of E-glass/Epon 828

Control shear strength: 43-44 MPa

Environment	Exposure time, hours	Shear strength, % of control value
Water, 88°C	0.5	0.56
	1.0	0.65
	2.0	0.64
	16.0	0.61
	72.0	0.67

A few experiments have been conducted to investigate the possible reversibility of shear strength decreases caused by environmental exposure. Substantial regain of composite properties has been reported for Kevlar/epoxy and other bulk composite systems when hydrothermal exposure was followed by drying (2). In addition, for certain bulk composite systems (graphite/epoxy), the temperature of hydrothermal exposure relative to the glass transition temperature of the matrix was found to have a major effect on regain of composite properties with drying: hydrothermal exposure above the matrix T_g resulted in much smaller property regain upon drying (3). Preliminary microbond results have been obtained for degraded Kevlar/Epon 828 specimens after subsequent drying above and below the resin T_g, which is about 70°C. To date, no measurable recovery of bond strength has been obtained with any combination of vacuum and heat drying for 24 hours.

REFERENCES

1. B. Miller, P. Muri, and L. Rebenfeld, Composites Science and Technology 28, 17 (1987).

2. C.J. Jones et al., Proceedings of the Royal Society of London Series A - Mathematical and Physical SC 396, N1811, 318 (1984).

3. L.T. Drzal, M.J. Rich, and M.F. Koenig, J. Adhesion 18, 49 (1985).

DESIGN AND FABRICATION OF BONDED JOINTS ON LARGE CANTILEVERED COMPOSITE TUBES

by Paul D. Wienhold and Richard L. Jarvis, AAI Corporation, Hunt Valley, Maryland.

OBJECTIVE

The utilization of remotely piloted vehicles (RPV's) aboard U.S. Navy ships is contingent on reliable methods of recovery. Currently, Pioneer RPV's are recovered on battle ships with a three mast net retrieval system developed by All American Engineering. However, this system requires considerable deck space and is not suitable for installation on destroyers and frigates.

AAI has developed a rotary shipboard net retrieval system (SNRS) illustrated in Figure 1 which has a relatively small footprint suitable for installation on ships with limited deck space. The base of the SNRS can be rapidly secured to standard deck fittings, thus eliminating the need for any shipboard modifications. The unit has a self-contained hydraulic power supply which can rapidly deploy or stow the net retrieval system. The mounting base has four retractable wheels to facilitate installation and stowage. The net retrieval arms have quick release connections which facilitate assembly and dismantling of the net support frame.

The AAI Shipboard Net Retrieval system is designed to recover the Mazlat/AAI Pioneer remotely piloted vehicle at gross weights up to 410 pounds and velocities from 30 to 60 knots. The SNRS uses a nylon cargo net supported by a lightweight, goal post frame. The net and support frame are allowed to pivot about a horizontal bearing as the RPV is recovered. The frame and net are decelerated by a caliper disc brake which is modulated by an electronic controller sensing frame rotational velocity.

AAI's baseline design used a 40 x 50 foot net supported by an aluminum tubular goal post frame. While the aluminum frame was suitable for recovering hardened dummy RPV's, its relatively high rotary inertia characteristics imposed excessive deceleration loads on the Pioneer RPV wing and tail sections. In order to reduce the recovery loads on the Pioneer RPV, AAI redesigned the goal post frame using advanced composite materials. The objective was to reduce the weight and rotary inertia of the frame by 50 percent or more and at the same time to increase the stiffness and fatigue life of the frame.

The composite frame had to be interchangeable with the aluminum baseline design. The thirty-six foot long vertical posts were 12.75 inches in diameter and had tapered walls for optimum strength and stiffness. Shipboard stowage and handling requirements dictated that each 36 foot long pole be assembled from two eighteen foot long sections with quick release connections. The quick release connections consisted of flanged aluminum fittings bonded to the ends of the 18 foot composite poles and two 180 degree annular aluminum clamps joined by two one-half inch diameter bolts. Since AAI's filament winding machine and curing ovens could not accommodate an 18 foot tube, it was necessary to fabricate two nine-foot composite tubes and joint them with a permanent bonded joint.

490

APPROACH

The requirement to recover the Pioneer at velocities between 30-60 knots at various approach angles and impact points represented considerable technical risk. Deceleration loads had to be limited to approximately 4 g's. Also, the possibility of the RPV either extending the net and impacting the dock, or rebounding from the net, had to be considered.

In order to assess these technical risks and optimize the design characteristics of the SNRS, AAI developed a computer model of the net retrieval system. Several hundred graphical simulations of the recovery dynamics were run resulting in refinements of the system inertia, stiffness and braking characteristics. Based on these simulations, AAI was able to complete the design, fabrication, and testing of the SNRS within a seven month period. Approximately one hundred successful recoveries were accomplished with minimal modifications to the system and with very good correlation between the computer model and test results as indicated in Figure 2.

The results of the graphical simulations were used as inputs to a NASTRAN finite element analysis of the net support arms which analyzed both static stresses and deflections and buckling behavior. The design chosen for the composite net retrieval arm consisted of four 9 foot graphite/epoxy tubes with wall thicknesses of 0.065, 0.098, 0.114, and 0.136 inches, from bottom to top respectively. The tubes were filament wound at AAI using +/- 15° and +/- 65° helix patterns onto 12-5/8 inch diameter by 10 foot long aluminum mandrels. Amoco T-300 graphite fibers and bisphenol-A resin with an acid anhydride hardener were used.

The joints discussed here were designed for the attachments between the tube sections.

DESIGN

Numerous bonded and bolted joint configurations could be applied to this application and were considered. Bolted joints would add too much weight, that of the fasteners themselves and the locally increased material thickness at the fastener holes. They would also suffer from possible fatigue and corrosion problems. Scarf and stepped lap joints are considered the highest strength and lightest weight bonded joints. However, they are impractical in this case due to the need for precise machining of the joint details on the large tube components. Simple lap joints have excessive peel and bending stresses due to the fact that the strap centerline is offset from that of the tubes.

The tapered double strap joint concept was selected. (See Figure 1.) It has low bending and peel stresses and correspondingly low stress concentrations. It has a high weight efficiency and requires little machining, all of which is done on the straps only. The assembly procedures are straightforward and require little tooling.

One or more layers of E-glass/epoxy fabric pre-preg were co-cured to the outside surface of the tubes in the area of the adhesive bonds to build up the outside diameter of the smaller of the tubes to that of the larger and to "soften" the joint. "Softening" means to put down a layer of intermediate stiffness between the strap and the first layer of the tube in which the fibers are nearly transverse to the load direction at

491

+/- 65°. In addition, the edges of the straps were tapered at 5° to reduce peel stresses and to reduce the stress concentrations in the tube walls. Peel stresses are reduced this way since the offset between the centerline of the strap and the tube wall is reduced down to the surface of the tube itself, greatly reducing the out-of-plane bending moment generated in the strap at its free edge. The stress concentration in the tube wall is reduced greatly over that which would occur at 90° corner at the free edge of a square-edged strap. Also, since the the stiffness of the strap increases gradually, the load transfer, too, is gradual.

The tapered double strap joint design was used at five locations on each net support arm. The detail at two of the locations, as shown in Figure 1a, consisted of a permanent joint between two composite tubes using graphite/epoxy straps on the inside and outside surfaces. The outside straps were in 120° segments for ease of assembly, while the inside strap was a full circle with a longitudinal split, again to facilitate assembly. At the other three locations a separable joint was required. An aluminum fitting with a flange for a ring-type clamp was bonded to the tubes using the tapered double strap joint concept. (See Figure 1b.) In these cases, however, the inside strap was a single graphite/epoxy part, as in the previous cases, but the outside strap was an integral part of the aluminum end fitting.

MATERIAL SELECTION

Graphite/epoxy fabric pre-preg was selected for the straps because of its high strength to weight ratio and its compatibility with the tubes themselves. It is also more damage tolerant and easier to work with than pre-preg tape. Fiberite HMF-322/714AH 250°F curing material was used. It is relatively low cost, is readily available, and has been used with good results at AAI. The low curing temperature allowed the use of sections of net support arm tubes, previously cured at 305°F, as lay-up tools. The elevated temperature wet (ETW) "B" allowables for the material are:

Ft = 57.3 ksi
Fc = 66.7 ksi
E1 = E2 = 8.6 msi

Two adhesives were selected, a two-part epoxy paste and an epoxy film adhesive. The room temperature curing paste was used for applications which required sliding fits or where the assembly could not be oven cured due to its size. The film, being easier to work with and higher strength, was used for all other applications.

Hysol 9309.2 epoxy paste adhesive was selected primarily for its high shear allowables of 5000 psi as-cured at room temperature and 4100 psi after conditioning for 90 days at 120°F and 98% relative humidity. In addition, it is has a low modulus which reduces peel stresses in a bond joint. It was used with a nylon scrim to control the bond line thickness. A handleable bond is achieved in 12 hours which is to be followed by a 6-1/2 day full cure.

American Cynamid FM-123-5-.06 epoxy film adhesive was selected for similar reasons. It cures at 225°F which makes it acceptable for use on the 305°F cured tubes. It is readily available and has been used with good success at AAI. It, too, is low modulus and has a shear strength of 5655 psi after conditioning for 30

days at 127°F and 95% relative humidity. It is supported with a knitted nylon carrier to control the bond line thickness.

STRESS ANALYSIS

Maximum tension and compression loads at each joint were calculated from the results of the NASTRAN finite element analysis of the net support arms. The greatest resultant force calculated at any of the nodes along the joint was assumed to be distributed along the 22.5° section of the diameter half way between it and the adjacent nodes. The result is the maximum load per unit width. Since it is assumed that the inner and outer straps share the load equally, one half of this value is the design load. The example shown here corresponds to the joint at the base of the net support arm which is the most highly loaded. The greatest load on this joint is 10460 pounds over the 22.5° arc section. The load per width (F/W) was calculated as follows:

$$F/W = \frac{10460 \text{ lb}}{2 \pi (13.36 \text{ in}) (22.5°/360°)}$$

$$= 1994 \text{ lb/in}$$

The strap overlap length was calculated using a conservative value for the adhesive shear strength of 3000 psi, a stress concentration factor of 2.0, and a factor of safety of 1.5. This results in a working shear stress allowable of 1000 psi. The overlap length (L) for one side of the joint was calculated as follows:

$$L = \frac{1994 \text{ lb/in}}{1000 \text{ psi}} = 1.994 \text{ in}$$

This value was rounded up to the nearest .10 inches or 2.00 inches.

The strap thickness was calculated using the lower of the tensile and compressive ETW "B" allowables, a stress concentration factor of 2.0, and a factor of safety of 1.5. This results in a working tensile/compressive stress allowable of 19.1 ksi. The strap thickness (T) was calculated as follows:

$$T = \frac{1994 \text{ lb/in}}{19.1 \text{ ksi}} = 0.104 \text{ in}$$

This value was rounded up to the nearest increment of the material ply thickness of 0.014 inches or 0.122 inches.

FABRICATION

The composite straps were hand layed up onto composite and aluminum tools and autoclave cured. All the edges were then ground to their final dimensions including the 5° tapers. Surface preparation for bonding was provided by the use of peel ply on the areas of the tubes and straps to be bonded. The peel ply was removed just prior to bonding. The aluminum fittings were FPL etched and primed with American Cyanamid BR-127 primer in the area to be bonded. All areas adjacent to the bonded joints were covered with polyester flash breaker tape to allow simple and thorough clean up of excess cured adhesive.

Pressure was applied to the outside straps during the cure of the adhesive using a standard vacuum bag with 27 inches of mercury applied. This was not possible for the inside straps so a pressure bladder was designed and built. It consisted of a spool-shaped aluminum fixture 10 inches long by 12 inches in diameter with silicone rubber walls bonded and clamped to the edges of the end plates. Pressure of 7 psi was applied by a continuous supply of regulated shop air through a hose connected to a fitting in one of the

end plates. The bladder was located at the joint in the middle of the 18 foot assemblies with an aluminum locating rod threaded to a tapped hole in the bladder's end plate. High temperature materials were used so that the bladder could be used in cure cycles of up to 350° F.

The aluminum end fittings were machined to an inside diameter which provides a tight fit with the tubes outside diameter such that no additional pressure was required. They were held in place in the axial direction during cure with a threaded aluminum rod extending through the tube with 3/8 inch aluminum end plates pulled up to both ends.

The bonding procedure began with the installation of the aluminum end fittings. The paste adhesive was applied to both surfaces to be bonded. The nylon scrim was layed into the wet adhesive on the tube. The fitting was slid onto the tube with a slight rotation and held in place with the two end plates drawn up to the threaded rod.

The graphite/epoxy inner straps at the joints with aluminum end fittings were bonded on next. The sheet of film adhesive was tacked to the inside surface of the tube with a heat gun. The strap was located on the tube and held in place with polyester tape. The pressure bladder was installed inside the tube over the strap and pressurized to 7 psi. The adhesive was then oven cured for one hour at 225°F.

The next assembly step was the bonding of the inside strap to one of the tubes at the permanent joints between composite tubes. The same basic procedure was used as with the other inner straps using film adhesive oven cured with the pressure bladder. Following that step, the exposed half of the inside strap was bonded to the other tube, assembling the two tubes. Again, Epoxy paste was applied to both surfaces with a layer of nylon scrim. Then the tubes were assembled and the pressure bladder located and inflated. The tubes were then aligned using a transit and adjusting the tripod tube support stands. The end plates were then drawn up on the treaded shaft to hold the tubes together.

Finally, the graphite/epoxy outside straps were bonded at the joint between the composite tubes. A similar procedure was followed using epoxy paste with nylon scrim. In this case pressure was applied with a vacuum bag installed over the joint area with a full vacuum applied for the 12 hour initial cure.

RESULTS

One complete net retrieval system was fabricated. Static proof tests were performed to working loads on one tube section with bonded joints while another tube section with an obsolete wall design was tested to failure. In both cases all adhesive bonds survived intact. Failures in the second test were restricted to the tube itself. Seventeen operational tests of the net retrieval system were performed with the composite net support arms installed. The tubes and bonded joints were undamaged and reduced RPV deceleration loads substantially.

FUTURE IMPROVEMENTS

The adhesive bond joints in the net support arms could be further optimized through the use of specialized

494

Air Force joint design software. These programs known as JOINT, BONJO, JTSDL, and A4EI are available from ASIAC (Aerospace Structures Information and Analysis Center) and have been transferred to AAI.

CONCLUSIONS

The tapered double lap joint is an efficient, reliable, and practical bonded joint concept for cantilevered composite tubes and other large structures. Its design and fabrication are straightforward when the appropriate materials are chosen and the correct procedures are followed.

ACKNOWLEDGMENTS

The authors wish to thank Dr. Young Kim, Michael Maher, and Vincent Myers for assistance in the design, material selection, and process development of the net support arm bonded joints. They would like to thank Terry Zeleny and Spencer Coogle for their work in fabricating the filament wound tubes and the bonded joints. They also thank Kent Jones for his fine illustrations.

REFERENCES

Perry, Henry Alexander; Adhesive Bonding of Reinforced Plastics; Naval Ordnance Laboratory, White Oak, MD; McGraw-Hill Book Co.; Copyright 1959.

Joining of Advanced Composites; Engineering Design Handbook; DARCOM Pamphlet No. 706-316; March 23, 1979.

Renton, W. James & Vinson, Jack R.; The Efficient Design of Adhesive Bonded Joints; Department of Mechanical and Aerospace Engineering, University of Delaware, Newark, DE; August 20, 1974; Gordon and Breach Science Publishers Ltd.; Copyright 1975.

Adams, R.D. & Peppiatt, N.A.; Stress Analysis of Adhesive Bonded Tubular Lap Joints; Dept. of Mechanical Engineering, University of Bristol, Bristol, England; July 30, 1976; Gordon and Breach Science Publishers Ltd.; Copyright 1977.

Hart-Smith, L.J.; Adhesive Bonding of Aircraft Primary Structures; Douglas Aircraft Co., McDonnell Douglas Corp., Long Beach, CA; Society of Automotive Engineers; Copyright 1980.
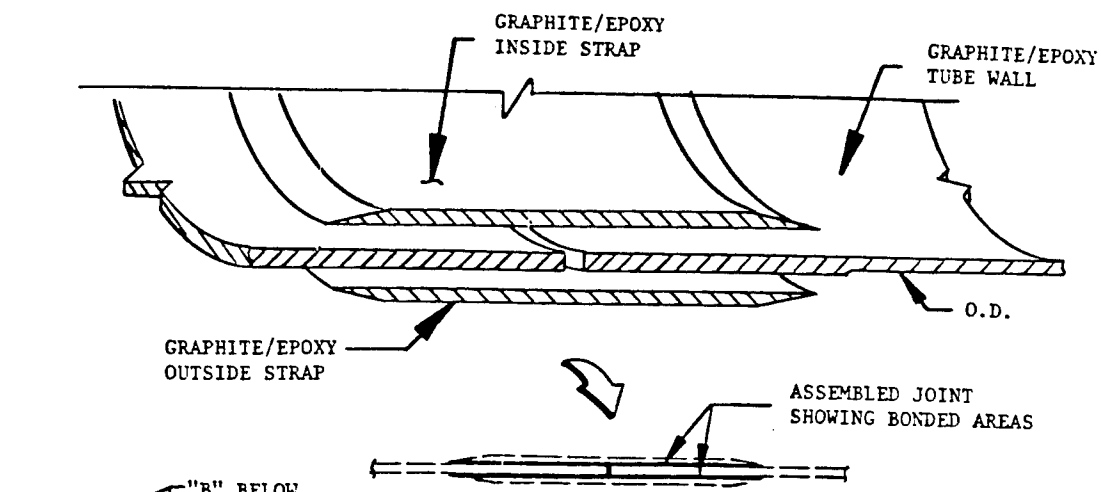
GRAPHITE/EPOXY
INSIDE STRAP

GRAPHITE/EPOXY
TUBE WALL

GRAPHITE/EPOXY
OUTSIDE STRAP

O.D.

ASSEMBLED JOINT
SHOWING BONDED AREAS

"B" BELOW

"A" ABOVE

"B" BELOW

Figure 1a. DOUBLE-LAP COMPOSITE STRAP JOINT

GRAPHITE/EPOXY INSIDE STRAP

GRAPHITE/EPOXY TUBE WALL
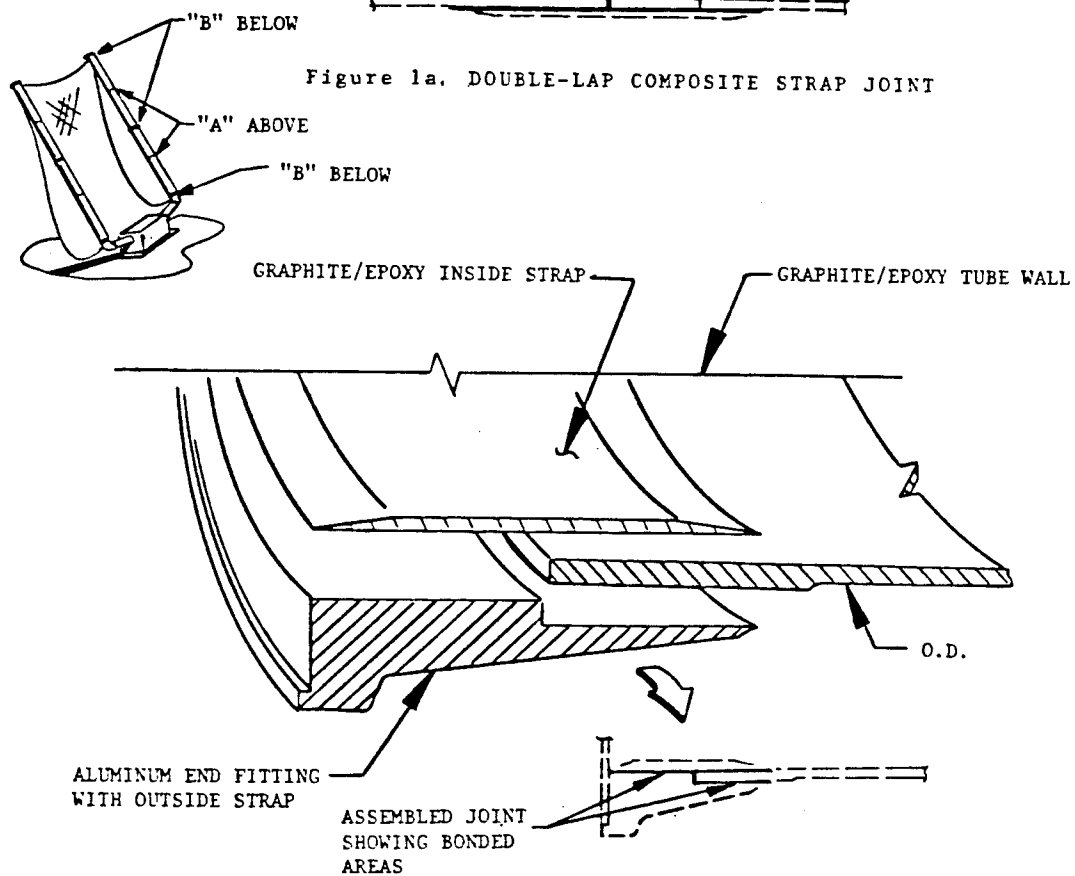
O.D.

ALUMINUM END FITTING
WITH OUTSIDE STRAP

ASSEMBLED JOINT
SHOWING BONDED
AREAS

Figure 1b. DOUBLE-LAP COMPOSITE/ALUMINUM STRAP JOINT

496
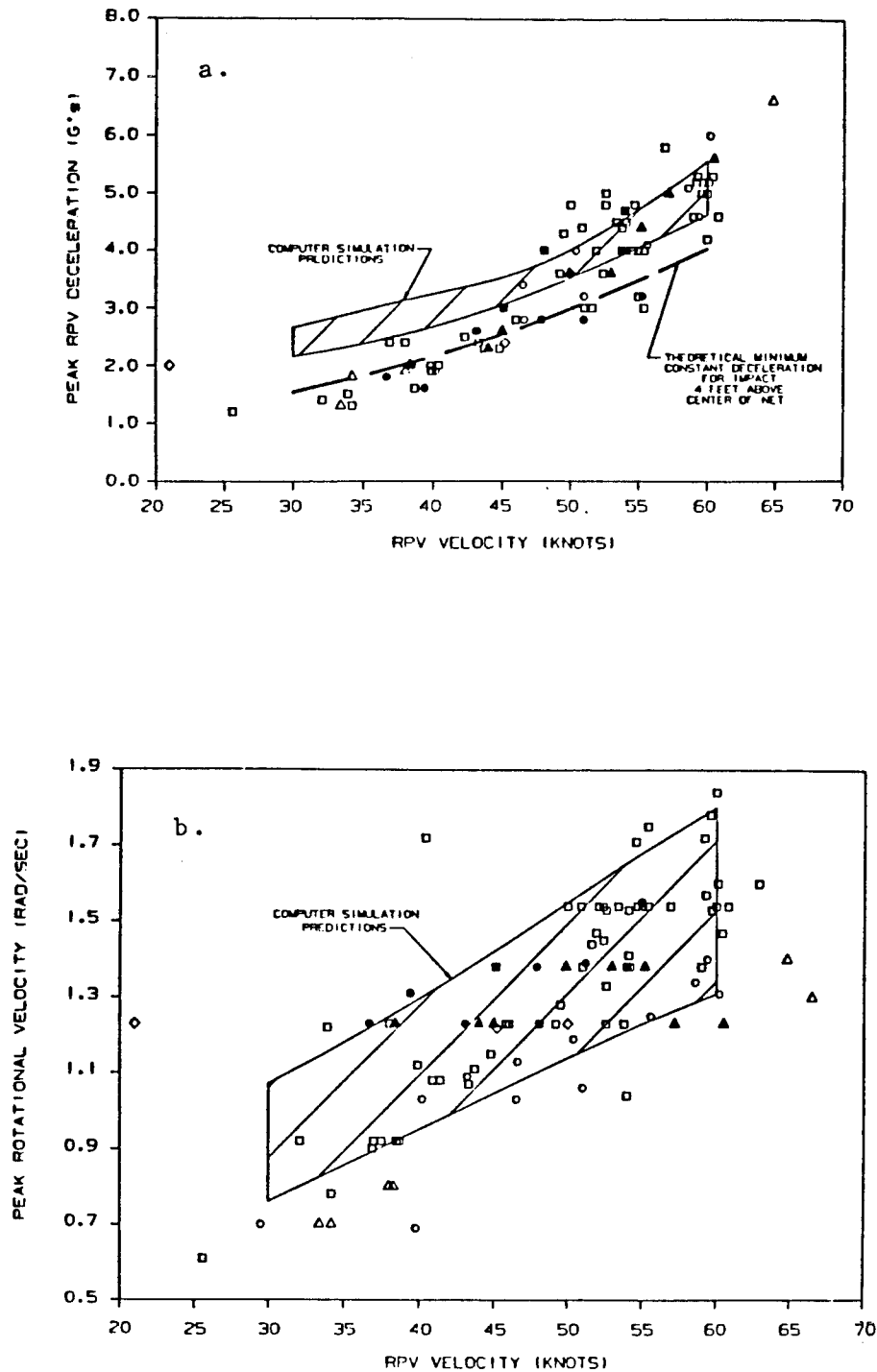
Figure 2. Computer Simulation Prediction and Actual Test
Data for AAI's Shipboard Net Recovery System

STRENGTH ESTIMATION OF ADHESIVE BONDED JOINTS BETWEEN CARBON STEEL SHAFT AND GFRP TUBE

Kozo Ikegami, Keizo Matsuo and Toshio Sugibayashi
Research Laboratory of Precision Machinery and Electronics
Tokyo Institute of Technology
Midoriku, Yokohama 227, Japan

The joining method of fiber reinforced plastics and metal is one of the most important problem for the practical use of fiber reinforced plastics The strength of joints between carbon steel shaft and glass fibe reinforced plastics(GFRP) tube with bonding epoxy resin is investigated analytically and experimentally. The stress and strain distributions in the joint are analysed by using the finite element method under axial load and torsional load. The high stress or strain concentrations occurrs at the edges of overlapping region between steel shaft and GFRP tube. The analysed strain distributions are compared with the experimental strain distributions. The strength of the shaft joint is predicted by applying the strength laws of GFRP, carbon steel, adhesive layer and their interfaces to the corresponding parts. The critical load of each part of the joint is determined. The initial failure load is determined by the smallest value among the critical loads in GFRP tube, carbon shaft, adhesive layer and their interfaces.

Figs. 1 and 2 show the joint model and the coordinates of the model. The elastic constants of the joint material are given in Table 1. The strength laws used for predicting the joint strength are as follows.
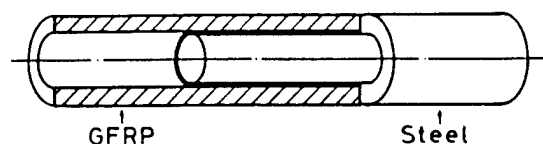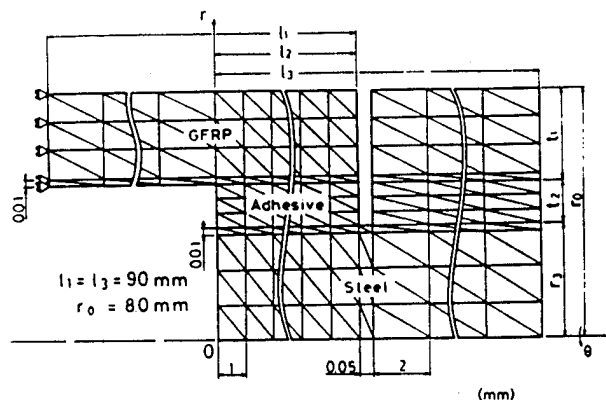

Fig. 1 Joint model

Fig. 2 Coordinates of joint

For GFRP,
$$F_f = c_1(\sigma_r - \sigma_\theta)^2 + c_2(\sigma_\theta - \sigma_z)^2 + c_3(\sigma_z - \sigma_r)^2$$
$$+ c_4\sigma_z + c_5\sigma_r + c_6\sigma_\theta + c_7\tau_{r\theta}^2 + c_8\tau_{z\theta}^2 + c_9\tau_{rz}^2 = 1$$

For carbon steel,
$$F_s = \{\sigma_z^2 + \sigma_r^2 + \sigma_\theta^2 - \sigma_r\sigma_\theta - \sigma_\theta\sigma_z$$
$$- \sigma_z\sigma_r + 3(\tau_{r\theta}^2 + \tau_{z\theta}^2 + \tau_{rz}^2)\}^{1/2}/343 = 1$$

For adhesive resin,
$$F_a = \{\sigma_z^2 + \sigma_r^2 + \sigma_\theta^2 - \sigma_r\sigma_\theta - \sigma_\theta\sigma_z$$
$$- \sigma_z\sigma_r + 3(\tau_{r\theta}^2 + \tau_{z\theta}^2 + \tau_{rz}^2)\}^{1/2}/64 = 1$$

For adhesive interfaces,
$$F_i = |\sigma_r/31.5|^{0.66} + |(\tau_{r\theta}^2 + \tau_{rz}^2)^{1/2}/30.8|^{0.66} = 1$$

The notations c in the strength law of GFRP are represented by the following equations.
$$c_1 = \{(F_{tr}F_{cr})^{-1} + (F_{t\theta}F_{c\theta})^{-1} - (F_{tz}F_{cz})^{-1}\}/2$$
The values c_2 and c_3 are obtained by changing circularly z, r and θ.
$$c_4 = (F_{tz})^{-1} - (F_{cz})^{-1}$$
The values c_5 and c_6 are obtained by changing circularly z, r and θ.

$$c_7 = (F_{sr\theta})^{-2}$$

The vaules c_8 and c_9 are obtained by changing circularly z, r and θ. The values of F are given in Table 2.

The failure stresses of the joint under tensile and torsional load and combined loads are shown in Figs. 3 to 5. The curves in Figs. 3 and 4 are the critial stresses in GFRP, steel shaft, adhesive layer and adhesive interfaces. In Fig. 5 the smallest critical stresses are illustrated for the joint of various ratioes $\bar{S} = (r_3/r_0)^2$ of cross sectional area between carbon steel and GFRP tube. The experimental initial and final failure stresses are solid marks and blank marks, respectively.

Table 1 Elastic constants of joint materials

		GFRP	Carbon steel	Adhesive resin
Ez , Eθ	GPa	9.98	206	3.33
Er	GPa	7.56		
Grz , Grθ	GPa	1.60	77.4	1.24
Gzθ	GPa	3.22		
Vrz , Vrθ		0.156	0.33	0.34
Vzθ		0.105		

Ez , Eθ , Er : Young's modulus
Grz , Grθ , Gzθ : Shear modulus
Vrz , Vrθ , Vzθ : Poisson's ratio

Table 2 Fundamental strength of GFRP

	Ftz Ftθ	Ftr	Fcz Fcθ	Fcr	Fsrz Fsrθ	Fszθ
Strength MPa	215	25.0	243	497	39.7	980

Ftz,Ftθ,Ftr : Tensile strength
Fcz,Fcθ,Fcr : Compressive strength
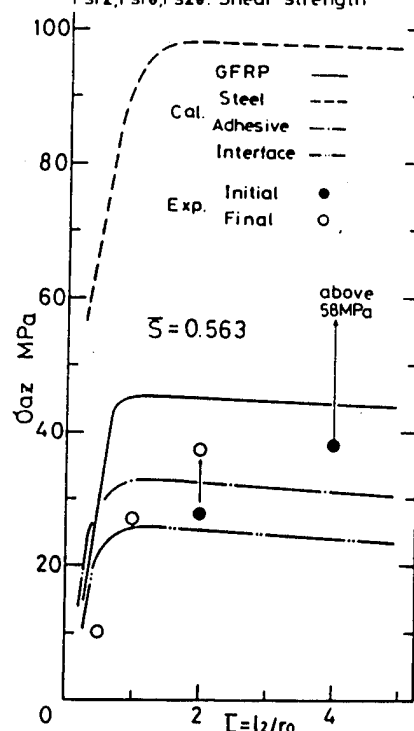Fsrz,Fsrθ,Fszθ : Shear strength
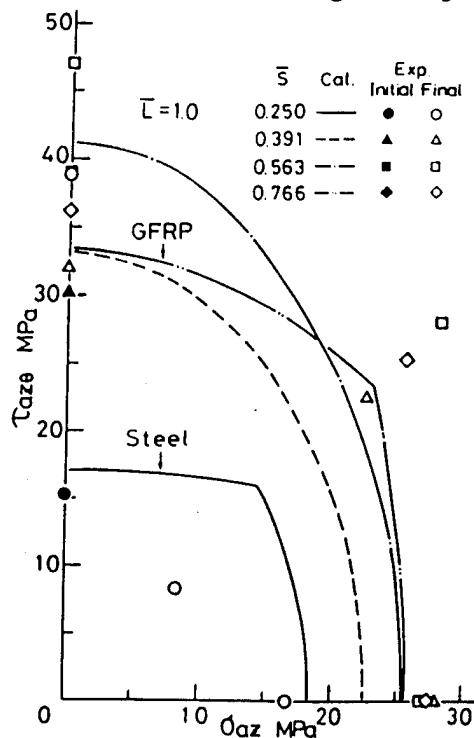

Fig. 3 Tensile strength of joint

Fig. 4 Torsional strength of joint

Fig. 5 Joint strength under combined laods

499